DIFFERENTIAL MODULATION OF THE STRUCTURAL AND

FUNCTIONAL CHARACTERISTICS OF HUMAN MATRIX

METALLOPROTEINASE ISOZYMES UPON BINDING TO

DIFFERENT LIGANDS

A Dissertation
Submitted to the Graduate Faculty
of the
North Dakota State University
of Agriculture and Applied Science

By

Bratati Ganguly

In Partial Fulfillment of the Requirements
for the Degree of
DOCTOR OF PHILOSOPHY

Major Department:
Chemistry and Biochemistry

September 2010

Fargo, North Dakota

North Dakota State University
Graduate School

Title

DIFFERENTIAL MODULATION OF THE STRUCTURAL AND FUNCTIONAL

CHARACTERISTICS OF HUMAN MATRIX METALLOPROTEINASE

ISOZYMES UPON BINDING TO DIFFERENT LIGANDS

By

BRATATI GANGULY

The Supervisory Committee certifies that this ***disquisition*** complies with North Dakota State University's regulations and meets the accepted standards for the degree of

DOCTOR OF PHILOSOPHY

ABSTRACT

Ganguly, Bratati, Ph.D., Department of Chemistry and Biochemistry, College of Science and Mathematics, North Dakota State University, September 2010. Differential Modulation of the Structural and Functional Characteristics of Human Matrix Metalloproteinase Isozymes upon Binding to Different Ligands. Major Professors: Dr. Derek Killilea and Dr. Sanku Mallik.

Matrix metalloproteinases (MMPs) are a family of Zn^{2+}-dependent, Ca^{2+}-containing endoproteinases involved in tissue remodeling and degradation of the extracellular matrix (ECM). Human MMP isozymes are known to be involved in the progression and metastasis of many diseases like cancer, Alzheimer's, and etc. The different nanoparticles (e.g. gold nanoparticles, liposomes, and charged quantum dots) used in this study provides insights into nanoparticle-induced differential modulation in the structural-functional characteristics of MMP 7, 9 and 10 for better therapeutic intervention.

To demonstrate the relationship between the rigid and flexible surfaces on the differential modulation of functional and structural characteristics of MMP-7, polylysine (PLL) and cationic gold nanoparticles (Au-CNP) were selected as representative examples. These cationic nano-structures were expected to serve as "soft" (flexible) and "rigid" (hard) ligands, respectively. Steady-state kinetic analysis demonstrated that PLL induces activation and inhibition of MMP-7 at stoichiometric and super-stoichiometric concentrations respectively. Circular Dichroism spectroscopy was used to confirm that binding of Au-CNP to MMP-7 induces denaturation of the protein.

In pursuit of understanding the molecular origin of the intrinsic selectivity in binding of human MMP isozymes to differently charged lipid membranes, steady-state kinetic studies and intrinsic tryptophan quenching studies were carried out. Results demonstrated that differently charged lipid membranes bind to all three MMPs;

phosphotidylserine (POPS) liposomes are selective for MMP-7. The bipolar distribution of negative and positive charges on the surface of this enzyme dictates the binding of liposomes and perturbation of catalytic activity.

An attempt to explain the molecular rationale for alternative binding modes of differently charged quantum dots (QDs) to the three MMPs, steady-state tryptophan quenching, steady-state kinetics, and time-resolved fluorescence measurements were carried out. Differently charged QDs bind to all the three MMP isozymes. Enzyme activity of these MMPs was perturbed upon binding to cationic and anionic QDs. Binding of MMPs to the differently charged QDs is reversible and is mediated via electrostatic interactions. Analysis of time-resolved fluorescence data indicates that the protein experiences different micro-environments, due to different distribution of intrinsic tryptophan residues (buried and exposed) on MMP isozymes or the existence of two distinct conformations of the protein. Binding to charged QDs perturbs enzyme activity of MMPs either by restricting the access of the substrate to the active-site or through allosteric modulation. In order to develop new isozyme-selective inhibitors, small molecule inhibitors (SMIs) were designed, synthesized and screened for MMP-7, 9 and 10. Results indicate that hydroxamates and carboxylates are preferred SMIs. Binding preference is based on either the micro-environments of the active-site pockets.

ACKNOWLEDGEMENTS

Dr. Glenn Dorsam's Research Team) have been very willingly helpful and prompt in their suggestions. Emilie DeKrey has always been available to help me take the photographs which have been used in this dissertation. Christopher Heth (from Dr. Rasmussen's Research Team) was always willing to share his synthesis skills with me. I am very grateful to him for the long helpful discussions.

I also extend my special thanks to Dr. Stuart Haring and his wife Dr. Jodi Haring for the helpful discussions regarding many molecular biology techniques included in this work which otherwise would not have been possible. The Department of Chemistry and Biochemistry at NDSU has been a great platform for me to develop my research skills and at the same time I got the opportunity to meet people from different countries and cultures. I have received immense support from most of the members of the department and this journey has been a very enriching experience of my life. Initially when I came to join NDSU it was very unfamiliar circumstances and a new environment for me but Dan and Mary Nelson were very quick to accept me as a part of their family. I am very grateful to them for bestowing love and letting me into their lives.

Without the good wishes, unconditional affection and prayers of family and close friends I would not have been the person I am today. My parents (Maa and Bapi) have been the driving force throughout my life. I would not have been able to accomplish anything without the sacrifices, support and motivation from my parents. It is their blessings and continuous prayers that have immensely helped me overcome my challenges.

DEDICATION

To my dearest Mother (MAA):
Smt. Sadhana Ganguly

"Unless you try to do something beyond what you have already mastered, you will never grow."

-- Ralph Waldo Emerson

This quote was constantly repeated by my mother to motivate me to conquer failures

and achieve success……………..

TABLE OF CONTENTS

LIST OF TABLES

LIST OF FIGURES

LIST OF SCHEMES

LIST OF ABBREVIATIONS

ALS...amyotrophic lateral sclerosis

Anx V... annexin V

AP1 ....activator protein-1

AQD.. anionic Quantum Dots

Au-CNPs.. cationic gold-nanoparticles

Au-NPs...gold-nanoparticles

Bam H .... *Bacillus amyloliquefaciens*

BCA .... bicinchoninic acid protein assay

BM ....basement membrane

BS ....benzenesulfonamide

BSA ....bovine serum albumin

CA... cysteine array

CA2...synaptotagmin C2A

CD .... circular dichroism

cDNA ....complementary DNA

CDS.. coding sequence

CF... cystic fibrosis

CHF.. congestive heart failure

CMTs .... chemically modified tetracyclines

CNS .... central nervous system

COPD...................................... chronic obstructive pulmonary disease

PEA3 ....polyomavirus enhancer A-binding protein-3 site

PE..phosphotidylethanolamine

Pfu ....*Pyrococcus furiosus*

Phe ....phenylalanine

PIP$_2$.........1,2-dioleoyl-sn-glycero-3-phosphoinositol-4,5-bisposphate

PLA ....phospholipid Assay

PL...photoluminescence

PLC ....phospholipase C

PLL ....polylysine

PMSF ....phenylmethylsulfonyl fluoride

PMN.. polymorphonuclear

POPC palmitoyl-2-oleoyl-sn-glycero-3-phosphocholine

POPS........... ....palmitoyl-2-oleoyl-sn-glycero-3-phosphotidylserine

PS .... phosptidylserine

PUMP.. putative uterine metalloproteinase

QDs ....quantum dots

RA..rheumatoid Arthritis

RCSB.............research collaboratory for structural bioinformatics

RFU..relative fluorescence units

RT-PCR .... reverse transcriptase PCR

s ....second

SA .... signal anchor

SDS...sodium dodecyl sulfate

SMI .... small molecule inhibitors

STAT .... signal transducer and activator of transcription

Tcf/Lef .... T-cell factor/lymphoid enhancer factor

TFA .... trifluoroacetic acid

TFPI2 .... tissue-factor pathway-inhibitor-2

TGA .... thioglycolate

THF .... tetrahydrofuran

TNF .... tumor necrosis factor

TIMP .... tissue inhibitors of metalloproteinases

TM .... trans membrane

TNB .... 2-nitro-5-mercaptobenzoic acid

tPA .... tissue plasminogen activator

TPL .... thiopeptolide

LT .... lifetime

Trp .... tryptophan

Ty .... tyrosine

uPA .... urokinase-type plasminogen activator

VEGF .... vascular endothelial growth factor

VPF .... vascular permeability factor

VM .... viral meningoencephalitis

Xho .... *Xanthomonas holcicola*

XMMP .... xenopus MMP

ZBG .... zinc binding group

CHAPTER 1. INTRODUCTION

1.1. Matrix Metalloproteases Family

1.1.1. Matrix metalloproteinase family background

Matrix metalloproteinases (MMPs) comprise a family of zinc-dependent, calcium-containing endoproteinases involved in tissue remodelling and degradation of all components of the extracellular matrix (ECM) at physiological pH. Researchers have been interested in the activity of tissue remodeling, both in physiological and disease processes, long before the individual enzymes were isolated and characterized. The earliest descriptions of MMPs in 1949 [1] was of depolymerising enzymes which could facilitate tumor growth by making connective tissue stroma and small blood vessels fill with more fluid. After 13 years, the first vertebrate MMP (collagenase) was isolated and characterized as the enzyme responsible for the resorption of tadpole tails. Several mammalian enzymes were partially purified but it was not until 1985, when structural homologies became apparent, allowing many new members to be identified through advancement in molecular biology [2].

1.1.2. Matrix metalloproteases evolution and diversification

At the time when MMPs were studied to resolve the mystery about the evolution, structure, and diversification of this large family of enzymes, two very prominent questions were posed: a) Why would such multiplicity of these enzymes be seen in nature? (b) What makes them different, and how does this difference in amino-acid sequence give rise to structural elements which can make each MMP a distinct enzyme? To address these questions, amino-acid sequences from 64 MMPs of various organisms,

vertebrates, invertebrates, and plants were compared. The three dimensional structures of several representative members of MMPs were modeled to gain insights into their similarities and differences using the available crystal structures for four MMPs [3-6]. Entire sequences, the catalytic domains, and the hemopexin-like domains of the 64 members of the MMP family were analyzed in terms of structures, evolution, and interactions with substrates/inhibitors. Analysis on the structural zinc-binding site and the calcium-binding sites were performed. These first comprehensive analyses of this important family of enzymes provided fundamental information on the evolution and properties of MMPs.

Analysis of the entire sequences and of the catalytic domains gave rise to 23 distinct subfamilies of MMPs [5]. To gain an insight into the similarities and differences, the available crystal structure of four MMPs were used to model the structures of the several representative members of the remaining MMPs. The data indicated that the origin of the MMPs could be traced prior to the emergence of vertebrates from invertebrates. The three main branches of the dendogram gave rise to the enzyme from vertebrates, invertebrates, and plants. The only exception was XMMP, which is from Xenopus. The XMMP was the least related. It possess a hemopexin domain that was absent in plant and nematode MMPs (Figure 1.1.A and B). This suggested that at some point in evolution, the genes encoding the primordial MMP and hemopexin-like domains were joined together leading to the origination of XMMP.

A

[2]	MMP2 mouse
[2]	MMP2 rat
[2]	MMP2 human
[2]	MMP2 rabit
[2]	MMP2 chicken
[9]	MMP9 mouse
[9]	MMP9 rat
[9]	MMP9 human
[9]	MMP9 rabit
[9]	MMP9 bovin
[9]	MMP9 newt
[12]	MMP12 rat
[12]	MMP12 mouse
[12]	MMP12 rabit
[12]	MMP12 human
[1]	MMP1 human
[1]	MMP1 rabit
[1]	MMP1 bovin
[1]	MMP1 pig
[1]	MMP1 Bull frog
[8]	MMP8 human
[13]	MMP13 mouse
[13]	MMP13 rat
[13]	MMP13 human
[13]	MMP13 frog (GB: U41824)
[13]	MMP13 frog (SW: Q10835)
[13]	MMP13 newt
[3]	MMP3 mouse
[3]	MMP3 rat
[3]	MMP3 human
[3]	MMP3 rabit
[3]	MMP3 horse
[10]	MMP10 human
[10]	MMP10 rat
[5]	MMP newt (GB: D82053)
[5]	MMP newt (GB: D82054)
[4]	collagenase-4 frog
[6]	CMMP chicken
[18]	Enamelysin bovin
[18]	Enamelysin pig
[7]	MMP7 mouse
[7]	MMP7 rat
[7]	MMP7 cat
[7]	MMP7 human
[11]	MMP11 rat
[11]	MMP11 mouse
[11]	MMP11 human
[11]	MMP11 frog
[16]	MT3-MMP chicken
[16]	MT3-MMP human
[14]	MT1-MMP human
[14]	MT1-MMP rat
[14]	MT1-MMP mouse
[14]	MT1-MMP rabit
[15]	MT2-MMP human
[17]	MT4-MMP human
[19]	MMP19 human
[23]	metalloprotease mouse-ear cress (TR: O04529)
[23]	metalloprotease soybean (GB: U63725)
[23]	metalloprotease mouse-ear cress (OD: E327511)
[20]	envelysin (GB: AB000719)
[20]	envelysin (SW: P22757)
[21]	MMP nematode (GB: U00038)
[22]	XMMP frog

Figure 1.1.A. The dendogram of the multiple-sequence analysis of the amino acid sequences for the 64 MMPs. The number in brackets represents the different classes. "v" represents the branch vertebrate MMPs, "i" represents invertebrate MMPs, and "p" represents plant MMPs. This figure has been adapted from the Ref 14.

3

B
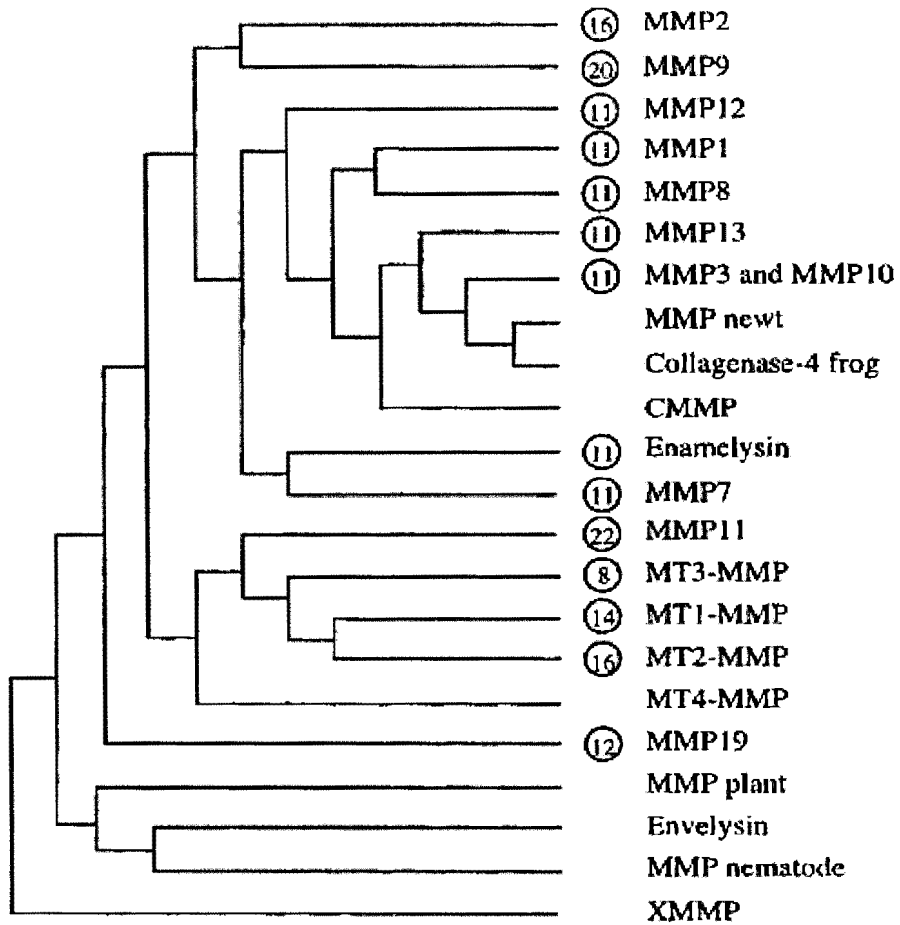
Figure 1.1.B. The simplified schematic diagram of the dendogram. The number in brackets represents the different chromosomal origins for human MMPs. This figure has been adapted from Ref 14. The amino acid sequences of MMPs were taken from Gene Bank, TREMBL, and SWISS-Prot data bank [7].

4

1.2. The Role of Matrix-degrading Proteases

Key functions of the basement membrane (BM) comprise cellular and tissue support, anatomical compartmentalization, and provision of a surface that enables the regulation of cellular function, differentiation, migration, and adhesion [8]. Interstitial connective tissue, adjacent to the BM, is composed of collagen fibers, proteoglycans, and glycoproteins and forms the major component of the extracellular matrix. Blood and lymphatic vessels are in close proximity to these tissues. Metastasis, facilitated by degradation of interstitial stroma by proteases, occurs when the cancer cells are able to break through these natural tissue barriers [8]. Specific proteolytic enzymes, produced by infiltrating leukocytes, stromal cells and tumor cells, are directly involved in the degradation and reorganization of the extracellular matrix, which in turn facilitates tumor cell invasion and metastasis. These proteolytic enzymes, termed matrix-degrading proteases, are classified into four major classes based on the nature of their active sites: (1) Matrix metalloproteinases (Gelatinases, Collagenases, Stromelysins, and Membrane Type MMPs); (2) Serine proteinases (plasminogen activators); (3) Cysteine proteinases (cathepsin B, cathepsin L); and (4) Aspartyl proteinases (cathepsin D). MMPs appear to be involved in the initial step of degradation of the extracellular matrix, although tumor invasion involves the interaction of several proteases in a complex processes.

The timely breakdown of the extracellular matrix (ECM) is necessary for embryonic development, reproduction, morphogenesis, tissue resorption, and remodeling. The matrix metalloproteinases (MMPs), also called matrixins, are thought to play a central role in these processes. The expression of most matrixins is transcriptionally regulated by

growth factors, hormones, cytokines, and cellular transformation [9-10]. The proteolytic activities of MMPs are accurately controlled during activation from their precursors and inhibition by endogenous inhibitors, such as α-macroglobulins and tissue inhibitors of metalloproteinases (TIMPs). Table 1.1 lists the currently known vertebrate matrixins. Additionally, non-vertebrate members have been identified in sea urchins [11], *Caenorhabditis elegans* [12], soybean [13], and *Arabidopsis thaliana* [14].

Table 1.1. The vertebrate members of the Matrixin family. A to H mean the domain composition of the different MMPs. The structures of the domains are shown in Figure 1.3. This table has been reproduced from Ref 15.

Protein	MMP	Domain Composition
Collagenase 1	MMP-1	B
Gelatinase A	MMP-2	C
Stromelysin 1	MMP-3	B
Matrilysin	MMP-7	A
Collagenase 2	MMP-8	B
Gelatinase B	MMP-9	D
Stromelysin 2	MMP-10	B
Stromelysin 3	MMP-11	E
Macrophage elastase	MMP-12	B
Collagenase 3	MMP-13	B
MT1-MMP	MMP-14	F
MT2-MMP	MMP-15	F
MT3-MMP	MMP-16	F
MT4-MMP	MMP-17	F
Collagenase 4 (Xenopus)	MMP-18	B
(No Trivial Name)	MMP-19	B
Enamelysin	MMP-20	B
XMMP(Xenopus)	MMP-21	G
CMMP(Chicken)	MMP-22	B
(No Trivial Name)	MMP-23	H

1.2.1. The extracellular matrix

The ECM, which contains collagens, non-collageneous glycoproteins, and proteoglycans, supports the adhesion of cells and transmits signal through the cell-surface

adhesive reporters (Figure 1.2). Alternative ECM constituents, such as tenascin, fibronectin, and variant isoforms of laminin, are found in tumors and might stimulate cancer progression. The BM is a specialized ECM that provides the first barrier against invasion of carcinomas and separates the epithelial cells from the underlying stroma.

(i)   Collagens

Collagen molecules consist of three α-chains, which form a triple helix [16]. Fibrillar collagens (type I, II, III, V and XI) form fibrils through interactions with integrins and influence cellular functions. BM collagens (type IV collagens) are network-forming collagens of the BM. Cells interact with collagen type IV molecules through integrins, laminin and heparan-sulphate proteoglycans. The 'multiple-triple-helix domains with interruption' collagens (type XV and XVIII) are primarily found in the BM of internal organs. A proteolytic fragment of the α1 chain of collagen type XVIII, known as endostatin, is an inhibitor of angiogenesis [17]. There are several other groups of collagens, including the transmembrane collagens that are a part of focal adhesion sites. It is interesting to note that gelatin is a denatured collagen and is a product of collagenase-digested collagens.

(ii)   Glycoproteins

Laminins composed of α, β and γ chains are heterotrimeric glycoproteins. They form networks with collagen IV and nidogen in the BMs. Laminins affect cellular functions by binding to integrins and non-integrin receptors [18]. Fibronectins and glycoproteins, that are present in the ECM and in the blood, form fibrils and affect cell morphology, adhesion, migration, and differentiation by binding to integrins [19-20].

(iii)   Proteoglycans

Proteoglycans have post-translational modifications of glycosaminoglycan chains such as heparan, keratin, and chondroitin sulphate. Perlecan, found in tumor stroma, is the most common heparan-sulphate proteoglycan of the BM. Other important proteoglycans are aggrecan, which is found as large 'aggregates' in cartilagenous tissues, and decorin. Versican is the main chondroitin-sulphate proteoglycan of non-cartilaginous tissues. Syndecans, glypicans, and CD44 are cell-surface proteoglycans [21]. Hyaluronan is also a glycosaminoglycan, but not a proteoglycan, and it is not covalently attached to any protein.
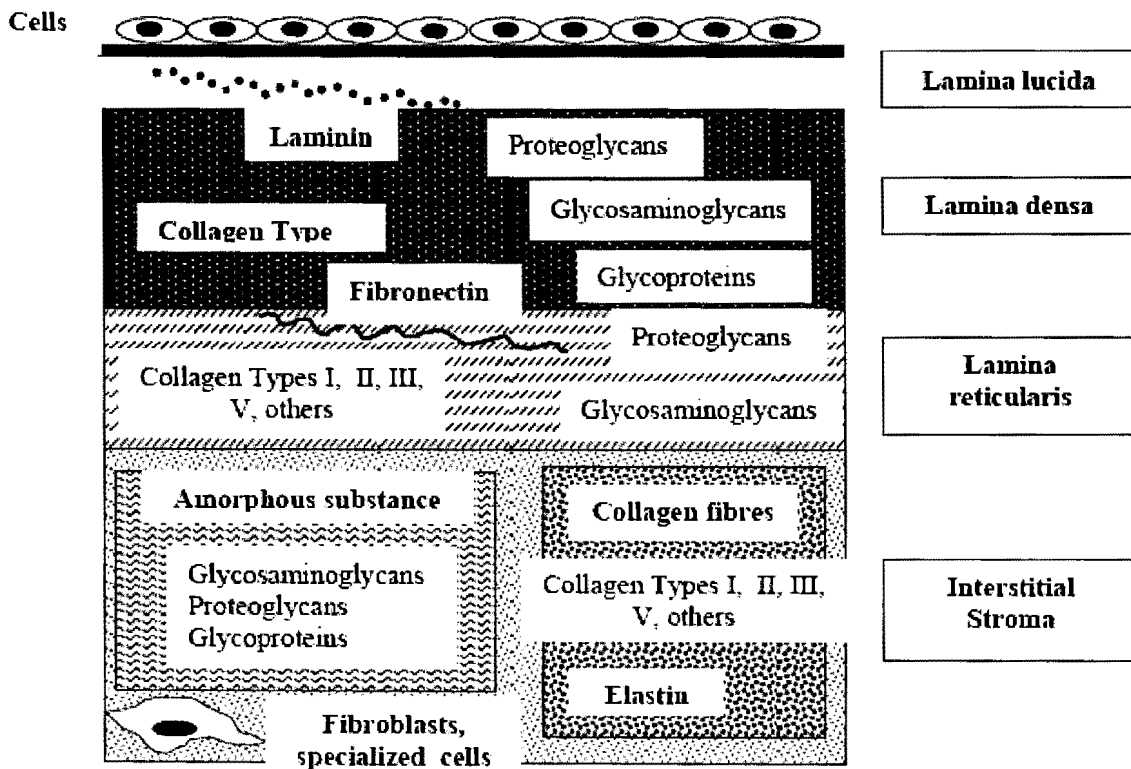
Figure 1.2. The diagram of the extracellular matrix (ECM), the basement membrane (BM), and the interstitial stroma (IS). This figure has been adopted Reference 21.

1.3. Classifications of MMPs

1.3.1. MMP classification based on domain structure and function

All matrixins are secreted as inactive pro-MMPs and synthesized as pro-enzymes. As illustrated in the Figure 1.3, the primary structures of 20 vertebrate matrixins comprises of several domain motifs. The peptide domain consists of about 80 amino acids with a unique conserved PRCG (V/N) PD sequence. To maintain latency of the pro–MMPs [22-23], the Cys within this sequence (the "cysteine switch") ligates the catalytic zinc. This sequence is missing in MMP-23 [24]. Stromelysin 3 (MMP-11), MT-MMPs, *Xenopus* MMP, and MMP-23 have a pro-protein processing sequence RX(K/R)R at the C-terminal end of the propeptide, and MMP-11 [25] and MMP-14 [26] were shown to be activated intracellularly by furin.
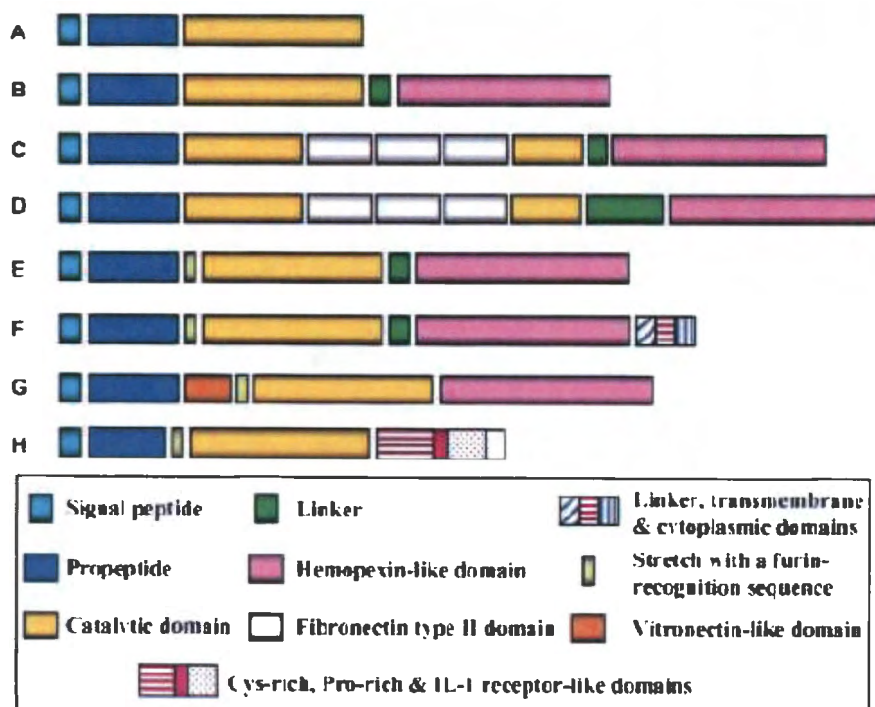
Figure 1.3. The domain arrangements of the vertebrate Matrixins. This figure has been reproduced from Ref 15.

9

The catalytic domain (about 170 amino acids) is made up of a zinc-binding motif HE*XX*H*XX*G*XX*H and a conserved methionine, forming a unique "Met-turn" structure [27]. This domain consists of three α-helices, five-stranded β-sheets, and bridging loops [26]. Members from other metalloproteinase families, *i.e.* astacins and reprolysins (ADAMs), are identical in having these backbone structures including the "Met-turn". These latter four families constitute the "metzincins" [27]. Stability and the expression of an enzymatic activity is provided by an additional structural Zn^{2+} ion and 2–3 Ca^{2+} ions present in the catalytic domains of matrixins (Figure 1.4). MMP-2 and MMP-9 have three repeats of the fibronectin-type II domain inserted in the catalytic domain. These repeats interact with collagens and gelatins [28-29].

The C-terminal hemopexin-like domain (about 210 amino acids) consists of an ellipsoidal-disk shape with a four-bladed β-propeller structure. Each blade is made up of four antiparallel β-strands and α-helix [30]. Although the catalytic domains alone can retain proteolytic activity toward other substrates [31], the hemopexin domain is an absolute requirement for collagenases to cleave triple-helical interstitial collagens [32]. The hemopexin domain of MMP-2 is also required for the cell surface activation of pro-MMP-2 by MT1-MMP [33-34]. Although its interaction with triple helical collagen is hypothesized, based on molecular modeling [34-35], the function of the proline-rich linker peptide that connects the catalytic and the hemopexin domains is not known. Instead of the hemopexin domain, MMP-23 has cysteine-rich, proline-rich, and IL-1 receptor-like regions [24]. A trans-membrane domain, found in the MT-MMPs, anchors these enzymes to the cell surface.

Seventeen different human MMPs have been identified and/or cloned and share significant sequence homology and a common multi-domain organization. Several MMPs have also been identified in other vertebrates, invertebrates, and from plant sources [36], collectively forming the MMP or matrixin subfamily A of the Metalloproteinase family [37]. The MMP family can be subdivided into five groups according to their structure and functional properties: (i) Collagenases (MMP-1, 8 and 13); (ii) Gelatinases A and B (MMP-2 and 9); (iii) Stromelysins 1 and 2 (MMP-3 and 10); (iv) a more heterogeneous subgroup containing Matrilysin (MMP-7), Enamelysin (MMP-20), the macrophage metalloelastase (MMP-12), and MMP-19 (together making up the 'classical' MMPs); and (v) the Membrane-Type MMPs (MT-MMPs-1 to 4 and stromelysin-3, MMP-11). These MMPs are glycosylated to different extents and at different sites but share a common multi-domain structure (Figure 1.5). According to sequence alignments [36, 38], the assembly of these domains can be attributed to evolutionary and diversification events. All MMPs are synthesized with a 20 amino-acid residue signal peptide and are (except probably the MT-MMP-like furin-processed proteinases) [39-41] secreted as latent pro-forms. These pro-proteinases, except Matrilysin, consist of an 80-residue N-terminal pro-domain followed by the 170-residue catalytic domain (see Figure 1.3), they are covalently connected through a 10 to 70 residue pro-rich linker to the 195-residue C-terminal hemopexin-like domain.

In the MT-MMPs, the polypeptide chain possesses an additional 75 to 100 residue extension, which presumably forms a trans-membrane helix and a small cytoplasmic domain [40]. Removal of the haemopexin-like domain in the collagenases eliminates their characteristic capability to cleave triple-helical collagen, but does not significantly affect

hydrolytic activity towards gelatin, casein or synthetic substrates [42]. In both gelatinases, the catalytic domains have an additional 175 amino-acid residue insert comprising three fibronectin-related type II modules conferring gelatin and collagen binding.

The TIMP family currently includes four different members (TIMPs-1 to -4), which after optimal topological superposition exhibit 41–52% sequence identity [43-44]. Besides their inhibitory role, these TIMPs seem to have other functions such as growth factor-like and anti-angiogenic activities [45-46]. Except for the weak interaction between TIMP-1, -2 and MMPs [40, 47-49], the TIMPs do not seem to significantly differentiate between the various MMPs [47]. TIMP-1 and -2 are unique, in a way, that they bind to the pro-forms of gelatinase A and B [48]. The complex between MT1-MMP and TIMP-2 seems to act as a cell-surface-bound 'receptor' for pro-gelatinase A in *in vivo* activation [47-49]. Removal of one-third of the TIMP polypeptide C-terminal chain gives rise to the N-terminal TIMP domains (N-TIMPs), which retain most of their reactivity toward their target MMPs [50-51].

1.3.2. MMP classification based on substrate specificity

The MMP endopeptidases, consisting of more than 21 human MMPs and the homologues from other species can cleave virtually any component of the ECM (Figure 1.5). Historically, the MMPs were divided into collagenases, gelatinases, stromelysins, and matrilysins on the basis of their specificity for ECM components. The common names of the MMPs reflect this classification (Table 1.2). A sequential numbering system for the MMPs has been adapted as the list of MMP substrates, and the MMPs are now grouped according to their structure. There are eight distinct structural classes of MMPs: three are

membrane-type MMPs (MT-MMPs) and five are secreted. They are discussed below.

1.3.2.1. Secreted MMPs

1.3.2.1.1. Minimal domain MMPs

Minimal-domain MMPs contain an amino-terminal signal sequence (Pre) that directs them to the endoplasmic reticulum. The propeptide (Pro) with a zinc-interacting thiol (SH) group maintains the inactive zymogens by interacting with the Zn^{2+} ion in the catalytic domain.
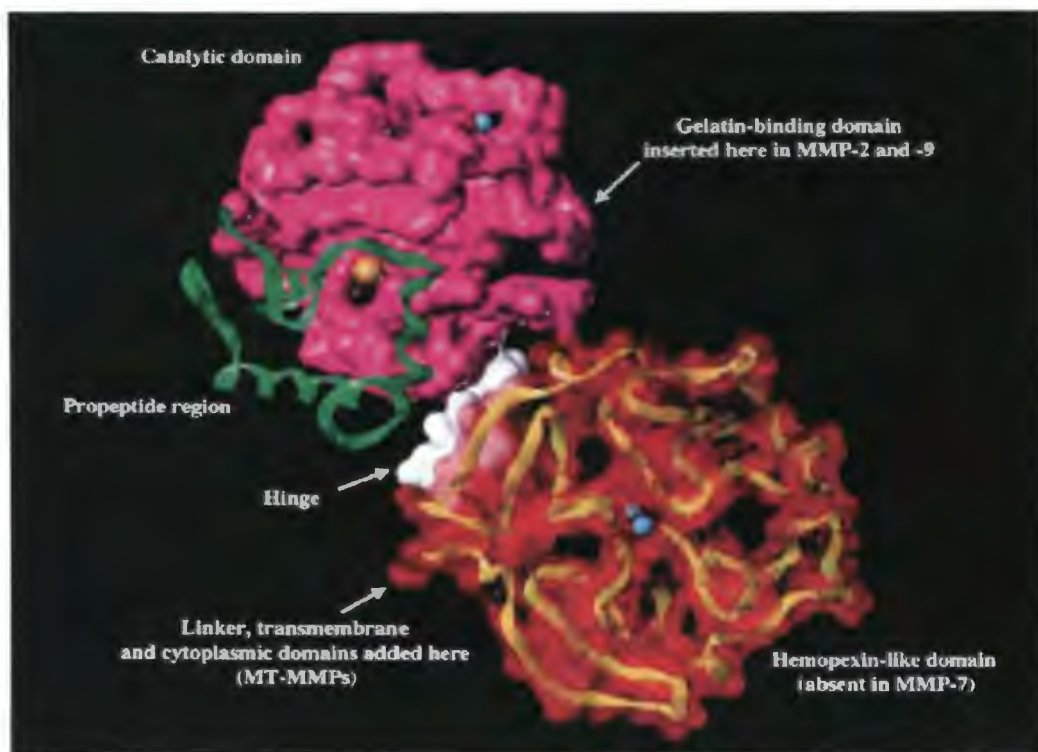
Figure 1.4. The different domain structures of MMPs. Crystallographic sources reveal the Pro-peptide domain, the catalytic domain and the hemopexin domain. The propeptide domain is representative from the X-ray structure of stomelysin (PDB - 1slm); the other regions are from collagenase (PDB - 1fbl). The catalytic zinc is shown as an orange sphere; calcium ions in the catalytic domain and the hemopexin-like domain are shown in cyan. The propeptide region is represented by the green ribbon, catalytic domain is shown as a pink surface, the hinge region is shown as a white surface and the hemopexin-like domain is shown as a yellow ribbon. This figure has been adopted from Ref 15.

13

1.3.2.1.2. Hemopexin domain MMPs

The simple hemopexin domain-containing MMPs have a hemopexin-like domain that is connected to the catalytic domain by a hinge (H). It mediates interactions with tissue inhibitors of metalloproteinases, cell-surface molecules, and proteolytic substrates in addition to the domains that are found in the minimal-domain MMPs. The first and the last of the four repeats in the hemopexin-like domains are linked by a disulphide bond (S–S).

1.3.2.1.3. Gelatin-binding domain MMPs

The gelatin-binding MMPs contain inserts that are similar to collagen-binding type II repeats of fibronectin (Fi).

1.3.2.1.4. The furin-activated secreted MMPs

Secreted MMPs, which are furin-activated, contain a recognition motif for intracellular furin-like serine proteinases (Fu) between their propeptide and catalytic domains that allows intracellular activation by these proteinases. This motif is also found in the vitronectin-like insert (Vn) MMPs and the membrane-type MMPs (MT-MMPs).

1.3.2.2. Non-secreted MMPs

1.3.2.2.1. Trans-membrane type MMPs

MT-MMPs include transmembrane MMPs that have a carboxy-terminal, single-span transmembrane domain (TM) and a very short cytoplasmic domain (Cy) on the glycosylphosphatidylinositol (GPI) anchor. MMP-23 represents a third type of membrane-linked MMP. It has an N-terminal signal anchor (SA) that targets it to the cell membrane, and hence is a type II transmembrane MMP. MMP-23 is also characterized by its unique cysteine array (CA) and immunoglobulin (Ig) like domains.
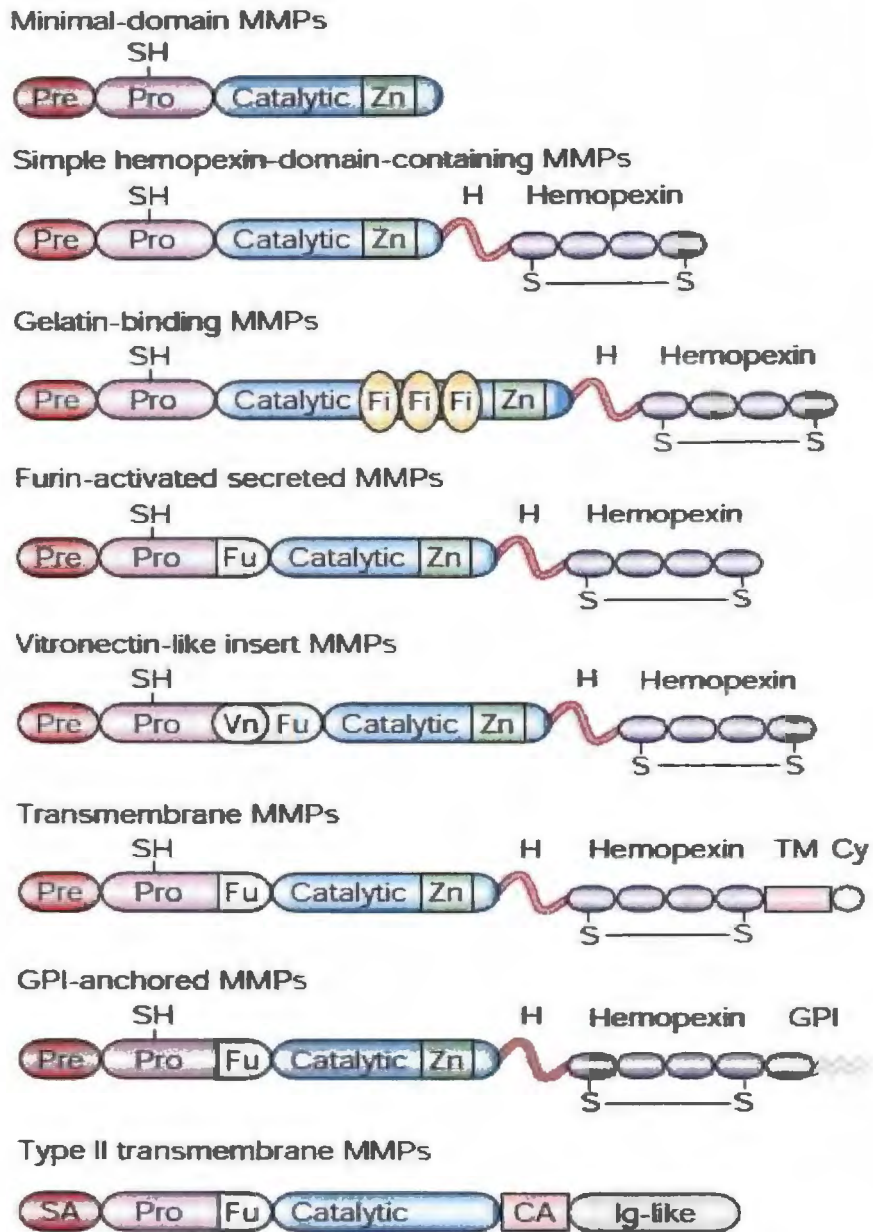
Figure 1.5. The structural organization of the MMPs. The figure has been reproduced from Ref 52.

Table 1.2 shows the classification of different types of MMPs based on substrate specificity and structural organization of the domains. Table 1.2 has been adopted from Ref 52.

Table 1.2. The classification of the different MMPs based on the type of substrate specificity and on the basis of structural organization.

MMP Designation	Classification based on Structure	Classification based on Substrate Specificity	Collagen Substrate Distribution	Additional Substrates	Mol. Wt. Collagen Additional Substrates
MMP-1	Simple hemopexin domain	Collagenase-1, interstitial collagenase, fibroblast collagenase, tissue collagenase	I, II, III, VII,VIII, X	Aggrecan, Gelatin, MMP-2, MMP-9	55,000/ 45,000
MMP-2	Gelatin-binding	Gelatinase A, 72-kDa gelatinase, 72-kDa type IV collagenase, neutrophil gelatinase	I, II, III, IV, V,VII, X, XI	Aggrecan, Elastin, Fibronectin Gelatin, Laminin, MMP-9, MMP-13	72,000/ 66,000
MMP-3	Simple hemopexin domain	Stromelysin-1, transin-1, proteoglycanase, procollagenaseactivating protein	II, III, IV, IX,X, XI	Aggrecan, Elastin, Fibronectin, Gelatin, Laminin, MMP-7, MMP-8, MMP-13	57,000/ 45,000
MMP-7	Minimal domain	Matrilysin, matrin, PUMP1, small uterine metalloproteinase	IV, X	Aggrecan, Elastin, Fibronectin, Gelatin, Laminin, MMP-1, MMP-2, MMP-9	28,000/ 19,000
MMP-8	Simple hemopexin domain	Collagenase-2, neutrophil collagenase, PMN collagenase, granulocyte collagenase	I, II, III, V, VII,VIII, X	Aggrecan, Elastin, Fibronectin,Gelatin, Laminin	75,000/ 58,000

16

Table 1.2. (continued)

MMP-9	Gelatin-binding	Gelatinase B, 92-kDa gelatinase, 92-kDa type IV collagenase	IV, V, VII, X,XIV	Aggrecan, Elastin, Fibronectin,Gelatin	92,000/ 86,000
MMP-10	Simple hemopexin domain	Stromelysin-2, transin-2	III, IV, V	Aggrecan, Elastin, Fibronectin,Gelatin, Laminin, MMP-1, MMP-8	57,000/ 44,000
MMP-11	Furin-activated and secreted	Stromelysin-3		Aggrecan, Fibronectin, Laminin	51,000/ 44,000
MMP-12	Simple hemopexin domain	Metalloelastase, macrophage elastase, macrophage metalloelastase	IV	Elastin, Fibronectin, Gelatin,Laminin	54,000/ 45,000 and 22,000
MMP-13	Simple hemopexin domain	Collagenase-3	I, II, III, IV	Aggrecan, Gelatin	60,000/ 48,000
MMP-14	Membrane-Type Metalloproteinase-14	MT1-MMP, MT-MMP1	I, II, III	Aggrecan, Elastin, Fibronectin,Gelatin, Laminin, MMP-2, MMP-13	66,000/ 56,000
MMP-15	Membrane-Type Metalloproteinase-15	MT2-MMP, MT-MMP2		Fibronectin, Gelatin, Laminin, MMP-2	72,000/ 60,000
MMP-16	Membrane-Type Metalloproteinase-16	MT3-MMP, MT-MMP3		MMP-2	64,000/ 52,000
MMP-17	GPI-linked Membrane-Type Metalloproteinase-17	MT4-MMP, MT-MMP4		Fibrin, Gelatin	57,000/ 53,000

17

Table 1.2. (continued)

MMP-18	Simple hemopexin domain	Collagenase-4 (*Xenopus;* no human homologue known)			70,000/ 53,000
MMP-19	Simple hemopexin domain	RASI-1, MMP-18	IV	Fibronectin, Aggrecan, COMP,Laminin, Gelatin	54,000/ 45,000
MMP-20	Simple hemopexin domain	Enamelysin		Aggrecan, Amelogenin, COMP	54,000/ 22,000
MMP-21	Vitronectin-like insert	Homologue of *Xenopus* XMMP			
MMP-22	Simple hemopexin domain	CMMP (chicken; no human homologue known)			
MMP-23	Type II transmembrane	Cysteine array MMP (CA-MMP), femalysin, MIFR, MMP-21/MMP-22			
MMP-24	Transmembrane	MT5-MMP, MT-MMP5			
MMP-25	GPI-linked	MT6-MMP, MT-MMP6 , Leukolysin	IV	Gelatin, Fibronectin, Laminin-I	
MMP-26	Minimal domain	Endometase, matrilysin-2	IV	Gelatin, Fibronectin	28,000/ 19,000
MMP-27	Simple hemopexin domain				
MMP-28	Furin-activated and secreted	Epilysin			

18

It can be observed that MMP-4, 5, and 6 nomenclature has been abandoned. It has also been reported that when MMP-19 was discovered, it was first reported as MMP-18 [54-55]; however, a MMP from xenopus had already been discovered and named MMP-18, it has been known as MMP-19 ever since. The human MMP-21 has not been characterized yet. MMP-23 has a gene sequence similar to MMP-21 and MMP-22; MMP-23 has hence been named as MMP-23A and B [56-57].

1.3.3. MMP catalytic domain

Out of all the domains in MMPs, the catalytic domain has been the most studied domain. The catalytic domain of the MMPs is an oblate ellipsoid. In the 'standard' orientation, in most MMPs, a small active-site cleft notched into the flat ellipsoid surface extends horizontally across the domain to bind peptide substrates from left to right (see Figure 1.6). The cleft, which stores the 'catalytic zinc', separates the larger 'upper subdomain' from the smaller 'lower subdomain'. The upper subdomain formed by the first three quarters of the polypeptide chain (up to Gly225) consists of a five-stranded β- pleated sheet, surrounded by three surface loops on its convex side and by two long regular α-helices on its concave side embracing a large hydrophobic core (Figure 1.6). The polypeptide chain starts on the molecular surface of the lower subdomain, passes strand sI, the amphipathic α-helix hA, and β-strands sII, sIII, sIV and sV, before entering the 'active-site helix' hB. Strands sII and sIII are connected by a relatively short loop bridging sI in classical MMPs. In MT-MMPs, this loop is expanded into the spur-like, solvent exposed MT-MMP- specific loop of unknown function [33-35, 40, 42, 48-49]. In all MMPs, strandsIII and sIV are linked via an 's-shaped double loop', that is clamped *via* the

'structural zinc' and the first of two to three bound Ca^{2+} ions to the β-sheet. This S-loop extends into the cleft sided 'bulge' continuing in the antiparallel 'edge strand' sIV. This bulge-edge segment is of prime importance for binding of peptidic substrates and inhibitors (see Figure 1.6). The sIV-sV connecting loop, along with the sII-sIII bridge sandwiches the second bound Ca^{2+} ion. After strand sV, the chain passes the large open sV-hB loop before entering the active-site helix hB. This helix provides the first (218) and the second His (222), which bind to the catalytic zinc, and the 'catalytic Glu-219', these residues represent the N-terminal part of the 'zinc-binding consensus sequence,' HEXXHXXGXXH, characteristic of the metzincin superfamily [27].

This active site helix stops abruptly at Gly-225, where the peptide chain bends down, and descends, presenting the third zinc liganding to histidine (His-228) and the following MMP-invariant Ser-229. The function of the helix cannot be judged from the catalytic domain structure alone. This helix runs through a wide right-handed spiral catalytic domain's 'chin' terminating in the 1,4-tight 'Met-turn' of the strongly conserved sequence (Ala234-Leu235-Met236-Tyr237) with an obligatory methionine residue at turn position 3.

The chain then returns back to the molecular surface to an (except in human stromelysin-3) invariant Pro-238, forms a conserved Pro 238-X-Tyr240 segment (the 'S1 outer wall of the pocket); runs through another wide loop of slightly variable length and conformation (called the 'specificity loop' [28-29]), before it passes the C-terminal-helix hC.
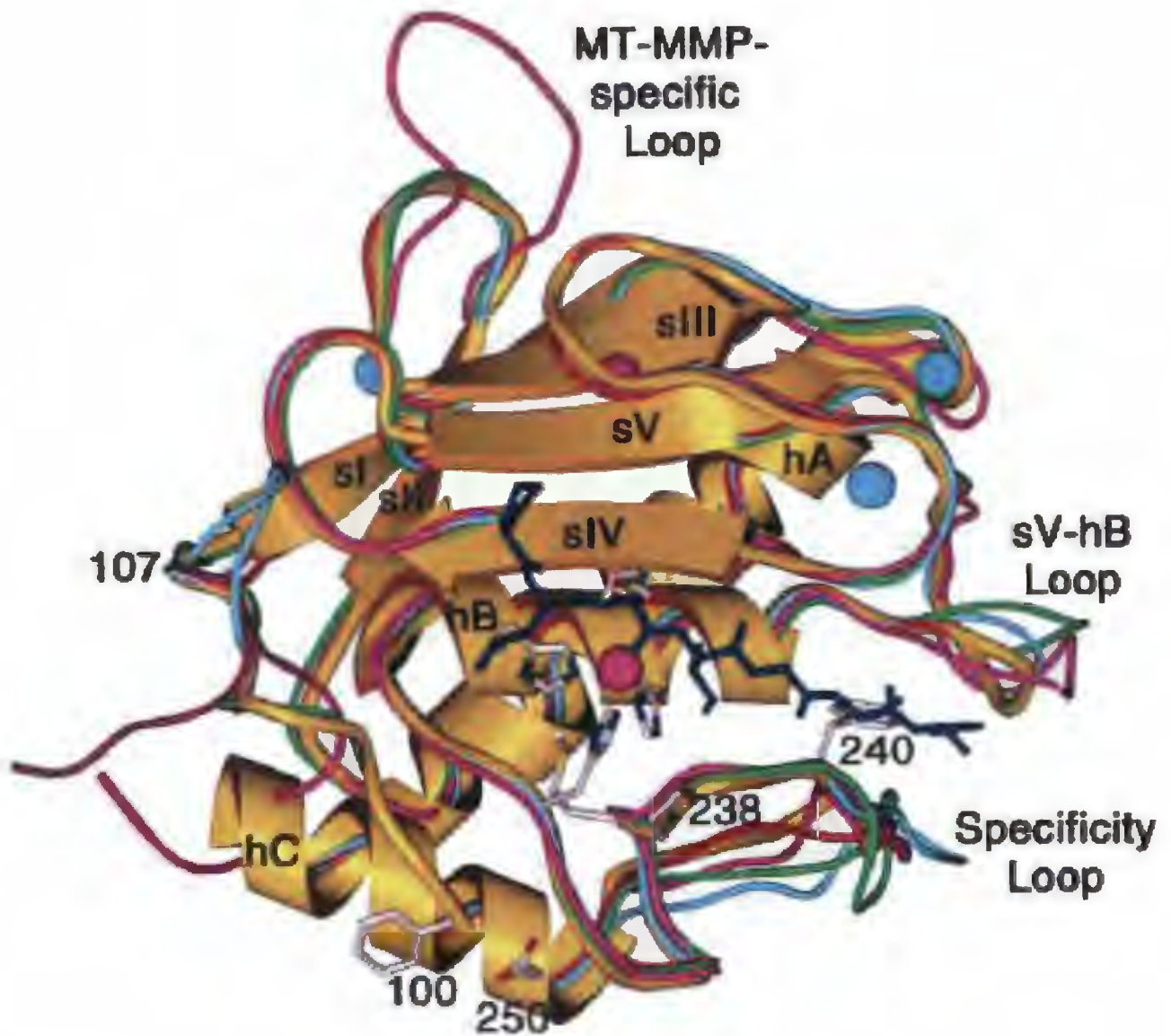
Figure 1.6. The catalytic domain of MMP isozymes. The catalytic domains of MMP-1 is shown in red, MMP-3 is shown in blue, MMP-7 is shown in green, MMP-8 is shown in dark blue and MMP-14 is shown in pink along with the heptapeptide substrate. The Zn^{2+} and Ca^{2+} ions have been displayed as pink and blue, respectively. This figure has been adopted from Ref 58.

1.4. MMP Catalysis and Mechanism

1.4.1. MMP enzyme activity

The reaction mechanism of MMPs with the proteolysis of ECM and non-ECM substrates has been delineated under the influence of the structural information available. It was believed that the catalytic Zn^{2+} of the MMP isozymes coordinates with the scissile amide carbonyl (Figure 1.7). The carbonyl gets attached by a water molecule found in the active site. This carbonyl bond has a hydrogen bond to one of the conserved residues, Glu-198 (in MMP-8) as well as coordinated to the Zn^{2+} in the active sites of almost all the MMP isozymes. The water molecule donates a proton to the Glu residue, which transfers it to the nitrogen of the scissile amide bond. This is followed by the Glu residue shuttling the remaining proton from the water molecule (acts as the solvent) to the nitrogen of the scissile amide leading to the cleavage of the peptide bond. The Zn^{2+} ion plays a vital role in stabilizing the negatively charged carbon of the scissile amide and conserved Ala-161 (in MMP-8), which in turn helps to stabilize the positive charge at the nitrogen of the scissile amide.

1.4.2. Cysteine switch

MMPs contain a conserved sequence (PRCGVPD) in the pro-domain that helps in maintaining the inactivity of the enzymes (Figure 1.8). The pro-domain in all MMPs fold in such a way that the cystein residue can coordinate with the catalytic Zn^{2+}. Cleavage of the cysteine–Zn^{2+} interaction replaces the thiol group by a water molecule. This makes the MMPs active for attacking peptide bonds of MMP targets and/or removal of the NH_2-terminal of its own pro-domain to become irreversibly activated (See 1.6.1.3 Section).
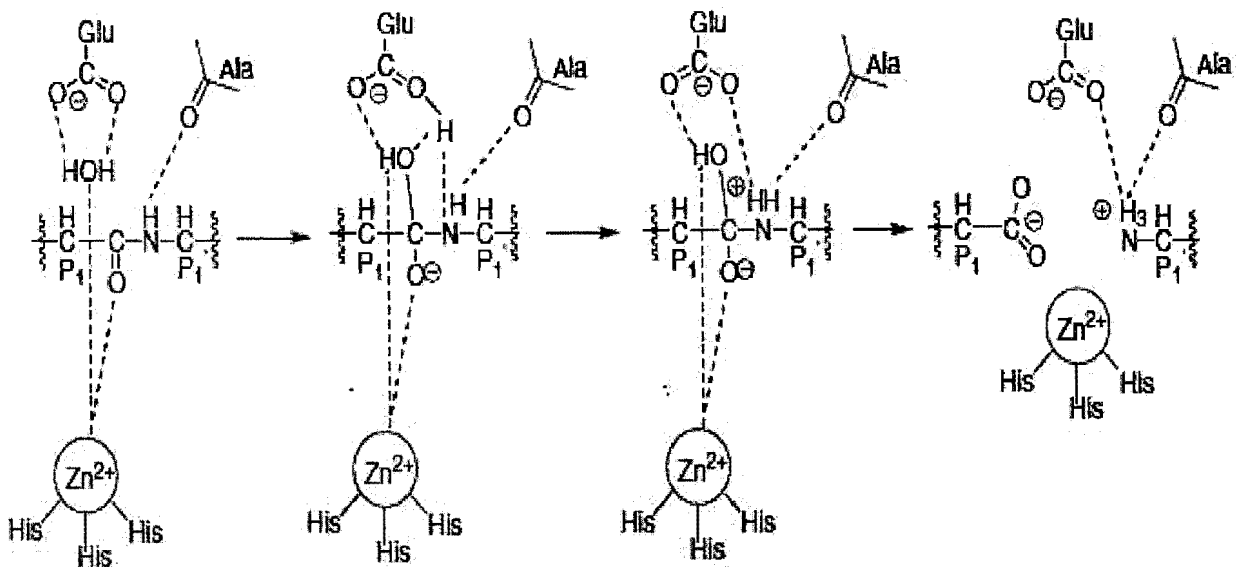
Figure 1.7. The reaction mechanism for the proteolysis by MMPs. This figure is adopted from Ref 59.

1.4.3. Detailed study of the active site of MMPs

The active site of MMP isozymes consists of two distinct regions: A) a groove in the protein surface with catalytic Zn^{2+} as the central point; and B) The S1' specificity site varies among all the members. Table 1.3 displays the residues that are found in the different isozymes of MMPs.

Most potent inhibitors like the hydroxamates adopt the extended conformations within the groove and manage to make a few β-structures like hydrogen bonds with the enzyme (Figure 1.7). The catalytic Zn^{2+} also plays a crucial role in binding to the bound inhibitors and stabilizing them in the MMP groove (Figure 1.9). The S1' holds the responsibility of recognizing substrate specificity in the active site.
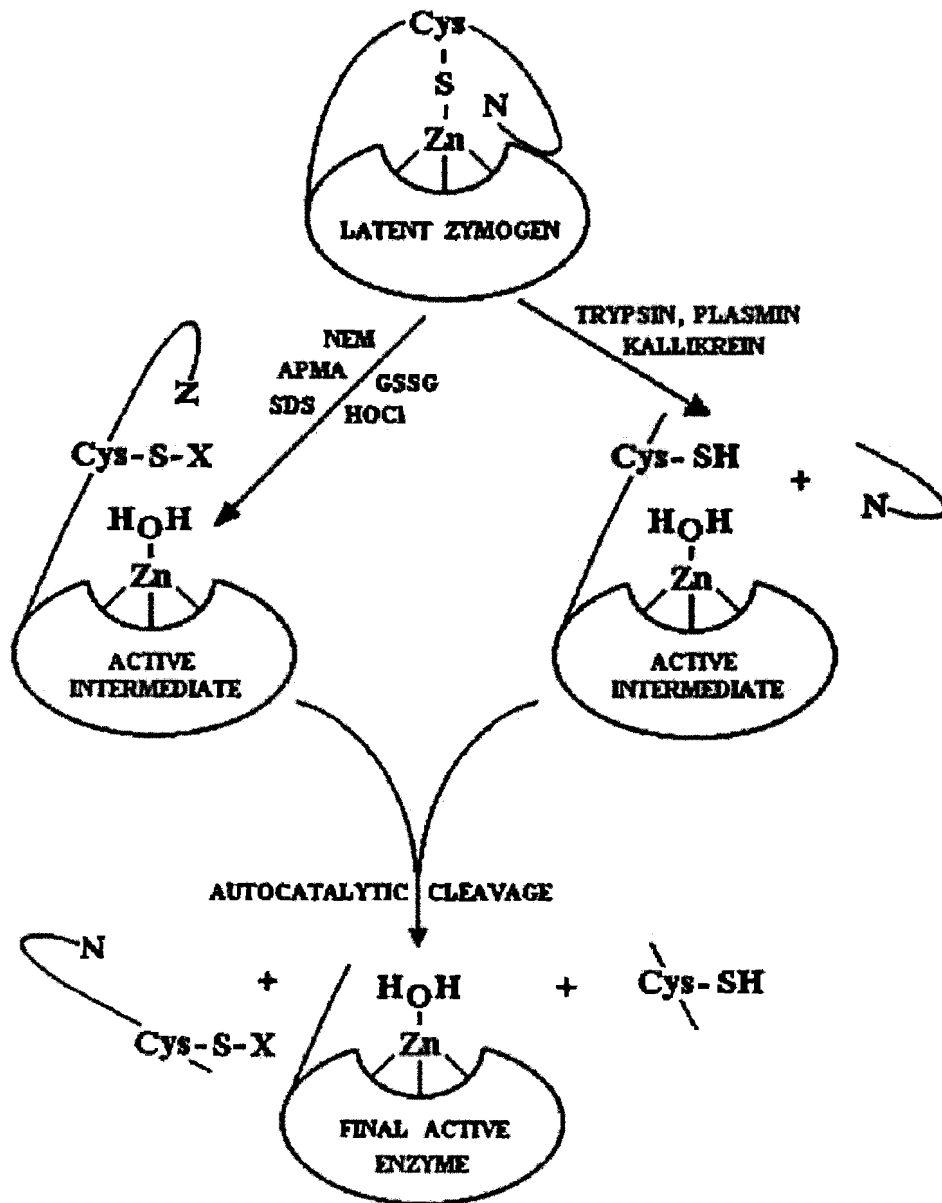
Figure 1.8. The cysteine switch model of MMP activation. This figure has been reproduced from Ref 60.

Table 1.3. The selected variable residues in the active site of MMPs. This table has been adopted from Ref 2.

Residue No	MMP 1	MMP 2	MMP 3	MMP 7	MMP 8	MMP 9	MMP 10	MMP 11	MMP 12	MMP 13	MMP 14
151	Ser	Tyr	Tyr	Tyr	Ser	Tyr	Tyr	Leu	His	Tyr	Thr
157	Gly	Asp	Gly	Gly	Asn	Asp	Gly	Gly	Gly	Ser	Gly
158	Gly	Gly	Asn	Asn	Gly	Gly	His	Gly	Gly	Gly	Gly
159	Asn	Leu	Val	Thr	Ile	Leu	Ser	Ile	Ile	Leu	Phe
165	Gln	Ala	Ala	Ala	Gln	Pro	Pro	Phe	Gly	Pro	Phe
188	Glu	Gly	Gly	Gly	Asn	Gly	Gly	Gly	Gly	Gly	Gly
189	Tyr	Tyr	Thr	Ile	Tyr	Tyr	Thr	Thr	Thr	Tyr	Asn
193	Arg	Leu	Leu	Tyr	Leu	Leu	Leu	Gln	Leu	Leu	Leu
194	Val	Val	Val	Ala	Val	Val	Val	Val	Thr	Val	Val
218	Ser	Ile	Ile	Thr	Asn	Met	Leu	Phe	Thr	Ile	Phe
220	Thr	Thr	His	Gly	Ala	Arg	Asn	Thr	Lys	Thr	Gln
222	Ser	The	Leu	Gly	Arg	Thr	Phe	Arg	Val	Thr	Met
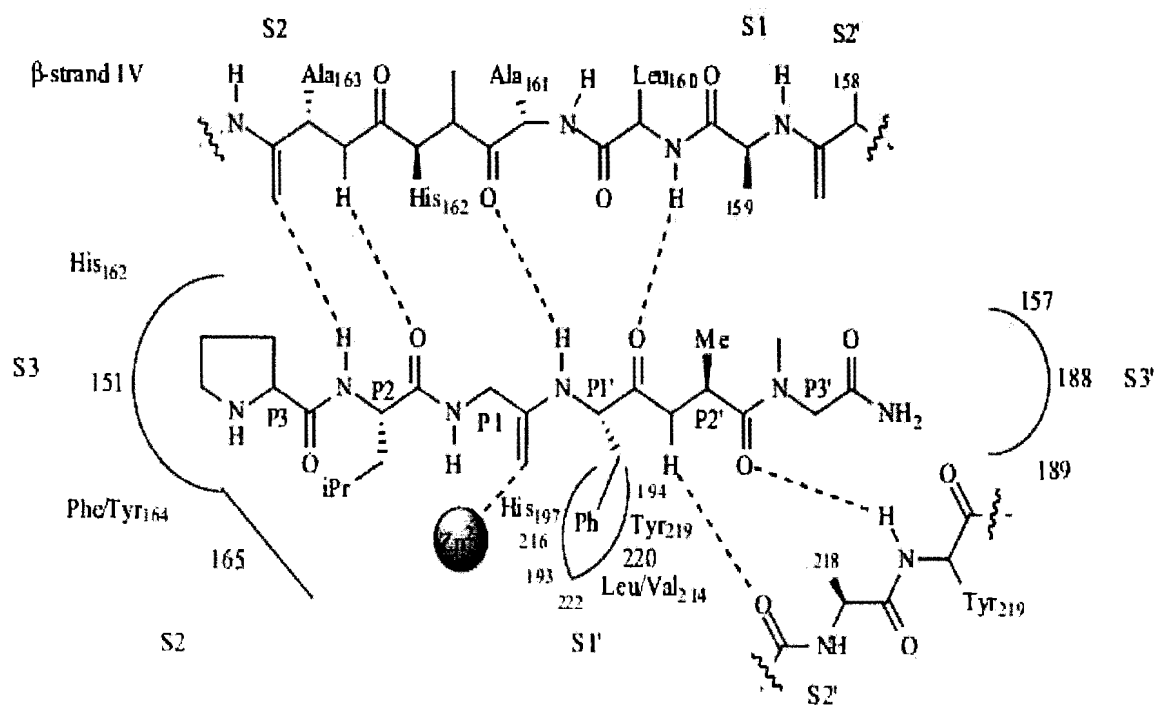
Figure 1.9. Schematic representation of the typical active site of MMP isozymes. This figure depicts the residues around MMP-8. This figure has been adopted from Ref 2.

The most important and crucial task in designing inhibitors or solving the rational

for the substrate specificity of these MMPs has been the correct understanding of the

different molecular subsite determinants (Figure 1.9). The substrate residues are named

P1, P2 and P1', P2' and similarly substrate recognition sites on the enzyme are named S1,

S2 and S1', S2' in N and C terminal directions of the scissile peptide bond, as per the

nomenclature designated by Schechter and Berger [61]. The substrate binding pockets

narrow from S3 to the S1' subsite. It is interesting to note that S1' appears to be a very well

notched out pocket.

1.5. Functions of MMPs

Growth and development are related to rapid cell movement and restructuring and

to reshaping of the extra-cellular matrix. A variety of studies have corroborated the

involvement of MMPs in physiological as well as pathological processes (Table 1.4).

Table 1.4. Involvement of MMPs in physiological and pathological conditions. This table
has been adopted from Ref 62.

Physiological Processes	Pathological Processes	Pathological Processes
Angiogenesis	Arthritis	Multiple sclerosis
Apoptosis	Alzheimer's disease	Nephritis
Blastocyst implantation	Atherosclerosis	Neurological disease
Bone remodeling	Breakdown of blood-brain barrier	Osteoarthritis (OA)
Cervical dialation	Cancer	Periodontal disease
Embryonic development	Cardiovascular disease	Rheumatoid
Endometrial cycling	Central nervous system disorders	Skin ulceration
Hair follicle cycling	Corneal ulceration	Sorby's fundus disease
Immune response	Emphysema	Vascular disease
Inflammation	Fibrotic lung disease	
Nerve growth	Gastric ulcer	
Organ morphogenesis	Guillian-Barre disease	
Ovulation	Liver cirrhosis	
Postpartum uterine involution	Liver fibrosis	
Wound healing	Metastasis	

1.5.1. Physiological conditions

1.5.1.1. Human endometrium

Menstruation, an event of tissue destruction, involves partial breakdown of the functional layer of the endometrium at the beginning of a normal reproductive cycle in women. Menstruation is similar to inflammatory responses, which include leukocyte infiltration, proliferation, and activation that occur in the endometrium before menstruation. It has been proposed that the leukocytes release MMPs during this stage. Interactions between leukocytes and the stromal and epithelial cells of the endometrium induce and activate MMPs resulting in tissue breakdown [63]. The mRNA for the MMPs, the interstitial collagenase, stromelysin-1, 2, and 3, matrilysin, gelatinase A, and gelatinase B are all expressed during the menstrual phase in the human endometrium [63-64]. Matrilysin is expressed in the epithelium and glandular epithelial cells throughout the tissue. Interstitial collagenase and gelatinase B are in stromal cells, but are concentrated in the luminal region of the tissue. The transcripts for stromelysin-3 and gelatinase A are localized throughout the stromal component of the tissue. The widespread expression of MMPs in all compartments of this tissue indicates that the coordinated effort of several MMPs may play a vital role in the breakdown and release of endometrial tissue during menstruation [65].

1.5.1.2. Wound repair

Wound repair is a physiological event in which tissue injury results in a repair process that finally leads to re-establishment of structure and function of the tissue. Cutaneous wound repair can be classified into three overlapping phases: (i) formation of a

fibrin clot followed by inflammation (early or late); (ii) re-epithelialization and granulation of tissue formation; and (iii) matrix formation and remodeling [66]. A fibrin clot is formed as a result of platelet aggregation and blood coagulation in the first phase of wound repair. Various growth factors and chemotactic factors, released from activated coagulation pathways, injured cells, and platelets, attract inflammatory cells to the wound area. Proteolytic degradation of the ECM is required in many stages of wound repair, such as degradation of the provisional matrix, angiogenesis, and keratinocyte migration. Following injury, MMP-1 is expressed by basal keratinocytes at the migration front of epidermis in several types of cutaneous wounds including incision wounds and blistering skin diseases [66]. The expression of MMP-1 in basal keratinocytes is rapidly induced after dermal injury, persists during healing, and subsides at re-epithelialization.

1.5.1.3. Cellular fibrinolytic activity

Interactions between the plasminogen/plasmin (fibrinolytic) system and MMP can affect cellular fibrinolysis (Figure 1.10). MMP-3 (stromelysin-1) specifically hydrolyzes urokinase (u-PA) giving rise to a 17 kDa NH_2 terminal fragment containing the functionally intact receptor (u-PAR)-binding sequence and a 72 kDa COOH terminal domain. MMP generates an angiotensin-like fragment from plasminogen. MMP-3 specifically hydrolyzes human α2-antiplasmin (α2-AP), the main physiological plasmin inhibitor. α2-AP cleaved by MMP-3 does not form a stable complex with plasmin and no longer interacts with plasminogen [67]. Cleavage and inactivation of α2-AP by MMP-3 may constitute a mechanism favoring local plasmin mediated proteolysis.

28
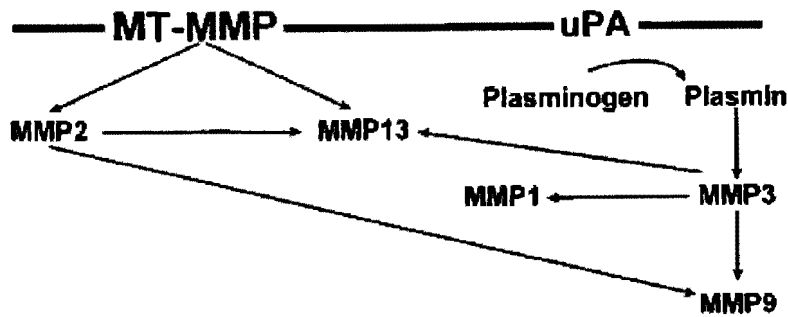
Figure 1.10. The activation cascade of MMPs. The MMPs involved in the activation cascade were MT1-MMP and MMP-2 and urokinase-type plasminogen activator (uPA). The figure has been adopted from Ref 53.

1.5.1.4. Epithelial remodeling

Matrilysin (the smallest, 28 kDa, of the known MMPs) gets expressed by non-injured, non-inflamed exocrine and mucosal epithelium in most tissues, i.e. in the lung. The expression of matrilysin in the normal epithelium indicates that this enzyme has a common homeostatic function among epithelia. All tissues in which matrilysin gets 'constitutively' expressed are open to the environment and hence vulnerable to bacterial exposure. Matrilysin has been prominently upregulated in tissues with a heavy bacterial load, such as in lungs with cystic fibrosis (CF). It has been suggested that matrilysin is responsible for the activation of pro-defensins, the precursor form of defensins that kill bacteria by membrane disruption [68].

A common role of the mucosal epithelium is to function as an active barrier against the external environment. The secretion of antimicrobial peptides by epithelial cells can be considered to be an important component of innate immunity. The α- and β- defensins consist of a family of cationic peptides that kill bacteria by membrane disruption [69]. The

pro-segment of α-defensin precursor retain them in an inactive state, and proteolysis at some point in the secretion pathway is required to remove the pro-domain. Paneth cells are specialized epithelial cells that secrete defensins and other antimicrobial molecules, and matrilysin activates these peptides in the secretion pathway.

1.5.1.5. Aging

Recent studies have confirmed that MMP-2 activity in smooth muscle cells is required in chemotactic invasion of a reconstituted basement [70]. The activity and expression of MT-MMP (MMP-14), MMP-2, and MMP-9 increase during mechanical injury to arteries [71]. MMP-2 has also been shown to be present within atherosclerotic lesions. The proteolytic activity results in rupture due to weakening of the fibrous cap [72-73]. In the aorta, in the absence of externally imposed experimental injury, age-associated disorganization of the internal elastic lamina has been observed [74]. Both MMP-2 and MMP-9, along with metalloelastase of macrophages [75] exhibit elastase activity [76]. It has been established that both latent and activated forms of MMP-2 are greater in the aortas of old than in young rats [74].

1.5.2. Pathological conditions

1.5.2.1. Angiogenesis

Angiogenesis or neo-vascularization can occur throughout the life span of an adult. During angiogenesis, capillary of parent venule are stimulated by an angiogenic stimulus, such as fibroblast growth factor (FGF), vascular permeability factor (VPF) and vascular endothelial cell growth factor (VEGF). The perivascular ECM is composed predominantly of type I collagen, and two specific MMPs, interstitial collagenase (MMP-1) and neutrophil

collagenase (MMP-8). They are capable of degrading type I collagen [77]. In a recent study, it has been demonstrated that MMP-1 activity appears to be required for angiogenesis [78]. MMPs facilitate EC (endothelial cell) release via the degradation of the venules basement membrane. Proteolytic activity is also required for the migration of EC into the perivascular stroma. These events are followed by sprout extension and subsequent lumen formation [79-80]. The finding represents a novel activation mechanism for MMPs by EC and smooth muscle cells. It has been suggested that the remodeling of the capillary endothelium that is required during angiogenesis can be induced by thrombin [81]. Tumor cell invasion and angiogenesis share a number of functional similarities. Initiation of cellular invasion in both processes requires attachment to a basement membrane, followed by creation of a proteolytic defect in the basement membrane and migration through this defect.

Cell proliferation and continued invasive behavior results in production of either a new vessel lumen or metastatic foci after invading cells cross this connective tissue barrier. Angiogenesis and tumorigenesis may be mutually stimulating in addition to sharing these functional similarities. Formation of new blood vessels helps in expansion of tumor foci in three dimensions [82]. Tumor foci exist as small, asymptomatic lesions restricted by the limitation of passive oxygen and nutrient diffusion, prior to vascularization. Following vascularization, the tumor foci undergo rapid local expansion and that in turn acquire enhanced metastatic potential that correlate directly with the degree of vasularization of the primary tumor [83]. Metastasis formation and tumor invasion are closely linked to tumor induced neo-angiogenesis.

1.5.2.2. Chronic ulcers

Chronic ulcers, which do not heal within the normal biological time range, are defined as "wounds". Examples of chronic wounds include ulcers, superficial surgical wounds, chemical burns, and burn wounds. The expression levels of MMP-2, MMP-9 and their activated forms are increased in wound fluids of chronic ulcers, compared to the normal healing process of acute wounds [84-85].

1.5.2.2.1. Liver fibrosis

Liver fibrosis is conventionally viewed as a progressive pathological process involving multiple molecular and cellular events that lead ultimately to deposition of excess matrix proteins in the extracellular space. There is increasing distortion of the normal liver architecture, with ineffective regeneration and repair, and the end result is cirrhosis.

1.5.2.3. Lung diseases

1.5.2.3.1. Chronic obstructive pulmonary disease (COPD)

The progressive structural damage associated with emphysema and other forms of chronic obstructive pulmonary disease (COPD) appears to be due to degradation of selective extra-cellular matrix components. The proteinases that can degrade elastin are involved in the development of COPD. The elastin content of the lung parenchyma is decreased in emphysema, while the collagen content is increased.

Exposing proteinase null mice to cigarette smoke provides a highly controlled model to assess the role of specific MMPs in emphysema. Long-term exposure of wild-type mice to cigarette smoke leads to inflammatory cell recruitment followed by alveolar

space enlargement that is quite similar to the lesions that develop in humans. Mice deficient in metalloelastase are markedly protected from development of emphysema due to long-term smoke exposure [86]. Metalloelastase is not the sole proteinase responsible for the human disease. There are probably several proteinases and inflammatory cells involved in the development of emphysema in humans. Human macrophages probably have a broader spectrum of MMPs (including metalloelastase). Collagenase-1, -2 and -3 also undoubtedly contribute to loss of the airspace and an increase in collagen deposition leading to airway obstruction [87]. Importantly, different enzymes from multiple families may act in concert in tissue remodeling. For example, metalloelastase as well as other MMPs degrades α1-proteinase inhibitor, and neutrophil elastase, a serine proteinase, degrades TIMPs. These enzymes can accentuate overall proteolytic activity by neutralizing each other's natural inhibitors [88].

1.5.2.4. Cardiovascular diseases

Atherosclerosis is an inflammatory process in which plaques are formed in the intimal layer of the vessel wall as a result of accumulation of lipid-rich macrophages, smooth muscle cells and lipids on these vessel walls. Clinical complications of atherosclerosis are often triggered by rupture of unstable plaques, triggering intravascular thrombosis and tissue ischemia [89-92]. Thinning of the atherosclerotic vessel wall due to elastin and collagen degradation and matrix necrosis may result in aneurysm formation and bleeding [90-91]. The MMP system has been implicated in the pathogenesis of atherosclerosis and aneurysm formation [92-94]. In animal models, over expression of TIMP-1 prevents aortic aneurysm formation and rupture. Human atherosclerosis appears to

be an important example of the potentially harmful effects of 92 kDa gelatinase production. Immuno-staining has shown that 92 kDa gelatinase productions in arteries is increased, whereas in normal arteries 92 kDa gelatinase is not expressed in both stable and unstable angina [94]. Increased production of 92kDa gelatinase in atherosclerosis may hence contribute to the matrix destruction and subsequently lead to plaque rupture. Interstitial collagenase and stromelysin have also been identified in atherosclerotic coronary arteries [73].

1.5.2.5. Inflammatory myopathy

MMPs have been found to play a role in inflammatory myopathies. These immune mediated disorders are characterized by loss of muscle fibres, invasion of mononuclear phagocytes and T-lymphocytes.

1.5.2.5.1. Congestive heart failure

MMPs such as collagenase-3 (MMP-13) are expressed at very low levels in normal myocardium. Membrane type-1 MMPs (MT1-MMP) are substantially upregulated in congestive heart failure (CHF). However, MMP species are not uniformly increased in patients with end-stage CHF, suggesting that a specific portfolio of MMPs is expressed in the failing myocardium. Recent studies in transgenic mice suggest that this MMP species plays a role in post infarction myocardial remodeling [104]. Clinical studies [95-96] have indicated the emergence of the interstitial collagenase MMP-13 in pathological remodeling states, such as human breast cell carcinoma and osteoarthritis. In a recent study [97] elevated MMP-13 levels were observed in end-stage of human heart failure. Increased myocardial MMP-13 levels were shown to occur with chronic pacing, which has been

34

suggested to be associated with the myocardial remodeling process [98-101,15].

1.5.2.6. Angiotensin

1.5.2.6.1. Rheumatoid arthritis

Progressive structural joint damage is one of the strongest predictors of long-term outcome in rheumatoid arthritis (RA) and osteoarthritis (OA). The rheumatic diseases possible to consistently prevent the progressive joint destruction that leads to chronic continue to symbolize a significant health care issue in the 21st century. It is still not disability, despite the best standards of care and recent therapeutic advances. In rheumatoid arthritis and osteoarthritis this progressive cartilage and bone destruction is considered to be driven by an excess of MMP enzymes [102]. MMPs contribute to joint destruction in rheumatoid arthritis (RA) in at least two ways. First, they can directly degrade the cartilage and bone. The major MMPs implicated in this process include stromelysin-1, collagenase-1, collagenase-3, gelatinase-A, and gelatinase-B. Second, MMPs are important during angiogenesis (the formation of new blood vessels), which is a prominent feature of rheumatoid arthritis. During angiogenesis, endothelial cells degrade at least two distinct barriers, the microvascular basement membrane and the interstitium. The gelatinases play a pivotal role during these stages [103].

1.5.2.7. Cancer

1.5.2.7.1. Role of MMPs in cancer dissemination

A positive correlation between the expression of multiple MMP family members (MMP-1, MMP-2, MMP-7, MMP-9, MMP-11, and MT1-MMP) and tumor progression has been demonstrated in numerous animal and human studies [104]. The ratio of activated to

35

total MMP levels, especially MMP-2, has also been correlated with tumor aggressiveness [105]. Based on numerous preclinical studies, it was proposed that targeting MMP activity may provide a mechanism to prevent cancer dissemination, [106].

1.5.2.7.2. Production of MMPs by tumor stromal cells

From studies of oncogene transformed cells, cancer cell lines, and experimental tumor models (Figure 1.11), it had long been assumed that cancer cells were responsible for producing the MMPs in human tumors [107-108]. The localization of MMP-1, MMP-2, MMP-3, and MT1-MMP mRNA primarily in stromal fibroblasts, especially in proximity to invading cancer cells led to this belief [109-110].

Inhibit endothelial MMPs & angiogenesis

(stimulates angiogenesis & tumor growth) IGF-II

Bind to ECM (cell migration)

IGF-BP

FAS Ligand   Degrade

INTEGRIN ◄──── Bind & activate MMP-2
αVβ3   SEPRASE ────────► ANGIOGENESIS

TIMPs

Cleavage   MMP-11   MT-MMP

Angiostatin   TIMP-2 (↑↓ proMMP activation)
(Inhibits Angiogenesis) MMP-7   STROMAL
CELL   Activation   Cleave LAMININ-5

Cleavage

Plasminogen   Fragment induces cancer cell migration

uPA bound-uPA receptor   proMMP-3   degrade

MMP-3   Collagen IV   proMMP-9   COLLAGEN IV, LAMININ,
CD44   binds   VITRONECTIN, FIBRONECTIN,
Decorin   MMP-1, 8, 13   ENACTIN

Activation   MT-MMP
proMMP-1, 3, 9 ◄── Plasmin

α1 protease inhibitor   IL1-β
(unleashes activity of serine proteases) perlecan   E-cadherin

Release of Growth Factors   binds   Degrade 3/4 & 1/4 fragments
(heparin binding-EGF)

FGF-2
(stimulates angiogenesis)   Cleave COLLAGENS I, II, III (enhance cancer invasion)

Stimulate cancer cell proliferation

FGF-BP

Figure 1.11. The potential influence of MMPs on the stromal cell secreted (plasminogen activator) cell surface proteinases and TIMPs during cancer progression. The effect of MMPs on the different factors like: integrins, cadherin, CD44, perlecan, cytokines (IL1-b), plasminogen, fibroblast growth factor (FGF), epithelial growth factor (EGF), insulin-like growth factor (IGF), binding proteins for growth factors (IGF-BP, FGF-BP), growth factor receptors (FGF-R),extracellular matrix proteins (collagen, laminin, vitronectin, fibronectin, enactin, decorin), and apoptosis factors (FAS ligand) are shown in this figure. Figure 1.11 has been adapted from Ref 111.

1.5.2.7.3. The role of MMPs in tumor invasion and metastasis

Metastasis, tumor cell invasion (involving proteolytic degradation of BM and ECM), altered cell adhesion and physical movement of tumor cells are now regarded as a multi-step phenomenon. The formation of new blood vessels (angiogenesis) is essential both for tumor growth, successful tumor invasion and metastasis. Angiogenesis is a complex and dynamic process that requires proliferation of endothelial cells from pre-existing blood vessels along with migration of endothelial cells and breakdown of the extracellular matrix (ECM). MMPs play a central role in the growth and development of blood vessels within tumors that require the same factors that are crucial to tumor cell invasion. Individual MMPs may have different, possibly contradictory, roles in angiogenesis. Proteolysis of the ECM is a pre-requisite for angiogenesis and activated MMPs (specifically, MMP-2) are present in endothelial cells of blood vessels near the sites of angiogenesis. However, several MMPs (MMP-2, MMP-7, MMP-9, and MMP-3) have recently been shown to be capable of proteolytic cleavage of plasminogen to form angiostatin, an endogenous angiogenesis inhibitor, which specifically inhibits proliferation of endothelial cells [112-114].

The MMPs are responsible for degradation of the constituents of BM and ECM. MMPs are implicated in altered adhesion between the tumor cell and its environment through interactions with an array of cell adhesion molecules. This implies that MMPs play a role in the movement of cells through the ECM. MMPs also have growth regulatory effects on both primary and secondary tumors in addition to their function in the breakdown of the ECM. *In vitro* studies have demonstrated the degradation of insulin-like

growth factor receptor binding proteins (IGFBP-3 and -5) by MMPs, which may contribute to the observed growth-regulatory functions of the MMPs [115]. There is experimental evidence (Figure 1.12) that proves that MMPs are involved in the early stages of tumor growth and development [116-117].
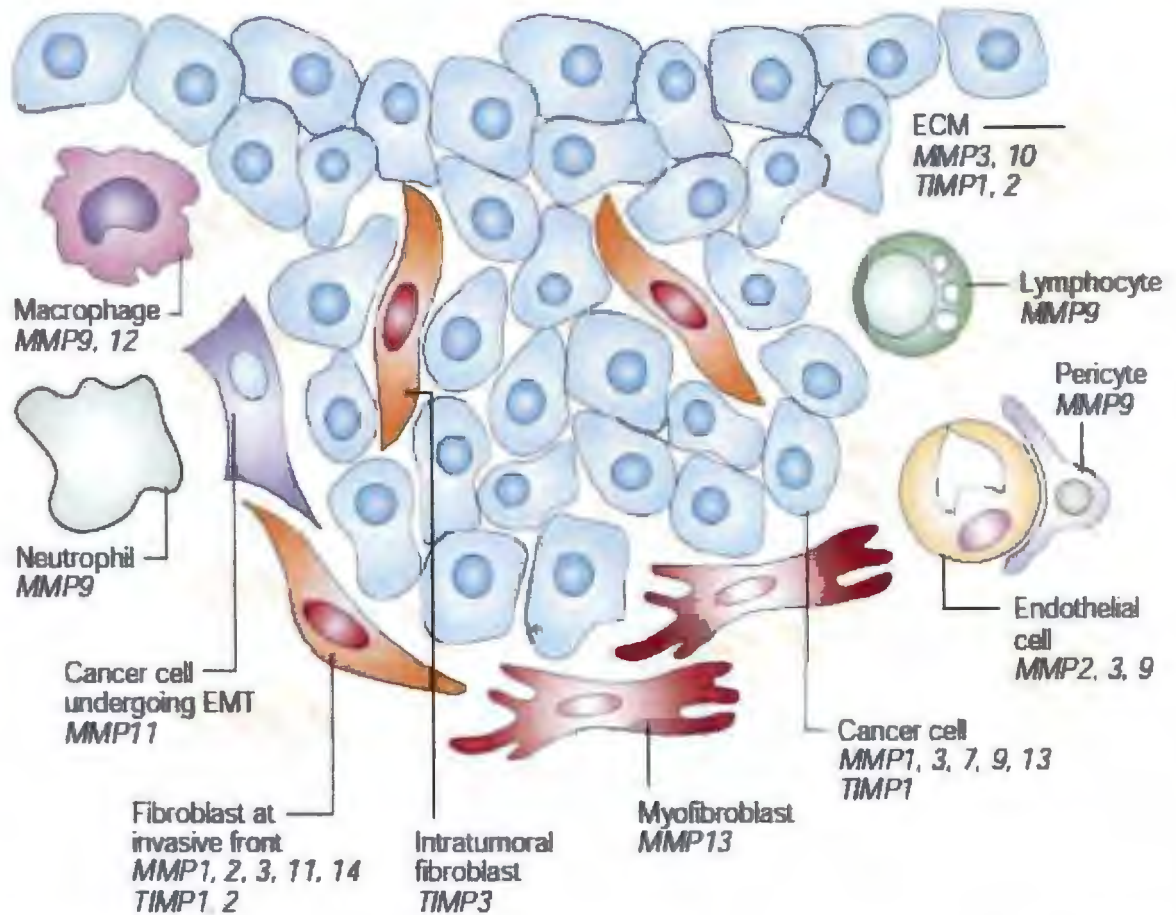
Figure 1.12. The expression of MMPs and TIMPs in the case of breast tumors. The breast cancer cells are proliferating in the stromal cells. It includes myofibroblasts, fibroblasts, pericytes, epithelial cells, macrophages, neutrophils and lymphopcytes in the stroma. MMP isozymes and TIMPs are also synthesized where the cancer cells undergo a transition from the epithelial to mesenchymal phase transition. The figure has been adapted from Ref 52.

The latency of the secreted enzymes and the presence of naturally occurring inhibitors tightly control the degradative activity of MMPs. The latter include general

plasma proteinase inhibitors such as α2-macroglobulin, as well as more specific inhibitors such as the tissue inhibitors of metalloproteinases, TIMP-1 [118], TIMP-2 [119], and TIMP-3 [120].

There appears to be a local and temporal imbalance between the levels of activated enzymes and their inhibitors in several diseases such as arthritis [121], neurodegenerative disease such as multiple sclerosis [122], and cancer [123] resulting in a breakdown of the extracellular matrix. Several studies have shown that in cancer models, the proportion of active MMPs overwhelms the local inhibitory activity surrounding the tumor. This MMP activity facilitates the local invasion and direct expansion of the primary tumor, the movement of tumor cells across the vascular basement membrane, and the local growth and invasion of any secondary tumors. MMP activity further contributes to the growth of new blood vessels, a requisite for malignant tumor growth. It is not likely that every type of cancer uses MMPs to break down matrix barriers, and other classes of proteases, such as the urokinase-type plasminogen activator, are known to be expressed in high levels in certain malignancies. Identifications of the relationship between cancer and MMPs are one of the major challenges in the development of matrix metalloproteinase inhibitors (MMPIs) as anticancer agents (Figure 1.12). It is extremely important to realize that very few human cancer cell lines and experimental *in vivo* models reflect the MMP expression of the tumor from which they were isolated. Hence, human tissues taken at the time of primary surgery provide the best insight into the role of MMPs in human cancer.

(i)   Collagenases

Fibrillar collagenase activity in epidermoid carcinomas of the oral cavity and larynx

was found to increase when compared to the activity in normal mucosa [124]. High levels of fibrillar collagenase activity were also found at the invading edge of gastric carcinomas [122]. In colorectal cancer, a correlation was detected with collagenolytic activity [124]. Interstitial collagenase in the connective tissue stroma of colorectal carcinomas was found to increase when compared to the staining in adenomas and normal mucosa [124].

(ii)   Stromelysins

Both in stromal and tumor cells, a high level of mRNA encoding for stromelysin-1 has been detected in lung, head and neck cancer [125]. It was not found in prostate [126], gastric, or colorectal cancer [127]. In contrast, high levels of PUMP-1 mRNA expression were revealed in gastric and colorectal cancers [127]. In the latter, it was localized in tumor tissue or in adjacent stroma, with little or no expression in surrounding normal tissue [52, 128-129]. High levels were also found in prostate cancers being localized to the malignant and non-malignant epithelial cells but not found to the associated stroma [127].

(iii)   Gelatinases

While the ratio of activated to latent gelatinase A was significantly higher in malignant versus benign breast lesions and a higher proportion of activated enzyme was related to increasing tumor grade [130], high levels of activated gelatinase A were demonstrated in invasive cancer of the breast [131]. The expression of gelatinase A was correlated with the progression of colorectal, gastric and breast cancer [132]; but failed to predict relapse or survival in patients with node-negative breast cancers [133]. Gelatinase A was also found to be higher in invasive ovarian cancer than in benign cystadenomas of the ovary, and was particularly intense around micro-invasive cells or clusters [134]. As

40

compared to normal sera, it was significantly elevated in sera of lung cancer patients and levels were also significantly higher in patients with distant metastases [135]. Gelatinase A was localized to the cells of the tumor associated stroma in both colorectal cancer [136] and infiltrating squamous cell cancer of the skin [137].

(iv)   Stromelysin-3

Several correlative studies in breast cancer have shown high levels of expression of stromelysin-3 mRNA in tumor tissue or in adjacent stroma, with little or no expression in surrounding normal tissue [138]. Low levels of stromelysin-3 mRNA were detected in colon, ovary, kidney and lung cancers. More recently stromelysin-3 mRNA and protein have been detected exclusively in the stromal cells surrounding squamous cell cancers of the head and neck, and these levels were significantly correlated to the invasiveness of the cancer cells. Transcripts for stromelysin-3 were localized in the samples exclusively in the neoplastic cells, while those for interstitial collagenase were found in both stromal and neoplastic cells [139]. The results point to an important role for stromelysin-3 in tumor progression and make it even more important to understand the proteolytic function of this metalloenzyme.

(v)   MT-MMP

MT-MMP, which appears to be a specific activator of progelatinase A, is a membrane-bound enzyme with a recognized transmembrane domain [140]. The expression of MT-MMP by cancer cells would grant the ability to activate gelatinase A, which is produced locally by stromal cells at the invasive tumor margins. In a study of gastric

41

cancer, MT-MMP was expressed exclusively in the tumor tissue and co-localised with activated gelatinase A in invasive carcinoma cell nests [141].

1.5.2.8. Neurodegenerative diseases

MMPs have been shown to degrade components of the basal lamina leading to disruption of the blood-brain-barrier in the central nervous system (CNS). MMPs contribute to the neuro-inflammatory response in many neurological diseases. Brain cells express both constitutive and inducible MMPs in response to cellular stress. MMPs are tightly regulated to avoid unwanted proteolysis. Secreted as inactive enzymes, the MMPs require activation by other proteases and free radicals. At the cell surface, they act as "sheddases" and release growth factors, which are important in cell survival and death [142]. The motor neurons in amyotrophic lateral sclerosis patients express significantly higher levels of MMP-9 as indicated by its increased levels in cerebrospinal fluid, suggesting a role in neurodegeneration [143]. In serum, however, MMP-9 was significantly increased in amyotrophic lateral sclerosis (ALS) patients similar to that of viral meningoencephalitis (VM) or bacterial meningitis (BM) patients [144]. It has recently been shown that axonal damage occurs within active plaques (localized area of myelin sheath destruction within the central nervous system) as a consistent consequence of demyelination in multiple sclerosis [145]. Demyelination not only damages neural transmission directly, but also increases axonal vulnerability to the proteolytic enzymes and cytokines produced by activated immune and glial cells. Increased MMP expression has also been associated with the pathologies of Alzheimer's disease, malignant gliomas and amyotrophic lateral sclerosis [146-147].

1.5.2.8.1. Parkinson's disease

MMP-2 levels in brain tissue from Parkinson's disease (PD) cases in substantia nigra were investigated post mortem. Levels of MMP-2 were not significantly changed in the cortex and hippocampus. MMP-9 levels remained unchanged in the investigated brain regions. Levels of TIMP-1, an endogenous tissue inhibitor of MMPs were significantly elevated in the substantia nigra, but not in the cortex and hippocampus. TIMP-2 levels were unchanged in PD. MMP-1 levels were unchanged in PD cases compared to controls. Collectively, these data showed alterations of MMP-2 and TIMP-1 in the substantia nigra, consistent with the possibility that alterations in MMPs/TIMPs may contribute to disease pathogenesis [148].

1.5.2.8.2. Alzheimer's disease

The neurons in the brain affected with Alzheimer disease expresses MMP-9 and uPAR. MMP-9 can be produced for the degradation of amyloid beta protein [149]. Among the non-gelatinase type isoforms in the brain, MT5-MMP (MMP-24) has been found to be the predominant species. As assessed biochemically and immune-histochemically, MT5-MMP has most strongly been expressed in cerebellum and localized in the membranous structure of expressing neurons. In cerebellum, its expression was regulated developmentally and was closely associated with dendritic tree formation of Purkinje cells, suggesting that MT5-MMP may contribute to neuronal development [150]. Additionally, its stable post developmental expression and co-localization with senile plaques in Alzheimer brain [151] indicates possible roles in neuronal remodeling naturally occurring inadulthood and in regulating patho-physiological processes associated with advanced age.

The increased activities of MMPs are a major cause of tissue breakdown and secondary damage in diseases such as rheumatoid arthritis, in peripheral inflammatory states. MMP-1 levels were considerably elevated in AD in all cortical areas by approximately 50%. It is, therefore, possible that MMP-1 activity in AD may contribute to the blood brain barrier dysfunction seen in AD [164]. There is considerable evidence to indicate that MMPs can play an important role in the pathogenesis of Alzheimer's disease (AD). Stromelysin-1 (MMP-3) plays an important role in activating latent type MMPs that were secreted originally as proenzymes. In case of degradation of β-amyloid protein, the selective distribution of MMP-3 in the human brain suggests that MMP-3 might play an important role in the pathogenesis of AD [152].

1.6. Regulation of MMPs

MMPs must be present in the right cell type and pericellular location, at the right time, and in the right amount, to accomplish their normal (or pathologic) functions and they must be activated or inhibited appropriately. MMPs are tightly regulated at the transcriptional and post-transcriptional levels and are also controlled at the protein level via their activators, inhibitors, and their cell surface localization. MMP proteolytic activity is regulated at three main levels — transcription, proenzyme activation and inhibition. Regulation of mRNA stability, translational efficiency, enzyme compartmentalization and secretion, cell-surface recruitment, substrate targeting, shedding, oligomerization, cellular uptake, and internalization, and finally, autolysis are the additional mechanisms by which MMP activity is fine-tuned. Since discussion at all these levels in detail would be impossible, hence, the major mechanism and regulation level of MMP activity is discussed

in this Dissertation. These mechanisms operate in coordination to assure that MMP expression and activity are only circumscribed to those sites and conditions in which proteolytic activity is necessary. However, malignant tumors have developed strategies to circumvent these regulatory mechanisms, and to generate the uncontrolled proteolytic activity that leads to cancer development and metastasis.

1.6.1. Regulation of MMP activity

1.6.1.1. Transcriptional regulation

The viewpoint in the early 1980s that MMPs are coordinately regulated at the transcriptional level is no longer valid. Instead, each cell displays a proteolytic phenotype in response to a particular stimulus and their transcription is independently regulated. There are numerous complex mechanisms by which cells control transcription of MMPs [153-154]. The transcription of MMP genes can be induced in tumor or stromal cells by various signals, such as cytokines, growth factors, and oncogene products, but cannot be expressed under normal quiescent conditions. These factors are typically released by the stroma, infiltrating host defense cells or by tumor cells themselves. MMP transcription can also be induced by other conditions such as alterations in cell shape or mechanical stress [155]. Although tumor necrosis factor-α (TNF-α) and interleukin (IL-1) are regularly implicated, no single factor has been identified to be exclusively responsible for the over-expression of MMPs in specific tumors [153]. Depending on the tumor-cell type, the same MMP can be transcriptionally induced or repressed by different agents. In MMP transcription, some factors such as TGF-β or retinoids, function as both positive and negative regulators [156-159].

Pro-MMPs are activated by different events (Figure 1.13 shows diverse regulatory signals). These active MMPs are involved in a number of processes that promote cancer development (red boxes), including promoting genetic instability, angiogenesis, cell growth, and invasion. They also interfere with apoptosis induction and host antitumor immune responses. MMP autolysis or inhibitors can interfere with the induction of these cellular effects. The levels of MMP regulation that might be therapeutically targeted are shown in orange boxes, and include cell responses to regulatory signals, transcriptional induction, signal transduction, post-transcriptional processing, MMP activation, and transport and secretion.
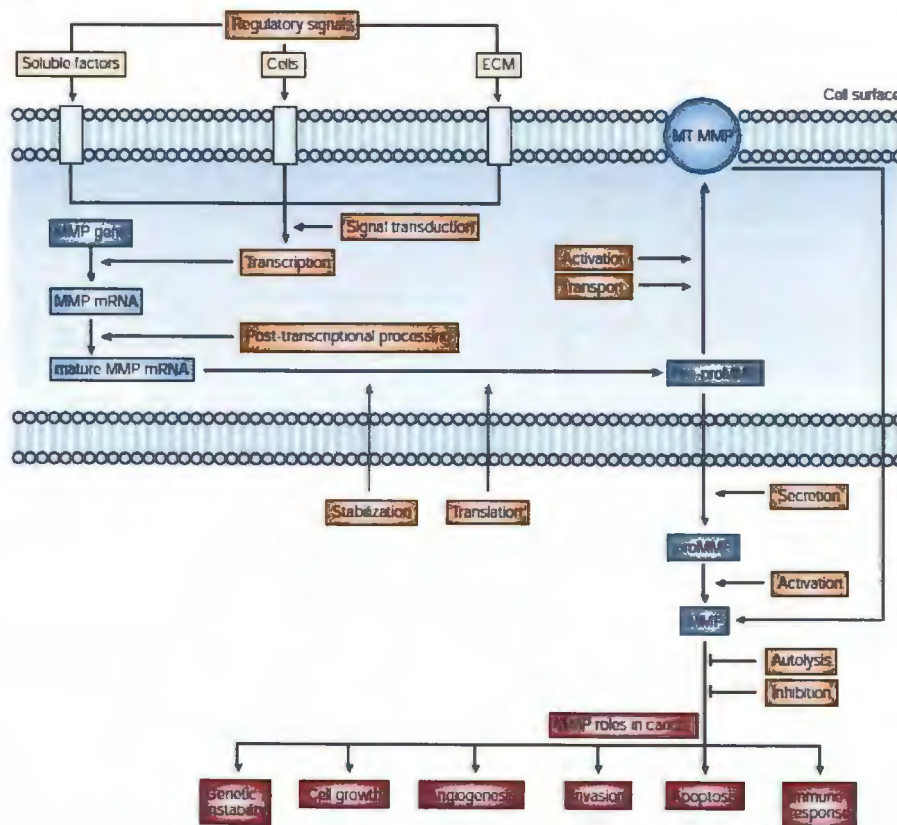
Figure 1.13. The levels of expression and MMP activity. This figure has been adopted from Ref 160.

1.6.1.2. Post-transcriptional regulation of MMP activity

Post-transcriptional mechanisms are vital to the control of MMP activity, as all the soluble MMPs are secreted as inactive zymogens requiring activation by cleavage of the N-terminal pro-domain (Figure 1.14). The membrane-type MMPs (MT-MMPs) are distinguished by the possession of a trans-membrane domain and differ in that they are activated intracellularly, prior to transport to the cell surface. The interaction of the MMPs with the urokinase-type plasminogen activator (uPA), also called the plasmin system is a complex process.
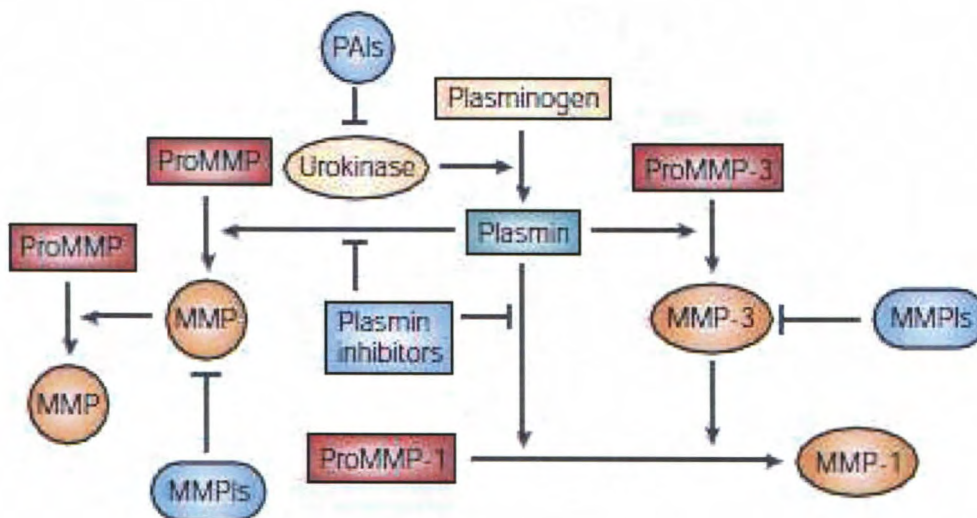
Figure 1.14. Strategies for blocking proMMP activation. This figure has been adapted from Ref 160.

Figure 1.14 shows the active MMPs that are generated through a multi-step proteolytic cascade and involves plasminogen cleavage by urokinase to create plasmin, which then cleaves proMMPs to create active MMPs. Some of these MMPs go on to cleave other proMMPs. MMP inhibitors (MMPIs) block MMP generation from proMMPs. Serineproteinase inhibitors (PAIs) of urokinase block plasmin generation while the plasmin

inhibitors block the proMMP conversion to MMPs.

1.6.1.3. MMP activation

Like many proteases, MMPs are synthesized as inactive zymogens (Figure 1.8). The mechanisms of MMP latency were originally uncertain, and were attributed to TIMP binding to the MMP active site. As it was found that the MMP prodomain masks the active-site cleft and prevents hydration of the active site Zn^{2+} ion, the idea was soon disregarded. A conserved unpaired cysteine residue in the prodomain of MMPs forms a cysteine-switch [161]. This concept has been supported by structural analysis of proMMP-2 [162] and proMMP-3 [163]. The site for MT1-MMP cleavage of proMMP-2 that initiates the activation lies on a surface-exposed loop within the prodomain [162]. This loop is likely to be present in other MMPs functioning as 'bait' for activating proteases, such as plasmin, chymase, and tryptase.

The prodomain structure partially unfolds, following initial cleavage, exposing additional sites for further cleavage by activating enzymes such as MMP-3. Binding to a ligand or to a substrate *in vivo* might also lead to a disengagement of the propeptide, causing protease activation [164]. Elucidating the requirement for a second MMP to perform the final activation cleavage, typically at a phenylalanine (Phe) or tyrosine (Tyr) at position 80 or 81 was a conceptual breakthrough in MMP research. Differences in the active site S1′ subsite and propeptide sequences of MMPs generate specificity for activating proteases. MMP-1 is an excellent example of an MMP that requires MMP-3 activation cleavage. This could not be due to an autocatalytic reaction. The shallow S1′ subsite pocket of MMP-1 cannot accommodate bulky side chains such as the amino-

terminal Phe of the correctly processed fully active enzyme. Other MMPs, such as MMP-2, have a deep pocket that can accommodate Tyr81, so activation can be completed autolytically by another active MMP-2, which must be tethered to the cell surface [165].

1.6.1.4. Regulation of MMP activity by inhibitors

1.6.1.4.1. Using TIMPs

MMP activity gets blocked by general inhibitors that are present in the plasma and tissue fluids, such as α2-macroglobulin and by more specific inhibitors, such as TIMPs. Four human TIMPs that are anchored in the ECM or secreted extracellularly have been identified [166]. The net balance between protease and inhibitor activities determines the proteolytic potential of tumors, and a decrease in TIMP levels are generally correlated with tumorigenesis [167]. Nevertheless, there are abundant examples in which TIMP expression, which would be expected to reduce tumorigenic potential, increases during tumor progression. This might be due to the host-protective stromal response [168].

1.6.1.4.2. Using endogenous inhibitors

Several recently described proteins contain domains that are homologous to the TIMP inhibitory domains, while some are novel MMP inhibitors, reversion-inducing cysteine-rich protein with Kazal motifs (RECK), a key regulator of ECM integrity and angiogenesis is a cell-surface MMP inhibitor [169]. This is also the case for tissue-factor pathway-inhibitor-2 (TFPI2) — a serine proteinase inhibitor that can function as an MMP inhibitor [170]. The procollagen C terminal proteinase enhancer (PCPE) releases a C-terminal fragment that is similar to the inhibitory domain of TIMPs, and possesses

significant MMP inhibitory activity [171-172]. As of now the physiological targets of these

putative MMP inhibitory activities remain unclear, as so is their relevance in cancer.

1.7. References

1. Gross, J., and Lapiere, C.M. (1962) Collagenolytic activity in amphibian tissues: A tissue culture assay, *Phys.* 48, 1015-1022.
2. Whittaker, M., Floyd, C. D., Brown, P., and Gearing, A. J. H. (1999) Design and therapeutic application of matrix metalloproteinase inhibitors, *Chem. Rev.* 99, 2735-2776.
3. Lovejoy, B., Cleasby, A., Hassell, A. M., Longley, K., Luther, M. A., Weigl, D., McGeehan, G., McElroy, A. B., Drewry, D., Lambert, M. H., and Jordan, S. R. (1994) Structure of the catalytic domain of fibroblast collagenase complexed with an inhibitor, *Science.* 263, 375–377.
4. Stams, T., Spurlino, J. C., Smith, D. L., Wahl, R. C., Ho, T. F., Qoronfleh, M. W., Banks, T. M., and Rubin, B. (1994) Structure of human neutrophil collagenase reveals large S1 specificity pocket, *Nature. Struct. Biol.* 1, 119–123.
5. Gooley, P. R., O'Connell, F., Marcy, A. I., Cuca, G. C., Salowe, S. P., Bush, B. L., Hermes, J. D., Esser, C. K., Hagmann, W. K., Springer, J. P., and Johnson, B. A. (1994) The NMR structure of the inhibited catalytic domain of human stromelysin-1. *Nature. Struct. Biol.* 1, 111–118.
6. Browner, M. F., Smith, W. W., and Castelhano, A. L. (1995) Matrilysin-inhibitor complexes: common themes among metalloproteases, *Biochemistry.* 34, 6602–6610.
7. Protein Data Bank http://www.pdb.org.
8. Duffy, M. (1992) The role of proteolytic enzymes in cancer invasion and metastasis, *Clin. Exp. Metastasis*, 10, 145–155.
9. Nagase, H. (1996) in Zinc Metalloproteases in Health and Disease (Hooper, N. M., Ed) pp. 153–204, *Taylor & Francis, London.*
10. Fini, M. E., Cook, J. R., Mohan, R., and Brinckerhoft, C. E. (1998) in *Matrix Metalloproteinases* (Parks, W. C., and Mecham, R. P., Ed) pp. 299–356, *Academic Press, San Diego.*
11. Lepage, T., and Gache, C. (1990) Early expression of a collagenase-like hatching enzyme gene in the sea urchin embryo, *EMBO. J.* 9, 3003–3012.
12. Wada, K., Sato, H., Kinoh, H., Kajita, M., Yamamoto, H., and Seiki, M. (1998) Cloning of three Caenorhabditis elegans genes potentially encoding novel matrix metalloproteinases, *Gene (Amst.).* 211, 57–62.
13. Pak, J. H., Liu, C. Y., Huangpu, J., and Graham, J. S. (1997) Construction and characterization of the soybean leaf metalloproteinase cDNA, *FEBS Lett.* 404, 283–288.
14. Massova, I., Kotra, L. P., Fridman, R., and Mobashery, S. (1998) Matrix metalloproteinases: structures, evolution, and diversification, *FASEB J.* 12, 1075–1095.

15. Nagase, H. and Woessner, J.F. Jr. (1999) Matrix metalloproteinases. *J. Biol. Chem.* 274, 21491-21494.

16. Sasaki, T., and Timpl, R. (1999) in *Guidebook to the Extracellular Matrix, Anchor and Adhesion Proteins* (Kreis, T. & Vale, R. Ed) pp: 434–443, *Oxford Univ. Press, Oxford, UK.*

17. O'Reilly, M. S. (1997) Endostatin: an endogenous inhibitor of angiogenesis and tumor growth, *Cell.* 88, 277–285.

18. Hynes, R. (1999) in *Guidebook to the Extracellular Matrix, Anchorand Adhesion Proteins* (Kreis, T. & Vale, R. Ed), pp: 422–425, *Oxford Univ. Press, Oxford, UK.*

19. Gustafsson, E., and Fassler, R. (2000) Insights into extracellular matrix functions from mutant mouse models. *Exp. Cell. Res.* 261, 52–68.

20. Cossins, J., Dudgeon, T. J., Catlin, G., Gearing, A. J., and Clements, J. M. (1996) Identification of MMP-18, a putative novel human matrix metalloproteinase. *Biochem. Biophys. Res. Commun.* 228, 494–498.

21. Mignatti, P., and Rifkin, D.B. (1993) Biology and biochemistry of proteinases in tumor invasion, *Physiol. Rev. 73*, 161-195.

22. Van Wart, H. E., and Birkedal-Hansen, H. (1990) The cysteine switch: a principle of regulation of metalloproteinase activity with potential applicability to the entire matrix metalloproteinase gene family, *Proc. Natl. Acad. Sci.U. S. A.* 87(14), 5578–5582.

23. Becker, J. W., Marcy, A. I., Rokosz, L. L., Axel, M. G., Burbaum, J. J., Fitzgerald, P. M., Cameron, P. M., Esser, C. K., Hagmann, W. K., Hermes, J. D., and Springer, J. P. (1995) Stromelysin-1: Three-dimensional structure of the inhibited catalytic domain and of the C-truncated proenzyme, *Prot. Sci.* 4, 1966–1976.

24. Gururajan, R., Grenet, J., Lahti, J. M., and Kidd, V. J. (1998) Isolation and characterize two novel metalloproteinase genes linked to Cdc2L on human Chromosome, *Genomics.* 52,101–106.

25. Pei, D., and Weiss, S. J. (1995) Furin-dependent intracellular activation of the human stromelysin-3 zymogen, *Nature.* 375, 244–247.

26. Pei, D., and Weiss, S.J. (1996). Transmembrane-deletion mutants of the membrane-type matrix metalloproteinase-1 process progelatinase A and express intrinsic matrix-degrading activity, *J. Biol. Chem.* 271, 9135–9140.

27. Bode, W., Gomis-Ruth, F. X., and Stocker, W. (1993) Astacins, serralysins, snake venom and matrix metalloproteinases exhibit identical zinc-binding environments (HEXXHXXGXXH and Met-turn) and topologies and should he grouped into a common family, the "metzincins," *FEBS Lett.* 331, 134–140.

28. Allan, J. A., Docherty, A. J. P., Barker, P. J., Huskisson, N. S., Reynolds, J. J., and Murphy, G. (1995) Binding of gelatinases A and B to type-I collagen and other matrix components, *Biochem. J.* 309, 299–306.

29. Steffensen, B., Wallon, U. M., and Overall, C. M. (1995) Extracellular Matrix Binding Properties of Recombinant Fibronectin Type II-like Modules of 72-kDa

51

Gelatinase/Type IV Collagenase: High Affinity Binding to Native Type I Collagen but not Native Type IV Collagen, *J. Biol. Chem.* 270, 11555–11566.

30. Gomis-Ruth, F. X., Gohlke, U., Betz, M., Knauper, V., Murphy, G., Lopez-Otin, C., and Bode, W. (1996) The helping hand of collagenase-3 (MMP-13): 2.7 A crystal structure of its C-terminal haemopexin-like domain, *J. Mol. Biol.* 264, 556–566.

31. Bode, W. (1995) A helping hand for collagenases: the haemopexin-like domain, *Structure.* 3, 527–530.

32. Clark, I. M., and Cawston, T. E. (1989) Fragments of human fibroblast collagenase: purification and characterization, *Biochem. J.* 263, 201–206.

33. Murphy, G., Willenbrock, F., Ward, R. V., Cockett, M. I., Eaton, D., and Docherty, A. J. P. (1992) The C terminal domain of 72 KDa gelatinase A is not required for catalysis, but is essential for membrane activation and modulates interactions with tissue inhibitors of metalloproteinase, *J. Biochem.* 328, 637–641.

34. Strongin, A. Y., Collier, I., Bannikov, G., Marmer, B. L., Grant, G. A., and Goldberg, G. I. (1995) Mechanism of cell surface activation of 72-kDa type IV collagenase. Isolation of the activated form of the membrane metalloprotease, *J. Biol. Chem.* 270 (10), 5331–5338.

35. de Souza, S. J., Pereira, H. M., Jacchieri, S., and Brentani, R. R. (1996) Collagen/collagenase interaction: does the enzyme mimic the conformation of its own substrate? *FASEB J.* 10, 927–930.

36. Massova, I., Kotra L. P., Fridman, R., and Mobashery, S. (1998) Matrix metalloproteinases: structures, evolution and diversification, *FASEB J.* 12, 1075–1095.

37. Rawlings, N. D., and Barrett A. J. (1995) Evolutionary families of metallopeptidases, *Methods Enzymol.* 248, 183–229.

38. Sang, Q. A., and Douglas, D. A. (1996) Computational sequence analysis of matrix metalloproteinases, *J. Prot. Chem.* 15, 137–160.

39. Sato, H., Takino, T., Okada, Y., Cao, J., Shinagawa, A., and Yamamoto, E. (1994) A matrix metalloproteinase expressed on the surface of invasive tumor cells, *Nature.* 370, 61–65.

40. Sato, H., Kinoshita, T., Takino, T., Nakayama, K., and Seiki, M. (1996) Activation of a recombinant membrane type 1-matrix metalloproteinase (MT1-MMP) by furin and its interaction with tissue inhibitor of metalloproteinases (TIMP)-2, *FEBS Lett.* 393, 101–104.

41. Pei, D., and Weiss, S. J. (1996) Transmembrane-deletion mutants of the membrane-type matrix metalloproteinase-1 process progelatinase A and express intrinsic matrix-degrading activity, *J. Biol. Chem.* 271, 9135–9140.

42. Murphy, G., and Knauper, V. (1997) Relating matrix metalloproteinase structure to function: why the 'hemopexin' domain? *Mat. Biol.* 15, 511–518.

43. Fernandez-Catalan, C., Bode, W., Huber, R., Turk, D., Calvete, J. J., and Lichte, A. (1998) Crystal structure of the complex formed by the membrane type 1-

matrix metalloproteinasewith the tissue inhibitor of metalloproteinases-2, the soluble progelatinase A receptor, *EMBO J.* 17, 5238–5248.

44. Douglas, D. A., Shi, Y. E., and Sang, Q. A. (1997) Computational sequence analysis of the tissue inhibitor of metalloproteinase family, *J. Prot. Chem.* 16, 237–255.

45. Gomez, D. E., Alonso, D. F., Yoshiji, H., and Thorgeirsson, U. P. (1997) Tissue inhibitors of metalloproteinases: structure, regulation and biological functions, *Eur. J. Cell. Biol.* 74, 111–122.

46. Cawston, T. (1998) Matrix metalloproteinases and TIMPs: properties and implications for the rheumatic diseases, *Mol. Med. Today.* 4, 130–137.

47. Murphy, G. and Willenbrock, F. (1995) Tissue inhibitors of matrix metalloendopeptidases. *Methods Enzymol.* 248, 496–510.

48. Strongin, A. Y., Marmer, B. L., Grant, G. A., and Goldberg, G. I. (1993) Plasma membrane-dependent activation of the 72-kDa type IV collagenase is prevented by complex formation withTIMP-2, *J. Biol. Chem.* 268, 14033–14039.

49. Kinoshita, T., Sato, H., Takino, T., Itoh, M., Akizawa, T., and Seiki, M. (1996) Processing of a precursor of 72-kilodalton type IV collagenase/gelatinase A by a recombinant membrane-type 1 matrix metalloproteinase, *Cancer Res.* 56, 2535–2538.

50. Huang, W., Meng, Q., Suzuki, K., Nagase, H., and Brew, K. (1997) Mutational study of the amino-terminal domain of human tissue inhibitor of metalloproteinases 1 (TIMP-1) locates an inhibitory region for matrix metalloproteinases, *J. Biol. Chem.* 272: 22086–22091.

51. Murphy, G., Houbrechts, A., Cockett, M. I., Williamson, R. A., O'Shea, M., and Docherty, A. J. P. (1991) The N-terminal domain of human tissue inhibitor of metalloproteinases retains metalloproteinase inhibitory activity, *Biochemistry.* 30, 8097–8102.

52. Egeblad, M., and Werb, Z. (2002) New functions for the matrix metalloproteinases in cancer Progression, *Nat. Rev.* 2, 161-174.

53. Curran, S., and Murray, G.I. (1999) Matrix metalloproteinase in tumour invasion and metastasis, *J. Pathol.* 189, 300-308.

54. Will, H., Atkinson, S. J., Butler, G. S., Smyth, B., and Murphy, G. (1996) The soluble catalytic domain of membrane type 1 matrix metalloproteinase cleaves the propeptide of progelatinase A and initiates autocatalytic activation, *J. Biol. Chem.* 271, 17119–17123.

55. Cossins, J., Dudgeon, T. J., Catlin, G., Gearing, A. J., and Clements, J. M. (1996) Identification of MMP-18, a putative novel human matrix metalloproteinase, *Biochem.Biophys.Res.Commun.* 228, 494–498.

56. Pei, D., Kang, T., and Qi, H. (2000) Cysteine array matrix metalloproteinase (CA-MP)/MMP-23 is a type II transmembrane matrix metalloproteinase regulated by a single cleavage for both secretion and activation, *J. Biol. Chem.* 275, 33988–33997.

57. Ohnishi, J. (2001) Cloning and characterization of a rat ortholog of MMP-23 (matrix metalloproteinase-23), a unique type of membrane-anchored matrix

metalloproteinase and conditioned switching of its expression during the ovarian follicular development, *Mol. Endocrinol.* 15, 747–764.

58. Bode,W., Catalan,C.F., Tschesche,H., Grams,F., Nagase,H., and Maskos,K. (1999) Structural properties of matrix metalloproteinase, *Cell. Mol. Life. Sci.* 55, 639-652.

59. Lovejoy, B., Hassell, A. M., Luther, M. A., Weigl, D., and Jordan, S. R. (1994) Crystal structures of recombinant 19-kDa human fibroblast collagenase complexed to itself, *Biochemistry.* 33, 8207-8217.

60. Springman, E.B., Angleton, E.L., Birkedal-Hansen, H., and Van Wart, H.E. (1990) Multiple modes of activation of latent human fibroblast collagenase: evidence for the role of a Cys73 active-site zinc complex in latency and a "cysteine switch" mechanism for activation, *Proc. Natl. Acad. Sci. U.S.A.* 87, 364-368.

61. Schechter, I. and Berger, A. (1967) On the size of the active site in proteases I Papain, *Biochem. Biophys. Res. Commun.* 27, 157-162.

62. Verma, R.P., and Corwin, H. (2007) Matrix metalloproteinases (MMPs): Chemical-biological functions and (Q) SARs, *Bioorg. Med. Chem.* 15, 2223-2268.

63. Salamonsen, L. A., Zhang, J., Hampton, A., Lathbury, L. (2000) Regulation of matrix metalloproteinases in human endometrium, *Hum. Reprod.* 15, 112–119.

64. Rodgers, W. H., Matrisian, L.M., Giudice, L.C., Dsupin, B., Cannon, P., Svitek, C., Gorstein, F., Osteen, K.G. (1994) Patterns of matrix metalloproteinase expression in cycling endometrium imply differential functions and regulation by steroid hormones, *J. Clin. Invest.* 94, 946–953.

65. Matrisian, L. M. (1994) Matrix metalloproteinase gene expression, *Ann. NY. Acad. Sci.*732: 42–50.

66. Ravanti, L., Kahari, V.M. (2000) Matrix metalloproteinases in wound repair, *Int. J. Mol. Med.* 6, 391–407.

67. Lijnen, H. R. (2002) Matrix metalloproteinases and cellular fibrinolytic activity, *Biochemistry.* 67, 92–98.

68. Wilson, C.L., Ouellette, A.J., Satchell. D.P., Ayabe, T., Lopez-Boado, Y.S., Stratman, J. L., Hultgren, S.J., Matrisian, L.M., and Parks, W.C. (1999) Regulation of intestinal α-defensin activation by the metalloproteinase matrilysin in innate host defense, *Science.* 286, 113–117.

69. Ganz,T. (1999) Immunology: Defensins and host defense, *Science.* 286: 420–421.

70. Pauly, R.R., Passaniti, A., Bilato, C., Monticone, R., Cheng, L., Papadopoulo, N., Gluzband, Y.A., Smith, L., Weinsterin, C., Lakatta, E.G., and Crow, M. (1994) Migration of cultured vascular smooth muscle cells through a basement membrane barrier requires type IV collagenase activity and is inhibited by cellular differentiation, *Circ. Res.* 75, 41–54.

71. Jenkins, G.M., Crow. M.T., Bilato. C., Gluzband. Y., Ryu. W.S., Li, Z., Stetlet-Stevenson, W., Nater, C., Froejlich, J.P., Lakatta. E.G., and Cheng, L. (1998) Increased expression of membrane-type matrix metalloproteinase-2 to the neointima of balloon-injured rat carotid arteries, *Circulation.* 97, 82–89.

54

72. Li, Z., Li, L., Zielke, H.R., Cheng, L., Xiao, R., Crow, M.T., Stetler-Stevenson, W.G., Froehlich, J., and Lakatta, E.G. (1996) Increased expression of 72 kD type IV collagenase (MMP-2) in human aortic atherosclerotic lesions, *Am. J. Pathol.* 148, 121–128.

73. Galis, Z.S., Sukhova, G. K., Lark, M.W., and Libby, P. (1994) Increased expression of matrix metalloproteinases and matrix degrading activity in vulnerable regions of human atherosclerotic plaques, *J. Clin. Invest.* 942, 2493–2503.

74. Li, Z., Froehlich, J., Galis, Z.S., and Lakatta, E.G. (1999) Increased expression of matrix metalloproteinase-2 in the thickened intima of aged rats, *Hypertension.* 33, 116–123.

75. Shapiro, S.D., Griffin, G.L., Gilbert, D.J., Jenkins ,N.A., Copeland, N.G., Welgus, H.G., Senior, R.M., and Ley, T.J. (1992) Molecular cloning, chromosomal localization and bacterial expression of a murine macrophage metallelastage, *J. Biol. Chem.* 267, 4664–4671.

76. Senior, R.M., Griffin, G.L., Fliszar, C.J., Shapiro, S.D., Goldberg, G.I., and Welgus, H.G. (1991) Human 92- and 72-kilodalton type IV collagenase are elastases, *J. Biol. Chem.* 266, 7870–7875.

77. Mignatti, P., and Rifkin, D.B. (1996) Plasminogen activators and matrix metalloproteinases in angiogenesis, *Enz. Prot.* 49, 117–137.

78. Fisher, C., Gilbertson-Beadling, S., Powers, E.A., Petzold, G., Poorman, R., and Mitchell, M.A. (1994) Interstitial collagenase is required for angiogenesis *in vitro*, *Dev. Biol.* 162, 499–510.

79. Ausprunk, D.H., and Folkman, J. (1977) Migration and proliferation of endothelin cells in preformed and newly formed blood vessels during tumor angiogenesis, *Microvasc. Res.* 14, 53–65.

80. Moses, M.A., and Langer, R. (1991) Angiogenesis inhibitors, *Biotechnology.* 9, 630–639.

81. Zucker, S., Conner, C., DiMassmo, B.I., Ende, H., Drews, M., Seiki, M., Bahou, W.F. (1995) Thrombin induces the activation of progelatinase A in vascular endothelial cells, *J. Biol. Chem.* 270, 23730–23738.

82. Stetler-Stevension, W.G., Aznavoorian, S., Liotta, L.A. (1993) Tumor cell interactions with the extracellular matrix during invasion and metastasis, *Annu. Rev. Cell. Biol.* 9, 541–573.

83. Weidner, N., Semple, J.P., Welch, W.R., and Folkman, J. (1991) Tumor angiogenesis and metastasis-correlation in invasive breast carcinoma, *New. Engl. J. Med.* 324, 1–8.

84. Yager, D.R., Zhang. L.Y., Liang. H.X., Diegclmann, R.F., and Cohen. I.K. (1996) Wound fluids from human pressure ulcers contain elevated matrix metalloproteinase levels and activity compared to surgical wound fluids, *J. Invest. Dermatol.* 207, 743–748.

85. Bullen, E.C., Langaker, M.T., Updike, D.L., Benton, R., Ludin, D., Hon, Z., and Howard, E.M. (1995) Tissue inhibitor of metalloproteinases-1 is decreased and

activated gelatinases are increased in chronic wounds, *J .Invest. Dermatol.* 104, 236–240.

86. Haumatani, R.D., Kobayashi, D.K., Senior, R.M., and Shapiro, S.D. (1997) Requirement for macrophage elastage for cigarette smoke induced emphysema, *Science.* 277, 2002–2004.

87. Parks, W.C., and Shapiro, S.D. (2001) Matrix metalloproteinases in lung biology, *Respir. Res.* 2, 110–119.

88. Liu, Z., Zhon, X., Shapiro, S.D., Shipley, J.M., Diaz, L.A., Senior, R.M., and Werb, Z. (2000) The serpin αl-protease inhibitor is a critical substrate for gelatinase B/MMP-9 *in vivo, Cell.* 102, 647–655.

89. Silence, J., Collen, D., and Lijnen, H.R. (2002) Reduced atherosclerotic plaque but enhanced aneurysm formation in mice with inactivation of the tissue inhibitor of metalloproteinase-1 (TIMP-1) gene, *Circ. Res.* 90, 897–903.

90. Davies, M.J., Richardson, P.D., Wolf. N., Katz, D.R., and Mann. J. (1993) Risk of thrombosis in human atherosclerotic plaques: Role of extracellular lipid, macrophage and smooth muscle cell content, *Br. Heart. J.* 69, 377–381.

91. Libby, P. (1995) Molecular basis of the acute coronary syndrome, *Circulation.* 91, 2844–2850.

92. Dollery, C.M., McEwan, J.R., and Henney, A.M. (1995) Matrix metalloproteinase and cardiovascular disease, *Circ. Res.* 77, 863–868.

93. Pyo, R., Lee, J.K., Shipley, J.M., Curci, J.A., Mao, D., Ziporin, S.J, Ennis, T.L., Shapiro, S.D., Senios, R.M., and Thompson, R.W. (2000) Targetted gene disruption of matrix metalloproteinase-9 (gelatinase B) suppresses development of experimental abdominal aortic aneurysms, *J. Clin. Invest.* 105, 1641–1649.

94. Brown, D.L., Hibbs. M.S., Kearney, M., Loushin, C., and Isner, J.M. (1994) Identification of 92 kDa gelatinase in human coronary atherosclerosis lesions: Association of active enzyme synthesis with unstable angina, *Circulation.* 21, 2125–2131.

95. Thompson, R.W., Holmes, D.R., Merters, R.A., Liau, S., Botney, M.D., Mecham, R.P., Welgus, H.G., and Parks, W.C. (1995) Production and localization of 92 kDa gelatinase in abdominal aortic aneurysms: An elastolytic metalloproteinase expressed by aneurysm-infiltrating macrophages. *J. Clin.Invest.* 96, 318–326.

96. Spinale, F.G., Coker, M.L., Thomas, C.V., Walker, J.D., Mukherjee, R., and Hebbar, L. (1998) Time-dependent changes in matrix metalloproteinase activity and expression during the progression of congestive heart failure; relation to ventricular and myocyte function, *Circ. Res.* 82, 482–495.

97. Thomas, C.V., Coker, M.L., Zellner, J.L., Handy, J.R., Crumbley, A.J., and Spinale, F.G. (1998) Increased matrix metalloproteinase activity and selective upregulation in LV myocardium from patients with end-stage dilated cardiomyopathy, *Circulation.* 97, 1708–1715.

98. Spinale, F.G., Krombach, R.S., Coker, M.L., Mukherjee, R., Thomas, C.V., Houck, W.V., Clair, M.J., Kribbs, S.B., Johnson, L.L., and Peterson, J.T. (1999) Matrix metalloproteinase inhibition during developing congestive heart failure in pigs; effects on left ventricular geometry and function, *Circ. Res.* 85, 364–376.

99. Tomita, M., Spinale, F.G., Crawford, F.A., and Zile, M.R. (1991) Changes in left ventricular volume, mass and function during development and regression of supraventricular tachycardia induced cardiomyopathy; disparity between recovery of systolic vs. diastolic function, *Circulation.* 83, 635–644.

100. Lee, R.T., and Libby, P. (2000) Matrix metalloproteinases: not-so-innocent bystanders in heart failure, *J. Clin. Invest.* 106, 827–828.

101. Li, Y.Y., Feng, Y.Q., Kadokmi, T., McTiernan, C.F., Draviam, R., Watkins, S.C., and Feldman, A.M. (2000) Myocardial extracellular matrix remodeling in transgenic mice were expression tumor necrosis factor-alpha can be modulated by anti-tumor necrosis factor alpha therapy, *Proc. Natl. Acad. Sci. USA.* 97, 2746–12751.

102. Hayakawa, T., Yamashita, K., Kodama, S., Iwata, H., and Iwata, K. (1991) tissue inhibitor of metalloproteinases and collagenase activity in synovial fluid of human rheumatoid arthritis, *Biomed. Res.* 12, 169–173.

103. Jackson, C., Nguyen, M., Arkell, J., and Sambrook, P. (2001) Selective matrix metalloproteinase (MMP) inhibitor in rheumatoid arthritis-targetting gelatinase A activation, *Inflamm. Res.* 50, 183–186.

104. Ellerbroek, S and Stack, M.S. (1999) Membrane-associated matrix metalloproteinases in metastasis, *BioEssays.* 21, 940-949.

105. Davies, B., Miles, D.W., Haperfield, L.C., Naylor, M.S., Bobrow, L.G., Rubens,R.D., and Balkwill, F.R. (1993) Activity of type IV collagenases in benign and malignant breast disease, *Br. J. Cancer.* 67, 1126-1131.

106. Stetler-Stevenson, W.G., Hewitt, R., and Corcoran, M. (1996) Matrix metalloproteinases and tumor invasion: from correlation and causality to the clinic, *Sem. Cancer. Biol.* 7, 147-152.

107. Liotta, L.A. (1992) Cancer cell invasion and metastasis, *Sci. American.* 266, 34-41.

108. Nicolson, G.L. (1991) Tumor and host molecules important in the organ preference of metastasis, *Sem. Cancer. Biol.* 2, 143-154.

109. Nelson, A.R., Fingleton, B., Rothenberg, M.L., and Matrisian, L.M. (2000) Matrix metalloproteinases: biologic activity and clinical implications, *J. Clin.Oncol.* 18 (5), 1135 -1149.

110. Olson, M.W., Toth, M., Gervasi, D.C., Sado, Y., Ninomiya, Y., and Fridman, R.(1998) High affinity binding of latent matrix metalloproteinase-9 to the alpha2(IV) chain of collagen IV, *J. Biol. Chem.* 273, 10672-10681.

111. Zucker,S., Cao,J., and Chen,Wen-Tien. (2000) Critical appraisal of the use of matrix metalloproteinase inhibitors in cancer treatment, *Oncogene.* 19, 6642-6650.

112. Lijnen, H.R., Ugwu, F., Bini, A., and Collen, D. (1998) Generation of anangiostatin-like fragment from plasminogen by stromelysin-1 (MMP-3), *Biochemistry.* 37, 4699-4702.

113. O'Reilly, M.S., Wiederschain, D., Stetler-Stevenson, W.G., Folkman, J., and Moses, M.A. (1999) Regulation of angiostatin production by matrix

metalloproteinase-2 in a model of concomitant resistance, *J .Biol. Chem.* 274, 29568-29571.

114. Fowlkes, J.L., Thrailkill, K.M., Serra, D.M., Suzuki, K., and Nagase, H.(1995) Matrix metalloproteinases as insulin-like growth factor binding protein-degrading proteinases, *Prog. Growth. Factor. Res.* 6, 255-263.

115. Goss, K.J., Brown, P.D., and Matrisian, L.M. (1998) Differing effects of endogenous and synthetic inhibitors of metalloproteinases on intestinal tumorigenesis, *Int. J. Cancer.* 78,629-635.

116. Patterson, B.C., and Sang, A.Q. (1997) Angiostatin-converting enzyme activities of human matrilysin (MMP-7) and gelatinase B/type IV collagenase (MMP-9), *J. Biol.Chem.* 272, 28823-28825.

117. Docherty, A.J.P., Lyons, A., Smith, B.J., Wright, E.M., Stephens, P.E., Harris, T.J.R. (1985) Sequence of human tissue inhibitor of metalloproteinases and its identity to erythroid-potentiating activity, *Nature.* 318, 66–69.

118. Stetler-Stevenson, W.G., Krutzsch, H.C., and Liotta. L. (1989b) Tissue inhibitor of metalloproteinase (TIMP-2): A new member of the metalloproteinase inhibitor family, *J. Biol. Chem.* 264, 17374–17378.

119. Leco, K.J., Khokha, R., Pavloff, N., Hawkes, S.P., and Edwards, D.R. (1994) Tissue inhibitor of metalloproteinases-3 (TIMP-3) as an extracellular matrix-associated protein with ad distinctive pattern of expression in mouse cells and tissues, *J. Biol.Chem.* 269, 9352–9360.

120. Gijbels, K., Masure, S., Carton, H., Opdenakker, G. (1992) Gelatinaseinthecerebrospinal fluid of patients with multiple sclerosis and other inflammatoryneurological disorders, *J. Neuroimmunol.* 41, 29–34.

121. Liotta, L.A., and Stetler-Stevenson, W.G. (1990) Metalloproteinases and cancer invasion, *Sem. Cancer. Biol.* 1, 99–106.

122. Van der Stappen, J.W.J., Hendriks, T., and Wobbest, T. (1990) Correlation between collagenolytic activity and grade of histological differentiation in colorectal tumors, *Int. J. Cancer.* 45, 1071–1078.

123. Hewitt, R.E., Leach, I.H., Powe, D.G., Clark, I.M., Cawston, T.E., and Turner, D.R. (1991) Distribution of colagenase and tissue inhibitor metalloproteinases (TIMP) in colorectal tumors, *Int. J. Cancer.* 49, 666–672.

124. Muller, D., Breathnach, R., Engelmann, A., Millon, R., Bronner, G., Flench,H., Dumont, P., Eber, M., and Abecassis, J. (1991) Expression of colagenase-related metalloproteinase genes in human lung or head and neck tumors, *Int. J. Cancer.* 48, 550–556.

125. McDonnel, S., Navre, M., Coffey, R.J., and Matrisian, L.M. (1991) Expression and localization of the matrix metalloproteinase pump-1 (MMP-7) in human gastric cancer and colon carcinomas, *Mol. Carcinogen.* 4, 527–533.

126. Siadat, P. M., Nagle, B.B., Breathnach, R., Finch, J.S., Brawer, M. K., and Bowden, G.T. (1991) Expression of metalloproteinase genes in human prostate cancer, *J.Cancer. Res. Clin. Oncol.* 117, 144–150.

127. Basset, P., Bellocqm J.P., Wolf, C., Stoll, I., Hutin, P., Limacher, J.M.,Poldhajcer, O.L., Chenard, M.P., Rio, M.C., and Chambon, P. (1990) A novel

metalloproteinase gene specifically expressed in stromal cells of breast carcinomas, *Nature.* 348, 699–704.

128. Yoshimoto, M., Itoh, F., Yamamoto, H., Himoda, Y., Imai, K., and Yachi, A. (1993) Expression of MMP-7 (Pump-1) mRNA in human colorectal cancers, *Int. J.Cancer.* 54, 614–618.

129. Brown, P.D., Bloxidge, R.E., Anderson, E., and Howell, A. (1993a) Expression of activated gelatinase in human invasive breast carcinoma, *Clin.Exp. Metastasis.* 11, 183–190.

130. Davies, B., Miles, D.W., Happerfeild, L.C.,Naylor, M.S., Bobrow,L.G., Rubens, R.D., and Balkwill, F.R. (1993a) Activity of type IV collagenases In benign and malignant breast disease, *Br. J.Cancer.* 67, 1126–1131.

131. D'Errico, A., Garbina, S., Liotta, L.A., Cantronovo, V., Stetler-Stevenson, W.G., and Grogioni, W.F. (1991) Augmentation of type IV collagenase, laminin receptor, and KI67 proliferation antigen associated with human colon, gastric and breast carcinoma progression, *Mol. Pathol.* 4, 239–246.

132. Daidone, M.G., Silvestrini, R., D'Errico, A., Di Fronzo, G., Benini, E., Mancini, A.M., Garbina, S., Liotta, L., and Grigioni, W.F. (1991) Laminin receptors, collagenase IV and prognosis in node-negative breast cancers, *Int. J. Cancer.* 48, 529–532.

133. Campo, E., Merino, M.J., Tavassoli, F.A., Charonis, A.S., Stetler-Stevenson, W.G., and Liotta, L.A. (1992) Evaluation of basement membrane components and the 72 kDa type IV collagenase in serous tumors of the ovary, *Am .J. Surg. Path.* 16, 500–507.

134. Garbisa, S., Scagliotti, G., Masiero, L., Di Francesco, C., Caenazzo, C., Onisto, M., Micela, M., Steler-Stevenson, W.G., and Liotta, L.A. (1992) Correlation of serum metalloproteinase levels with lung cancer metastasis and response to therapy, *Cancer. Res.* 52: 548–549.

135. Brown, P.D., Bloxidge, R.E., Stuart, N.S.A., Gatter, K.C., and Carmichael,J. (1993b) Correlation between expression of activated 72 kDa gelatinase and tumour spread in non-small cell lung carcinoma, *J. Natl. Cancer. Inst.* 85, 574–578.

136. Poulson, R., Pignatelli, M., Stetler-Stevenson, W.G., Liotta, L.A., Wright, P.A., Jeffery, R.E., Longcroft, J.M., Rogers, L., and Stamp, G.W. (1992) Stromal expression of 72 kDa type IV collagenase (MMP-2) and TIMP-2 mRNAs in colorectal neoplasia, *Am. J. Pathol.* 141, 389–396.

137. Pyke, C., Ralfklaer, E., Huhtala, P., Hurskainen, T., Dano, K., and Tryggvason, K. (1992) Localization of messenger RNA for Mr 72,000 and 92,000 type IV collagenases in skin cancers by *in situ* hybridization, *Cancer. Res.* 52, 1336–1341.

138. Miller, L.B. (1993) Structure and function of the urokinase receptor, *Blood. coagul.Fibrinolysis.* 4, 292–303.

139. Strongin, A., Collier, I., Bannikov, G., Marmer, B.L., Grant, G.A., and Goldberg, G.I. (1995) Mechanism of cell surface activation of 72 kDa type IV collagenase, *J. Biol.Chem.* 270, 5331–5338.

140. Nomura, H., Sato, H., Seiki, M., Mai, M., and Okada, Y. (1995) Expression of the membrane-type matrix metalloproteinase in human gastric carcinomas, *Cancer. Res.* 55, 3263–3266.

141. Rosenberg, G.A. (2002) Matrix metalloproteinases in neuroinflammation, *Glia.* 39, 279–291.

142. Ilzecka, J., Stelmasiak, Z., and Dobosz, B. (2001) Matrix metalloproteinase-9 (MMP-9) activity in cerebrospinal fluid of amyotrophic lateral sclerosis patients, *Neurol.Neurochir. Pol.* 35, 1035–1043.

143. Beuche, W., Yushchenko, M., Mader, M., Maliszewska, M., Felgenhauer, K., and Weber, F. (2000) Matrix metalloproteinase-9 is elevated in serum of patients with amyotrophic lateral sclerosis, *Neuroreport.* 11, 3419–3422.

144. Trapp, B., Peterson, J., Ranasohalf, R., Rudick, R., Mork, S., and Bo, L. (1998) Axonal transection in the lesions of multiple sclerosis, *N. Engl. J. Med.* 338, 278–285.

145. Clements, J., Cossins, J., Wells, G., Corkill, D., Hellrich, K., Wood, L., Piggot, R., Stablar, G., Ward, G., Gearing, A., and Miller, K. (1997) Matrix metalloproteinase and tumor necrosis factor-α inhibitor, *J. Neuroimmunol.* 74, 85–94.

146. Johnson, L.L., Dyer, R., and Hupe, D.J. (1998) Matrix metalloproteinases, *Curr .Opin. Chem. Biol.*2, 466–471.

147. Lorenzl, S., Albers, D.S., Narr, S., Chirichigno, J., and Beal, M.F. (2002) Expression of MMP-2, MMP-9, and MMP-1 and their endogenous counter regulators TIMP-1 and TIMP-2 in postmortem brain tissue of Parkinson's disease, *Exp. Neurol.* 178, 13–20.

148. Asahina, M., Yoshiyama, Y., and Hattori, T. (2001) Expression of matrix metalloproteinase-9 and urinary-type plasminogen activator in Alzheimer's disease brain, *Clin. Neuropathol.* 20, 60–63.

149. Sekine-Aizawa, Y., Hama, E., Watanabe, K., Tsubuki, S., Kanai-Azuma, M.,Kanai, Y., Arai. H., Aizawa, H., Iwata, N., and Saido, T.C. (2001) Matrix metalloproteinase (MMP) system in brain: Identification and characterization of brain-specific MMP highly expressed in cerebellum, *Eur. J. Neurosci.* 13, 935–948.

150. Leake, A., Morris, C.M., and Whateley, J. (2000) Brain matrix metalloproteinase 1 levels are elevated in Alzheimer's disease, *Neurosci. Lett.* 291, 201–203.

151. Yoshiyama, Y., Asahina, M., and Hattori, T. (2000) Selective distribution of matrix metalloproteinase-3 (MMP-3) in Alzheimer's disease brain, *Acta. Neuropathol. (Berl).* 99, 91–95.

152. Fini, M. E., Cook, J. R., Mohan, R., and Brinckerhoff, C. E. (1998) in *Matrix Metalloproteinases* (Parks, W. C. & Mecham, R. P. Ed), pp: 299–356, *Academic Press, New York.*

153. Westermarck, J., and Kähäri, V. M. (1999) Regulation of matrix metalloproteinase expression in tumor invasion, *FASEB J.* 13, 781–792.

154. Kheradmand, F., Werner, E., Tremble, P., Symons, M., and Werb, Z. (1998) Role of Rac1 and oxygen radicals in collagenase-1 expression induced by cell shape change, *Science.* 280, 898–902.

155. Overall, C. M., Wrana, J. L., and Sodek, J. (1989) Independent regulation of collagenase, 72-kDa progelatinase, and metalloendoproteinase inhibitor expression in human fibroblasts by transforming growth factor-β, *J. Biol.Chem.* 264, 1860–1869.

156. Uría, J. A., Jiménez, M. G., Balbín, M., Freije, J. M. P., and López-Otín, C. (1998) Differential effects of transforming growth factor-β on the expression of collagenase-1 and collagenase-3 in human fibroblasts, *J.Biol.Chem.* 273, 9769–9777.

157. Overall, C. M. (1995) Repression of tissue inhibitor of matrix metalloproteinase expression by all-*trans*-retinoic acid in rat bone cell populations: comparisons with transforming growth factor-β1, *J. Cell. Physiol.*164, 17–25.

158. Jiménez, M. J. (2001)A regulatory cascade involving retinoic acid, Cbfa1, and matrix metalloproteinases is coupled to the development of a process of osteogenic differentiation during bone formation, *J.Cell.Biol.* 155, 1333–1344.

159. Overall, C.M., and Otin, C.L. (2002) Strategies for MMP inhibition in cancer: Innovations for the post-trial era, *Nat. Rev.* 657-672.

160. Springman, E. B., Angleton, E. L., Birkedal-Hansen, H., and Van Wart, H. E. (1990) Multiple modes of activation of latent human fibroblast collagenase: evidence for the role of a Cys73 active-site zinc complex in latency and a 'cysteine switch' mechanism for activation, *Proc. Natl. Acad. Sci. USA.* 87, 364–368.

161. Morgunova, E. (1999) Structure of human pro-matrix metalloproteinase-2: activation mechanism revealed, *Science.* 284, 1667–1670.

162. Becker, J. W. (1995) Stromelysin-1: three-dimensional structure of the inhibited catalytic domain and of the C-truncated proenzyme, *Prot. Sci.* 4, 1966–1976.

163. Bannikov, G. A., Karelina, T. V., Collier, I. E., Marmer, B. L., and Goldberg, G. I. (2002) Substrate binding of gelatinase B induces its enzymatic activity in the presence of intact propeptide, *J. Biol. Chem.* 277, 16022–16027.

164. Overall, C. M. (2000) Domain interactions in the gelatinase A:TIMP-2:MT1-MMP activation complex: the ectodomain of the 44-kDa form of membrane type-1 matrix metalloproteinase does not modulate gelatinase A activation, *J.Biol. Chem.* 275, 39497–39505.

165. Brew, K., Dinakarpandian, D., and Nagase, H. (2000) Tissue inhibitors of metalloproteinases: evolution, structure and function, *Biochim. Biophys. Acta.* 1477, 267–283.

166. Khokha, R. (1989) Antisense RNA-induced reduction in murine TIMP levels confers oncogenicity on Swiss 3T3 cells, *Science.* 243, 947–950.

167. Jiang, Y., Goldberg, I. D., and Shi, Y. E. (2002) Complex roles of tissue inhibitors of metalloproteinases in cancer, *Oncogene.* 21, 2245–2252.

168. Oh, J. (2001) The membrane-anchored MMP inhibitor RECK is a key regulator of extracellular matrix integrity and angiogenesis, *Cell.* 107, 789–800.

169. Herman, M. P. (2001) Tissue factor pathway inhibitor-2 is a novel inhibitor of matrix metalloproteinases with implications for atherosclerosis, *J. Clin. Invest.* 107, 1117–1126.
170. Mott, J. D. (2000) Post-translational proteolytic processing of procollagen C-terminal proteinase enhancer releases a metalloproteinase inhibitor, *J. Biol. Chem.* 275, 1384–1390.
171. Stetefeld, J. (2001) The laminin-binding domain of agrin is structurally related to N-TIMP-1, *Nat. Struct. Biol.* 8, 705–709.

CHAPTER 2. STATEMENT OF PROBLEM

2.1. Questions Addressed in this Dissertation

The focus of this disquisition is the structural-functional behavior of the three different hMMP isozymes upon binding to various types of ligands. The three hMMP isozymes, hMMP-7, 9 and 10, chosen for these studies are one of the most important and disease intriguing members of the MMP family. These three hMMP isozymes were cloned, expressed and purified; and used for different biophysical and kinetic studies. The three important questions which invoked this study were: (A) MMP-7 is predominantly secreted, but it also cleaves a variety of non-ECM substrates such as E-cadherin, TNF-α, Fas ligand, insulin-like growth factors, and raises the question : Why would MMP-7 be recruited to the cell surface to hydrolyze its cognate non-ECM substrates? (B) Despite its well recognized patho-physiological roles, MMP-7 has not been rigorously investigated from the point-of-view of its structural-functional and mechanistic features, and (C) The bipolar distribution of the positive and negative charges in the vicinity of the active-site pocket and on the opposite end of the protein structure is an interesting characteristic of MMP-7 and 10. This study is important from the point-of-view of regulation of MMP isozymes by electrostatic interactions with its cognate partners in an aqueous solvent.

In addition, the choice of these three human MMP isozymes (MMP-7, 9 and 10) were based on the fact that MMP-7 (belongs to the subfamily of matrilysin), MMP-9 (belongs to subfamily of gelatinases), and MMP-10 (belongs to the subfamily of stromelysins) causes varied range of diseases which include multiple scelrosis, chronic ulcers, lung diseases, cardiovascular diseases, alzheimer's, rheumatoid arthriritis, and

various forms of cancer, such as stomach, pancreas, esophageal, ovarian, lungs, and uterine to mention a few. Also, the future application of this work would be that gold-nanoparticles (Au-NPs), liposomes (LNPs), and quantum dots (QDs) are the different biocompatible nanoparticles (NPs) which bear excellent potential to mimic the "antibodies", are delivered to the target site, in case of metastasis. These NPs can interact with the cognate proteins; in this case, the three hMMP isozymes were used to develop a highly specific diagnostic and desensitized protocol for the MMP family of biomedical relevance. This research establishes the mechanism by which the hMMP isozymes bind and interact with Au-NPs, LNPs, QDs and small molecule inhibitors (SMIs). This leads to the structural-functional consequences the hMMP isozymes upon binding to the different ligands. The successful completion of this research provide future insights into developing nano-particle based, highly specific and facile diagnostics as well as desensitizing tools for MMPs and other biomarker proteins. In an attempt to answer the unresolved questions the following objectives were undertaken:

[1]. To demonstrate the relationship between "rigid" and "flexible" surfaces on the differential modulation of functional and structural characteristics of human Matrilysin (hMMP-7).

[2]. To study the molecular origin of the intrinsic selectivity in binding of hMMP isozymes to differently charged lipid membranes.

[3]. To elucidate the alternative binding modes of hMMP isozymes to cationic and anionic QDs.

[4]. High throughput screening of the SMIs with the hMMP isozymes.

CHAPTER 3. MATERIALS AND METHODS

3.1. Materials

3.1.1. Chemical reagents used for the study

Plasmid pOTb7 containing the full length cDNA clones of human Matrix Metalloproteinase-7 (ATCC #: MGC- 3913), human Matrix Metalloproteinase-9 (ATCC #: MGC- 12688) and human Matrix Metalloproteinase-10 (ATCC #: MGC-1704) were purchased. *Nde I* and *Xho I* Restriction Endonuclease and T_4 DNA Ligase were obtained from New England Biolabs (Ipswich, MA). Miniprep, maxiprep and Qiaquick® purification kits were purchased from Qiagen (Valencia, CA). Primers were designed and the sequences were checked for hair-pin loop formation and secondary structure formations before having them synthesized at Integrated DNA Technologies (IDT, San Diego, California). Agarose (Molecular Biology grade) was purchased from Bio-Rad (Hercules, CA). $ZnCl_2$, $CaCl_2$, Tris, HEPES, phosphate, ampicillin, chloramphenicol and IPTG were purchased from Life Science Resources (Milwaukee, WI). Yeast extract, tryptone, PMSF, and DMSO were purchased from Becton Dickinson (Sparks, MD). Standard Dialysis bags of MCWO of 8000 Da and MCWO 14,000 Da came from Spectrum® Bio Labs (Texas, USA). Urea, NaCl, bovine serum albumin (BSA) were purchased from Thermo Fisher Scientific Inc. (Rockford, IL), Molecular weight standards for SDS-PAGE and Chelex® 100 were purchased from Bio-Rad (Hercules, CA). BCA Protein Assay Kit was purchased from Thermo Fisher Scientific Inc. BL21-CodonPlus® DE3 (RIL), Recombinant *Pfu* DNA polymerase and DH5α *E. coli* competent cells were purchased from Stratagene (La Jolla, CA). The Commercial MMP substrates: Mca-Pro-Leu-Gly-Leu-Dpa-Ala-Arg-NH_2 and

Ac-Pro-Leu-Gly-SCH [CH$_2$CH(CH$_3$)$_2$]-CO-Leu-Gly-OC$_2$H$_5$ were purchased from known

Calbiochem (Gibbstown, NJ). MCA standard as control was purchased from Calbiochem.

The differently charged cationic and anionic AuNPs were provided by Dr Rotello,

(Department of Chemistry at University of Massachusetts at Amherst). Polylysine (PLL), vydac

C$_{18}$ reverse phase column, acetonitrile, 0.1% TFA were purchased from Sigma ® (Saint

Louis, MO). Lipids were purchased from Avanti ® Polar Lipids, (Alabaster, AL). Cationic

and anionic quantum dots were provided by Dr. Chen (Department of Physics at University

of Texas at Arlington). Inhibitors that were screened for MMPs were synthesized by Dr.

Manas Haldar, Rajesh Subramaniam and Mike Scott and were supplied from Dr. Sanku

Mallik (Department of Pharmaceutical Sciences at NDSU). Inhibitors screened were

synthesized and supplied by Dr. Cook's Laboratory (Department of Chemistry and

Biochemistry at NDSU). All other chemicals were of reagent grade, and were used without

further purification.

3.2. Methods

3.2.1. Cloning, expression and purification of recombinant hMMP-7

Human MMP-7, hMMP-9 and hMMP-10 were cloned in Dr. Srivastava's

laboratory at North Dakota State University by Donald Klocke. The cloning of human

hMMP isozymes (hMMP-7, 9 and 10) was carried out using the following method:

3.2.1.1. Cloning of hMMP-7

The cDNA of human matrilysin (hMMP-7) cloned into mammalian expression

vector pOTB7 was obtained from ATCC (MGC- 3913). The nucleotide fragment encoding

the catalytic domain of hMMP-7 corresponding to residues Tyr 94-Lys 267 was amplified

by the thermocycler using DNA as a template and purified using the QIAquick® gel extraction kit. The following oligonucleotides: the sense primer contained the *Nde I* at the 5' end (5'- GGAATTCCATATGTACTCACTATTTCCAAATAGCC -3') and the antisense primer which contained the *Bam HI* at the 3' end (5'- CGCGGATCCTCACTATTTCTTTCTTGAATTACTTCT -3') in order to introduce the translational initiating methionine (Met). The 3' end provides the stop codon and the *Bam HI* site respectively to facilitate the cloning in pET 20b (+) expression vector. The PCR reaction mixture contained the template DNA (~ 50 ng), primers (4 µl of 25 µM), dNTPs (1 µl of 10 mM), MgCl$_2$ (10 µl of 25 mM), and Pfu DNA polymerase (5 units) in a total volume of 100 µl. The PCR reaction conditions were set as follows: 30 seconds at 94°C for denaturation, 1 minute and 30 seconds at 55°C for annealing, 15 minutes at 72°C for extension, for a total number of 25 reaction cycles. The PCR reaction product and the expression vector pET 20b (+) were digested with *Nde I* and *Bam HI* and purified from an agarose gel using the QIAquick gel extraction kit. The purified products were ligated with T$_4$ DNA ligase (forming the hMMP-7 pET plasmid) and transformed into DH5α cells for plasmid propagation [1]. The cloning of the coding regions of hMMP-7 in the pET 20b (+) vector was confirmed by sequencing the plasmid at the University of Chicago, Cancer Research Center. The plasmid was transformed into *E.coli* BL21 (DE3) for protein expression.

3.2.1.2. Expression and induction of hMMP-7

The pET expression system was grown in Luria Broth (Trypton-10g, yeast extract-5g, NaCl-10g in 1L), supplemented with 100 µg of ampicillin/ml, 50 µg/ml of

chloramphenicol at 37°C until A_{600} was 0.6. The expression of hMMP-7 was induced by addition of 400 μM IPTG. The cells were incubated further at 37°C for 5 hours. The cell suspension was centrifuged at 8000 r.p.m using a Sorvall SLA 1500 fixed angle rotor for 20 minutes.

3.2.1.3. Sonication and urea washes to the inclusion bodies of hMMP-7

The pellet was washed in 50 mM Tris buffer, pH 7.5, and 1mM PMSF in 2-propanol was added prior to sonication. The cells were sonicated for a total time of 10 minutes in a Branson bath sonifier utilizing 40% duty cycle in an ice cold bath. The sonicated extract was centrifuged at 15,000 rpm using a Sorvall SS34 fixed angle rotor for 30 minutes, and the pellet was collected. The pellet containing inclusion bodies was washed with buffer containing 50 mM Tris, pH 7.5, and then the resuspended solution was centrifuged at 8000 r.p.m using a Sorvall SLA 1500 fixed angle rotor for 15 minutes. The pellet obtained from this step was subjected to 2 M urea buffer wash containing 50 mM Tris, 10 mM $CaCl_2$, 10 μM $ZnCl_2$ and 150 mM NaCl, pH 7.5. Again, the resuspended solution was centrifuged at 8000 r.p.m using a Sorvall SLA 1500 fixed angle rotor for 15 minutes. The pellet was then dissolved in 6 M urea buffer containing 50 mM Tris, 10 mM $CaCl_2$, 10 μM $ZnCl_2$ and 150 mM NaCl, pH 7.5   by stirring overnight at 4°C. The 6 M urea extract was centrifuged at 15,000 r.p.m using a Sorvall SS34 fixed angle rotor for 30 minutes and its supernatant extract was collected for further purification.

3.2.1.4. Refolding using serial dilution of the 6 M urea extract of hMMP-7

This step consisted of refolding the hMMP-7 contained in the 6 M urea supernatant fraction in 50 mM Tris, 10 mM $CaCl_2$, 10 μM $ZnCl_2$, 6 M urea and 150 mM NaCl, pH 7.5

by sequential dialysis. The concentration of the 6 M supernatant fraction was determined by BCA assay. The 6 M supernatant was diluted to 0.1 mg/ml concentration of the protein, by using 50 mM Tris, 10 mM $CaCl_2$, 10 μM $ZnCl_2$ and 150 mM NaCl, pH 7.5 and this diluted supernatant was packed in a membrane dialysis bag with MCWO of 5,000 Da. This sample was dialyzed for 24 hours by changing 3 times (for 8 hours at 4°C) into the refolding buffer (50 mM Tris, 10 mM $CaCl_2$, 10 μM $ZnCl_2$ and 150 mM NaCl, pH 7.5). The refolding buffer was placed in a 1000 ml cylinder and the dialysis bag was placed inside the cylinder for equilibrium to be established.

3.2.2. Cloning, expression and purification of recombinant hMMP-9

3.2.2.1. Cloning of hMMP-9

The cloning of hMMP-9 has been performed the same way as hMMP-7. The cDNA of human Gelatinase B (hMMP-9) cloned into mammalian expression vector pOTB7 was obtained from ATCC (MGC-12688). The nucleotide fragment encoding the catalytic domain of hMMP-9 corresponding to residues Phe-106 – Leu-442 was amplified by PCR using DNA as a template and purified using the QIAquick® gel extraction kit. The following oligonucleotides: The sense primer contained the *Nde I* restriction site at the 5' end (5' –GGAATTCCATATGTTCCAAACCTTTGAGGGCGAC-3') and the anti-sense primers which contained the restriction enzyme Xho *I* at the 3' end of the primer (5'-CCGCTCGAGTTAATAGAGGTGCCGGATGC-3') respectively. These primers contained the *Nde I* restriction enzyme sequence in the sense primer and *Xho I* restriction enzyme sequence in the antisense primer. There are additional sequences added in both sense and anti-sense primers for the easy recognition by their respective enzymes.

The PCR reaction mixture contained the template DNA (~ 50 ng), primers (4 µl of 25 µM), dNTPs (1 µl of 10 mM), MgCl$_2$ (10 µl of 25 mM), and pfu DNA polymerase (5 units) in a total volume of 100 µl. The PCR reaction conditions were set as follows: 30 seconds at 94°C denaturation, 1 minute and 30 seconds at 55°C for annealing, 15 minutes at 72°C for extension, for a total number of 25 reaction cycles. The PCR reaction product and the expression vector pET 20b (+) were digested with *Nde I* and *Xho I* and purified from an agarose gel using the QIAquick gel extraction kit. The purified products were ligated with T$_4$ DNA ligase (forming the hMMP-9-pET plasmid) and transformed into DH5α cells for plasmid propagation. The cloning of the coding regions of hMMP-9 in the pET 20b (+) vector was confirmed by sequencing the plasmid at the University of Chicago Cancer Research Center. The plasmid was transformed into *E.coli* BL21 (DE3) for protein expression.

3.2.2.2. Expression and induction of hMMP-9

The protocol for expression and induction of hMMP-9 was similar to hMMP-7.

3.2.2.3. Sonication and urea washes to the inclusion bodies of hMMP-9

The protocol for sonication and urea washes to the inclusion bodies of hMMP-9 was similar to hMMP-7.

3.2.2.4. Refolding using snap dilution of the 6 M urea extract of hMMP-9

The 6 M urea supernatant extract was snap diluted by ten fold in 50 mM Tris, 10 mM CaCl$_2$ and 10 µM ZnCl$_2$, pH 7.5. The 6 M urea extract was diluted into the buffer drop-wise with slow stirring at 4°C. The non-homogenous solution was stirred for 30 minutes and eventually put off the stirrer (kept undisturbed) for 12 to 14 hours at 4°C.

3.2.3. Cloning, expression and purification of recombinant hMMP-10

3.2.3.1. Cloning of hMMP-10

The cloning of hMMP-10 was similar to the purification procedure followed in case of hMMP-7 and 9. The cDNA of human stromelysin 2 (hMMP-10) cloned into mammalian expression vector pOTB7 was obtained from ATCC (MGC- 1704). The nucleotide fragment encoding the catalytic domain of hMMP-10 corresponding to residues Phe-99 – Lys-277 was amplified by PCR using DNA as a template and purified using the QIAquick® gel extraction kit. The following oligonucleotides: The sense primer contained *Nde I* at the 5' end (5' – GGAATTCCATATGTTCAGCTCCTTTCCTGGCATGCC-3' and and anti-sense primers 5'-CCGCTCGAGTCACTATTTTGTGGGCACCAGGGGT - 3'. These primers contained the *Nde I* restriction enzyme sequence in the sense primer and *Xho I* restriction enzyme sequence in the antisense primer. There are additional sequences added in both sense and anti-sense primers for the easy recognition by their respective enzymes (*Nde I* and *Xho I*).

The PCR reaction mixture contained the template DNA (~ 50 ng), primers (4 µl of 25 µM), dNTPs (1 µl of 10 mM), MgCl$_2$ (10 µl of 25 mM), and pfu DNA polymerase (5 units) in a total volume of 100 µl. The PCR reaction conditions were set as follows: 30 seconds at 94°C denaturation, 1 minute and 30 seconds at 55°C for annealing, 15 minutes at 72°C for extension, for a total number of 25 reaction cycles. The PCR reaction product and the expression vector pET 20b (+) were digested with *Nde I* and *XhoI* and purified from an agarose gel using the QIAquick gel extraction kit. The purified products were ligated with T$_4$ DNA ligase (forming the hMMP-9-pET plasmid) and transformed into

DH5α cells for plasmid propagation. The cloning of the coding regions of hMMP-9 in the pET 20b (+) vector was confirmed by sequencing the plasmid at the University of Chicago Cancer Research Center. The plasmid was transformed into *E.coli* BL21 (DE3) for protein expression.

3.2.3.2. Expression and induction of hMMP-10

The protocol for expression and induction of hMMP-10 was similar to hMMP-7.

3.2.3.3. Sonication and urea washes to the inclusion bodies of hMMP-10

The protocol for sonication and urea washes to the inclusion bodies of hMMP-10 was similar to hMMP-7.

3.2.3.4. Refolding using serial dilution of the 6 M urea extract of hMMP-10

The 6 M urea supernatant was treated exactly the same way as hMMP-7. The 6 M urea extract using serial dilution was refolded.

3.2.4. Checking the purity of the expressed protein by SDS polyacrylamide gel electrophoresis showing different fractions obtained during purification process

The refolded protein along with all the fractions obtained during the purification process was aliquoted and samples were separated by SDS-PAGE. This step is used for the estimation of the yield of the protein collected at each step. The protein samples taken as aliquots were analyzed by SDS-PAGE electrophoresis, using 12% resolving and 4% stacking gels [1]. The 12% resolving gel comprised of 12% acrylamide prepared in 1.5 M Tris, pH 8.8, 0.1% SDS and the stacking gel of 4% prepared in 0.5 M Tris, pH 6.8, 0.1% SDS. Samples were dissolved in loading dye (comprised of 10% SDS, 25% glycerol, 5 mM β-mercaptoethanol, 0.015% bromophenol blue, and 300 mM Tris, pH 6.8) and denatured by boiling for 5 minutes in a water bath.

The gels were electrophoresed at 200 V using a buffer (0.1% SDS, 25 mM tris, 190 mM glycine, pH 8.3), stained with a mixture of 0.1% coomassie blue in 10% acetic acid and 10% methanol for 20 minutes and destained by mixture of 10% acetic acid and 40% methanol for 20 minutes. The purity of the expressed enzymes (specific activity) was estimated by comparising to the number and the degree of the intensity of the individual protein bands in the standard protein ladder (Protein™ ladder, EMD; Madison, WI).

3.2.5. Steady state experiments for the determination of kinetic parameters (K_m, V_{max}, K_{cat} and K_{cat}/K_m) for hMMP isozymes

Life depends on the well orchestrated series of different chemical reactions. Many of these life sustaining reactions proceed too slowly on their own. In order to accelerate these slow reactions; nature evolved catalysts also known as "enzymes". As time progressed, the enzymes discovered were obtained in pure or partially pure forms; hence scientists became anxious in attaining a better understanding of the details of the mechanistic properties of these enzymes during the catalysis of a reaction. The concept of enzyme forming a complex with their cognate substrate was first demonstrated by Emil Fisher during the nineteenth century, about the "Lock and Key Model" [2] for the stereo-chemical relationship between the enzyme and its cognate substrate.

3.2.5.1. Assays and steady-state characterizations of the enzyme catalyzed reaction

Kinetics is the study of the rates at which chemical reactions occur. A major importance of this study is that it gives a detailed understanding of the various steps in the reaction process and the sequence in which they occur. The advantages of studying the kinetics of an enzyme catalyzed reaction are as mentioned: (a) Using the kinetic studies, the binding affinities of ligands and the other cognate inhibitors to the enzyme can be

determined. This information would give us an idea about the maximum catalytic rate of the enzyme; (b) The rate of the reaction varies with different parameters like temperature, pH etc, etc; hence, upon combined study of the chemical rate and structural studies done on the enzyme, the catalytic mechanism of the enzyme can be established; (c) The understanding of the enzyme's rate, which may play an important role in the metabolic pathways, would help us understand the role of the enzyme in the physiological conditions.

3.2.5.1.1. Spectrophotometric assay for MMP isozymes catalyzed reaction

The spectrophotometric assay for MMPs were performed using a substrate known as thiopeptolide TPL [Ac-Pro-Leu-Gly-(2-mercapto-4-methylpentanoyl)-Leu-Gly-OE], originally developed for vertebrate collagenase [3]. The experimental conditions maintained are similar for all the hMMP isozymes. The enzyme activity of hMMP-7, 9 and 10 were measured in 25 mM HEPES, 10 mM $CaCl_2$, pH 7.5. The hMMP isozymes (7, 9 and 10) have a preferred mechanism to cleave the Thiolpeptide (TPL) and release free thiol groups [4]. The released thiol groups react with the 5, 5'-dithiobis-(2-nitrobenzoic acid) (DTNB) to produce a mixed disulfide and 2-nitro-5-mercaptobenzoic acid (TNB), the newly released reactive groups ionize TNB anion in water at neutral and alkaline pH (Scheme 3.1). The yellow color generated by TNB anion is monitored spectrophotometrically by monitoring the absorbance at 412 nm ($\varepsilon = 13,600$ M^{-1} cm^{-1}).

In a typical experiment, the initial slope of the progress curve is measured via a Molecular Devices SpectraMax® Plus microplate reader in a polystyrene microplate or a 1-cm path length quartz cuvette. The buffer used in the assay is 25 mM HEPES, 10 mM $CaCl_2$, and pH 7.5 at 25°C. Reaction volumes were restricted to 200 µl for reliability and

sensitivity of the instrument. According to the typical experimental setup, the reaction mixture contained 1 mM DTNB and 20 μM TPL of the substrate. The enzyme concentration varied depending on the hMMP isozyme used. The concentrations of the hMMP used were 0.3 μM, 0.16 μM, and 2 μM for hMMP-7, 9 and 10, respectively.

The monitoring time of the reaction was 300 seconds and the calculation of the product formation as a function of time was based on an extinction coefficient of 13.6 mM^{-1} cm^{-1} (at 412 nm) for 2-nitro-5-mercaptobenzoic acid (TNB) anion generated. The data collected were converted in terms of the "units" of activity. The unit of the hMMP activity is defined as the "amount of enzyme required to convert one micromole of the substrate to product per min under the standard experimental conditions"
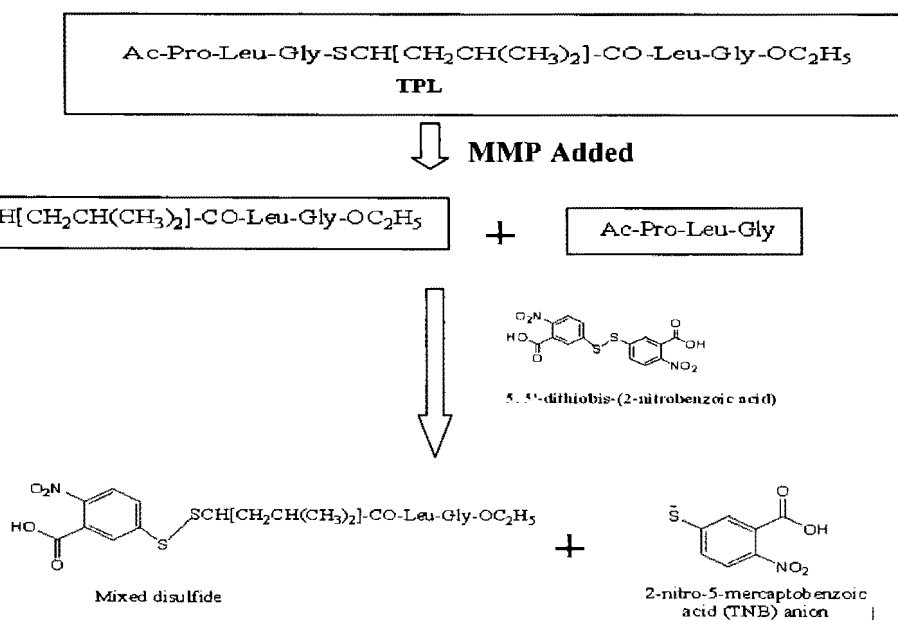
Scheme 3.1. Spectrophotometric assay for MMP isozymes using TPL and DTNB.

3.2.5.1.2. Spectrofluorometric assay for MMP isozymes catalyzed reaction

The spectrofluorometric assays for MMPs are performed using a peptide substrate, Mca-Pro-Leu-Gly-Leu-Dpa-Ala-Arg-NH$_2$. This substrate was developed by Knight *et al.*

[5-7]. The experimental conditions maintained are similar for all the hMMP isozymes. The enzyme activity of hMMP-7, 9 and 10 were measured in 25 mM HEPES, 10 mM CaCl$_2$, pH 7.5. In the mentioned substrate MCA and Dpa represents (7-Methoxycoumarin-4-yl) acetyl and N-3-(2,4-dinitrophenyl)-L-2,3-diaminopropionyl, respectively. In this substrate, the highly fluorescent MCA group is very efficiently quenched by energy transfer (RET) by the 2,4-dinitrophenyl group. The hMMP isozymes (7, 9 and 10) used in the assay, have a preferred mechanism to cleave the Gly-Leu [G - L] bond releasing the MCA group (fluorophore group) from the 2,4-dinitrophenyl (quencher group), resulting in an increase in fluorescence. This is shown in Scheme 3.2. In a typical experiment, the initial slope of the progress curve is measured via a Molecular Devices SpectraMax Plus microplate reader in a black polystyrene microplate. The buffer used in the assay is 25 mM HEPES, 10 mM CaCl$_2$, and pH 7.5 at 25°C. Reaction volumes were restricted to 200 µl for reliability and sensitivity of the instrument.

In a typical experimental setup, the reaction mixture contained 25 µM of the substrate. The enzyme concentration varied depending on the hMMP isozyme used. The concentrations of the hMMP used were 0.3 µM, 0.16 µM, and 2 µM for hMMP-7, 9 and 10, respectively. As the enzyme hydrolyzed the substrate, the release of the AMC was indicated by increase in fluorescence at 395 nm. The excitation wavelength was maintained at 335 nm. The stock solution of the substrate was carefully prepared in 25 mM HEPES buffer at pH 7.5. The monitoring time of the reaction was 300 seconds and the absorbance maximum of the unquenched peptide at 324 nm (ε = 12, 900 M^{-1} cm^{-1}) was taken into

account as the control. The data collected were converted in terms of the "units" of activity (similar to Scheme 3.1.).

Mca-Pro-Leu-Gly-Leu-Dpa-Ala-Arg-NH$_2$

⇓ + **MMP Added**

Mca-Pro-Leu-Gly   Leu-Dpa-Ala-Arg-NH$_2$
(Fluorophore)   (Quencher)
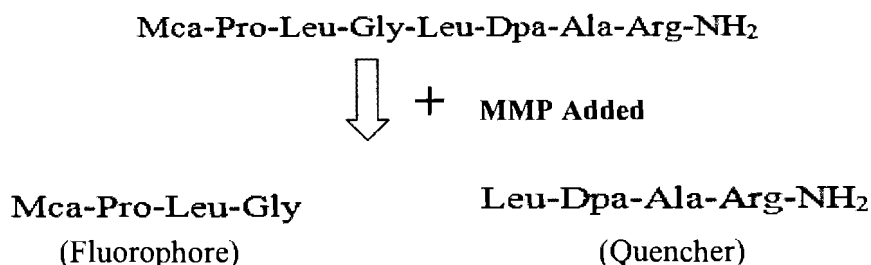
Scheme 3.2. Spectrofluorometric assay for MMP using a commercial fluorogenic substrate.

3.6. Relationship between "rigid" and "flexible" surfaces on the differential modulation of functional and structural characteristics of Matrilysin (hMMP-7)

3.2.6.1. Preparation of Au-NPs

The Au-NPs, prepared in Dr.Rotello's laboratory (University of Massachusetts at Amherst), were tested with different buffers and were found to be most stable in 10 mM Phosphate buffer, pH 8.0. The stock of the Au-NPs was dissolved in this buffer and small amounts of these NPs were diluted in the respective buffer and used for subsequent experiments.

3.2.6.2. Determination of the effect of cationic macro clusters on the hMMP-7 catalyzed cleavage of florogenic substrate

The effect of cationic macro clusters like polylysine (PLL) on enzymatic activity of hMMP-7 was monitored by measuring the initial rate of the hMMP-7 catalyzed reaction using a fluorogenic peptide (obtained from Calbiochem, CA) of the following composition: MCA-Pro-Leu-Gly-Leu-Dpa-Ala-Arg-NH$_2$ [Where MCA and Dpa stand for (7-Methoxycoumarin-4-yl) acetyl and N-3-(2,4-dinitrophenyl)-L-2,3-diaminopropionyl, respectively] while maintaining the excitation and emission wavelengths of 335 nm and

77

395 nm, respectively. The time course of the reaction was monitored for about 5 minutes. Human MMP-7 in the reaction mixture was maintained at 0.3 μM, while PLL varied between 0 - 500 μM in the reaction mixture in 25 mM HEPES, 10 mM CaCl$_2$, pH 7.5.

3.2.6.3. Determination of the effect of cationic nano particles (Au-CNP) on the hMMP-7 catalyzed cleavage of florogenic substrate

The effect of cationic Nano particles (Au-CNPs) on the hMMP-7 activity was determined by using the same fluorogenic peptide as employed with PLL. The excitation and emission wavelengths of the fluorogenic peptide were maintained at 335 nm and 395 nm, respectively. The concentration range for cationic gold nanoparticles (Au-CNP) was varied between 0 and 1 μM. The hMMP-7 concentration during the above experiment was maintained at 0.3 μM in a reaction mixture of 25 mM HEPES, 10 mM CaCl$_2$, pH 7.5.

3.2.6.4. Evaluating the secondary structural changes in hMMP-7 and PLL *via* Circular Dichroism (CD) spectroscopic studies

The binding of hMMP-7 to polylysine (PLL) was evaluated using the Circular Dichroism System (Jasco J-815 spectropolarimeter) with spectral changes in the far UV region (250-200 nm) using 1 mm path length in a quartz cuvette by systematically titrating with increasing concentrations of PLL (0 - 100 μM) to hMMP-7 (5 μM) in the cuvette. The secondary structural changes / local organization of the *unstructured protein* were indicated by the double peaks at 222 nm and 210 nm. In order to delineate the hypothesis, the origin of the significant portion of the CD signal (contributed from the changes in the secondary structure of PLL and protein) was monitored; under the same experimental conditions, systematic titration of PLL (0 - 100 μM) in 5 mM HEPES, pH 7.5 was monitored as a control experiment to correct the CD signal as the background of PLL in the absence of

hMMP-7. In order to reduce spectroscopic noise, five scans were done and averaged, and the inbuilt program was used to analyze the data.

3.2.6.5. Evaluating the Au-CNP mediated secondary structural changes of hMMP-7 via Circular Dichroism spectroscopic studies

Circular dichroism spectra of hMMP-7 (50 µM) in the presence of increasing concentration of Au-CNP were monitored. The experiment was performed in 5 mM phosphate buffer, pH 7.5 between 210-270 nm regions using a Jasco J-815 spectropolarimeter. The concentration of Au-CNP was varied from 0 to 5 µM.

3.2.6.6. Ascertaining whether the the activation / inhibitory feature of hMMP-7 with high concentrations of PLL was denaturation or inhibition of the enzyme

In a typical experiment, 39 µM of hMMP-7 and PLL each were pre-incubated and then a fixed aliquot was withdrawn every time and transferred to the reaction mixture for measuring the enzyme activity using fluorogenic peptide (obtained from Calbiochem, CA) of the following composition: MCA-Pro-Leu-Gly-Leu-Dpa-Ala-Arg-NH$_2$ [Where MCA and Dpa stand for (7-Methoxycoumarin-4-yl) acetyl and N-3-(2,4-dinitrophenyl)-L-2,3-diaminopropionyl, respectively]. The excitation and emission wavelengths of 335 nm and 395 nm, respectively were maintained. In this process, the PLL concentration was diluted to 0.3 µM (activation concentrations) and 50 µM (inhibitory concentrations) in the reaction mixture respectively; and then the initial rate of hMMP-7 catalyzed reaction was measured using the fluorogenic substrate for different time intervals. The initial rates were compared to the rates when the PLL were mixed instantly without any pre-incubation period.

3.2.6.7. Ascertaining whether the the activation / inhibitory feature of hMMP-7 with high concentrations of Au-CNP was denaturation or inhibition of the enzyme

This experiment was performed to ascertain the potencies of Au-CNP on the act of

inhibition versus inactivation of hMMP-7. In this typical experiment, a relatively high concentration of hMMP-7 (~ 8 μM) was pre-incubated with 2.1 μM Au-CNP, and 6 μl was withdrawn from the stock sample and transferred to the reaction mixture for measuring the enzyme activity as already described in the above experiment. In this approach, the Au-CNP was diluted in the reaction mixture, and the concentrations were similar to the ones that were used during the inhibition experiment. The initial rates were compared to the rates when the Au-CNP was mixed instantly without any pre-incubation period.

3.2.7. Molecular origin of the intrinsic selectivity in binding of *human* Matrix Metalloproteinase (hMMP) isozymes to differently charged lipid membranes

3.2.7.1. Preparation of differently charged liposomes (LUVs)

Appropriate volumes of chloroformic solutions of desired lipids were transferred to a round bottom flask. A 9:1 mixture of spectroscopic grade chloroform: methanol (total volume = 20 ml) was added to achieve complete dissolution of the lipids. The organic solvent was removed under vacuum in a rotary evaporator (Yamato® RE 450) at 42°C with rotation of the flask at 220 rpm. After its formation, the thin film was kept under vacuum for 24 hours to remove residual organic solvent.

Buffer (5 ml of 20 mM HEPES, pH 7.5 containing 150 mM NaCl) was added to the flask, and the thin lipid film was detached by continuous rotation at 220 rpm for 1 hour in a water bath at 70°C. The resulting hydrated lipid suspension was sonicated for 1 hour in a heating block at 70°C using a probe sonicator (Branson® 150 continuous pulse level #3). A clear and uniform dispersion of the lipid vesicles was obtained. This solution was filtered through a 220 μm filter to remove any shavings introduced during sonication.

After one hour at room temperature, the suspension of lipid vesicles became hazier, confirming their aggregation into larger vesicles. At this stage, the vesicles were extruded through a 100 nm polycarbonate filter (Avanti® Polar Lipids, AL) to obtain large unilamellar vesicles.

3.2.7 2. Phosphate assay on the LUVs

This assay was performed for determining the phospholipid content. 5 mM KH_2PO4 was prepared as a stock solution and dilutions were made varying from 0 to 63.0 nmoles inorganic phosphate into clean 13 * 100 mm disposable glass test tubes. 200 µl 10% H_2SO4 was heated for 1 hr @ 200°C in a heating block. 25 µl 30% H_2O_2 was then added to each tube and heated for 40 min@ 200°C. The tubes were cooled and later color reagent (Ammonium Molybdate, ddH_2O and Vit C) and ddH_2O was added. This solution was heated to 45°C for 20 minutes. The test tubes were cooled down to room temperature and the Absorbance at A_{820} was measured using a Molecular Devices SpectraMax® Plus microplate reader using a quartz cuvette (1-cm path length). The control samples and test samples were prepared in triplicates. The A_{820} values from the standard control samples were plotted as a function of nmoles of inorganic phosphate. The slope from this plot was used to calculate the amount of inorganic phosphate in the different liposome samples.

3.2.7.3. Determination of hMMP isozymes liposome interaction *via* fluorescence of dansylPE (dPE)

The interaction of the liposomes with hMMP isozymes was measured with 10 mol % dansylPE (Avanti® Polar Lipids, Alabaster, AL) as reporter using an LSB50 spectroflourimeter. In a typical experiment, 1 µM of hMMP-7 was taken in the cuvette and titrated with increasing concentrations of dansylPE-containing anionic, cationic or neutral

liposomes (LNPs). The excitation wavelength was set at 283 nm and the intensities of the emission peak at 343 nm, 335 nm, and 330 nm corresponding to the protein's tryptophan residues of hMMP-7, hMMP-9, and hMMP-10, respectively. The corresponding dansyl reporter was monitored at 513 nm. The 513 nm peak was corrected for increasing background fluorescence due to increasing dansylPE by performing a blank titration of dansylPE containing liposomes into buffer-only and subtracting the background from corresponding intensities in the presence of hMMP-7. Fractional saturation was determined as the ratio of the fluorescence intensity change observed at the given concentration of lipid to the maximum fluorescence change observed for 343 nm, 335 nm, or 330 nm for hMMP-7, 9, and 10, respectively, along with 513 nm peaks. K_d values were determined by nonlinear regression using the hyperbola equation.

As described above, titration of increasing aliquots of dansylPE containing anionic, cationic or neutral liposomes into hMMP isozymes in the cuvette led to a decrease in the fluorescence intensity at 343 nm and a corresponding increase of the corrected dansyl fluorescence at 525 nm. Hence, the decrease in the peak intensity of 343 nm, 335 nm, and 330 nm in case of hMMP-7, hMMP-9, and hMMP-10, respectively, was plotted as a function of increasing outer leaflet lipid concentration. The K_d was then determined via non-linear regression analysis as mentioned above.

3.2.7.4. Evaluating the thermograms of different mol % of DMPS using Differential Scanning Calorimetry (DSC)

The LUVs constituted of varying composition of DMPC: DMPS. The DMPS varied from 5%, 25%, 30% and 40%. DSC studies were performed on Microcal VP-DSC (Microcal Inc, Northampton, MA) system. The major component was DMPC. The total

phospholipid concentration was maintained approximately at 3.5 to 4.0 mM in 20 mM

HEPES, 150 mM NaCl, pH 7.5, similar to the buffer used to prepare the liposomes. The

LUVs were heated at a scan rate 10°C/ hr (from 10°C to 45°C). Each scan was repeated

seven times.

3.2.7.5. Analysis of the effect of liposomes on the activity of hMMP isozymes

The interaction of liposomes with hMMP isozymes were monitored by measuring

the rate of hMMP isozymes hydrolysis of the fluorogenic peptide MMP-2 / MMP-7,

MCA-Pro-Leu-Gly-Leu-Dpa-Ala-Arg-NH$_2$·TFA [Dpa = N-3-(2,4-dinitrophenyl)-L-2,3-

diaminopropionyl], using an LSB50 fluorimeter with excitation wavelength set at 335 nm.

The intensity of emission of the fluorescent product was monitored at 395 nm for 5

minutes. The concentrations of hMMP-7, hMMP-9, or hMMP-10 in the cuvette/

fluorescence plate reader were maintained at 1 µM, 0.3 µM, and 2 µM, respectively, while

the liposome concentration (total lipid) was varied between 0 and 250 µM. Graphs showing

the rate of product formation as a function of increasing concentration of liposomes were

plotted. The K$_i$ value of the enzyme–liposome complex formed was determined via non-

linear regression analysis of the experimental data as described by Banerjee *et.al.* [8] using

the Grafit® 4.0 software.

3.2.7.6. Probing the possible interaction between hMMP-7 substrate and cationic liposomes

To confirm that the cationic liposomes mediated inhibition of hMMP-7 was due to

formation of hMMP-7-liposomes complex, and not due to interaction of the enzyme's

substrate with liposomes, an analytical HPLC (using a vydac C$_{18}$ reverse-phase column)

experiment was carried out. During this experiment, 20 µM substrate in the absence and

presence of 200 μM liposomes was loaded to the column and subsequently eluted by a linear gradient of 0–70% acetonitrile in water (containing 0.1% TFA) over a 60 minutes time period. The flow rate of the column was maintained at 1.5 ml/min. The peak elution time of the substrate would suggest whether or not the liposome sequestered the substrate and yielded artifactual results about the cationic liposomes mediated inhibition of hMMP-7.

3.2.7.7. Plotting the osmolality as a function of increasing concentration of NaCl

A 1 ml volume of stock 1 M NaCl concentration was prepared in 25 mM HEPES Buffer, pH 7.5 in a falcon tube. Subsequent dilutions were made in 1 ml eppendorf tubes varying from 0 to 250 mM NaCl. The osmolality of these NaCl solutions was measured using an Advanced Instuments Micro-Osmometer. The osmolality as a function of NaCl concentrations (mM) was plotted. The slope of the plot was used further to calculate and adjust the osmolality of the liposomes prepared for salt dependent experiments.

3.2.8. To unravel the alternative binding modes of *human* Matrix Metalloproteinase (hMMP) isozymes to cationic and anionic quantum dots

3.2.8.1. Excitation and emission spectra of CQD and AQD

The absorbance spectra were measured in a Molecular Devices SpectraMax® Plus microplate reader using a quartz cuvette (1-cm path length). The excitation spectra measured was represented after subtraction of the buffer background and the difference data is represented in absorbance units. All measurements were performed in a standard quartz cuvette or 96 well plates at room temperature.

The steady state spectrofluorometric emission studies were performed on a Beckman DU 7400 spectrofluorimeter or Molecular Devices SpectraMax® Plus microplate

reader (path length approximately 0.3 cm) or in Perkin Elmer lambda 50-B spectrofluorometer, equipped with a magnetic stirrer and thermostated water bath. The emission spectra measured were represented after subtraction of the buffer background and the difference data is represented in relative fluorescence units (RFU). All measurements were performed in a standard quartz cuvette or in 96 well plates at room temperature.

3.2.8.2. Determination of the dissociation constant (K_d) of hMMP-CQD complex

The steady state spectrofluorometric studies were performed on a Beckman DU 7400 spectrofluorimeter or Molecular Devices SpectraMax® Plus microplate reader (path length approximately 0.3 cm). As the CdTe cationic quantum dots (CQD) were stable in 10 mM Tris, pH 8.0, these experiments were done in the mentioned buffer. The CQD (λ_{ex} = 570 nm, λ_{em} = 595 nm), with excitation and emission slit widths of 5 mm, using 4*4 mm quartz cuvette or fluorescent well plate. The dissociation constant (K_d) of hMMP-Isozymes - CQD complex was determined by titrating hMMP-7 , 9 or 10 into a fixed concentration of CQD in 10 mM Tris, pH 8.0 buffer. The excitation wavelength was fixed at 280 nm and the quenching of the tryptophan florescence was monitored at 343 nm, 335 nm and 330 nm for hMMP-7, hMMP-9, and hMMP-10, respectively. A fixed concentration of CQD (0.3 µM) was used to titrate with hMMPs. A blank titration of hMMP isozyme into the buffer was performed to subtract the contribution of protein from that of the sample. The difference in signal at 343 nm, 335 nm, or 330 nm; after the subtraction, was plotted as a function of increasing concentration of hMMP isozymes. The dissociation constant was determined as described by Banerjee.et.al. [8]. However, as the stock concentration of CQD was not known, the fitting parameter determining the concentration of CQD used in the cuvette was

85

not constrained. The dissociation constants (K$_d$) of the MMP-CQD complexes were determined by analyzing the binding isotherm with the classical quadratic equation for the enzyme-ligand interactions using Grafit 4.0 (Erithacus software) and representing the following equation:

$$\Delta F = C * \frac{(E_t * n + L_t + K_d) - \sqrt{(E_t * n + L_t + K_d)^2 - 4E_t * n * L_t}}{2} \quad \text{............Eq (3.5)}$$

where n, L$_t$, E$_t$ and C refer to the stoichiometry of the enzyme-ligand complex, total ligand concentration, total enzyme concentration, and capacity (amplitude of the difference in the signal change), respectively. The difference in fluorescence of the complex after subtraction of its individual components would relate to the dissociation constant (K$_d$). However, the association constant (K$_a$) of the enzyme-ligand complex was represented here in the equation as the reciprocal of the dissociation constant (K$_d$) in the binding studies.

3.2.8.3. Determination of the dissociation constant (K$_d$) of hMMP-AQD complex

The steady state spectrofluorometric studies were performed on a Beckman DU 7400 spectrofluorimeter or Molecular Devices SpectraMax® Plus microplate reader (path length approximately 0.3 cm). As the CdTe/ TGA anionic quantum dots (AQD) were stable in 10 mM Tris, pH 8.0, these experiments were done in the mentioned buffer. The AQD (λ_{ex} = 570 nm, λ_{em} = 625 nm), with excitation and emission slit widths of 5 mm, using 4*4 mm quartz cuvette or fluorescent well plate. The dissociation constants (K$_d$) of hMMP-isozymes-CdTe AQD complex were determined by titrating hMMP isozymes 7, 9, or 10 into a fixed concentration of AQD in 10 mM Tris, pH 8.0 buffer. The excitation wavelength was fixed at 280 nm and the quenching of the tryptophan fluorescence was

monitored at 343 nm, 335 nm, and 330 nm for hMMP-7, hMMP-9, and hMMP-10, respectively. A fixed concentration of AQD (0.57 µM) was used to titrate with increasing concentrations of hMMPs. A blank titration of hMMP isozyme into the buffer was performed to subtract the contribution of protein from the sample. After the subtraction, the difference in signal at 343 nm, 335 nm, or 330 nm for hMMP-7, hMMP-9, and hMMP-10, respectively, was plotted as a function of increasing concentration of hMMPs. The dissociation constant was determined as described by Qin and Srivastava [9]. However, as the stock concentration of AQD was not known, the fitting parameter determining the concentration of AQD used in the cuvette was not constrained. The same equation was used to determine the dissociation constant of the hMMP isozymes to the AQD.

3.2.8.4. Determination of the inhibition constant (K_i) of hMMP-CQD complex

The effects of CQDs on enzymatic activity of hMMP isozymes were performed by measuring the initial rate of the hMMP isozymes catalyzed reaction using the fluorogenic substrate of the following composition: MCA-Pro-Leu-Gly-Leu-Dpa-Ala-Arg-NH_2 [Where MCA and Dpn stand for (7-Methoxycoumarin-4-yl)acetyl and N-3-(2,4-dinitrophenyl)-L-2,3-diaminopropionyl, respectively], maintaining the excitation and emission wavelengths of 335 nm and 395 nm, respectively. The progress curve of the hMMP catalyzed reaction was monitored for about 300 seconds. The CQD concentrations were varied between 0 and 2.2 µM and the concentrations of 0.3 µM, 0.16 µM and 1 µM for hMMP-7, 9, and 10 respectively, was maintained in the reaction mixture in 50 mM Tris, 10 mM $CaCl_2$, pH 7.5.

3.2.8.5. Determination of the inhibition constant (K_i) of hMMP-AQD complex

The effect of AQDs on enzymatic activity of hMMP isozymes were determined by

measuring the initial rate of the hMMP isozymes catalyzed reaction using the fluorogenic substrate MCA-Pro-Leu-Gly-Leu-Dpa-Ala-Arg-NH$_2$ [Where MCA and Dpn stand for (7-Methoxycoumarin-4-yl)acetyl and the other component is N-3-(2,4-dinitrophenyl)-L-2,3-diaminopropionyl, respectively]. The excitation and emission wavelengths of 335 nm and 395 nm, respectively, were maintained. The progress curve of the hMMPs, was a catalyzed reaction monitored for about 300 seconds. The AQD concentrations were varied between 0 and 3.3 μM, and the concentrations of 0.3 μM, 0.16 μM and 1 μM of hMMP-7, 9, and 10 respectively, was maintained in the reaction mixture in 50 mM Tris, 10 mM CaCl$_2$, pH 7.5.

3.2.8.6. To probe the effect of inhibition vs inactivation of hMMP isozymes using CQD

This experiment was performed to ascertain the potencies of differently charged CQD on inhibition versus inactivation of hMMP isozymes. In a typical experiment, approximately 4 μM of hMMP-7, 9, or 10 was pre-incubated with 6 μM CQD respectively in separate eppendorf tubes for 20 minutes. 10 μl was withdrawn from the stock sample and transferred to the reaction mixture for measuring the enzyme activity at different time intervals. In the case of reversal studies, the CQD and hMMP isozymes were diluted by 25 fold in the reaction mixture, and their concentrations became similar to the ones that were in the enzyme assay and the inhibition studies. The initial rates were compared to the rates when the CQD were mixed instantly without any pre-incubation period.

3.2.8.7. To probe the effect of inhibition vs inactivation of hMMP isozymes using AQD

This experiment was performed to ascertain the potencies of differently charged AQD on inhibition versus inactivation of hMMP isozymes. In this typical experiment, approximately 4 μM of hMMP-7, 9, and 10 was pre-incubated with 6 μM AQD

respectively in separate eppendorf tubes for 20 minutes. 10 μl was withdrawn from the stock sample and transferred to the reaction mixture for measuring the enzyme activity at different time intervals. In the case of reversal studies, the AQD and hMMP isozymes were diluted by twenty-fold in the reaction mixture, and their concentrations became similar to the ones that were in the enzyme assay and the inhibition studies. The initial rates were compared to the rates when the AQD were mixed instantly without any pre-incubation period.

3.2.8 8. Time resolved fluorescence decay of CQD in absence and presence of hMMP isozymes

Fluorescence Lifetime Decay measurements were carried out using a custom designed Photon Technology International (PTI) Easy Life® instrument. The excitation source for measuring the time resolved fluorescence decay was the Light Emitting Diode (LED) with maximum power output at 280 and 340 nm respectively. The experiments were done under setting 1-ST 1_{CQD} (Ex 280 nm, Em 335 nm) and setting II –ST II_{CQD} (Ex 340 nm, Em 570 nm) for CQD. The emission slits were maintained at 6.0 nm. The emitted light was detected by stroboscopic emission monochromator set at specific wavelengths. The data were collected using 200 channels, 1sec as the integration time, and ten averages were taken to obtain the highest resolution of the fluorescence traces. The instrument response time was recorded by using a starch suspension to measure the scatter. The time resolved fluorescence decay curves were analyzed by using the inbuilt exponential decay equations in the PTI analysis software. A single exponential decay equation was attempted for each decay curve, and a bi-exponential decay equation was used wherein the resulting residuals were high [4].The kinetic traces were fitted using the following equations:

$$I(t) = \sum_{i=1}^{n} \alpha_i \exp(-t/\tau_i) \quad \text{............................Eq (3.6)}$$

where α_i and τ_i are amplitude and fluorescence lifetime for the ith component, respectively. The relative contribution of component i (f_i) was calculated derived from the above mentioned relationship, which when modified can be represented in the following format:

$$f_i = (\alpha_i \tau_i / \sum_{i=1}^{n} \alpha_i \tau_i) * 100\% \quad \text{...............................Eq (3.7)}$$

The goodness of the exponential fit of fluorescence curves was determined by the reduced χ^2, the Durbin Watson, and Z values. All measurements were conducted under ambient environmental conditions.

3.2.8.9. Time resolved fluorescence decay of AQD in the absence and presence of hMMP isozymes

Fluorescence lifetime decay measurements were performed using a custom designed Photon Technology International (PTI) Easy Life® instrument. The excitation source for measuring the time resolved fluorescence decay was the Light Emitting Diode (LED) with maximum power output at 280 and 340 nm, respectively. The experiments were done under setting I- $ST1_{AQD}$ (Ex 280 nm, Em 335 nm) and setting II-ST II $_{AQD}$ (Ex 340 nm, Em 625 nm) for AQD. The emission slits were maintained at 6.0 nm. The emitted light was detected by stroboscopic emission monochromator set at specific wavelengths. The data were collected using 200 channels, 1sec as the integration time and ten averages were taken to obtain the highest resolution of the fluorescence traces. The instrument response time was recorded by using a starch suspension to measure the scatter. The time resolved fluorescence decay curves were analyzed by using the inbuilt exponential decay equations in the PTI analysis software. A single exponential decay equation was attempted

for each decay curve, and a bi-exponential decay equation was used where the resulting residuals were high. The goodness of the exponential fit of fluorescence curves was determined by the reduced χ^2, the Durbin Watson, and Z values. All measurements were conducted under ambient environmental conditions.

3.2.9. High throughput screening of the small molecule inhibitors (SMI) with the hMMP isozymes

3.2.9.1. Analysis on the effect on the enzyme activity for hMMP isozymes with the small molecule inhibitors (SMIs)

The effects of the different small molecule inhibitors on enzymatic activity of hMMP-7, 9, and 10 were performed by measuring the initial rate of the hMMP isozymes catalyzed reaction using the fluorogenic substrate MCA-Pro-Leu-Gly-Leu-Dpa-Ala-Arg-NH$_2$ [Where MCA and Dpa stand for (7-Methoxycoumarin-4-yl)acetyl and N-3-(2,4-dinitrophenyl)-L-2,3-diaminopropionyl, respectively]. The excitation and emission wavelengths of 335 nm and 395 nm, respectively, were maintained. The progress curve of the hMMP isozymes catalyzed reaction was monitored for about 300 seconds. The Inhibitors are first screened at 10 μM concentration; and if the % inhibition was 50% or more of the enzyme activity, then the K_i for the inhibitor of the enzyme was determined, while the concentration of hMMP-7, 9, and 10 was maintained at 0.3 μM, 0.16, and 2 μM respectively in reaction mixture in 25 mM HEPES, 10 mM CaCl$_2$, pH 7.5. The K_i value of the enzyme–inhibitor complex formed was determined via non-linear regression analysis of the experimental data as described by Banerjee $et.al.$ [8] using the Grafit® 4.0 software. The initial slopes of the progress curves were noted but for easy representation, the rate of the hMMP isozymes is represented as % activity. The inhibition constant (K_i) and the mode

of inhibition was determined by using a double-reciprocal plot analysis of the data for the hMMP isozymes with the SMIs. It is known that the Michaelis-Menten equation relies on the free concentration of the substrate and the SMIs, rather than the total concentration of each; the fraction bound $[I]_b$ must be subtracted from the total $[I]_t$ to find out the total concentration available in the reaction $[I]_f$. This information becomes very crucial for the analysis of the kinetic data. This information is carefully fed into the quadratic equation, representing the enzyme-inhibitor binding. The built in quadratic equation is a classic steady-state equation for the competitive inhibitors. First, the simplest forms of the equations were used, and if the data did not fit the simple competitive equation, then the other complex forms like un-competitive or non- competitive equations were used.

$$v = \frac{V_{max}}{1 + K_m/[S]\,(1 + [I]_f/K_i)} \quad\text{..Eq (3.8)}$$

where $[I]_f$ represents the free concentration of the inhibitor. In some inhibition experiments, the $[S]_{total} \leq K_m$, the equation would be simplified as:

$$v = \frac{V_{max}}{K_m(1+[I]_f/K_i)} \quad\text{...Eq (3.9)}$$

The final form of the competitive steady-state model can be represented as:

$$v = \frac{v_0*K_i}{K_i + \left([I]_t - 0.5\{([I]_t + [E]_t + K_i) - \sqrt{([I]_t + [E]_t + K_i)^2 - 4*[I]_t*[E]_t}\}\right)} \quad\text{....................Eq (3.10)}$$

The calculations for the SMI inhibition data [Eq (3.10)] were used to calculate the K_i for the hMMP isozymes using the non-linear regression analysis software, Grafit 4.0.

3.2.9.2. Analysis of the spatio-temporal distribution of the functional groups in the inhibitor using Gaussian 3.0

The molecular modeling and the computational methods available for the different estimation of the interaction between two molecules (ligands) are categorized as molecular mechanics or electronic structure methods. The simplest and easiest method for us to obtain the spatio-temporal distribution of the functional groups, as well as their individual distribution, which dictated the dynamics of the interaction between the enzyme and the side groups and their geometry optimization inside the enzyme active-site cavity was captured by Gaussian 3.0 software package. The parameters used make these methods computationally inexpensive, making them suited for small and large systems where other methods are not very practical and sensitive.

3.3. References

1. Sambrook, E., Fritsch, E. and Maniatis, T. (1989) Small-scale preparations of plasmid DNA in: Molecular Cloning: A Laboratory Manual (2nd Ed), *Cold spring Harbor Laboratory: Cold spring Harbor, NY.*
2. Koshland, D.E. (1958) Application of a Theory of Enzyme Specificity to Protein Synthesis, *Proc. Natl. Acad. Sci.* 44(2): 98–104.
3. Garnero, P., Borel, O., Byrjalsen, I., Ferreras, M., Drake, F.H., McQueney, M.S., Foged, N.T., Delmas, P.D., and Delaisse, Jean-M. (1998) The Collagenolytic Activity of Cathepsin K Is Unique among Mammalian Proteinases, *J. Biol. Chem.* 273, 32347-32352.
4. Weingarten, H., Martin, R., and Feder, J. (1985) Synthetic substrates of vertebrate collagenase, *Biochemistry.* 24, 6730-6734.
5. Knight, C.G., Willenbrock, F. and Murphy, G. (1992). A novel coumarin-labelled peptide for sensitive continuous assays of the matrix metalloproteinases. *FEBS Lett.* 296, 263-266.
6. Neumann, U., Kubota, H., Frei, K., Ganu, V. and Leppert, D. (2004) Characterization of Mca-Lys-Pro-Leu-Gly-Leu-Dpa-Ala-Arg-NH2, a fluorogenic substrate with increased specificity constants for collagenases and tumor necrosis factor converting enzyme, *Anal. Biochem.* 328, 166-173.
7. Welch, A.R., Holman, C.M., Browner, M.F., Gehring, M.R., Kan, Chen-Chen., and Van Wart, H.E. (1995) Purification of human matrilysin produced in Escherichia

coli and characterization using a new optimized fluorogenic peptide substrate, *Arch. Biochem.* 324 (1), 59-64.

8. Banerjee, A.L., Eiler, D., Roy, B.C., Jia, X., Haldar, M.K., Mallik, S. and Srivastava, D.K. (2005). Spacer-based selectivity in the binding of "two-prong" ligands to recombinant human carbonic anhydrase I. *Biochemistry.* 44, 3211-3224.

9. Qin, L., and Srivastava, D.K. (1998) Energetics of two-step binding of a chromophoric reaction product, trans-3-indoleacryloyl-CoA, to medium-chain acyl-coenzyme-A dehydrogenase, *Biochemistry.* 37, 3499-3508.

CHAPTER 4. PHYSIOCHEMICAL CHARACTERIZATION OF THE RECOMBINANT HUMAN MATRIX METALLOPROTEINASE ISOZYMES (hMMP-7, 9 and 10)

4.1. Introduction

The hMMP isozymes were sub-cloned, expressed and purified in order to use these isozymes for the characterization and the analysis of their kinetic parameters.

4.2. Results and Discussion

4.2.1. Cloning, expression and purification of hMMP -7

4.2.1.1. Checking the purity of the expressed protein by SDS-PAGE showing different fractions obtained during the purification process of hMMP-7

The refolded protein along with all the fractions obtained during the purification process was aliquoted, and samples were separated by SDS-PAGE to estimate the yield of the protein collected at each step. It would exhibit the natural progressive steps in increasing the purity of the protein (specific activity) with the help of the different techniques used throughout the purification process of hMMP-7. Figure 4.1 shows that the hMMP-7 is approximately 95% pure protein.

Estimation of the protein concentration of hMMP-7 was achieved by using the BCA protein assay wherein BSA was used as the standard protein marker. The absorbance at A_{562} was measured in a Molecular Devices SpectraMax® Plus microplate reader in a polystyrene microplate in duplicate with varied concentrations of the standard (varied from 50 ng to 500 ng). A new standard plot was prepared each time the Bradford or BCA assay was used to measure the protein content of hMMP-7 stock concentration [1]. The refolded hMMP-7 has a molecular weight of 19 kDa.
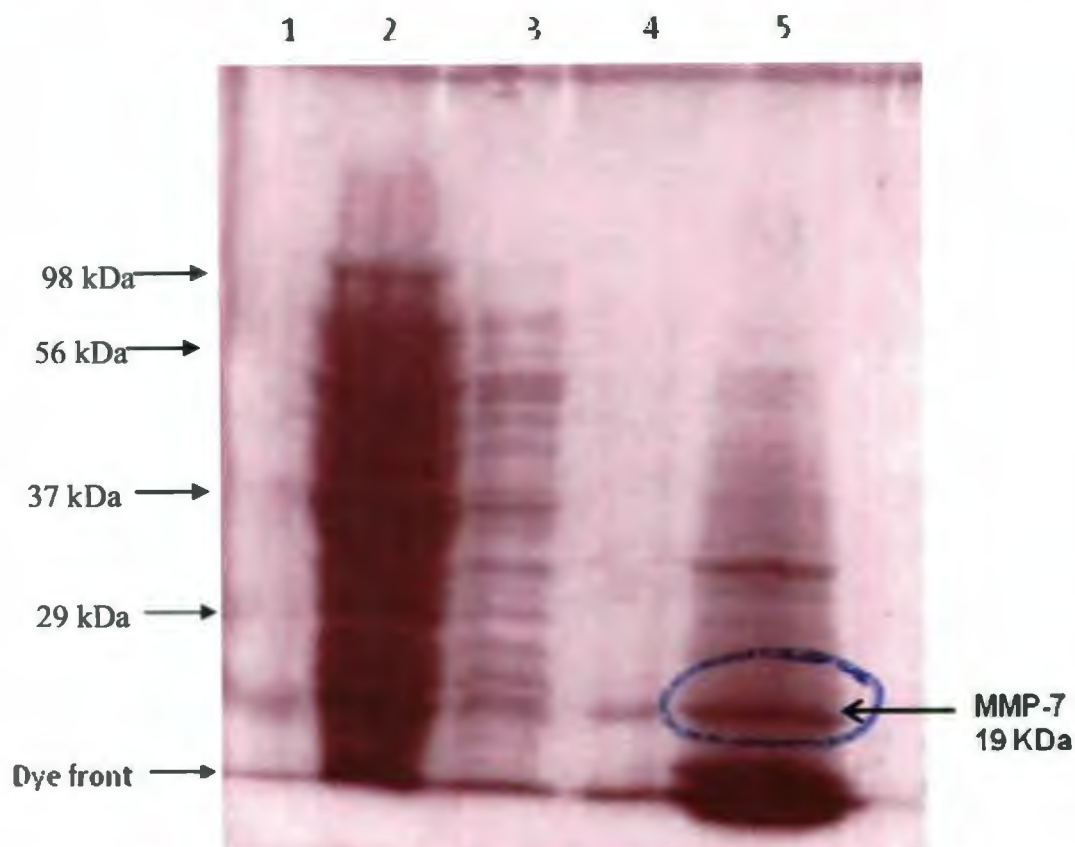
Figure 4.1. The SDS PAGE analysis of hMMP-7 at various stages of purification. Electrophoresis was on a 12% resolving gel with a 4% stacking gel and proteins were stained with coomassie blue. *Lane 1*: Standard Protein™ ladder, *Lane 2*: crude extract, *Lane 3*: 2M urea wash, *Lane 4*: refolded protein, *Lane 5*: 6 M urea supernatant.

.
4.2.1.2. Measurement of enzyme activity and protein estimation of hMMP-7 using Bradford method / BCA method

The enzyme activity of the recombinant hMMP-7 was measured by following the initial rate of hydrolysis of the fluorogenic peptide MMP-2/MMP-7 flourogenic peptide using an LSB50 Elmer fluorimeter in 25 mM HEPES, 10 mM $CaCl_2$, pH 7.5 (Figure 4.2). The purified enzyme was subjected to SDS-PAGE analysis to confirm the homogeneity of the protein. The enzyme concentrations were determined according to BCA assay, utilizing

BSA as the standard protein. Enzyme fractions were then pooled and dialyzed in storage

buffer (25 mM HEPES, 10 mM CaCl₂, 150 mM NaCl and 10 µM ZnCl₂, pH 7.5) and

stored at -20°C until used.
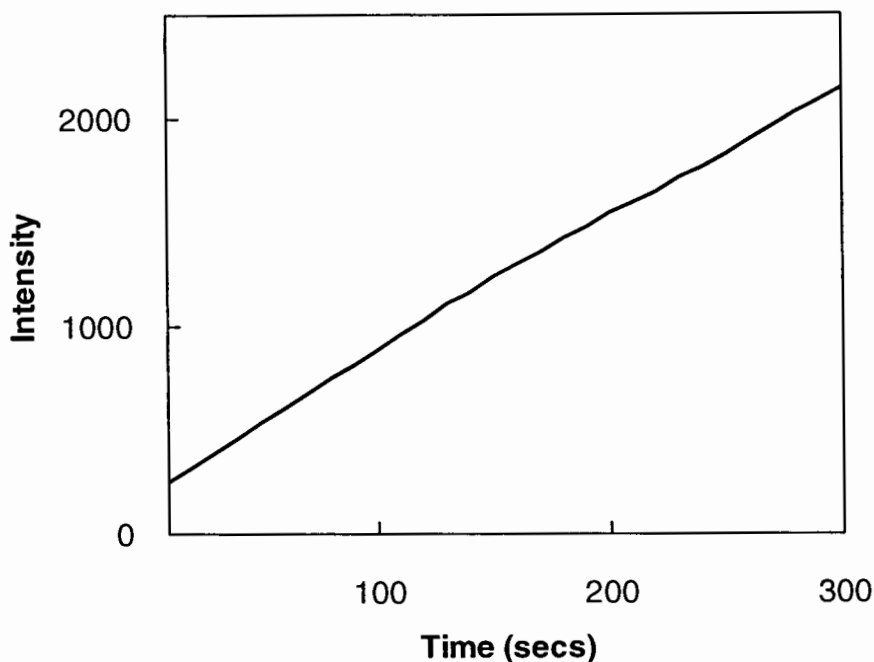
Figure 4.2. Spectrofluorometric assay of hMMP-7 catalyzed enzymatic reaction in presence of MCA-Dpa fluorogenic substrate. The reaction mixture included 25 mM HEPES, 10 mM CaCl₂, pH 7.5. The initial rate (represented as $\Delta F.s^{-1} = 4.9$) of the progress curve was measured in a polystyrene microplate (path length = 3 mm) for 300 secs; excitation and emission wavelengths were 335 nm and 395 nm, respectively. [hMMP-7]= 300 nM, [S] = 25 µM.

After cloning and expressing hMMP-7, the active hMMP-7 was purified with a

high specificity, and also the total yield of hMMP-7 from 1 L of LB medium was

estimated. Table 4.1 shows the summary table for the purification process of hMMP-7. The

6 M urea yielded 10.6 mg/ml of the protein, the protein concentration was estimated by

BCA assay method, the concentration dropped significantly. It was very evident that this is

a major step where protein is lost.

Table 4.1. Summary table of one-step purification of hMMP-7.

Sample	Total volume (ml)	Protein conc (mg/ml)	Total protein (mg)	Activity (μM. min^{-1})	Specific activity (μM. min^{-1}. mg-^{1})	% Recovery
6 M urea extract	15	10.6	159	-	-	-
Refolded hMMP-7	224	0.256	57.3	900	576923.08	36%

Obviously, in the refolding process there is a large probablility that all of the newly folded protein might not have folded into the native conformation. In the heterogeneous population of the newly refolded protein sample, the conformation that has acquired the native active-site conformation would eventually catalyze the reaction. Only 36% of the total protein refolded correctly and was active. Moreover, with hMMP isozymes, it is an established fact that there is protein precipitation during serial or snap dilution. Even though 150 mM NaCl concentrations have been maintained, still there has been nucleation and aggregation occurring during the equilibration of the refolding process leading to the protein "falling out" of the solution in the form of visible aggregates [2].

The high catalytic activity and high specific activity indicates the efficient refolding in the recovered protein. However, comparison of the yield of other proteins recovered from inclusion bodies to recovering 57 mg of hMMP-7 per liter of LB broth, the yield shown in Table 4.1 is considered good. Hence, purified hMMP-7 was used for the experiments included in this Dissertation. It has been reported that in other laboratories 18-20 mg/ L of LB has been produced [3]. Calbiochem (Gibbstown, NJ), commercially sells

hMMP-7 (active, human, recombinant MMP-7), 100 µg for $299, whereas Enzo® Life

Sciences sells 10 µg for $ 309.

4.2.2. Cloning, expression and purification of hMMP -9

4.2.2.1. Checking the purity of the expressed protein by SDS-PAGE showing different fractions obtained during purification process of hMMP-9

The refolded protein along with all the fractions obtained during the purification

process has been aliquoted, the samples were separated by SDS-PAGE, and the yield of the

protein collected was estimated at each step. The procedure followed was similar to that for

hMMP-7. The refolded hMMP-9 has a molecular weight of 42 kDa (Figure 4.3).
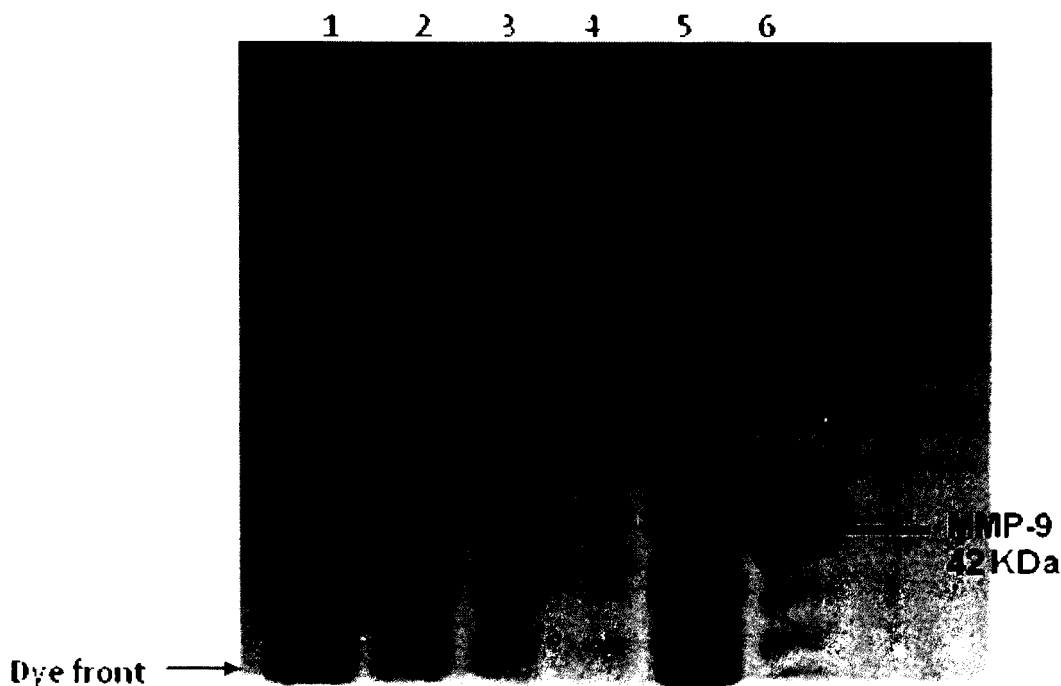
Figure 4.3. The SDS PAGE analysis of hMMP-9 at various stages of purification. Electrophoresis was on a 12% resolving gel with a 4% stacking gel and proteins were stained with coomassie blue. *Lane 1*: crude extract, *Lane 2*: lysis buffer wash, *Lane 3*: 2M urea wash, *Lane 4:* refolded protein, Lane 5: 2M urea wash (Repeat), *Lane 6*: 6M urea supernatant.

4.2.2.2. Measurement of the enzyme activity and protein estimation of hMMP-9 using Bradford method / BCA method

The enzyme activity of the recombinant hMMP-9 was measured by following the rate of hydrolysis of the fluorogenic peptide MMP-2/MMP-7 using an LSB50 Elmer fluorimeter in 25 mM HEPES, 10 mM $CaCl_2$, pH 7.5 (Figure 4.4). The purified enzyme was subjected to SDS-PAGE analysis to confirm the homogeneity of the protein. In Figure 4.3, lane 4 shows the presence of a single band representing a 42 KDa molecular weight. In Figure 4.3, lane 6, a dark band corresponding to the similar molecular weight indicates the presence of hMMP-9 in the denatured state in 6 M urea extract. The enzyme concentrations were determined according to BCA assay, utilizing BSA as the standard protein. Enzyme fractions were then pooled and dialyzed in storage buffer (25 mM HEPES, 10 mM $CaCl_2$, 150 mM NaCl and 10 μM $ZnCl_2$, pH 7.5) and stored at -20°C until used.
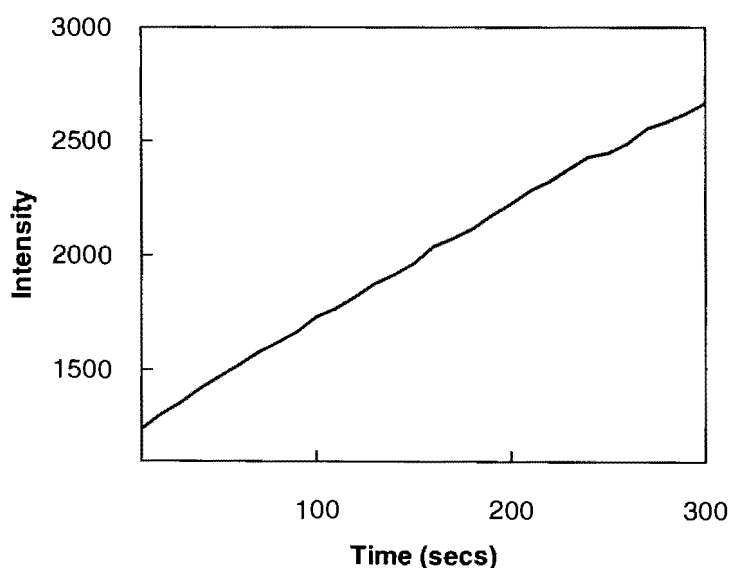
Figure 4.4. Spectrofluorometric assay of hMMP-9 catalyzed enzymatic reaction in presence of MCA-Dpa fluorogenic substrate. The reaction mixture included 25mM HEPES, 10 mM $CaCl_2$, pH 7.5. The initial rate (represented as $\Delta F.s^{-1} = 5.2$) of the progress curve was measured in a polystyrene microplate (path length = 3 mm) for 300 secs; excitation and emission wavelengths were 335 nm and 395 nm, respectively. [hMMP-9]= 160 nM, [S] = 25 μM.

After cloning and expressing hMMP-9, it was important to know whether the active hMMP-9 (Figure 4.4) purified possessed a high specificity and also to estimate the total yield of hMMP-9 from 1 L of LB medium. Table 4.2 shows the summary table for the purification process of hMMP-9.

Table 4.2. Summary table of one-step purification of hMMP-9.

Sample	Total volume (ml)	Protein conc (mg/ml)	Total protein (mg)	Activity ($\mu M. min^{-1}$)	Specific activity ($\mu M. min^{-1}. mg^{-1}$)	% Recovery
6 M urea extract	15	15.9	238.5	-	-	-
Refolded hMMP-9	188	0.34	63.92	1966.67	655556.67	26.8

The 6 M urea yielded 15.9 mg/ml of the protein, but when refolded, a significant amount of protein was lost. Only 26.8% of the total protein yielded was refolded correctly and was active. Moreover, with hMMP isozymes it is a very well established fact that there is huge amount of precipitation during the snap dilution step. In presence of 150 mM NaCl, there was nucleation and aggregation occurring during the equilibration of the refolding process leading to the formation of visible aggregates. Another very striking event during the purification and refolding of hMMP-9 was auto-degradation [4]. hMMP-9 acts like a triple helicase; preferentially cleaving a specific sequence existing in a triple-helical conformation [5]. Hence, this feature makes purification of hMMP-9 in the active form even more difficult. But with few of the modifications in the purification protocol this problem has been solved (refer to the steps in the purification process-Chapter 3 section 3.2). The catalytic activity (Figure 4.4) and high specific activity indicates the efficient

refolding in the recovered protein (Table 4.2). However, it was noticed that the yield of hMMP-9 was 63.9 mg/L LB broth. Moreover, the purified enzyme exhibited high activity and specific activity. It has been reported that in other laboratories 10-12 mg/ L of LB is generally recovered [6]. Calbiochem (Gibbstown, NJ) commercially sells hMMP-9 (active, human, recombinant MMP-9) for 5 μg for $289, whereas Enzo ® Life Sciences sells 10 μg for $369.

4.2.3. Cloning, expression and purification of hMMP -10

4.2.3.1. Checking the purity of the expressed protein by SDS-PAGE showing different fractions obtained during purification process of hMMP-10

The refolded protein along with all the fractions obtained during the purification process has been aliquoted, and the samples were separated by SDS-PAGE to estimate the yield of the protein collected at each step. The procedure followed was similar to that of hMMP-7 and hMMP-9. The molecular weight of hMMP-10 was determined to be 20 kDa (Figure 4.5).

4.2.3.2. Measurement of enzyme activity and Protein estimation of hMMP-10 using Bradford method / BCA method

The enzyme activity of the recombinant hMMP–10 was measured by following the rate of hydrolysis of the fluorogenic peptide MMP-2/MMP-7 flourogenic peptide using an LSB50 Elmer fluorimeter in 25 mM HEPES, 10 mM $CaCl_2$, pH 7.5 (Figure 4.6). The purified enzyme was subjected to SDS-PAGE analysis to confirm the homogeneity of the protein. The enzyme concentrations were determined according to BCA assay, utilizing BSA as the standard protein.

Figure 4.5. The SDS PAGE analysis of hMMP-10 at various stages of purification. Electrophoresis was on a 12% resolving gel with a 4% stacking gel and proteins were stained with coomassie blue. *Lane 1*: Standard Protein™ ladder, *Lane 2*: crude extract, *Lane 3*: lysis buffer wash, *Lane 4*: 2M urea wash, *Lane 5*: 6 M urea wash, *Lane 6*: refolded protein.
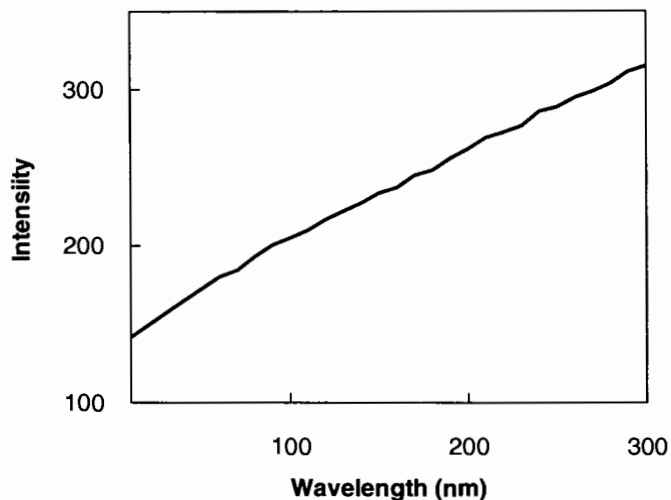
Figure 4.6. Spectrofluorometric assay of hMMP-10 catalyzed enzymatic reaction in presence of MCA-Dpa fluorogenic substrate. The reaction mixture included 25 mM HEPES, 10 mM CaCl$_2$, pH 7.5. The initial rate (represented as $\Delta F.s^{-1} = 0.5$) of the progress curve was measured in a polystyrene microplate (path length = 3 mm) for 300 secs; excitation and emission wavelengths were 335 nm and 395 nm respectively. [hMMP-10]= 2 µM, [S] = 25 µM.

Enzyme fractions were then pooled and dialyzed in storage buffer (25 mM HEPES, 10 mM CaCl$_2$, 150 mM NaCl and 10 μM ZnCl$_2$, pH 7.5 and stored at -20°C until used. After cloning, expressing, and purifying hMMP-10, it was very satisfying to record that the active hMMP-10 showed a high specificity and also estimated the total yield of hMMP-10 from 1 L of LB medium. Table 4.3 shows the summary table for the purification process of hMMP-10. The 6 M urea yielded 14.7 mg/ml of the protein but once refolded the protein concentration was estimated by BCA assay method was to be 1.09 mg/ml. It was this step that there was major loss in protein concentration.

In the heterogeneous population of the sample, the only conformation which acquired the native conformation eventually catalyze the reaction and in this case, only 38 % of the total protein refolded correctly and was active.

Table 4.3. Summary table of one-step purification of hMMP-10.

Sample	Total volume (ml)	Protein conc (mg/ml)	Total protein (mg)	Activity (μM. min^{-1})	Specific activity (μM. min^{-1}. mg^{-1})	% Recovery
6M urea extract	15	14.7	220.5	-	-	-
Refolded hMMP-10	77.5	1.09	83.9	504.38	63047.5	38

The high catalytic activity (Figure 4.6) and high specific activity indicate the efficient refolding in the recovered protein (Table 4.3). However, if the yield of other proteins is compared to the recovery from this purification procedure, 83.9 mg from 1L LB broth is considered good. Hence, it has been very satisfying in observing the activity and

specific activity of the purified hMMP-10. It has been reported that other laboratories have produced 20-25 mg/ L of LB [7]. It has been noted that Enzo® Life Sciences sells hMMP-10 for 10 μg for $ 309.

4.2.4. Distribution of Typtophan / Tyrosine residues on the surfaces of hMMP isozymes

Tryptophan (W) is very sensitive to the micro-environment as a fluorophore based on which emission maxima for the protein is determined. To carry out the biophysical studies discussed in this dissertation, the following criteria are important: (a) the knowledge about the distribution of the W residues; (b) the extent of their surface exposure (actively reacting with the solvent); (c) The spatio-temporal arrangement of the heterogeneous population (both the buried and exposed) W residues from the active-site pocket are very critical and sensitive to the interaction with different ligands. Therefore, a detailed study of the W residues in the hMMP isozymes was studied using the UCSF Chimera® software and the structures of MMP isozymes have been obtained as PDB files [8].

4.2.4.1. Solid surface representation of the ribbon structure of hMMP-7 showing the distribution of Typ / Tyr residues

Upon analysis of the crystal structure of the catalytic domain of hMMP-7, it was noted that hMMP-7 bears four tryptophan and eight tyrosine residues. Out of the four tryptophan residues, three were fully exposed and the other one was partially buried. Figure 4.7 shows all the exposed and one partially exposed W residues in hMMP-7.

4.2.4.2. Solid surface representation of the ribbon structure of hMMP-9 showing the distribution of the Typ / Tyr residues

Upon analysis of the crystal structure of the catalytic domain of hMMP-9, eight of

tryptophan residues are present in hMMP-9 with varying degrees of exposure to the aqueous environment. A careful analysis of the catalytic domain shows three tryptophan residues that were partially exposed, with one residue being fully buried in the interior core of the protein. Figure 4.8.A shows the front view of the catalytic domain of hMMP-9. It shows the three partially exposed as well as one of the fully buried W residues. Figure 4.8.B shows the side view of the same protein.
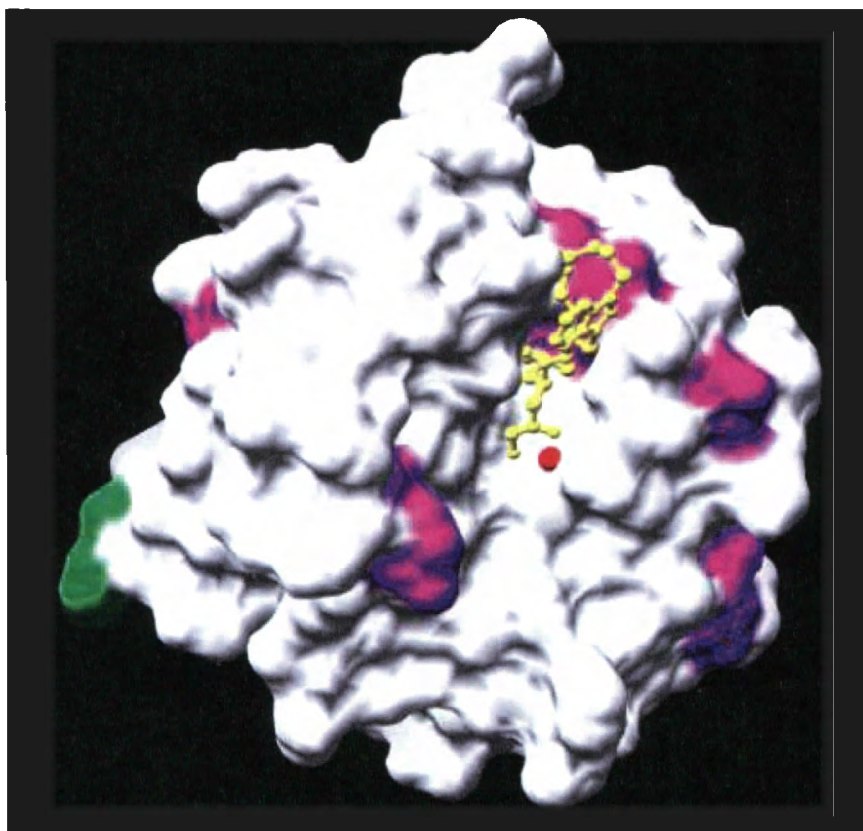
Figure 4.7. Solid surface representation of the ribbon structure of hMMP-7 (1Q3A), showing the tyrosine and tryptophan residues. The highlighted portion in purple indicates the tryptophan residues around the active site. There are 4 tryptophan residues (W), 3 are fully exposed and 1 is partially buried. The red colored ball indicates the catalytic Zn^{2+} ion and the yellow colored ball and stick represents the inhibitor in the active site pocket. The green colored region represents the tyrosine residues. This figure has been developed using UCSF Chimera[R] software [9].
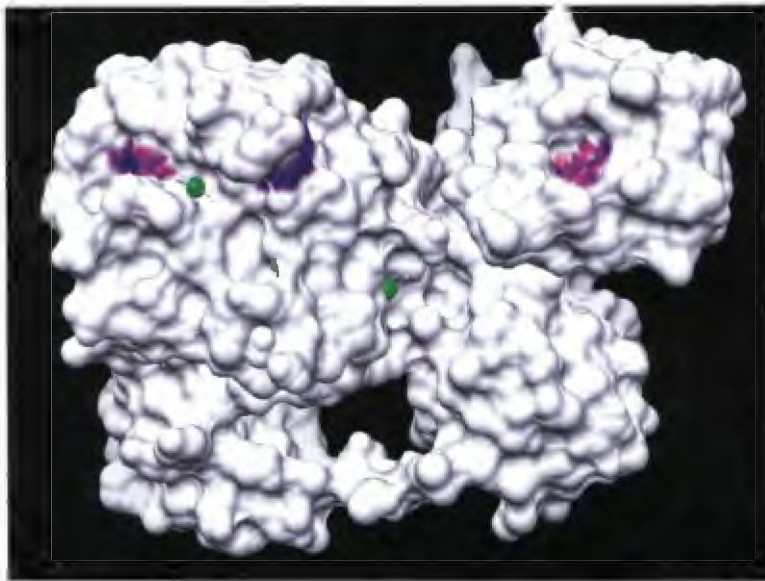
Figure 4.8.A. Solid surface representation of the ribbon structure of hMMP-9 (PDB ID: 1l6j) showing tryptophan residues (frontal view). The highlighted portion in purple indicates the tryptophan residues around the active site. There are 3 are partially exposed and 1 is fully buried tryptophan residues (W). The green colored balls indicate the catalytic Ca^{2+} ions. This figure has been developed using UCSF Chimera® software.
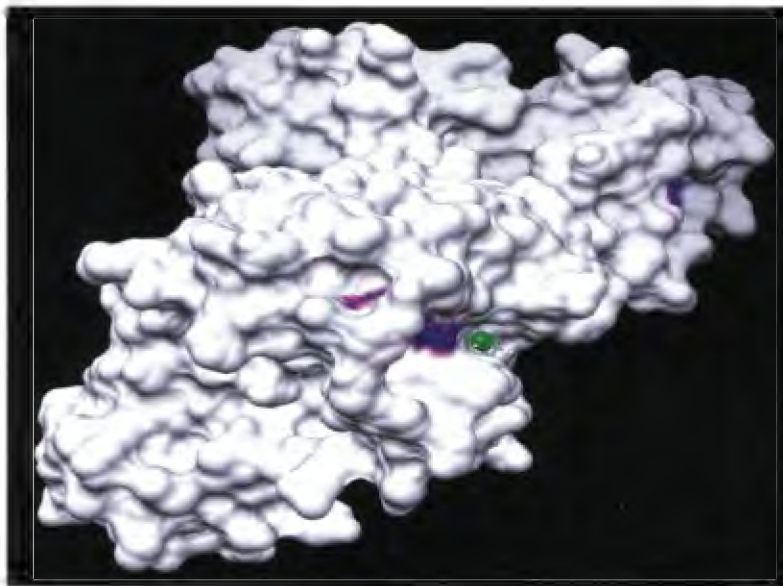
Figure 4.8.B. Solid surface representation of the ribbon structure of hMMP-9 (PDB ID: 1l6j) showing the tryptophan residues (side view). There are 3 are partially exposed (purple colored) and 1 is fully buried tryptophan residues (W). The green colored ball indicates the catalytic Ca^{2+} ion in the active site pocket. This figure has been developed using UCSF Chimera® software.

4.2.4.3. Solid surface representation of the ribbon structure of hMMP-10 showing the distribution of the Typ / Tyr residues

Analysis of the crystal structure of the fibronectin domain and the catalytic domain of hMMP-10 (Figure 4.9) shows that it harbor 8 tryptophan residues with varying degrees of exposure to the aqueous environment. However, two tryptophan residues were found to be fully buried in the analysis of the catalytic domain, while one residue was partially exposed to the interior core of the protein.
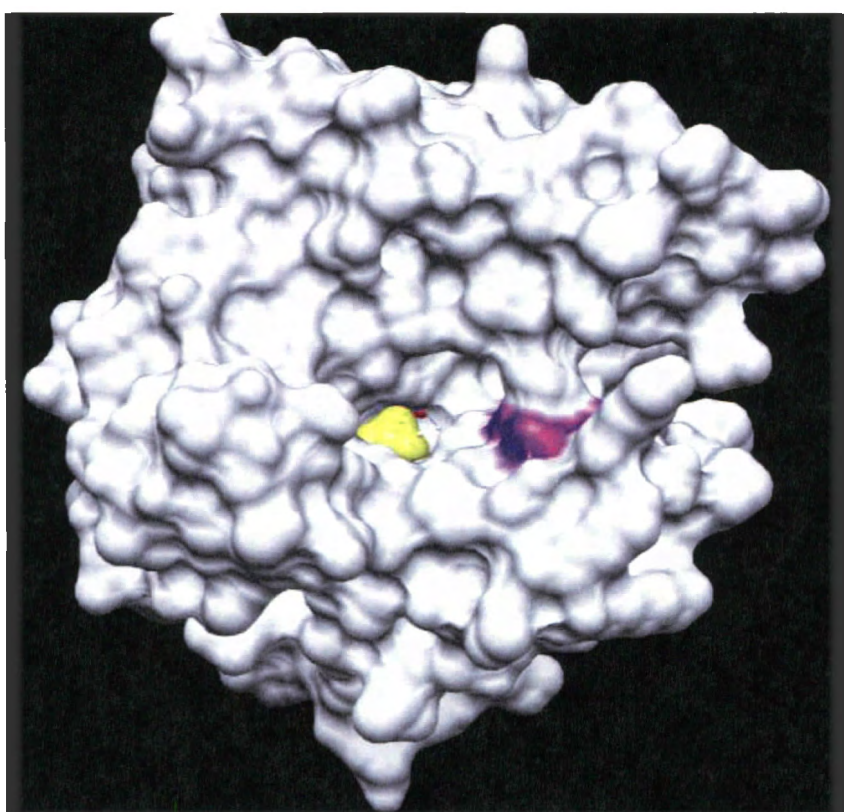
Figure 4.9. Solid surface representation of the ribbon structure of hMMP-10 (PDB: 1jcz) showing the tryptophan residues. The highlighted portion in purple indicates the tryptophan residues around the active site. There are 3 tryptophan residues (W), 2 are buried and 1 is partially exposed. The red colored ball indicates the catalytic Zn^{2+} ion and the yellow colored ball and stick represents the inhibitor in the active site pocket. This figure has been developed using UCSF Chimera[R] software.

4.2.4.4. Steady state experiments for the determination of the kinetic parameters (K_m, V_{max}, K_{cat} and K_{cat} / K_m) for hMMP isozymes

The kinetic parameters that were considered were K_m (affinity for the substrate), V_{max} (maximal velocity of the enzyme), K_{cat} (turn over number of the enzyme) and K_{cat}/K_m (specificity of the enzyme for the substrate) for the three hMMP isozymes. The obvious question asked in this study was what would these kinetic constants add to the understanding of these enzymes?

The value of K_m varies considerably from one enzyme to another. K_m is known as the substrate concentration that results in half-maximal velocity for the enzymatic reaction. K_m also represents the substrate concentration at which half of the active sites in the sample are saturated with the substrate molecules in the steady-state. K_{cat} is referred to as the turnover number of the enzyme. It defines the number of catalytic turnover events that occur per unit time (s^{-1}).

In the laboratory, the turn over number as K_{cat} can be easily determined, by measuring the reaction velocity under conditions [S] $>>$ K_m, so that v (initial rate) equals V_{max} (maximal velocity). But in physiological condition, generally [S] $<<$ K_m is known to exist. In the laboratory, where, [S] $>>$ K_m, the formation of ES complex is rapid and often is not the rate-limiting step. However, *in vivo* condition, where [S] $<<$ K_m mostly exists, the overall reaction may be restricted by diffusion rate of the encountering molecules (i.e. the enzyme and the substrate). Nonetheless, the measurement of K_{cat} (velocity under saturating substrate condition) gives us the most consistent medium of comparing rates of different enzymatic reactions. Changes in K_{cat} indicate the perturbations in the chemical steps

subsequent to the initial substrate binding. Indeed K_{cat} provides the lower limit on the first-order rate constant of the slowest step following substrate binding which eventually leads to product release.

The catalytic efficiency of an enzyme is best defined by the ratio of the kinetic constants; K_{cat}/K_m. The ratio has a second order rate constant and is generally used to compare the efficiencies of different enzymes. It has often been observed that there are large differences in K_{cat} rather than K_m. The only reason being substrate specificity often results from differences in transition states rather than ground state binding interactions. The K_{cat}/K_m ratio is the best measure of substrate specificity.

4.2.4.4.1. Determination of K_m of MCA

To investigate the individual kinetic parameters (like K_m, K_{cat} and K_{cat}/K_m values) of the fluorogenic substrate with the three hMMP isozymes in catalyzing the reaction, at first the standard plot had to be prepared to determine the nmoles of product formed / sec using the fluorogenic substrate. MCA was chosen as the control substrate (commercially available). The progress curves for the hMMP isozymes, i.e. the initial rates were obtained in the units of Flu units/sec ($\Delta F.s^{-1}$). For the construction of the MCA plot, a stock solution of MCA was prepared in 25 mM HEPES, 10 mM $CaCl_2$, pH 7.5. MCA has excitation and emission wavelengths of λ_{ex} = 335 nm and λ_{em} = 395 nm, respectively, with a cutoff filter at 350 nm. The slope of the fluorescence intensity vs. concentration of MCA was then used to convert the initial rates of the catalyzed reaction from Fl units/sec to nM product/sec. Upon analyzing the data, using the linear equation, the slope of the standard MCA plot was found to be 0.11 Flu/nM MCA (Figure 4.10).
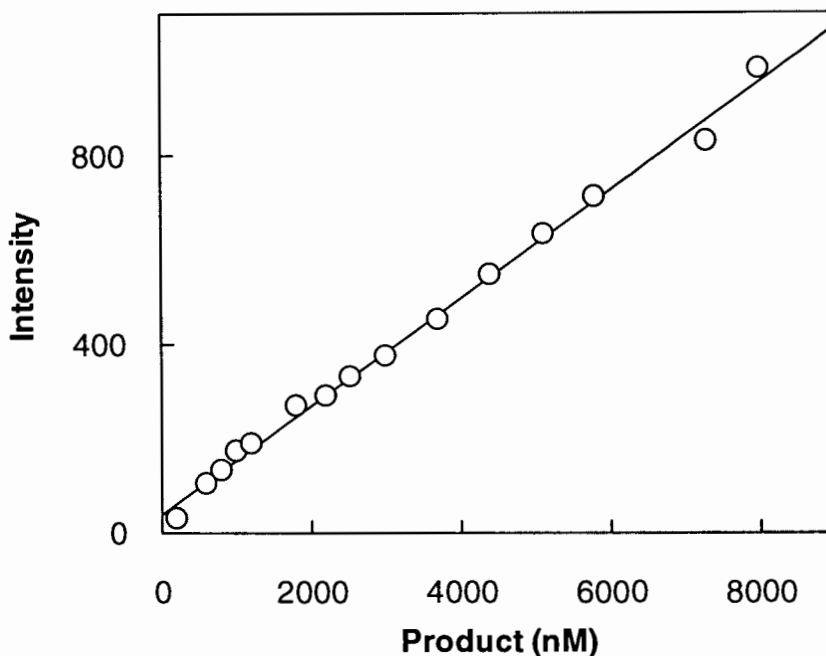
Figure 4.10. The standard plot for MCA. Stock solution of MCA was prepared in 25 mM HEPES, 10 mM CaCl$_2$, pH 7.5. MCA has an excitation and emission wavelength as λ_{ex} = 335 nm and λ_{em} = 395 nm, respectively, with a cutoff filter at 350 nm. The solid smooth line is the best fit of the data by linear regression with slope = 0.11 (Fluorescence units/nM of MCA).

A "unit" of MMP activity can be defined as the amount of enzyme required to convert one micromole (μM) of the substrate to product per min under the standard experimental conditions of buffer and temperature. The enzyme activity was calculated using the given formulae (obtained from Calbiochem, CA):

$$\text{Activity (U/ml)} = \frac{\Delta F * C * V}{F * v} \quad \text{..Eq (4.1)}$$

where ΔF represents the change in flu during peptide hydrolysis/min, C represents the concentration of product used for standard, V indicates the volume of peptide hydrolysis reaction, F represents the Flu at the C used from the standard plot, v indicates the volume of enzyme added.

111

To determine the other kinetic parameters (For example K_m, V_{max}, k_{cat} and K_{cat} / K_m) the initial slopes of the progress curves (Fl units/sec) were recorded and were analyzed using the classic Michaelis-Menten equation (Eq 4.3). The V_{max} values obtained from the plots were represented as Flu units/sec. they were converted into nM product formed /sec for each of the cases and subsequently used in the following equation to obtain the required V_{max} values.

$$K_{cat} = \frac{V_{max}}{[E]_T}$$ ....Eq (4.2)

where K_{cat} is the turn over number for the enzyme, V_{max} is the maximum velocity (rate) obtained by the enzyme and $[E]_T$ is the total concentration of the enzyme available in the reaction. K_{cat} is represented in unit of sec^{-1}. All the data reported herein were analyzed by Grafit Software (version 4.0).

The above kinetic data were expressed as the reactions were initiated by the addition of the enzyme and the initial rates were plotted as a function of substrate concentration. The data were analyzed via the classic Michaelis-Menten equation:

$$v = V_{max} / (1 + K_m / [S])$$ ....Eq (4.3)

where v is the initial rate, K_m is the apparent binding constant of the substrate with the enzyme (represented in µM) and V_{max} is the maximal steady-state rate (represented in µM sec^{-1}). Figure 4.11 shows the Michaelis-Menten hyperbolic plot for hMMP-7 catalyzed hydrolysis of the fluorogenic substrate.

Figure 4.11. The Michaelis-Menten hyperbolic plot for hMMP-7 catalyzed hydrolysis of the fluorogenic substrate in 25 mM HEPES, 10 mM $CaCl_2$, pH 7.5 at 25°C. [hMMP-7] = 300 nM and substrate concentration varied from 1-45 μM. Product formation was measured in arbitrary fluorescence units as a function of time ($\Delta F.s^{-1}$), which was then converted to concentration of MCA released. A MCA standard curve was used for calculating other kinetic parameters. The excitation and emission wavelengths were λ_{ex} = 335 nm and λ_{em} = 395 nm, respectively. The solid smooth line is the best fit of the hMMP-7 data according to the Michaelis Menten equation (Eq 4.3). The K_m was determined to be 10.3 μM.

The data represented in Figure 4.11 can be plotted as 1 / v versus 1 / [S] and can also be analyzed by the linearized Michaelis-Menten equation, which is also known as the Lineweaver–Burk plot (or double reciprocal plot), it can be represented in a simplistic manner as follows:

$$1 / v = K_m / V_{max} * 1 / [S] + 1 / V_{max} \quad \ldots\ldots\ldots\ldots\ldots\ldots\ldots\ldots\ldots\ldots\ldots\ldots\ldots\ldots Eq\ (4.4)$$

where the K_m / V_{max} is given by the slope and $1 / V_{max}$ is given by the y-intercept.

From the data (Figure 4.11), the K_m of hMMP-7 for the commercial fluorogenic substrate could reliably be determined. According to the Michaelis-Menten equation, the K_m was determined to be 10.3 µM. As known in the literature, the K_m has been reported to be 24-26 µM by Knight *et. al.* [10-12]. The reason for the K_m being almost threefold lower than the reported data, it can be rationalized that hMMP-7 was homogenous and of high purity with very high specific activity (Refer to Table 4.1). Moreover, the commercial fluorogenic substrate was specific for MMP-2/MMP-7. Hence, that justifies the low K_m value of hMMP-7 for the fluorogenic substrate.

4.2.4.4.3. Determination of K_m of hMMP-9 for fluorogenic substrate

The condition under which hMMP-9 catalyzed hydrolysis of the fluorogenic substrate were carried out were similar to experimental setup of hMMP-7. Figure 4.12 shows the Michaelis-Menten hyperbolic plot for hMMP-9 catalyzed hydrolysis of the fluorogenic substrate.

According to the Michaelis-Menten equation, the K_m was determined to be 9.2 µM. As known in literature [13], the K_m has been reported to be varying between 15-30 µM. The K_m appears to be similar to the reported data; it simply means that hMMP-9 was very homogenous and of high purity with very high specific activity (Refer to Table 4.2). Even though the commercial fluorogenic substrate was specific for MMP-2/MMP-7, the specificity of hMMP-9 for the substrate was very good, as MMP-2 and MMP-9 both belong to the gelatinase family.
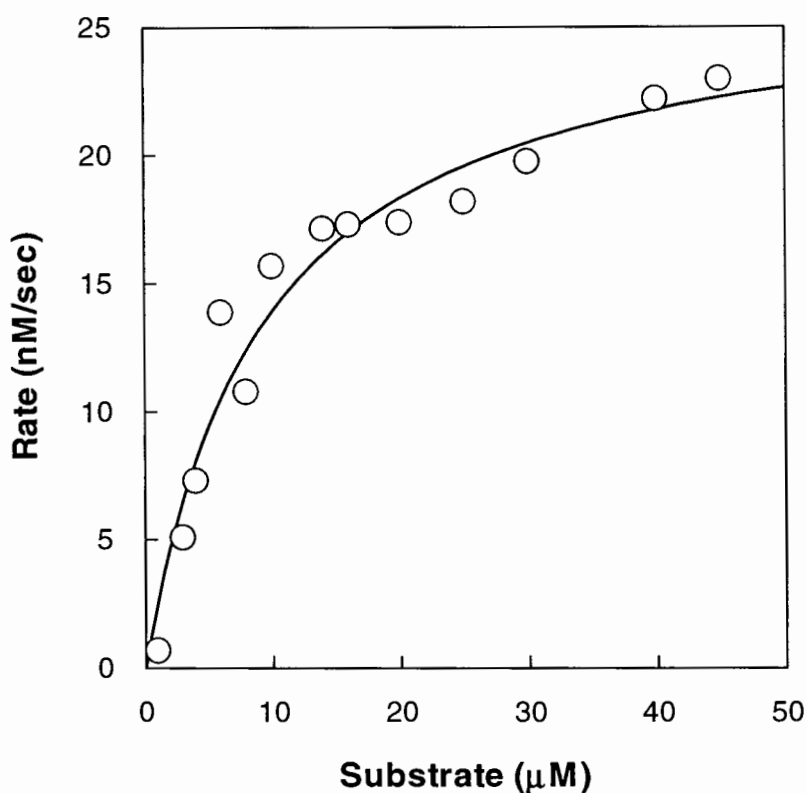
Figure 4.12. The Michaelis-Menten hyperbolic plot for hMMP-9 catalyzed hydrolysis of the fluorogenic substrate in 25 mM HEPES, 10 mM $CaCl_2$, pH 7.5 at 25°C. [hMMP-9] = 160 nM and substrate concentration varied from 1-45 μM. Product formation was measured in arbitrary fluorescence units as a function of time $(\Delta F.s^{-1})$, which was then converted to concentration of MCA released. A MCA standard curve was used in calculation of other kinetic parameters. The excitation and emission wavelengths were λ_{ex} = 335 nm and λ_{em} = 395 nm, respectively. The solid smooth line is the best fit of the hMMP-9 data according to the Michaelis Menten equation (Eq 4.3). The K_m was determined to be 9.2 μM.

The reason for the specificity of hMMP-7 and 9 being so good for this fluorogenic substrate is due to the presence of the conserved residues at the active-site and nature of the active site amongst the hMMP isozymes [14]. Hence, that justifies the low K_m value of hMMP-9 for the fluorogenic substrate.

Figure 4.13 shows the Michaelis-Menten hyperbolic plot for hMMP-10 catalyzed

hydrolysis of the fluorogenic substrate.
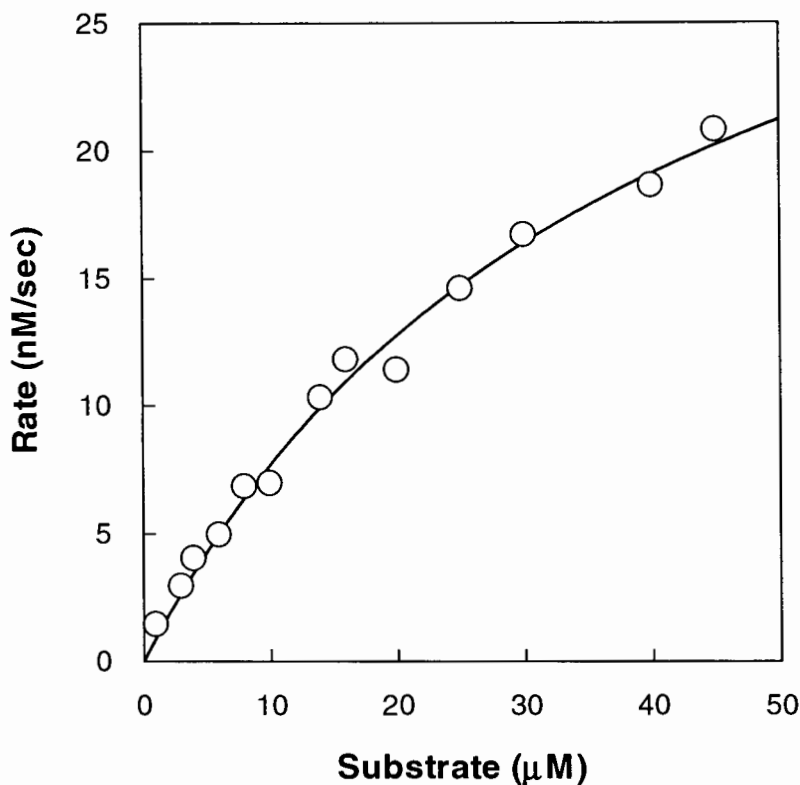
Figure 4.13. The Michaelis-Menten hyperbolic plot for hMMP-10 catalyzed hydrolysis of the fluorogenic substrate in 25 mM HEPES, 10 mM $CaCl_2$, pH 7.5 at 25°C. [hMMP-10] = 2 μM and substrate concentration varied from 1-45 μM. Product formation was measured in arbitrary fluorescence units as a function of time ($\Delta F.s^{-1}$), which was then converted to concentration of MCA released. A MCA standard curve was used in calculation of other kinetic parameters. The excitation and emission wavelengths were λ_{ex} = 335 nm and λ_{em} = 395 nm, respectively. The solid smooth line is the best fit of the hMMP-10 data according to the Michaelis Menten equation (Eq 4.3). The K_m was determined to be 39.3 μM.

These data reliably determine the K_m of hMMP-10 for the commercial fluorogenic

substrate. According to the Michaelis-Menten equation, the K_m was determined to be 39.3

μM. However, it was observed in Figure 4.13, the hMMP-10 catalyzed hydrolysis of this commercial fluorogenic substrate was very slow as compared to hMMP-7 and 9. However, in this case the substrate concentration could not be varied any higher than 45 μM due to two reasons: (a) The highest concentration in a typical experiment chosen should be experimentally reasonable; and (b) If a concentration of substrate higher than 45 μM was used, in this experiment there would be a contribution of an inner filter effect, which would incorporate an additional complexity in the system. A higher K_m value, compared to the other hMMP isozymes used under the same experimental settings, indicates hMMP-10 has less affinity towards the commercial substrate. Moreover, the commercial fluorogenic substrate was specific for MMP-2/MMP-7. Hence, that justifies the high K_m value of hMMP-10 for the fluorogenic substrate as compared to hMMP-7 or 9.

4.2.4.4.5. Determination of K_{cat} of hMMP-7 for fluorogenic substrate

The V_{max} value obtained from Figure 4.11 was converted to nM/sec and used in the Eq 4.2. Eq 4.3 was used to convert the V_{max} into nM/sec, and it was found to be 116.11 nM/sec. Thus, the K_{cat} value could be calculated inserting the values of V_{max} and $[E]_T$ of 116.11 nM/sec and 300 nM, respectively. The K_{cat} value for hMMP-7 for the hydrolysis of the fluorogenic substrate was 0.387 s^{-1}.

4.2.4.4.6. Determination of K_{cat} of hMMP-9 for fluorogenic substrate

The V_{max} value obtained from Figure 4.12 was converted into nM/sec and used in Eq 4.2. The V_{max} obtained from Eq 4.3 was 26.8 nM/sec. Thus, the K_{cat} value could be calculated by using V_{max} and $[E]_T$ values of 26.8 nM/sec and 160 nM, respectively. The K_{cat} value for hMMP-9 towards the hydrolysis of the fluorogenic substrate was 0.17 s^{-1}.

4.2.4.4.7. Determination of K_{cat} of hMMP-10 for fluorogenic substrate

The V_{max} value obtained from Figure 4.13 was converted into nM/sec and used in

Eq 4.2. The V_{max} from Eq 4.3 was 37.92 nM/sec. Thus, the K_{cat} value could be calculated

by using the values of V_{max} and $[E]_T$ of 37.92 nM/sec and 2 μM, respectively. The K_{cat}

value for hMMP-9 towards the hydrolysis of the fluorogenic substrate was 0.019 s^{-1}. The

Summary table (Table 4.4) represents the kinetic parameters for hydrolysis of the

fluorogenic substrate by the MMP isozymes.

Table 4.4. The summary table for the kinetic parameters for hMMP isozymes. The comparison of the kinetic parameters for the commericial fluorogenic substrate hydrolysis by hMMP-7, 9 and 10 at pH 7.5. The kinetic parameters K_m, K_{cat} and K_{cat} /K_m have been reported.

hMMP Isozymes	K_m (μM)	k_{cat} (s^{-1})	k_{cat}/K_m ($M^{-1}s^{-1}$)
hMMP-7	10.3	0.387	38,000
hMMP-9	9.2	0.170	20,000
hMMP-10	39.3	0.019	484

Table 4.4 shows that the K_m values for hMMP-7 and 9 were comparable towards

the commercial fluorogenic substrate, but hMMP-10 shows almost a threefold lower

affinity towards the fluorogenic substrate. The K_{cat} values are highest for hMMP-7

followed by hMMP-9 and lowest for hMMP-10. K_{cat} value indicates the turnover number

of the enzyme for the substrate. It was obvious from Figure 4.13 and also from Table 4.4,

that hMMP-10 bears a very low affinity for the commercial substrate. The K_{cat}/K_m values

are an indication of the substrate specificity of the different hMMP isozymes. hMMP-7 has

a value of 38,000 $M^{-1}.s^{-1}$ and hMMP-9 bears a value of 20,000 $M^{-1}.s^{-1}$; however, the

K_{cat}/K_m value for hMMP-10 has a very low specificity for this particular substrate. The

reported K_{cat}/K_m value for hMMP-7 by Calbiochem (Gibbstown, NJ) were 1.7 x 10^5 M^-

^{1}sec^{-1}, it has been well noted that this result appears to be very similar to the result reported

herein for hMMP-7.

4.3. References

1. Bradford, M.M. (1976). A rapid and sensitive method for the quantitation of microgram quantities of protein utilizing the principle of protein-dye binding, *Anal. Biochem.* 72, 248-254.
2. Dill, K.A. (1990) Dominant forces in protein folding, *Biochemistry.* 29, 7133-7155.
3. Ou, Li., Ma, J., Zheng, X., Chen, X., Li, G., and Wui, H. (2006) The expression and refolding of isotopically labeled recombinant Matrilysin for NMR studies, *Prot. Express. Purif.* 47(2), 367-373.
4. Ye, Qi-Zhuang., Johnson, L.L., Hupe, D.J., and Baragi, V. (1992) Purification and characterization of the human stromelysin catalytic domain expressed in *Escherichia coli, Biochemistry.* 31, 11231-11235.
5. Lauer-Fields, J.L., Juska, D., and Fields, G.B. (2002) Matrix metalloproteinases and collagen catabolism, *Biopolymers (Pep. Sci).* 66, 19-32.
6. Cheng, D., Shen, Q., Nan, F., Qian, Z. and Ye, Q. (2003) Purification and characterization of catalytic domains of gelatinase A with or without fibronectin insert for high-throughput inhibitor screening. *Prot. Expr. Purif.* 27, 63-74.
7. Harrison, R.K., Chang, B., Niedzwiecki, L., and Stein, R.L. (1992) Mechanistic studies on the human matrix metalloproteinase stromelysin, *Biochemistry.* 31, 10757-10762.
8. Protein Data Bank http://www.pdb.org.
9. T.E. (2004) UCSF Chimera--a visualization system for exploratory research and analysis, *J. Comput. Chem.* 25, 1605-1612.
10. Knight, C.G., Willenbrock, F. and Murphy, G. (1992). A novel coumarin-labelled peptide for sensitive continuous assays of the matrix metalloproteinases. *FEBS Lett.* 296, 263-266.
11. Neumann, U., Kubota, H., Frei, K., Ganu, V. and Leppert, D. (2004) Characterization of Mca-Lys-Pro-Leu-Gly-Leu-Dpa-Ala-Arg-NH2, a fluorogenic substrate with increased specificity constants for collagenases and tumor necrosis factor converting enzyme, *Anal. Biochem.* 328, 166-173.
12. Welch, A.R., Holman, C.M., Browner, M.F., Gehring, M.R., Kan, Chen-Chen., and Van Wart, H.E. (1995) Purification of human matrilysin produced in Escherichia coli and characterization using a new optimized fluorogenic peptide substrate, *Arch. Biochem.* 324 (1), 59-64.
13. Shingleton, W.D., Hodges, D.J., Brick, P. and Cawston, T.E. (1996) Collagenase: a key enzyme in collagen turnover, *Biochem.Cell.Biol.* 74, 759-775.
14. Bode, W., Catalan, C. F., Tschesche, H., Grams, F., Nagase, H., and Maskos, K. (1999) Structural properties of matrix metalloproteinases, *Cell. Mol. Life. Sci.* 55, 639-652.

CHAPTER 5. RELATIONSHIP BETWEEN "RIGID" AND "FLEXIBLE" SURFACES ON THE DIFFERENTIAL MODULATION OF FUNCTIONAL AND STRUCTURAL CHARACTERISTICS OF MATRILYSIN (hMMP-7)

5.1. Introduction

The transformation of normal cells to cancerous cells accompanies a wide range of changes in the macro-molecular components of the cell [1]. Some of these changes involve expression of a new class of enzymes and proteins that interact differently with their cognate partners. For example, there are changes in lipid structures, metabolic processes, and gene expression [2-3]. Electrostatic interactions serve as one of the important mediators of macromolecular interactions, such as observed with proteins, protein-lipid, and protein–nucleic acid complexes [4-6]. Understanding of the electrostatic forces in aqueous solution, which control chemical processes and give rise to biological structure, is essential for a variety of biotechnological applications, ranging from chemical synthesis to unraveling the physiological processes involved in drug design, signal transduction, protein folding, localization, and function related to health and disease [7-9].

5.1.1. Use of LNPs as biosensors and as a diagnostic tool

Over the past several years, sensitive, selective, and convenient methods have been sought to detect proteins in physiological systems [10]. However, protein detection is a challenging problem due to protein structural diversity as well as the inability to selectively interact with their putative ligand molecules. Several physiological processes are mediated through protein-lipid interactions, and the molecular mechanisms by which such interactions regulate the cellular function is of considerable interest and importance from the point-of-view of developing a wide range of biotechnological applications [11].

The mechanistic studies on protein-lipid interactions have been customarily pursued using liposomes as the representative lipid nanoparticles (LNP). Apart from lipid nanoparticles, protein detection and desensitizations have recently been pursued using differently decorated gold nanoparticles (Au-NPs) and quantum dots (QDs) [12-14]. Due to the size-and-shape-controlled architecture of these metallic nanoparticles (NPs), detection and desensitization of protein biomarkers of many diseases have been facilitated [8]. Besides their growth and proliferation, cancer cells also have the potential to dislodge from their residual tissues and migrate to other organs and start proliferating [15]. These "metastatic" processes are accomplished through a series of biochemical reactions including disruption of extracellular matrix proteins [16].

5.1.2. Patho-physiological roles of MMPs

The level of extracellular matrix (ECM) assembly is dynamically controlled physiologically by synthesis of individual components (such as collagens, elastin, etc.) and degradation by matrix metalloproteinases (MMPs). Under normal conditions, these processes are well "coordinated" but during metastasis, several MMPs are over-expressed, and their increased levels can be indicative markers of a variety of cancers [17-18]. Amongst the 26 members of the MMPs family, unlike most MMPs [17-19], which are involved in both normal physiological as well as pathological processes, matrilysin (MMP-7) has been ascribed to be primarily involved in the inflammatory diseases and cancers, although some physiological roles of this enzyme have also been alluded to in the literature [20]. Hence, it appears likely that MMP-7 is representative of the "true" pathological enzyme of the matrix types of human diseases [21].

Despite its well recognized patho-physiological roles, MMP-7 has not been rigorously investigated from the point-of-view of its structural-functional and mechanistic features. Although MMP-7 is structurally the simplest and smallest enzyme of the MMP family [22], it poseses certain experimental challenges, including increasing the yield and stability of the enzyme and characterizing the structure of the enzyme. Since MMP-7 preferentially cleaves some of the non-ECM substrates [23-24], which are confined to the cell membrane (e.g., E-cadherin, TNF-α, Fas ligand, insulin-like growth factors), its confinement to the biological membrane has been sporadically considered [24].

One of the interesting features of MMP-7 is its electrostatic surface potentials, exhibiting somewhat bipolar distribution of the positive and negative charges in the vicinity of the active-site pocket and on the opposite end of the protein structure [25]. Hence, it was very interesting to investigate the influence of cationic surface binding groups on the catalytic properties of the enzyme.

These studies are important from the point-of-view of the regulation of MMP-7 by electrostatic interactions with its cognate partners in an aqueous solvent. Toward this goal, polylysine (PLL) and cationic gold nano-particles (Au-CNP) were utilized as representative surface binding groups. With the long term goal of desensitizing and alleviating the onset of carcinogenesis and metastasis, the structural and functional consequences of interactions of hMMP-7 with different surface types of cationic macro-clusters is very interesting. In this endeavor, besides utilizing a charged homo-polypeptide system like PLL (representative of a "flexible" surface), and cationic Au-NPs (representative of a "rigid" surface) were utelized. The objective was to probe the degree to which the catalytic and

structural features of hMMP-7 changed in the presence of either rigid or flexible charged surfaces. It was observed that in addition to the charges, flexibility as well as surface curvatures of the different types of charged surfaces (rigid or flexible) modulated the structural-functional characteristics of hMMP-7.

5.2. Results and Discussion

To probe the influence of cationic macro-clusters on hMMP-7 catalyzed reaction, polylysine (PLL) and cationic gold nanoparticles (Au-CNP) were selected as representative examples. These cationic macro-structures were expected to serve as "soft" (flexible) and "rigid" (hard) ligands, respectively, and thus had the potential to exhibit their entropic advantage/disadvantage upon binding with the enzyme.

Figure 5.1.A shows the structure of the differently functionalized gold nano particles (Au-NPs). Dr. Vincent Rotello's laboratory (Department of Chemistry at University of Massachusetts at Amherst) provided the cationic Au-NPs. Figure 5.1.B shows the schematic diagram of the cationic gold nanoparticle (Au-CNP). Figure 5.2 shows the monomer structure of cationic macro-cluster of PLL.
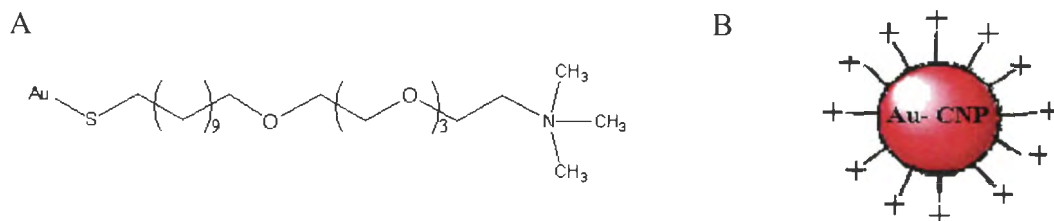
Figure 5.1.A. Structure of the cationic gold Nanoparticles. B. Schematic diagram of cationic Nanoparticle (Au-CNP).
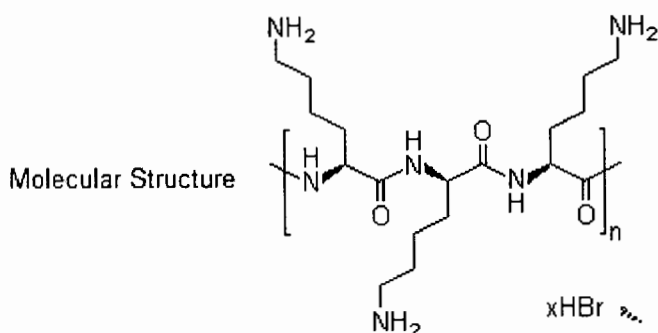
Figure 5.2. Monomer structure of the Polylysine (PLL).

Figure 5.3 shows the effect of increasing the concentration of PLL on the hMMP-7 catalyzed cleavage of a fluorogenic substrate (see Materials and Methods) in 25 mM HEPES, 10 mM $CaCl_2$, pH 7.5. The initial rate of the enzymatic reaction was determined by monitoring the time dependent formation of the fluorophoric reaction product at 395 nm (λ_{ex} = 335 nm). Note, that as the concentration of PLL increased, the rate of the hMMP-7 catalyzed reaction initially increased, attained a maximum value, and then started decreasing. Evidently, PLL served both as an activator and as an inhibitor at low and high concentrations, respectively. Interestingly, the magnitude of activation was not trivial; it was about 25% higher than the activity of the enzyme in the absence of the ligand. Interestingly, the concentration of PLL required to attain the maximum activity of hMMP-7, was equal to the concentration of the enzyme. Hence, the PLL mediated activation occurred at the stoichiometric ratio of 1:1. There have been many precedents in the literature of PLL having two modes of binding site for ligands [26-28]. The charged homo-polypeptide of PLL can attain several secondary structural conformational states leading to two distinct binding sites [28].

124
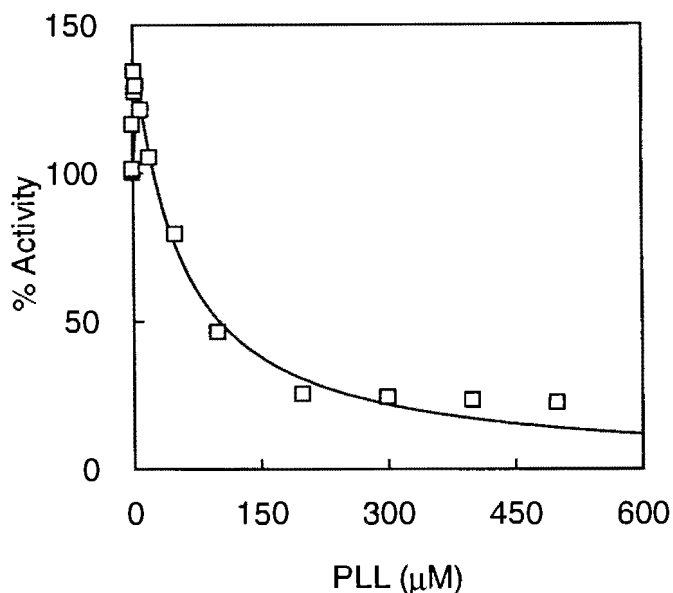
Figure 5.3. Effect of PLL on enzyme activity of hMMP-7. Activation of hMMP-7 activity at stoichiometric concentration of PLL (0.3 μM) followed by inhibition at higher concentration of PLL (ranging from 10 μM – 450 μM). The initial rates of the enzyme catalyzed hydrolysis of Fluorogenic substrate were measured as a function of the Ligand concentrations. [hMMP-7] = 0.3 μM, [S] = 25 μM. The solid smooth line is the best fit of the experimental data according to Eq 1.1 for the K_i values of K_1 (activation constant) and K_2 (inhibition constant). K_1 and K_2 values are 0.34 ± 0.2 μM and 2.4 ± 0.04 μM, respectively.

In the absence of any definitive model for the activation and inhibition data of Figure 5.3, a general equation [29] was resorted to analyze them by using the following format (Eq 5.1).

$$V = \frac{B_0 + B_1[L]}{1 + A_1[L] + A_2[L]^2}$$ ....(Eq 5.1)

Where B and A are the macroscopic constants pertaining to the catalytic and binding features of the enzyme, and L represents the concentration of PLL. B_0 refers to the enzyme activity in the absence of any ligand. For the microscopic 2-step model (containing one activation and one inhibition site) the activation constant (K_1) and inhibition constant (K_2) for the binding of ligand to first and second sites will be equal to $1/A_1$ and A_1/A_2, respecti-

vely. The solid line on Figure 5.3 shows the non-linear regression analysis of the data according to Eq 5.1 with the magnitudes of B_1, A_1, and A_2 being equal to 476.66, 3.26, and 0.06, respectively. It resulted in Activation constant (K_1) and Inhibition constant (K_2) for the binding of ligand to be 0.34 ± 0.2 μM and 2.4 ± 0.04 μM, respectively.

To probe the generality or specificity of PLL-dependent activation and inhibition of hMMP-7, a similar experiment in the presence of increasing concentrations of Au-CNP (Figure 5.4) was carried out.
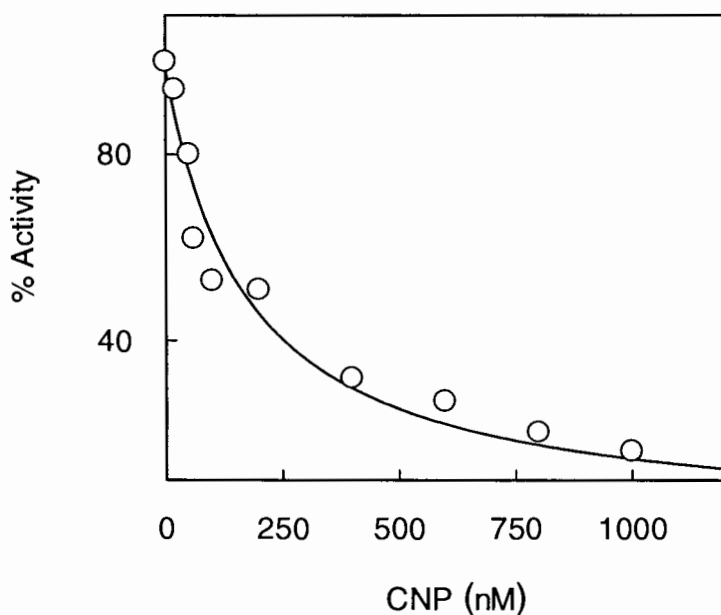
Figure 5.4. Effect of Au-CNP on enzyme activity of hMMP-7. Higher concentration of Au-CNP (1 μM) inhibits the enzyme activity of hMMP-7. The initial rates of the enzyme catalyzed hydrolysis of fluorogenic substrate were measured as a function of the Ligand concentrations. [hMMP-7] = 0.3 μM, [S] = 25 μM. IC_{50} value for Au-CNP was obtained by fitting by Eq. 1.2 and found to be 0.173 ± 0.030 μM; the solid smooth line represents the trend of the data points.

In contrast to PLL, Au-CNP molecules were conceived to be non-flexible (i.e. "rigid") ligands. Hence, if the surface charges were the only determinants for inhibiting hMMP-7, both PLL and Au-CNP would be expected to yield an identical result. On the

126

other hand, if the surface curvature and/or rigidity of cationic macro-clusters exhibited additive functions in inhibiting hMMP-7, these cationic macro-clustered ligands would behave differently even when they carried identical charges.

To this end, the effect of Au-CNP on the catalytic activity of hMMP-7 under the same conditions used for cationic PLL mediated inhibition was investigated. Figure 5.4 shows the inhibition of the hMMP-7 catalyzed reaction using an increasing concentration of Au-CNP. Note that unlike PLL, Au-CNP inhibits the hMMP-7 catalyzed reaction at low concentrations of Au-CNP. The solid smooth line is the best fit for the data where the IC_{50} value is 0.173 ± 0.030 µM.

$$y = \frac{100\%}{\left(1 + \frac{(x)}{IC_{50}}\right)^s}$$ .... (Eq 5.2)

Where, Eq 5.2 fits inhibition data to a two parameter equation, with the lower and upper limits of the background corrected as being equal to 0 and 100, respectively. The slope factor is 1.

The experimentally determined IC_{50} values were ascribed (from the data of Figure 5.4) to the inhibitory potency of PLL (Figure 5.3). On comparing the IC_{50} value of the above Au-CNP with the K_i value of the cationic PLL ("K_2 value" – Inhibitory constant), it is apparent that the former was more potent in inhibiting hMMP-7 than the latter. The origin of the above difference is likely to partly lie in the "rigidity" as well as the surface curvature of Au-CNP as compared to the cationic PLL. It has been suspected that PLL and Au-CNP would differently modulate the ionic micro-environment of the enzyme's active

site small pocket (via long range interaction), and such a feature is likely to be manifested by the "rigidity" and "flexibility" of these cationic macro-clusters.

At this point, it becomes very important to investigate why the similarly charged cationic macro-clusters of macro molecules (PLL and Au-CNP) differentially affect the micro-environment of the hMMP-7 active site. To probe more into this interesting feature of whether the binding of PLL to hMMP-7 causes CD spectral changes in the far UV region (arising from the secondary structural changes); a study was conducted to determine the CD spectra of hMMP-7 in the presence of increasing concentrations of cationic PLL. As shown in Figure 5.5, hMMP-7 showed a broad negative elliptical peak in the 245 nm to 200 nm region, which is primarily dominated by the β-sheet structure of the protein. The magnitude of negative helicity increased with the concomitant emergence of double peaks at 222 nm and 219 nm (characteristics of α-helical structure) as the concentration of PLL increased. It was interesting to note that maximal helicity was obtained when the concentration of PLL became nearly ten-fold higher than the concentration of hMMP-7 during the course of titration. Moreover, from Figure 5.3, it was very evident that the highest activity in hMMP-7 was observed at stoichiometric concentration of PLL; however, in the CD signal the magnitude of negative helicity of hMMP-7 diminished only after reaching ten-fold stoichiometric concentration of PLL. This suggests that the secondary structural changes are much slower, and it takes super stoichiometric concentrations of PLL to drastically exhibit the change (α-helical population to random coil conformation).

These data initially led to the conclusion that the PLL-mediated activation of hMMP-7 was due to the marked secondary structural changes (from predominantly β-

sheet to α-helix) in hMMP-7. But it was soon realized that a significant fraction of CD signal was originating due to the conversion of PLL from the random coil structure to a helical structure upon binding with the negatively charged surface of hMMP-7 at physiological pH. This was confirmed by taking the CD spectra of PLL in the presence of negatively charged gold nanoparticles (Au-ANP) as well as in a buffer solution of pH 11.0. In both these cases, the diminution of positive charges from the ε-NH$_2$ group of lysine residues resulted in the transformation of the random coil of PLL to α-helix. Since changes in CD signals were observed upon the binding of PLL to Au-ANP, it was concluded that the data of Figure 5.5 contain an elliptical contribution from both hMMP-7 and PLL, and it was difficult to segregate their individual contributions. Irrespectively, the formation of the helical content in PLL (in the presence of hMMP-7) attests to their physical interactions, and such interactions are electrostatically mediated via complementary positive and negative charges of PLL and hMMP-7, respectively.

PLL at neutral pH is known to exist as a disordered random coil due to unfavorable charge–charge repulsions operative among the charged side-chain groups of lysine residues [30]. Consequently, an increase in the repulsive forces may favor the backbone to conform to a random coil rather than a helical conformation. The interactions between the –NH– and the –CO– groups in the backbone of the polypeptide chain constitute the attractive forces.

At pH 7.5, PLL exists in a random coil conformation; the repulsive forces among the charged side-chain groups of the homo polypeptide appear to dominate over the attractive forces. However, in the presence of hMMP-7 the dielectric constant of the

medium decreases, the attraction forces among the backbone –NH– and –CO– groups seem to supercede the repulsive forces among the charged side chains, and thus, finally resulting in the transformation of the backbone of the charged PLL from a random coil to the α-helix conformation.

At pH 11.0, PLL is known to exist in α-helical conformation, as the side-chain ε-amino groups of PLL are expected to be uncharged at this pH. The attractive forces among the –NH– and –CO– groups of the backbone are expected to be strengthened resulting in the induction of helical conformation. At this juncture, it appears that it is difficult to offer a concrete explanation for the destabilization of the helical conformation, but it is likely that a very high concentration of PLL propels a condition commonly referred as "over-crowding" [31]. Overcrowding eventually leads to the disorganization of the induced helical conformation to a random coil when the interactions between the exposed amide groups in the polypeptide and bulk water molecules get strengthened. The promotion of the "inter-hydrogen bonds" and destabilization of "intra-hydrogen bonds" among the backbone –NH– and –CO– groups of the homo polymer were also likely to be stabilized. Such an action could indirectly explain the increased stability or fresh induction of a β-sheet transitory conformation and finally stabilizing a loose structure of random coil.

It was further probed whether incubation of hMMP-7 with Au-CNP resulted in changes in the secondary structure of the protein using Circular Dichroism spectroscopy. Figure 5.6 shows the changes in the molar ellipticity of hMMP-7 as a function of increasing concentration of Au-CNP. Note that as the concentration of Au-CNP increases, the amplitude of the α-helical peak (at 222 nm) of hMMP-7 decreases, suggesting that the

enzyme gradually loses its secondary structure, which can be easily ascribed to the Au-CNP mediated denaturation of the enzyme.
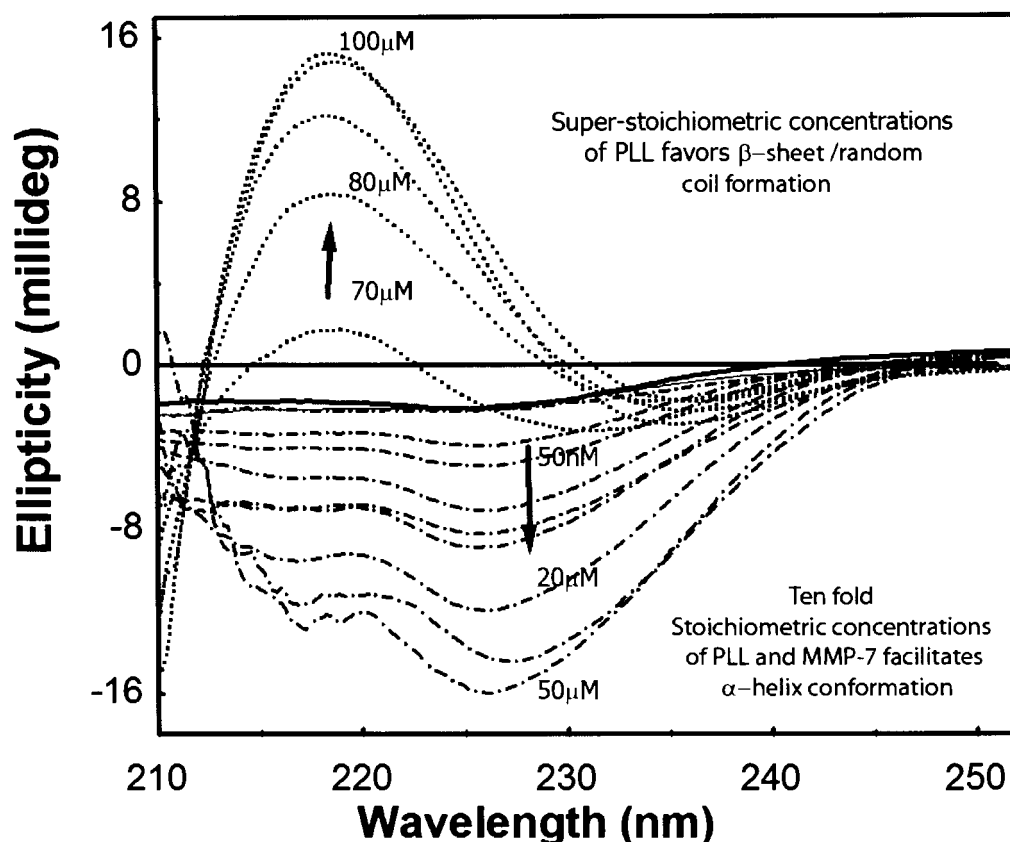
Figure 5.5. Conformational changes in hMMP-7 upon binding to PLL. The binding of polylysine to hMMP-7 was detected by the Circular Dichroism System (Jasco J-815 spectropolarimeter) with spectral changes in the far UV region (250-200 nm) in the presence of increasing concentrations of polylysine. The negative elliptical peak in the 240 to 200 nm region was predominantly β-sheet structure. But with increasing concentration of polylysine (0 - 100 μM), there is an enhancement in the double peak at 222 and 210 nm. Interestingly, the maximal ellipticity was observed at the concentration of hMMP-7 and polylysine being 5 μM of hMMP-7, and 50 μM of PLL. The solid bold line (−) indicates the CD spectra of 5 μM hMMP-7 and the dotted line (...) indicates the spectra of hMMP-7 and PLL complex as a function of increasing concentration of PLL. Until the ten-fold stoichiometric concentration of PLL to hMMP-7 was reached, the negative helicity gradually increased. Upon reaching the super-stoichiometric concentration, the CD signal above 60 μM of PLL (inhibitory concentration) gave positive spectra at 219 nm.
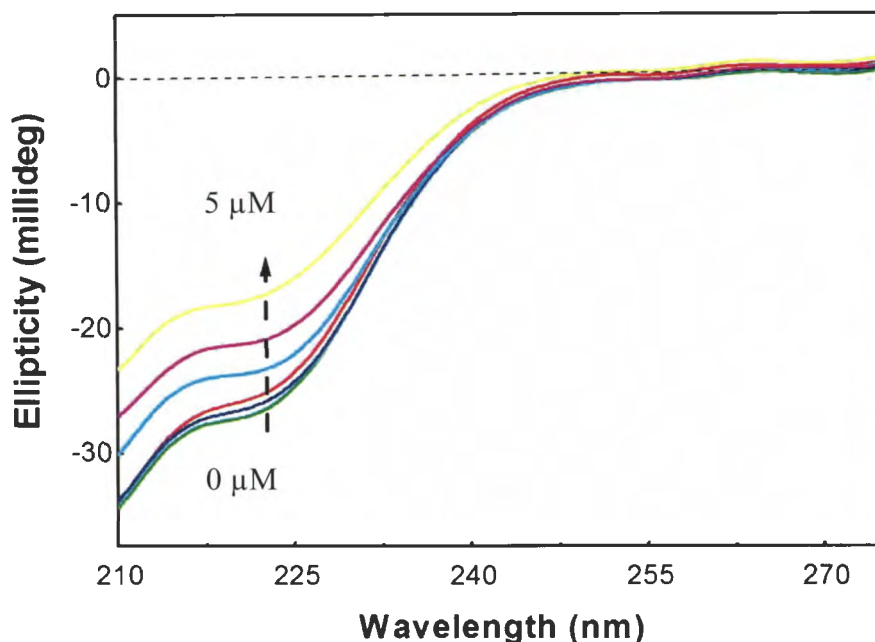
Figure 5.6. Conformational changes in hMMP-7 upon binding to Au-CNP. hMMP-7 undergoes denaturation upon interacting with Au-CNP. CD spectra of hMMP-7 in the presence of increasing concentrations of Au-CNP. The experiment was performed in 5 mM phosphate buffer, pH 7.5 between 210–270 nm region using a Jasco J-815 spectropolarimeter. The concentration of Au-CNP varied from 0-5 μM. The solid green line indicates the CD spectra of 50 μM hMMP-7 alone. The increasing concentration of Au-CNP results in the decrease in the magnitude of the negative ellipticity as shown by the vertical arrow.

However, the amplitude of the α-helical peak (at 222 nm) of hMMP-7 diminished when hMMP-7 was titrated systematically with super stoichiometric concentrations of PLL (Figure 5.5) indicating the collapse of the stable structure and a concomitant increase in the positive peak (at 205 nm). These data are further supportive of the fact that apart from charge [32], the rigidity/flexibility [33] and the surface curvature [34] of the cationic Au-NPs modulates the structural features of hMMP-7.

It was also contemplated whether or not the observed inhibition of hMMP-7 at high concentrations of cationic macro-clusters like PLL was due to denaturation of the enzyme.

To ascertain this, hMMP-7 (11 μM) and PLL (10.7 μM) were incubated for 10 minutes, and a 7 μl aliquot was withdrawn and transferred to the reaction mixture (total volume = 0.25ml) cuvette for measuring the enzyme activity. In this way, the concentration of PLL in the reaction mixture was reduced to 0.3 μM (similar to that required for the full activation of the enzyme). The experimental data revealed (Figure 5.7.A) that the above dilution restored the enzyme activity to the level (even after Pre-incubation), initially observed in the presence of 0.3 μM PLL when instantly mixed. Similar results were observed when 8 μM hMMP-7 and PLL (1.25 mM) were incubated for different time intervals, and 10 μl aliquots were withdrawn and transferred to the reaction mixture (total volume = 0.25 ml) cuvette for measuring the enzyme activity. The concentration of PLL in the reaction mixture was 50 μM (similar to that condition where only 45% activation of the enzyme remained when instantly mixed). A control experiment was performed in the absence of PLL.

The black line represents the progress curve for hMMP-7 alone (0.3 μM), the green line represents the hMMP-7 + PLL (0.3 μM) Set 1(Pre-Incubation), the red line represents the hMMP-7 + PLL (0.3 μM) Set 2 (No Pre-Incubation), the blue line represents hMMP-7 (0.3 μM) + PLL (50 μM) Set 1 (Pre-Incubation), and the pink line represents hMMP-7 (0.3 μM) + PLL (50 μM) Set 2 (No- Pre-Incubation), respectively. Figure 5.7.A shows the enzyme catalyzed reaction progress curves under three different conditions. The black line represents the progress curve for hMMP-7 alone (0.3 μM), the green line represents the hMMP-7 + PLL (0.3 μM) Pre-Incubation, and the pink line represents hMMP-7 (0.3 μM) +

PLL (50 μM) No-Pre-Incubation respectively. The slopes of progress curves are designated

by black line (------), green line (----), and the pink line (----) for comparison.
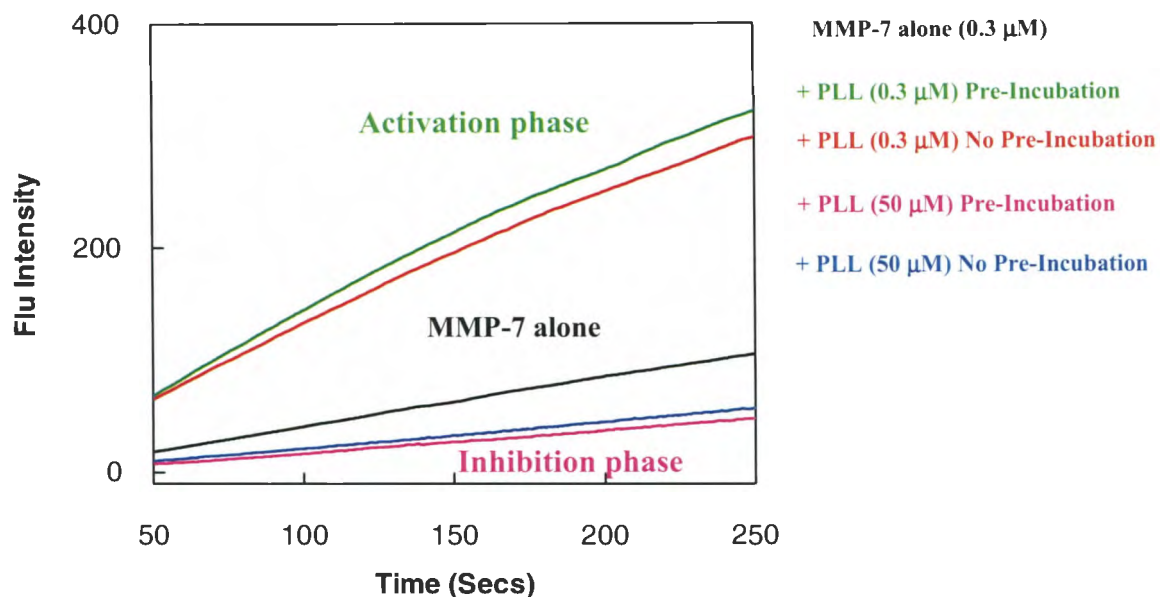
Figure 5.7.A. Inhibition or inactivation of hMMP-7 with PLL. hMMP-7 binds to PLL reversibly. The enzymatic activity of hMMP-7, maintained at 0.3 μM in the reaction mixture was monitored by measuring the initial rate of the hMMP-7 catalyzed reaction using fluorogenic peptide of the following composition: MCA-Pro-Leu-Gly-Leu-Dpa-Ala-Arg-NH_2 [Where MCA and Dpa stand for (7-Methoxycoumarin-4-yl)acetyl and N-3-(2,4-dinitrophenyl)-L-2,3-diaminopropionyl, respectively] while maintaining the excitation and emission wavelengths of 335 nm and 395 nm, respectively. The time course of the reaction was monitored for about 250 secs.

The slopes ($\Delta F.s^{-1}$) of the progress curves calculated for the above data were 0.44 (black line), 1.32 (green line), and 0.198 (pink line). Clearly, the activation and inhibition feature of hMMP-7 by PLL (at stoichiometric and super-stoichiometric concentrations) was fully reversible, and thus the inhibitory phase of Figure 5.3 was not due to inactivation of the enzyme. Similarly, to ascertain whether the inhibition exhibited by Au-CNP was a true inhibition phenomenon and not due to partial inactivation of the enzyme, the following experiment was performed (Figure 5.7.B). The enzyme hMMP-7 (~ 8 μM) and Au-CNP

(2.1 µM) were pre-incubated for different time intervals and 6 µl aliquots were withdrawn

and transferred to the reaction mixture for measuring the enzyme activity.
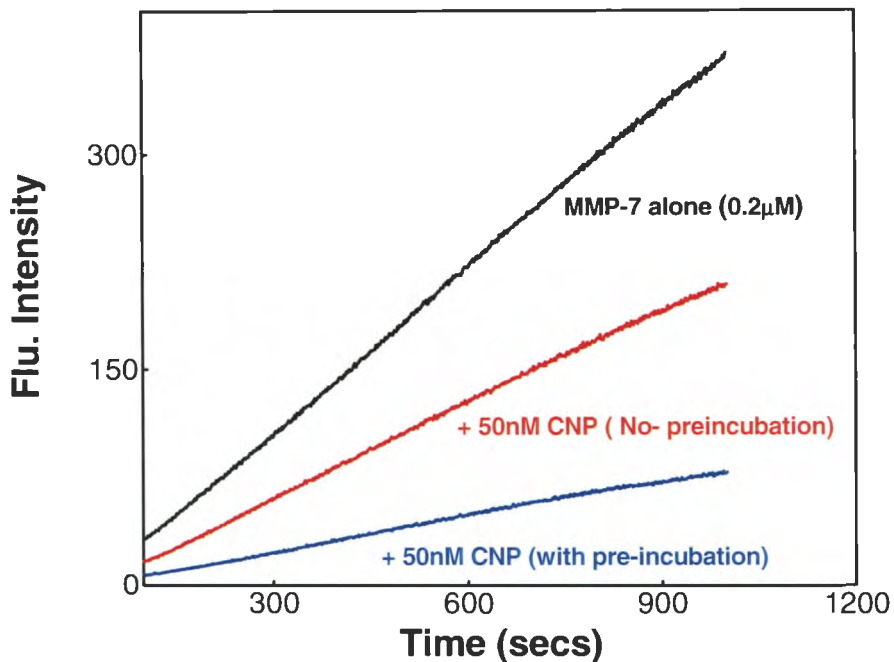
Figure 5.7.B. Inhibition versus inactivation of hMMP-7 by Au-CNP. The time course of the hMMP-7 catalyzed reaction in the presence of Au-CNP is shown. A control experiment was performed in the absence of Au-CNP. The time course of the reaction was monitored for about 1000 sec. Other conditions are the same as in Figure 24 A. The black solid line, the red solid line and the blue solid line indicate the progress curves of hMMP-7 alone, hMMP-7 with 0.050 µM Au-CNP (0 time incubation) and hMMP-7 (10 minutes pre-incubation time), respectively. The slopes ($\Delta F.s^{-1}$) of the progress curves were calculated for the above data 0.38 (black line), 0.28 (red line), and 0.087 (blue line). Note that the incubation of hMMP-7 with Au-CNP for 10 minutes resulted in an additional 70% loss in the enzyme activity.

A control experiment was performed in absence of Au-CNP. Figure 5.7.B shows

the enzyme catalyzed reaction progress curves under three different conditions: control

(Black line); incubation with Au-CNP for 0 time (Red line); and 10 minutes (Blue line).

The rates of reactions (slopes) under the above conditions for the black (----), red (----), and

the blue (----) lines were determined to be 0.38, 0.28, and 0.087 $\Delta F.s^{-1}$, respectively.

On comparison of these reaction rates it was apparent that when the enzyme was pre-incubated with Au-CNP for 10 minutes, and an aliquot was transferred to the reaction mixture (such that hMMP-7 and Au-CNP concentrations were similar to those utilized in the 0 time incubation experiment; red line), the enzyme's activity was impaired by 70%. Hence, besides Au-CNP dependent inhibition of hMMP-7 (compare the slopes of the control and 0 time incubation experiments), the former inactivates the enzyme in a time dependent manner. It should be emphasized that such a slow denaturation process was not observed in presence of inhibitory concentrations of cationic PLL (Figure 5.7.A).

Scheme 5.1 shows the proposed mechanism for the differential influence of cationic Au-NP and PLL on the structural-functional features of hMMP-7. The negative electrostatic potentials in the vicinity of the active-site pocket of the enzyme have been shown to form favorable contacts with both cationic PLL as well as Au-CNP.

However, due to a marked difference in the rigidity as well as the dimension (in the form of surface curvature) of PLL (being a flexible, meshy and fluffy network) and Au-CNP (rigid spheres of 2.0 nm diameters), the latter induces a change in the enzyme conformation and thus leads to the partial denaturation of the protein. Hence, Au-CNP causes both inhibition (due to complementary electrostatic interaction at the active-site pocket) as well as inactivation of the enzyme. On the other hand, the lack of an extensive surface curvature coupled with the flexibility of the meshy network of PLL, it was surmised that the cationic macro-cluster of PLL only elicits the activation and inhibitory influence on the hMMP-7 catalyzed reaction. Although this is the first demonstration of the influence of rigid versus flexible cationic macro-clusters on the catalytic and structural

features of hMMP-7, there are literature precedents of this type of findings with other proteins [35-38].
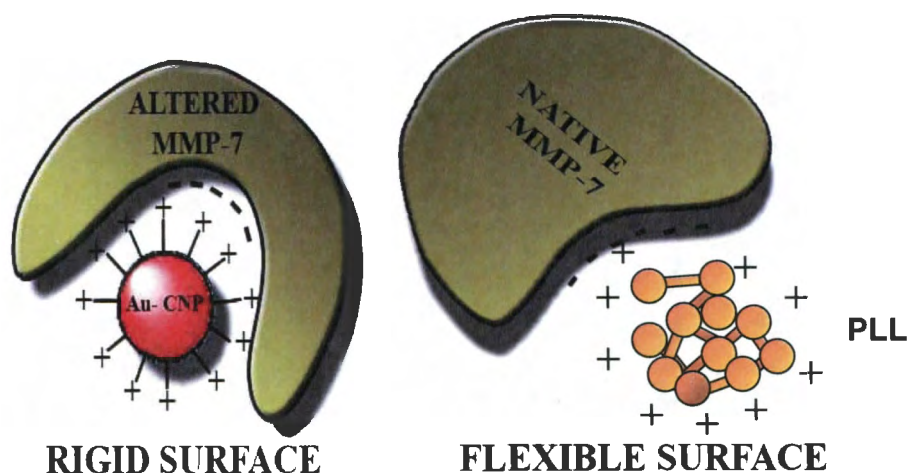
Scheme 5.1. The schematic model showing the influence of "flexible" versus "rigid" cationic surfaces on the structural feature of hMMP-7.

The electrostatic interaction existing between the complementary surfaces of the enzyme and the NPs were contemplated to vary from being non-reactive to enhancing inhibition and inactivation of the enzyme [39]. Of all the possibilities, one of the plausible reasons of PLL-mediated interaction elicits the protein to read just its tertiary structure; thereby mutual adjustment of the PLL-hMMP-7 complex leads to a flexible, stable "Binary Associative Complex" [40] (Scheme 5.1); eventually leading to the prevention of distortion of the protein's native conformation. On the other hand, Au-CNP upon binding to hMMP-7 is able to bend / distort the active-site pocket of the enzyme, resulting in the "arched shaped" conformation. In spite of the entropic favorability, the inhibition constant (K_I value) of PLL is lower than IC_{50} value of Au-CNP. The data thrust on the fact that the entropic penalty for the Au-CNP mediated changes in the enzyme conformation is compensa-

ted by the favorable enthalpic involvement. Irrespectively, the activation and inhibition of hMMP-7 occurs by positive charges present on the above (PLL and Au-CNP) macro-clusters rather than by their specific nature.

Besides, it has been known that proteins can attach to the Au-CNP surface via direct chemical cross linking or by "self assembly" via electrostatic interactions [32, 41–45] such as that observed in the case of hMMP-7. The proteins adsorbed on the "rigid" NPs surfaces often induce conformational changes, which are manifested in the changes of the local tertiary structures of the protein followed by gradual unfolding to a comparatively loose configuration, often leading to the denaturation of proteins. Hence, it is not surprising that Au-CNP (rigid, spherical), unlike PLL (flexible, meshy network), causes inactivation of the enzyme presumably due to thermodynamic drive imposed by the preferential interaction of the denatured (vis a vis native) form of hMMP-7 to the Au-CNP surface [46-47].

A cumulative account of the experimental data presented in this Chapter leads to the following conclusions: (1) The enzyme activity of hMMP-7 is enhanced by stoichiometric concentrations of PLL and inhibited at higher concentrations of PLL; (2) Au-CNP acts as a very strong inhibitor for hMMP-7; (3) There are secondary conformational changes observed in hMMP-7 upon binding to positively charged PLL indicating the protein becoming more helical and compact in structure; (4) There are secondary changes observed in hMMP-7 upon binding to Au-CNP but the protein loses its secondary helical structure indicating that Au-CNP denatures hMMP-7; and (5) PLL binds reversibly to hMMP-7 whereas Au-CNP denatures hMMP-7. At the same time, in

conjunction with other indirect literature precedents, this work strengthens the idea that apart from the charges, rigidity/flexibility and/or surface curvature of the cationic macro-clusters produce a different influence on the catalytic and structural characteristics of hMMP-7. There will be more detailed studies on the interaction of hMMP isozymes to differently charged surfaces in the subsequent Chapters.

5.3. References

1. Overall, C. M., and Kleifeld, O. (2006) Tumor microenvironment-opinion: validating matrix metalloproteinases as drug targets and anti-targets for cancer therapy. *Nat. Rev. Cancer.* 6, 227-239.
2. Davenport, E. L., Morgan, G. J., and Davies, F. E. (2008) Untangling the unfolded protein response. *Cell Cycle.* 7 (7), 865-869.
3. Bhattacharya, R., and Mukherjee, P. (2008) Biological properties of "naked" nanoparticles. *Adv. Drug Deliv Rev.* 60, 1289-1306.
4. Korolev, N., Vorontsova, O.V., and Nordenskiold, L. (2007) Physico-chemical analysis of electrostatic foundation for DNA-protein interactions in chromatin transformations. *Prog. Biophys. Mol. Biol., Biopolymers.* 88 (3), 325-339.
5. Arcesi, L., Penna, G. L., and Perico, A. (2007) Generalized electrostatic model of the wrapping of DNA around oppositely charged proteins. *Biopolymers.* 86 (2), 127-135.
6. Winn, P. J., Zahran, M., Battey, J. N. D., Zhou, Y., Wade, R. C., and Banerjee, A. (2007) Structural and electrostatic properties of ubiquitination and related pathways. *Front. Biosci.* 12, 3419-3430.
7. Tanaka, T., and Rabbitts, T. H. (2008) interfering with protein-protein interactions: Potential for cancer therapy, *Cell Cycle.* 7 (11), 1569-1574.
8. Jain, K. K. (2007) Applications of nanobiotechnology in clinical diagnostics. *Clin. Chem.* 53 (11), 2002-2009.
9. Brewer, S. H., Glomm, W. R., Johnson, M. C., Knag, M. K., and Franzen, S. (2005) Probing BSA to citrate-coated gold nanoparticles and surfaces. *Langmuir.* 21, 9303-9307.
10. Verma, A., and Rotello, V. M. J. (2005) Surface recognition of biomacromolecules using nanoparticle receptors. *Chem. Commun.* 3, 303-312.
11. Willner, I., Basnar, B., and Willner, B. (2007) Nanoparticle-enzyme hybrid systems for nanobiotechnology. *FEBS. J.* 274, 302-309.
12. Zhao, M. and Ghosh, I. (2007) Quantum dots and peptides: A bright future together. *Biopolymers.* 88 (3), 325-339.
13. Huo, Q. (2007) A perspective on bioconjugated nanoparticles and quantum dots. *Colloids. Surf. B Biointerfaces.* 59 (1), 1-10.

14. Maxwell, D. J., Taylor, J. R., and Nie, S. (2002) Self-assembled nanoparticle probes for recognition and detection of biomolecules. *J. Am. Chem. Soc.* 124, 9606- 9612.
15. Sternlicht, M. D., and Werb, Z. (2001) How matrix metalloproteinases regulate cell behavior. *Ann. Rev. Cell. Dev. Biol.* 17, 463-516.
16. Li, M., Yamamoto, H., Adachi, Y., Maruyama, Y., and Shinomura, Y. (2006) Role of matrix metalloproteinase-7 (matrilysin) in human cancer invasion, apoptosis, growth, and angiogenesis. *Exp. Biol. Med. (Maywood).* 231, 20-27.
17. Lauer-Fields, J. L., Juska, D., and Fields, G. B. (2002) Matrix metalloproteinases and collagen catabolism. *Biopolymers.* 66, 19-32.
18. Matter, H., and Schudok, M. (2004) Recent advances in the design of matrix Metalloprotease inhibitors, *Curr. Opin. Drug. Discov. Devel.* 7, 513–535.
19. Nagase, H., and Woessner, J. F. (1999) Matrix metalloproteinases, *J. Biol. Chem.* 274, 21491-21494.
20. Wielockx, B., Libert, C., and Wilson, C. (2004) Matrilysin, from cancer to inflammation and back, a promising drug target? Cytokine. *Growth. Factor. Rev.* 15(2-3), 111-115.
21. Hsieh, M.S., Ho, H.C., Chou, D.T., Pan, S., Liang, Y.C., Hsieh, T.Y., Lan, J.L., and Tsai, S.H. (2003) Expression of matrix metalloproteinase-9 (gelatinase B) in gouty arthritis and stimulation of MMP-9 by urate crystals in macrophages, *J. Cell Biochem.* 89, 791-799.
22. Yu, W.H., and Woessner Jr, F.J. (2000) Heparan sulphate proteoglycans as extracellular docking molecules for matrilysin (matrix metalloproteinase 7), *J. Biol. Chem.* 275, 4183–4191.
23. Kahari, V., and Saarialho-Kere, U. (1997) Metalloproteinases in skin, *Exp. Dermatol.* 6, 199-213.
24. Saarialho-Kere, U. (1998) Patterns of matrix metalloproteinase and TIMP expression in chronic ulcers, *Arch. Dermatol.* 294, S47-S54.
25. Ganguly, B., Banerjee, J., Elegbede, AI., Klocke, D. J., Mallik, S., and Srivastava, D. K. (2007) Intrinsic selectivity in binding of matrix metalloproteinase-7 to differently charged lipid membranes, *FEBS Lett.* 581(29), 5723-5726.
26. Elegbede, A. I., Haldar, M. K., Manokaran, S., Kooren, J., Roy, B. C., Mallik, S., and Srivastava, D. K. (2007) A strategy for designing "multi-prong" enzyme inhibitors by incorporating selective ligands to the liposomal surface, *Chem. Commun.* 32, 3377-3379.
27. Richards, F.M. (1997) Protein Stability: Still an unsolved Problem, *Cell. Mol. Life. Sci.*53, 790-802.
28. Liu, Ge., Molas, M., Grossmann, G.A., Pasumarthy, M., Peraless, J.C., Cooper, M.J., and Hanson, R.W. (2001) Biological Properties of Poly-L-Lysine-DNAComplexes generated by cooperative binding of the Polycation, *J. Biol. Chem.* 276 (37), 34379-34387.
29. Wang, Z. X., and Srivastava, D. K. (1994) A graphical method for determining the number of essential sites in enzymes with multiple binding sites for a ligand, *Anal Biochem.* 216 (1), 15-26.

30. Fukushima, K., Sakamoto, T., Tsuji, J., Kondo, K., and Shimozawa, R. 1994 The Transition of α-helix to β-structure of poly(L-Lysine) induced by phosphatidic acid vesicles and its kinetics at alkaline pH, *Biochim. Biophys. Acta.* 1191, 133-140.

31. Hu, Z., Jiang, J., and Rajagopalan, R. (2007) Effects of macromolecular crowding On biochemical reaction Equilibria: A molecular Thermodynamic perspective, *Biophys. J.* 93, 1464-1473.

32. Abecassis, B., Testard, F., Arleth, L., Hansen, S., Grillo, I., and Zemb, T. (2007) Electrostatic control of spontaneous curvature in cationic reverse micelles, *Langmuir.* 23, 9983-9989.

33. Chah, S., Hammond, M. R., and Zare, R. N. (2005) Gold nanoparticles as a colorimetric sensor for protein conformational changes, *Chem. Biol.* 12, 323-328.

34. Ikai, A. 2005 Local rigidity of a protein molecule, *Biophys. Chem.* 116, 187-191.

35. Hantgan, R. R., Stahle, M. C., Connor, J. H., Horita, D. A., Rocco, M., MClane, M. A., Yakovlev, S., and Medved, L. (2006) Integrin αIIbβ3: Ligand interactions are linked to binding-site remodeling. *Protein. Sci.* 15, 1893-1906.

36. Wangoo, N., Bhasin. K. K., Mehta, S. K., and Suri, C. R. (2008) Synthesis and capping of water-dispersed gold nanoparticles by an amino acid: Bioconjugation and binding studies. *J. Colloid Interface Sci.* 323, 247-254.

37. Kang, T., Hong, S., Choi, I., Sung, J. J., Kim, Y., Hahn, J-S., and Yi, J. (2006) Reversible pH-driven conformational switching of tethered superoxide dismutase with gold nanoparticle enhanced surface plasmon resonance spectroscopy. *J. Am. Chem. Soc.* 128, 12870-12878.

38. Chen, J., Zheng, A., Chen, A., Gao, Y., He, C., Kai, X., Wu, G., and Chen, Y. (2007)A functionalized gold nanoparticles and rhodamaine 6G based fluorescent sensor for high senstitive and selective detection of mercury (II) in environment water samples. *Anal. Chim. Acta.* 599, 134-142.

39. Zhaochun, Wu., Zhang, B., and Yan, B. (2009) Regulation of enzyme activity through interactions with nanoparticles. *Int. J. Mol. Sci.* 10, 4198-4209.

40. Voet, D., Voet, J. G., and Pratt, C. (1995) In Fundamentals of Biochemistry: Life at the Molecular Level, *John Wiley and Co*, Vol. 3.

41. Nylund, M., Fortelius, C., Palonen, E. K., Molotkovsky, J. G., and Mattjus, P. (2007) Membrane curvature effects of glycolipid transfer protein activity. *Langmuir.* 23, 11726-11733.

42. Lins, L., Decaffmeyer, M., Thomas, A., and Brasseur, R. (2008) Relationships between the orientation and the structural properties of peptides and their membrane interactions. *Biochim. Biophys. Acta.* 1778 (7-8), 1537-1544.

43. Wangoo, N., Bhasin, K. K., Mehta, S. K., and Suri, C. R. (2008) Synthesis and capping of water-dispersed gold nanoparticles by an amino acid: Bioconjugation and binding studies. *J. Colloid Interf. Sci.* 323, 247-254.

44. Kang, T., Hong, S., Choi, I., Sung, J. J., Kim, Y., Hahn, J-S., and Yi, J. (2006) Reversible pH-driven conformational switching of tethered superoxide dismutase with gold nanoparticle enhanced surface plasmon resonance spectroscopy. *J. Am. Chem. Soc.* 128, 12870-12878.

45. Vartak, D., and Gemeinhart, R. (2007) Matrix metalloproteases: Underutilized targets for drug delivery, *J. Drug. Targ.* 15(1), 1–20.
46. Mandal, H. S., and Kraatz, H. B. (2007) Effect of the surface curvature on the secondary structure of peptides adsorbed on nanoparticles. *J. Am. Chem. Soc.* 129, 6356-6357.
47. Teichroeb, J. H., Forrest, J. A., Ngai, V., and Jones, L. W. (2006) Anomalous thermal denaturing of proteins adsorbed to nanoparticles. *Eur. Phy. J. E.* 21, 19-24.
48. Huang, C. Z., Liao, Q. G., and Gan, L. H. (2007) Telomere DNA conformational change induced aggregation of gold nanoparticles as detected by Plasmon resonance light scattering technique. *Anal. Chim. Acta.* 604 (2), 165-169.

CHAPTER 6. MOLECULAR ORIGIN OF THE INTRINSIC SELECTIVITY IN BINDING OF HUMAN MATRIX METALLOPROTEINASE (hMMP) ISOZYMES TO DIFFERENTLY CHARGED LIPID MEMBRANES

6.1. Introduction

Each tissue is an organized assembly of cells held together by cell-cell adhesion, cell-matrix adhesion, and an extracellular matrix (ECM) assembly, which is primarily constituted of different types of collagen fibers [1]. Under physiological conditions, the level of extracellular matrix (ECM) assembly is dynamically controlled by synthesis of its individual components (such as collagens, elastin, etc.) and its degradation by proteolytic enzymes, such as metalloproteinases (MMPs). Under normal conditions, these "coordinated" processes are responsible for embryonic development, reproduction, wound healing, and angiogenesis [2-6]. Any factor (genetic and/or environmental), which obviates the above dynamic control; either results from an excessive accumulation of the ECM assembly or its degradation, thereby, causing a variety of human diseases. For example, depending upon the tissue type or excessive ECM degradation leads to the onset of a variety of pathological conditions such as: chronic wounds, dermal photo-ageing, bullous skin diseases, atherosclerosis, rheumatoid arthritis, pulmonary fibrosis, cancer and metastasis, all of which are [7-8] caused by MMPs.

6.1.1. Brief description of the types of MMPs

Based on the structural features (including the amino-acid sequences, domain organizations, etc.), 26 different types of MMPs [9-10] have been recognized in human tissues, which fall into six major classes: (i) collagenases (MMP-1, MMP-8, MMP-13, MMP-18); (ii) gelatinases (MMP-2, MMP-9); (iii) stromelysins and stromelysin like

MMPs (MMP-3, MMP-10, MMP-11); (iv) matrilysins (MMP-7; Putative Uterine metalloproteinase or PUMP-1; MMP-26); (v) membrane type MMPs (MMP-14, MMP-15, MMP-16, MMP-17, MMP-24, MMP-25); and (vi) other MMPs (viz., MMP-12, MMP-19, MMP-20, MMP-23A, and MMP-27). Although MMP-7 and MMP-26 both fall in the matrilysin category, and they are often referred to as matrilysin-1 and matrilysin-2, respectively, MMP-7 is taken as the sole representative of matrilysin due to its association with different diseases and its detailed physiological studies.

6.1.2. MMP-7 binding to cell membrane

The localization of secreted MMPs on the surface of the cell membrane is believed to be needed for metastatic "selfish" cells to process and degrade the other cell surface macro-molecules [11-12]. For the cancer to progress; the anchoring of the secreted MMPs on the membrane surface probably has been invoked as a benefit either in preventing rapid diffusion of the proteases or in their active interaction with other non-ECM substrates. A hemopexin domain is believed to be a pre-requisite for such successful association. This work has echoed other researcher's suggestions that MMP-7 (known to lack a hemopexin domain) binds to cell surfaces [13]. Previous studies have suggested that rat MMP-7 binds to heparan sulfate proteoglycans on rat uterine cell tissue [14] providing a strong indication that MMP-7 and it's cognate substrate partners might be mediated by third molecules such as heparin sulfate proteoglycans.

6.1.3. Importance of liposomes as a diagnostic tool

Following the classical demonstration of Singer and Nicholson that the lipid moieties of biological membranes are highly mobile, there have been several lines of

advancements on the structural-functional aspects of membrane fluidity in modulating the physiological functions of cells. The original view of the membrane lipid structure as the "sea of fluid lipid molecules in which proteins float" has been revised, due to the realization that the lipid molecules often exist in highly ordered states and such states are presented in the form of micro-domains. Due to varied degrees of interactions (both attractive as well as repulsive) among lipid "head" and "tail" groups, lipid membranes are known to prevail in a "gel" phase, an ordered (crystalline) liquid phase, and a disordered liquid phase [15].

It is not surprising that any subtle aberration in these physiological processes can be manifested in the pathogenesis of a variety of human diseases. A few of the most prevelant ones, such as obesity, diabetes, cardiovascular diseases, cancer, Alzheimer's disease, asthma, and others are currently studied and efforts are being made to treat these diseases at membrane levels. Due to the feasibility of altering the lipid composition and consequently investigating the influence of different types of lipid moieties, liposomes serve as an excellent model [16] for undertaking biophysical studies of the lipid-protein interactions.

6.1.4. Characteristics of differently charged liposomes

The distribution of the lipids between the inner and the outer leaflet of a biological membrane is asymmetric. The outer surface is enriched in Phosphotidylcholine (PC) while the inner, cytosolic surface is rich in phosphotidylethanolamine (PE) and phosptidylserine (PS). The outer lipid membrane surface, as a result, is electrically neutral while the inner membrane surface is negatively charged. Lipid asymmetry is known to play a role for the proper orientation of the membrane proteins. The crystal structure of lipids like PC, PG and

PE, amongst all the anionic lipids, has been well demonstrated, but a crystal structure of a PS lipid has not been available. POPS measured at neutral pH in the absence of ions is similar to the other phospholipids with respect to the glycerol backbone, but it differs significantly in its head group orientation and motion. The POPS head group is rigid and exhibits internal flexibility [16].

In a recent review of membrane lipids, Mclaughlin and Murray [17] indicated the observation of a subclass of signaling proteins that spend a considerable fraction of time diffusing through the cytosol in search of binding partners. Mclaughlin and Murray [17] further argued that the cells utilize several biophysical mechanisms to facilitate the flow of information from the interior to the surface of the cells. Distinguished physiologist, Knut Schmidt-Nielsen coined the term "cheap tricks' to describe this motion [18].

Phosphatidylinositol 4,5-bisphosphate (PI(4,5)P_2 or PIP$_2$) is uniquely important among membrane-bound lipids as a regulator of cell function. PIP$_2$ is a critical mediator of a variety of cellular processes in spite of its structural simplicity and relative scarcity in cells (<1% of all membrane lipids). The most widely recognized function of PIP$_2$ is as a substrate for hydrolytic cleavage by Phospholipase C (PLC) into diacylglycerol (DAG) and inositol trisphosphate (IP$_3$). These are effectors of protein kinase C and calcium signaling, respectively. PIP$_2$ itself participates in several signaling pathways and is implicated in the regulation of proteins responsible for the maintenance and dynamics of the actin cytoskeleton [18-19], attachment of these cytoskeletal structures to the plasma membrane, regulation of membrane trafficking and attachment [20-21], ion channel activity[22], and synaptic vesicle fusion [23].

6.1.5. Non-covalent forces influencing the binding of protein liposome interactions

Over many years of research on the interactions between proteins and their cognate ligand molecules, it is now evident that a large amount of credit goes to the non-covalent forces, which enhance and stabilize these intermolecular interactions [24,26]. Modeling electrostatic interactions of linear polyelectrolytes with counter macro ions of different three-dimensional structures, such as spheres or cylinders [25], are increasingly being employed to understand non-trivial contributions in these interactions. These models will bring out the interesting aspects of DNA–protein interactions as well as the polyelectrolytes and oppositely charged nano-particle interactions. One of the major applications of atomic-scale models is to detect DNA-protein interactions in order to quantitatively explain the experimental data and give hints to structural questions of immense biological interest [27].

The interesting feature in the latter area was explored in this study from the point-of- view of developing "multi-prong" inhibitors [28] for the pathogenic enzymes as well as developing diagnostic tools for the disease marker proteins. Liposomes of varied compositions were formulated such that they could be utilized as diagnostics as well as therapeutic tools for treating various human diseases. Unlike conventional usage of liposomes (i.e., serving as drug carriers), the approach has been to introduce selective ligands on the liposomal surface (as head groups) and "tap" the potentials of the lipid mobility (within liposomes) in promoting the "multivalent" interactions between the liposomal ("reporter") head groups and the complementary proteins. The objective has been pursued via formulating liposomes containing sensitized-dansyl as the fluorescent probe.

The balance between hydrogen-bonding and electrostatic repulsion can regulate PIP_2-mediated signaling, thereby moderating the pools of PIP_2 available for single-lipid binding protein domains versus those that bind multi-molecular assemblies [21]. A detailed study about PIP_2 [24] reveals that when the basic peptide binds to the membrane surface rich in PIP_2, very low concentrations of lipid POPS in the plane of the membrane was found. This can happen only if the peptide sequesters several PIP_2 lipids in its immediate neighborhood when it binds to a $POPC/PIP_2$ membrane [24].

Biosensors based on antibody array technology have made rapid progress as a possible means of quick and direct protein detection [16]. However, most recently, metallic films and gold nanoparticles have been proposed as sensing platforms to exploit the surface plasmon phenomenon and its application in biospecific interaction assays [29]. Although, the antibody array methodology can provide quick and simultaneous protein detection, nonetheless, it has its own limitations. It is known that metal and glass substrates are not the most desirable approach for *in vivo* applications.

Despite the wealth of studies on MMPs and the enormous amount of knowledge available on the inhibitors of this family of enzymes, the persistent efforts for many decades in developing diagnostic tools for the disease marker proteins still remains to be defined. Upon consideration that the catalytic and regulatory features of hMMP isozymes (especially hMMP-7) would be fine-tuned if it were to be localized on the plasma membrane, the main goal was to investigate their potential interactions with model biological membranes and discern the functional consequences of such interactions.

6.2. Results and Discussion

The data reveal that all three Matrix Metalloproteinase isozymes (hMMP-7, 9 and 10) interact with anionic, cationic and neutral lipid membranes, although hMMP-7 interacts strongest with anionic membranes. While the catalytic activity of hMMP-7 remains unaffected upon binding to neutral and negatively charged membranes, it is drastically impaired upon binding to the positively charged membranes. The structural data reveal that the origin of these features lies in the "bipolar" distribution of the electrostatic surface potentials on the crystallographic structure of hMMP-7.

Figure 6.1 shows the structure of the lipids used to formulate the differently charged Liposomes (LUVs). The LUVs were prepared with zwitterionic 1-palmitoyl-2-oleoyl-sn-glycero-3-phosphocholine (POPC) as a major (75–95%) component and other lipids (contributing different net charges) as minor components. For formulating negatively charged liposomes, we utilized anionic lipids; POPS and 1,2-dioleoyl-sn-glycero-3-phosphoinositol-4,5-bisposphate (PIP$_2$), which harbor -1 and -3 net charges, respectively, in their head groups at neutral pH. For positively charged liposomes, the cationic lipid; 1-palmitoyl-2-oleoyl-sn-glycero-3-ethylphosphocholine (EPOPC), containing +1 net charge on its head group at neutral pH were utilized.

The Phospholipid Assay (PLA) was performed for determining the phospholipid content in differently charged LUVs so that the mol % of each constituent incorporated into the lab prepared LUVs can be measured and considered while calculating the K_d values in the binding studies for the different hMMP isozymes. The assumption, that the lipid molecules are distributed equally between the outer and the inner leaflets of the LUVs, was

used to calculate the effective concentration of POPS, PIP$_2$, EPOPC and POPC along with Dansyl PE head groups on the outer surface of LUVs (which would be supposedly involved in the interaction with hMMP isozymes). All the steady-state fluorescence experiments were repeated in triplicates, and consistent results were obtained.
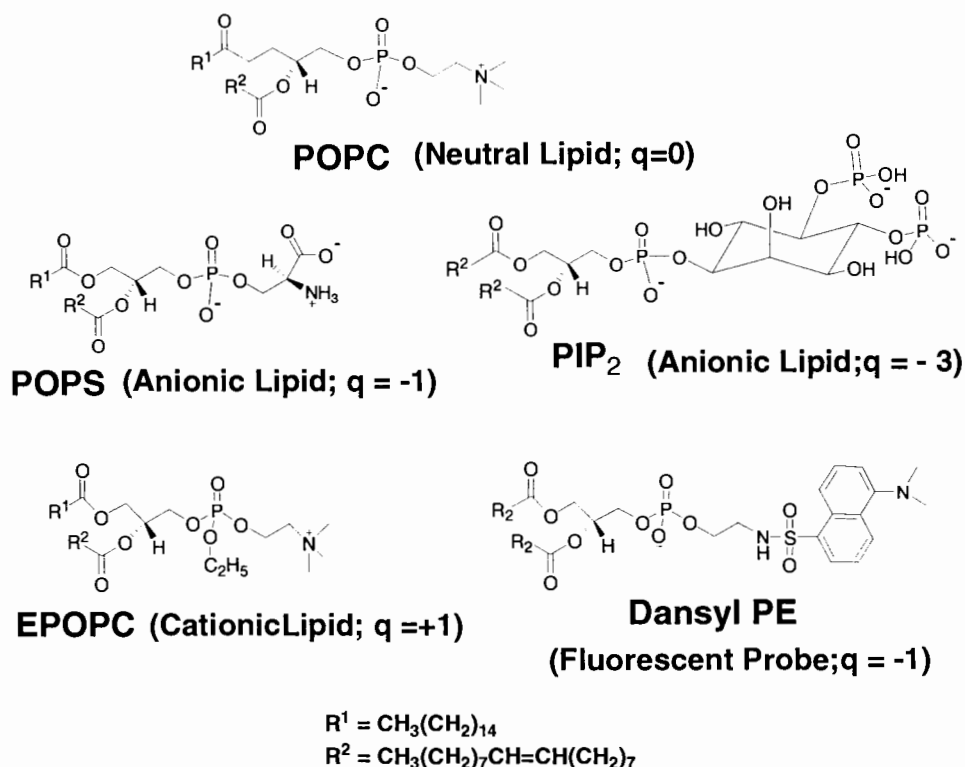

Figure 6.1. Structure of different lipids used in formulating liposomes.

To probe whether hMMP isozymes selectively interact with negative, neutral or cationic liposomes, we performed binding studies of these differently charged liposomes as the Model membrane system. Moreover, this appeared feasible based on the electrostatic potentials on the surface of hMMP-7, 9, and 10 (Figure 6.2). It is very striking that in case of hMMP-7, the surface around the active site pocket has negative potential, while the distal end (opposite side) of the enzyme surface is predominantly positive. Similarly, the

electrostatic surface potential of the other hMMP isozymes (hMMP-9 and 10) were tested. It was discovered that hMMP-10 shared a common scenario with hMMP-7 (the bipolar distribution of charge).
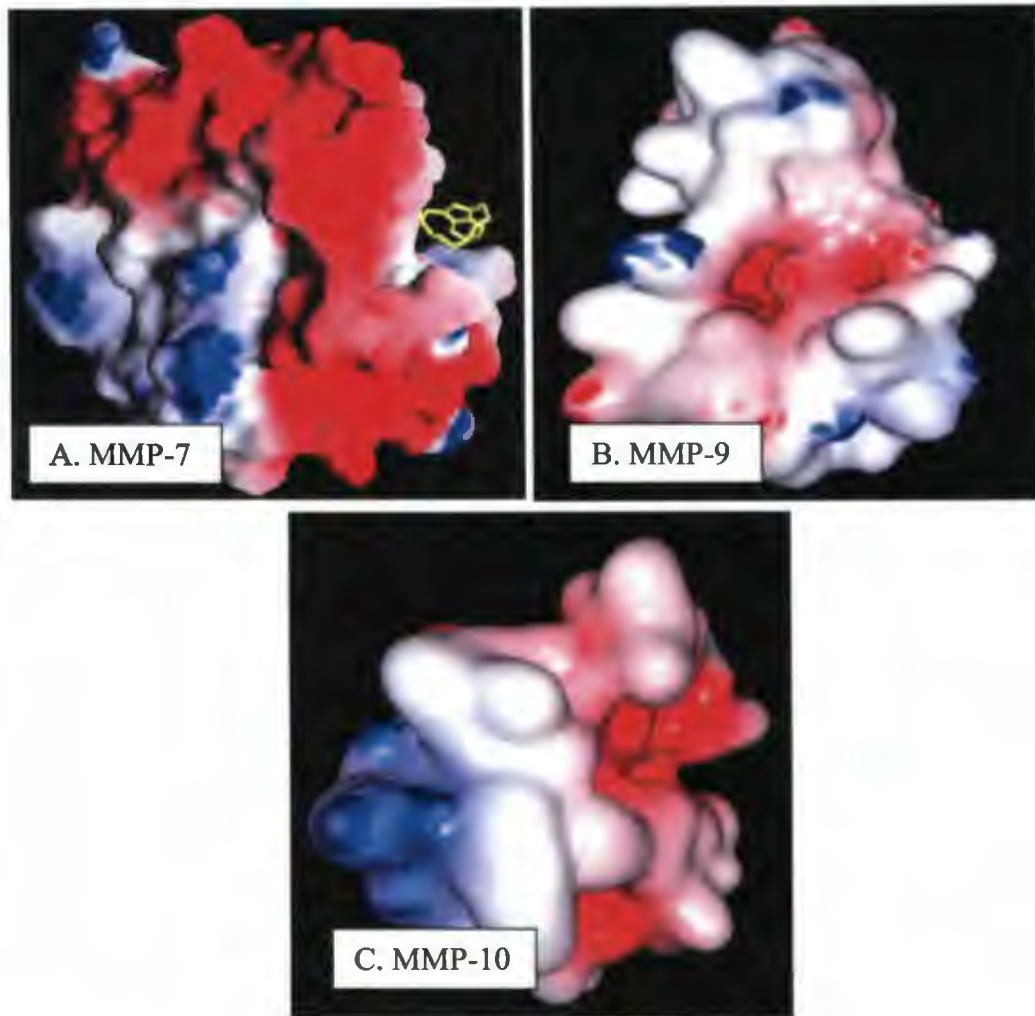

Figure 6.2. Electrostatic potential of MMP isozymes. The red and blue colors represent the negative and positive potentials, respectively; calculated via the aid of the GRASP software on a SGI molecular modeling workstation.

However, hMMP-9 has scattered clusters of positive and negative charge density on the protein surface. The distinct and different patterns of distribution of "surface charge density" on the hMMP isozymes (especially that of hMMP-7 and 10 with respect to

hMMP-9) were helpful in speculating on the effects of anionic and cationic membrane surfaces on the micro-environment of the active site of the hMMP isozymes and their effect on the efficiency to catalyze the reaction.

Figure 6.3 shows the binding of hMMP-7 to anionic LUVs (POPS 5 mol %), which was quantified by monitoring the fluorescence signals of the liposome-dansyl probe as well as that of the enzyme's tryptophan/tyrosine residues. Further note, the systematic decrease in the enzyme's fluorescence emission intensity (λ_{cm} = 343 nm) with concomitant increase in the intensity of the dansyl peak (at 513 nm). The overall spectral changes conform to a single isobestic point at 397 nm, indicating the origin of the presence of an equilibrating liposome-hMMP-7 complex. However, it was also closely noted that after the subtraction of the background dansyl signal; there was no Fluorescence Resonance Energy Transfer (FRET) [30] from the excited state of the enzyme's tryptophan/tyrosine residues to the liposome-resident dansyl probe. FRET is a process whereby energy is non-radiatively transferred from a donor molecule to an acceptor molecule through long-range dipole interactions. FRET has recently been used for many applications that include DNA sensing, proteomics, and probing various processes in living cells [31]. The liposomes were formulated with the hope of manipulating the differently charged liposomes to invoke FRET from the excited state of the protein tryptophan to the stable dansyl probe of the protein-dansyl resident liposome complex. In addition, the dissociation constant (K_d) calculated from the liposome concentration-dependent changes in the fluorescence intensities at 343 nm (due to quenching of the enzyme's fluorescence) was found to be 55.0 ± 0.73 µM.
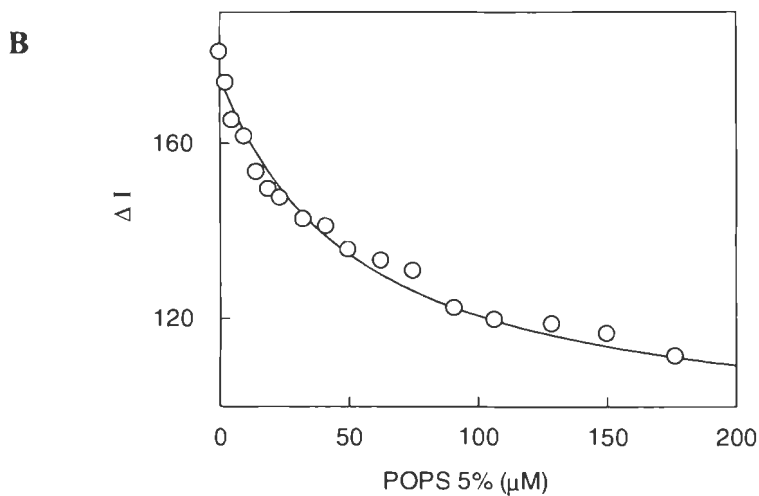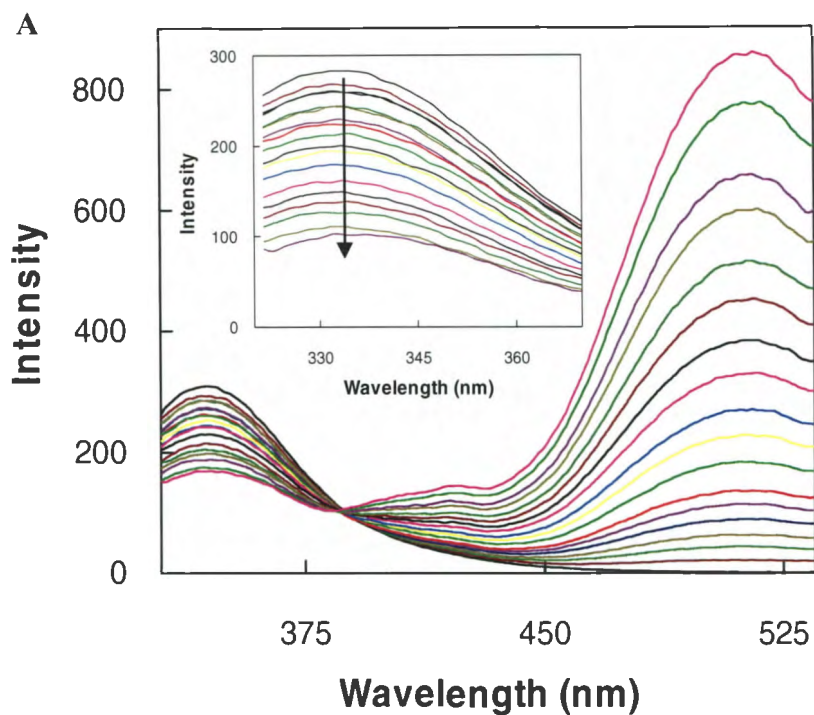
Figure 6.3. Interaction of hMMP-7 with anionic liposome containing POPC: POPS: DPE (85:5:10) mol %. A. Spectra of POPS 5% in presence of protein, the inset shows the difference spectra after subtraction of the background dansyl signal B. The binding isotherm for the POPS – MMP-7 complex. The solid smooth line is the best fit of the data for K_d value 55.0 ± 0.73 μM.

To investigate the interaction of hMMP-7 with anionic liposomes (POPS) but different mol %, a similar experimental setup was used. Figure 6.4 shows the interaction of hMMP-7 with anionic liposome containing POPC: POPS: DPE (80:10:10) mol %. The binding isotherm (Figure 6.4) shows that K_d value to be 21.3 ± 0.24 µM. Similarly, K_d values determined by the systematic decrease in the fluorescence intensities at 343 nm due to the interaction of hMMP-7 with anionic liposomes (containing POPS of different compositions such as 25 mol %, 30 mol % and 40 mol %) were 5.5 ± 0.1 µM, 10.0 ± 0.2 µM and 1.73 ± 0.4 µM, respectively.

As noted in the case of POPS (5 mol %), after subtraction of the background dansyl signal, there was no significant signal from the liposome-resident dansyl probe at 10 mol %. But, as the concentration of POPS per unit area in the liposomes increased, i.e. in case of 25 mol % (Figure 6.5), 30 mol % (Figure 6.6) and 40 mol % (Figure 6.7) LUVs, there was concomitant increase in the dansyl peak (λ_{em}= 513 nm) after the elimination of the background probe (dansyl) signal as the fluorescence intensities at 343 nm decreased due to quenching of the enzyme's fluorescence. Due to high scatter in the resultant dansyl signal (λ_{ex}= 280 nm, λ_{em}= 513 nm), it was difficult to reliably confirm the dissociation constants (K_d) of hMMP-7 with POPS liposomes using progressive different mol fractions. To further investigate, the probe was directly excited to determine the dissociation constants of hMMP-7 with these sets of anionic liposomes (λ_{ex}= 340 nm, λ_{em}= 513 nm). The spectral difference did not give a reliable signal to conclude, and thereby confirm, about the probe mediated changes in the micro-environment of the enzyme's tryptophan/tyrosine residues or alteration in the micro-environment of the dansyl probe.

Figure 6.4. Interaction of hMMP-7 with anionic liposome containing POPC: POPS: DPE (80:10:10) mol %. A. Spectra of POPS 10% in presence of protein, the inset shows the difference spectra after subtraction of the background dansyl signal B. The binding isotherm for the POPS – MMP-7 complex. The solid smooth line is the best fit of the data for K_d value 21.3 ± 0.24 μM.

Figure 6.5. Interaction of hMMP-7 with anionic liposome containing POPC: POPS: DPE (65:25:10) mol %. A. Spectra of POPS 25% in presence of protein, the inset shows the difference spectra after subtraction of the background dansyl signal B. The binding isotherm for the POPS – MMP-7 complex. The solid smooth line is the best fit of the data for K_d value 5.5 ± 0.1 μM.
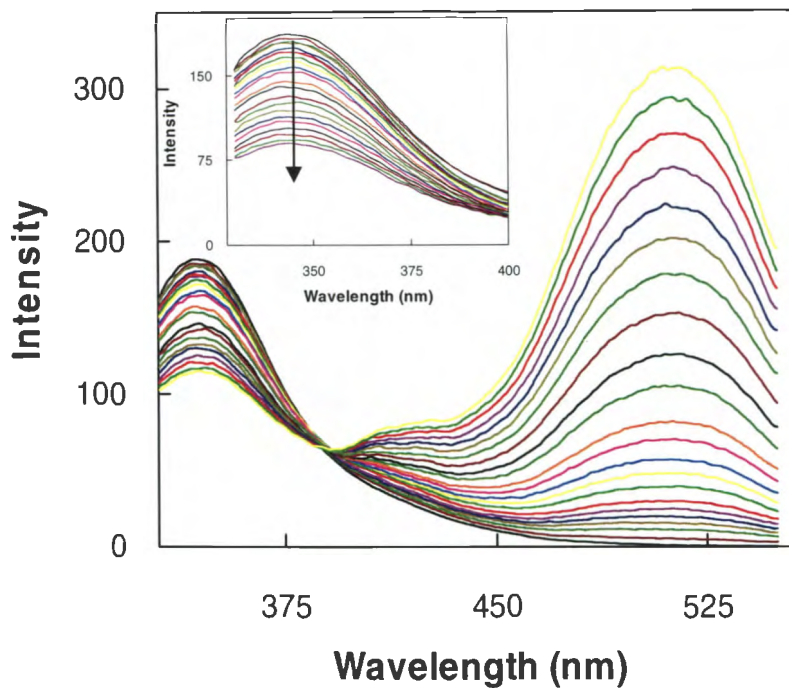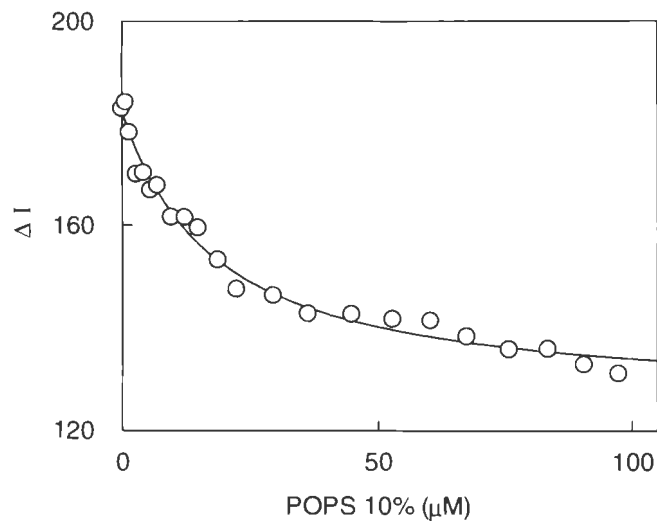
Figure 6.6. Interaction of hMMP-7 with anionic liposome containing POPC: POPS: DPE (60:30:10) mol %. A. Spectra of POPS 30% in presence of protein, the inset shows the difference spectra after subtraction of the background dansyl signal B. The binding isotherm for the POPS – MMP-7 complex. The solid smooth line is the best fit of the data for K_d value 10.0 ± 0.2 μM.
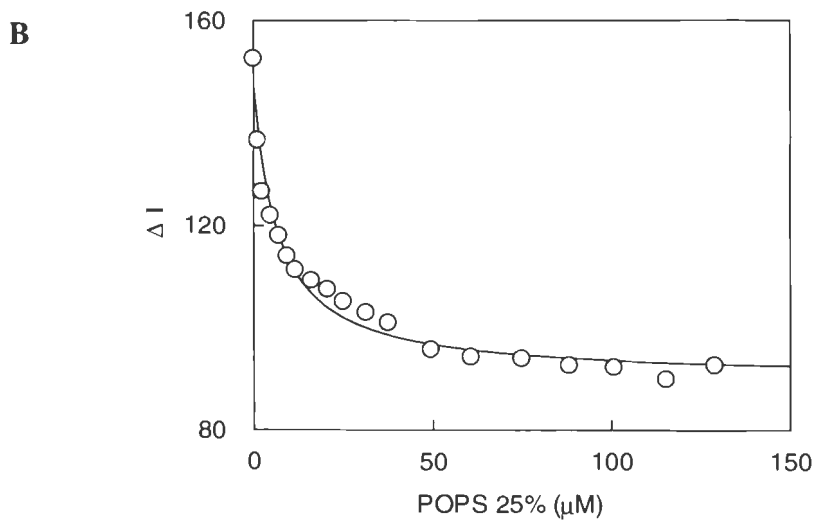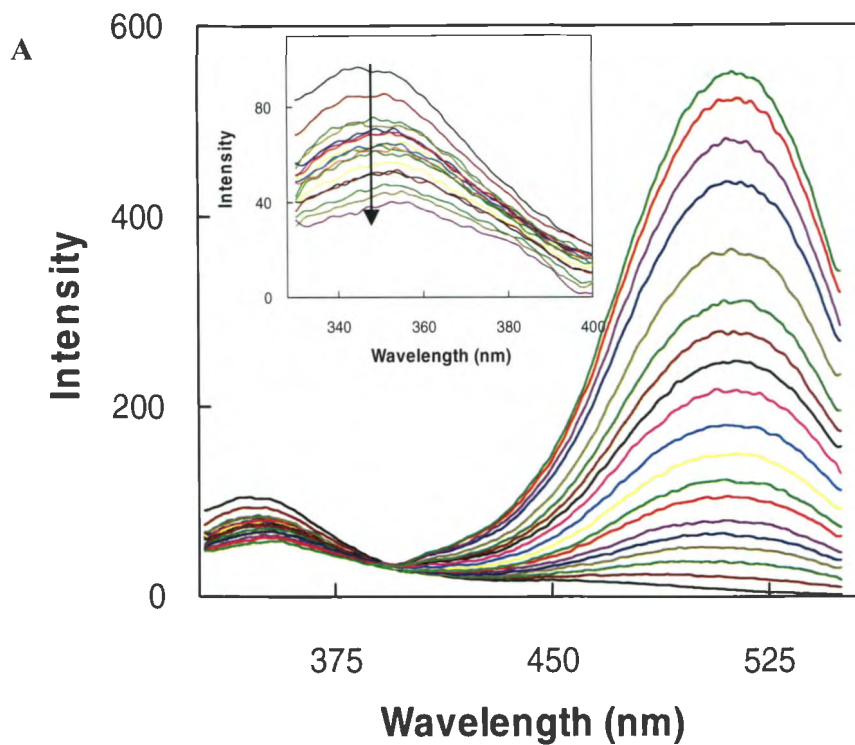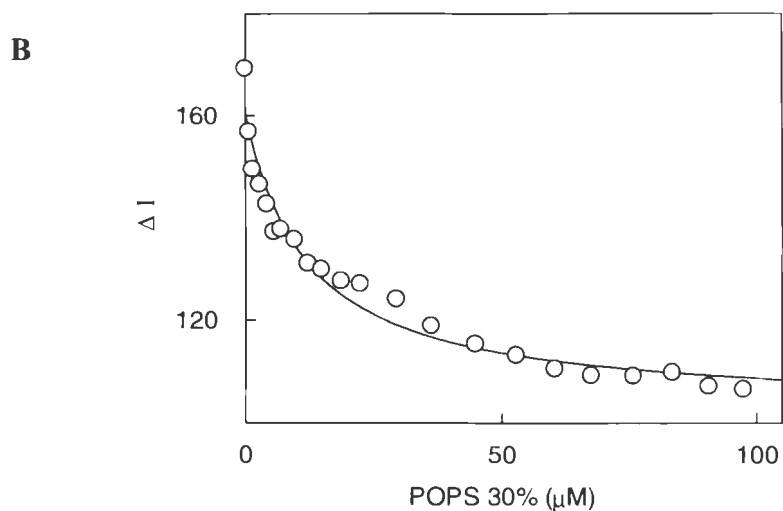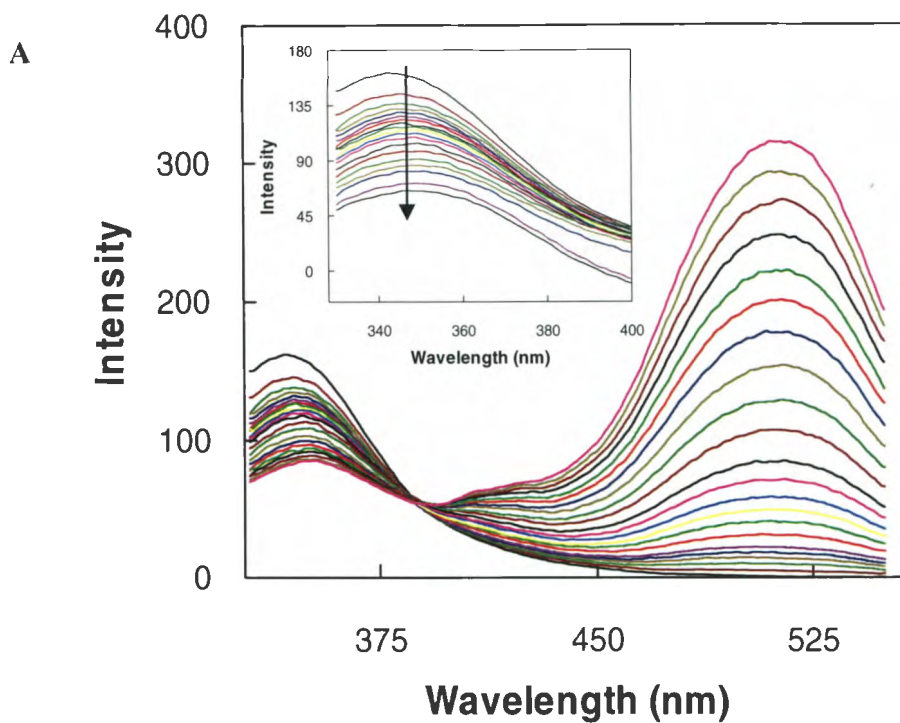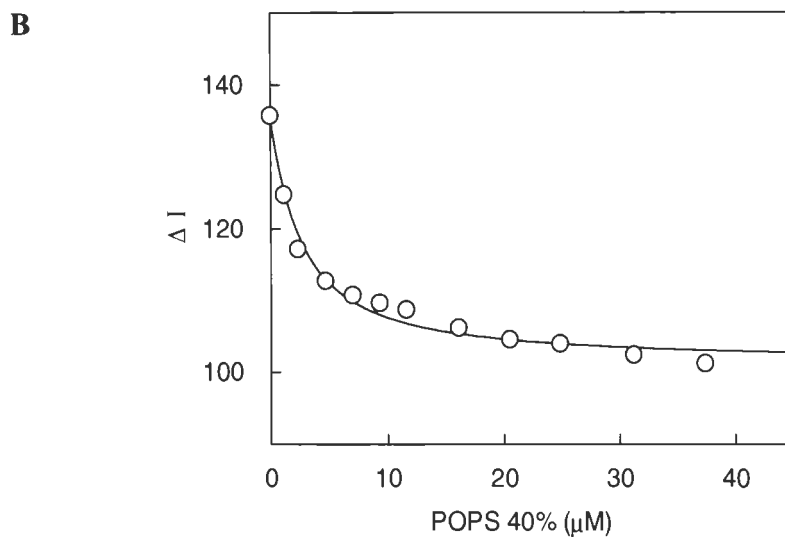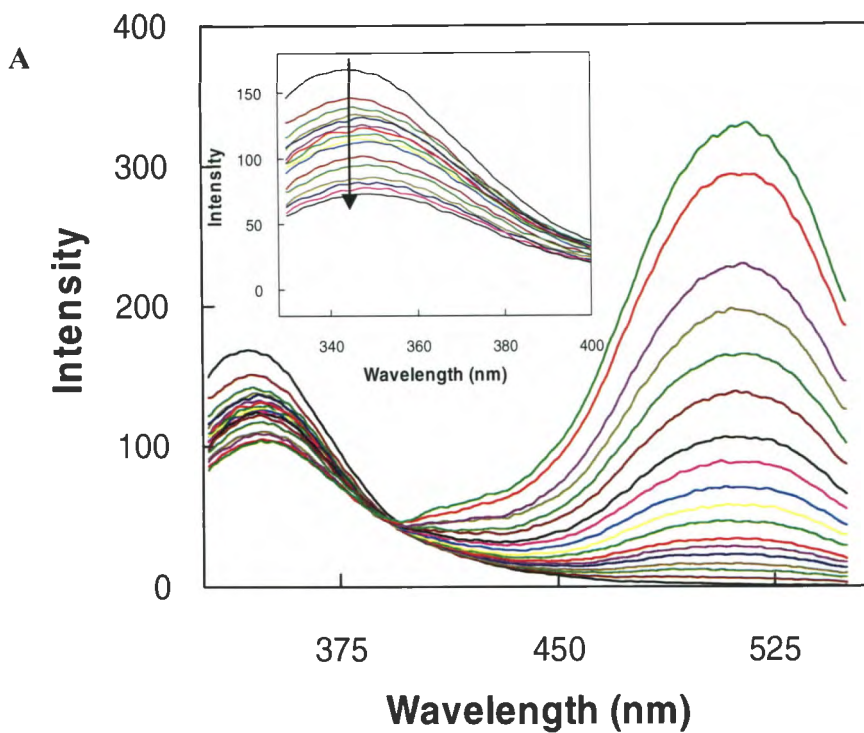
Figure 6.7. Interaction of hMMP-7 with anionic liposome containing POPC: POPS: DPE (50:40:10) mol %. A. Spectra of POPS 40% in presence of protein, the inset shows the difference spectra after subtraction of the background dansyl signal B. The binding isotherm for the POPS – MMP-7 complex. The solid smooth line is the best fit of the data for K_d value 1.73 ± 0.4 μM.

The lipid titrations were carried out in the presence of 5 mol % and 10 mol %

Dansyl PE (DPE). The spectral difference did not show a significant signal in case of 5 mol

% DPE incorporated in the differently charged LUVs as compared to 10 mol % DPE. For

clarity and reliability of the signal from the probe 10 mol % DPE was used for all the

experiments. As observed for Carbonic Anhydrase [32], the response of hMMP isozymes

to the dansyl probe was checked as a preliminary control experiment. The data indicated

that none of the hMMP isozymes binds to the dansyl probe with the consideration that the

net negative charge of the dansyl-PE may perturb the observed binding. It was quite

possible that the enhanced binding could be due to the fact that an additional negative

charge contributed from the DPE played a role to the offset by the bulky dansyl head group

region of the lipid. However, it was negated out by the fact that the acyl chain (bearing the

negative charge) would be embedded within the bilayer [33].

With the improvement of the sensitivity of fluorescent probes, diagnostics, and

imaging in biomedical sciences have immensely benefited. The dansyl probe exhibits

changes in polarity of the micro-environment active-site pocket of proteins like CA I and II

upon binding [32]. The fluorescence emission intensity and the quantum yield of the dansyl

probe is known to be enhanced upon binding to hCA I and II leading to the changes in the

hydrophobicity of the active site of the enzyme [33]. The local polarity of the polar head

group of the dansyl probe resident in the lipid vesicle has been used in many instances to

measure the changes of different parameters like polarity, packing constraints and

hydration degree [34].

Figure 6.8 shows the relationship between K_d (hMMP-7) and varying POPS mol %.

It is evident that as the mol % of POPS LUVs increases, the dissociation constant (K_d)

values decrease attempting to exhibit a saturating trend indicating the progressive increase

in the binding affinity of hMMP-7 towards the densely populated POPS liposomes.
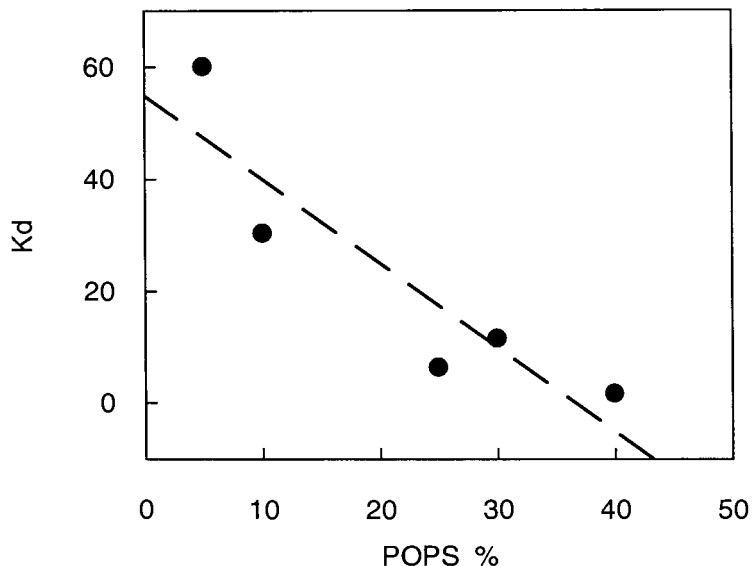
Figure 6.8. Relationship between K_d (hMMP-7) vs POPS %. There is loss of linearity between the binding affinity of hMMP-7 and between the POPS rich anionic liposome.

This kind of relationship has been demonstrated for the first time in the case of

hMMP-7. The exponential decrease of the intrinsic membrane dissociation constant as a

function of POPS content of the anionic lipid vesicles has already been pointed out

indicating the specificity of POPS liposomes to CA2 [35]. At this point, two major

questions arose: A) Does the Local Charge Density (LCD) of the POPS liposome

(complementing the large positively charged macro-cluster residues on the distal end of

hMMP-7) solely dictate the binding affinity of liposome –hMMP-7 associative complex; or

B) Does the different innate organization of the LUVs with different mol % of POPS

composition have an important role to play?

The thermogram of the 10, 25, 30 and 40 mol % DMPS liposomes has been shown in Figure 6.9. DMPC was used as the major lipid component. For easy visualization, the scan range for all the thermograms was from 10°C to 45°C. Membrane lipids might exist in many different phases and temperature induced inter-conversions between the existing different phases can readily occur. In order to probe the thermodynamic characterization of these non-perturbing thermotropic phase transitions in biological membranes, DSC has been utilized. The thermograms indicate that the T_m of the LUV (5 mol % DMPS) and LUV (40 mol % DMPS) is 25.2°C and 29.7°C, respectively. There is a shift in the T_m by 4.5°C. The POPS LUVs with 5, 25, 30 and 40 mol % showed no transition in the range of 8°C to 20°C. The scenario was mimicked by preparing the POPS analogues and the DMPS LUVs with the 5, 25, 30 and 40 mol %. The calculations of T_m, ΔH_{cal}, ΔH_v indicated the existence of the DMPS LUVs in their predominant "fluid" phase [36]. This posed a question on the influence of lipid organization with different mol fractions of DMPS (i.e. POPS) on the thermodynamic parameters for the native stability of the LUVs.

DMPC was used as a major lipid to prepare different mol % of DMPS (5, 25, 30 and 40), while DMPS (analog to POPS) provided the charge to the LUV. T_m values for the different PS mol % constituted LUVs were analyzed to answer the above question. A shift of 4.5°C (from 25.2°C to 29.7°C) was observed. The mol % of the anionic head group and the membrane fluidity along with the absolute chemical nature (e.g. POPS versus DMPS) of the lipid constituents dictated the thermodynamics of the organization of the LUVs. Such a scenario can only originate due to the facile movement of lipid moieties in the liposomal bilayers [36].

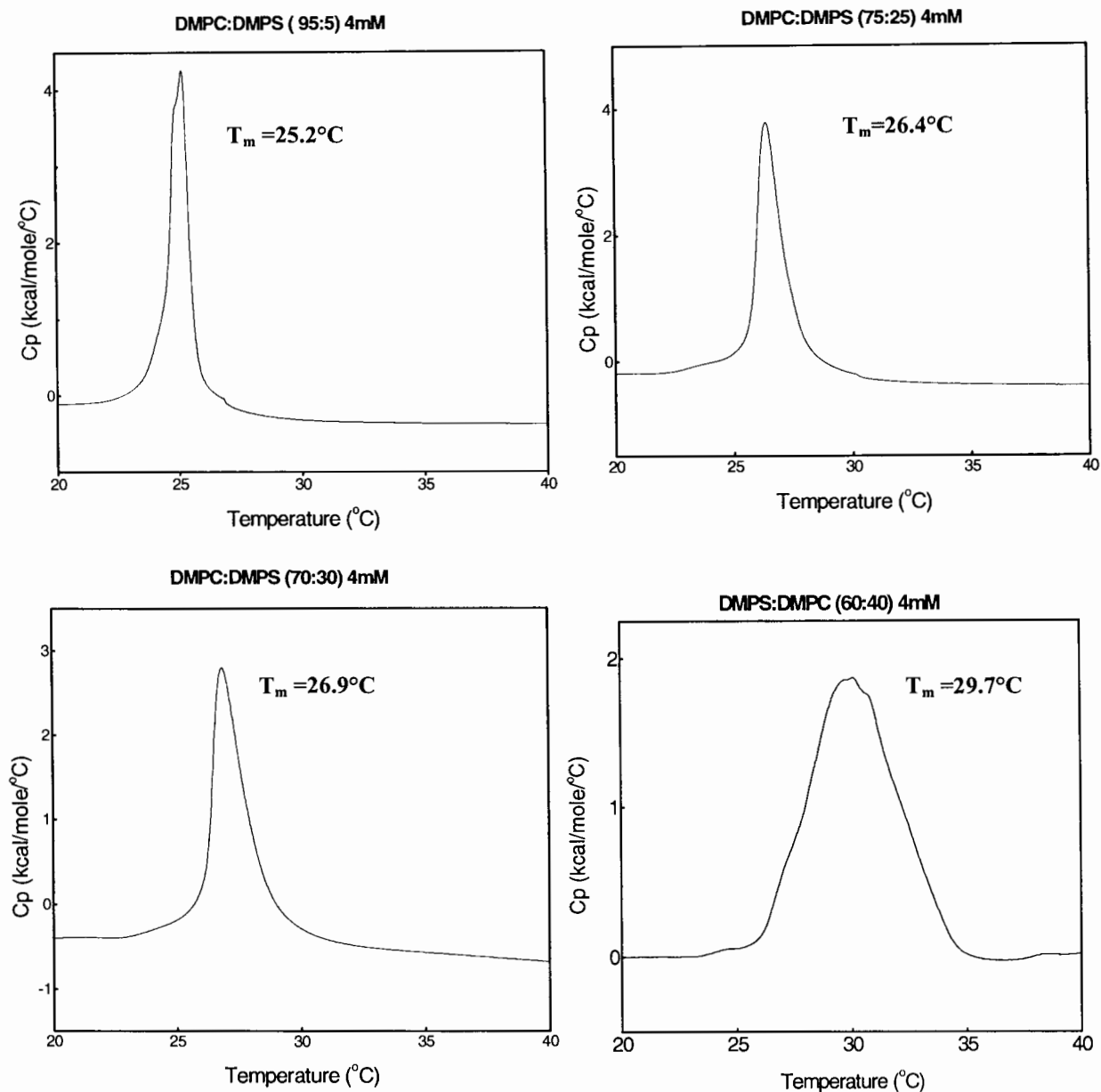Figure 6.9. Thermograms of different mol % of DMPS using Differential Scanning Calorimetry (DSC). There is a shift of 4.5°C in the T_m of the DMPS liposomes with increase in mol % of POPS liposomes. The total phospholipid concentration was maintained approximately at 3.5 to 4.0 mM in 20 mM HEPES, 150 mM NaCl, pH 7.5. The LUVs were heated at a scan rate 10°C / hr (from 10°C to 45°C). Each scan was repeated seven times.

These are the first detailed differential scanning calorimetric studies for the organizational distribution of POPS LUVs formulated with varying POPS composition under the exact experimental conditions as that of Figure 6.3, 6.5-6.7. The experiments provided useful insights into the role of mutual cooperation between the lipid "head" and "tail" groups in the overall energetics of the lipid organization (Table 6.1). POPS is expected to contain a negative charge on its head group. The lipids are expected to reside at he farthest possible distance from each other to optimize the energy due to electrostatic repulsion between the negatively charged flexible head groups of POPS [36]. This scenario fitted well with DMPS (5, 25 and 30 mol %) although DMPS 5 mol % has a sharper peak than DMPS 25 and 30 mol %. The DSC profile of DMPS 40 mol % was different.

The main transition peak gradually broadens and shifts upward, and there is a decrease in peak amplitude as DMPS is incorporated into the DMPC bilayers at progressively higher mole fractions. The main transition broadened significantly as the PS content was increased to 40 mol %. Considering these results, it becomes very tempting to speculate on the induction of demixing/organization of the lipid components, resulting in the re-organization of the (PC/PS rich region) of the individual lipid components as part of the liposome integrity. However, one possible speculative explanation for this scenario would be that there was a re-organization of the lipid tails as the anionic LUVs formulated had more and more POPS rich liposomes within the bilayer. Literature precedents indicate the presence of entrapped water molecules [37] around the lipid tail regions in the crystalline liquid state (but not in the gel state), which might be released upon the re-adjustment of the lipid structures. More so, for the POPC liposomes as the extent of

hydration is more pronounced in POPS rich liposomes than POPC. That scenario can impart an influence on the degree of hydration of the POPS lipid head groups differently as the POPS liposomes get richer in PS content.

Explanations for the observed effects of lipid structure on membrane fall into two broad categories. An explanation in terms of the chemical interactions (hydrogen bonding, charge, hydrophobicity, and size) between the lipid and the protein at the microscopic level, and an explanation in terms of changes in bulk properties of the lipid bilayer such as viscosity, internal pressure, and stored curvature elastic stress at the macroscopic level.

A phosphatidylethanolamine (PE) head group can be both a hydrogen bond acceptor through its phosphate group and a hydrogen bond donor through its $-NH_3^+$ group, while a phosphatidylcholine (PC) head group can act as a hydrogen bond acceptor through its phosphate group. Interactions of the PC head groups with surrounding water molecules differ in comparison with PE head groups. As indicated by molecular dynamics simulations [38], direct hydrogen bonds are formed between the $-NH_3^+$ group and the water molecules while the hydrophobic $-NMe_3^+$ group induces formation of a "clathrate"-like hydration shell [36] around the head groups in order to optimize inter-water hydrogen bonding. The presence of intrinsic membrane proteins and the bilayer-preferring lipids in a biological membrane would force the PE to adopt a bilayer structure, which might be in a state of curvature stress. Since insertion of a protein into the bilayer surface will reduce the curvature stress, it has been argued that this curvature elastic energy could enhance binding of extrinsic membrane proteins to the surface of the membrane. These changes arise due to changes in lateral mobility and head group hydration of the POPS within the bilayer, which

modulates the ΔH_{cal}, ΔH_v and T_m values of the LUVs.

The temperature range over which the transition occurs and the energy associated with the transition between states provide information about the stability and the cooperativity within the structure [37]. The existence of large aggregates of lipid molecules in the ordered bilayer structure dictates gel and liquid crystalline states of lipids. There is less long-range ordering in the system as the aggregate gets smaller. The extent of long-range interactions determines the degree of cooperativity in the gel to liquid crystalline transition in the aggregated bilayer. The limit of cooperativity is achieved when all the molecules of the bilayer are placed between states together at a single temperature. The size of the "cooperative unit" (c.u.) tends to be less than 1 when the number of lipid molecules defining the bilayer has heterogeneity and the existence of discrete domains in the bilayers [39].

Intuitively, $\Delta H_{van't\ Hoff}$ is the enthalpy associated with the transition of the entire cooperative unit. ΔH_{cal} reflects the enthalpy associated with overcoming the intermolecular forces between molecules. Hydrated macromolecular systems characterized by a macroscopic extended network of homogeneous intra-segmental and intermolecular forces are cooperative in nature. One non 2-step model (using Origin® 5.0) was used to analyze ΔH_{cal} and ΔH_v values. It indicated that as T_m increases, the ΔH_{cal} values increase systematically corresponding to the decrease in the ΔH_v values. The calculation of ΔH_v / ΔH_{cal} (indicating the "cooperation unit" c.u. in the phase transition of the liposomes) was much lower than 1 suggesting the existence of more than one intermediate state. Theoretical and experimental studies suggest the counterbalance of the attractive and

repulsive forces among the head groups of LUVs by encouraging complementary

interactions among the tail groups [36].

Table 6.1. The T_m, ΔH_{cal} and ΔH_v values of the DMPC: DMPS (with progress varying mol fractions of PS) LUVs. A one non 2-step model using Origin® 5.0 was used to calculate the thermodynamic parameters for these lipid membranes.

Mol %	T_m	ΔH_{cal}	ΔH_v
DMPS 5	25.2 ± 0.002	4614 ± 18.3	6.63 ± 0.3
DMPS 25	26.4 ± 0.004	6056 ± 29.4	4.62 ± 0.8
DMPS 30	26.9 ± 0.004	5369 ± 24.0	3.91 ± 0.2
DMPS 40	29.7 ± 0.005	9188 ± 19.2	1.52 ± 0.9

For example, if a negatively charged head group (like POPS anionic group) on the

surface of LUVs is neutralized (by repulsively being thrown away to the farthest possible

distance) with the increase in the mol % of POPS LUVs, the POPS density per unit area

would increase. There will be new contacts created between the POPS lipid head and the

bulk water molecules. The tail rearrangement and their individual interaction with the bulk

water molecules will alter each other's spatio- temporal arrangements via intrinsic "cross-

talk" [40] with rich concentrations of POPS repulsive head groups.

Figure 6.10 depicts the binding of hMMP-9 to anionic liposomes (POPS 5 mol %),

which was quantified by monitoring the fluorescence signals of the liposome-dansyl probe

as well as that of the enzyme's tryptophan/tyrosine residues. The experimental setup was

similar to Figure 6.3. The K_d values determined by the systematic decrease in the

fluorescence intensities at 335 nm due to the interaction of hMMP-9 with anionic

liposomes [containing POPS of different compositions such as 5 mol %, 25 mol % (Figure

6.11) and 40 mol % (Figure 6.12)] were 147.03 ± 0.14 μM, 33.3 ± 0.24 μM and $24.04 \pm$

0.063 μM, respectively. It was very interesting to note that after subtraction of the

background dansyl signal, there was no significant signal from the liposome-resident dansyl probe at 10 mol %, 25 mol % or 40 mol % with the interaction of hMMP-9 and POPS liposomes.

Figure 6.13 shows the relationship between K_d (hMMP-9) and varying POPS mol %. The trend appears to be similar to hMMP-7. Figure 6.14 shows binding of hMMP-10 to anionic liposomes (POPS 5 mol %) and was quantified by monitoring the fluorescence signals of the liposome-dansyl probe as well as that of the enzyme's tryptophan/tyrosine residues. The experimental conditions have been setup similar to Figure 6.10. The K_d values determined by the systematic decrease in the fluorescence intensities at 330 nm due to the interaction of hMMP-10 with anionic liposomes [containing POPS of different compositions such as 5 mol %, 25 mol % (Figure 6.15) and 40 mol % (Figure 6.16)] were 64.5 ± 0.09 μM, 40.2 ± 0.06 μM and 26.0 ± 0.08 μM, respectively. Interestingly, in Figure 6.14, we can observe in the inset that there is a gradual red shift by 10 nm (from 330 nm to 340 nm) in the resultant spectra of the interaction of hMMP-10 with POPS (5 mol %). There is a red shift upon binding of hMMP-10 with POPS (25 mol %) by 8 nm (from 330 nm to 338 nm) as shown in Figure 6.15. It can be observed that there is no red shift (in Figure 6.16) with interaction of hMMP-10 and POPS (40 mol %). Solvent polarity and the local environment have profound effects on emission spectral properties of fluorophores [41]. One common use of solvent effects is to determine the polarity of the probe binding site on the macromolecule. Binding is usually accompanied by spectral shift or change in quantum yield due to the different environment for the bound ligand. These spectral shifts can also be used in retrospect the extent of binding.
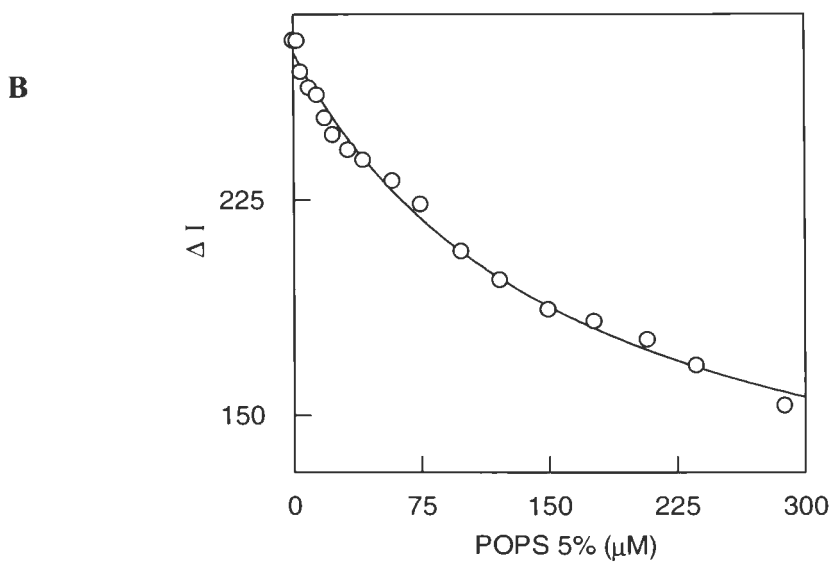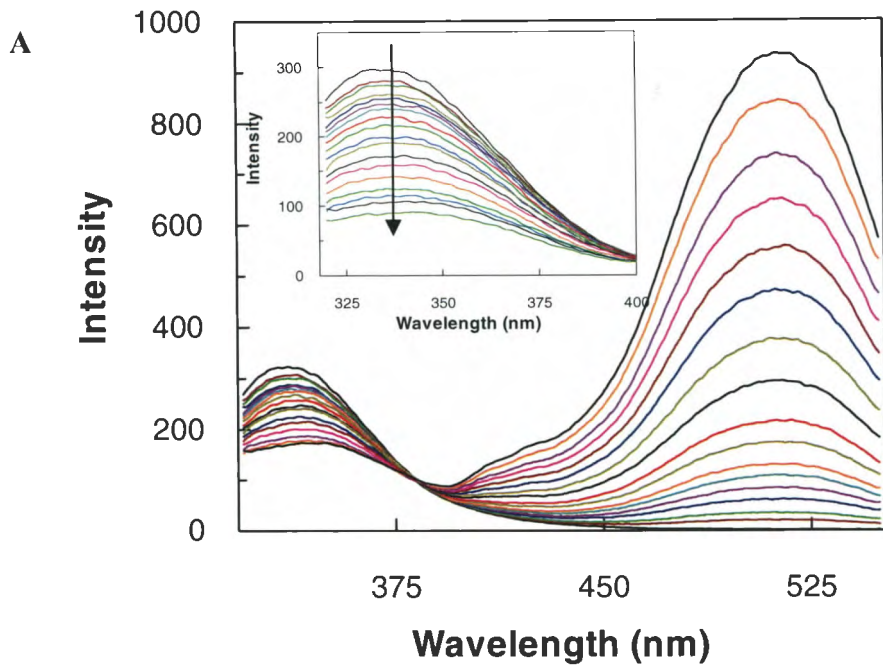
Figure 6.10. Interaction of hMMP-9 with anionic liposome containing POPC: POPS: DPE (85:5:10) mol %. A. Spectra of POPS 5% in presence of protein, the inset shows the difference spectra after subtraction of the background dansyl signal B. The binding isotherm for the POPS – MMP-9 complex. The solid smooth line is the best fit of the data for K_d value 147.03 ± 0.14 μM.

Figure 6.11. Interaction of hMMP-9 with anionic liposome containing POPC: POPS: DPE (65:25:10) mol %. A. Spectra of POPS 25% in presence of protein, the inset shows the difference spectra after subtraction of the background dansyl signal B. The binding isotherm for the POPS – MMP-9 complex. The solid smooth line is the best fit of the data for K_d value 33.3 ± 0.24 µM.
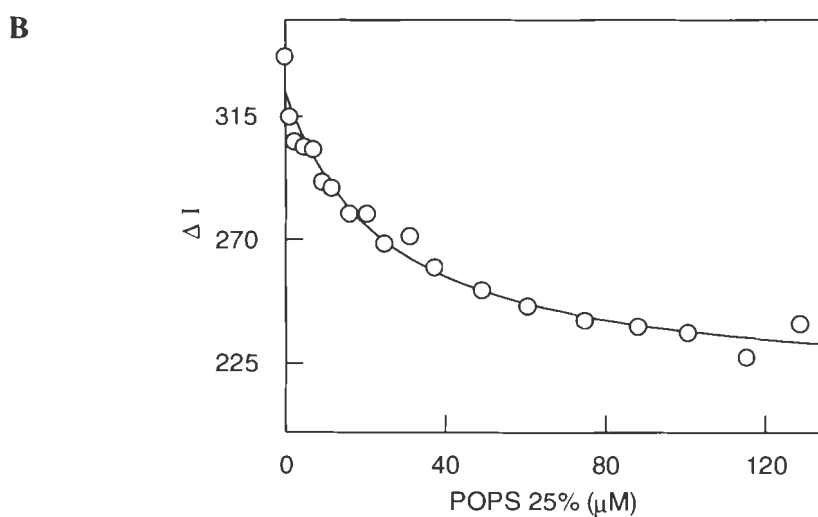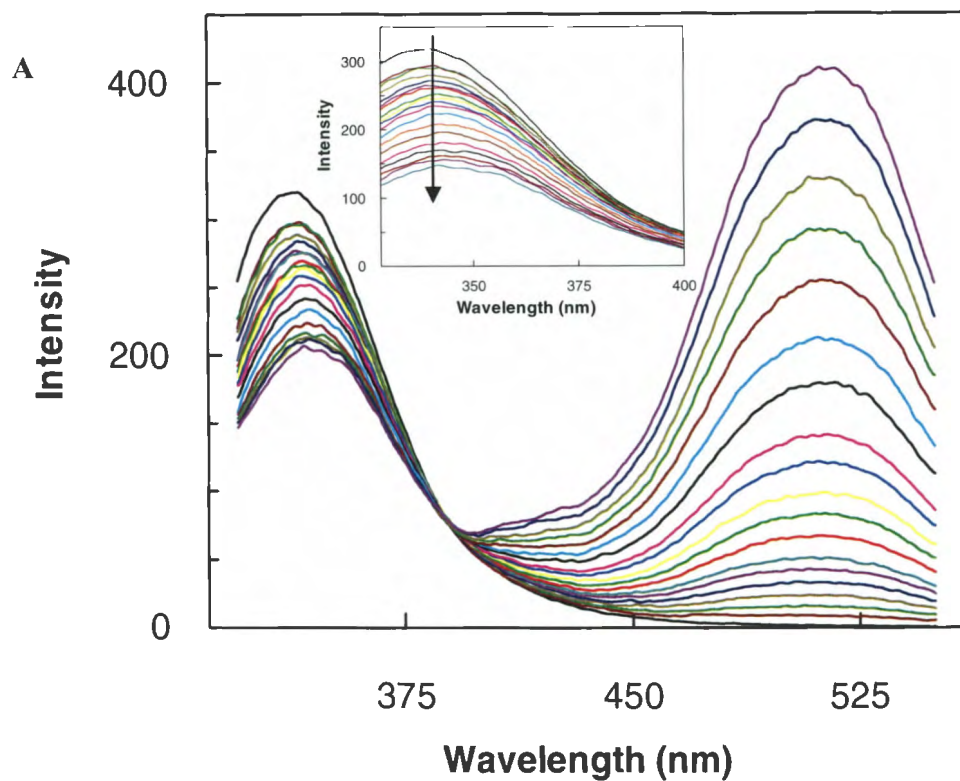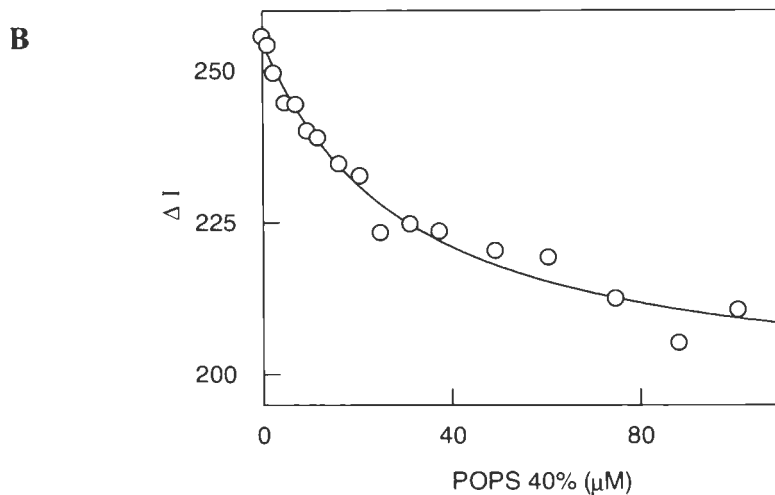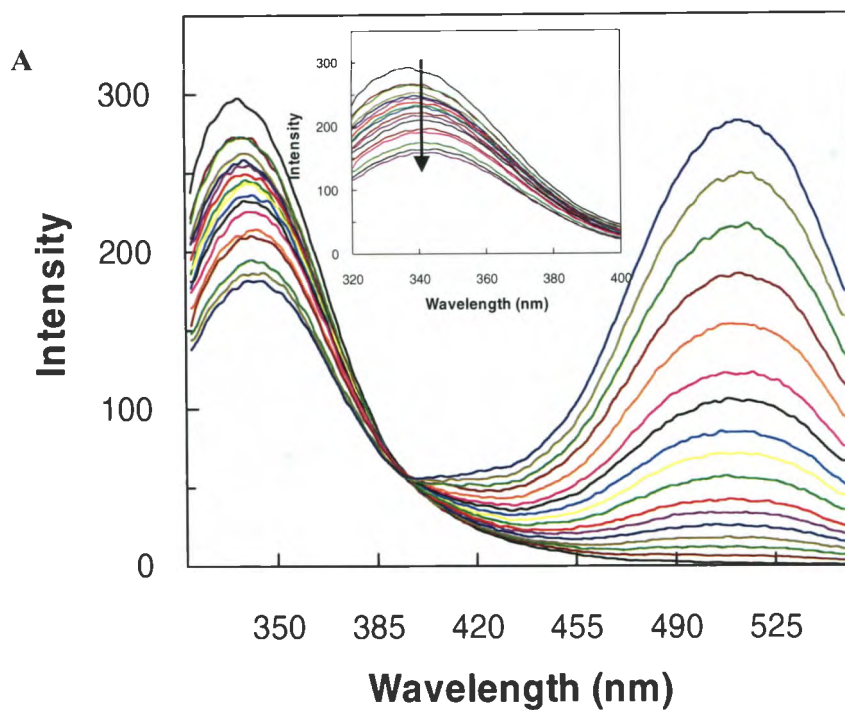
Figure 6.12. Interaction of hMMP-9 with anionic liposome containing POPC: POPS: DPE (50:40:10) mol %. A. Spectra of POPS 40% in presence of protein, the inset shows the difference spectra after subtraction of the background dansyl signal B. The binding isotherm for the POPS – MMP-9 complex. The solid smooth line is the best fit of the data for K_d value 24.04 ± 0.063 μM.
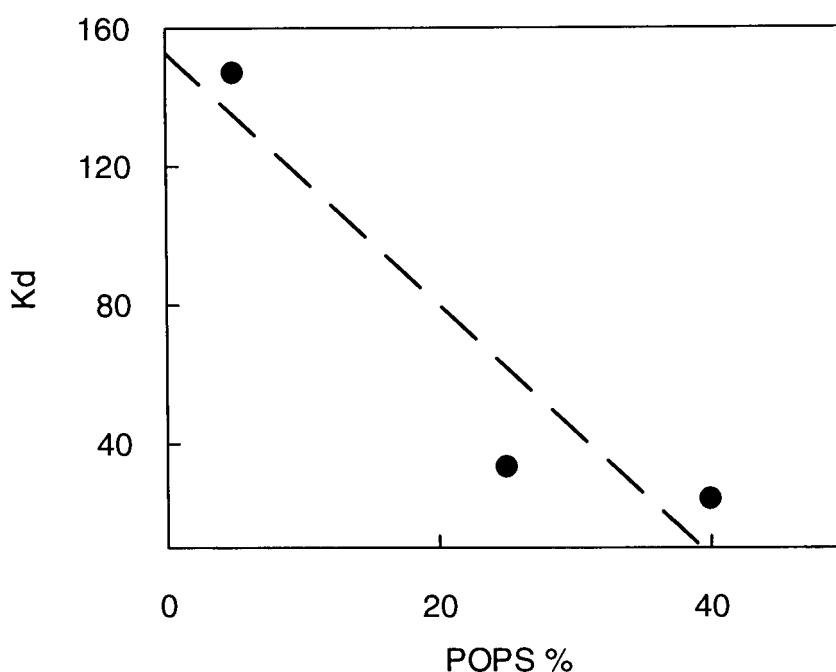
Figure 6.13. Relationship between K_d (hMMP-9) vs POPS %. There is loss of linearity between the binding affinity of hMMP-9 and between the POPS rich anionic liposome.

This special feature provides many opportunities to probe the local environment surrounding a fluorophore. However, it can be difficult to know which effect is dominant in a particular experimental system, and usually more than one effect will simultaneously affect the fluorophores. It intuitively appears that such electronic spectral changes have been attributed to the polar micro-environment of the active-site of the enzyme. However, after subtraction of the background dansyl signal, there was no significant signal from the liposome-resident dansyl probe at 10 mol %, 25 mol % or 40 mol % POPS liposomes with the interaction of hMMP-10, which is strikingly similar to what was observed with hMMP-9. The variation in the dansyl signal in case of the interaction of hMMP-7 with increasing POPS concentration in the lipsomes was a unique feature observed in hMMP-7 but not in hMMP-9 or hMMP-10.

Figure 6.14. Interaction of hMMP-10 with anionic liposome containing POPC: POPS: DPE (85:5:10) mol %. A. Spectra of POPS 5% in presence of protein, the inset shows the difference spectra after subtraction of the background dansyl signal B. The binding isotherm for the POPS – MMP-10 complex. The solid smooth line is the best fit of the data for K_d value 64.5 ± 0.09 µM.

Figure 6.15. Interaction of hMMP-10 with anionic liposome containing POPC: POPS: DPE (65:25:10) mol %. A. Spectra of POPS 25% in presence of protein, the inset shows the difference spectra after subtraction of the background dansyl signal B. The binding isotherm for the POPS – MMP-10 complex. The solid smooth line is the best fit of the data for K_d value 40.2 ± 0.06 μM.
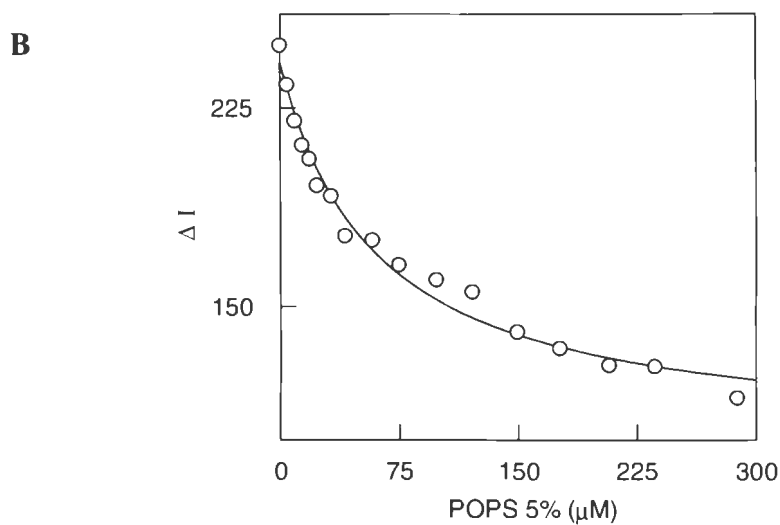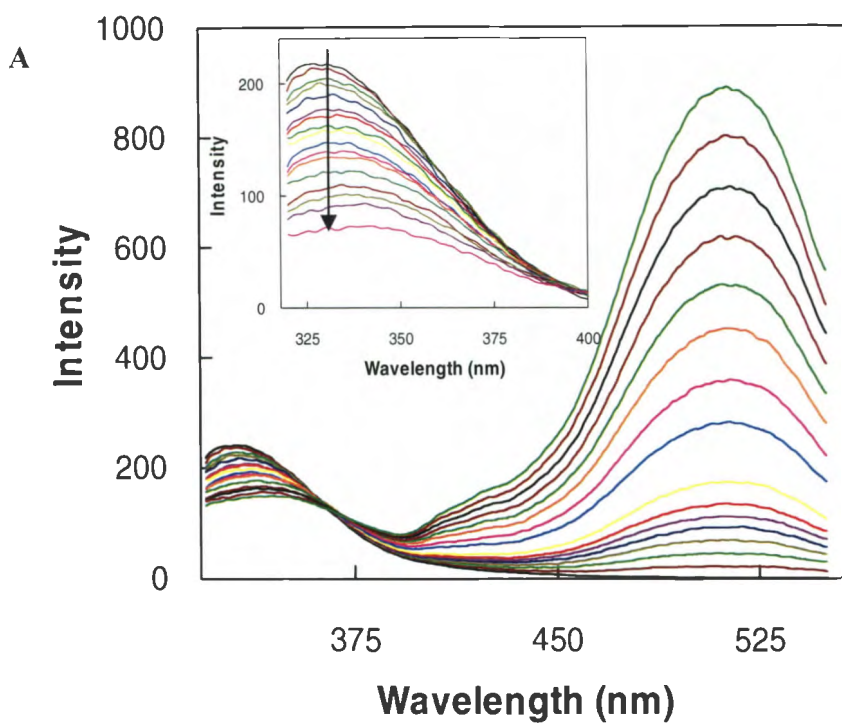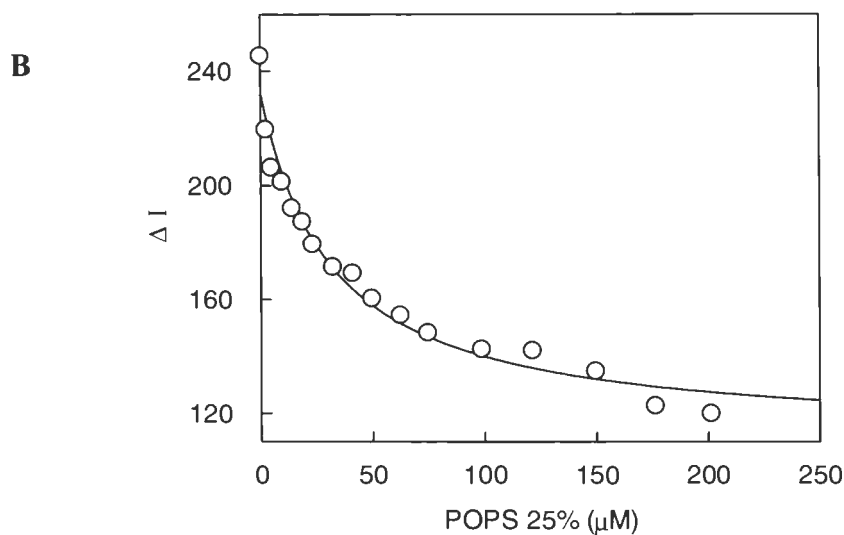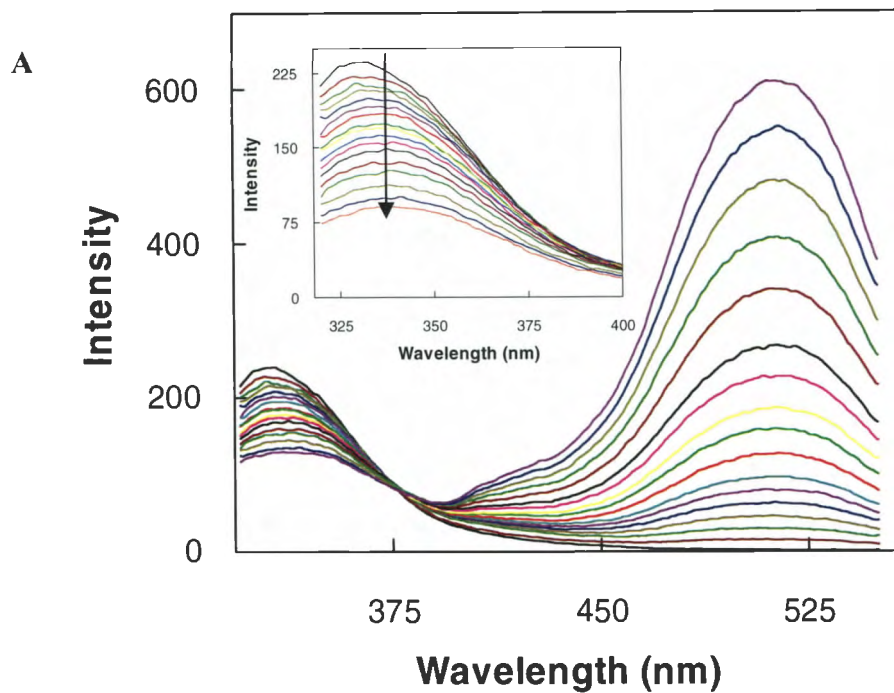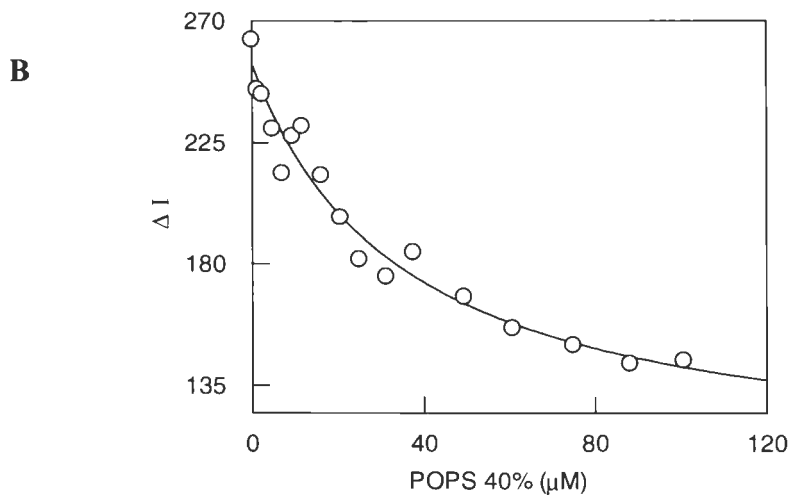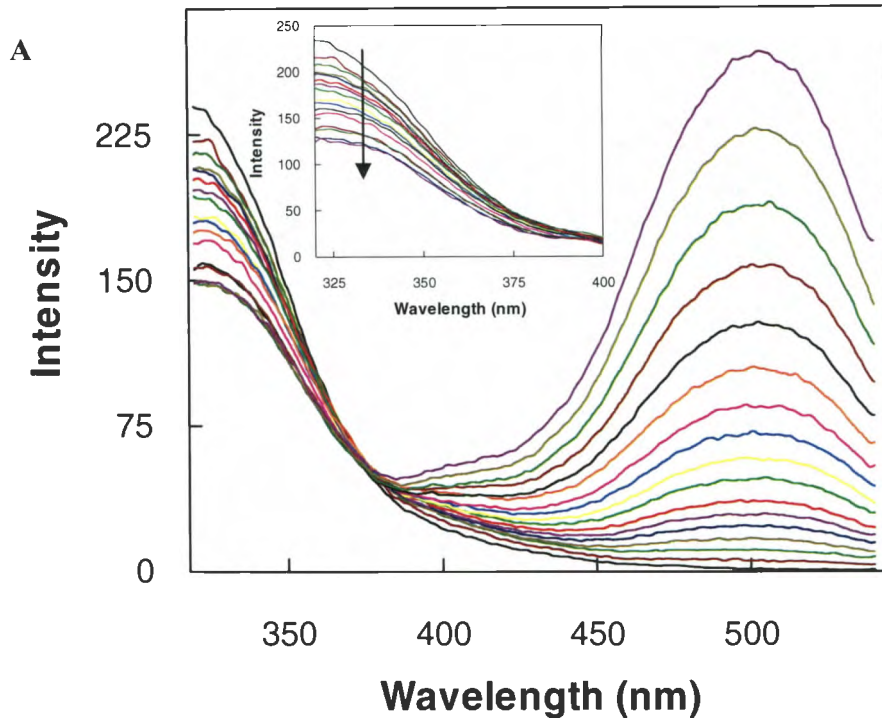
Figure 6.16. Interaction of hMMP-10 with anionic liposome containing POPC: POPS: DPE (50:40:10) mol %. A. Spectra of POPS 40% in presence of protein, the inset shows the difference spectra after subtraction of the background dansyl signal B. The binding isotherm for the POPS – MMP-10 complex. The solid smooth line is the best fit of the data for K_d value 26.0 ± 0.08 μM.

There can be two scenarios in this situation. (a) Firstly, this could be attributed to the difference in the distribution of the surface macro-clusters of the homogenous charge densities in hMMP-7 as compared to the scattered charges in hMMP-9 (Figure 6.2). That however, does not eliminate the fact that hMMP-10 shares a comparative macro-cluster surface charge distribution with hMMP-7, but such a feature has not been observed with the dansyl probe in case of hMMP-10. Given these facts; it raises a strong thrust on the existence of other weak forces (like electrostatics, hydrophobic forces, etc) also contributing to the stability of the protein-ligand (their cognate partner) complexes formed [42]. Figure 6.17 shows the relationship between K_d (MMP-10) and varying POPS mol %. There is a direct linear relationship between the binding affinity of hMMP-10 and the POPS rich anionic liposomes.
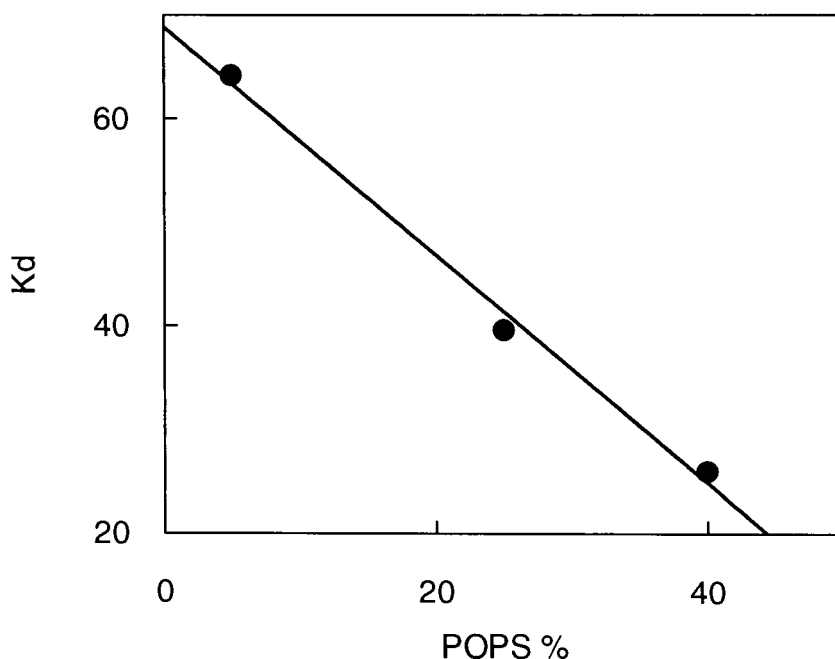
Figure 6.17. Relationship between K_d (MMP-10) vs POPS %. There is a direct linear relationship between the binding affinity of hMMP-10 and between the POPS rich anionic Liposomes. The binding affinity increases as the mol % POPS increases.

Table 6.2 shows the relationship between K_d (hMMP isozymes) and POPS (25 mol %). hMMP-7 shows the tightest binding affinity for POPS liposomes (25 mol %). This became very clear upon comparing the data for the three hMMP isozymes at physiological pH 7.5 as well as mimicking the physiological membrane conditions (25 mol % of POPS in brain cells), it tentatively suggests that eventhough hMMP-7 is a secreted protein it migrates to the sites where these non-ECM substrates are located near the membrane and hMMP-7 binding to membrane promotes it's activity [43].

Table 6.2. Relationship between K_d (hMMP isozymes) vs POPS (25 mol %). hMMP-7 has the most tight binding affinity to POPS (25 mol %) liposome.

MMP Isozymes	K_d (25 % POPS) μM
hMMP-7	5.5
hMMP-9	33.3
hMMP-10	40.2

Recent studies have indicated that binding of Cholesterol Sulfate (CS) incorporated into liposomes, which mimics a cell membrane, facilitates the MMP-7 catalyzed proteolysis of the cell bound proteins eventually inducing a cell-cell aggregation and significantly enhancing metastatic potential [44].

Having established that hMMP-7 holds a strong specificity for POPS liposomes, an important question still remains. Does hMMP-7 exclusively interact with the negatively charged membranes (POPS) or does it also interact with positively charged (EPOPC 25 mol %) and/or neutral (POPC 90 mol %) membranes? Recent studies have shown that Annexin V (Anx V) binds preferentially to POPS incorporated in lipid vesicles vis-a-vis the POPC component of the LUVs [45-46]. To probe the generality of the above findings,

176

several binding studies of hMMP-7 to differently charged LUVs as a model membrane system were performed.

Figure 6.18 shows the interaction of hMMP-7 with cationic liposome containing POPC: EPOPC: DPE (65:25:10) mol %. The binding isotherm for the EPOPC–MMP-7 complex has a K_d value 20.6 ± 0.02 μM. As similar experiment was performed on the interaction of hMMP-9 (Figure 6.19) with cationic liposome containing POPC: EPOPC: DPE (65:25:10) mol % and the interaction of hMMP-10 (Figure 6.20) with cationic liposome containing POPC: EPOPC: DPE (65:25:10) mol %. The binding isotherm for the EPOPC – MMP-9 complex and EPOPC-MMP-10 complex predicts the K_d values to be 14.5 ± 0.013 μM and 8.2 ± 0.015 μM, respectively.

Upon titration with cationic liposomes, it was observed that the intrinsic fluorescence of hMMP-7 was quenched, but there was no significant increase in the dansyl peak at 513 nm. This was presumably due to the absence of energy transfer (due to "distance" or "orientation") from the enzyme's tryptophan/tyrosine residues to the liposome resident dansyl-PE probe. Considering the close distance interaction required for quenching, the extent of quenching is sensitive to the molecular factors that affect the rate and probability of contact, including steric shielding, and charge-charge interactions [41]. In contrast, FRET is a through space interaction that occurs over long distances and is insensitive to these factors. Furthermore, the theory of Forster predicts that FRET depends on the distance and the final factor (the orientation factor). The dependence of the orientation factor ($κ^2$) on the direction of the emission dipole of the donor and the absorption dipole of the acceptor play a very important role.

Figure 6.18. Interaction of hMMP-7 with cationic liposome containing POPC: EPOPC: DPE (65:25:10) mol %. A Spectra of EPOPC 25% in presence of protein, the inset show the difference spectra after subtraction of the background dansyl signal B. The binding isotherm for the POPS – MMP-7 complex. The solid smooth line is the best fit of the data for K_d value 20.6 ± 0.02 μM.

Figure 6.19. Interaction of hMMP-9 with cationic liposome containing POPC: EPOPC: DPE (65:25:10) mol %. A. Spectra of EPOPC 25% in presence of protein, the inset shows the difference spectra after subtraction of the background dansyl signal B. The binding isotherm for the POPS – MMP-9 complex. The solid smooth line is the best fit of the data for K_d value 14.5 ± 0.013 μM.
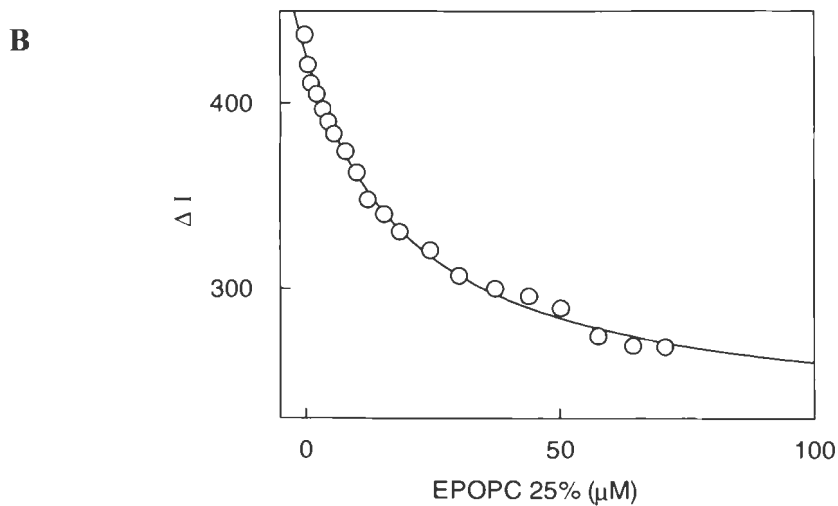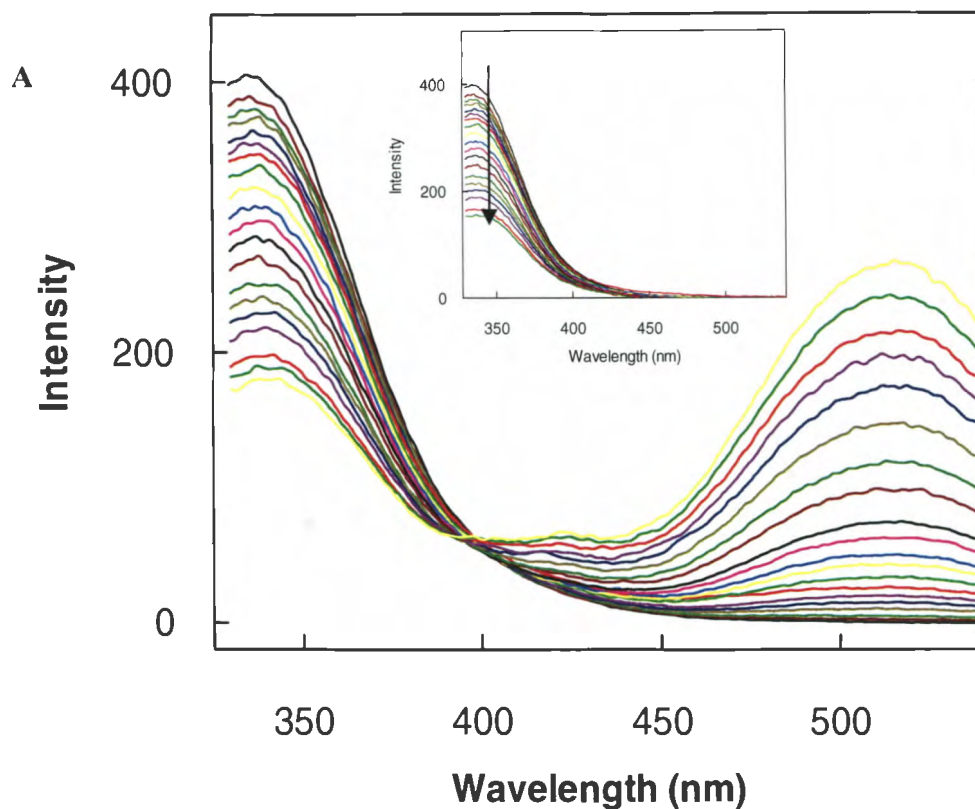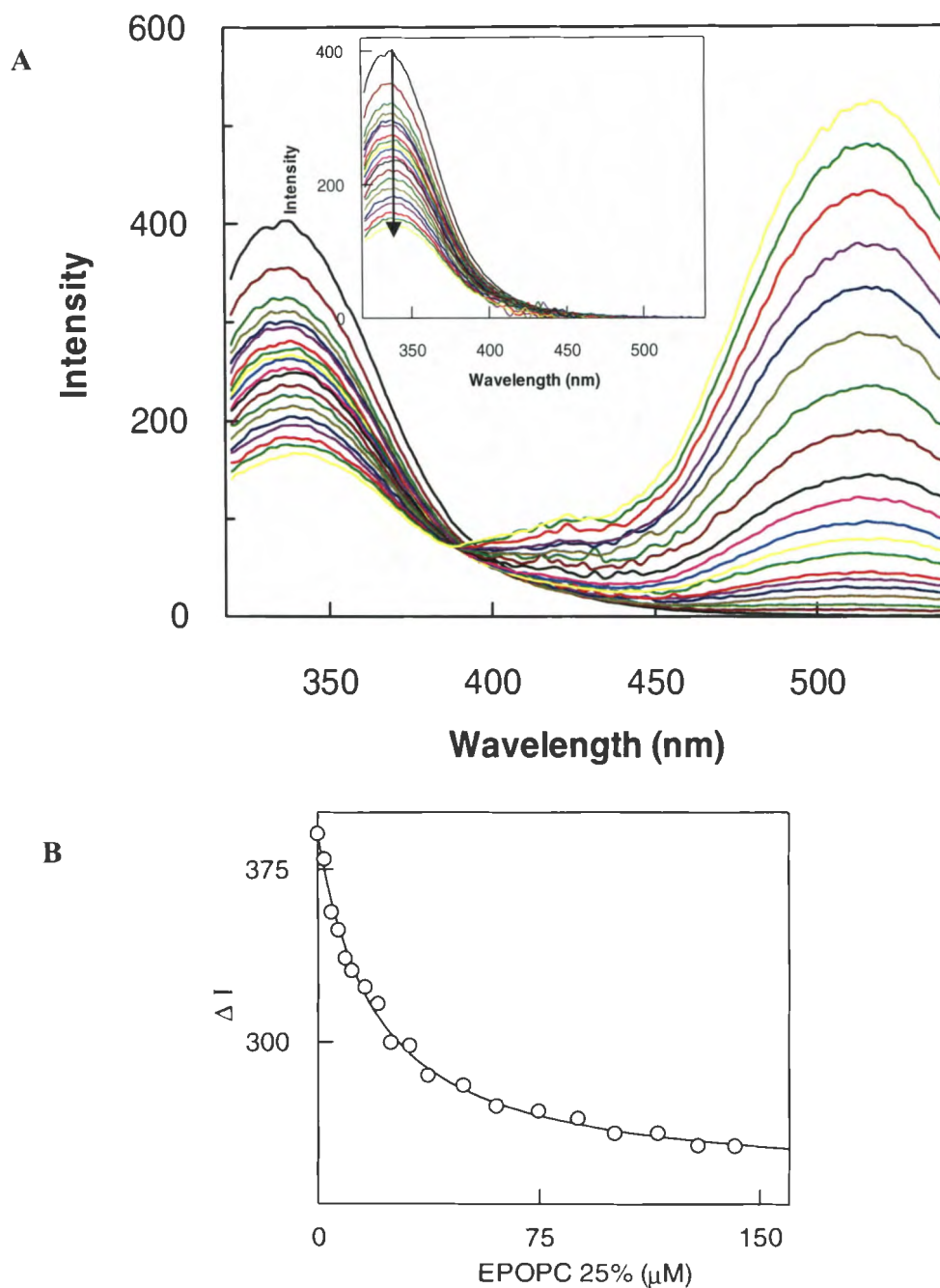
Figure 6.20. Interaction of hMMP-10 with cationic liposome containing POPC: EPOPC: DPE (65:25:10) mol %. A. Spectra of EPOPC 25% in presence of protein, the inset shows the difference spectra after subtraction of the background dansyl signal B. The binding isotherm for the POPS – MMP-10 complex. The solid smooth line is the best fit of the data for K_d value 8.2 ± 0.015 μM.

Table 6.3 shows the relationship between K_d (MMP isozymes) and EPOPC (25 mol %) liposomes. hMMP-10 shows a two-fold tighter binding than hMMP-7 and 9. Figure 6.21 shows the binding isotherm of hMMP-7 with neutral liposomes containing POPC: DPE (90:10) mol %. The K_d value was 13.8 ± 0.04 µM. POPC liposomes bind to hMMP-7. Upon a closer look at the electrostatic surface potential (Figure 6.2), it was obvious that the binding of liposomes occurred near and/or around the positive cluster of residues (on the rear side of the active site pocket).

Table 6.3. Relationship between K_d (MMP isozymes) vs EPOPC (25 mol %). hMMP-10 shows two-fold tighter binding than hMMP-7 and 9.

MMP Isozymes	K_d (25 % EPOPC) µM
hMMP-7	20.6
hMMP-9	14.5
hMMP-10	8.2

Although the putative binding region of neutral liposomes was still not clearly apparent, upon titrating POPC rich liposomes to both hMMP-9 and 10 (Figure 6.22, 6.23), both of the hMMP isozymes responded by quenching [47] of the fluorescence signals of Typ/Tyr residues. The K_d values for hMMP-9 and hMMP-10 were 46.5 ± 0.07 µM and 25.8 ± 0.03 µM, respectively. Table 6.4 shows relationship between K_d (MMP isozymes) and POPC (90 mol %). hMMP-7 has the tightest binding affinity amongst MMPs.

Table 6.4. Relationship between K_d (MMP isozymes) vs POPC (90 mol %). hMMP-7 has the tightest binding affinity amongst the MMP isozymes.

MMP Isozymes	K_d (90 % POPC) µM
hMMP-7	13.8
hMMP-9	46.5
hMMP-10	25.8

Figure 6.21. Interaction of hMMP-7 with neutral liposomes containing POPC: DPE (90:10) mol %. A. Spectra of POPC 90% in the presence of protein, the inset shows the difference spectra after subtraction of the background dansyl signal B. The binding isotherm for the POPS – MMP-7 complex. The solid smooth line is the best fit of the data for K_d value 13.8 ± 0.04 μM.

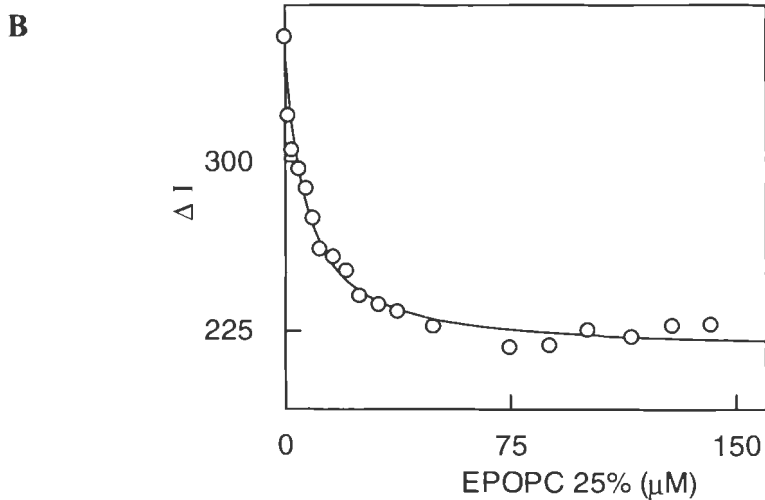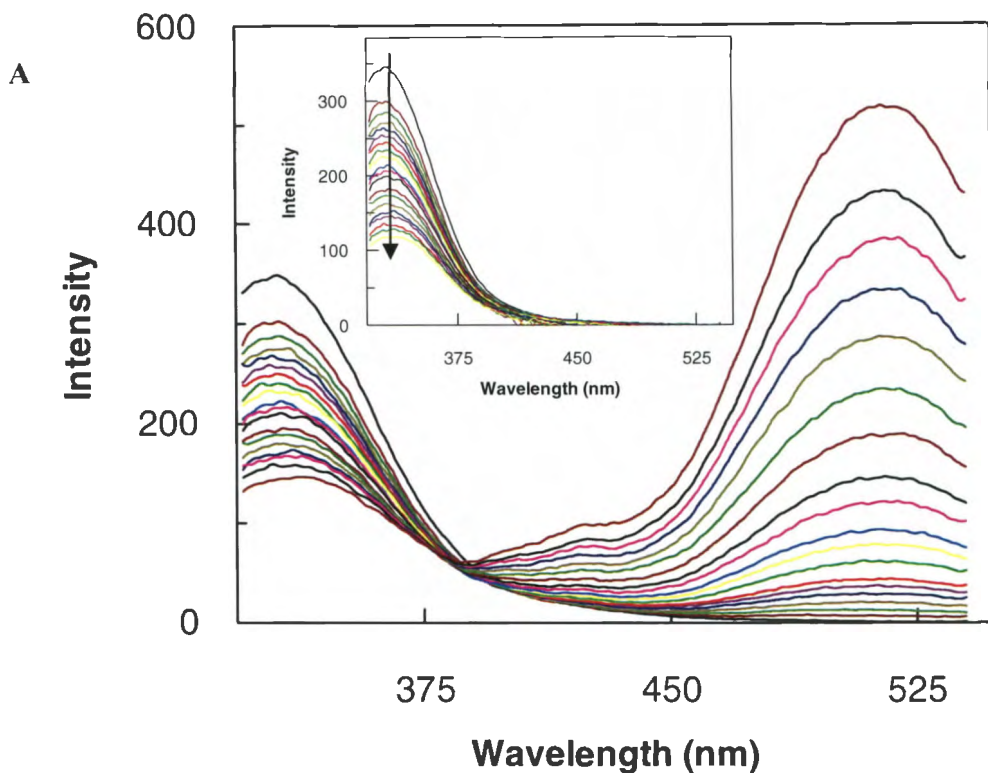Figure 6.22. Interaction of hMMP-9 with neutral liposomes containing POPC: DPE (90:10) mol %. A. Spectra of POPC 90% in the presence of protein, the inset shows the difference spectra after subtraction of the background dansyl signal B. The binding isotherm for the POPS – MMP-9 complex. The solid smooth line is the best fit of the data for K_d value 46.5 ± 0.07 μM.
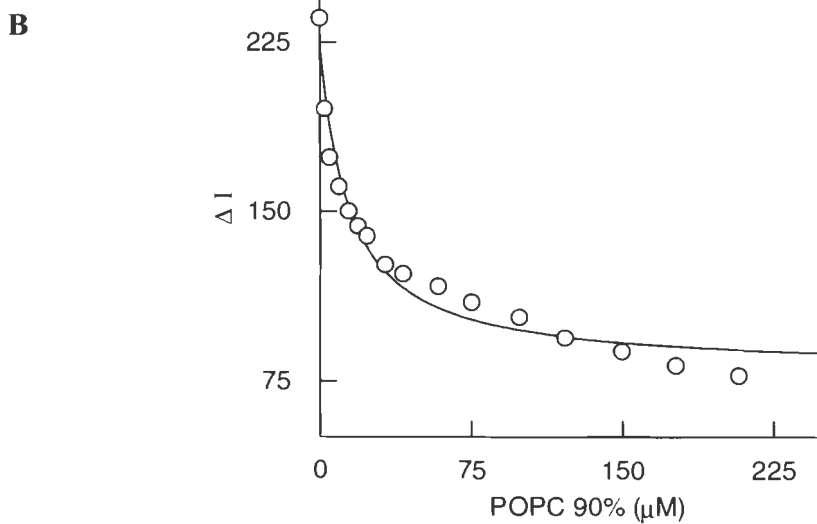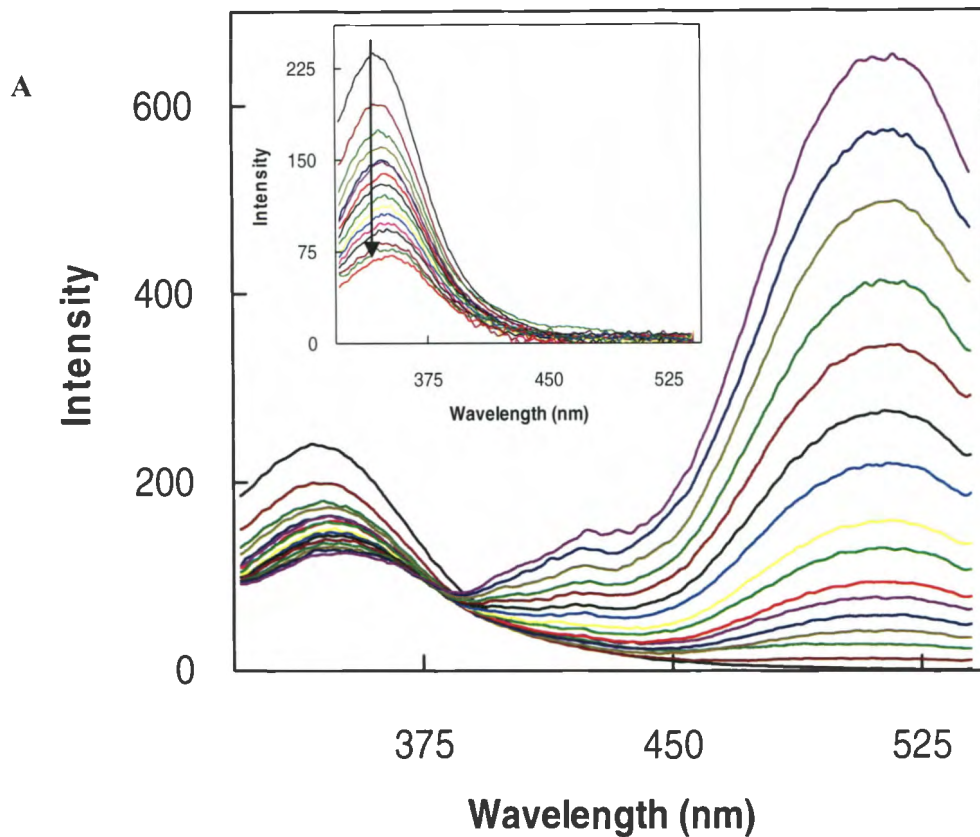
Figure 6.23. Interaction of hMMP-10 with neutral liposomes containing POPC: DPE (90:10) mol %. A. Spectra of POPC 90% in the presence of protein, the inset shows the difference spectra after subtraction of the background dansyl signal B. The binding isotherm for the POPS – MMP-10 complex. The solid smooth line is the best fit of the data for K_d value 25.8 ± 0.03 μM.

Figure 6.24 shows the structure of the two important lipid components used for these studies. PIP$_2$ and POPS lipid constituents were used to formulate anionic liposomes. These two lipids contribute to negative charge, POPS and 1,2-dioleoyl-sn-glycero-3-phosphoinositol-4,5-bisposphate (PIP$_2$), which harbors (q= -1) and (q= -3) net charges, respectively, in their head groups at neutral pH.

PIP$_2$ (Anionic Lipid;q = - 3)   **POPS** (Anionic Lipid; q = -1)
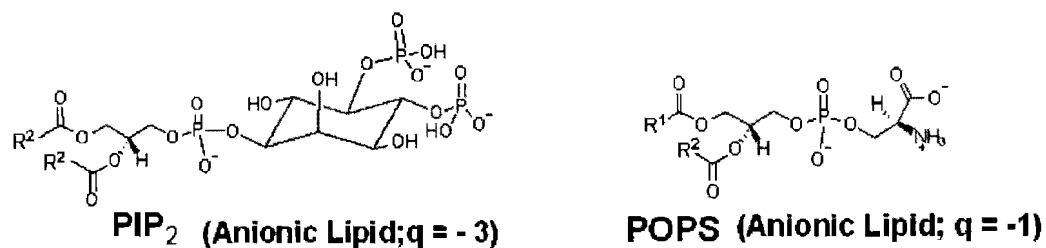
Figure 6.24. Structure of the PIP$_2$ and POPS lipids showing the net charges in their head groups at neutral pH (7.0).

Although, this work clearly exhibits that hMMP-7 has immense specificity for phospholipid head groups vis-a-vis POPS as a specific binder there still is a need to determine whether or not hMMP-7 binds with equal specificity to any other negatively charged liposomes. In order to do this, three different types of anionic liposomes were formulated. Here, the anionic liposomes had POPC as the major component, but the PIP$_2$ concentration was varied to include 1 mol %, 2 mol % and 4 mol %. Clearly, it was intended to strategically increase the LCD with the subsequent increase in the mol % of the PIP$_2$ constructed LUVs.

Figure 6.25 shows the interaction of hMMP-7 with anionic liposomes containing POPC: PIP$_2$: DPE (89:1:10) mol %. With an identical experimental setup, POPC: PIP$_2$: DPE (88:2:10) mol % and POPC: PIP$_2$: DPE (86:4:10) mol % were used to determine the K$_d$ values of hMMP-7 towards these liposomes. The K$_d$ values for the interaction of PIP$_2$ (1

mol %), PIP$_2$ (2 mol %) in Figure 6.26 and PIP$_2$ (4 mol %) in Figure 6.27 with hMMP-7

were 2.6 ± 0.014 μM, 5.2 ± 0.02 μM and 5.5 ± 0.2 μM, respectively. Figure 6.28 shows the

relationship between K$_d$ and PIP$_2$ mol %. Based on the observation, it becomes evident that

with slight variation like 1 mol %, 2 mol % and 4 mol % PIP$_2$, there was no significant

change in the K$_d$ values.

When the chemical structures of POPC and PIP$_2$ were closely compared (Figure

6.1), it was obvious that the orientation of the head group of PIP$_2$ projects perpendicular

with respect to the plane of the membrane surface. The potentially erect structure and large

head group size implies that it may protrude further into the aqueous phase than a typical

phospholipid [44]. There has been a conscious attempt to strictly vary the PIP$_2$ mol %

within a very narrow range because: (A) The typical effective concentration of PIP$_2$ in a

mammalian cell is about of 1 mol % of phospholipids, which is ~ 10 μM in a human

erythrocyte [48]; and (B) Above 5 mol % of PIP$_2$, there is induction of domain formation

even with little membrane stress, which would contribute to unnecessary complications in

the liposome organization while formulating the native PIP$_2$ liposomes.

Table 6.5 summarizes the K$_d$ values of hMMP-7 interaction with different mol % of

POPS LUVs with the K$_d$ values for hMMP-7 interaction with different mol % of PIP$_2$

LUVs. A casual perusal of the comparative data reveals that the binding of hMMP-7 with

25 mol % POPS has a similar K$_d$ as that of binding to only 4 mol % PIP$_2$ LUVs. There is

more favorable binding of PIP$_2$ than POPS lipid head groups.
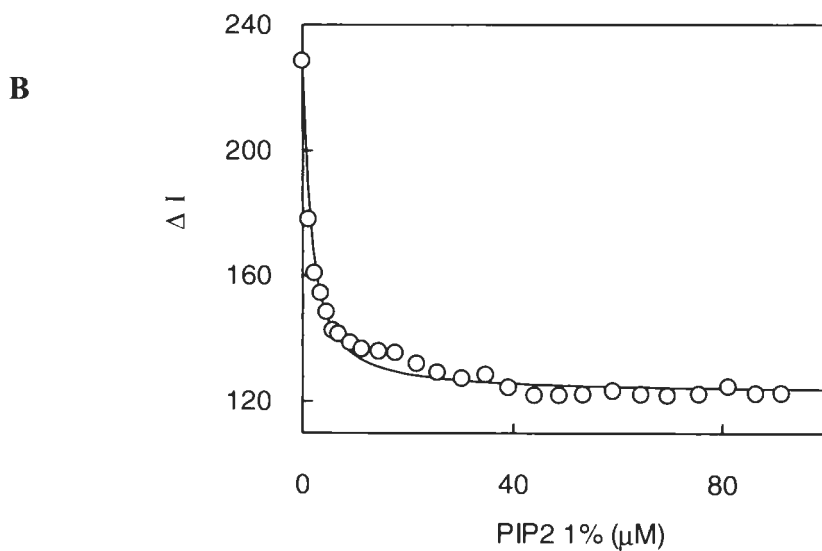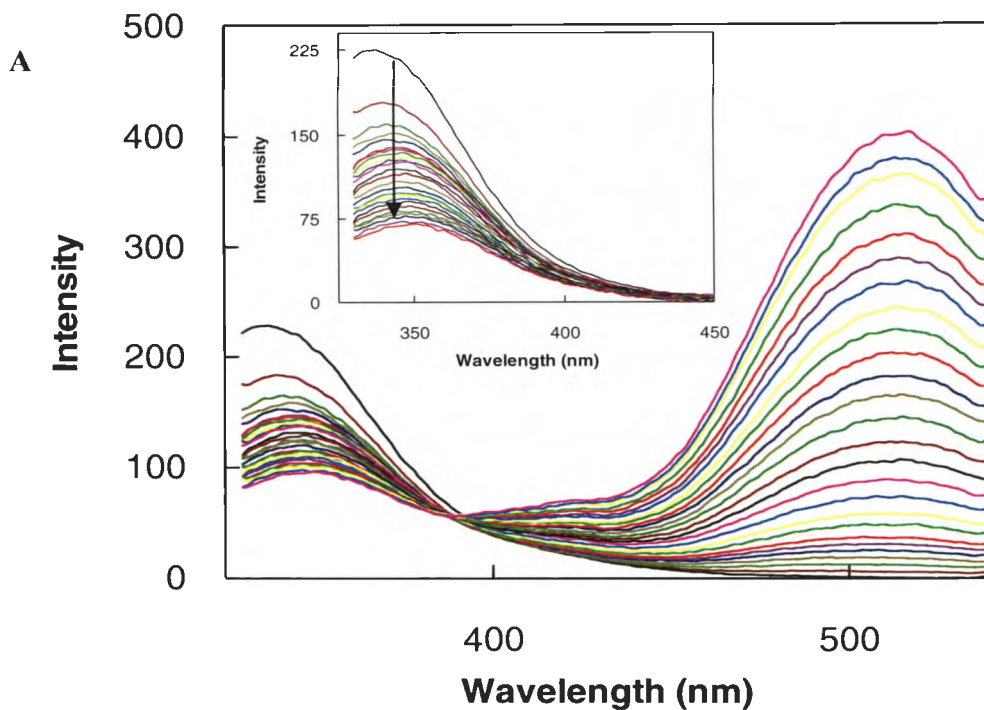
Figure 6.25. Interaction of hMMP-7 with anionic liposomes containing POPC: PIP_2: DPE (89:1:10) mol %. A. Spectra of PIP_2 1 mol % in presence of protein, the inset shows the difference spectra after subtraction of the background dansyl signal B. The binding isotherm for the PIP_2 – MMP-7 complex. The solid smooth line is the best fit of the data for K_d value 2.6 ± 0.01 μM.
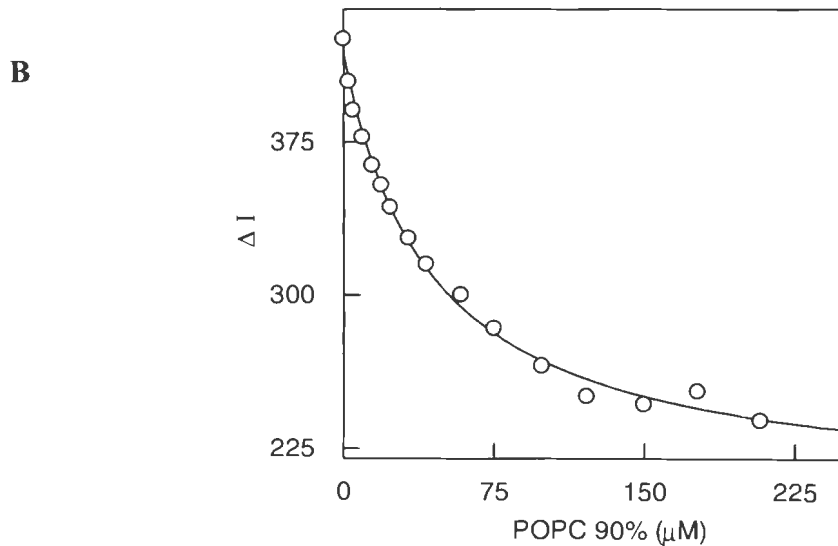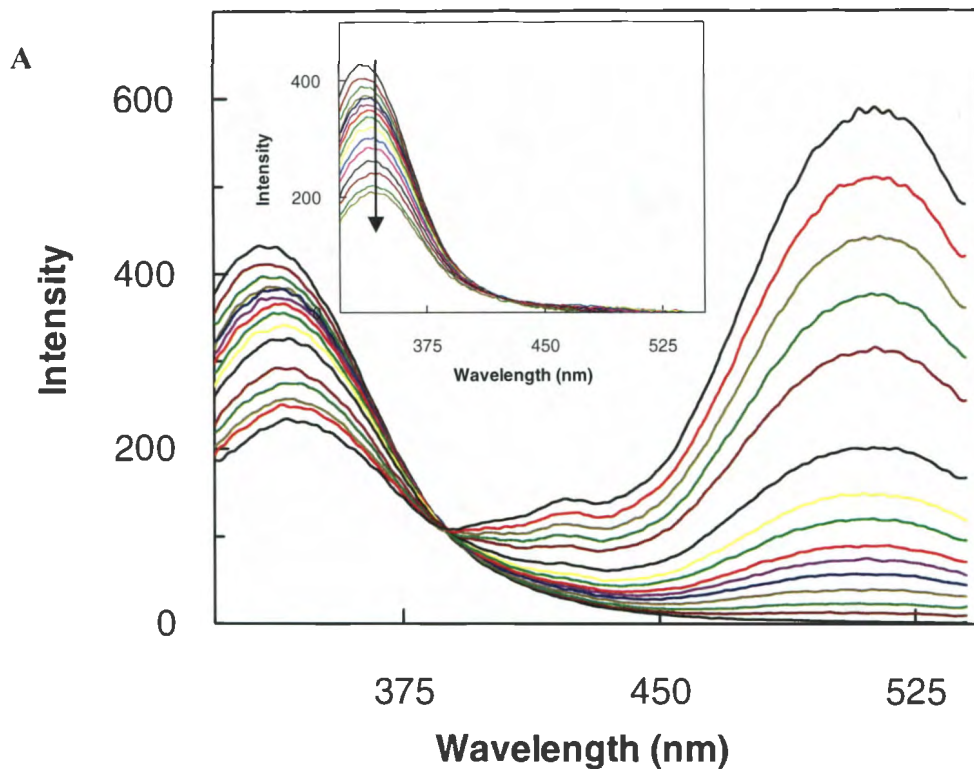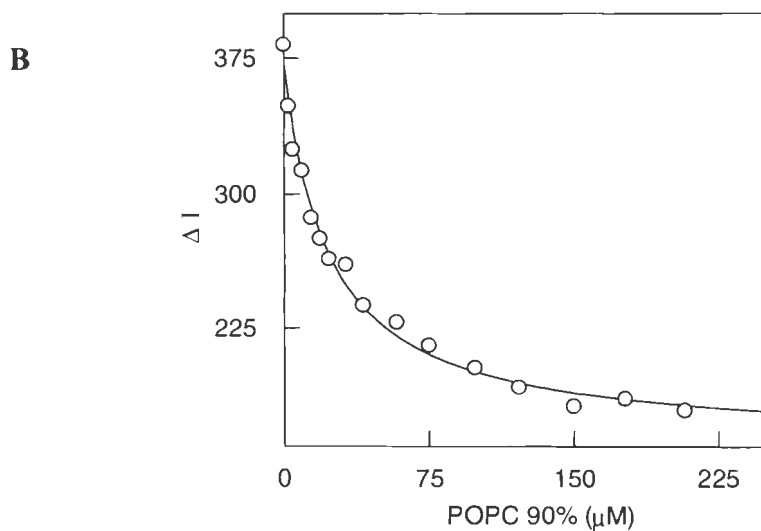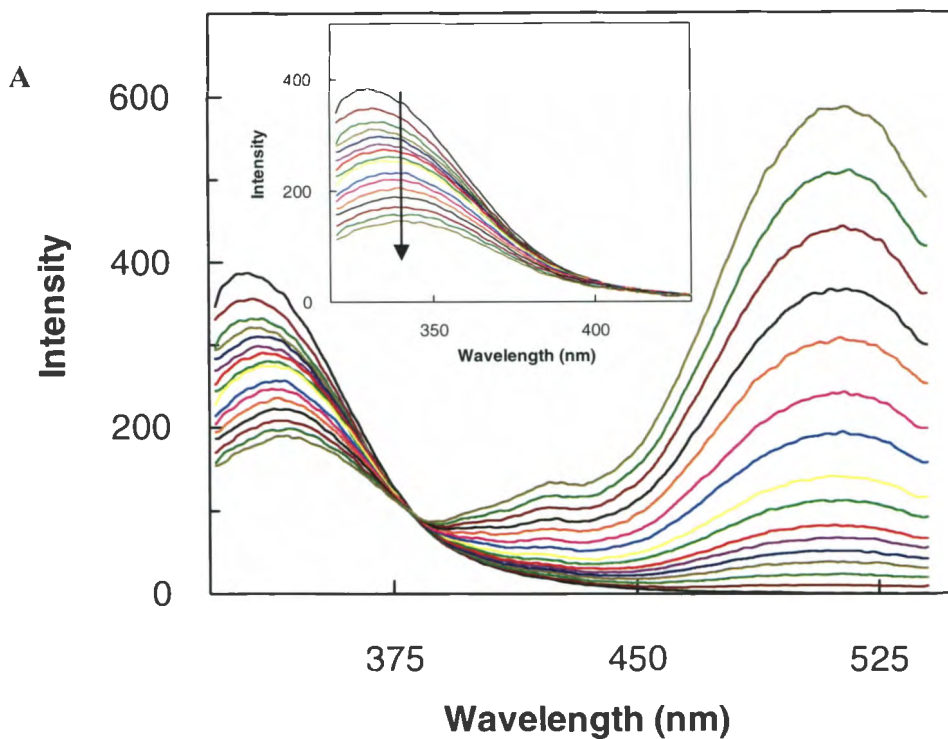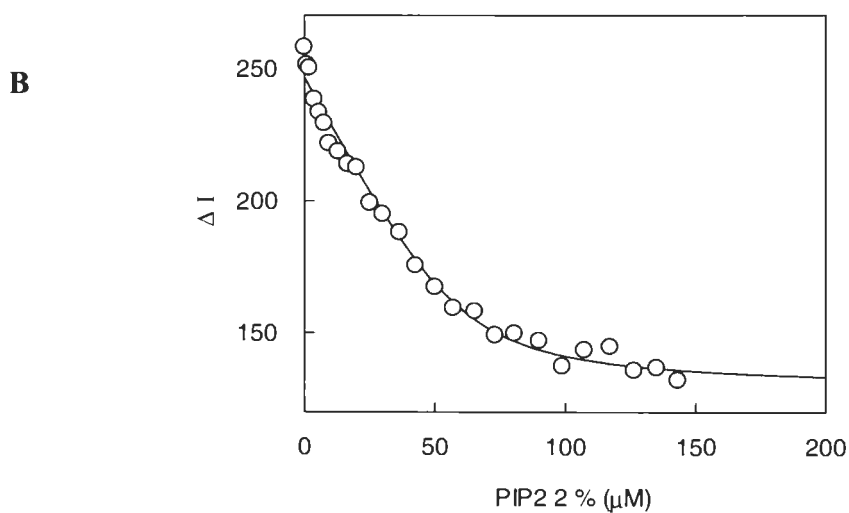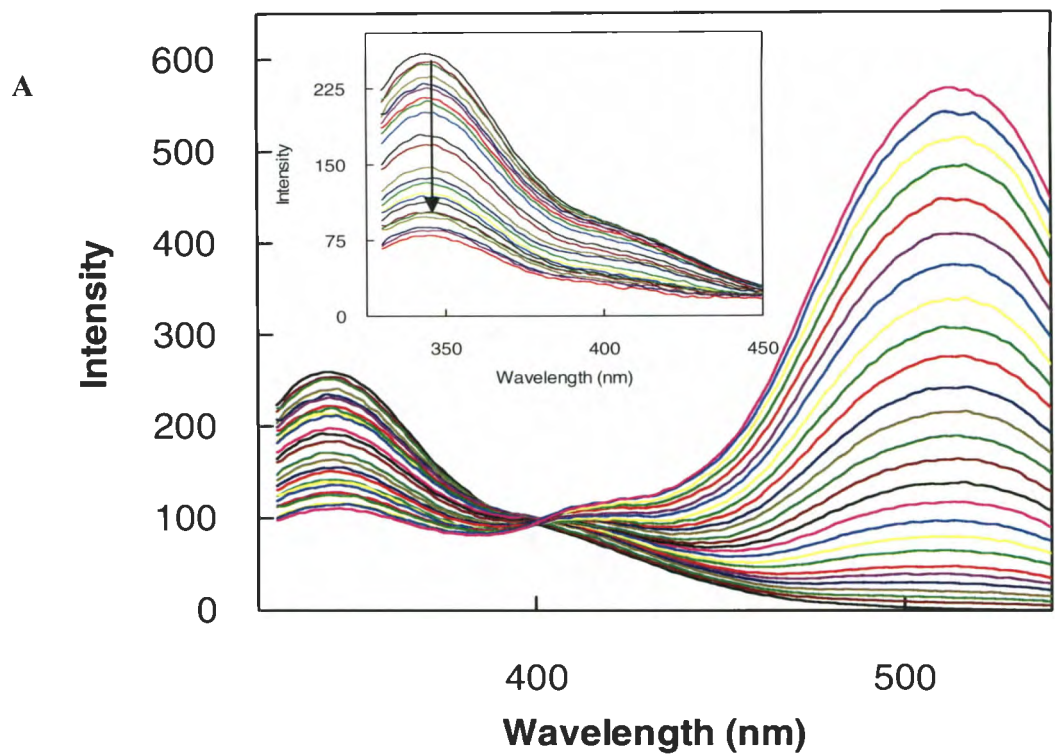
Figure 6.26. Interaction of hMMP-7 with anionic liposomes containing POPC: PIP$_2$: DPE (88:2:10) mol %. A. Spectra of PIP$_2$ 2 mol % in presence of protein, the inset shows the difference spectra after subtraction of the background dansyl signal B. The binding isotherm for the PIP$_2$ – MMP-7 complex. The solid smooth line is the best fit of the data for K$_d$ value 5.2 ± 0.02 μM.
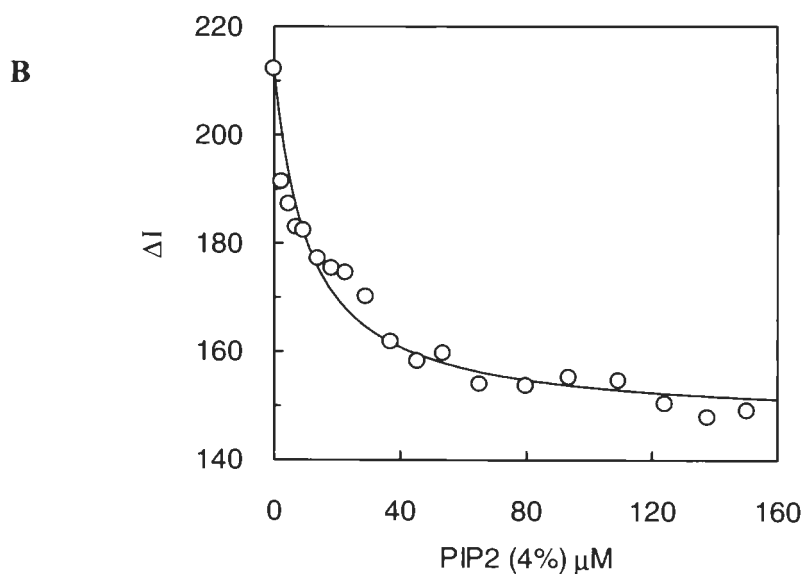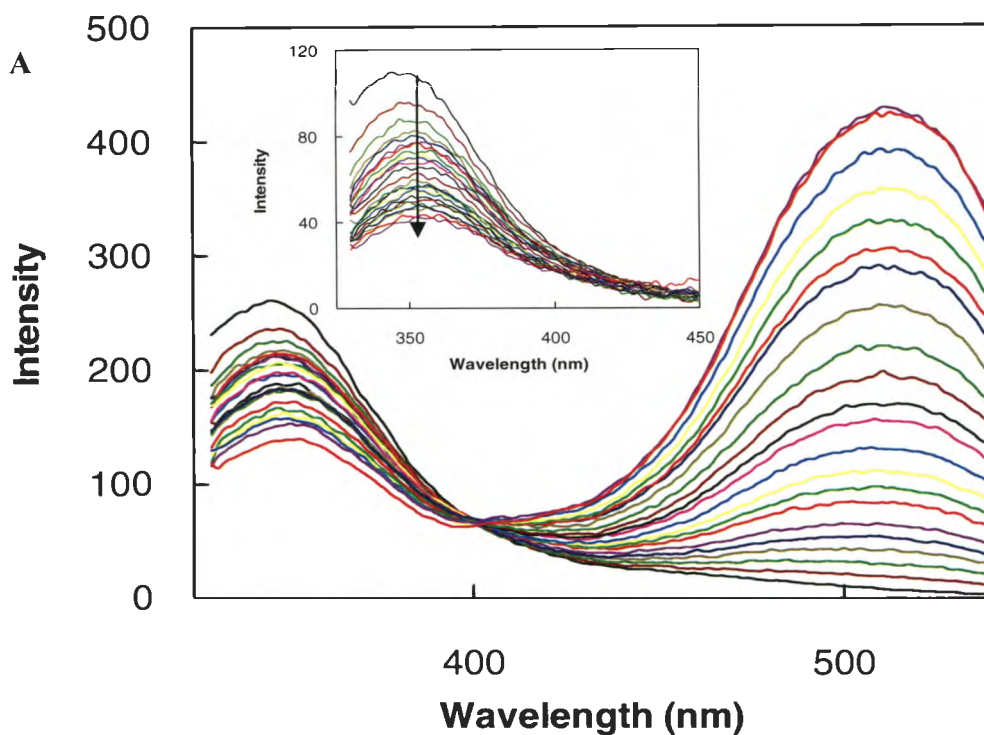
Figure 6.27. Interaction of hMMP-7 with anionic liposomes containing POPC: PIP_2: DPE (86:4:10) mol %. A. Spectra of PIP_2 4 mol % in presence of protein, the inset shows the difference spectra after subtraction of the background dansyl signal B. The binding isotherm for the PIP_2 – MMP-7 complex. The solid smooth line is the best fit of the data for K_d value 5.8 ± 0.2 µM.
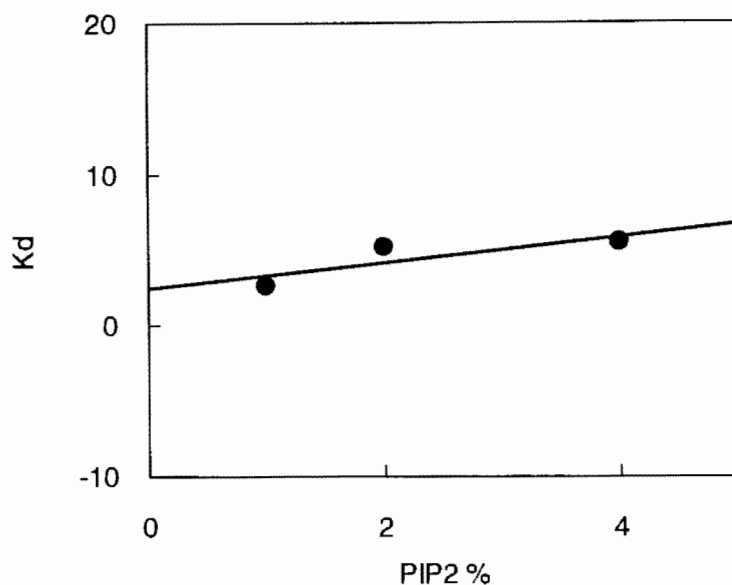
Figure 6.28. Relationship between K_d (hMMP-7) vs PIP_2 mol %.

Such a scenario could originate when protein containing clusters enriched with basic and hydrophobic residues bind to negatively charged lipids like PIP_2. They might control the local free concentration of PIP_2 in the plasma membrane by sequestration of these anionic lipids [49] which are commonly found in the plasma membrane, like the ones already mentioned in the Chapter.

Table 6.5. Comparison of K_d (hMMP-7) values between POPS % and PIP_2 % LUVs.

POPS %	K_d (μM)
POPS 5 %	55
POPS 10 %	21.3
POPS 25%	**5.5**
POPS 30 %	10.1
POPS 40%	1.73

PIP_2 %	K_d (μM)
PIP_2 1 %	2.6
PIP_2 2 %	5.2
PIP_2 4%	**5.8**

Many recent precedents and theoretical analyses [50] throw light on the fact that when the monovalent acidic lipids (like POPS) are subjected to such interactions the POPS lipids are sequestered minimally, if at all. Despite the mounting evidence for the existence of spatially distinct pools of PIP_2 [49], the precise mechanism for the formation of such domains has yet to be defined.

Now that the binding specificities of hMMP-7 towards anionic liposomes have been resolved, it was of prime importance to investigate the effect of the differently charged LUVs on the functional aspect of these enzymes. To test the above hypotheses, the influence of liposomes bearing different charges on the catalytic activity of hMMP-7 was determined.

Figure 6.29 shows the effect of differently charged liposomes on enzyme activity of hMMP-7. Since the negative charges appeared to be clustered in the vicinity of the active-site pocket of hMMP-7 (see Figure 6.2), it was logical to expect that the enzyme activity would be impaired upon binding of hMMP-7 to the positively (but not negatively) charged liposomes.

As expected, the data clearly show that the neutral and negatively charged liposomes do not inhibit the hMMP-7 catalyzed reaction. However, the positively charged liposomes exhibit a pronounced inhibitory effect. The analysis of the inhibition data yielded a K_i value of 18.6 $\pm$ 0.4 μM for the positively charged (EPOPC-containing) liposomes, which is comparable to their direct binding affinity (K_d = 20.6 $\pm$ 0.02 μM; Table 6.3).

It should be pointed out that the above similarity suggests that the inhibition of the

hMMP-7 by cationic liposomes is due to their "physical-proximity" interaction. However, to exclude the possibility that the above inhibition is due to the binding of substrates to the cationic liposomes (such that the substrates are not available to the enzyme), we performed an analytical HPLC (using a C_{18} reverse phase column) experiment. In this experiment (Figure 6.30), the elution profiles of the substrate (20 μM) in the absence and presence of cationic liposomes (200 μM) were compared under the condition where about 90% hMMP-7 was inhibited (see Figure 6.29). The experimental data revealed that the elution time of the substrate remained unchanged in the presence of cationic liposomes suggesting that the substrate did not interact with the liposomes.

Figures 6.31 and 6.32 show the effect of differently charged liposomes on enzyme activity of hMMP-9 and 10. Surprisingly, none of the differently charged liposomes perturbed the enzyme activity of hMMP-9 and hMMP-10. In the light of the data presented herein, it appears plausible that the coulombic interaction between the negatively charged active site surface of hMMP-7 and the cationic phospholipid head groups of the liposomes exists. The cationic LUVs probably block the accessibility of the substrate to the active-site pocket of the enzyme, causing the inhibition of the enzyme. Since the negatively charged liposomes are unlikely to block the accessibility of the enzyme's active site pocket for its substrate (due to potential coulombic repulsion), they do not exhibit the inhibitory effect. The different "site specific binding" of anionic versus cationic liposomes is also apparent from the difference in steady-state fluorescence emission profiles of the hMMP-7-liposome complexes (compare the Figure 6.5 and 6.18).

Because of all the lack of an extensive surface curvature coupled with the flexibility

Figure 6.29. Effect of differently charged liposomes on enzyme activity of hMMP-7. The enzyme-catalyzed hydrolysis of the fluorogenic peptide (λ_{ex} = 335 nm, λ_{em} = 395 nm) was measured as a function of the liposome concentrations exposed in the outer leaflet of LUVs. The symbols (□-□), (o-o) and (●-●) represents Anionic (POPS - 25 mol %), Neutral (POPC - 90 mol %) and Cationic (EPOPC - 25 mol %) liposomes, respectively. Only EPOPC (25 mol %) inhibits the enzyme activity of hMMP-7. The solid smooth line is the best fit of the data for the K_i value of MMP-7–cationic liposome complex equal to 18.6 ± 0.4 μM.
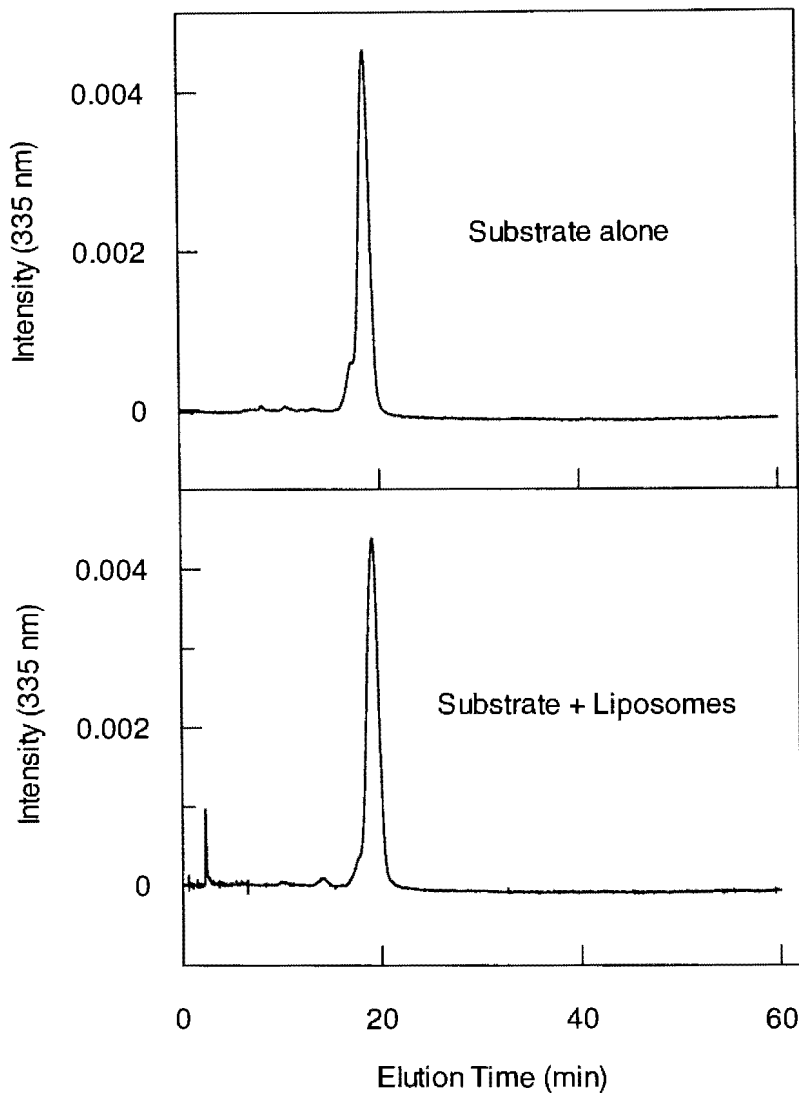
Figure 6.30. HPLC fluorescence spectra of substrate alone and substrate along with cationic liposomes (EPOPC-25 mol %) as a function of retention time. 20 μM substrate in the absence (Figure 55; top panel) and presence of 200 μM liposomes (Figure 55; bottom panel) was loaded onto the a vydac C_{18} reverse phase column, on an analytical HPLC and subsequently eluted by a linear gradient of 0-70% acetonitrile in water (containing 0.1% TFA) over a 60 minutes time period. The flow rate of the column was maintained at 1.5 ml/min. the peak elution time of the substrate remained unchanged upon its incubation with the cationic liposomes, suggesting that the latter did not sequester the substrate. Hence, the inhibition of hMMP-7 by cationic liposomes is a consequence of direct interaction between the above species.

of the lipid bilayer, it is conceivable that the cationic LUVs elicit the inhibitory influence on the hMMP-7 catalyzed reaction. There are literature precedents of these findings with other proteins [51-53]. It has been argued that when proteins bind to flexible surfaces like liposome nanoparticles (LNPs), they adjust their conformations in response to the dynamic "re-organization" of the membrane.
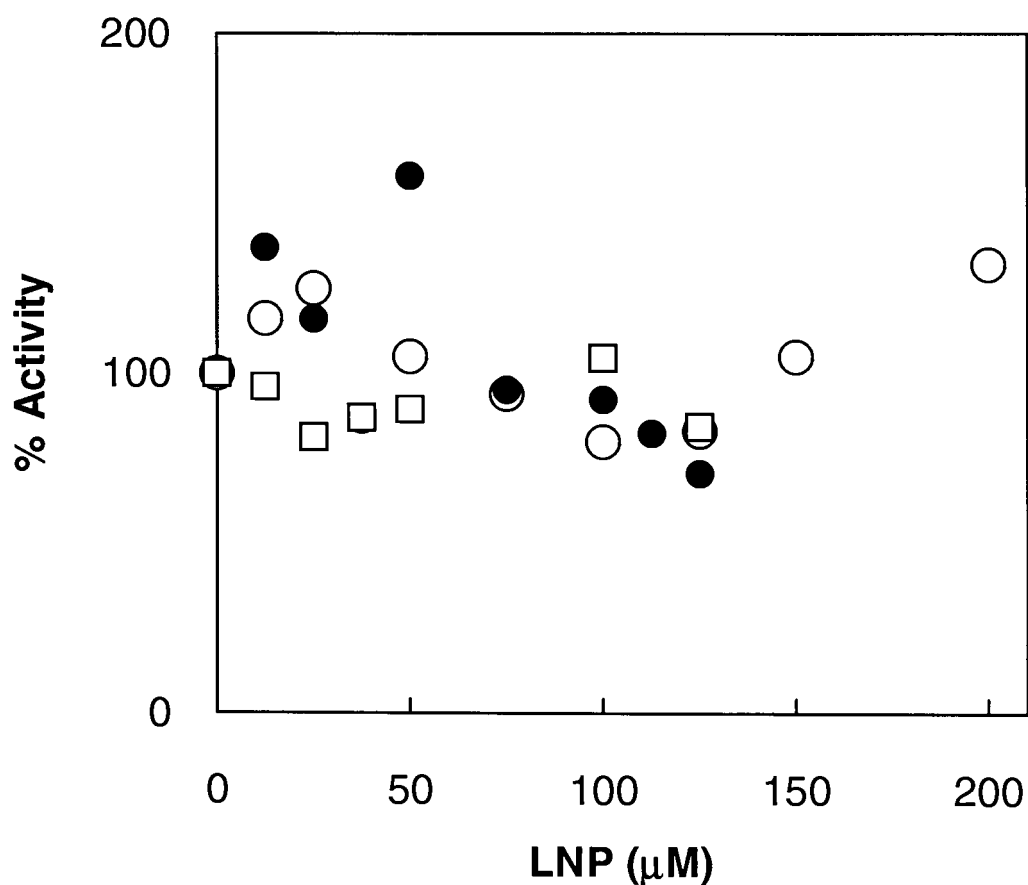
Figure 6.31. Effect of differently charged liposomes on enzyme activity of hMMP-9. The enzyme-catalyzed hydrolysis of the fluorogenic peptide (λ_{ex} = 335 nm, λ_{em} = 395 nm) was measured as a function of the liposome concentrations exposed in the outer leaflet of LUVs. The symbols (□-□), (o-o) and (●-●) represents anionic (POPS - 25 mol %), neutral (POPC - 90 mol %) and cationic (EPOPC - 25 mol %) liposomes, respectively. None of the differently charged liposomes perturbed the enzyme activity of hMMP-9.
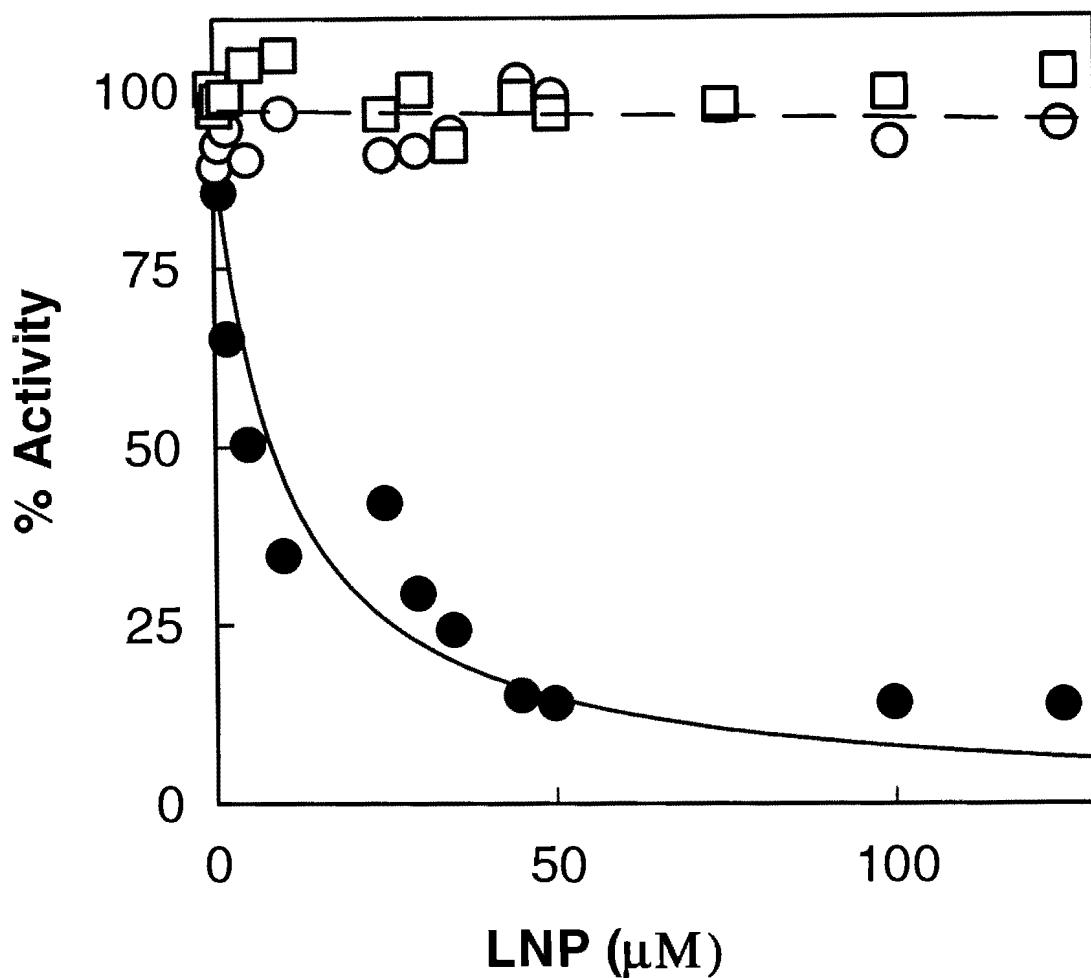
195
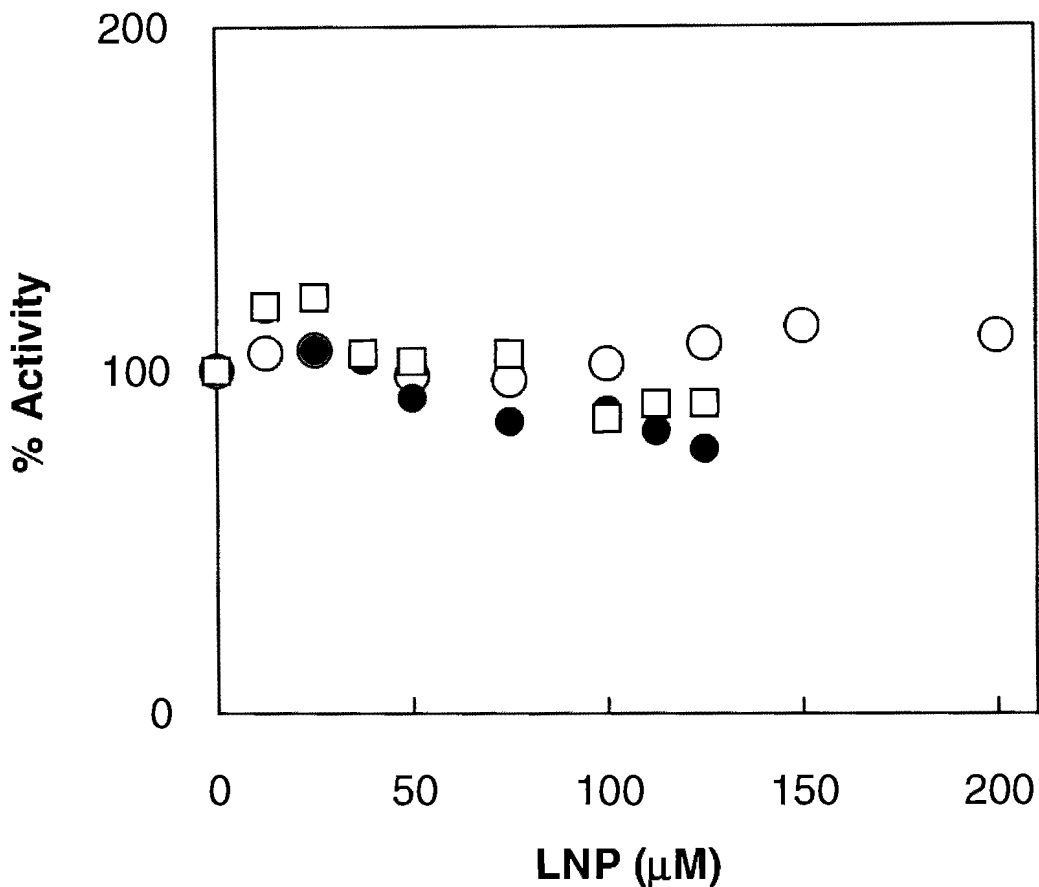
Figure 6.32. Effect of differently charged liposomes on enzyme activity of hMMP-10. The Enzyme-catalyzed hydrolysis of the fluorogenic peptide (λ_{ex} = 335 nm, λ_{em} = 395 nm) was measured as a function of the liposome concentrations exposed in the outer leaflet of LUVs. The symbols ($\square$-$\square$), (o-o) and (●-●) represents anionic (POPS - 25 mol %), neutral (POPC - 90 mol %) and cationic (EPOPC - 25 mol %) liposomes, respectively. None of the differently charged liposomes perturbed the enzyme activity of hMMP-10.

Depending on their intrinsic thermodynamic stabilities, both LNPs and their interacting protein partners can mutually cause structural deformities (Scheme 6.1); such phenomena are often referred to as the "bending-dominated deformation" of flexible LNPs and "stretching-dominated response" of the intrinsically flexible protein [54].

Streching response in MMP-7

NATIVE MMP-7

Cationic Liposome

Bending deformation in LNP
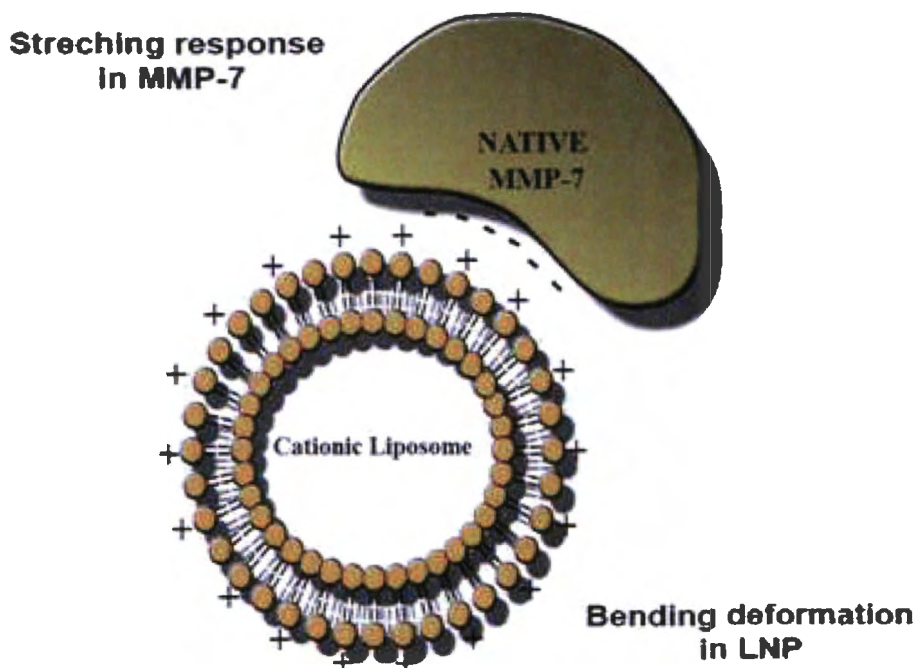
Scheme 6.1. Schematic representation of the effect of surface curvature and flexibility of LUVs on the differential mode of binding of hMMP-7 to cationic liposome and influence on the catalytic activity of the enzyme. This figure has been taken from Ref 60.

Weak interactions of proteins and their cognate ligand partners (eg. van der Waals, electrostatic and hydrogen bonding forces, etc.) may contribute to the binding of hMMP isozymes binding to the differently charged lipid membranes. The hypothesis that interaction of hMMP with their cognate partners is driven by electrostatic and/or hydrophobic interactions which can be derived from the fact that hMMP isozymes interact with both anionic and cationic LUVs. There are examples of such phenomena happening with other proteins [55], but no such study has been reported for hMMP isozymes. Many important biochemical processes involve reactions in which no covalent bonds are made or broken; only weaker bonds and interactions are involved [56]. Examples include the reaction of an antigen with its cognate antibody, the binding of many hormone proteins,

denaturation of proteins and nucleic acids, and so on. In order to understand the structure and dynamics of biological macromolecules, one needs to understand the molecular forces that act within a macromolecule [55-56].

Many studies support the hypothesis that the interactions between neighboring PIP_2 molecules occur by electrostatic repulsion between the charge-dense poly-anionic head groups. It was also worth noting, the importance of hydrogen bonding or lipid head group hydration in maintaining the physical state of PIP_2 in planar systems. The specificity of $PI(4,5)P_2$ may be because of an unique ability to form hydrogen-bonded networks resulting in structural and functional sequestration. Because of their large negative charge (q = -3), these lipids may display only mutually repulsive interactions within the plane of the bilayer that keeps them dispersed unless they are anchored to specific proteins [57].

To ascertain the influence of ionic strength of the buffer on the local charge distribution and organization of the native conformation of the LUVs upon physically interacting with the hMMP isozymes, the K_d values for the binding of hMMP isozymes to POPS (25 mol %) and EPOPC (25 mol %) LUVs with varying concentrations of NaCl were carried out. As shown in Figure 6.33, 1 ml standard stock of 1 M NaCl concentration was prepared in 25 mM HEPES buffer, pH 7.5 in a falcon tube. Subsequent dilutions were prepared in 1 ml eppendorf tubes varying from 0 to 250 mM NaCl. The osmolality of these NaCl concentrations was measured and the osmolality as a function of NaCl concentrations (mM) was plotted. The slope of the plot was used to calculate and adjust the osmolality of these liposomes formulated separately for maintaining the osmotic pressure and preventing the LUVs from bursting.
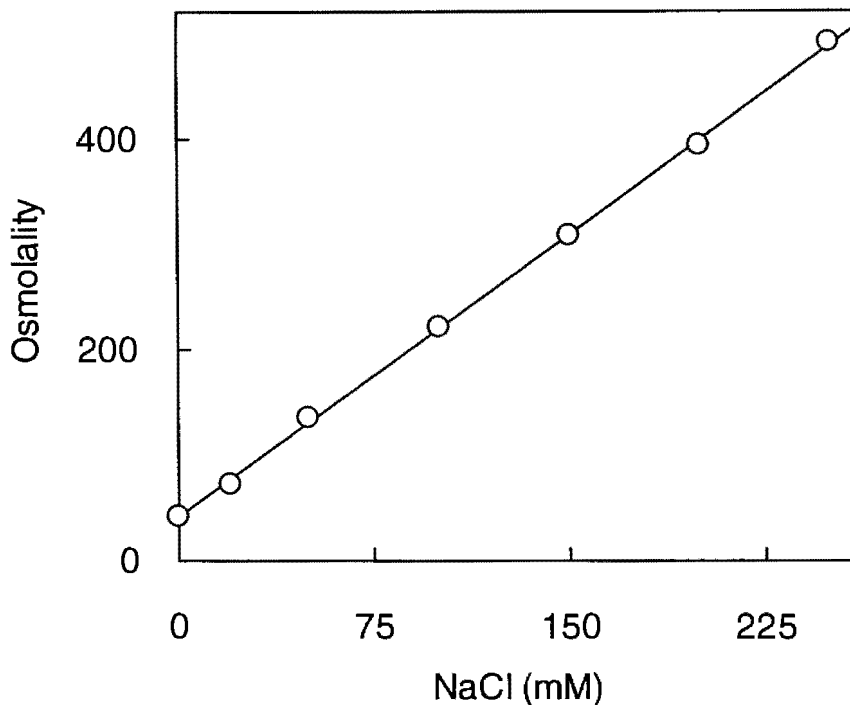
Figure 6.33. Standard plot for osmolality as a function of increasing concentration of NaCl.

Osmotic pressure balance between the molar osmotic strength inside the inner vesicle layer and in the bulk buffer can be achieved by using sucrose, PEG, or dextran while formulating liposomes with varying ionic strength [58]. Figure 6.34 A, B and C shows the binding isotherm of POPC: POPS: DPE (65:25:10) and hMMP-7 complex formation at 150 mM NaCl, 100 mM NaCl and 50 mM NaCl, respectively. It was purported to delineate the relationship between the effect of the dissociation constants (K_d values) of hMMP-7 upon binding to the POPS liposomes and varied NaCl concentration. The K_d values were 5.5 ± 0.1 μM, 2.3 ± 0.7 μM and 1.5 ± 0.5 μM for 150 mM NaCl, 100 mM NaCl and 50 mM NaCl, respectively. Note that these values show that as the ionic strength of the buffer decreases the binding of hMMP-7 to the anionic POPS liposomes increases.

Figure 6.34.A. Binding isotherm of POPC: POPS: DPE (65:25:10) and hMMP-7 at 150 mM NaCl B. Binding isotherm of POPC: POPS: DPE (65:25:10) and hMMP-7 at 100 mM NaCl C. Binding isotherm of POPC: POPS: DPE (65:25:10) and hMMP-7 at 50 mM NaCl. The excitation wavelength was set at 280 nm. A, B and C represents the binding constants derived by conducting the titration in 25 mM HEPES, pH 7.5 with varying NaCl concentrations from (A)150 mM, (B) 100 mM and (C) 50 mM. The solid smooth lines are the best fit of the data with the K_d values of $5.5 \pm 0.1 \mu M$, $2.3 \pm 0.7 \mu M$ and $1.5 \pm 0.5 \mu M$ for A, B and C, respectively.

200

There is a five-fold decrease in the K_d values when the ionic strength was varied from 150 mM NaCl concentration to 50 mM NaCl concentration (Figure 6.35). This is a clear indication of the prevalence of pure electrostatics in the physical binding of hMMP-7 and POPS (25 mol % LUVs).

Figure 6.35. Relationship between the dissociation constant (K_d) of hMMP-7 and POPS (25 mol %) as a function of salt concentration.

Proteins constantly interact with other macromolecules in the vicinity and are an essential component of a living cell. Understanding the nature of forces involved in protein-protein interaction will lead to vital clues in the functioning of cells [59].

Although complex interactions between two cognate macro-molecules are driven by hydrophobic effects and van der Waals interactions, the contributions of entropy and electrostatics cannot be neglected. Similar experiments of ionic strength dependent binding effects on hMMP-9 (see Figure 6.36 A, B and C) and hMMP-10 (Figure 6.37 A, B and C)

were carried out. The K_d values for hMMP-9 were 33.3 ± 0.24, 74.6 ± 0.12 μM and 53.0 ±

0.06 μM for 150 mM NaCl, 100 mM NaCl and 50 mM NaCl, respectively. However, the

K_d values for hMMP-10 were 40.2 ± 0.06 μM, 48.1 ± 0.12 μM and 44.0 ± 0.07 μM for 150

mM NaCl, 100 mM NaCl and 50 mM NaCl, respectively.

With the decrease in the ionic strength of the buffer, K_d values increased,

establishing the fact that binding of hMMP-9 to POPS liposomes is mediated via

hydrophobic interactions. For hMMP-10 and POPS liposomes; the K_d values did not vary.

Table 6.6 shows the relationship between the dissociation constant of hMMP-9 and

POPS (25 mol %) as a function of increasing salt concentration. Table 6.7 results further

advocate the relationship between the dissociation constant of hMMP-10 and POPS (25

mol %) as a function of increasing salt concentration. In contrast to the hMMP-7 data,

hMMP-9 and 10 experimental results do not display the explicit specific forces involved

behind the interaction of differently charged liposomes. It is suggestive of the relevant fact

that the hMMP-7-POPS complex formation is at least most prominently mediated by

electrostatic forces [56]. However, the hMMP-9-POPS or hMMP-10-POPS complexes

were partly or completely dictated by hydrophobic forces [56]. Figure 6.38 A, B and C

shows the binding isotherm of POPC: EPOPC: DPE (65:25:10) and hMMP-7 complex

formation at 150 mM NaCl, 100 mM NaCl and 50 mM NaCl, respectively. The

relationship between the effects on the dissociation constants (K_d values) of hMMP-7 upon

binding to the EPOPC liposomes at varied NaCl concentration were investigated. The K_d

values were 20.6 ± 0.02 μM, 10.0 ± 0.02 μM and 0.99 ± 0.048 μM for 150 mM NaCl, 100

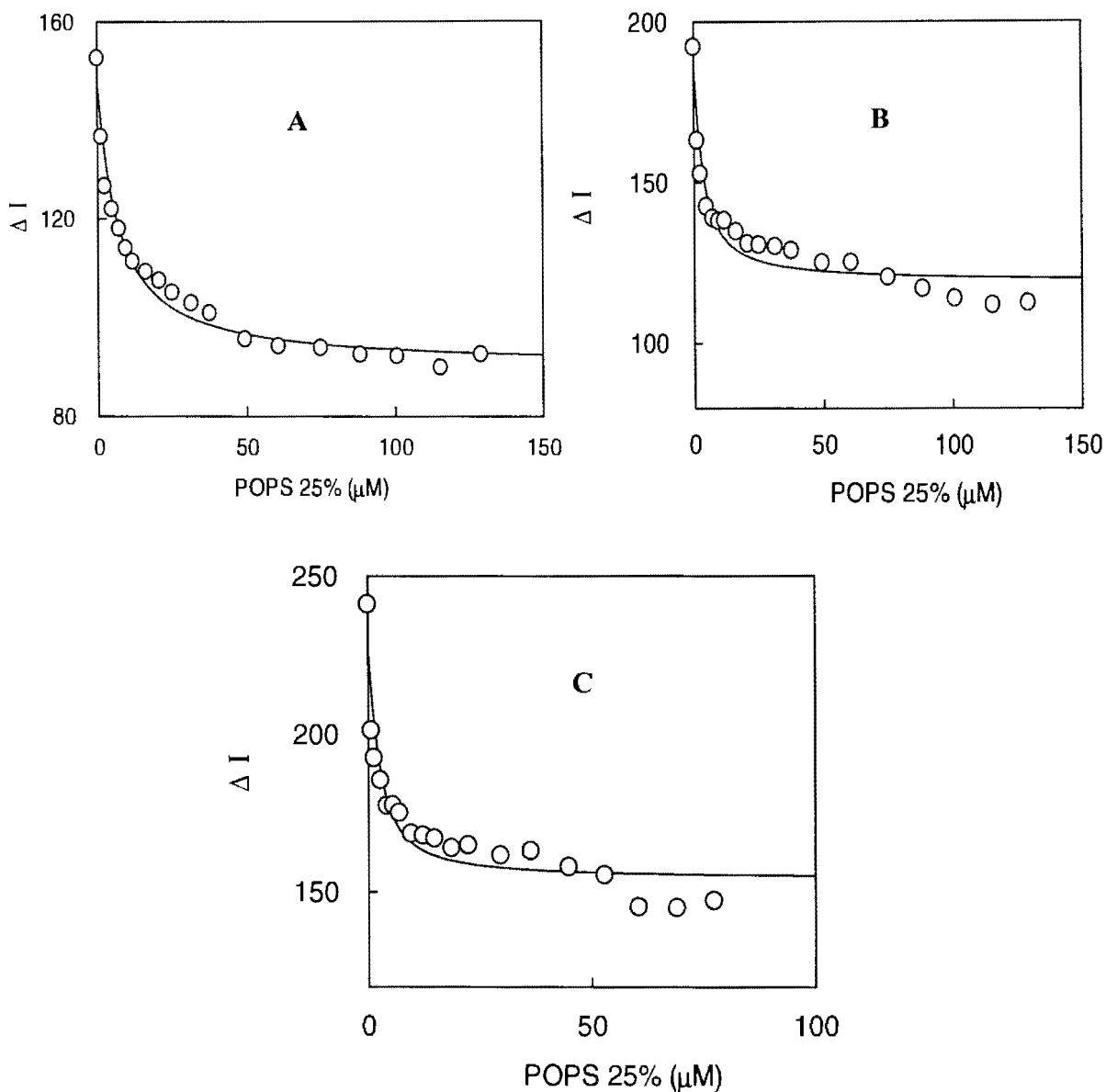mM NaCl and 50 mM NaCl, respectively.
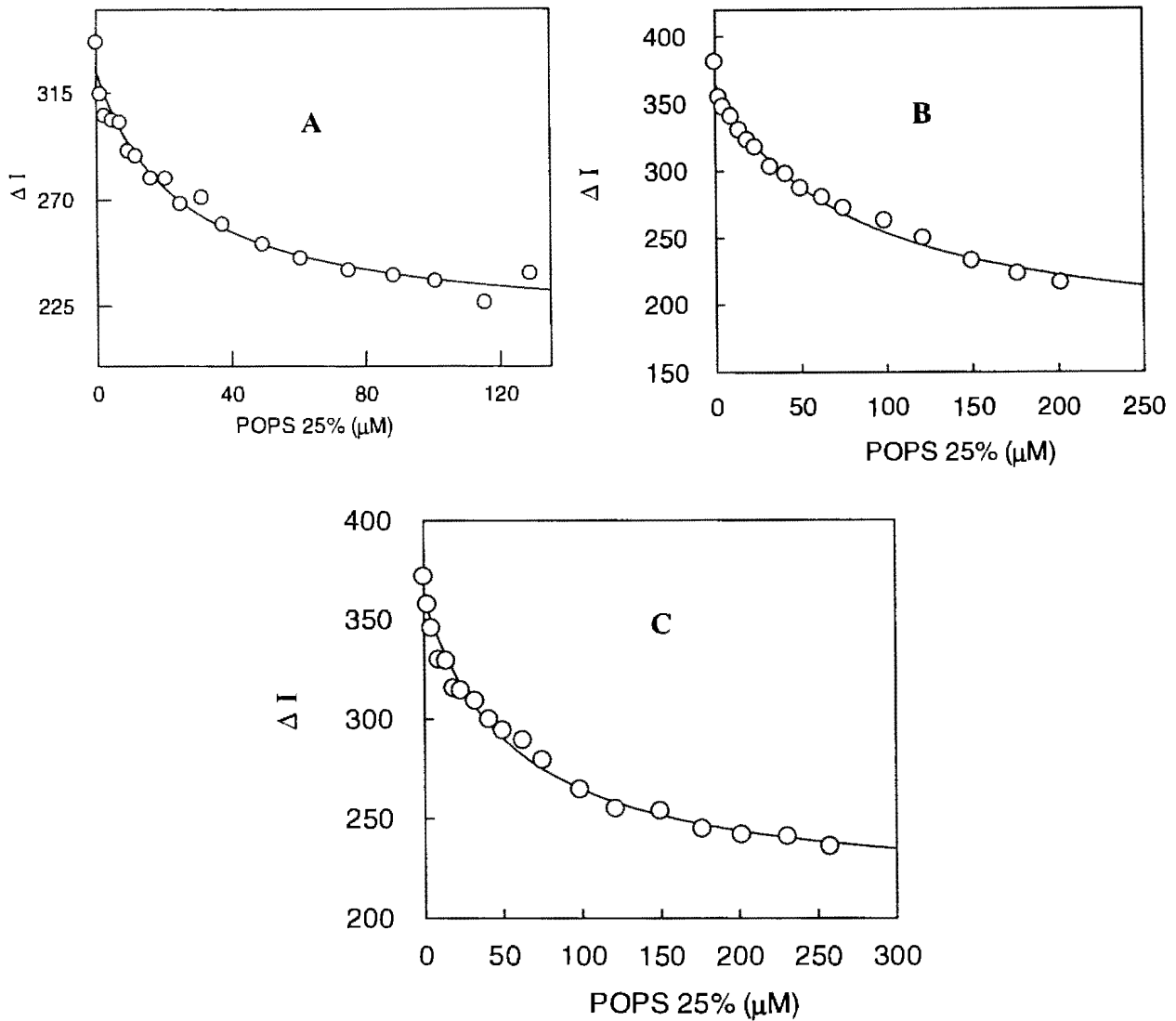
Figure 6.36.A. Binding isotherm of POPC: POPS: DPE (65:25:10) and hMMP-9 at 150 mM NaCl B. Binding isotherm of POPC: POPS: DPE (65:25:10) and hMMP-9 at 100 mM NaCl C. Binding isotherm of POPC: POPS: DPE (65:25:10) and hMMP-9 at 50 mM NaCl. The excitation wavelength was set at 280 nm. A, B and C represents the binding constants derived by conducting the titration in 25 mM HEPES, pH 7.5 with varying NaCl concentrations from (A)150 mM, (B) 100 mM and (C) 50 mM. The solid smooth lines are the best fit of the data with the K_d values of 33.3 ± 0.24, 74.6 ± 0.12 μM and 53.0 ± 0.06 μM for A, B and C, respectively.
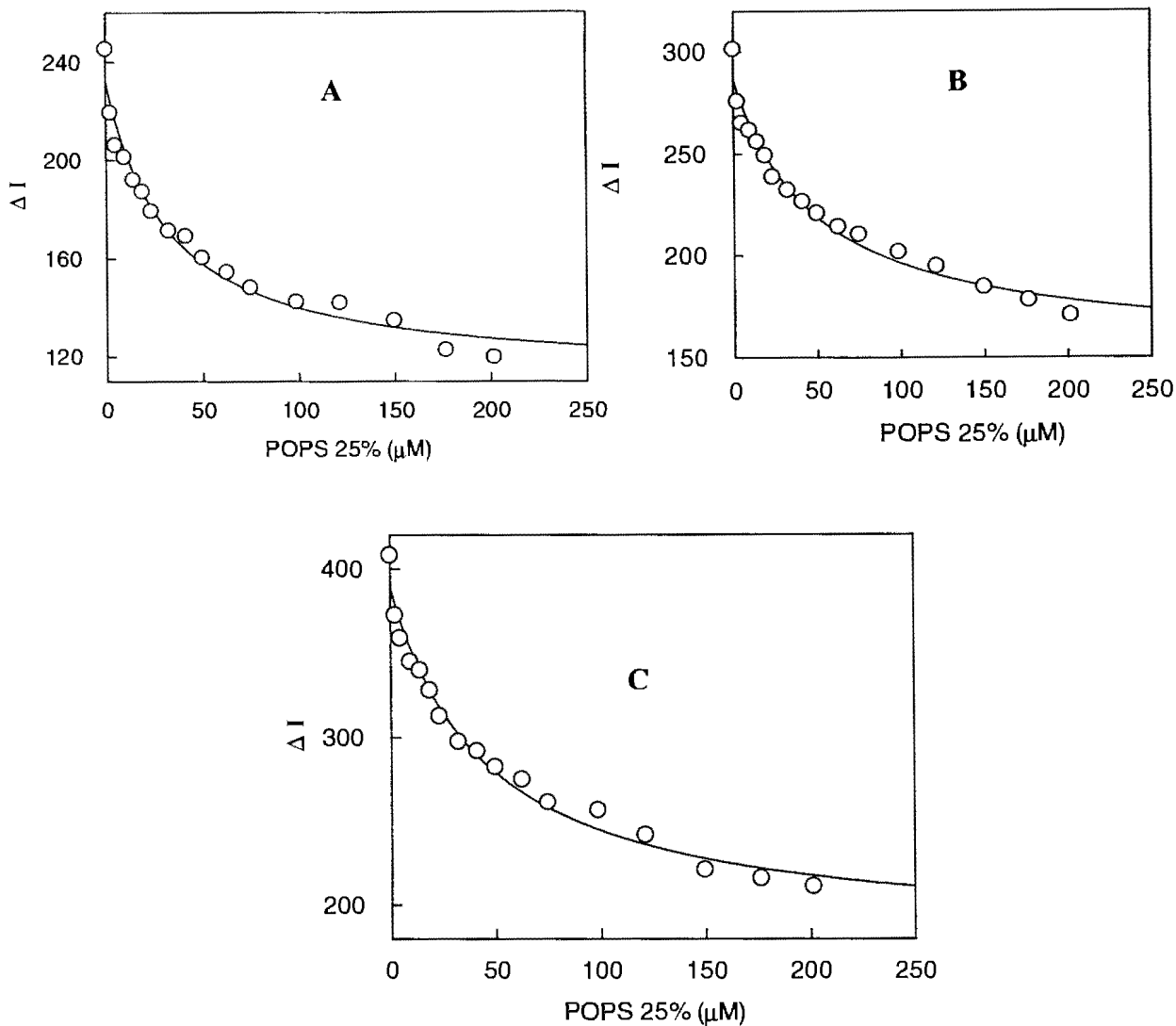
Figure 6.37.A. Binding isotherm of POPC: POPS: DPE (65:25:10) and hMMP-10 at 150 mM NaCl B. Binding isotherm of POPC: POPS: DPE (65:25:10) and hMMP-10 at 100 mM NaCl C. Binding isotherm of POPC: POPS: DPE (65:25:10) and hMMP-10 at 50 mM NaCl. The excitation wavelength was set at 280 nm. A, B & C represents the binding constants derived by conducting the titration in 25 mM HEPES, pH 7.5 with varying NaCl concentrations from (A)150 mM, (B) 100 mM and (C) 50 mM. The solid smooth lines are the best fit of the data with the K_d values of 40.2 ± 0.06 μM, 48.1 ± 0.12 μM and 44.0 ± 0.07 μM for A, B and C, respectively.

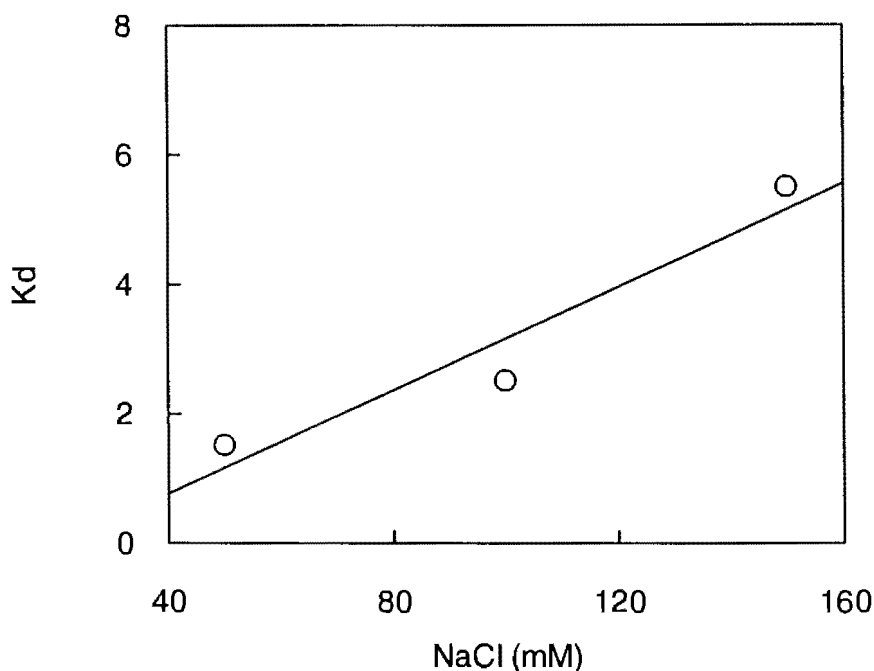Table 6.6. Relationship between the dissociation constants of hMMP-9 and POPS (25 mol %) as a function of salt concentration.

NaCl concentration	K_d (25 % POPS) µM hMMP-9
150 mM NaCl	33.3
100 mM NaCl	74.6
50 mM NaCl	53.0

Figure 6.39 indicates the binding of hMMP-7 and EPOPC (25 mol %) liposomes are mediated via strong electrostatics. Similar experiments of ionic strength dependent binding effects on hMMP-9 (see Figure 6.40 A, B and C) and for hMMP-10 (Figure 6.41 A, B and C) were carried out. The K_d values for hMMP-9 were 14.0 ± 0.013 µM, 12.0 ± 0.02 µM and 30.0 ± 0.05 µM for 150 mM NaCl, 100 mM NaCl and 50 mM NaCl, respectively. However, The K_d values for hMMP-10 were 8.2 ± 0.015 µM, 15.0 ± 0.025 µM and 8.7 ± 0.09 µM for 150 mM NaCl, 100 mM NaCl and 50 mM NaCl, respectively.

Table 6.7. Relationship between the dissociation constants of hMMP-10 and POPS (25 mol %) as a function of salt concentration.

NaCl concentration	K_d (25 % POPS) µM hMMP-10
150 mM NaCl	40.2
100 mM NaCl	48.1
50 mM NaCl	44.0
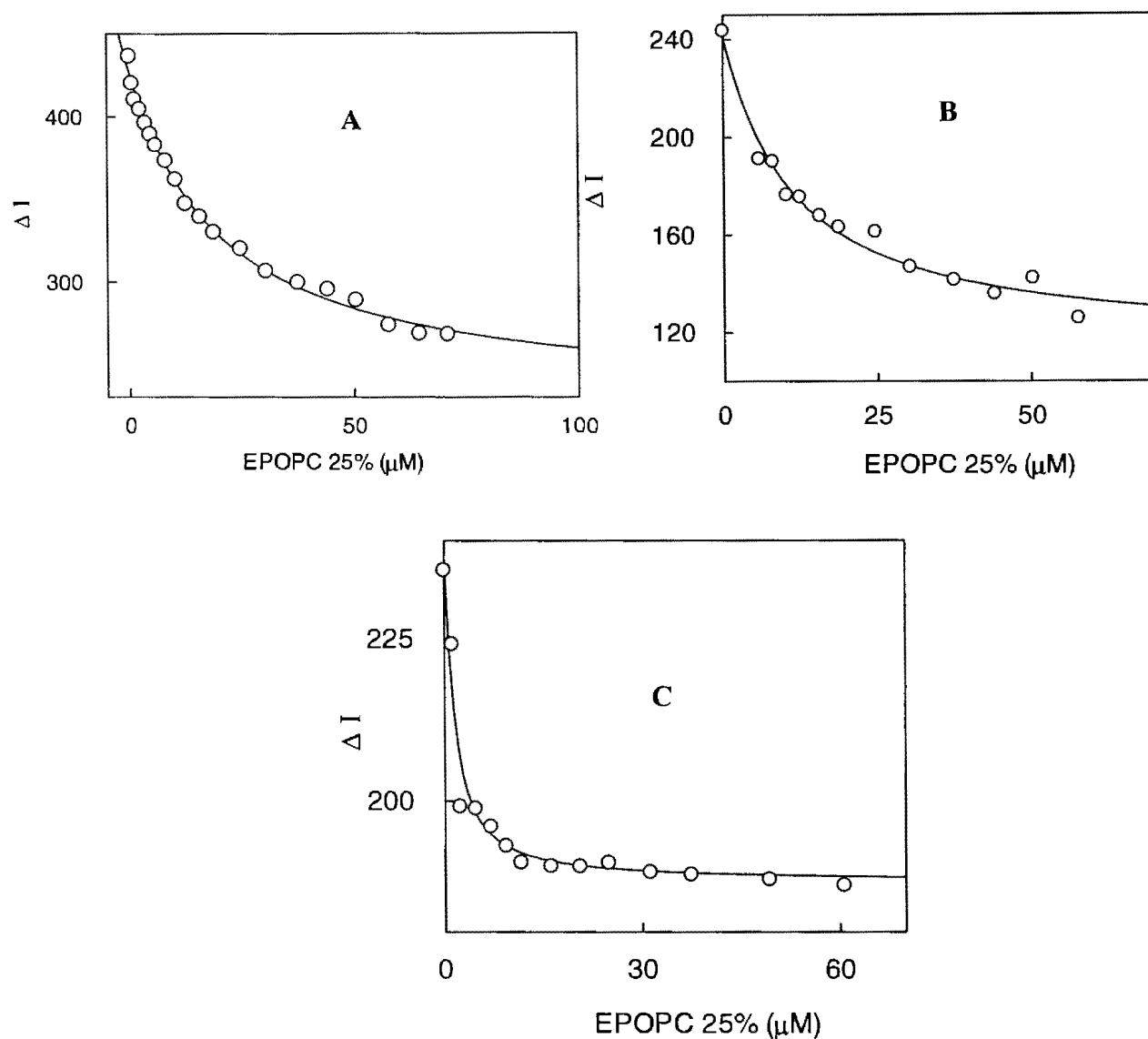
Figure 6.38.A. Binding isotherm of POPC: EPOPC: DPE (65:25:10) and hMMP-7 at 150 mM NaCl B. Binding isotherm of POPC: EPOPC: DPE (65:25:10) and hMMP-7 at 100 mM NaCl C. Binding isotherm of POPC: EPOPC: DPE (65:25:10) and hMMP-7 at 50 mM NaCl. The excitation wavelength was set at 280 nm. A, B & C represents the binding constants derived by conducting the titration in 25 mM HEPES, pH 7.5 with varying NaCl concentrations from (A)150 mM, (B) 100 mM and (C) 50 mM. The solid smooth lines are the best fit of the data with the K_d values of 20.6 ± 0.02 μM, 10.0 ± 0.02 μM and 0.99 ± 0.048 μM for A, B and C, respectively.

Figure 6.39. Relationship between the dissociation constants (K_d) of hMMP-7 and EPOPC (25 mol %) as a function of salt concentration.

Figure 6.39 shows that strong electrostatic forces drive the binding of EPOPC (25 mol %) LUVs to hMMP-7. In Table 6.8, the interaction between hMMP-9 and EPOPC (25 mol %) LUVs are mediated by hydrophobic interaction while Table 6.9 predicts that the interaction between hMMP-10 and EPOPC (25 mol %) LUVs are mediated by mixed forces [60-61].

Table 6.8. Relationship between the dissociation constants of hMMP-9 and EPOPC (25 mol %) as a function of salt concentration.

| NaCl concentration	K_d (25 % EPOPC) µM hMMP-9
150 mM NaCl	14.0
100 mM NaCl	12.0
50 mM NaCl	30.0
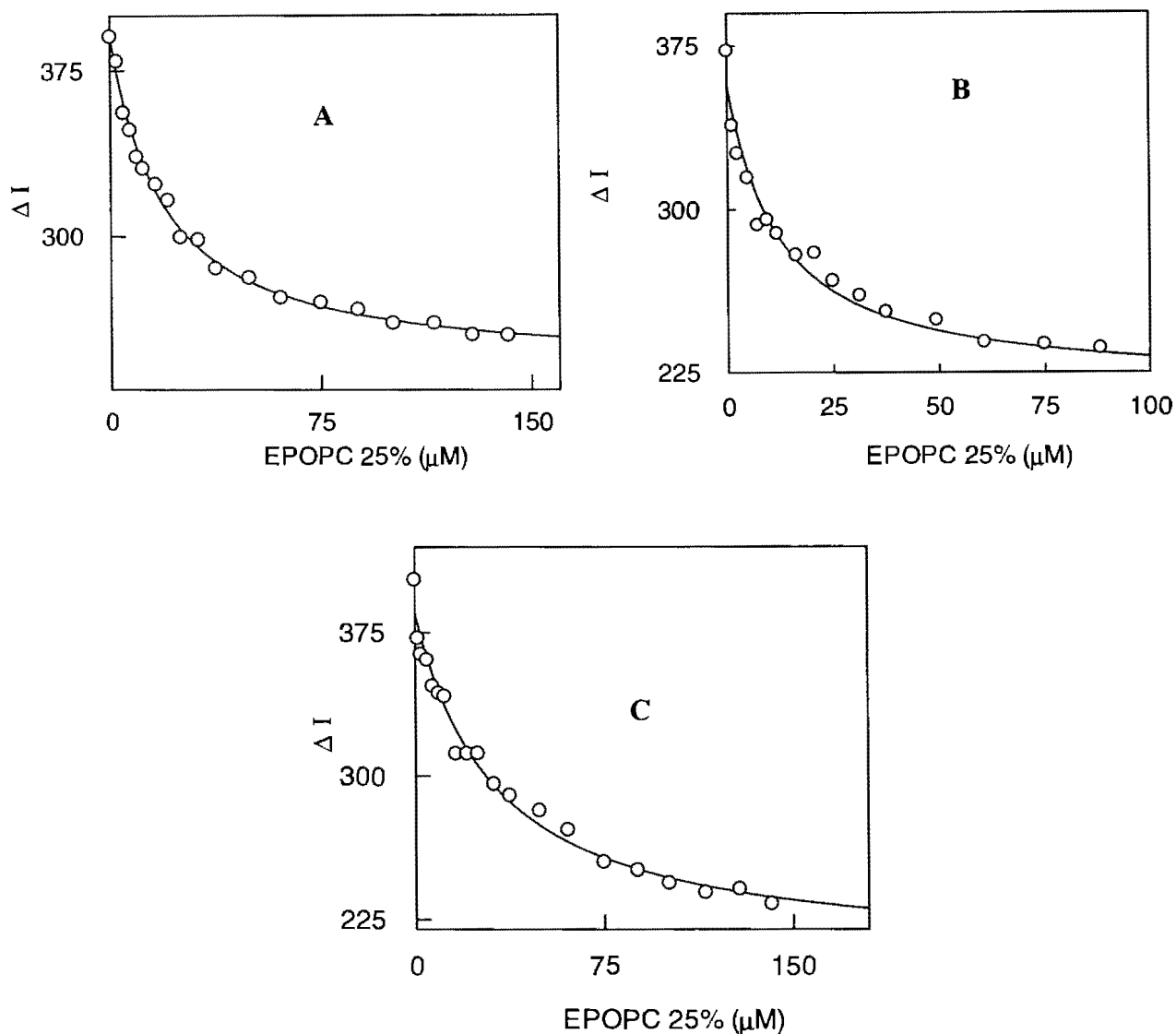
Figure 6.40.A. Binding isotherm of POPC: EPOPC: DPE (65:25:10) and hMMP-9 at 150 mM NaCl B. Binding isotherm of POPC: EPOPC: DPE (65:25:10) and hMMP-9 at 100 mM NaCl C. Binding isotherm of POPC: EPOPC: DPE (65:25:10) and hMMP-9 at 50 mM NaCl. The excitation wavelength was set at 280 nm. A, B & C represents the binding constants derived by conducting the titration in 25 mM HEPES, pH 7.5 with varying NaCl concentrations from (A)150 mM, (B) 100 mM and (C) 50 mM. The solid smooth lines are the best fit of the data with the K_d values of 14.0 ± 0.013 µM, 12.0 ± 0.02 µM and 30.0 ± 0.05 µM for A, B and C, respectively.
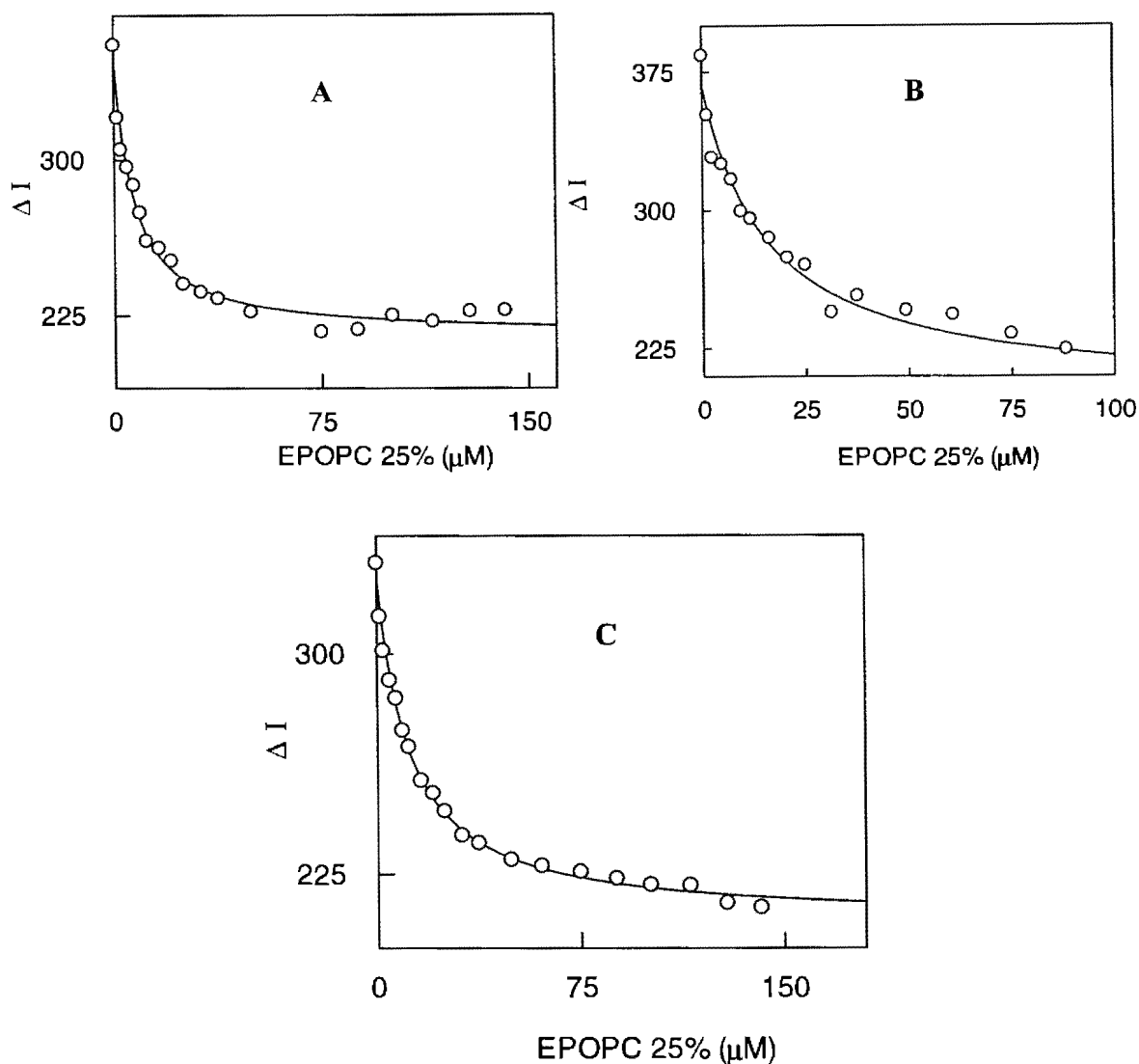
Figure 6.41.A. Binding isotherm of POPC: EPOPC: DPE (65:25:10) and hMMP-10 at 150 mM NaCl B. Binding isotherm of POPC: EPOPC: DPE (65:25:10) and hMMP-10 at 100 mM NaCl C. Binding isotherm of POPC: EPOPC: DPE (65:25:10) and hMMP-10 at 50 mM NaCl. The excitation wavelength was set at 280 nm. A, B and C represents the binding constants derived by conducting the titration in 25 mM HEPES, pH 7.5 with varying NaCl concentrations from (A)150 mM, (B) 100 mM and (C) 50 mM. The solid smooth lines are the best fit of the data with the K_d values of 8.2 ± 0.02 µM, 15.0 ± 0.03 µM and 8.7 ± 0.09 µM for A, B and C, respectively.

Table 6.9. Relationship between the dissociation constants of hMMP-10 and EPOPC (25 mol %) as a function of salt concentration.

NaCl concentration	K_d (25 % EPOPC) µM hMMP-10
150 mM NaCl	8.2
100 mM NaCl	15.0
50 mM NaCl	8.17

Table 6.10.A and B establishes the relationship between the dissociation constants (K_d) of hMMP isozymes and POPS (25 mol %) as a function of increasing salt concentration and EPOPC (25 mol %) as a function of increasing salt concentration, respectively.

In view of these findings, the proposed hypothesis states that due to electrostatic features, when bound to the negatively charged or neutral membranes, the active-site pocket of the hMMP-7 remains unobstructed and the enzyme stays fully active. In contrast, when hMMP-7 binds to the positively charged membranes, it is drastically inhibited and this is presumably due to the orientation of the enzyme's active-site pocket toward the positively charged membrane surface.

Consistent with this hypothesis, Scheme 6.2 represents the schematic diagram showing the electrostatic potentials on the surface of hMMP-7 (pdb1MMQ) containing bound hydroxamate inhibitor and putative binding surfaces for anionic and cationic LUVs. The structural coordinates of hMMP-7 were obtained from the Research Collaboratory for Structural Bioinformatics (RCSB) and Protein Data Bank (PDB). The surface potentials i.e. (negative and positive potentials) were calculated with the aid of the GRASP software on a SGI molecular modeling workstation [62-64].
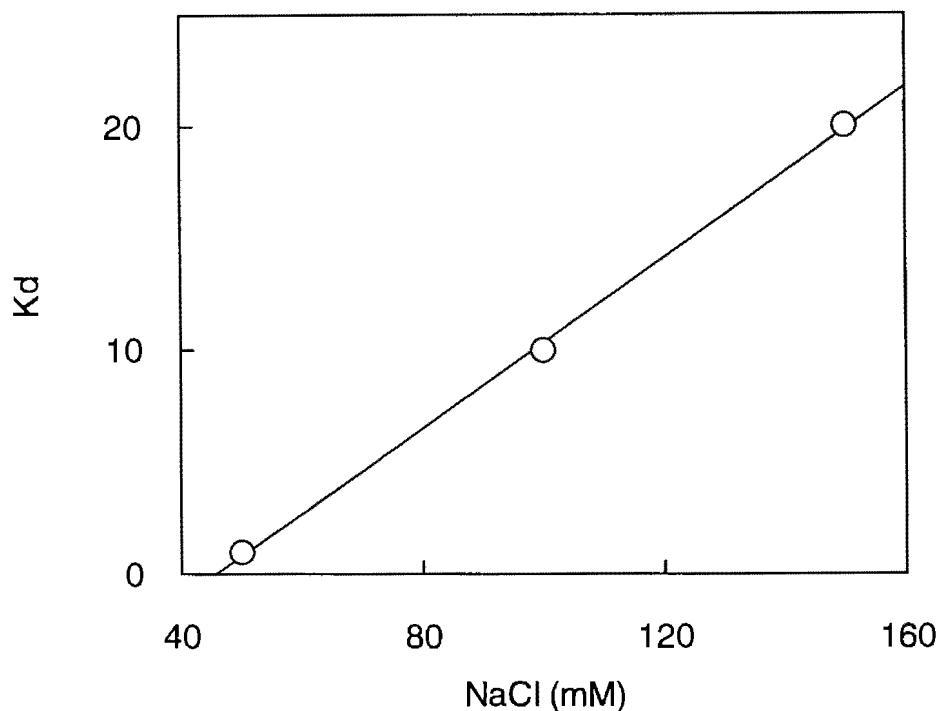
Table 6.10.A. Relationship between the dissociation constants (K_d) of hMMP isozymes and POPS (25 mol %) as a function of salt concentration. B. Relationship between the dissociation constants (K_d) of hMMP isozymes and EPOPC (25 mol %) as a function of salt concentration.

A

NaCl concentration	MMP-7 (K_d µM)	MMP-9 (K_d µM)	MMP-10 (K_d µM)
POPS (25%) 150mM NaCl	5.5	33.3	40.2
POPS (25%) 100mM NaCl	2.5	74.6	48.1
POPS (25%) 50mM NaCl	1.5	53	44
	Prominently Electrostatics	Mixed Electrostatics + Hydrophobic Interactions	Mixed Electrostatics + Hydrophobic Interactions

B

NaCl concentration	MMP-7 (K_d µM)	MMP-9 (K_d µM)	MMP-10 (K_d µM)
EPOPC (25%) 150mM NaCl	20	14	8.2
EPOPC (25%) 100mM NaCl	10	12	15
EPOPC (25%) 50mM NaCl	0.99	30	8.17
	Strong Electrostatics	Hydrophobic Interaction	Mixed Electrostatics + Hydrophobic Interactions

In summary, it is reported herein, for the first time, a few of the novel conclusions about the interaction of the hMMP isozymes and the differently charged lipid membranes: (1) All of the three hMMP isozymes bind to the differently charged LUVs with varying affinity, but hMMP-7 has more specificity to the POPS liposomes; (2) Enzyme activity of hMMP-7 is perturbed upon binding to the EPOPC (25%) liposomes due to strong electrostatics; (3) Enzyme activity of hMMP-9 or 10 is not perturbed upon binding to the

differently charged LUVs; (4) hMMP-7 binds to cationic liposomes via strong electrostatics, unlike MMP-9 and 10; (5) Both local negative charge density (LCD) and organization of the LUVs dictate the specificty with which hMMP-7 binds to anionic POPS LUVs; and (6) Poly anionic PIP$_2$ (4 mol %) shows binding affinity similar to mono anionic POPS with 25 mol %.
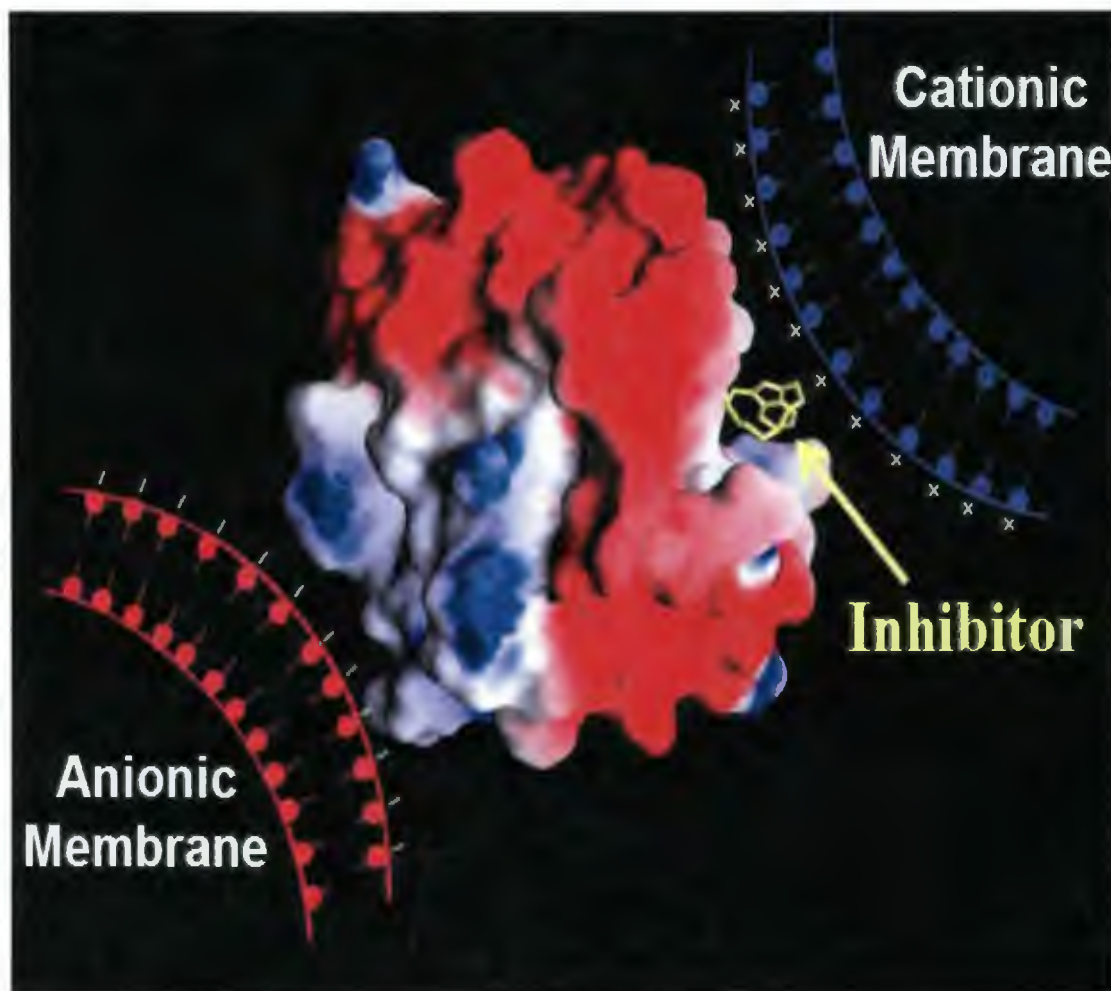
Scheme 6.2. Schematic model illustrating the electrostatic potentials on the surface hMMP-7 (pdb1MMQ) containing bound Hydroxamate inhibitor and putative binding surfaces for anionic and cationic lipid membranes. The red (1.9 kcal/mol) and blue (9.8 kcal/mol) colors represent the negative and positive potentials, respectively, calculated with the aid of the GRASP software on a SGI molecular modeling workstation.

Under physiological and pathological conditions, the catalytic activity of hMMP-7 could be fine-tuned by selective interaction with membranes of different charge and/or membrane-resident proteins. Further, the outcome of these studies may lead to the development of therapeutic/diagnostic tools for the selective detection of hMMP-7 from the pool of MMP isozymes, which is known to be over-expressed in a variety of chronic pathological conditions, including cancers [65].

6.3. References

1. Kahari, V., and Saarialho-Kere, U. (1997) Metalloproteinases in skin, *Exp. Dermatol.* 6, 199-213.
2. Saarialho-Kere, U. (1998) Patterns of matrix metalloproteinase and TIMP expression in chronic ulcers, *Arch. Dermatol.* 294, S47-S54.
3. Nagase, H., and Woessner, J. F. (1999) Matrix metalloproteinases, *J. Biol. Chem.* 274, 21491-21494.
4. Kerkela, E., and Saarialho-K, U. (2003) Matrix metalloproteinases in tumor progress: focus on basal and squamous cell skin cancer, *Exp. Dermatol.* 12, 109-125.
5. Nelson, A. R., Fingleton, B., Rothenberg, M. L., and Matrisian, L. M. (2000) Matrix metalloproteinases: biological activity and clinical implications, *J. Clin. Oncol.* 18, 1135-1149.
6. Liotta, L. A., Tryggvason, K., and Garbisa, S. (1980) Metastatic potential correlates with enzymatic degradation of basement membrane collagen, *Nature.* 284, 67-68.
7. Hsieh, M.S., Ho, H.C., Chou, D.T., Pan, S., Liang, Y.C., Hsieh, T.Y., Lan, J.L., and Tsai, S.H. (2003) Expression of matrix metalloproteinase-9 (gelatinase B) in gouty arthritis and stimulation of MMP-9 by urate crystals in macrophages, *J. Cell. Biochem.* 89, 791-799.
8. Winberg, J., Berg, E., Kolset, S., and Uhlin-Hansen, L. (2003) Calcium Induced activation and truncation of promatrix metalloproteinase-9 linked to the core protein of chondroitin sulfate proteoglycans, *Eur. J. Biochem.* 270 (19), 3996-4007.
9. Verma, R., and Hansch, C. (2007) Matrix metalloproteinases (MMPs): Chemical–biological functions and (Q) SARs, *Bioorg. Med. Chem.* 15, 2223–2268.
10. Vartak, D., and Gemeinhart, R. (2007) Matrix metalloproteases: Underutilized targets for drug delivery, *J. Drug. Target.* 15(1), 1–20.
11. Li, Q., Park, P. W., Wilson, C. L., and Parks, W. C. (2002) Matrilysin shedding of syndecan-1 regulates chemokine mobilization and transepithelial efflux of neutrophils in acute lung injury, *Cell.* 111, 635–646.

12. Yu, Q., and Stamenkovic, I. (2000) Cell surface-localized matrix metalloproteinase-9 proteolytically activates TGF-β and promotes tumor invasion and angiogenesis, *Genes Dev.* 14, 163–176.

13. Yamamoto, K., Higashi, S., Kioi, M., Tsunezumi, J., Honke, K., and Miyazaki, K. (2006) Binding of active matrilysin to cell surface cholesterol sulfate is essential for its membrane-associated proteolytic action and induction of homotypic cell adhesion, *J. Biol. Chem.* 281 (14), 9170-9180.

14. Yu, W. H., and Woessner, and J. F., Jr. (2000) Heperan sulfate proteoglycans as extracellular docking molecules for Matrilysin (Matrix Metalloproteinase 7), *J. Biol. Chem.* 275, 4183–4191.

15. Silvius, J. R. (2005) Partitioning of membrane molecules between raft and non-raft domains: Insight from model-membrane studies, *Biochimica et Biophysica Acta.* 1746, 193-202.

16. Mbamala, E. C.; Shaul, A. B.; and May, S. (2005) Domain formation induced by the adsorption of charged proteins on mixed lipid membranes, *Biophys. J.* 88 (3), 1702-1714.

17. Mclaughlin, S., Wang, J., Gambhir, A., and Murray, D. (2002) PIP$_2$ and proteins: Interactions, organization, and information flow, *Ann. Rev. Biomol. Struct.* 31, 151-175.

18. Janmey, P. A., and Lindberg, U. (2004) Cytoskeletal regulation: rich in lipids, *Nat. Rev. Mol. Cell. Biol.* 5, 658–666.

19. Yin, H. L., and Janmey, P. A. (2003) Myosin-1c, the hair cells adaptation motor, *Annu. Rev. Physiol.* 65, 761–789.

20. Martin, T. F. J. (2001) PI(4,5)P$_2$ regulation of surface membrane traffic, *Curr. Op. Cell Biol.* 13 (4), 493-499.

21. Varnai, P., Lin, X., Lee, S. B., Tuymetova, G., Bondeva, T., Spat, A., Rhee, S. G., Hajnoczky, G., and Balla, T. (2002) Inositol Lipid Binding and Membrane Localization of Isolated Pleckstrin Homology (PH) Domains, *J. Biol. Chem.* 277, 27412–27422.

22. Hilgemann, D. W., Feng, S., and Nasuhoglu, C. (2001) The complex and intriguing lives of PIP$_2$ with ion channels and transporters, *Sci. STKE.* 2001, RE19.

23. Cremona, O., and De Camilli, P. J. (2001) Phsophoinositides in membrane traffic at the synapse, *Cell. Sci.* 114, 1041–1052.

24. Levental, I., Cembers, A., and Janmey, P.A. (2008) Combined electrostatics and hydrogen bonding determine intermolecular interactions between polyphosphoinositides, *J. Am. Chem. Soc.* 130 (28), 9025-9030.

25. Arcesi, L., Penna, G. L., and Perico, A. (2006) Generalized electrostatic model of the wrapping of DNA around oppositely charged proteins, *Biopolymers.* 86 (2), 127-135.

26. Davey, C. A., Sargent, D. F., Luger, K., Maeder, A. W., and Richmond T. J. (2002) Solvent mediated interactions in the structure of the nucleosome core particle at 1.9 Å resolution, *J. Mol. Biol.* 319, 1097–1113.

27. Talley, K., Ng, C., Shoppell, M., Kundrotas, P., and Alexov, E. (2008) On the electrostatic component of protein-protein binding free energy, *PMC Biophysics.* 1:2, 1-23.

28. Norel, R., Sheinerman, F., Petrey, D., and Honig, B. (2001) Electrostatic contributions to protein-protein interactions: fast energetic filters for docking and their physical basis, *Protein. Sci.* 10, 2147-2161.

29. Elegbede, A. I., Haldar, M. K., Manokaran, S., Kooren, J., Roy, B. C., Mallik, S., and Srivastava, D. K. (2007) A strategy for designing "multi-prong" enzyme inhibitors by incorporating selective ligands to the liposomal surface, *Chem. Commun.* 32, 3377-3379.

30. Marras, S.A.E. Selection of fluorophore and quencher pairs for Fluorescent Nucleic acid hybridization probes, In Methods in Molecular Biology: Fluorescent energy transfer nucleic acid probes: Designs and protocols, Ed V.V. Didenko © *Humana Press Inc., Totowa, NJ.*

31. Li, X., McCarroll, M., and Kohli, P. (2006) Modulating fluorescence resonance energy transfer in conjugated liposomes, *Langmuir: Journal of Surfaces and Colloids.* 22(21), 8615-8617.

32. Banerjee. A.L., Tobwala, S., Ganguly, B., Mallik, S., and Srivastava, D.K. (2005) Molecular Basis for the Origin of Differential Spectral and Binding Profiles of Dansylamide with Human Carbonic Anhydrase I and II, *Biochemistry.* 44(10), 3673-3682.

33. Banerjee, J., Haldar, M. K., Manokaran, S., Mallik, S., and Srivastava, D.K. (2007) New fluorescent probes for carbonic anhydrase, *Chem. Commun.* 2723-2725.

34. Bernik, D.L., and Negri, R.M. (1998) Local polarity at the polar head level of lipid vesicles using dansyl fluorescent probes, *J of Colloidal and Interface Science.* 203, 97-105.

35. Kertz, J.A., Almeida, P.F.F., Frazier, A.A., Berg, A.K., and Hinderliter, A. (2007) The cooperative response of synaptotagmin I C2A. A hypothesis for a Ca^{2+} driven molecular hammer, *Biophysical. J.* 92, 1409-1418.

36. Cheng, Q., and Stevens, R. C. (1998) Charge-induced chromatic transition of amino acid- derivatized polydiacetylene liposomes, *Langmuir.* 14, 1974-1976.

37. Cevc, G., Watts, A., and Marsh, D. (1981) Titration of the phase transition of phosphatidylserine bilayer membranes. Effects of pH, surface electrostatics, ion binding, and head-group hydration, *Biochemistry.* 20, 4955-4965.

38. Lewis, R. N.A. H., Mannock, D.A., and McElhaney, R.N. (2007) Differential scanning calorimetry in the study of lipid phase transitions in model and biological membranes, In *Methods in Molecular Biology.* 400, 171-195.

39. Bach, D., and Miller, I.R. (1998) Hydration of phospholipid bilayers in the presence and absence of cholesterol, *Biochim. Biophys. Acta.* 1368, 216-224.

40. Silvius, J. R., and Gagne, J. (1984) Calcium-induced fusion and lateral phase separations in phosphatidylcholine-phosphatidylserine vesicle. Correlation by calorimetric and fusion measurements, *Biochemistry.* 23, 3241-3247.

41. Lakowicz, J.R. (1999) In Principles of Fluorescence Spectroscopy, Ed *Springer, Hoboken,* Vol. 3.

42. Voet, D., Voet, J. G., and Pratt, C. (1995) In Fundamentals of Biochemistry: Life at the Molecular Level, *John Wiley and Co*, Vol. 3.

43. Berton, A., Selvais, C., Lemoine, P., Henriet, P., Courtoy, P.J., Marbaix, E., and Emonard, H. (2007) Binding of matrilysin-1 to human epithelial cells promotes it's activity, *Cell. Mol. Life. Sci.* 64, 610-620.

44. Higashi, S., Oeda, M., Yamamoto, K., and Miyazaki, K. (2008) Identification of amino acid residues of matrix metalloproteinase-7 essential for binding to cholesterol sulfate, *J. Biol. Chem.* 281 (14), 9170-9180.

45. Gerke, V., Creutz, C.E., and Moss, S.E. (2005) Annexins: linking Ca^{2+} signaling to membrane dynamics, *Nat. Rev. Mol. Cell. Biol.* 6, 449-461.

46. Meers, P., and Mealy, T. (1993) Calcium-dependent annexin V binding to phospholipids: stoichiometry, specificity, and the role of negative charge, *Biochemistry.* 32, 11711-11721.

47. Eftink, M.R., and Ghiron, C.A. (1981). Fluorescence quenching studies with protein, *Anal. Biochem.* 114, 199-227.

48. Wang, J., Gambhir, A., Mihalyne, G.H., Murray, D., Golebiewska, U., and McLaughlin, S. (2002) Lateral sequestration of phosphatidylionsitol 4.5-bisphosphate by the basic effector domain of myristoylated alanine-rich C kinase substrate is due to nonspecific electrostatic interactions, *J. Biol. Chem.* 277 (37), 34401-34412.

49. Rauch, M.E., Ferguson, C.G., Prestwich, G.D., and Cafiso, D.S. (2002) Myristoylated alanine-rich C kinase substrate (MARCKS) sequesters spin-labeled phosphatidylinositol 4,5-bisphosphate in lipid bilayers. *J. Biol. Chem.* 277 (16), 14068-14076.

50. Golebiewska, U., Gambhir, A., Mihalyne, G.H., Zaitseva, I., Radler, J., and McLaughlin, S. (2006) Membrane-bound basic peptides sequester multivalent (PIP_2), but not monovalent (PS), acidic lipids, *Biophysical. J.* 91, 588-599.

51. Hantgan, R. R., Stahle, M. C., Connor, J. H., Horita, D. A., Rocco, M., MClane, M. A., Yakovlev, S., and Medved, L. (2006) Integrin αIIbβ3: Ligand interactions are linked to binding-site remodeling, *Protein. Sci.* 15, 1893-1906.

52. Das, S., and Du, Q. (2008) Adhesion of vesicles to curved substrates, *Phys. Rev. E Stat. Nonlin. Soft Matter Phys.* 77 (1 Pt 1).

53. Ohki, S., and Arnold, K. (2008) Experimental evidence to support a theory of lipid membrane fusion, *Coll. Surf. B. Biointerfaces.* 63 (2), 276-281.

54. Sanii, B., Smith, A. M., Butti, R., Brozell, A. M., and Parikh, A. N. (2008) Bending membranes on demand: Fluid phospholipid bilayers on topologically deformable substrates, *Nano. Lett.* 8 (3), 866-871.

55. Golemis, E., and Adams, P.D. (2002) In Protein-Protein interactions: A Molecular Cloning Manual, Ed *Cold Spring Harbor Laboratory Press*, Vol 2.

56. Buckinghaamn, A.D., and Utting, B. D. (1970) Intermolecular forces. *Annu. Rev. Phys. Chem.* 21, 287-316.

57. Lins, L., Decaffmeyer, M., Thomas, A., and Brasseur, R. (2008) Relationships between the orientation and the structural properties of peptides and their membrane interactions, *Biochim. Biophys. Acta.* 1778, 1537-1544.

58. Montaville, P., Coudevylle, N., Radhakrishnan, A., Leonov, A., Zweckstertter, M., and Becker, S. (2008) The PIP$_2$ binding mode of C2 domains of rabphilin-3A, *Protein. Sci.* 17, 1025-1034.

59. MacDonald, R. I. (1985) Membrane fusion due to dehydration by polyethylene glycol, dextran, or sucrose, *Biochemistry.* 24 (15), 4058-4066.

60. Ganguly, B., and Srivastava, D.K. (2008). Influence of "Flexible" versus "Rigid" Nanoparticles on the Stability of Matrix Metalloproteinase-7, *J. Biomed. Nanotechnol.* 4, 457–462.

61. Dickey, A., and Faller, R. (2008) Examining the contributions of lipid shape and head group charge on bilayer behavior, *Biophys. J.* 95, 2636-2646.

62. Browner, M.F., Smith, W.W., and Castelhano, A.L. (1995) Matrilysin-inhibitor complexes: common themes among metalloproteases, *Biochemistry.* 34, 6602–6610.

63. Johnson, L.N., and Barford, D. (1994) Electrostatic effects in the control of glycogen phosphorylase by phosphorylation, *Prot. Sci.* 3, 1726–1730.

64. Nicholls, A., Sharp, K.A., and Honig, B. (1991) Protein folding and association: insights from the thermodynamic properties of hydrocarbons, *Proteins.* 11, 281–296.

65. Ii, M., Yamamoto, H., Adachi, Y., Maruyama, Y., and Shinomura, Y. (2006) Role of matrix metalloproteinase-7 (Matrilysin) in human cancer invasion, apoptosis, growth, and angiogenesis, *Exp. Biol. Med.* (Maywood). 231, 20–27.

CHAPTER 7. MECHANISTIC STUDIES TO UNRAVEL THE ALTERNATIVE BINDING MODES OF HUMAN MATRIX METALLOPROTEINASE (hMMP) ISOZYMES TO CATIONIC AND ANIONIC QUANTUM DOTS

7.1. Introduction

7.1.1. Application of QDs in various fields of research

Semiconductor quantum dots (QDs) are increasingly being incorporated into various biological applications ranging from tumor targeting to multiplexed fluorescent detection *in vivo* after being first reported as improved fluorophores for biological imaging applications in 1998 [1]. Quantum dots are the tailored form of semiconductor nano-crystals that possess outstanding electronic and spectral properties [2]. Size distribution, shape, and their surface defects dictate the spectroscopic properties of the quantum dots. QDs are increasingly being used to visualize trafficking dynamics of individual proteins [2]. However, the inorganic composition of QDs causes robust size- dependent optical properties that are not conducive to their direct integration into biological assays.

Significant advancements have been made over the past two decades in controlling the size and surface of chemically-synthesized semiconductor nanoparticles. Photonic crystals, thin-film light-emitting devices, and biological labels are the potential applications of water-soluble semiconductor nanoparticles with high photoluminescence (PL) quantum efficiency [3]. Semiconductor nanoparticles exhibit unique physical and chemical properties, which are distinctly different from their corresponding individual molecules or bulk materials [4], due to quantum confinement.

7.1.2. Functional modifications made on QD surfaces

The presence of functional modifications and the presence of various reactive to the

chemical functionalities determine the possibility of a net positive or negative surface charge on the surface of the QD [5-7]. Many researchers have concentrated on identifying suitable blocking strategies and surface modifications of features which restrict biological recognition of nanoparticles and reduce their nonspecific binding to cellular membranes. Protein adsorption can result in unwanted interference or desirable outcomes depending on the nature of the biological assay under investigation. An improved understanding of the potentially reactive surface will result in the elimination of undesirable biological interferences and improved surface passivation [8]. Most of the fluorescent imaging applications utilizing QD probes use antibody conjugation to introduce biological specificity.

The biologically active small molecule QD conjugates have been targeted for membrane associated receptors by Warenment *et.al* [9]. Small molecule conjugates, unlike antibody recognition, have several advantages. Small molecule attachment provides minimal additional bulk whereas the large size of antibodies (approximately 150 kDa) adds significant steric bulk to an already sizable QD probe [10-12]. The antibody-antigen interaction varies dramatically from antibody to antibody, despite the fact that antibodies can be designed to recognize virtually any specific biological target, and the associated cost of antibody production considerably limits their utility [13-14].

7.1.3. The non-covalent binding forces dictating the binding of QDs to protein surfaces

Hard proteins (proteins with a high internal cohesion) have a stronger resilience against structural rearrangements during adsorption as compared to soft proteins (proteins which are structurally labile), which change their structure readily upon adsorption to the

QD surface [15]. Dehydration of the sorbent surface, being a strong entropically driven force for adsorption, enables both hard and soft proteins to adsorb on hydrophobic surfaces. In the case of hard proteins, electrostatic attraction is responsible for adsorption to hydrophilic surfaces. In case of soft proteins, the adsorption is due to hydrophilic electrostatic repulsion, where the gain in conformational entropy (associated with a decrease in secondary structure) of the protein is sufficiently large to overcome the electrostatic repulsion [16]. Adsorption behavior in the case of bovine serum albumin (BSA) is not controlled by the hydrophobicity of the sorbent surface. Other studies have also indicated that BSA adsorption is primarily determined by the protein itself [17-18] rather than the sorbent surface. These studies contributed to in the understanding of electrostatic interactions used to induce self-assemblies of water-dispersed NPs with polymers [19].

7.1.4. Studies done using QDs to exploit the conformational changes in the protein structure

About 300 papers per year in Biological Abstracts Report present studies on changes in tryptophan (Trp) fluorescence of proteins using QDs as fluorescence markers [11]. The fluorescence intensity observed for a range of wavelengths using tryptophan properties such as emission maximum wavelength (λ_{max}), time resolved fluorescence lifetime (LT), anisotropy, and Resonance Energy Transfer (RET) has been studied in detail. Using these results, new studies on the changes in protein conformation, quencher accessibility to proteins, and enzyme-ligand binding studies have been carried out. Monitoring the tryptophan signals associated with the diffusion of different solutes within their interior core has been one of the approaches of experimentally evaluating the

contributions of conformational dynamics in proteins [12]. The changes in the protein conformation depend on the smooth and rigid surfaces. The primary contributions to the protein adsorption originate from (i) co-adsorption of small ions arising from the electrostatic interactions between the protein and the sorbent surface, (ii) dispersion interaction, (iii) changes in the state of hydration of the sorbent surface and parts of the protein molecule, and (iv) structural re-organizations in the protein [14-15]. These studies have not revealed a great deal of information on MMPs, although several details on the molecular level of these proteins have been obtained.

7.1.5. Allosteric site in proteins

The capacity to modulate physiologically significant interactions is more widespread and frequent among proteins possesing "Allosteric sites" [21]. Many of the approaches like steady-state and time-resolved fluorescence lifetime (LT) measurements have been used to experimentally evaluate the contributions of conformational changes in MMPs in order to unravel the two different binding modes of hMMP isozymes while binding to cationic and anionic quantum dots. This study provides a more detailed insight of the interaction of MMP isozymes binding and interacting with differently charged QDs for the multi-faceted and efficient use in medical therapy, industrial processes, and as diagnostic tools for detection of different stages of cancer.

7.2. Results and Discussion

In an attempt to explain the molecular mechanisms for alternative modes of binding of hMMP isozymes (hMMP-7, 9 and 10) to differently charged quantum dots (i.e. CQD and AQD), binding studies, kinetic studies and time resolved fluorescence

measurement studies were carried out. Results of these studies indicate that CQD and AQD both bind to all of the hMMP isozymes via both strong electrostatic and hydrophobic interactions.

Figure 7.1.A shows the absorption spectra of cationic quantum dots (CQD). The CQDs used were 3.0 nm in diameter and made by cadmium telluride (CdTe) QD functionalized by cystamine. The CQDs show a broad absorption band from 250 nm to 610 nm. Figure 7.1.B shows the glass vial containing the pale yellow colored CQDs. The absorption peak at 340 nm was chosen to excite the QD in order to contribute the least from the CQD.

Figure 7.1.A. Absorption spectra of cationic quantum dots. B. Photo of a glass vial containing cationic quantum dots. The CQD shows a broad absorption band from 250 nm to 610 nm. But the absorption peak at 340 nm was chosen to excite the QD in order to have minimized contribution from QD as hMMP isozymes would also absorb significantly in the UV region. CQDs used were 3.0 nm in diameter and made by cadmium telluride (CdTe) QD functionalized by cystamine.

Figure 7.2.A shows the absorption spectra of anionic quantum dots (AQD). The AQDs used were 4.5 nm diameter and made by cadmium telluride (CdTe) QD

functionalized by Thioglycolate (TGA). The AQD shows a broad absorption band from 250 nm to 600 nm. Figure 7.2.B shows the glass vial containing the deep red colored AQD. The absorption peak at 340 nm was chosen to excite the QD in order to contribute the least from the AQD.
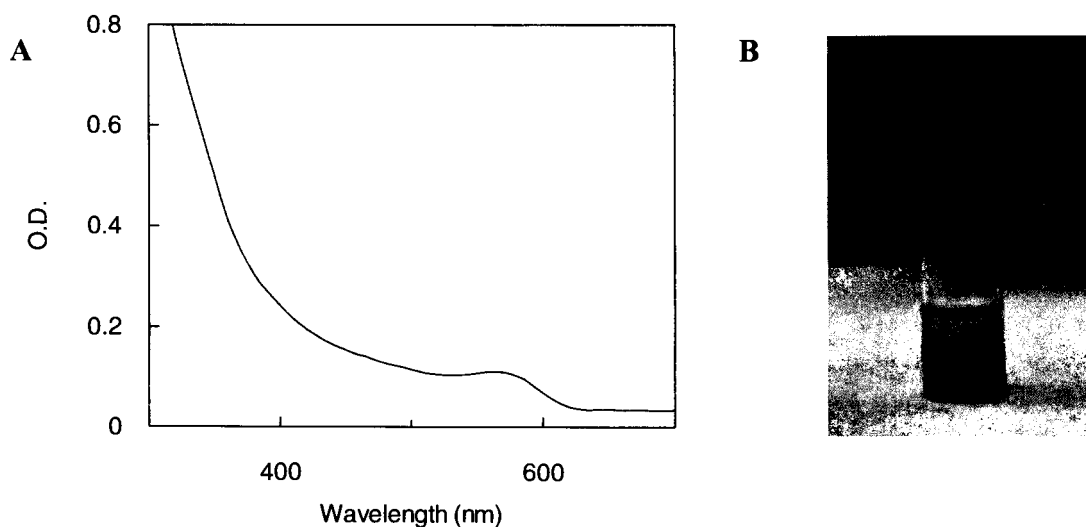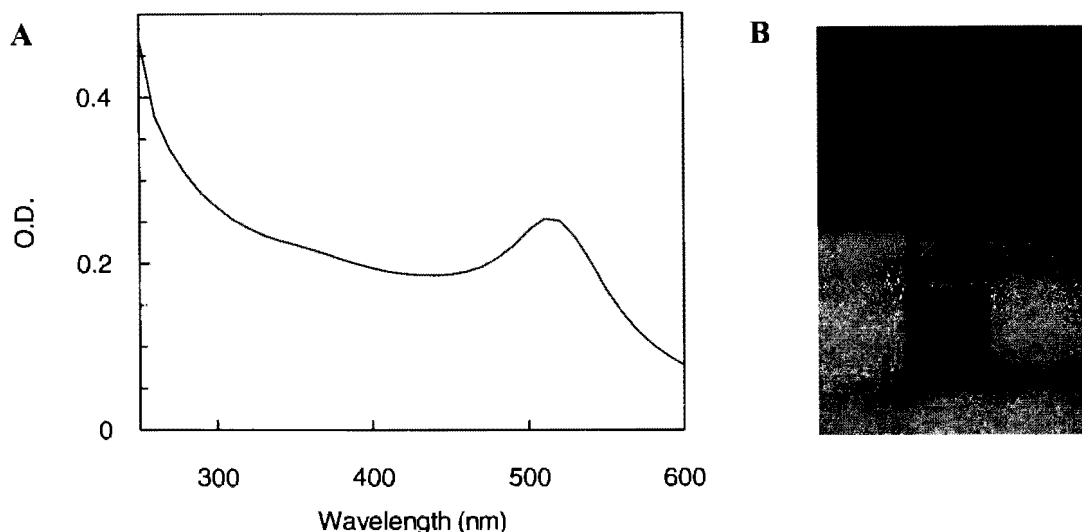

Figure 7.2.A. Absorption spectra of anionic quantum dots. B. Photo of a glass vial containing anionic quantum dots. The AQD shows a broad absorption band from 250 nm to 600 nm. But the absorption peak at 340 nm was chosen to excite the QD in order to have minimized contribution from QD as hMMP isozymes would also absorb significantly in the UV region. AQD used is nearly 4.5 nm diameter and made by Cadmium telluride (CdTe) QD functionalized by Thioglycolate (TGA).

Recent studies on NPs have opened new avenues to a host of new bio-molecular conjugates with applications in drug delivery, biocompatibility, "smart" materials in diagnostics and sensors [22]. Although semiconductor particles (e.g. CdSe) have been used primarily as quantum dots providing an intrinsic fluorescence label to proteins, the most common particles used for protein attachment are gold and silver. The size of these NPs typically varies about < 10 nm diameter. This makes them suitable as labels rather than immobilization matrixes.

Although particle size plays a vital role in modulating protein structure and function, no systematic study on the effect of particle size on the structure and function of adsorbed proteins has been performed till date. Recent studies [22] have shown that smaller NPs strongly favor binding to protein structure that result in higher intrinsic enzyme activity as compared to larger NPs. In this study, the two differently charged QDs with different sizes were compared. The CQD and AQD used in this study were about 3.0 nm and 4.5 nm, respectively.

Figure 7.3 shows the emission spectra of the CQD. Based on the absorption and emission spectra for CQDs, the excitation and emission wavelengths chosen for future experiments were 340 nm and 570 nm, respectively.
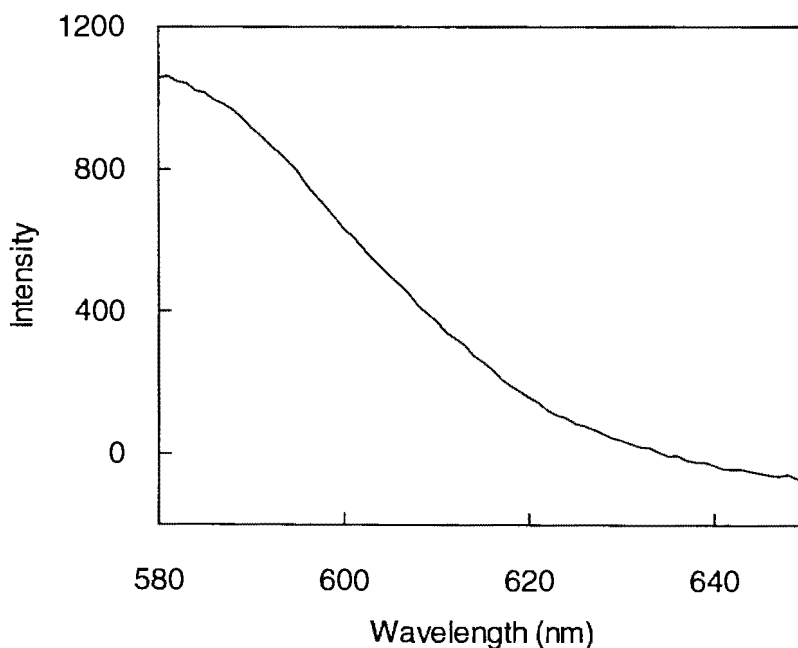

Figure 7.3. Emission spectra of cationic quantum dot (CdTe-Cys). The CdTe QD was diluted fifty-fold in 10 mM Tris, pH 8.0 using a plate reader with 3 mm diameter. The emission spectrum of the sample was corrected against the buffer blank. λ_{ex} and λ_{em} was 340 nm and 570 nm respectively.

Figure 7.4 shows the emission spectra of the AQDs. Based on the absorption and emission spectra for the AQDs, the excitation and emission wavelengths chosen for future experiments were 340 nm and 625 nm, respectively.
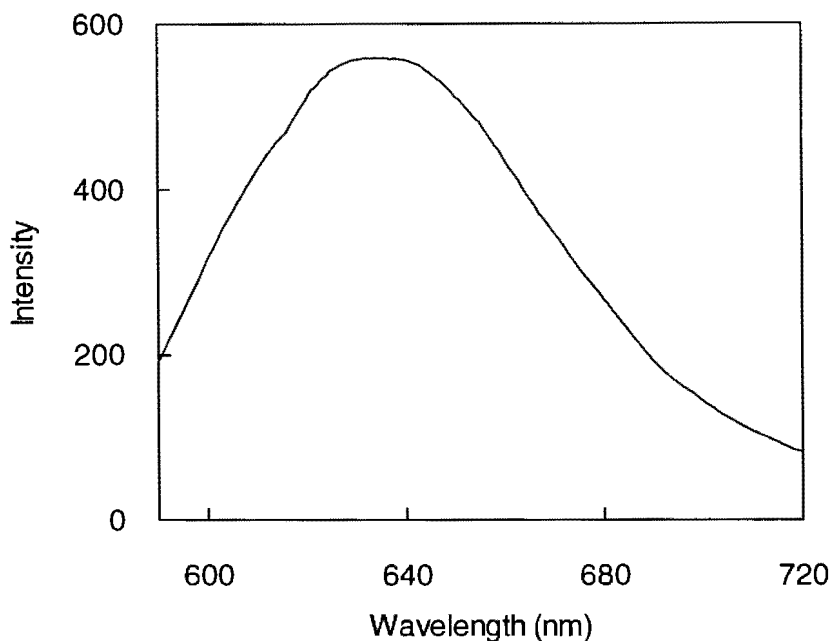
Figure 7.4. Emission spectra of anionic quantum dot (CdTe-TGA). The CdTe/ TGA QD were diluted 50 fold in 10 mM Tris, pH 8.0 using a plate reader with 3 mm diameter. The emission spectrum of the sample was corrected against the buffer blank. λ_{ex} and λ_{em} was 340 nm and 625 nm respectively.

Many researchers have studied the structures of the different hMMP isozymes depicting the size of the active site of these different hMMP isozymes by using the UCSF Chimera® software [23]. The crystal structures of many new members of the human MMP family have been discovered continuously in the last 20 years, until the final deposition of the human genome has fixed the final number at 24, five of which possess an additional shorter isoform. All MMPs have in common a catalytic domain constituted by about 170 amino acid residues. X-ray crystallographic structures of several MMP catalytic domains have shown that the active site is a domain which is an oblate sphere, measuring around 20

Å (2 nm), that runs across the domain. This piece of information indicates the size of the active site of the different hMMPs (hMMP-7, 9 and 10) leading to an idea about the comparative account of the size difference (considering the circumference) of the CQD or AQD compared to the active site of these hMMP isozymes. There have been many reports that support that MMP-7 [24], being the smallest in the family, has a catalytic domain around the size of 27 Å (2.7 nm). The size of MMP-9 [25] and MMP-10 [26] catalytic domains are 35 Å (3.5 nm) and 25 Å (2.5 nm), respectively. We can clearly observe that all three hMMP isoforms are comparable in size with the two differently charged QDs. However, AQD is a little larger (4.5 nm in diameter).

In order to find the effect of CQD and AQD to hMMP isozymes, binding studies were carried out. Figure 7.5 shows the dissociation constant (K_d) of the hMMP-7-CQD complex. The steady-state spectrofluorometric studies were performed in a Molecular Devices SpectraMax[®] Plus microplate reader (path length approximately 0.3 cm). The CQD used in these experiments were found to be most stable in 10 mM Tris, pH 8.0 and were prepared in Dr. Chen's laboratory.

This experiment was carried out by fixing the CQD concentration (0.3μM), while titrating with increasing concentrations of hMMP-7 from a known stock. The quenching of the tryptophan/tyrosine signal was monitored keeping the excitation and emission wavelength as 280 nm and 343 nm, respectively. The blank titration of protein into the buffer was performed to find the difference in the protein signal (ΔF) to be used to determine the dissociation constant (K_d) for the hMMP-7-CQD complex formation. This experiment was carried out by fixing the CQD concentration (0.3μM), while titrating with

increasing concentrations of hMMP-7 from a known stock. The quenching of the tryptophan/tyrosine signal was monitored keeping the excitation and emission wavelength as 280 nm and 343 nm, respectively. The blank titration of protein into the buffer was performed to find the difference in the protein signal (ΔF) to be used to determine the dissociation constant (K_d) for the hMMP-7-CQD complex formation.

Figure 7.5. Determination of the dissociation constant (K_d) of the hMMP-7-CQD complex. The excitation was at 280 nm and the tryptophan signal was monitored at 343 nm. A fixed concentration of CQD (0.3 µM) was titrated with known concentrations of hMMP-7. The corrected signal from the blank titration of protein into buffer was used to calculate the binding constant. The solid smooth line is the best fit of the data showing the k_d to be 1.25 ± 0.3 µM.

The binding isotherm was plotted using the fluorescence difference signal as a function of the protein concentration. The stock concentration of the CQD could not be determined *a priori*, so it seemed a valid approach to use a quadratic binding equation, which would account for both the concentration of CQD used as well as determine the K_d for the complex formation. The k_d was determined to be 1.25 ± 0.3 µM. There was a 12 nm

red shift observed in the tryptophan fluorescence emission maxima. The shift can be attributed to an Internal Stark effect (ISE) [27].

The large red shift in fluid solvents with high dielectric constants can also be attributed to the stark effect [28-33]. The strong electric field at the solute is due to the partial orientation of solvent dipoles around the larger solute dipoles. The magnitude of the field and the orientation of the indole ring determine the spectral shift. The extent to which the maximum fluorescence is governed by solvent and protein residues depends on: (1) Polarization (orientation) of water molecules by charged and polar protein; and (2) Polarization (electronic) of the Trp ring by an electric field arising from water and protein.

In most cases, with oriented regions of water, 15-25 Å from Trp collectively contribute to 5-10 nm blue and red shifts [34]. This is due to the ordering of the domains of water to the charged groups of the protein. The contribution of water and protein is found to increase with increasing wavelengths. Figure 7.6 shows the binding isotherm for the determination of dissociation constant (K_d) of a hMMP-9-CQD complex. Under identical conditions the dissociation constant for hMMP-9 to the CQD was determined. The quenching of the tryptophan/tyrosine signal was monitored keeping the excitation and emission wavelength as 280 nm and 335 nm, respectively. The k_d was determined to be 0.2 ± 0.08 µM.

Figure 7.7 shows the dissociation constant (K_d) of hMMP-10-CQD complexes. The quenching of the tryptophan/tyrosine signal was monitored keeping the excitation and emission wavelength as 280 nm and 330 nm. The k_d was determined to be 2.0 ± 0.23 µM. There was a 15 nm red shift observed in the tryptophan fluorescence emission λ_{max}.
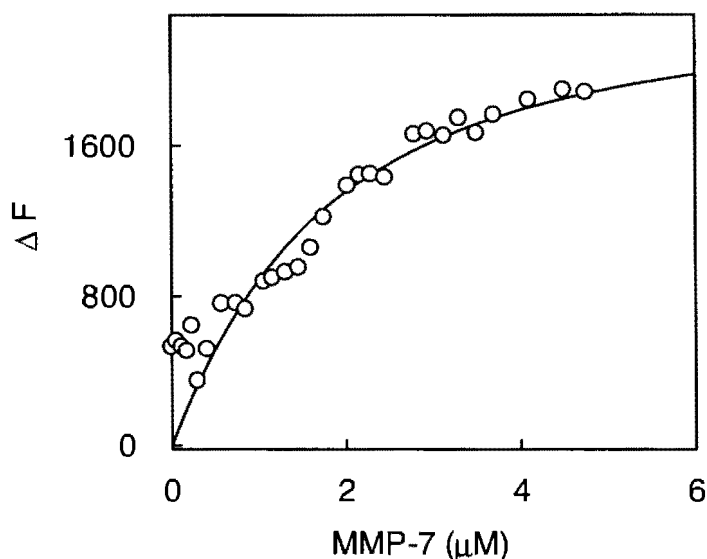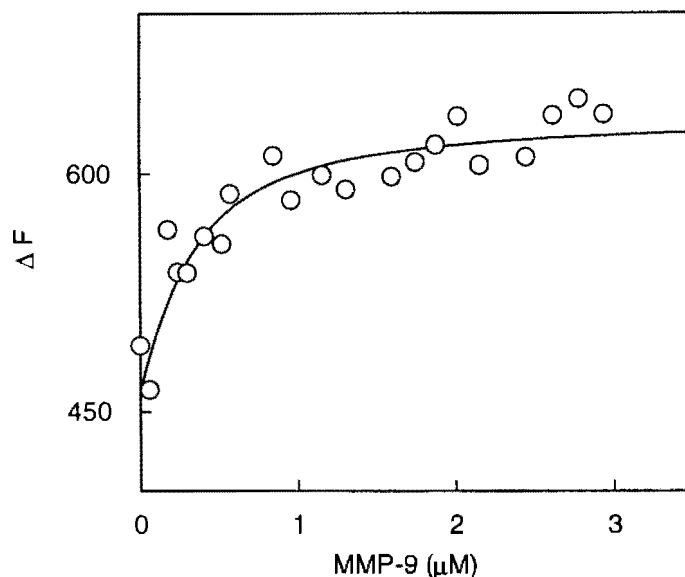
Figure 7.6. Determination of the dissociation constant (K_d) of hMMP-9-CQD complex. The excitation was at 280 nm and the W signal was monitored at 335 nm. A fixed concentration of CQD (0.3 µM) was titrated with known concentrations of hMMP-9. The corrected signal from the blank titration of protein into buffer was used to calculate the binding constant. The solid smooth line is the best fit of the data showing the k_d to be 0.2 ± 0.08 µM.

Figure 7.7. Determination of the dissociation constant (K_d) of the hMMP-10-CQD complex. The excitation was at 280 nm and the W signal was monitored at 330 nm. A fixed concentration of CQD (0.3 µM) was titrated with known concentrations of hMMP-10. The corrected signal from the blank titration of protein into buffer was used to calculate the binding constant. The solid smooth line is the best fit of the data showing the k_d to be 2.0 ± 0.23 µM.
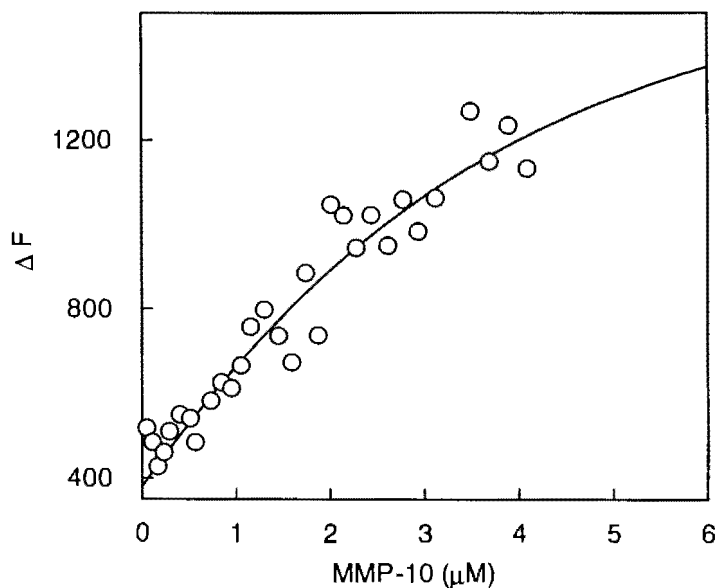
229

Table 7.1 shows the comparative account of the K_d of the hMMP isozymes with CQD. hMMP-7 and 10 show a comparable binding affinity to CQD but hMMP-9 exhibits a ten-fold higher binding affinity, which reflects a non-trivial interaction existing between hMMP-9 and CQD. The interaction of hMMP isozymes with CQD demonstrate that hMMP-9 binds to the CQD most strongly while hMMP-7 and 10 share comparable binding affinity.

Figure 7.8 shows the dissociation constant (K_d) of the hMMP-7-AQD complex. The steady-state spectrofluorometric studies were performed on a Molecular Devices SpectraMax® Plus microplate reader (path length of approximately 0.3 cm). Similar to the CQD, the AQD was also found to be stable in 10 mM Tris, pH 8.0.

Table 7.1. Comparative account of the dissociation constants (K_d) of hMMP isozymes with CQD.

MMP Isozymes	CQD K_d (μM)
hMMP-7	1.25
hMMP-9	0.2
hMMP-10	2.0

A fixed concentration of AQD (0.57 μM) was titrated with known concentrations of hMMP-7. The excitation was at 280 nm and the tryptophan signal was monitored at 354 nm. The blank titration of protein into the buffer was performed to find the difference in the protein signal (ΔF) to be used to determine the dissociation constant (K_d) for the hMMP-7-AQD complex formation. The fluorescence difference signal as a function of the protein concentration was used to construct the binding isotherm. It can be observed the

saturating hyperbolic profile, showing the K_d value to be 0.6 ± 0.16 μM. Note that the AQD binds to hMMP-7 two-fold tighter than CQD.

Figure 7.9 shows the dissociation constant (K_d) of the hMMP-9-AQD complex. Under the same setting as hMMP-7, the K_d value for hMMP-9 with AQD was determined to be 0.13 ± 0.11 μM. When compared with the K_d value of hMMP-9-CQD complex formation ($k_d = 0.2 \pm 0.08$ μM) it is clear that the binding affinities were easily comparable.
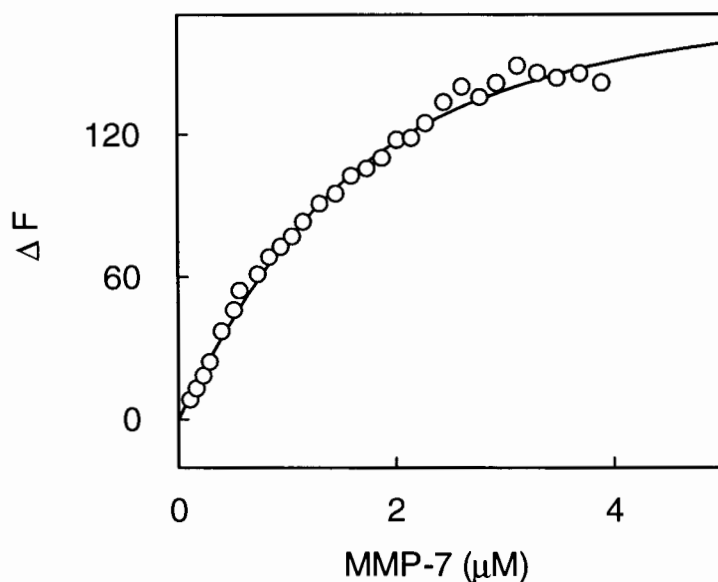
Figure 7.8. Determination of the dissociation constant (K_d) of the hMMP-7-AQD complex. A fixed concentration of AQD (0.57 μM) was titrated with known concentrations of hMMP-7. The excitation was at 280 nm and the tryptophan signal was monitored at 354 nm. The corrected signal from the blank titration of protein into buffer was used to calculate the binding constant. The solid smooth line is the best fit of the data showing the k_d was determined to be 0.6 ± 0.16 μM.

Figure 7.10 shows that the determination of the dissociation constant (K_d) of the hMMP-10-AQD complex. The k_d was determined to be 0.03 ± 0.02 μM. The K_d of hMMP-10 with CQD is 2.0 ± 0.23 μM. The binding affinity of hMMP-10 with AQD is sixty-

sixfold tighter than with CQD. The AQD binds to hMMP-10 even with higher affinity

(twenty-fold higher) than hMMP-7.

Protein contributions such as charged side chains, polar side chains, Trp backbone

and other backbones cause the shift in protein fluorescence [29, 35-36]. Backbone and

polar side chains contribute to short range (van der Waals contact) shifts of 5-10 nm by

dipole-dipole interactions reaching 20 nm in some extreme cases.

Figure 7.9. Determination of the dissociation constant (K_d) of the hMMP-9-AQD complex. A fixed concentration of AQD (0.57 μM) was titrated with known concentrations of MMP-9. The excitation was at 280 nm and the tryptophan signal was monitored at 354 nm. The corrected signal from the blank titration of protein into buffer was used to calculate the binding constant. The solid smooth line is the best fit of the data showing the k_d was determined to be 0.13 $\pm$ 0.11 μM.

Charged amino-acid residues (Lys, Arg, Asp, Glu, and any C-terminal residue)

make the largest contribution to the fluorescence shift for proteins [36-37]. The largest red

shift of 78 nm was observed for the Lys-133 of *Staphylococcus* and 67 nm for the Asp-26

of thioredoxin, while the largest blue shift was observed at 38 nm for Arg-22 in monomer

232

of melittin and 39 nm for Lys-57 in thioredoxin [37]. The largest shifts of 20 nm due to the neutral side chains were observed from Asn-117 of subtilisin and 7 nm for Gln-105 of
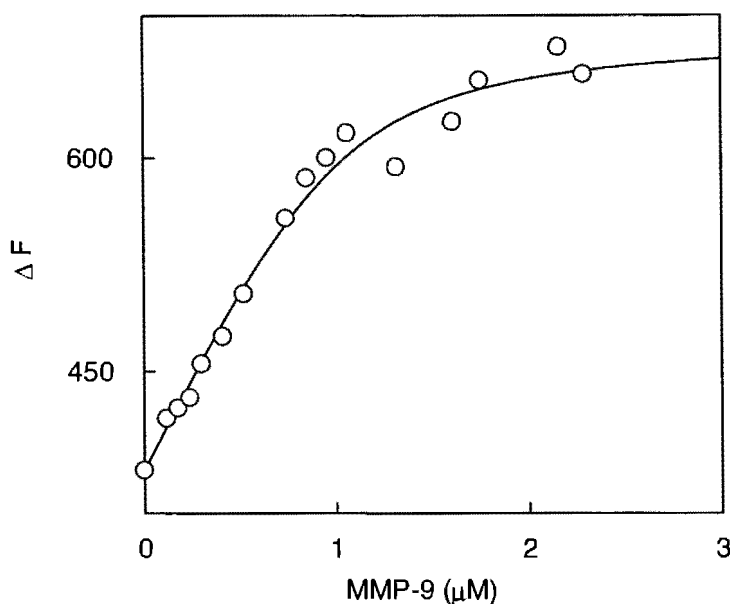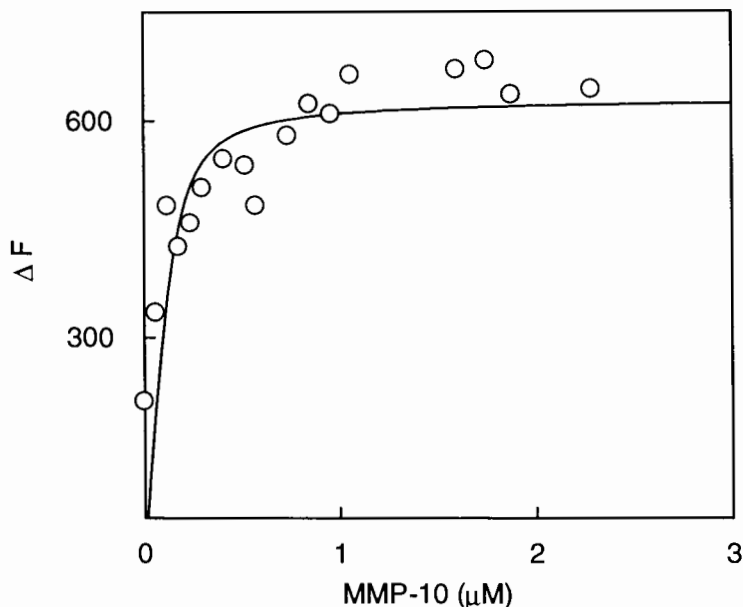

Figure 7.10. Determination of the dissociation constant (K_d) of the hMMP-10-AQD complex. A fixed concentration of AQD (0.57 μM) was titrated with known concentrations of MMP-10. The excitation was at 280 nm and the tryptophan signal was monitored at 354 nm. The corrected signal from the blank titration of protein into buffer was used to calculate the binding constant. The solid smooth line is the best fit of the data showing the k_d was determined to be 0.03 ± 0.02 μM.

T4 lysozyme (W-138). The Trp backbone atoms contribute significantly to the shift [38]. The contributions range from a 9 nm blue shift (for Trp-118 of azurin) to a 6 nm red shift (for monellin).

Table 7.2 shows a comparative account of the K_d of hMMP isozymes with AQD. Except for hMMP-9, where there was no variation in the binding affinity for the differently charged QD. Other hMMP isozymes (hMMP-7 and hMMP-10) exhibit good specificity for AQD (negatively charged QD) as compared to CQD (positively charged QD). But hMMP-

10 binds tightly with AQD. The interactions of hMMP isozymes with AQD demonstrated that hMMP-10 binds to the AQD most strongly, followed by hMMP-9 and hMMP-7. This result contrasts the findings in the liposome mediated interactions with hMMP isozymes. One plausible rationale would be the comparable size of the two molecules involved (hMMP-7 and AQD). As noted above, the size of hMMP-7 active site and AQD were 2.7 nm and 4.5 nm, respectively, indicating that unlike anionic LUVs (100 nm diameter), the AQDs were two times the size of the enzyme. Hence, the dynamics of the binding would get affected due to surface curvature and availability of the surface area for the hMMP-7 to spread or bend on the QDs [16].

Table 7.2. Comparative account of the dissociation constants (K_d) of hMMP isozymes with AQD.

MMP Isozymes	AQD K_d (μM)
hMMP-7	0.6
hMMP-9	0.13
hMMP-10	0.03

The two parameters that decide the emission maximum are degree of exposure of the tryptophan residues and solvent properties. The orientation of the water molecules and electronic polarization of the indole ring in the trytophan imposed by the surrounding water plays a vital role in the determination of the shifts observed in the fluorescence emission maxima [39]. Tryptophan is very sensitive to the micro-environment as a fluorophore based on which emission maxima for the protein is monitored. If $\lambda_{max} \leq 330$ nm, a tryptophan residue is considered buried in a non-polar environment, while $\lambda_{max} \geq 330$ nm suggests the tryptophan is exposed and in a polar environment. The mere presence of water

or any buffer solvent does not influence the position of λ_{max}, whereas the orientation of the water dipole does influence it. A red shift, with the size of the shift being inversely proportional to the distance from the center of the tryptophan ring, is created by the relative direction of a charge from the tryptophan bearing positive charges on the end of the benzene ring while the reverse holds true for negative charges. The red shift is caused by the extent of exposure of the faces of the benzene ring of tryptophan to water. A modest red shift occurs if the edge is exposed to the face of the benzene ring while a large red shift occurs if the face is exposed. Water, on the other hand can cause a significant red shift (10-20 nm) for buried tryptophan's due to the collective action of regions of water up to 25 nm distance that are favorably oriented by the charges and/or shape of the protein [40].

Upon analysis of the crystal structure of the catalytic domain of hMMP-7, it was noted that hMMP-7 contains four tryptophan residues and eight tyrosine residues. Out of the four tryptophan residues, three were fully exposed and the other one was partially exposed (See Chapter 4). Eight tryptophan residues are present in hMMP-9 with varied degrees of exposure to the aqueous environment. A careful analysis of the catalytic domain shows three tryptophan residues that were partially exposed with one residue being fully buried in the interior core of the protein [41]. A red shift was observed and extensive hypochromicity can be credited for the formation of a more open structure in the presence of QDs by either partial or complete revelation of one or more exposed tryptophan residues. The binding of QDs differently modulates the micro-environment of hMMP-9 resident tryptophan. It is known that λ_{max} and q (quantum yield) tryptophan residues can separate in proteins into two different classes, one of which is exposed and the other

235

buried. The exposed tryptophan residues, with the position of λ_{max} towards the longer wavelength side (λ_{max} of approximately 350 nm) and the quantum yield equal or higher than that of free aqueous tryptophan (approximately 0.13-0.17), are in a high-polar aqueous environment [42].

The other tryptophan residues, which are buried inside the protein in a low-polar hydrophobic environment, with the position of λ_{max} toward the shorter wavelength side (λ_{max} of approximately 330 nm), have low quantum yield (0.04 to 0.07). The shift in the protein spectrum towards 350-353 nm upon denaturation by urea and 330-332 nm upon addition of anionic detergents in acidic solutions supports the hypothesis [43]. The characterization of hMMP-10 was done using a tryptophan fluorescence probe. Human MMP-10 harbors 8 tryptophan residues with varied degrees of exposures to the aqueous environment together in the fibronectin domain and the catalytic domain [44]. However, two tryptophan residues were found to be fully buried in the analysis of the catalytic domain, while one residue was partially buried to the interior core of the protein.

With this knowledge, it was tempting to delve into the question of whether or not the interaction of the hMMP isozymes has any effect on their functional aspect of catalyzing a reaction. To answer this question inhibition studies using the three available hMMP isozymes and the two differently charged QDs were conducted.

Figure 7.11 shows the inhibition constant (K_i) of the hMMP-7-CQD complex. When the fluorogenic substrate was cleaved by hMMP-7 in the presence of increasing concentrations of CQD, the enzyme was inhibited upto 80% at higher concentrations of CQD (varied from 0 to 3 μM) used. The K_i was 0.24 $\pm$ 0.04 μM. When the K_d (1.25 $\pm$ 0.3

μM) and K$_i$ (0.24 ± 0.04 μM) values were compared for hMMP-7 and CQD, the difference in K$_d$ and K$_i$ was five-fold, which indicates that there would be some conformational changes in the protein followed by inhibition of the enzyme activity.

Figure 7.12 shows the inhibition constant (K$_i$) of the hMMP-9-CQD complex. The enzyme was inhibited more than 90% at lower concentrations of CQD (varying from 0 to 2 μM) used. The K$_i$ was 0.32 ± 0.037 μM. When the K$_d$ (0.2 ± 0.08 μM) and K$_i$ (0.32 ± 0.037 μM) values were compared for hMMP-9 and CQD, the similarity in K$_d$ and K$_i$ showed that there was binding and subsequent inhibition of the enzyme due to physically binding at the active site and blocking the accessibility of the substrate.
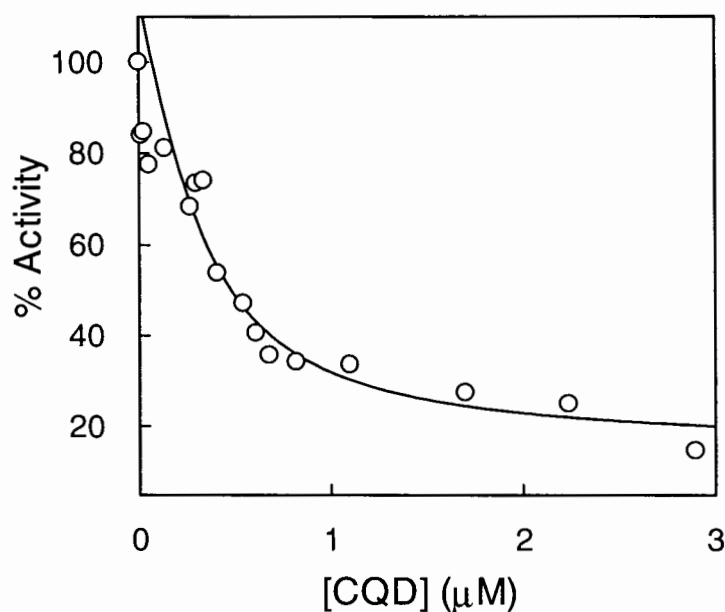

Figure 7.11. Determination of the inhibition constant (K$_i$) of hMMP-7-CQD complex. The enzyme-catalyzed hydrolysis of the fluorogenic peptide (λ_{ex} = 335 nm, λ_{cm} = 395 nm) was measured as a function of the CQD concentrations. The symbol (o-o) represent data obtained in the presence of CQD. [hMMP-7] = 0.3μM, [Substrate] = 25 μM. The activity of hMMP-7 decreases as a function of increasing concentrations of CQD. The solid smooth line is the best fit of the data for the CQD-MMP-7 complex. The K$_i$ value was determined to be 0.24 ± 0.04 μM.

Figure 7.13 shows the inhibition constant (K_i) of the hMMP-10-CQD complex. The enzyme was inhibited more than 80% at higher concentrations of CQD (varying from 0 to 4 μM) used. The K_i was 1.11 ± 0.07 μM. When the K_d (2.0 ± 0.23 μM) and K_i (1.11 ± 0.07 μM) values were compared for hMMP-10 and CQD, the comparative values of K_d and K_i showed that there was binding and inhibition of the enzyme due to just binding and proximity of the active-site and blocking the accessibility of the substrate.
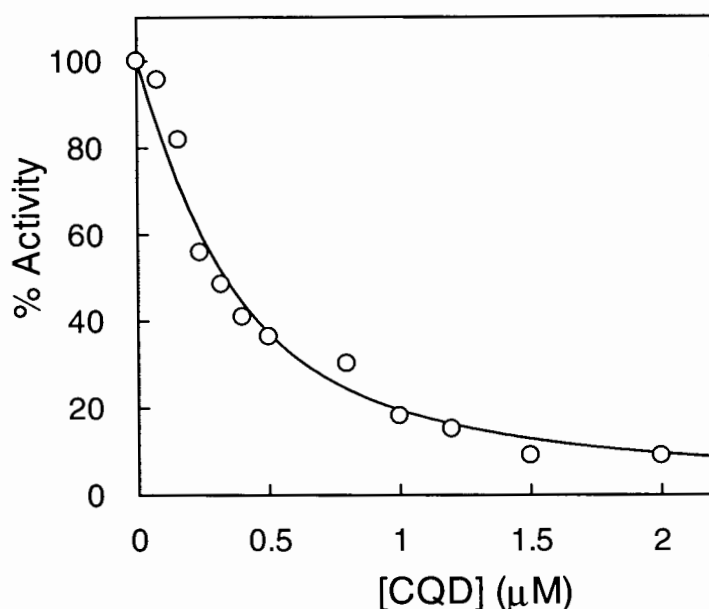

Figure 7.12. Determination of the inhibition constant (K_i) of hMMP-9-CQD complex. The enzyme-catalyzed hydrolysis of the fluorogenic peptide (λ_{ex} = 335 nm, λ_{em} = 395 nm) was measured as a function of the CQD concentrations. The symbol (o-o) represent data obtained in the presence of CQD. [hMMP-9] = 0.16 μM, [Substrate] = 25 μM. The activity of hMMP-9 decreases as a function of increasing concentrations of CQD. The solid smooth line is the best fit of the data for the CQD-MMP-9 complex. The K_i value was determined to be 0.32 ± 0.04 μM.

Table 7.3 shows the comparative account of the K_i of hMMP isozymes with CQD. It reflects the similar inhibition constants for hMMP-7 and 9, unlike hMMP-10. Human MMP-7 and 9 are inhibited by CQD four-fold more than hMMP-10. The interactions of

hMMP isozymes with CQD demonstrated that CQD acts as a potent inhibitor for hMMP-7 and hMMP-9 to a comparable degree. On the other hand, hMMP-10 binds strongly to CQD, but it does not act as a very potent inhibitor. This feature hints at some conformational changes that potentially might be occurring upon binding to the CQD.
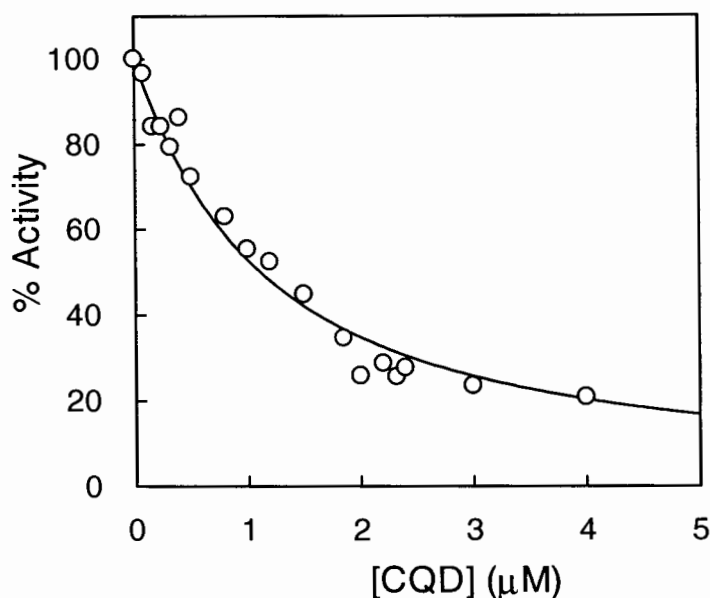

Figure 7.13. Determination of the inhibition constant (K_i) of hMMP-10-CQD complex. The enzyme-catalyzed hydrolysis of the fluorogenic peptide (λ_{ex} = 335 nm, λ_{em} = 395 nm) was measured as a function of the CQD concentrations. The symbol (o-o) represent data obtained in the presence of CQD. [hMMP-9] = 1.0 μM, [Substrate] = 25 μM. The activity of hMMP-10 decreases as a function of increasing concentrations of CQD. The solid smooth line is the best fit of the data for the CQD-MMP-10 complex. The K_i value was determined to be 1.11 ± 0.07 μM.

Table 7.3. Comparative account of the inhibition constants (K_i) of hMMP isozymes with CQD.

MMP Isozymes	CQD K_i (μM)
hMMP-7	0.24
hMMP-9	0.32
hMMP-10	1.11

Figure 7.14 shows the inhibition constant (K_i) of the hMMP-7-AQD complex. The enzyme was inhibited 80% at higher concentrations of AQD (varying from 0 to 2.5 μM) used. The K_i was 0.04 ± 0.08 μM. When the K_d (0.6 ± 0.16 μM) and K_i (0.04 ± 0.08 μM) values were compared for hMMP-7 and AQD it was found that the difference in K_d and K_i was seventeen-fold. This indicated that subtle conformational changes in the protein were contributing to the inhibition of the enzyme activity.
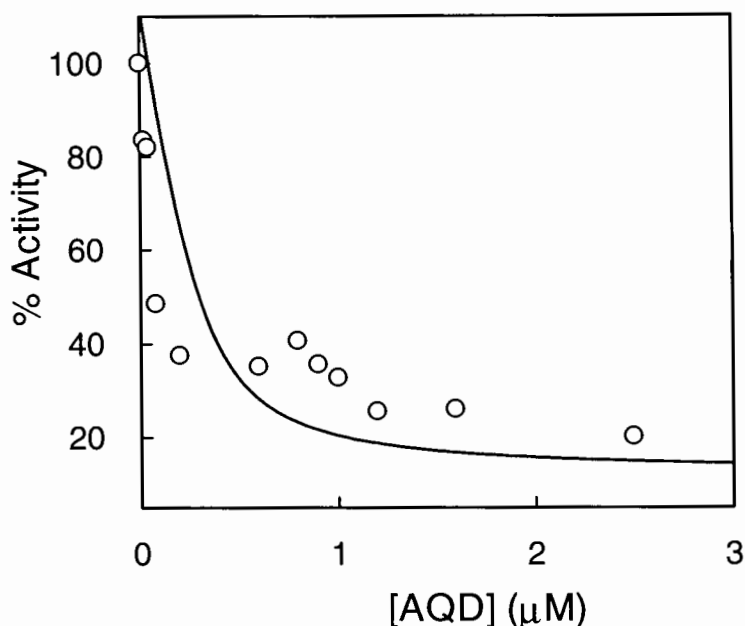

Figure 7.14. Determination of the inhibition constant (K_i) of the hMMP-7-AQD complex. The enzyme-catalyzed hydrolysis of the fluorogenic peptide (λ_{ex} = 335 nm, λ_{em} = 395 nm) was measured as a function of the AQD concentrations. The symbol (o-o) represents data obtained in the presence of AQD. [hMMP-7] = 0.3 μM, [Substrate] = 25 μM. The activity of hMMP-7 decreases as a function of increasing concentrations of AQD. The solid smooth line is the best fit of the data for the AQD-MMP-7 complex. The K_i value was determined to be 0.04 ± 0.08 μM.

Figure 7.15 shows the inhibition constant (K_i) of the hMMP-9-AQD complex. The enzyme was inhibited a little less than 80% at higher concentrations of AQD (varying from 0 to 1.2 μM) used. The K_i was 0.15 ± 0.02 μM. When the K_d (0.14 ± 0.11 μM) and K_i (0.15

± 0.02 µM) values were compared for hMMP-9 and AQD, the close association in K_d and

K_i implies that AQD binding leads to conformational changes in the overall enzyme,

thereby distorting the globular tertiary structure of the protein due to the presence of an

allosteric binding site for the AQD.

Figure 7.16 shows the inhibition constant (K_i) of the hMMP-10-AQD complex. The

enzyme was inhibited a little less than 80% at higher concentrations of AQD (varying from

0 to 2 µM) used. The K_i was 0.27 ± 0.03 µM. When the K_d (0.03 ± 0.02 µM) and K_i (0.27 ±

0.03 µM) values were compared for hMMP-10 and AQD, the difference in K_d and K_i

implies that upon binding to AQD there are conformational changes in the native enzyme.

Figure 7.15. Determination of the inhibition constant (K_i) of hMMP-9-AQD complex. The enzyme-catalyzed hydrolysis of the fluorogenic peptide (λ_{ex} = 335 nm, λ_{em} = 395 nm) was measured as a function of the AQD concentrations. The symbol (o-o) represents data obtained in the presence of AQD. [hMMP-9] = 0.16 µM, [Substrate] = 25 µM. The activity of hMMP-9 decreases as a function of increasing concentrations of AQD. The solid smooth line is the best fit of the data for the AQD-MMP-9 complex. The K_i value was determined to be 0.15 ± 0.02 µM.

Nanoparticles, as compared to traditional materials, have a larger surface area that can be tailored with organic molecules through covalent or non-covalent modifications to form functionalized NPs [45]. These tailored NPs possess abilities to prevent non-specific binding and recognize specific bio-macromolecules, so that, enzyme activities can be specifically regulated when bound to surface modified NPs.
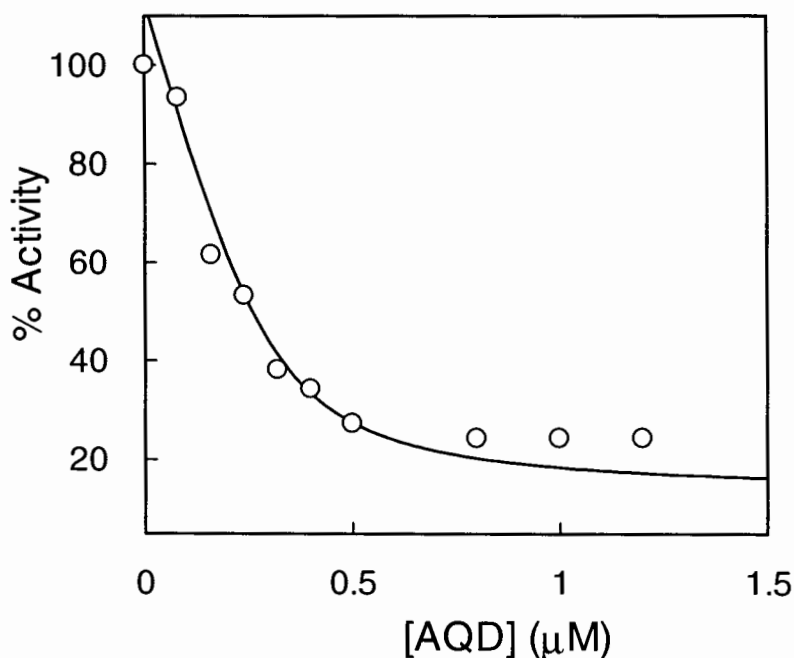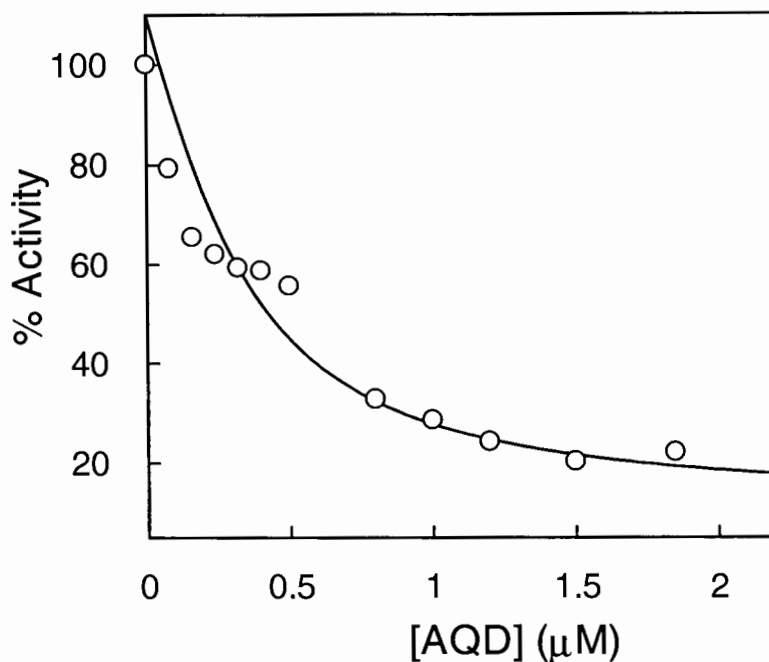

Figure 7.16. Determination of the inhibition constant (K_i) of hMMP-10-AQD complex. The enzyme-catalyzed hydrolysis of the fluorogenic peptide (λ_{ex} = 335 nm, λ_{em} = 395 nm) was measured as a function of the AQD concentrations. The symbol (o-o) represents data obtained in the presence of AQD. [hMMP-10] = 1.0 μM, [Substrate] = 25 μM. The activity of hMMP-10 decreases as a function of increasing concentrations of AQD. The solid smooth line is the best fit of the data for the AQD-MMP-10 complex. The K_i value was determined to be 0.27 ± 0.03 μM.

In accordance with the above results, a range of studies of protein or peptide adsorption on Au or SiO_2 NPs of different sizes have been reported. Proteins, including lysozyme, horseradish peroxidase, catalase, and trypsin [22], adsorb strongly to SiO_2 NPs (sizes ranging from 9 to 40 nm). In the process, these proteins undergo a partial loss of the

structure and generally a significant loss in enzyme activity.

Table 7.4 shows the comparative account of the K_i of hMMP isozymes with AQD. It shows that hMMP-7 is inhibited most potently compared to hMMP-9 and 10. Even though the K_d value is seventeen-fold higher than the K_i value, it appears that hMMP-7 binds to AQD, and then with conformational adjustment, a stable complex of the hMMP-7-AQD complex is reached leading to the potent inhibition. This scenario is in contrast to the case of hMMP-10, where formation of the complex causes the potency of inhibition to decrease. This is a very interesting facet that the isozymes exhibited, leading to the conclusion that these flexible hMMPs undergo conformational changes upon binding the the QDs, especially the AQD.

Table 7.4. Comparative account of the inhibition constants (K_i) of hMMP isozymes with AQD.

MMP Isozymes	AQD K_i (μM)
hMMP-7	0.04
hMMP-9	0.15
hMMP-10	0.27

The findings in the above experiments showed that CQD and AQD both bind and inhibit the three hMMP isozymes with varying potencies. But, to know whether or not the inhibition observed was a "true" inhibition or it was newly formed irreversible binary hMMP-QD complex, a snap dilution tests were carried out to check the reversibility of the formed complex. Figure 7.17.A and 7.17.B shows whether CQD and AQD respectively inhibits or inactive the enzyme activity of hMMP-7. Figure 7.17.B shows whether or not AQD inhibits or inactives the enzyme activity of hMMP-7. The progress curve of the

hMMP-7 catalyzed reaction was monitored in the presence of CQD or AQD under different conditions. The conditions were (1) the progress curves of hMMP-7 (0.3 μM) alone, (2) hMMP-7 with 0.24 μM CQD/AQD (0 time incubation), and (3) hMMP-7 with 0.24 μM CQD/AQD (20 minutes pre-incubation time). The slopes ($\Delta F.s^{-1}$) of the progress curves calculated for the above data were 6.88 (black line), 4.67 (red line), 3.66 (green line) and 3.83 (blue line) $\Delta F.s^{-1}$, respectively, for CQD, while 9.55 (black line), 2.03 (red line), 2.05 (green line) and 3.0 (blue line) $\Delta F.s^{-1}$, respectively, were calculated for AQD. Upon incubation of hMMP-7 with CQD, there was a loss of 17% enzyme activity. But, that trivial loss in activity is often expected when enzymes are pre-incubated with very high inhibitor concentrations (CQD in this case) and then snap diluted. The enzyme is forced to refold back to its native structure. But there is a very good possibility that the enzyme does not refold back to its compact native conformation. It might have a close resemblance with it's native structure but probably attains a different conformation. However, in case of AQD, upon pre-incubation with hMMP-7, the enzyme activity is enhanced [46]. This result led to the conclusion that AQD helped hMMP-7 to become a more compact structure.

Figure 7.18.A and B shows whether CQD and AQD respectively inhibits or inactive the enzyme activity of hMMP-9. The progress curve of the hMMP-9 catalyzed reactions are shown in presence of CQD and AQD under different conditions and monitored for 200 secs. The conditions were (1) the progress curves of hMMP-9 (0.16 μM) alone, and (2) hMMP-9 with 0.24 μM CQD/AQD (0 time incubation), and hMMP-9 with 0.24 μM CQD/AQD (20 minutes pre-incubation time). The slopes ($\Delta F.s^{-1}$) of the progress curves were calculated for the above data were 5.3 (red line), 0.27 (blue line), 0.28 (green line)

$\Delta F.s^{-1}$, respectively, for CQD, and 5.2 (black line), 0.22 (red line), 0.27 (green line) $\Delta F.s^{-1}$, respectively, were calculated for AQD.

Figure 7.19.A and B shows whether CQD and AQD respectively inhibit or inactive the enzyme activity of hMMP-10. The progress curve of the hMMP-10 catalyzed reaction is shown in presence of CQD and AQD under different conditions and monitored for 200 secs. The conditions were 1) the progress curves of hMMP-10 (1.0 µM) alone, and 2) hMMP-10 with 0.240 µM CQD/AQD (0 time incubation), and hMMP-10 (20 min pre-incubation time) respectively. The slopes for MMP-10 ($\Delta F.s^{-1}$) of the progress curves calculated for the above data were 0.38 (black line), 0.14 (red line), and 0.18 (green line) $\Delta F.s^{-1}$, respectively, for CQD, while 0.38 (black line), 0.09 (red line), 0.11 (green line) $\Delta F.s^{-1}$, respectively, were calculated for AQD.

Table 7.5.A shows the comparative account of the effect for inhibition/ inactivation of hMMP isozymes with CQD. Table 7.5.B shows the comparative account of the effect for inhibition/ inactivation of hMMP isozymes with AQD. The hMMP-7 becomes a more compact structure after incubation with AQD. Moreover, the binding of QDs to hMMP isozymes are all reversible. Even though both QDs and Au-NPs (See Chapter 5) were rigid molecules with high surface curvature, Au-NPs denatured the proteins while QDs physically bind to the hMMPs in a reversible manner.

Electrostatic force plays a key role in the design of nanostructures and biomolecules that have high efficiency and self-targeting selectivity [16]. The conformation of DNA molecules change from coiled long chains to compact globules when CTAB-modified QDs induces a DNA condensation process [47-48].
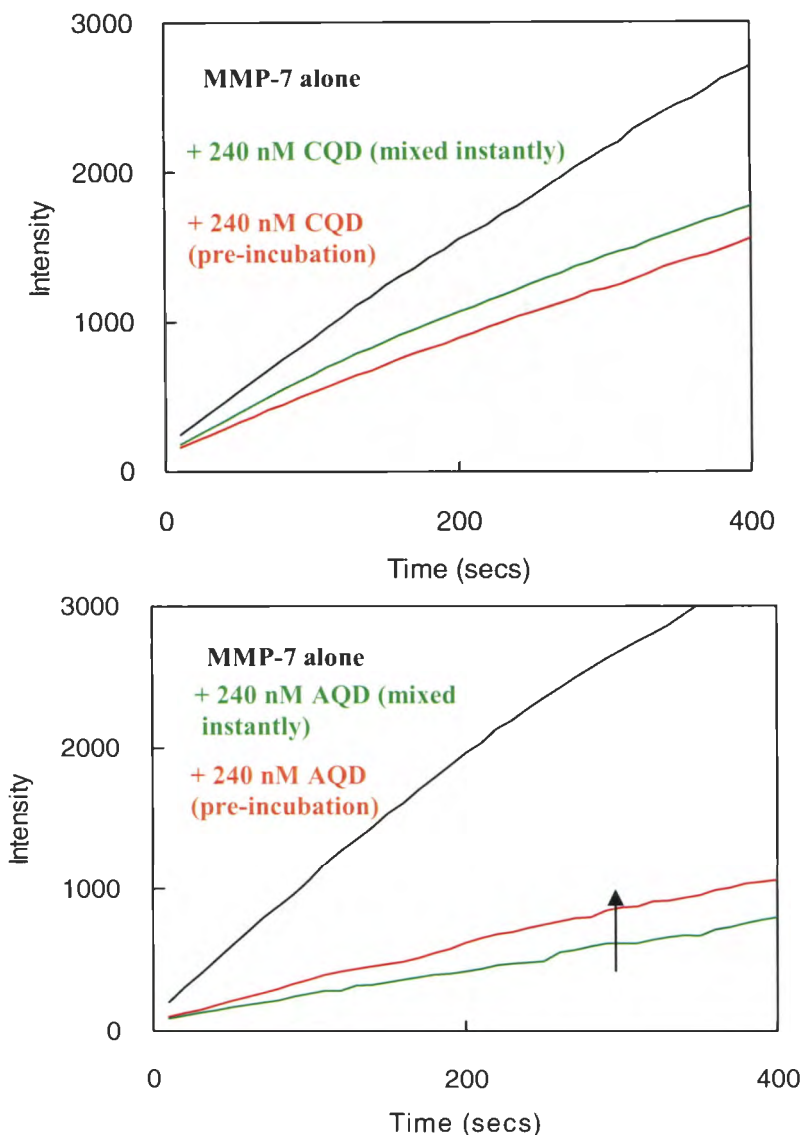
Figure 7.17.A. Inhibition / inactivation of the enzyme activity of hMMP-7 by CQD. B. Inhibition / inactivation of the enzyme activity of hMMP-7 by AQD. The time course of hMMP-7 catalyzed reaction in the presence of CQD / AQD has been shown. A control experiment was performed in the absence of QDs. The black solid line, the red solid line, the green solid line and the blue solid line indicates the progress curves of hMMP-7 alone (0.3 μM, hMMP-7 with 0.240 μM CQD/AQD (0 time incubation), and hMMP-7 (20 min pre-incubation time) and hMMP-7 (1 hr pre-incubation time) respectively. The slopes ($\Delta F.s^{-1}$) of the progress curves were calculated for the above data were 6.88 (black line), 4.67 (red line), 3.66 (green line) and 3.83 (blue line) $\Delta F.s^{-1}$, respectively, for CQD, while 9.55 (black line), 2.03 (red line), 2.05 (green line) and 3.0 (blue line) $\Delta F.s^{-1}$, respectively, for AQD. The incubation of hMMP-7 with CQD for 20 mins resulted in 17 % loss in the enzyme activity while the enzyme activity increases upon longer pre-incubation with AQD.
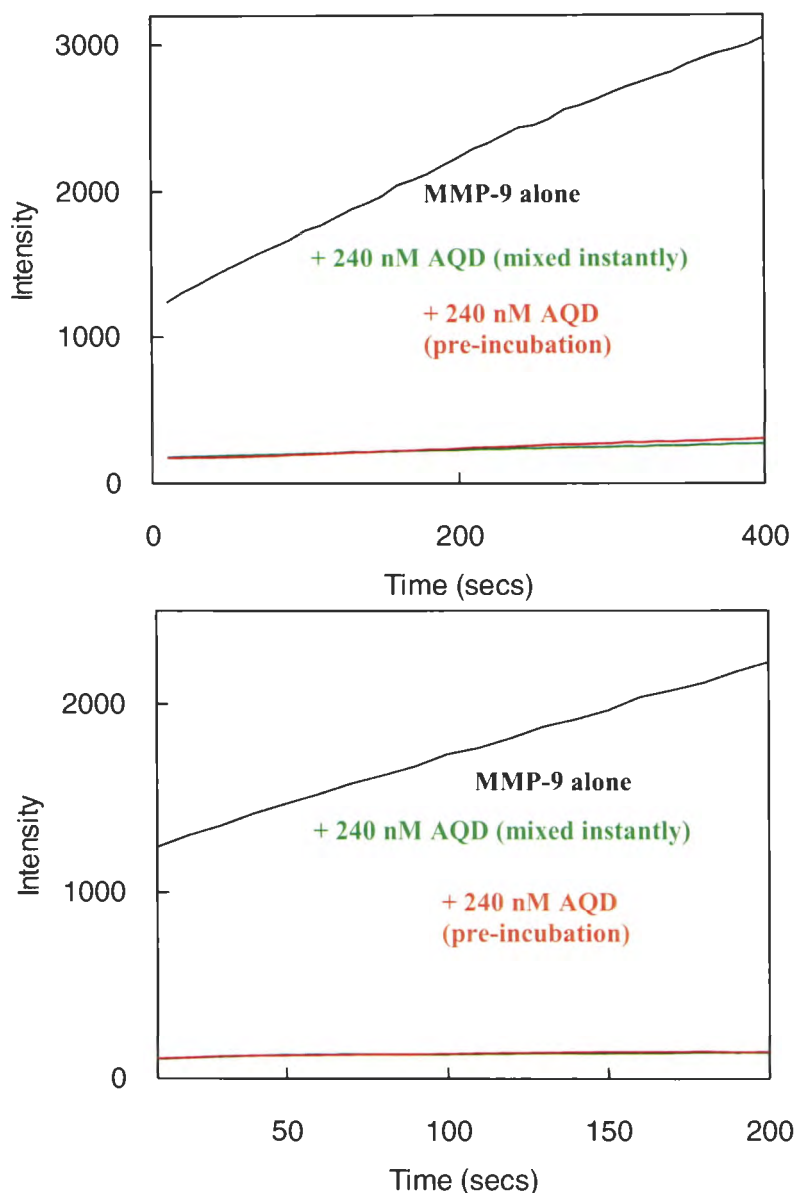
Figure 7.18.A. Inhibition / inactivation of the enzyme activity of hMMP-9 by CQD. B. Inhibition / inactivation of the enzyme activity of hMMP-9 by AQD. The time course of the MMP-9 catalyzed reaction in the presence of CQD / AQD has been shown. Control experiment has been performed in the absence of QDs. The time course of the reaction was monitored for about maximum 200 sec. For MMP-9 the red solid line, the blue solid line, the green solid line indicates the progress curves of hMMP-9 alone (0.16 μM, hMMP-9 with 0.240 μM CQD/AQD (0 time incubation) hMMP-9 with the same concentration of QDs (20 min pre-incubation time) respectively. The slopes ($\Delta F.s^{-1)}$ of the progress curves were calculated for the above data were 5.3 (red line), 0.27 (blue line), 0.28 (green line) $\Delta F.s^{-1}$, respectively for CQD while 5.2 (black line), 0.22 (red line), 0.27 (green line) $\Delta F.s^{-1}$, respectively, for AQD.
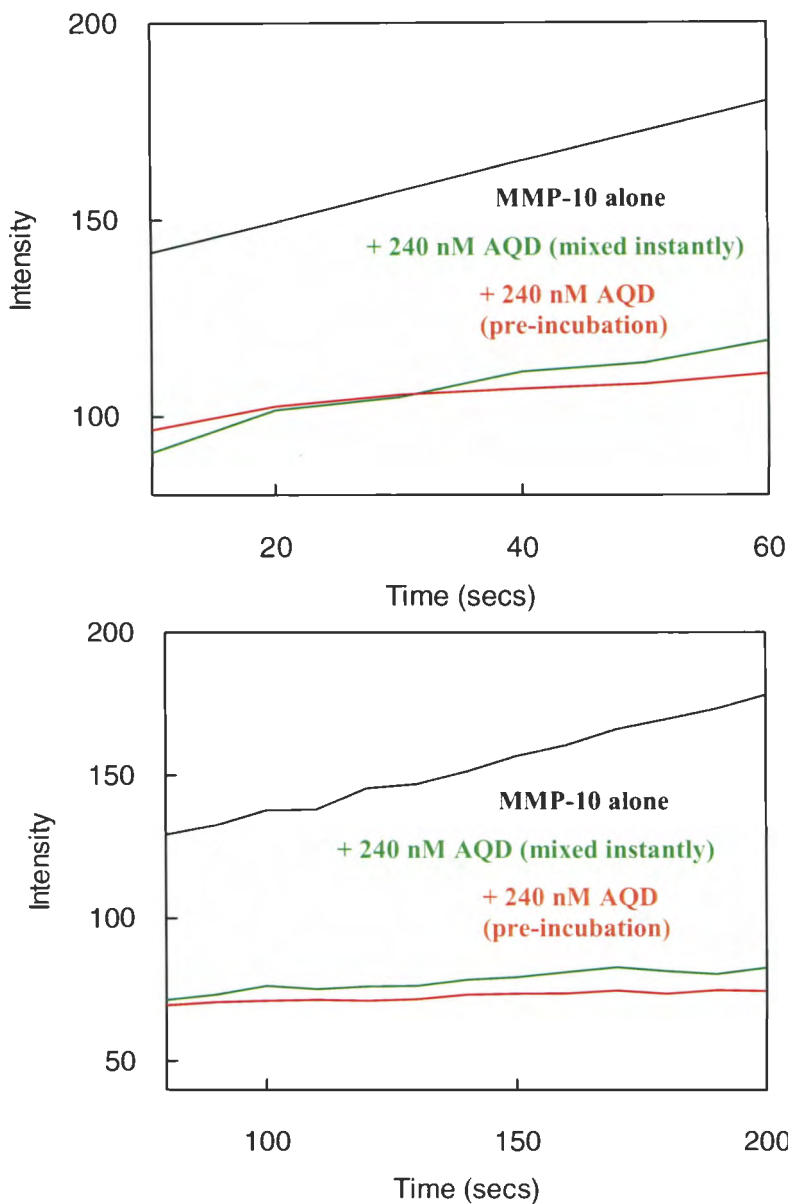
247

Figure 7.19.A. Inhibition / inactivation of the enzyme activity of hMMP-10 by CQD. B. Inhibition / inactivation of the enzyme activity of hMMP-10 by AQD. The time course of the reaction was monitored for about maximum 200 sec. For hMMP-10 the red solid line, the blue solid line, the green solid line indicates the progress curves of hMMP-10 alone (1.0 μM, hMMP-10 with 0.240 μM CQD/AQD (0 time incubation) hMMP-10 with the same concentration of QDs (20 min pre-incubation time) respectively. The slopes for MMP-10 ($\Delta F.s^{-1}$) of the progress curves were calculated for the above data were 0.38 (black line), 0.14 (red line), 0.18 (green line) $\Delta F.s^{-1}$, respectively, for CQD while 0.38 (black line), 0.09 (red line), 0.11 (green line) $\Delta F.s^{-1}$, respectively, for AQD.

Table 7.5.A. Comparative account of the effect for inhibition/ inactivation of hMMP isozymes with CQD. B. Comparative account of the effect for inhibition/ inactivation of hMMP isozymes with AQD.

A

MMP Isozymes	CQD
hMMP-7	98 % reversible
hMMP-9	100% reversible
hMMP-10	100% reversible

B

MMP Isozymes	AQD
hMMP-7	More than 100 % reversible
hMMP-9	100% reversible
hMMP-10	100% reversible

Electrostatic force plays a key role in the rate of arrival of the protein molecules at the sorbent surface is slower at lower protein concentration in solution, corresponding to lower surface coverage, allowing the molecules more time to adjust their structure to the new environment before a neighboring site becomes occupied by molecules arriving at a later stage. This results in more severe structural arrangement at lower surface coverage. Studies are available in the literature [49] that suggests that the structural characteristics of BSA molecules in aqueous solution remain unaffected after being exchanged from a hydrophilic silica surface. BSA molecules with altered structural properties are obtained after release from hydrophobic PS-surfaces.

There have been recent studies [50] that demonstrate the use of a QD biosensor for detection of activity of matrix metalloproteinases. Quantum dots (QDs) are often cell-impermeable and require transporters to facilitate crossing over the cell membranes. There is a simple and versatile method that utilizes enzymes, matrix metalloproteases like MMP-2 and MMP-7, to modulate the cellular uptake of QDs [51]. QD-peptide conjugates could be efficiently taken up into cells after MMP treatment. This enzyme-modulated cellular

uptake of QDs may be applied to other nanoparticles for biological imaging and selective drug delivery into tumor cells.

Interactions between QDs and hMMP isozymes can also change the lifetime of the intrinsic tryptophan residues and confirm the steady-state binding experiments. The lifetime of hMMP-7, 9 and 10 in the presence or absence of CQD and AQD were measured to confirm the binding interactions of the hMMP isozymes with the cationic and anionic QDs.

Figure 7.20 depicts the lifetime of hMMP-7 in the presence and absence of CQD. The time resolved fluorescence decay profiles of hMMP-7 in the absence and presence of CQD are shown. Fluorescence of tryptophan residues is known to be responsive to the polarity of the local environment [51]. Thus, it shows great potential in the study of electronic properties with the limitation that it requires microscopic information, which is not easily accessible. To exploit this signal and infer from the experiment, the idea was to envisage whether the binding and overall quenching of the tryptophan/tyrosine residues manifested in the steady-state fluorescence studies were due to the formation of hMMP-7-CQD complex, to a transition from the ground state to excited state phenomena [52-53] or the formation of a ground state complex? The protein sample was measured using λ_{ex} and λ_{em} at 280 nm and 340 nm, respectively. The excited state lifetime traces of hMMP-7 in the absence and presence of CQD were recorded. The lifetime data confirm that both of the lifetime traces exhibit a biphasic rate equation, leading to the conclusion that hMMP-7 has two lifetimes, the τ_s (shorter lifetime) and τ_l (longer lifetime), in the absence and in the presence of CQD. According to the best fit data (smooth lines) $\tau_s = 0.1 \pm 0.1$ ns and α_s

(amplitude) = 0.2 ± 0.1; τ_l = 2.3 ± 0.2 ns and α_l = 0.05 ± 0.0 for hMMP-7 alone, and τ_s = 0.06 ± 0.0 ns and α_s = 0.1 ± 0.0; τ_l = 2.4 ± 0.0 ns and α_l = 0.01 ± 0.0 in the presence of CQD. The bottom panels show the residuals of the fit of hMMP-7 lifetime traces in the absence and presence of CQD. It is very interesting to note that, the shorter lifetime decreases drastically. However, the longer lifetime remains comparable in both cases. Moreover, the other components (amplitudes) do show changes in the longer lifetime data.

Figure 7.21 depicts the lifetime of hMMP-7 in the presence and absence of AQD. The time resolved fluorescence decay profiles of hMMP-7 in the absence and presence of AQD was shown. The protein sample was measured using λ_{ex} and λ_{em} at 280 nm and 340 nm, respectively. The excited state lifetime traces of hMMP-7 in the absence and presence of AQD were recorded. The lifetime data confirms that both the lifetime traces exhibit a biphasic rate equation leading to the conclusion that there are two lifetimes. The analysis of the experimental data indicates τ_s (shorter lifetime) and τ_l (longer lifetime), both with and without AQDs. According to the best fit data (smooth lines) τ_s = 0.1 ± 0.1 ns and α_s (amplitude) = 0.2 ± 0.1; τ_l = 2.3 ± 0.2 ns and α_l = 0.05 ± 0.0 for hMMP-7 alone, and τ_s = 0.06 ± 0.0 ns and α_s = 0.04 ± 0.02; τ_l = 2.6 ± 0.0 ns and α_l = 0.01 ± 0.0 in the presence of AQD. The bottom panels show the residuals of the fit of hMMP-7 lifetime traces in the absence and presence of AQD. Interestingly, again the longer lifetime did not change but the shorter lifetime decreased. Amplitude for both the components decreased.
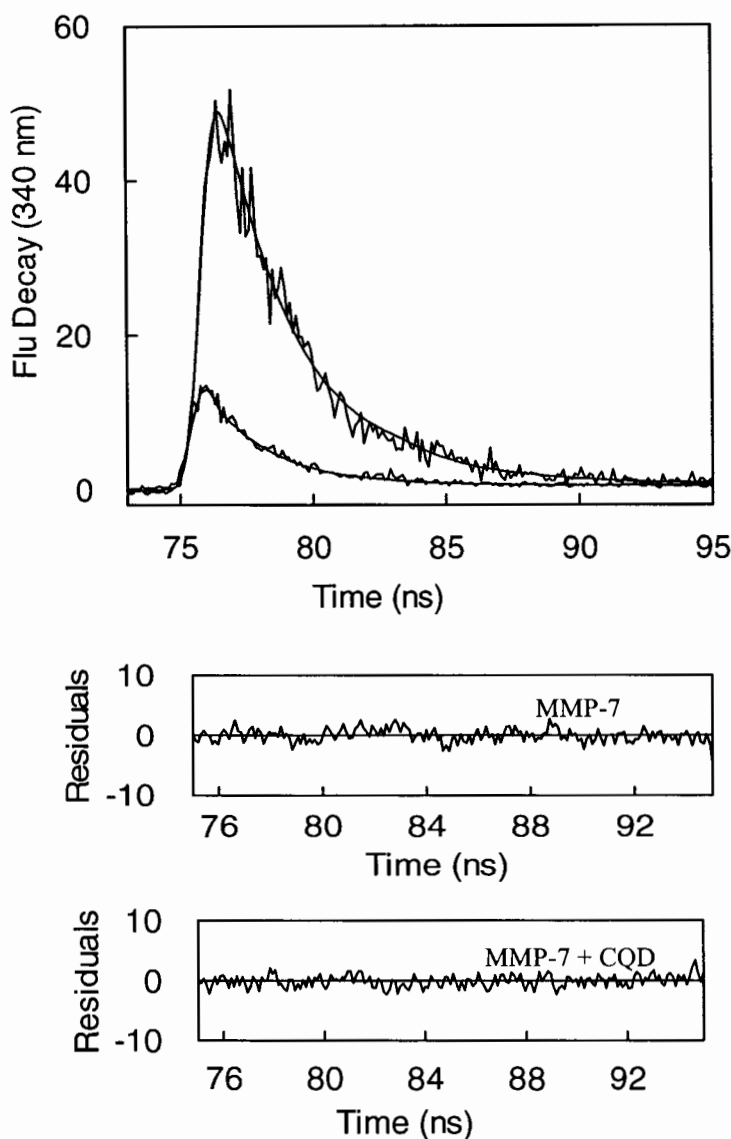
Figure 7.20. Lifetime of hMMP-7 in presence and absence of CQD, λ_{ex}= 280 nm, λ_{em}= 340 nm. Time resolved Fluorescence decay profiles of hMMP-7 in absence and presence of CQD. The protein sample was measured using λ_{ex} and λ_{em} at 280 nm and 340 nm respectively. [hMMP-7] = 5 μM, [CQD] = 1.6 μM. The solid smooth lines are the best fit of the data according to Eq 3.6 with τ_s = 0.1 ± 0.1 ns and α_s (amplitude) = 0.2 ± 0.1; τ_l = 2.3 ± 0.2 ns and α_l = 0.05 ± 0.0 for hMMP-7 alone, and τ_s = 0.06 ± 0.0 ns and α_s = 0.13 ± 0.0; τ_l = 2.4 ± 0.0 ns and α_l = 0.01 ± 0.0 in the presence of CQD. The bottom panels show the residuals of the fit of hMMP-7 lifetime traces in the absence and presence of CQD.
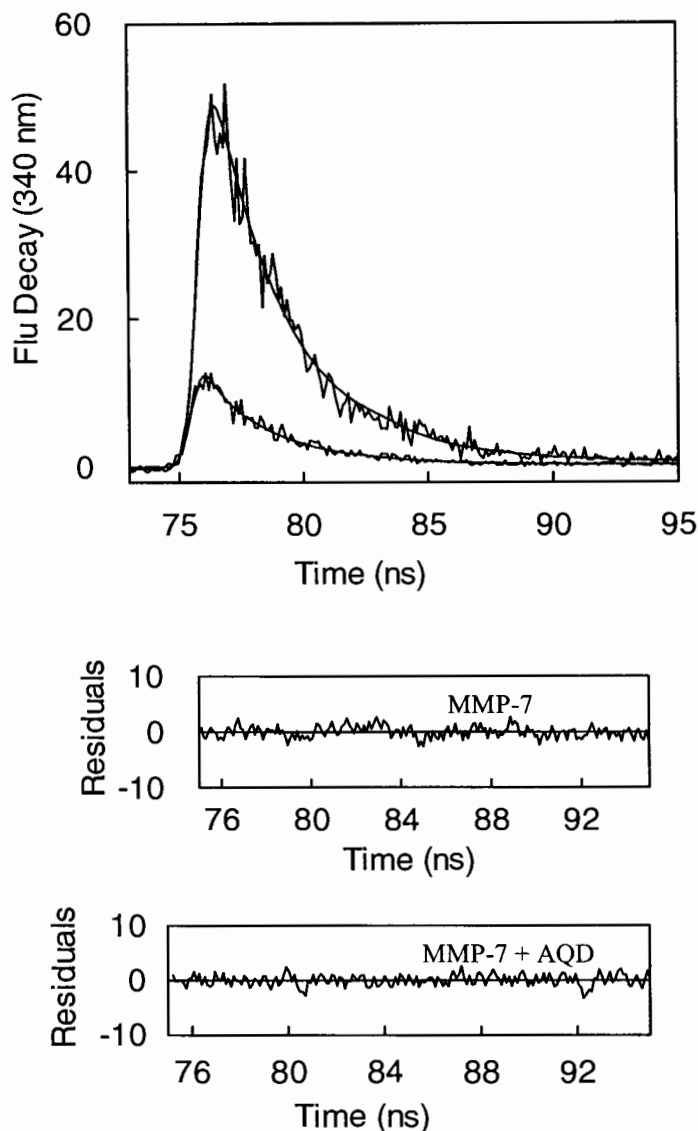
Figure 7.21. Lifetime of hMMP-7 in presence and absence of AQD, λ_{ex}= 280 nm, λ_{em}= 340 nm. Time resolved Fluorescence decay profiles of hMMP-7 in absence and presence of AQD. The protein sample was measured using λ_{ex} and λ_{em} at 280 nm and 340 nm respectively. [hMMP-7] = 5 μM, [AQD] = 1.85 μM. The solid smooth lines are the best fit of the data according to Eq 3.6 with $\tau_s = 0.1 \pm 0.1$ ns and α_s (amplitude) = 0.2 ± 0.1; $\tau_l = 2.3 \pm 0.2$ ns and $\alpha_l = 0.05 \pm 0.0$ for hMMP-7 alone, and $\tau_s = 0.06 \pm 0.0$ ns and $\alpha_s = 0.04 \pm 0.02$; $\tau_l = 2.6 \pm 0.0$ ns and $\alpha_l = 0.01 \pm 0.0$ in the presence of AQD. The bottom panels show the residuals of the fit of hMMP-7 lifetime traces in the absence and presence of AQD.

Figure 7.22 depicts the lifetime of hMMP-9 in the presence and absence of CQD. The time resolved fluorescence decay profiles of hMMP-9 in the absence and presence of CQD was shown. The protein sample was measured using λ_{ex} and λ_{em} at 280 nm and 340 nm respectively.The lifetime data confirms that both of the lifetime traces exhibit a biphasic rate equation leading to the conclusion that there are two lifetimes. The analysis of the experimental data indicates τ_s (shorter lifetime) and τ_l (longer lifetime), both with and without CQDs. According to the best fit data (smooth lines) $\tau_s = 0.8 \pm 0.0$ ns and α_s (amplitude) $= 0.06 \pm 0.1$; $\tau_l = 3.3 \pm 0.0$ ns and $\alpha_l = 0.03 \pm 0.0$ for hMMP-9 alone, and $\tau_s = 0.13 \pm 0.0$ ns and $\alpha_s = 0.05 \pm 0.0$; $\tau_l = 2.2 \pm 0.0$ ns and $\alpha_l = 0.01 \pm 0.0$ in the presence of CQD. The bottom panels show the residuals of the fit of hMMP-9 lifetime traces in the absence and presence of CQD. Both shorter and longer lifetime values decreased. The amplitudes corresponding to shorter and longer lifetime exhibits no significant change.

Figure 7.23 depicts the lifetime of hMMP-9 in presence and absence of AQD. The time resolved fluorescence decay profiles of hMMP-9 in absence and presence of AQD is shown. The protein sample was measured using λ_{ex} and λ_{em} at 280 nm and 340 nm, respectively. The lifetime data confirms that both the lifetime traces exhibit a biphasic rate equation leading to conclusion that there are two lifetimes. The analysis of the experimental data indicates τ_s (shorter lifetime) and τ_l (longer lifetime); both with and without AQDs. According to the best fit data (smooth lines) $\tau_s = 0.8 \pm 0.0$ ns and α_s (amplitude) $= 0.06 \pm 0.1$; $\tau_l = 3.3 \pm 0.0$ ns and $\alpha_l = 0.03 \pm 0.0$ for hMMP-9 alone, and $\tau_s = 0.17 \pm 0.0$ ns and $\alpha_s = 0.05 \pm 0.0$; $\tau_l = 2.3 \pm 0.0$ ns and $\alpha_l = 0.02 \pm 0.0$ in the presence of AQD. The bottom panels show the residuals of the fit of hMMP-9 lifetime traces in the

absence and presence of AQD. The drastic decrease in the shorter lifetime was observed. The amplitudes for both the components did not vary in this case.

Similarly, the lifetime changes in the hMMP-10 in the presence and absence of CQD and AQD was determined. Figure 7.24 shows $\tau_s = 1.2 \pm 0.0$ ns and α_s (amplitude) = 0.05 ± 0.0; $\tau_l = 3.8 \pm 0.0$ ns and $\alpha_l = 0.04 \pm 0.0$ for hMMP-10 alone, and $\tau_s = 0.3 \pm 0.0$ ns and $\alpha_s = 0.03 \pm 0.0$; $\tau_l = 2.8 \pm 0.0$ ns and $\alpha_l = 0.01 \pm 0.0$ in the presence of CQD. The bottom panels show the residuals of the fit of hMMP-10 lifetime traces in the absence and presence of CQD. The shorter lifetime decreases with changes in both the amplitude values. Figure 7.25 shows the lifetime of hMMP-10 in presence and absence of AQD. The lifetime data showed biphasic profiles in presence and absence of AQD. The values were τ_s = 1.2 ± 0.0 ns and α_s (amplitude) = 0.05 ± 0.0; $\tau_l = 3.8 \pm 0.0$ ns and $\alpha_l = 0.04 \pm 0.0$ for hMMP-10 alone, and $\tau_s = 0.7 \pm 0.0$ ns and $\alpha_s = 0.02 \pm 0.01$; $\tau_l = 3.4$ ns ± 0.0 ns and $\alpha_l =$ 0.01 ± 0.0 in the presence of AQD. The bottom panels show the residuals of the fit of hMMP-10 lifetime traces in the absence and presence of AQD. There was slight decrease in the shorter lifetime, however, both the amplitudes decreased.

Lifetime data help probe many scenarios as compared to steady-state data. Lifetime measurements can be used to distinguish between static and dynamic quenching. Events that occur in the lifetime of a singlet excited state, with a time-scale range from a few picoseconds to a few hundred nanoseconds, can be monitored by time resolved fluorescence spectroscopy [54].
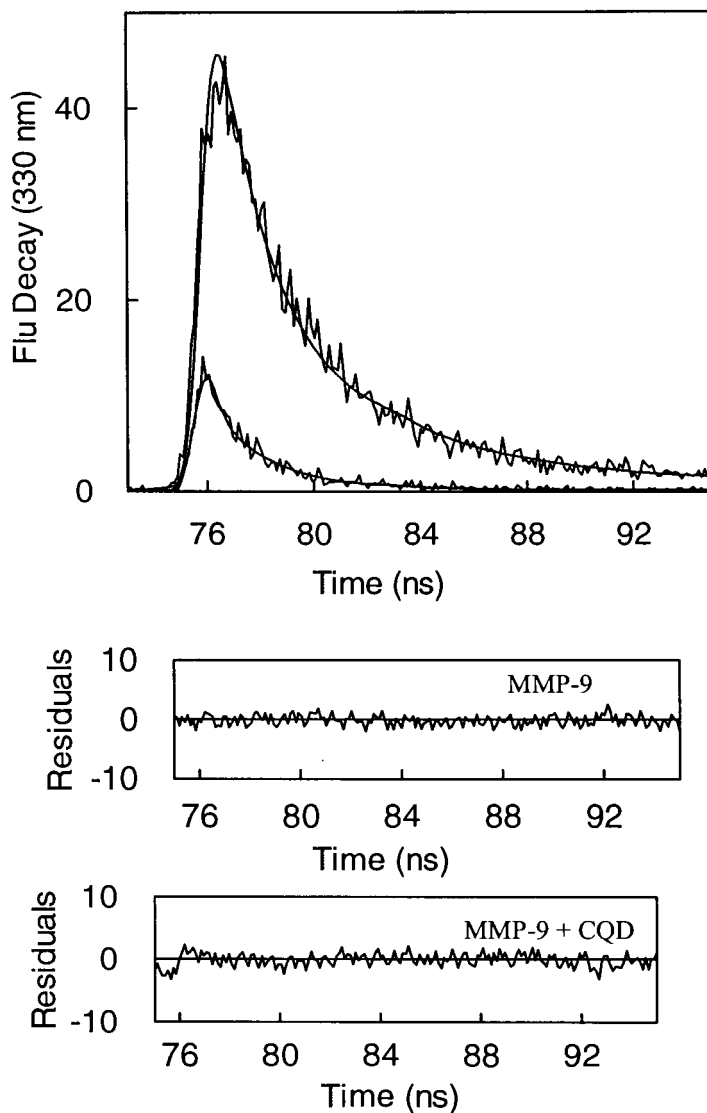
Figure 7.22. Lifetime of hMMP-9 in the presence and absence of CQD, λ_{ex}= 280 nm, λ_{cm}= 340 nm. Time resolved Fluorescence decay profiles of hMMP-9 in absence and presence of CQD. The protein sample was measured using λ_{ex} and λ_{cm} at 280 nm and 340 nm respectively. [hMMP-9] = 5 μM, [CQD] = 0.84 μM. The solid smooth lines are the best fit of the data according to Eq 3.6 with τ_s = 0.8 $\pm$ 0.0 ns and α_s (amplitude) = 0.06 $\pm$ 0.1; τ_l = 3.3 $\pm$ 0.0 ns and α_l = 0.03 $\pm$ 0.0 for hMMP-9 alone, and τ_s = 0.13 $\pm$ 0.0 ns and α_s = 0.05 $\pm$ 0.0; τ_l = 2.2 $\pm$ 0.0 ns and α_l = 0.01 $\pm$ 0.0 in the presence of CQD. The bottom panels show the residuals of the fit of hMMP-9 lifetime traces in the absence and presence of CQD.
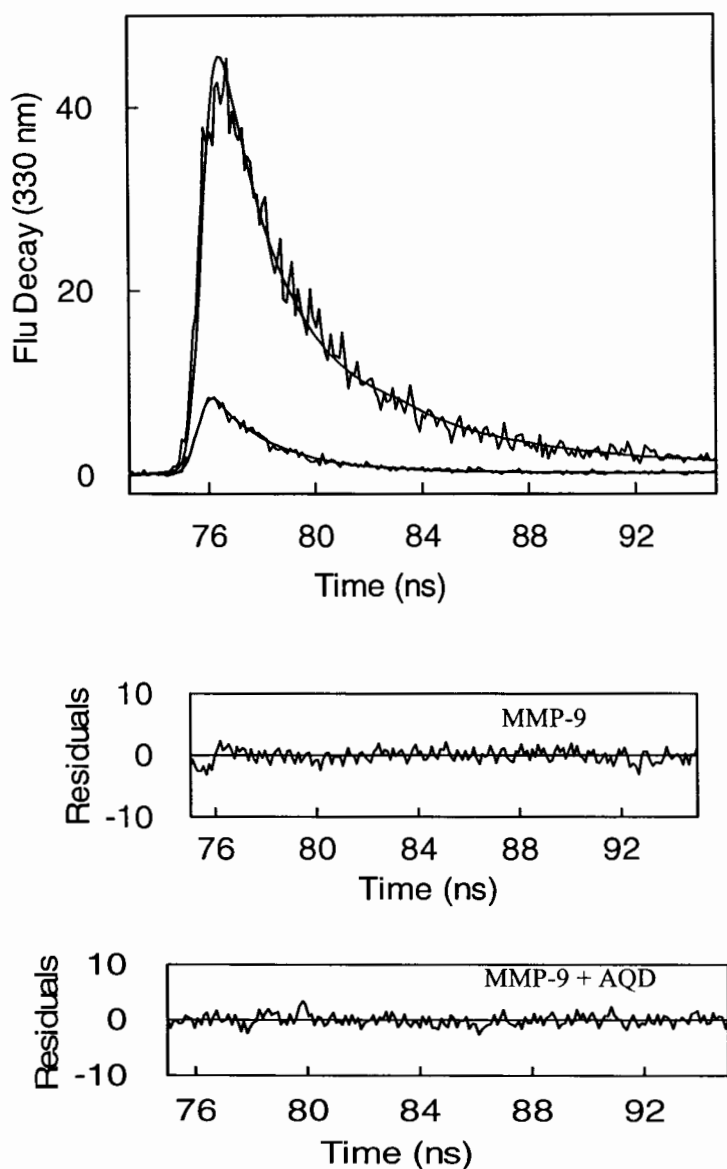
256

Figure 7.23. Lifetime of hMMP-9 in the presence and absence of AQD, λ_{ex}= 280 nm, λ_{em}= 340 nm. Time resolved Fluorescence decay profiles of hMMP-9 in absence and presence of AQD. The protein sample was measured using λ_{ex} and λ_{em} at 280 nm and 340 nm respectively. [hMMP-9] = 5 μM, [AQD] = 1.85 μM. The solid smooth lines are the best fit of the data according to Eq 3.6 with τ_s = 0.8 ± 0.0 ns and α_s (amplitude) = 0.06 ± 0.1; τ_l = 3.3 ± 0.0 ns and α_l = 0.03 ± 0.0 for hMMP-9 alone, and τ_s = 0.17 ± 0.0 ns and α_s = 0.05 ± 0.0; τ_l = 2.3 ± 0.0 ns and α_l = 0.02 ± 0.0 in the presence of AQD. The bottom panels show the residuals of the fit of hMMP-9 lifetime traces in the absence and presence of AQD.
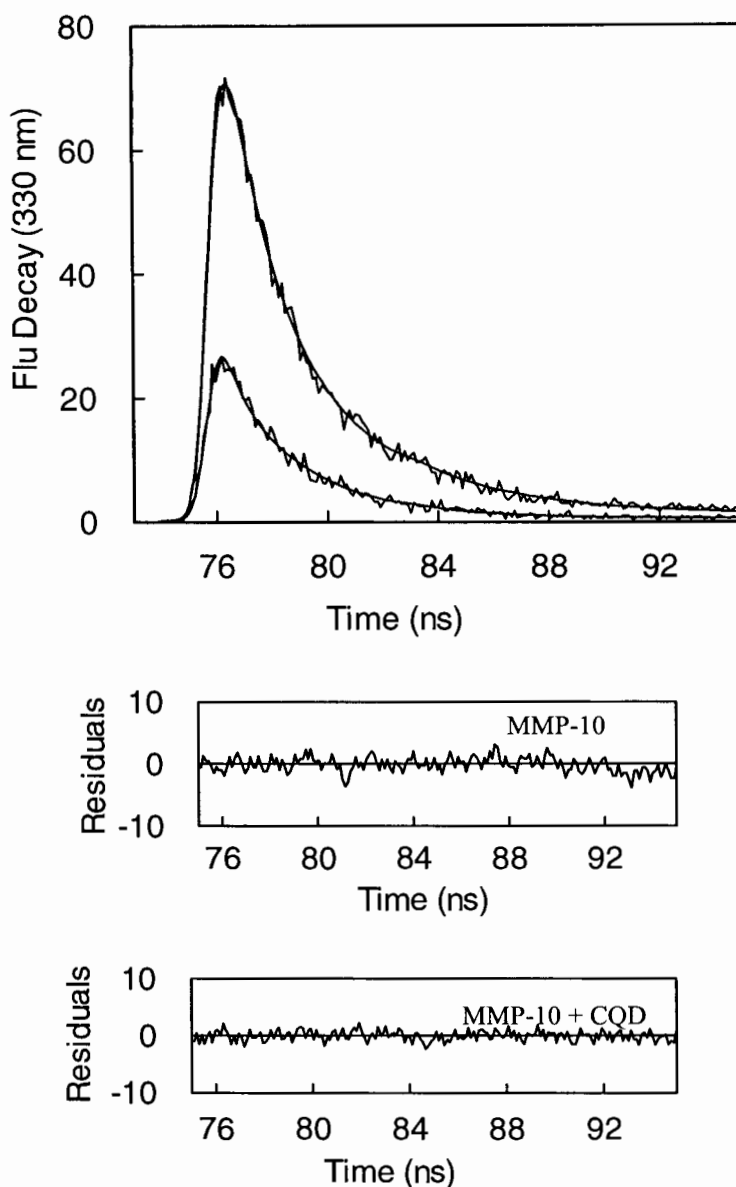
Figure 7.24. Lifetime of hMMP-10 in the presence and absence of CQD, λ_{ex}= 280 nm, λ_{em}= 340 nm. Time resolved Fluorescence decay profiles of hMMP-10 in absence and presence of CQD. The protein sample was measured using λ_{ex} and λ_{em} at 280 nm and 340 nm respectively. [hMMP-10] = 30 μM, [CQD] = 0.57 μM. The solid smooth lines are the best fit of the data according to Eq 3.6 with τ_s = 1.23 $\pm$ 0.0 ns and α_s (amplitude) = 0.05 $\pm$ 0.0; τ_l = 3.8 $\pm$ 0.0 ns and α_l = 0.04 $\pm$ 0.0 for hMMP-10 alone, and τ_s = 0.34 $\pm$ 0.0 ns and α_s = 0.03 $\pm$ 0.0; τ_l = 2.8 $\pm$ 0.0 ns and α_l = 0.01 $\pm$ 0.0 in the presence of CQD. The bottom panels show the residuals of the fit of hMMP-10 lifetime traces in the absence and presence of CQD.
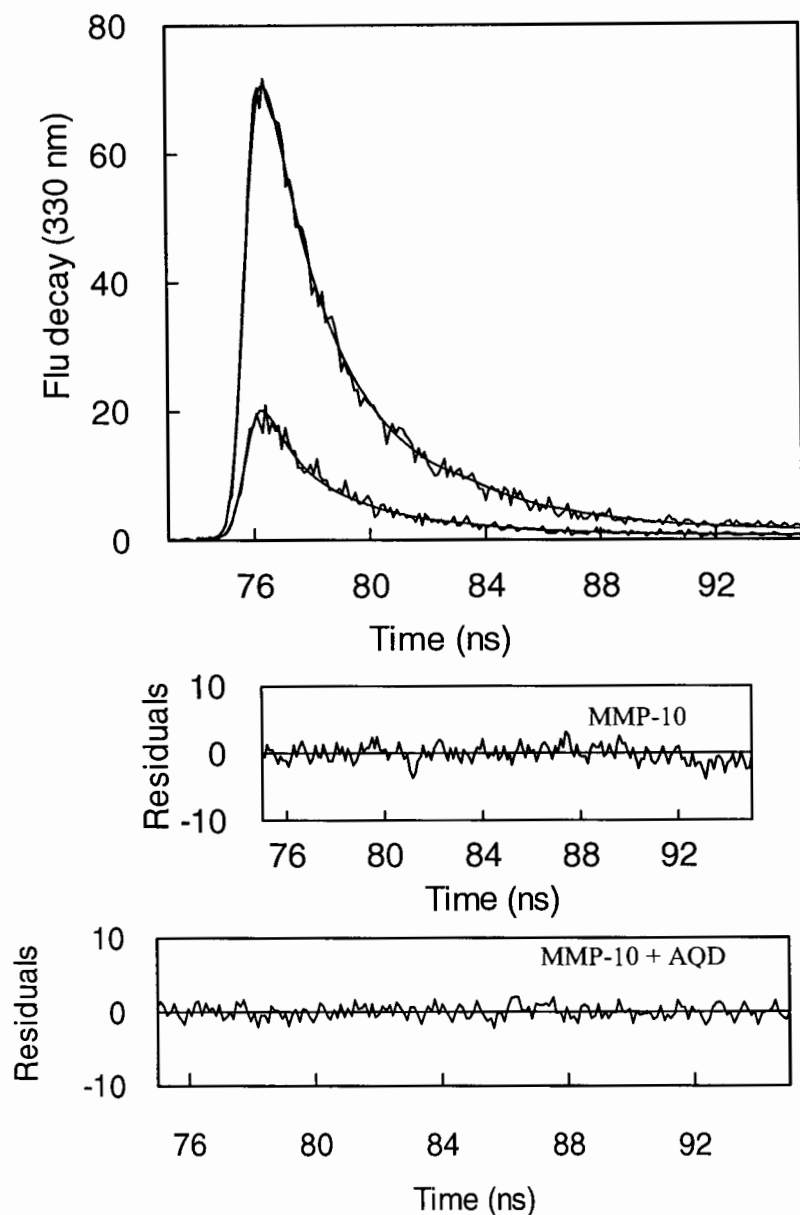
258

Figure 7.25. Lifetime of hMMP-10 in the presence and absence of AQD, λ_{ex}= 280 nm, λ_{em}= 340 nm. Time resolved Fluorescence decay profiles of hMMP-10 in absence and presence of AQD. The protein sample was measured using λ_{ex} and λ_{em} at 280 nm and 340 nm respectively. [hMMP-10] = 30 µM, [AQD] = 0.96 µM. The solid smooth lines are the best fit of the data according to Eq 3.6 with τ_s = 1.23 ± 0.0 ns and α_s (amplitude) = 0.05 ± 0.0; τ_l = 3.8 ± 0.0 ns and α_l = 0.04 ± 0.0 for hMMP-10 alone, and τ_s = 0.7 ± 0.0 ns and α_s = 0.02 ± 0.01; τ_l = 3.4 ns ± 0.0 ns and α_l = 0.01 ± 0.0 in the presence of AQD. The bottom panels show the residuals of the fit of hMMP-10 lifetime traces in the absence and presence of AQD.

259

The 280 nm LED was used as the excitation source and an emission wavelength was 340 nm. In the case of hMMP-7 and CQD, there was a decrease in the smaller lifetime component and in the longer amplitude component. This result invites the conclusion that some of the surface exposed tryptophan residues from the interior core of the protein are more exposed to the solvent. This is further corroborated by a 12 nm red shift in the steady-state fluorescence emission band of the enzyme's tryptophan residues (Figure 7.5). In the case of hMMP-7 and AQD, it is observed that the smaller lifetime component decreases leading to a decrease in both of the amplitudes. This can be explained by the fact that the decay time of the uncomplexed fluorophore is not decreased by formation of static ground-state complexes, since the unquenched fluorophores are observed in both cases. Dynamic quenching, on the other hand, decreases the mean decay time, measures the entire excited state population. This feature corroborates with the reversibility experiment attempted on hMMP-7 and AQD (Figure 7.17.B). There too it is observed that upon incubation the reversibility of the enzyme activity is more than 100%. This remarkable feature elicits only towards the fact that upon binding to AQD, hMMP-7 forms a complex in the excited state and the flexible native conformation of the active site undergoes a conformational change in order to stabilize the associative complex.

In the case of hMMP-9 and CQD, we observed the same scenario as for hMMP-7. The shorter lifetime component of hMMP-9 changes in the presence of AQD. The shorter lifetime decreases drastically, but no change in their corresponding amplitudes was observed. This observation leads to the conclusion that there is micro-heterogeneity within the hMMP-9 protein molecules. Complex decay can be treated in terms of micro-heteroge-

neity if the kinetics of the excited-state reaction is rapid as compared to the time-scale of measurement. The dynamic approach to the excited-state equilibrium is reflected in the observed decay. In the case of hMMP-10 and CQD, we observed that not only is there a change in both the lifetimes, but the amplitude for the longer lifetime component decreases too. Some of the surface exposed tryptophan residues of MMP-10 get exposed to the solvent more from the interior core of the protein. This fact corroborates with 15 nm red shift in the steady-state fluorescence emission band.

Still there is an ongoing debate about the capacity of lifetime of the tryptophan residues that can be exploited. Many researchers believe that the rotation of whole proteins, segments of polypeptide chains and individual amino acid side chains are biological events that occur in this time frame [55]. A chromophore in an excited state can interact with neighboring amino acid residues or solvent molecules. A single chromophore in different micro-environments can be treated as a fluorophore mixture, with two decay constants found in a protein containing two tryptophan residues. Bi-exponential decay kinetics can reflect two states of the protein and can be used to investigate the interconversion, if a protein has only one tryptophan residue and two conformations. Microheterogeneity can be subtle [56]. The bi-exponential decay in tryptophan zwitterions can be interpreted from the fact that tryptophan exists in micro-heterogeneous forms.

All of these results when taken together suggest that hMMP isozymes respond differently to CQD and AQD, but they bind to both these QDs which very nicely validate the observations noted. Hence, the contribution of the differential binding modes of hMMP-7 and hMMP-10 to CQD and AQD (due to their clustered positive and negative

charges) together in synergy with the role of strong electrostatics or hydrophobic interactions would be sequentially determined. Tables 7.6, 7.7 and 7.8 show the comparative account of the lifetime of the hMMP isozymes in the presence and absence of differently charged QDs.

Table 7.6.A. The comparative account of the lifetime of hMMP-7 in the presence and absence of CQD, λ_{ex} = 280 nm and λ_{em} = 340 nm. B. The comparative account of the lifetime of hMMP-7 in presence and absence of AQD, λ_{ex} = 280 nm and λ_{em} = 340 nm.

A

Ex 280 nm, Em 330 nm	τ_s	α_s	τ_l	α_l
MMP-7 alone	0.1	0.2 ± 0.1 (82 %)	2.3	0.05 (18 %)
+ 1.85 µM AQD	0.06	0.04 ± 0.02 (89%)	2.6	0.01 (11%)

B

Ex 280 nm, Em 330 nm	τ_s	α_s	τ_l	α_l
MMP-7 alone	0.1	0.2 ± 0.1 (82 %)	2.3	0.05 (18 %)
+ 1.6 µM CQD	0.06	0.13 ± 0.03 (93 %)	2.4	0.01 (7 %)

Table 7.7.A. The comparative account of the lifetime of hMMP-9 in the presence and absence of CQD, λ_{ex} = 280 nm and λ_{em} = 340 nm. B. The comparative account of the lifetime of hMMP-9 in presence and absence of AQD, λ_{ex} = 280 nm and λ_{em} = 340 nm.

A

Ex 280 nm, Em 330 nm	τ_s	α_s	τ_l	α_l
MMP-9 alone	0.8	0.06 ± 0.1 (64 %)	3.3	0.03 (36 %)
+ 0.84 µM CQD	0.13	0.05 ± 0.0 (86%)	2.2	0.01 (14 %)

B

Ex 280 nm, Em 330 nm	τ_s	α_s	τ_l	α_l
MMP-9 alone	0.8	0.06 ± 0.07 (64 %)	3.3	0.03 (36 %)
+ 1.85 µM AQD	0.2	0.05 ± 0.02 (68%)	2.3	0.02 (32%)

Table 7.8.A. The comparative account of the lifetime of hMMP-10 in the presence and absence of CQD, λ_{ex} = 280 nm and λ_{em} = 340 nm. B. The comparative account of the lifetime of hMMP-10 in presence and absence of AQD, λ_{ex} = 280 nm and λ_{em} = 340 nm.

A

Ex 280 nm, Em 330 nm	τ_s	α_s	τ_l	α_l
MMP-10 alone	1.2	0.05 ± 0.0 (56 %)	3.9	0.04 (44 %)
+ 0.57 µM CQD	0.3	0.03 ± 0.0 (58%)	2.8	0.01 (42%)

B

Ex 280 nm, Em 330 nm	τ_s	α_s	τ_l	α_l
MMP-10 alone	1.2	0.05 ± 0.0 (56%)	3.9	0.04 (44 %)
+ 0.96 µM AQD	0.7	0.02 ± 0.01 (60%)	3.4	0.01 (40 %)

To monitor the lifetime of the QDs, the probe was excited and the protein was titrated. The probes (CQD and AQD) were excited in absence and presence of the MMP isozymes, and then with the change in the micro-environment of the sensitive probe the lifetime of the probe changes. We determined the fluorescence lifetime of CQD and AQD either in the absence or presence of hMMP-7, 9 or 10. A 340 nm LED was the excitation source and the emission monochromator was set at 570 nm (CQD) and 625 nm (AQD).

Figure 7.26 shows the lifetime of CQD in presence and absence of hMMP-7. The time resolved fluorescence decay profiles of CQD in the absence and presence of hMMP-7 is shown. The CQD sample was measured using λ_{ex} and λ_{em} at 340 nm and 570 nm, respectively. The excited-state lifetime traces of CQD in the absence and presence of hMMP-7 were recorded. The τ_s = 1.6 ± 0.0 ns and α_s (amplitude) = 0.01 ± 0.0; τ_l = 13.7 ± 0.0 ns and α_l = 0.03 ± 0.0 for CQD in the absence of hMMP-7, and τ_s = 1.6 ± 0.0 ns and α_s

$= 0.01 \pm 0.0$, $\tau_l = 12.7 \pm 0.00$ ns and $\alpha_l = 0.01 \pm 0.0$ in the presence of hMMP-7. These results indicate that none of the lifetimes varied. However, the amplitude of the longer lifetime drastically decreased. Figure 7.27 shows the lifetime of AQD in the presence and absence of hMMP-7. The time resolved fluorescence decay profiles of AQD in the absence and presence of hMMP-7 are shown. The AQD sample was measured using λ_{ex} and λ_{em} at 340 nm and 625 nm, respectively. The excited-state lifetime traces of AQD in the absence and presence of hMMP-7 were recorded. The $\tau_s = 1.9 \pm 0.0$ ns and α_s (amplitude) $= 0.01 \pm 0.0$; $\tau_l = 16.6 \pm 0.0$ ns and $\alpha_l = 0.01 \pm 0.0$ for AQD in the absence of hMMP-7, and $\tau_s = 0.01 \pm 0.0$ ns and $\alpha_s = 0.01 \pm 0.0$, $\tau_l = 9.4 \pm 0.0$ ns and $\alpha_l = 0.01 \pm 0.0$ in the presence of hMMP-7. The bottom panels show the residuals of the fit for AQD lifetime traces in the absence and presence of hMMP-7. Both the shorter and longer lifetimes decreased. The amplitude of the shorter lifetime increased but the amplitude for longer lifetime decreased.

Figure 7.28 shows the lifetime of CQD in the presence and absence of hMMP-9. The time resolved fluorescence decay profiles of CQD in the absence and presence of hMMP-9 was shown. The CQD sample was measured using λ_{ex} and λ_{em} at 340 nm and 570 nm, respectively. The excited state lifetime traces of CQD in the absence and presence of hMMP-9 were recorded. The $\tau_s = 1.6 \pm 0.0$ ns and α_s (amplitude) $= 0.01 \pm 0.0$; $\tau_l = 13.7 \pm 0.0$ ns and $\alpha_l = 0.02 \pm 0.0$ for CQD in the absence of hMMP-9, and $\tau_s = 0.05 \pm 0.0$ ns and $\alpha_s = 0.03 \pm 0.0$, $\tau_l = 10.0 \pm 0.0$ ns and $\alpha_l = 0.01 \pm 0.0$ in the presence of hMMP-9 respectively. The bottom panels show the residuals of the fit of CQD lifetime traces in the absence and presence of hMMP-9. Both the shorter and longer lifetime decreased. The shorter lifetime amplitude increased while the amplitude for the longer lifetime decreased.
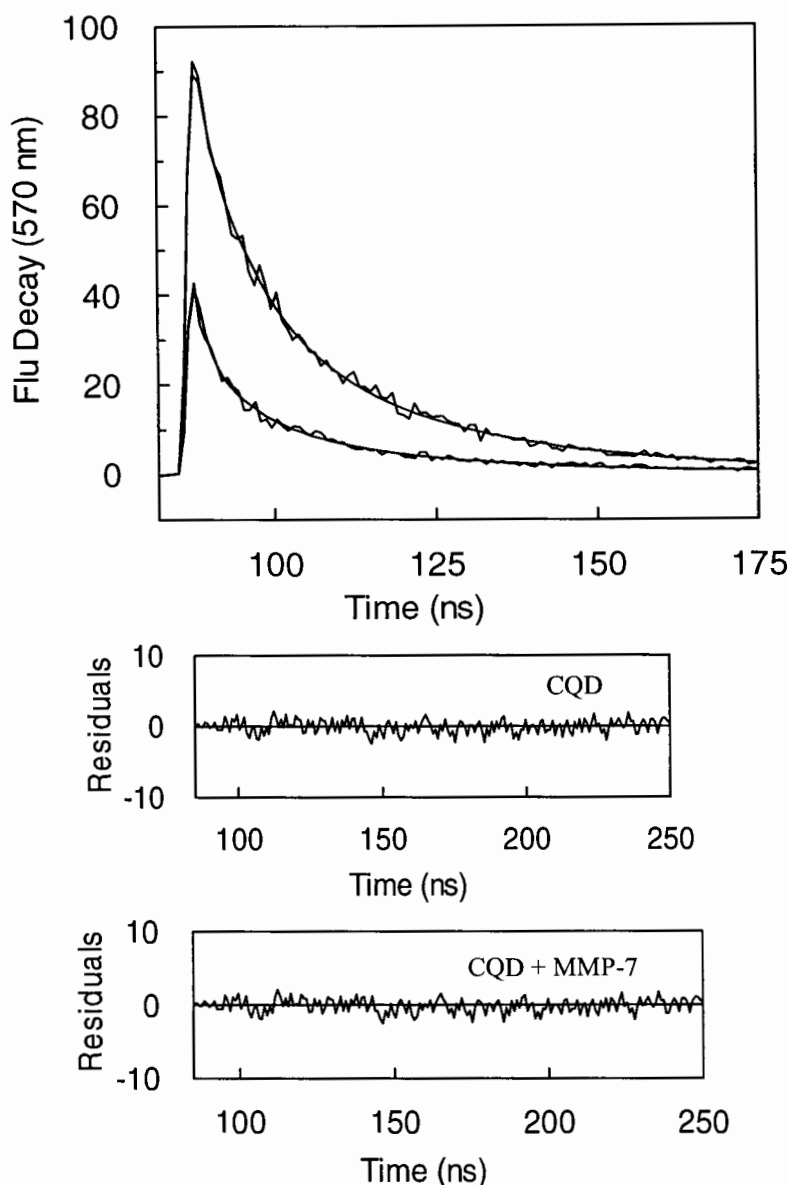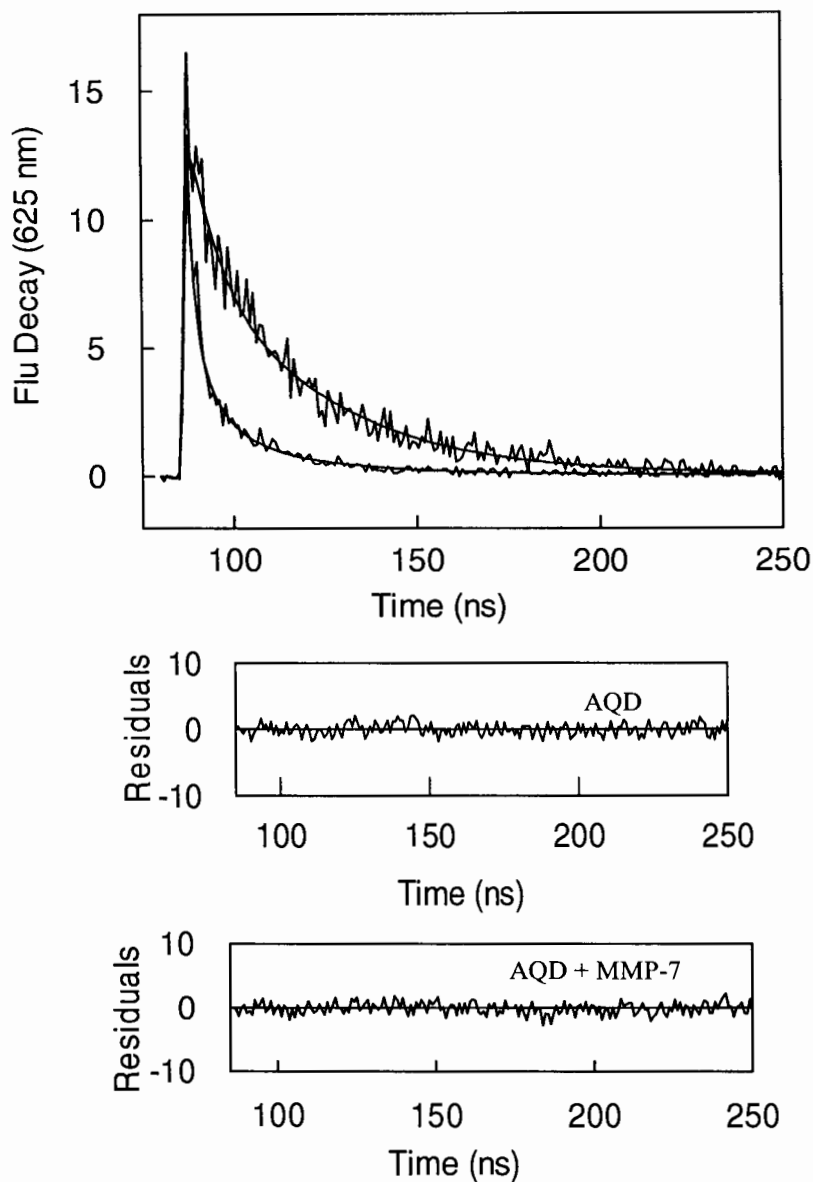
Figure 7.26. Lifetime of CQD in the presence and absence of hMMP-7, λ_{ex}= 340nm, λ_{em}= 570 nm. The time resolved fluorescence decay of CQD was measured in the absence and presence of hMMP-7. The CQD was monitored at and λ_{em} = 570 nm when excited at λ_{ex} = 340 nm. [CQD] = 1 μM, [hMMP-7] = 1.9 μM. The solid smooth lines are the best fit of the data according to Eq 3.6 with τ_s = 1.6 ± 0.0 ns and α_s (amplitude) = 0.01 ± 0.0; τ_l = 13.7 ± 0.0 ns and α_l = 0.02 ± 0.0 for CQD in the absence of hMMP-7, and τ_s = 1.6 ± 0.0 ns and α_s = 0.01 ± 0.0, τ_l = 12.7 ± 0.0 ns and α_l = 0.01 ± 0.0 in the presence of hMMP-7. The bottom panels show the residuals of the fit of CQD lifetime traces in the absence and presence of hMMP-7.

Figure 7.27. Lifetime of AQD in the presence and absence of hMMP-7, λ_{ex}= 340 nm, λ_{em}= 625 nm. The time resolved fluorescence decay of AQD was measured in the absence and presence of hMMP-7. The AQD was monitored at and λ_{em} = 625 nm when excited at λ_{ex} = 340 nm. [AQD] = 2 μM, [hMMP-7] = 3.0 μM. The solid smooth lines are the best fit of the data according to Eq 3.6 with τ_s = 1.9 ± 0.0 ns and α_s (amplitude) = 0.01 ± 0.0; τ_l = 16.6 ± 0.0 ns and α_l = 0.01 ± 0.0 for AQD in the absence of hMMP-7, and τ_s = 0.01 ± 0.0 ns and α_s = 0.01 ± 0.0, τ_l = 9.4 ± 0.0 ns and α_l = 0.002 ± 0.00 in the presence of hMMP-7 respectively. The bottom panels show the residuals of the fit of AQD lifetime traces in the absence and presence of hMMP-7.

Figure 7.29 shows the lifetime of AQD in the presence and absence of hMMP-9. The time resolved fluorescence decay profiles of AQD in the absence and presence of hMMP-7 was shown. The AQD sample was measured using λ_{ex} and λ_{em} at 340 nm and 625 nm, respectively. The excited state lifetime traces of AQD in the absence and presence of hMMP-9 were recorded. The $\tau_s = 1.9 \pm 0.0$ ns and α_s (amplitude) $= 0.01 \pm 0.0$; $\tau_l = 16.6 \pm 0.0$ ns and $\alpha_l = 0.01 \pm 0.0$ for AQD in the absence of hMMP-9, and $\tau_s = 2.2 \pm 0.0$ ns and $\alpha_s = 0.01 \pm 0.0$, $\tau_l = 18.3 \pm 0.0$ ns and $\alpha_l = 0.01 \pm 0.0$ in the presence of hMMP-9. The bottom panels show the residuals of the fit for AQD lifetime traces in the absence and presence of hMMP-9. Both shorter and longer lifetime slightly increase. The amplitude for longer lifetime however decreases while no change in the amplitude for the shorter lifetime.

Figure 7.30 shows the lifetime of CQD in the presence and absence of hMMP-10. The time resolved fluorescence decay profiles of CQD in the absence and presence of hMMP-10 are shown. The CQD sample was measured using λ_{ex} and λ_{em} at 340 nm and 570 nm, respectively. The excited-state lifetime traces of CQD in the absence and presence of hMMP-10 were recorded. The $\tau_s = 1.6 \pm 0.0$ ns and α_s (amplitude) $= 0.01 \pm 0.0$; $\tau_l = 13.7 \pm 0.0$ ns and $\alpha_l = 0.02 \pm 0.0$ for CQD in the absence of hMMP-10, and $\tau_s = 0.1 \pm 0.0$ ns and $\alpha_s = 0.02 \pm 0.0$, $\tau_l = 10.5 \pm 0.0$ ns and $\alpha_l = 0.02 \pm 0.0$ in the presence of hMMP-10. The bottom panels show the residuals of the fit of CQD lifetime traces in the absence and presence of hMMP-10. Both the shorter and the longer lifetime values decrease, more so for the shorter lifetime. There was no significant change in the amplitude values.
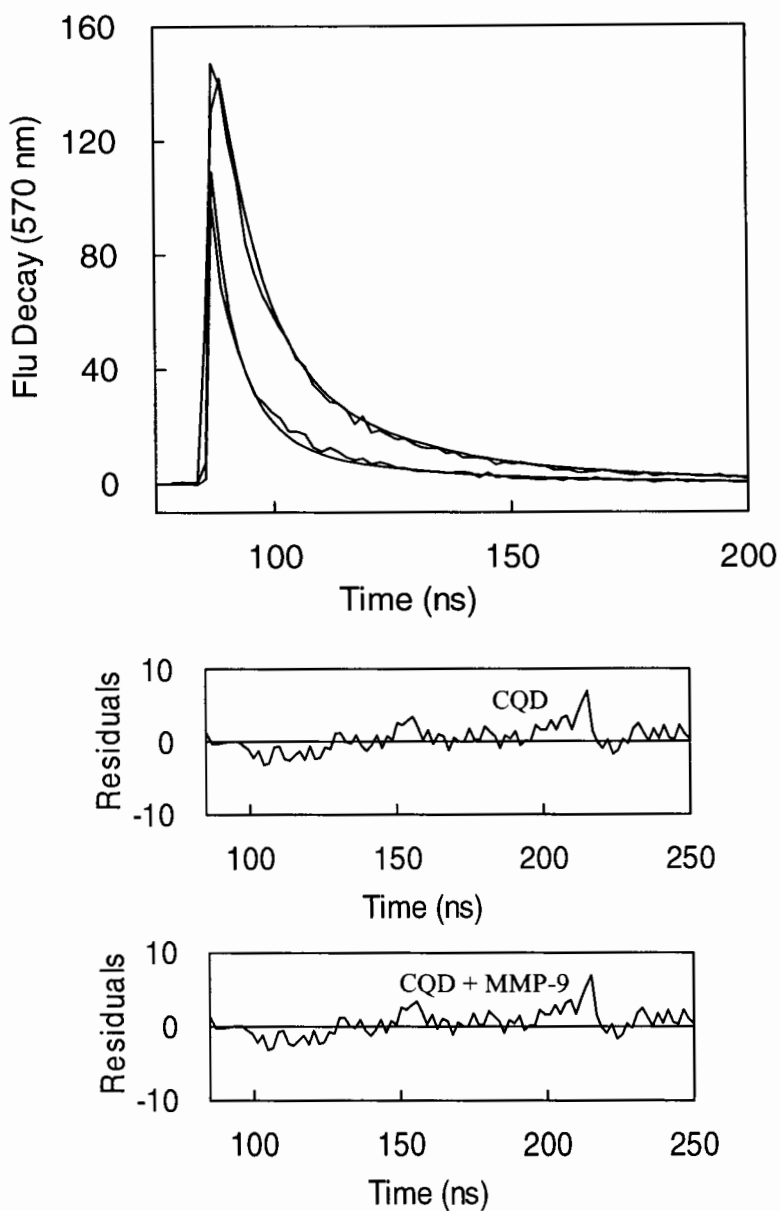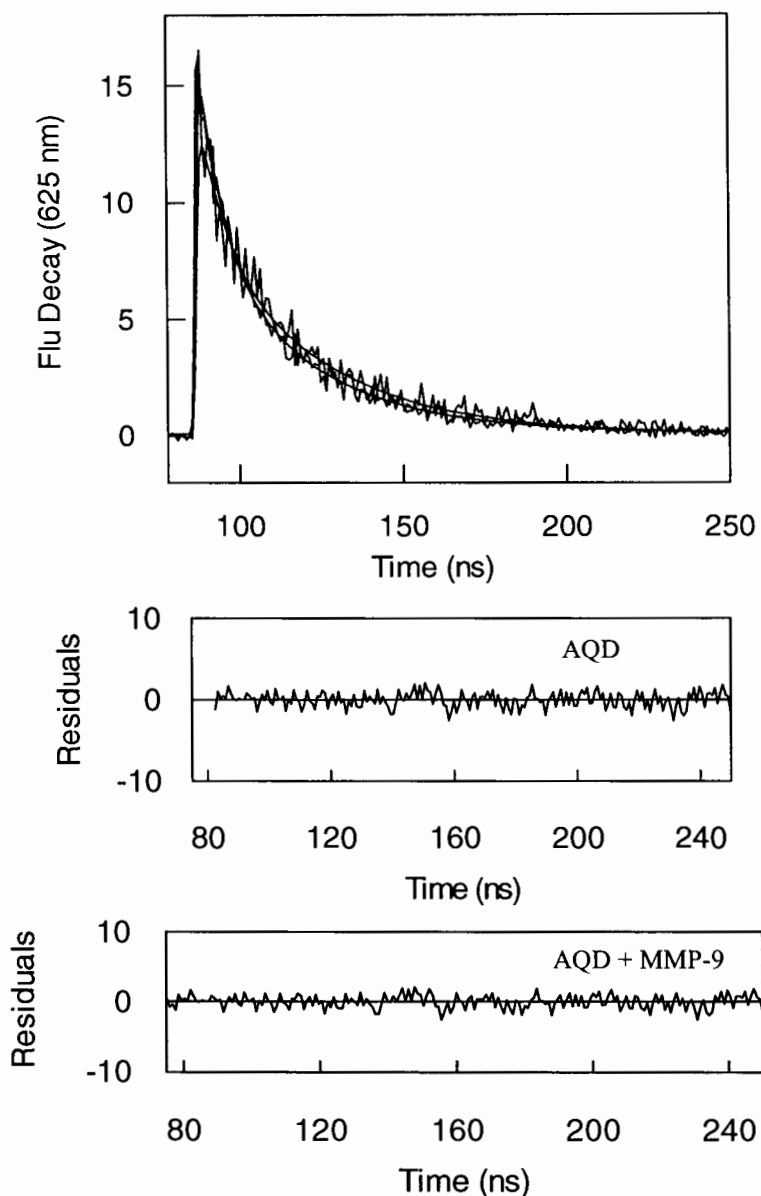
Figure 7.28. Lifetime of CQD in the presence and absence of hMMP-9, λ_{ex}= 340nm, λ_{em}= 570 nm. The time resolved fluorescence decay of CQD was measured in the absence and presence of hMMP-9. The CQD was monitored at and λ_{em} = 570 nm when excited at λ_{ex} = 340 nm. [CQD] = 1 μM, [hMMP-9] = 2.7 μM. The solid smooth lines are the best fit of the data according to Eq 3.6 with τ_s = 1.6 ± 0.00 ns and α_s (amplitude) = 0.01 ± 0.0; τ_l = 13.7 ± 0.0 ns and α_l = 0.02 ± 0.0 for CQD in the absence of hMMP-9, and τ_s = 0.05 ± 0.0 ns and α_s = 0.03 ± 0.0, τ_l = 10.0 ± 0.0 ns and α_l = 0.01 ± 0.0 in the presence of hMMP-9. The bottom panels show the residuals of the fit of CQD lifetime traces in the absence and presence of hMMP-9.

268

Figure 7.29. Lifetime of AQD in the presence and absence of hMMP-9, λ_{ex}= 340 nm, λ_{em}= 625 nm. The time resolved fluorescence decay of AQD was measured in the absence and presence of hMMP-9. The AQD was monitored at and λ_{em} = 625 nm when excited at λ_{ex} = 340 nm. [AQD] = 2 μM, [hMMP-9] = 4.8 μM. The solid smooth lines are the best fit of the data according to Eq 3.6 with τ_s = 1.9 ± 0.00 ns and α_s (amplitude) = 0.01 ± 0.0; τ_l = 16.6 ± 0.0 ns and α_l = 0.01 ± 0.0 for AQD in the absence of hMMP-9, and τ_s = 2.2 ± 0.0 ns and α_s = 0.01 ± 0.0, τ_l = 18.3 ± 0.0 ns and α_l = 0.01 ± 0.0 in the presence of hMMP-9. The bottom panels show the residuals of the fit of AQD lifetime traces in the absence and presence of hMMP-9.

Figure 7.31 shows the lifetime of AQD in the presence and absence of hMMP-10. The time resolved fluorescence decay profiles of AQD in the absence and presence of hMMP-7 was shown. The AQD sample was measured using λ_{ex} and λ_{em} at 340 nm and 625 nm, respectively. The excited state lifetime traces of AQD in the absence and presence of hMMP-10 were recorded. The τ_s = 1.9 ± 0.0 ns and α_s (amplitude) = 0.01 ± 0.0; τ_l = 16.6 ± 0.0 ns and α_l = 0.01 ± 0.0 for AQD in the absence of hMMP-10, and τ_s = 5.9 ± 0.0 ns and α_s = 0.01 ± 0.0, τ_l = 18.7 ± 0.0 ns and α_l = 0.01 ± 0.0 in the presence of hMMP-10 respectively. The bottom panels show the residuals of the fit of AQD lifetime traces in the absence and presence of hMMP-10. There is an increase in the smaller and longer lifetime data. The amplitude for the longer lifetime data decreases.

In the case of hMMP-7 and CQD, it was found that the lifetime for the shorter and the longer phases do not change, however, the amplitude for the longer phase decreases drastically. This indicates that the the tryptophan residues from the interior core of the protein are more exposed to the solvent. The fact that QDs quench the intrinsic steady-state fluorescence of hMMP-7 but do not alter the lifetimes of the tryptophan moieties implies that the overall quenching process is a ground-state phenomenon. A plausible reason could be that hMMP-7-CQD complex was unable to make the transition of the complex from the ground state to the excited state.

In the case of hMMP-7 and AQD, it was observed that the lifetime decreases (in both the phases). The smaller amplitude seems to increase whereas the longer amplitude decreases. The origin of the shorter amplitude decrease and longer increase substantiates the fact that the protein opens up more and the polarity around the AQD changes.
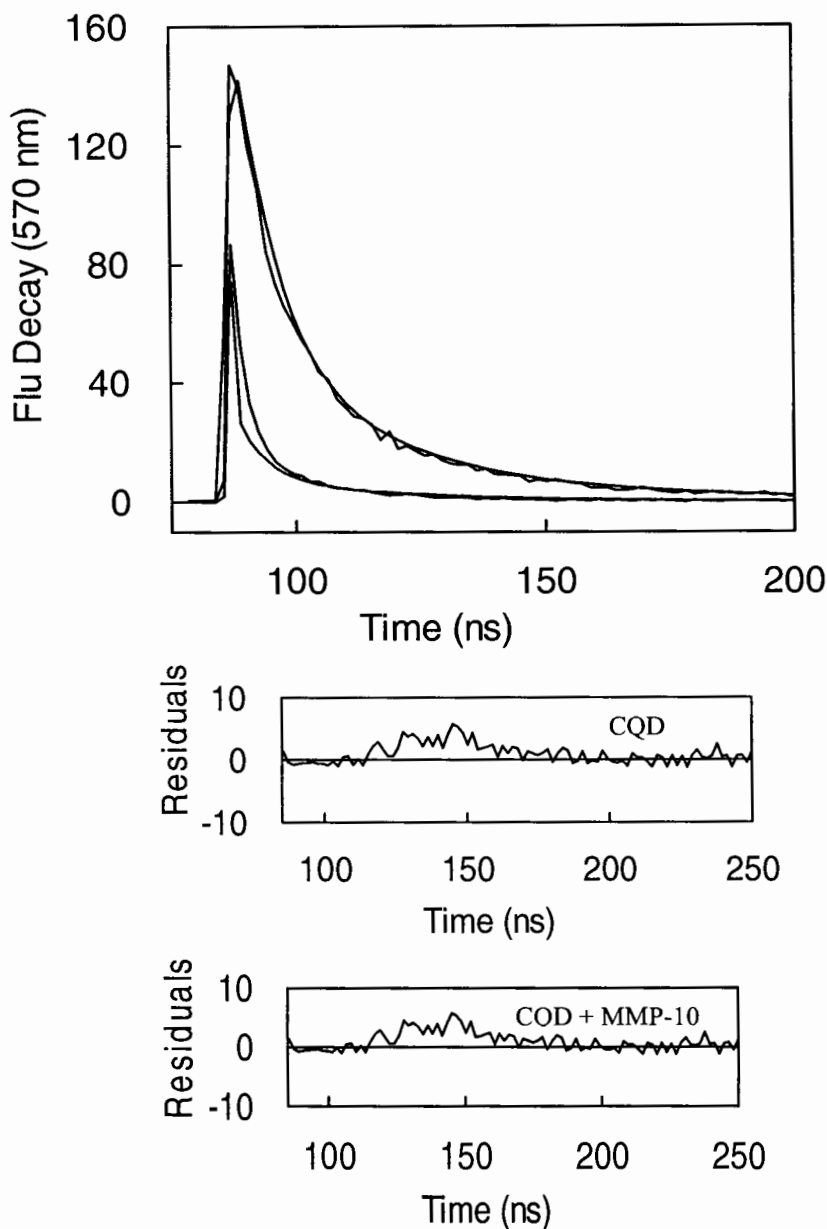
Figure 7.30. Lifetime of CQD in the presence and absence of hMMP-10, λ_{ex}= 340nm, λ_{em}= 570 nm. The time resolved fluorescence decay of CQD was measured in the absence and presence of hMMP-10. The CQD was monitored at and λ_{em} = 570 nm when excited at λ_{ex} = 340 nm. [CQD] = 1 µM, [hMMP-7] = 1.9 µM. The solid smooth lines are the best fit of the data according to Eq 3.6 with τ_s = 1.6 ± 0.0 ns and α_s (amplitude) = 0.01 ± 0.0; τ_l = 13.7 ± 0.0 ns and α_l = 0.02 ± 0.0 for CQD in the absence of hMMP-10, and τ_s = 0.1 ± 0.0 ns and α_s = 0.02 ± 0.0, τ_l = 10.5 ± 0.0 ns and α_l = 0.02 ± 0.0 in the presence of hMMP-10. The bottom panels show the residuals of the fit of CQD lifetime traces in the absence and presence of hMMP-10.
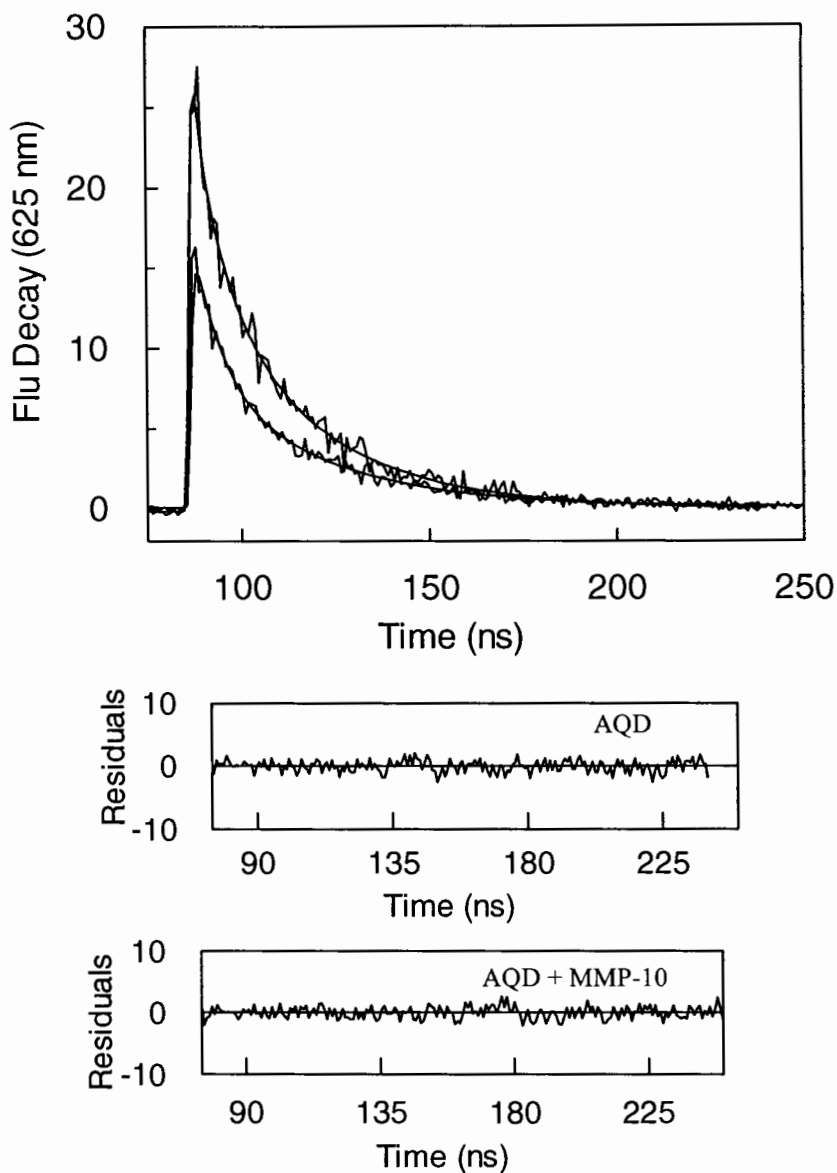
271

Figure 7.31. Lifetime of AQD in the presence and absence of hMMP-10, λ_{ex}= 340 nm, λ_{em}= 625 nm. The time resolved fluorescence decay of AQD was measured in the absence and presence of hMMP-10. The AQD was monitored at λ_{em} = 625 nm and λ_{ex} = 340 nm. [CQD] = 2 μM, [hMMP-7] = 0.8 μM. The solid smooth lines are the best fit of the data according to Eq 3.6 with τ_s = 1.9 ± 0.0 ns and α_s (amplitude) = 0.01 ± 0.0; τ_l = 16.6 ± 0.0 ns and α_l = 0.01 ± 0.0 for AQD in the absence of hMMP-10, and τ_s = 5.9 ± 0.0 ns and α_s = 0.01 ± 0.0, τ_l = 18.7 ± 0.0 ns and α_l = 0.01 ± 0.0 in the presence of hMMP-10. The bottom panels show the residuals of the fit of AQD lifetime traces in the absence and presence of hMMP-10.

272

The electronic configuration of the AQD core shell gets distorted due to the change in the solvent polarity. In the case of CQD and AQD with hMMP-9, in both of these scenarios, it can be contemplated that the decrease in the longer component of the amplitude exposes the QDs to a different polarity of the solvent molecules upon binding to hMMP-9. In case of hMMP-10 and CQD, the lifetime component decreases, while there is no change in the amplitudes. This is a clear indication of the transition of the hMMP-10 and CQD complex transiting from the ground-state to the excited-state due to dynamic quenching. However, an interesting aspect of the above analytical outcome is the apparent lack of the "static" contribution. For hMMP-10, upon binding to AQD, there was exactly an opposite scenario. It was observed that the lifetime of both the phases increase, leading to a decreased in the longer amplitude component. This suggests that hMMP-10 upon binding to the AQD, undergoes conformation distortion from the native compact structure and as MMPs are known to be "soft" flexible proteins [57], it bends on the surface of AQD to obtain stability after forming the complex. In light of these observations, it was believed that the partially buried Trp residues were completely buried and the exposed ones were more exposed. Table 7.9, 7.10 and 7.11 shows the comparative account of lifetime of CQD /AQD in presence and absence of hMMP isozymes (Ex 340 nm, Em 570 nm / 625 nm for CQD and AQD, respectively). It can be concluded from the lifetime data that either of the following scenarios may exist: (A) It is possible that the tryptophan residues of the enzymes are in different micro-environments and as such would decay with different lifetime values; or (B) The protein exists in two distinct conformations that exhibit different average lifetime decays.

Table 7.9.A. The comparative account of lifetime of CQD in the presence and absence of hMMP-7, λ_{ex} = 340 nm and λ_{em} = 570 nm. B. The comparative account of lifetime of AQD in the presence and absence of hMMP-7, λ_{ex} = 340 nm and λ_{em} = 625 nm.

A

Ex 340 nm, Em 570 nm	τ_s	α_s	τ_l	α_l
CQD alone	1.6	0.01 ± 0.0 (30 %)	13.7	0.02 ± 0.0 (70 %)
+ 1.9 µM MMP-7	1.6	0.01 ± 0.0 (56%)	12.7	0.01 ± 0.0 (44 %)

B

Ex 340 nm, Em 625 nm	τ_s	α_s	τ_l	α_l
AQD alone	1.9	0.01 ± 0.0 (29 %)	16.59	0.01 ± 0.0 (71 %)
+3 µM MMP-7	0.01	0.01 ± 0.0 (71 %)	9.41	0.01 ± 0.0 (29%)

Table 7.10.A. The comparative account of lifetime of CQD in the presence and absence of hMMP-9, λ_{ex} = 340 nm and λ_{em} = 570 nm. B. The comparative account of lifetime of AQD in the presence and absence of hMMP-9, λ_{ex} = 340 nm and λ_{em} = 625 nm.

A

Ex 340 nm, Em 570 nm	τ_s	α_s	τ_l	α_l
CQD alone	1.6	0.01 ± 0.0 (30%)	13.7	0.02 ± 0.0 (70 %)
+ 2.7 µM MMP-9	0.1	0.03 ± 0.0 (83%)	10.0	0.01 ± 0.0 (17 %)

B

Ex 340 nm, Em 625 nm	τ_s	α_s	τ_l	α_l
AQD alone	1.9	0.01 ± 0.0 (29 %)	16.6	0.01 ± 0.0 (71 %)
+4.8 µM MMP-9	2.2	0.01 ± 0.0 (71 %)	18.3	0.01 ± 0.0 (29%)

Table 7.11.A. The comparative account of lifetime of CQD in the presence and absence of hMMP-10, λ_{ex} = 340 nm and λ_{em} = 570 nm. B. The comparative account of lifetime of AQD in the presence and absence of hMMP-10, λ_{ex} = 340 nm and λ_{em} = 625 nm.

A	Ex 340 nm, Em 570 nm	τ_s	α_s	τ_l	α_l
	CQD alone	1.6	0.01 ± 0.0 (30%)	13.7	0.02 ±0.0 (70 %)
	+ 0.9 µM MMP-10	0.1	0.02 ± 0.0 (50 %)	10.5	0.02 ± 0.0 (50 %)

B	Ex 340 nm, Em 625 nm	τ_s	α_s	τ_l	α_l
	AQD alone	1.9	0.01 ± 0.0 (29 %)	16.6	0.01 ± 0.0 (71%)
	+0.8 µM MMP-10	5.9	0.01 ± 0.0 (34 %)	18.7	0.01 ± 0.0 (66 %)

Electronic interactions are crucial to the structural and functional properties of proteins [58-60]. In order to establish or refute the concept of binding of hMMP isozymes (specially hMMP-7 and 10) via strong electrostatics and hMMP-9 via more prominent hydrophobic interactions (inferred from other experimental data), the study of the effect on the binding affinity of the hMMP isozymes to the two differently charged QDs (CQD and AQD) by varying the NaCl concentration was performed. At first, the experimental setup for Figure 7.5 was repeated. This facilitates the formation of hMMP-CQD or hMMP-AQD complex, and then to this complex, increasing concentrations of NaCl was titrated. Qualitatively, it was estimated whether upon increasing the NaCl concentration, the quenched fluorescence of the tryptophan (when λ_{ex} and λ_{em} were 280 nm and 343 nm respectively) returns back to the original hyperchromic intensity of the tryptophan when QDs were not present. It was observed that in all the cases (both for CQD and AQD), with hMMP-7 and 10, more than 80% of the fluorescence intensity returned to the native

intensity of these proteins, but for hMMP-9, the changes were not be correlated to the original native fluorescence signal. This corroborates the hypothesis of the "clustered" charge distribution of positive and negative charges at the surfaces of the hMMP-7 and 10 (Scheme 6.2) playing a key role in the interaction between the proteins and QDs (Scheme 7.1). Due to the "scattered' charge distribution of positive and negative charges in hMMP-9, it would be plausible to conclude that the interactions of hMMP-9 with QDs was dictated by a mixed effect of electrostatics as well as hydrophobic forces. Energy transfer between oppositely charged CdSe/ZnS core-shell NCs with electrostatic attraction in aqueous solution was reported by Nabiev *et al.* [61-62]. Rogach *et al.* [63] reported an efficient FRET in bilayers of water-soluble CdTe NCs capped with thiol surfactants, forming a layer-bilayer assembly. The use of electrostatic forces for assembly extends to charged biomacromolecules such as proteins and DNA [64]. The exhibition of electrostatic interactions in the formation of lipid-nanoparticle conjugate materials of variable composition and topological structure has also been reported [62].

The two major factors that contribute in the determination of minimum size of enzymes were: (1) Enzyme conferring enough "rigidity" [16], and (2) A protein should not tend to associate indiscriminately with other cellular proteins. Apart from one or two possible exceptions, the same general argument may be used to account for the fact that allosteric proteins have been found to mediate both homotropic and heterotropic interactions implying that they are oligomers. Heterotropic interactions can *a priori* be me-diated by a monomeric protein possessing two different binding sites (proposed in Scheme 7.1), associated with two different "tautemeric" states of the molecule [21].
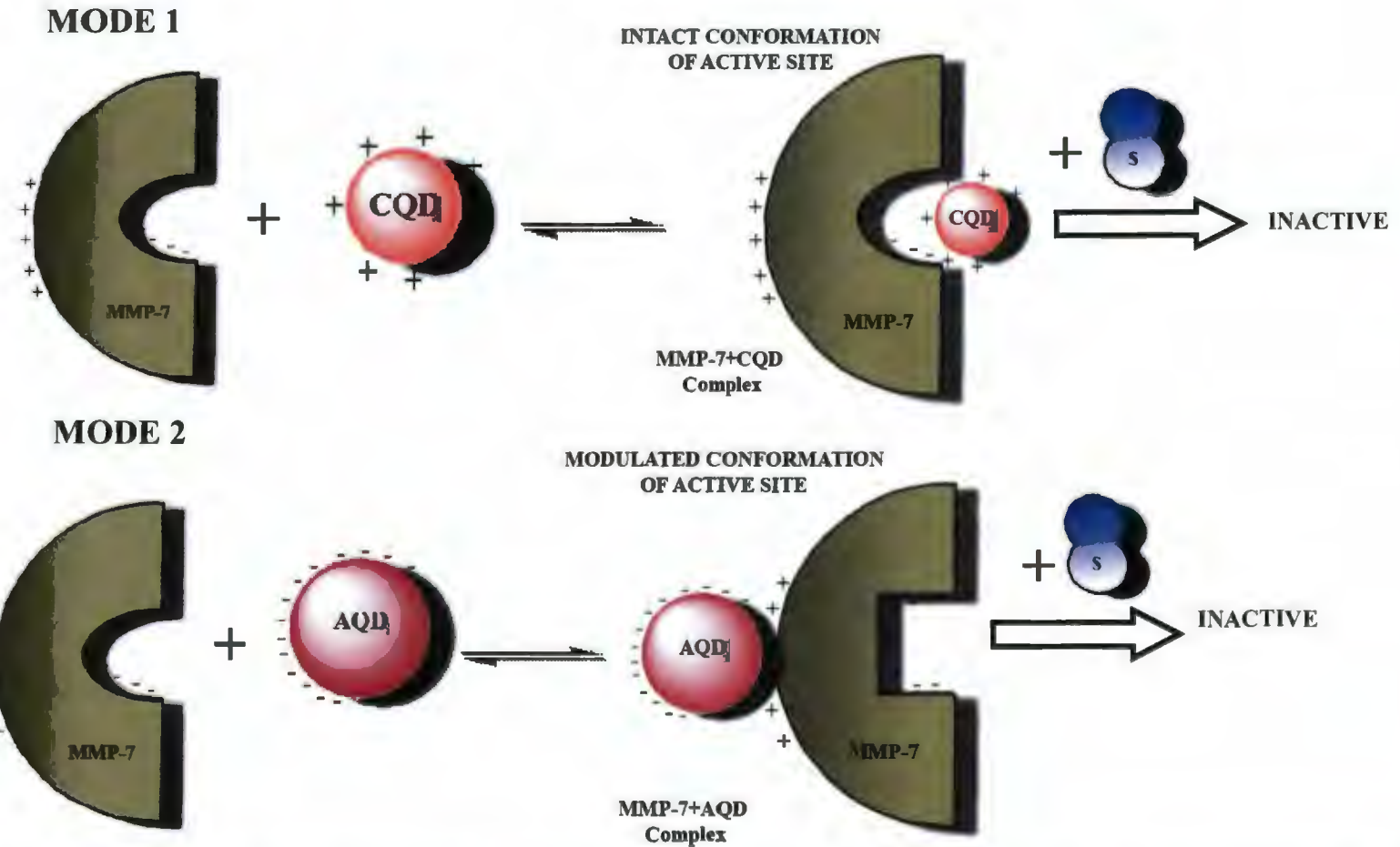
Scheme 7.1. The schematic model hypothesized to conceptualize as hMMP-7 bears two alternative modes of binding to CQD and AQD. Upon binding to CQD (Mode 1), the enzyme activity of hMMP-7 gets perturbed due to the inaccessibility of the substrate at the active site, whereas upon binding to AQD (Mode 2) at the alternative site (Allosteric site), the enzyme undergoes a subtle modulation in the native conformation of the active site, which leads to the inability of the enzyme to catalyze the reaction. The double reversible arrow demonstrates that the binding of hMMP-7 can dissociate from the complex in a reversible manner. "S" stands for the Substrate.

Scheme 7.1 illustrates the proposed hypothesis that when hMMP-7 (taken as an example, a similar situation exists for hMMP-10) binds and forms hMMP-7-CQD complex, the complex gets stabilized via electrostatic forces. Due to the existence of strong electrostatics, the CQD (which is positively charged) binds at the active site and blocks substrate accessibility; hence hMMP-7 when bound to CQD does not catalyze the reaction. A perturbation in the enzyme activity is again observed upon binding and forming a complex with AQD. Due to strong electrostatics, the clustered positively charged residues at the opposite side of the active site would attract the AQD. The binding of the AQD at the distal end of the hMMP-7 modulates the active-site pocket (which is flexible), leading to a conformation of the active site that no longer can fit the substrate according to the "Induced fit hypothesis" [21], thereby the "allosteric site" at the distal end leads to an inactive enzyme.

A detailed analysis of the data from the experimental results presented herein, leads to the following conclusions: (1) Differently charged QDs bind to hMMP-7, 9 and 10; (2) Enzyme activity of all three hMMPs gets perturbed due to binding to cationic as well as anionic QDs; (3) Binding of the hMMPs to the differently charged QDs is reversible; (4) Binding of the hMMP to CQD and AQD were mediated via electrostatics; and (5) Lifetime data indicates: [A]. It is possible that the tryptophan residues of the enzymes are in different micro-environments and as such would decay with different lifetime values, and [B]. The proteins exists in two distinct conformations that exhibit different average lifetime decays. MMPs are involved in tumor formation in many types of human cancers, hence QDs imaging *in vivo*, modulation of uptake of these QDs in cells with tumor specific

enzymes may lead to selective accumulation of nanoparticles in tumor cells. Another application, which is quite likely to bring a revolution in multiplexed applications, is utilizing several QD-peptide ligands to target multiple cellular receptors. In addition, this proposal may emerge as a powerful imaging method for dissecting complex receptor distributions and cell trafficking. Given the rapid growth in new QD based materials and the well-established utility of peptides in biology and chemistry, the overlap between these fields will certainly be quite bright.

7.3. References

1. Murray, C.B., Norris, D.J., and Bawendi, M.G. (1993) Synthesis and characterization of nearly monodisperse CdE (E=sulfur, selenium, tellurium) semiconductor nanocrystallites, *J. Am. Chem. Soc.* 115, 8706–8715.
2. Unni, C., Philip, D., and Gopchandran, K.G. (2008) Studies on optical absorption and photoluminescence of thiolglycerol-stabilized CdS quantum dots, *Spectrochimica Acta Part A.* 71, 1402–1407.
3. Zhang, H., Zhou, Z., and Yang, B. (2003) The influence of carboxyl groups on the photoluminescence of mercaptocarboxylic acid-stabilized CdTe nanoparticles, *J. Phys.Chem. B.* 107, 8-13.
4. Dabbousi, B.O., Rodriguez-Viejo, J., Mikulec,F.V., Heine, J.R., H. Mattoussi, Ober, R., Jensen, K.F., and Bawendi, M.G. (1997) (CdSe)ZnS Core–shell quantum dots: synthesis and characterization of a size series of highly luminescent nanocrystallites, *J.Phys Chem. B.* 101, 9463–9475.
5. Ji, M., Jin, l., Guo, J., Yang, W., Wang, C., and Fu, S. (2008) Formation of luminescent nanocomposite assemblies via electrostatic interaction, *J. Coll. Interf. Sci.* 318, 487-495.
6. Shenhar, R., and Rotello, V.M. (2003) Nanoparticles: scaffolds and building blocks, *Acc. Chem. Res.* 36, 549-561.
7. Tam-Chang, S.-W.; Biebuyck, H. A.; Whitesides, G. M.; Jeon, N.; and Nuzzo, R. G. (1995) Self-Assembled Monolayers on Gold Generated from alkanethiols with the Structure RNHCOCH2SH, *Langmuir.* 11, 4371-4382.
8. Wu, Y., Lopez, G.P., Sklar, L.A., and Buranda, T. (2007) Spectroscopic characterization of streptavidin functionalized quantum dots, *Anal. Biochem.* 364, 193-203.
9. Warnement, M. R., Tomlinson, I. D., Chang, J. C., Schreuder, M.A., Luckabaugh, C.M., and Rosenthal, S.J. (2008) Controlling the reactivity of ampiphilic quantum dots in biological assays through hydrophobic assembly of PEG derivatives, *Bioconj. Chem.* 19, 1404-1413.

10. Kley, N., Ivanov, I., and Meier-Ewert, S. (2004) Genomics and proteomics tools for compound mode-of-action studies in drug discovery, *Pharmacogenomics.* 5, 395-404.

11. Boldt, K., Bruns, O.T., Gaponik, N., and Eychmiiller, A. (2006) Comparative examination of the stability of semiconductor quantum dots in various biochemical buffers, *The J. Phys. Chem. B.*110, 1959-1963.

12. Nygren, P., Lundqvist, M., Broo, K., and Jonsson, B. H. (2008) Fundamental design principles that guide induction of helix upon formation of stable peptide-nanoprticle complexes, *Nano. Lett.* 8(7), 1844-1852.

13. Stobiecka, A. (2005) Acrylamide-quenching of Rhizomucor miehei lipase, *J. Photochem. Photobiol. B., Biol.* 80, 9-18.

14. Norde, W., and Haynes, C.A. (19960 Thermodynamics of protein adsorption. In: Brash, J.L., Wojciechowski, P.W. (Eds.), Interfacial Phenomena and Bioproducts. *Marcel Dekker, New York, NY,* pp: 123–144.

15. Norde, W. (1998) Driving forces for protein adsorption at solid surfaces. In: Malmsten, M. Jr (Ed.), Biopolymers at Interfaces. In: Surfactant Sci, vol. 75. *Marcel Dekker, New York,* pp: 27–54.

16. Norde, W., and Giacomelli, C.E. (2000) BSA structural changes during homomolecular exchange between the adsorbed and the dissolved states, *J. Biotechnol.* 79, 259–268.

17. Osovsky, R., Shavel, A., Gaponik, N., Amirav, L., Eychmiiller, A., Weller, H., and Lifshitz, E. (2005) Electrostatic and covalent interactions in CdTe nanocrystalline assemblies, *J.Phy.Chem. B.* 109, 20244-20250.

18. Artemyev, M. V., Bibik, A. I., Gurinovich, L. I., Gaponenko, S. V., and Woggon, U. (1999) Evolution from individual to collective electron states in a dense quantum dot ensemble, Physical *Review B: Cond. Matt. and Mat. Phys.* 60(3), 1504-1506

19. Micic, Olga I., Ahrenkiel, S. P., and Nozik, Arthur J. (2001) Synthesis of extremely small InP quantum dots and electronic coupling in their disordered solid films *Appl. Phys. Lett.* 78(25), 4022-4024.

20. Star, A., Liu, Yi., Grant, K. Ridvan, L., Stoddart, J.F., Steuermman, D.W., Diehl, M.R., Boukai, A., and Heath, J.R. (2003) Noncovalent side-wall functionalized of single-wall carbon nanotubes, *Macromolecules.* 36, 553-560.

21. Monod, J., Wyman, J., and Changeux, J. P. (1965) On the nature of allosteric transitions: a plausible model, *J. Mol. Biol.* 12, 88–118.

22. Vertegel, A.A., Siegel, R.W., and Dordick, J.S. (2004) Silica nanoparticle size influences the structure and enzymatic activity of adsorbed lysozyme, *Langmuir.* 20, 6800–6807.

23. Pettersen, E.F., Goddard, T.D., Huang, C.C., Couch, G.S., Greenblatt, D.M., Meng, E.C., and Ferrin, T.E. (2004) UCSF Chimera-a visualization system for exploratory research and analysis, *J. Comput. Chem.* 25, 1605-1612.

24. Bode, W., Catalan, C. F., Tschesche, H., Grams, F., Nagase, H., and Maskos, K. (1999) Structural properties of matrix metalloproteinases, *Cell. Mol. Life. Sci.* 55, 639-652.

25. Elkins, P.A., Ho, Y.S., Smith, W.W., Janson, C.A., D'Alessio, K.J., McQueney, M.S., Cummings, M.D., and Romanic, A.M. (2002) Structure of the C-terminally truncated human ProMMP9, a gelatin-binding matrix metalloproteinase, *Acta. Crystallogr. D. Biol. Crystallogr.* 58, 1182-1192.

26. Bertini, I., Calderone, V., Fragai, M., Luchinat, C., Mangani, S. and Terni, B. (2004) Crystal structure of the catalytic domain of human matrix metalloproteinase 10, *J. Mol. Biol.* 336, 707-716.

27. Vivian, J.T., and Callis, P.R. (2001) Mechanisms of tryptophan fluorescence Shifts in proteins, *Biophysical J.* 80, 2093-2109.

28. Shen, X., Liou, X., Ye, L., Liang, H., and Wang, Z. (2007) Spectroscopic studies on the interaction between human hemoglobin and CdS quantum dots, *J. Coll. Interf. Sci.* 311, 400–406.

29. Demchenko, A.P. (1986) Ultraviolet Spectroscopy of Proteins. Springer-Verlag, Berlin.. *Ultraviolet Spectroscopy of Proteins. Springer-Verlag, Berlin.*

30. Eftink, M.R., and Ghiron, C.A. (1976) Exposure of tryptophanyl residues in proteins: Quantitative determination by fluorescence quenching studies, *Biochemistry.* 15, 672-680.

31. Eftink, M.R., and Ghiron, C.A. (1981). Fluorescence quenching studies with proteins, *Anal. Biochem.* 114, 199-227.

32. Lakowicz, J.R., and Weber, G. (1973) Quenching of protein fluorescence by oxygen: Detection of structural fluctuations in proteins on the nanosecond time scale, *Biochemistry.* 12, 4171-4179.

33. Chang, Y.C., and Ludescher, R.D. (1993) Tryptophan fluorescence quenching in rabbit skeletal myosin rod, *Biophys. Chem.* 48, 49-59.

34. Stack, M.S., Itoh, Y., Young, T.N., and Nagase, H. (1996) Fluorescence quenching studies of matrix metalloproteinases (MMPs): evidence for structural rearrangement of the proMMP-2/TIMP-2 complex upon mercurial activation, *Arch. Biochem. Biophys.* 333, 163-169.

35. Szabo,G., and Rayner,D. (1980) Fluorescence Decay of Tryptophan Conformers in Aqueous Solution. *J. Am. Chem. Soc.* 102 (2), 554-563.

36. Lehrer, S.S. (1971) Solute perturbation of protein fluorescence: The quenching of the tryptophyl fluorescence of model compounds and of lysozyme by iodide ion, *Biochemistry.* 10, 3254-3263.

37. Michalet, X., Pinaud, F.F., Bentolila, L.A., Tsay, J.M., Doose, S., Li, J.J., Sundaresan, G., Wu, A.M., Gambhir, S.S., and Weiss, S. (2005) Quantum dots for live cells, in vivo imaging, and diagnostics, *Science.* 307, 538–544.

38. Beechem, J.M., and Brand, L. (1985) Time-resolved fluorescence of proteins, *Annu. Rev. Biochem.* 54, 43-71.

39. Lauer-Fields, J.L., Tuzinski, K.A., Shimokawa, K.I., Nagase, H., and Fields, G.B. (2000) Hydrolysis of triple-helical collagen peptide models by matrix metalloproteinases, *J. Biol. Chem.* 275, 13282-13290.

40. Nicholls, A., Sharp, K.A., and Honig, B. (1991) Protein folding and association: insights from the interfacial and thermodynamic properties of hydrocarbons, *Proteins.* 11, 281-296.

41. Tochowicz, A., Maskos, K., Huber, R., Oltenfreiter, R., Dive, V., Yiotakis, A., Zanda, M., Bode, W., and Goettig, P. (2007) Crystal structures of MMP-9 complexes with five inhibitors: contribution of the flexible Arg424 side-chain to selectivity, *J. Mol. Biol.* 371, 989-1006.

42. Weber, J., and Senior, A.E. (2000) Features of F(1)-ATPase catalytic and noncatalytic sites revealed by fluorescence lifetimes and acrylamide quenching of specifically inserted tryptophan residues, *Biochemistry.* 39, 5287-5294.

43. Volotovskiĭ, I.D. and Konev, S.V. (1967) Relation between the conformation and UV luminescence of proteins, *Biofizika.* 12, 200-205.

44. Emonard, H., and Grimaud, J.A. (1990) Matrix metalloproteinases. A review. *Cell. Mol. Biol.* 36, 131-153.

45. Chao, P., and Chow, C.S. (2007) Monitoring aminoglycoside-induced conformational changes in 16S rRNA through acrylamide quenching, *Bioorg. Med. Chem.* 15, 3825-3831.

46. Wu, X., and Narsimhan, G. (2008) Effect of surface concentration on secondary and tertiary conformational; changes of lysozyme adsorbed on silica nanoparticles, *Biochim. Biophys. Acta.* 1784, 1694-1701.

47. Sastry, M., Rao, M., and Ganesh, K.N. (2002) Electrostatic assembly of nanoparticles and biomolecules, *Acc. Chem. Res.* 35, 847-855.

48. Day, Y.S.N., Baird, C. L., Rich, R.L., and Myszka, D.G. (2002) Direct comparison of binding equilibrium, thermodynamic, and rate constants determined by surface- and solution-based biophysical methods, *Protein. Sci.* 11, 1017–1025.

49. Wu, Z., Zhang, B., and Yan, B. (2009) Regulation of enzyme activity through interactions with nanoparticles, *Int. J. Mol. Sci.* 10, 4198–4209.

50. Zhang, Y., So, M.K., and Rao, J. (2006) Protease-modulated cellular uptake of quantum dots, *Nano. Letts.* 6, 91988-91992.

51. Yao. H., Zhang, Y., Xiao, F., Xia, Z., and Rao, J. (2007) Quantum dot/bioluminescence resonance energy transfer based highly sensitive detection of proteases, *Angew. Chem. Int. Ed.* 46, 4346 –4349.

52. Lakowicz, J.R. (1999) In: Principles of Fluorescence Spectroscopy, 2nd Ed., *Kluwer Academic/ Plenum Publishers, New York.*

53. Konev, S.V. (1967) Fluorescence and Phosphorescence of Proteins and Nucleic Acids, *Plenum Press, New York.*

54. Morgan, N.Y., English, S., Chen, W., Chernomordik, V., Russo, A., Smith, P.D., and Gandjbakhche, A. (2005) Real time in vivo non-invasive optical imaging using near-infrared fluorescent quantum dots, *Acad. Radiol.* 12, 313-323.

55. Teague, S.J. (2003) Implications of protein flexibility for drug discovery, *Nat. Rev. Drug. Discov.* 2, 527-541.

56. Chattopadhyay, K., and Frieden, C. (2006) Steady-state and time-resolved fluorescence studies of the intestinal fatty acid binding protein, *Proteins.* 63, 327-335.

57. Ganguly, B., and Srivastava, D.K. (2008). Influence of "Flexible" versus "Rigid" Nanoparticles on the Stability of Matrix Metalloproteinase-7, *J. Biomed. Nanotechnol.* 4, 457–462.

58. Chen, W. (2008) Nanoparticle fluorescence based technology for biological applications, *J. Nanosci. Nanotechnol.* 8, 1019–1051.

59. Shao, L., Dong, C., Sang, F., Qian, H., and Ren, J. (2009) Studies on interaction of CdTe quantum dots with bovine serum albumin using fluorescence correlation spectroscopy, *J. Fluoresc.* 19, 151–157.

60. Chen, R.J., Zhang, Y., Wang, D., and Dai, H. (2001) Noncovalent sidewall functionalization of single-walled carbon nanotubes for protein immobilization, *J. Am. Chem. Soc.* 123, 3838–3839.

61. Nabiev, R.F., and Yeh, P. (1993) Dynamics of the spontaneous emission of an atom into the photon-density-of-states gap: Solvable quantum-electrodynamical model, *Phys. Rev. A.* 47 (4), 3880-3884.

62. Woggon, U., Giessen, H., Gindale, F., Wind, O., Fluegel, B., and Peyghambarian, N. (1996) Ultrafast energy relaxation in quantum dots, *Phys. Rev. B.* 54 (24), 17681-17690.

63. Rogach, A. L., Nagesh, D., Ostrander, J.W., Giersig, M., and Kotov, N.A. (2000) "Raisin Bun"-Type Composite Spheres of Silica and Semiconductor Nanocrystals, *Chem. Matter.* 12, 2676-2685.

64. Liu, Yi., Zhang, M.Xi., Zhang, Z.L., Xie, H.Y., Tian, Zhi.Q., Wong, Kwok-Y., and Pang, Dai-W. (2008) Controlled and reversible binding of positively charged quantum dots to lambda DNA, *Front. Biosci.* 13, 923-928.

CHAPTER 8. HIGH THROUGHPUT SCREENING OF THE SMALL MOLECULE INHIBITORS (SMI) WITH THE hMMP ISOZYMES

8.1. Introduction

Matrix metalloproteinases (MMPs) are a large family of calcium-dependent zinc-containing endopeptidases that are responsible for tissue remodeling and degradation of the extracellular matrix (ECM), which includes collagens, elastins, gelatin, matrix glycoproteins, and proteoglycans. Homeostasis is usually maintained since MMPs are minimally expressed under normal physiological conditions. These enzymes are strictly controlled by endogenous MMP inhibitors (MMPIs) and tissue inhibitors of MMPs (TIMPs). Imbalance between the activity of MMPs and TIMPs is a result of over-expression of MMPs and can lead to variety of pathological disorders [1-5].

8.1.1. Background of the discovery of inhibitors for MMPs

The earliest description of MMPs in 1949 was that of depolymerizing enzymes, which could facilitate tumor growth by making connective tissue stroma. Collagenase, the first vertebrate MMP, was isolated 13 years later from a tadpole tail and was eventually characterized. Although several mammalian enzymes were partially purified over the next 20 years, it was not until 1985 that the field really developed and structural homologies became apparent, allowing new members to be identified through molecular biological techniques [6]. It was confirmed in a recent study that smoking alters the levels of several MMPs in skin tissue, serum, and saliva, and thus may in turn affect the turnover of the extracellular matrix (ECM) of skin possibly leading to carcinogenesis [7]. MMPs have been considered a promising target for cancer therapy, and a large number of synthetic and natural MMP inhibitors (MMPIs) have been identified as the cytostatic and anti-angiogenic

agents and have begun to undergo clinical trials.

8.1.2. Substrate specificity of the MMPs

A groove on the protein surface centered on the catalytic zinc ion and a S1' specificity site are the two distinct regions of the active-site that varies considerably among members of the family. Bound inhibitors make several hydrogen bonds with the enzyme by adopting extended β-structure-like conformations within the groove and provide a fourth ligand for the catalytic Zn^{2+} ion. The S1' subset plays a pivotal role in determining the substrate specificity in the active enzyme. The volume of this subsite varies widely, with a relatively small hydrophobic site in MMP-7 and MMP-1 as compared with a very large site in MMP-8 and a site that extends all the way through the MMP-3 molecule [8], open to solution at both ends. There is variation in the MMPs in the amino-acid residues that form the S1' pocket (Figure 8.1.A).

It has been confirmed that different MMPs exhibit different selectivity for different matrix proteins. Thus, understanding of such substrate selectivity to identify optimized peptide substrates to be used in assay development and design of selective MMP inhibitors is of significant importance. Studies have been conducted to determine the sequence of the cleavage site in protein substrates for individual enzymes [9-11].

Proline is the preferred amino acid at the P3 position for all examined MMP isozymes. Leu and Met are preferred at P2 position for MMP-7 while Arg is preferred at P2 for MMP-2 selectivity. Glu provides significant cleavage by MMP-7 and MMP-8, and negligible cleavage by MMP-1, MMP-2, and MMP-9 at the P1 position. At P1', the presence of a Tyr residue results in highly selective cleavage by MMP-8 and Leu and Met

appear to be preferred for broad-spectrum cleavage. Studies suggest that for efficient cleavage there is very little selectivity for the tryptophan residue at the P2' position [10].

Figure 8.1.A. Binding between an inhibitor and MMP-3 in the catalytic domain. This figure has been adopted from Ref 12.

The same is true for amino-acid changes at P3'. The S3–S1 subsites form a shallow region bordered on one side by β-strand IV that features a hydrophobic proline binding cleft at S3. The selective replacement of the catalytic zinc in MMP-3 with other transition metals such as Mn^{2+}, Co^{2+}, Cd^{2+}, and Ni^{2+} results in the retention of protease activity. However, substitution of the catalytic metal influences the substrate specificity of the enzyme since the active-site geometry is altered, and affects the substrate binding site [13]. The selectivity of the most known MMP inhibitors relies on the two dominant molecular features: (a) a chelating moiety that interacts with the catalytic zinc ion; and (b) hydrophobic extensions protruding from the catalytic site into the large and hydrophobic

the inhibitor selectivity since the structural differences between members of the MMP families occur mainly in the S1' subsite [14]. The specificity at those particular sites can also be defined by the Structure-Activity Relationships (SARs) in Figure 8.1.B.

R₁: P₁' Substituent
Major determinant of activity and selectivity
Small groups selective for MMP-1 and larger
spares MMP-1 and MMP-7
Charged and polar groups not tolerated

R₃: P₃' Substituent
Wide range of substituents tolerated
Aromatic groups improve MMP-3 selectivity

Zinc Binding Group

Rₐ: α Substituent
Increases activity against
MMP-1 and -3
Can be cyclized to R₂

R₂: P₂' Substituent
Wide range of substituents tolerated
Aromatic groups preferred
Bulky groups increase oral bioavailability
Can be cyclized to Ra and R₂

Figure 8.1.B. The importance of the structure-activity relationships of the Hydroxamate MMP inhibitor. This figure is adopted from Ref 5.

8.1.3. Types of MMPs inhibitors (MMPIs) synthesized

The criteria for a molecule to qualify as an effective inhibitor of MMP are: (a) at least one functional group that provides a hydrogen bond interaction with the enzyme backbone; (b) A functional group (e.g. carboxylic acid, hydroxamic acid and sulfydryl etc.) capable of chelating the active site zinc (II) ion (this will be referred to as zinc binding group or ZBG); and (c) one or more side chains which undergo effective van der Waals interactions with the enzyme subsites [15-17]. It is evident that these requirements can be fulfilled by a variety of structural classes of MMP inhibitors, which have been discovered

by various methods including combinatorial chemistry [18-20].

8.1.4. Types of MMPIs screened for therapeutics

There are several MMPIs that have been screened and they have been categorized into different classes as discussed below.

(i)   Hydroxamates

The Hydroxamates (CHNHOH) moiety has proved to be the most potent Zn^{2+} binding group. It acts as a bidentate ligand with the active site Zn^{2+} ion, having distorted trigonal bipyramidal geometry. In this conformation, the two oxygen atoms coordinate with the Zn^{2+} ion present in the active site. While the amide nitrogen forms a hydrogen bond with the carbonyl group of the amino-acid residue in the active site. There are three distinct types of hydroxamate inhibitors; Succinyl Hydroxamate, Malonic acid based derivatives, and Sulfonamide and Sulfone based inhibitors.

(ii)   Carboxylates

The Carboxylate group has proved to be a less potent binding group towards the Zn^{2+} ion. Binding of the inhibitor releases water molecules bound to the catalytic Zn^{2+}.

(iii)   Thiol zinc-binding groups

The potency of the Thiol zinc-binding group of inhibitors is intermediate between hydroxamates and carboxylates. The Thiol (SH) moiety is monodentately coordinated to the catalytic Zn^{2+} ion of the enzyme.

(iv)   Thiadiazoles/ Thiadiazine group

Thiadiazoles were discovered as MMP inhibitors through a broad screening of many inhibitors. The thiadiazoles form a hydrogen bond with the secondary pleated sheets

288

in Stromelysins. There is rearrangement of the structure and the inhibitor, it obtains a very stable structure due to the π-π stacking inside the active site of MMP-3.

(v)   Phosphorous based ligands (PBL)

PBL becomes coordinated to the catalytic Zn^{2+} via oxygen atoms either monodentately or bidentately. Extended substitutions in the P3 region and P1' region enhanced potency of the inhibitors. The binding mode of the PBL prefers the phenyl group :o be occupied in the S2 pocket and the isobutyl group filled in the S1' pocket.

(vi)   Chemically modified tetracyclines (CMT)

CMTs bind to metal ions. The preferred metal ions are Ca^{2+} or Zn^{2+}.

(vii)   Natural inhibitors

Ageadine A is the best known amongst the natural inhibitors for structure-activity relationships of the Succinyl Hydroxamate MMP inhibitors. Pyrrole imidazole alkaloid isolated from marines Agelas sponges has been the most promising anti-cancer agent with potent anti-angiogenic activity. It appears to posses a broad inhibition spectrum.

8.1.5. Destiny of the MMPIs in clinical trials

Preliminary evaluation of most chemotherapeutic agents involves successive dose escalation to identify the maximum-tolerated dose and to describe dose-limiting toxicities. Conversely, because of their non-cytotoxic effects on the tumor, Phase I studies with MMPIs have sought to establish tolerable doses of drug, suitable for protracted administration, that produce serum levels that exceed the inhibitory concentration of targeted MMPs without causing unacceptable normal tissue toxicity. Another formidable challenge faced in the clinical development of MMPIs has been the quantification of anti-

tumor effects. Single-agent phase II clinical trials of new anticancer agents typically have objective response rates as their primary end point [21]. Although preclinical models have demonstrated the impact of MMPIs on delaying growth of the primary tumor, decreasing the number and volume of metastatic lesions, prolonging time to tumor progression or recurrence and increasing life span. The primary impact of MMPIs has not been substantial regression of large primary tumors. Given the limitations of secondary end points of response, the development of MMPIs has proceeded rapidly to Phase III trial design with the end point of survival. Batimastat was the first synthetic MMPI to enter human clinical trials but poor solubility limited oral administration. The Phase I and Phase I/II trials [22] involved intraperitoneal and intrapleural administration to patients with cytology-proven malignant ascites and malignant pleural effusions.

In retrospection, it can be concluded that the lack of efficacy of most MMPIs tested in cancer clinical trials was not surprising [23-24]. It is an established fact that MMPs are vital in the early aspects of cancer progression and their contribution might be minimal once metastases have been generated [25-26]. It is important to design new clinical trials for MMPIs in selected early-stage of cancers in combination with other drugs. Lack of success might also have been a result of problems in the selection of either the inhibitors or the protease targets by preventing autolytic degradation. MMPIs target proteases such as the ADAMTSs, with slow tumor growth through their anti-angiogenic activities [27-28]. Although, the use of these new MMPIs for cancer therapy must be used cautiously, it needs to be noted that many of these paradoxical *in vitro* or animal model results have not been demonstrated in man and might not work once subjected to humans as prescribed drugs.

Other proteases from other families might also be involved and even compensate for MMP actions blocked by MMPIs [29-31]. These proteases should therefore also be identified and targeted in combination therapy.

8.2. Results and Discussion

The exhaustive study of all these small molecule inhibitors has been targeted as the potential therapeutic MMP inhibitors for the varied range of diseases like extracellular matrix degradation or angiogenesis. With the additional knowledge about the potency of these SMIs for the different hMMP isozymes; the rationale for designing the SMIs was to discover a few potent inhibitors that might prove to exhibit preference of one isozyme over the others. In addition, to discover the "drug" that would inhibit MMP isozymes from a pool of pathogenic proteins.

In this project 250 compounds, synthesized by Dr Mallik's laboratory (Department of Pharmaceutical Sciences, NDSU) and Dr Cook's laboratory (Department of Chemistry and Biochemistry, NDSU), were tested as inhibitors with the three hMMP isozymes (hMMP-7, 9 and 10). The enzyme assay was performed under the standard experimental conditions (See Materials and Method Section). For compounds obtained from Dr Mallik's laboratory, the data for hMMP-9 and 10 were taken from Shakila Tobwala's PhD Dissertation [32] and compared and contrasted with the results obtained for hMMP-7 (which was carried out as a part of this project). The idea behind this comparison was to point out the selectivity and preferred potency exhibited by some the SMIs synthesized in Dr Mallik's laboratory, for hMMP-7 as compared to hMMP-9 and 10. For the compounds obtained from Dr Cook's laboratory, assays using hMMP-7, 9 and 10 were carried out as a

part of this dissertation. As an integral part of this project, 24 classes of SMIs were synthesized and screened against the hMMPs. They were classified as: DAPA Hydroxamate inhibitors, Ornithine Hydroxamate inhibitors, Lysine Hydroxamate inhibitors, Miscellaneous Hydroxamate inhibitors, DAPA Carboxylate inhibitors, Ornithine Carboxylate inhibitors, Lysine Carboxylate inhibitors, Cinnamic acid O-Phenylene Diamine Derivative inhibitors, Cinnamic acid O-Phenylene Diamine Cyclene Derivative inhibitors, Urea-2-amino-5 mercapto-Thiadiazole derivative inhibitors, Thio Urea derivative inhibitors, Urea-2-amino-5 mercapto-Thiadiazole Cyclene derivative inhibitors, Mercapto Pyridine derivative inhibitors, Pyrimidine Trione derivative inhibitors, Pyridinol inhibitors, Thioxopyrimidine Dione derivative inhibitors, Phenol derivative inhibitors, Phenyl Sulfonyl derivative inhibitors, Hydrazono Methyl phenol inhibitors, Benzyl Ester inhibitors, Benzamide derivative inhibitors, Benzene Thiol inhibitors, Dimethyl Pyrimidine Trione (DPT) derivative inhibitors.

Figure 8.2 shows the classification of the 24 different classes into these distinct categories and they are further discussed in the Chapter with respect to the selective potency against the different hMMP isozymes. The measurement of the initial velocity of the enzyme reaction was measured from the progress curve and similar experimental conditions were maintained for all the tested SMIs (See Methods Section). In the Tables depicting the results of the different screened inhibitors, NI would stand for "Non-Inhibitory", ND would represent "Not Determined", % respresents the percentage of inhibition observed at 10 µM concentration of the inhibitor and the numerical values represents the K_i values in µM.

Figure 8.2. Classification of the different classes of the small molecule MMP isozyme inhibitors screened by the high throughput screening of this study.

DAPA Hydroxamate Inhibitors

DAPA Carboxylate Inhibitors

Mercapto Pyridine Derivative Inhibitors

Ornithine Hydroxamate Inhibitors

Ornithine Carboxylate Inhibitors

Pyrimidine Trione Derivative Inhibitors

Pyridinol Inhibitors

Lysine Carboxylate Inhibitors

Lysine Hydroxamate Inhibitors

Thioxopyrimidine Dione Derivative Inhibitors

MMP INHIBITORS

Miscellaneous Hydroxamate Inhibitors

Phenol Derivatives Inhibitors

Phenyl Sulfonyl Derivative Inhibitors

Methyl Red Inhibitors

Urea 2-Amino-5-Mercapto -Thiadiazole Derivatives Inhibitors

Hydrazono Methyl Phenol Inhibitors

Benzyl Ester Inhibitors

Cinnamic Acid O-Phenylene Diamine Derivatives Inhibitors

Thio Urea Derivative Inhibitors

Benzamide Derivative Inhibitors

Benzene Thiol Inhibitors

Cinnamic Acid O-Phenylene Diamine Cyclene Derivatives Inhibitors

Urea 2-Amino-5-Mercapto -Thiadiazole Cyclene Derivatives Inhibitors

Dimethyl Pyrimidine Trione Derivatives [DPT] Inhibitors

Figure 8.3 shows the Inhibition constant (K_i) of hMMP-7 with DAPA Hydroxamate

inhibitors. The K_i values for RS-V-93, RS-V-90 and RS-II-75 are 6.0 ± 0.9 µM, 0.6 ± 0.08
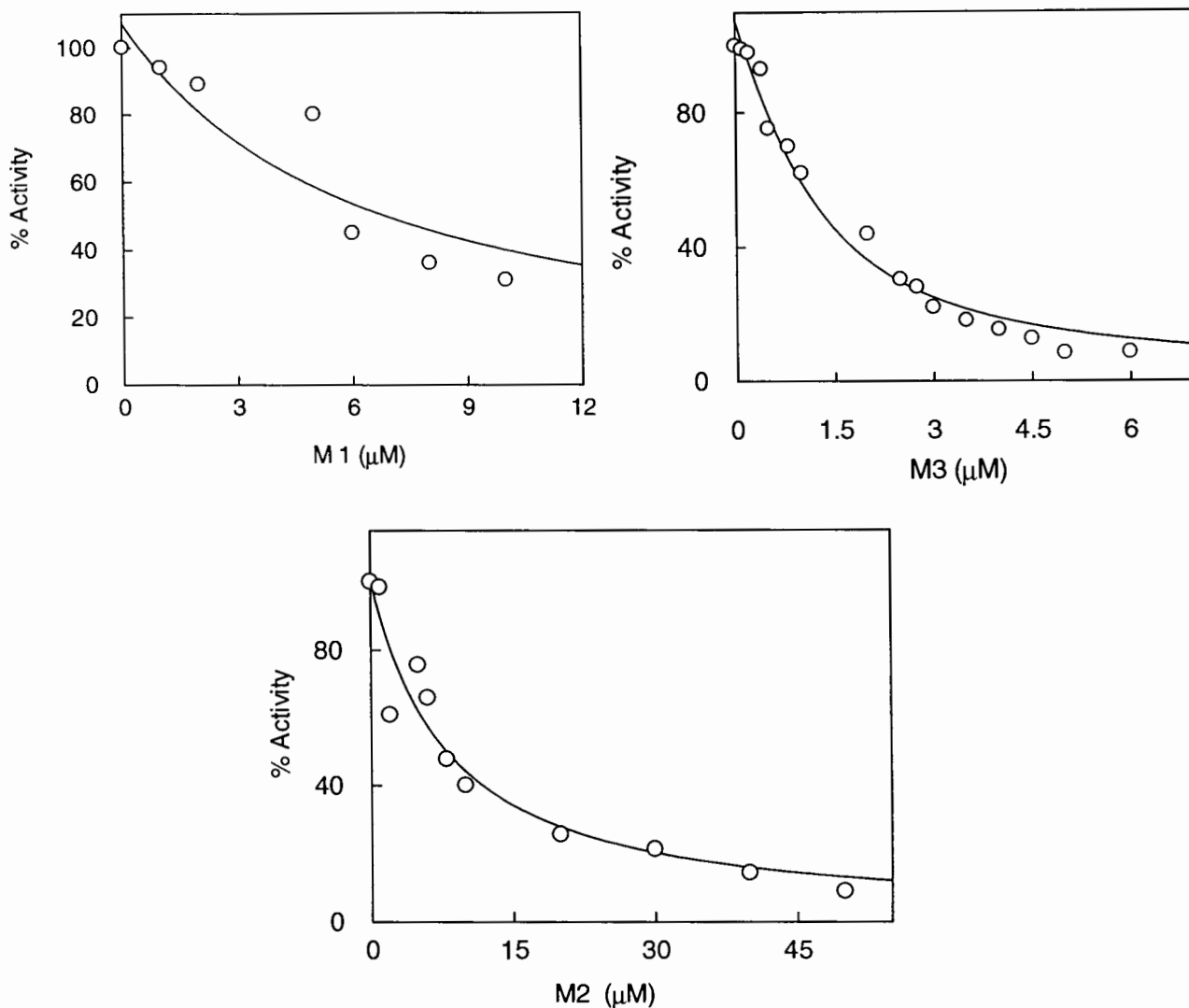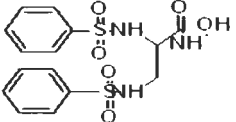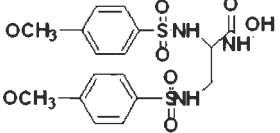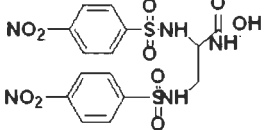
µM and 10 ± 0.1 µM, respectively.
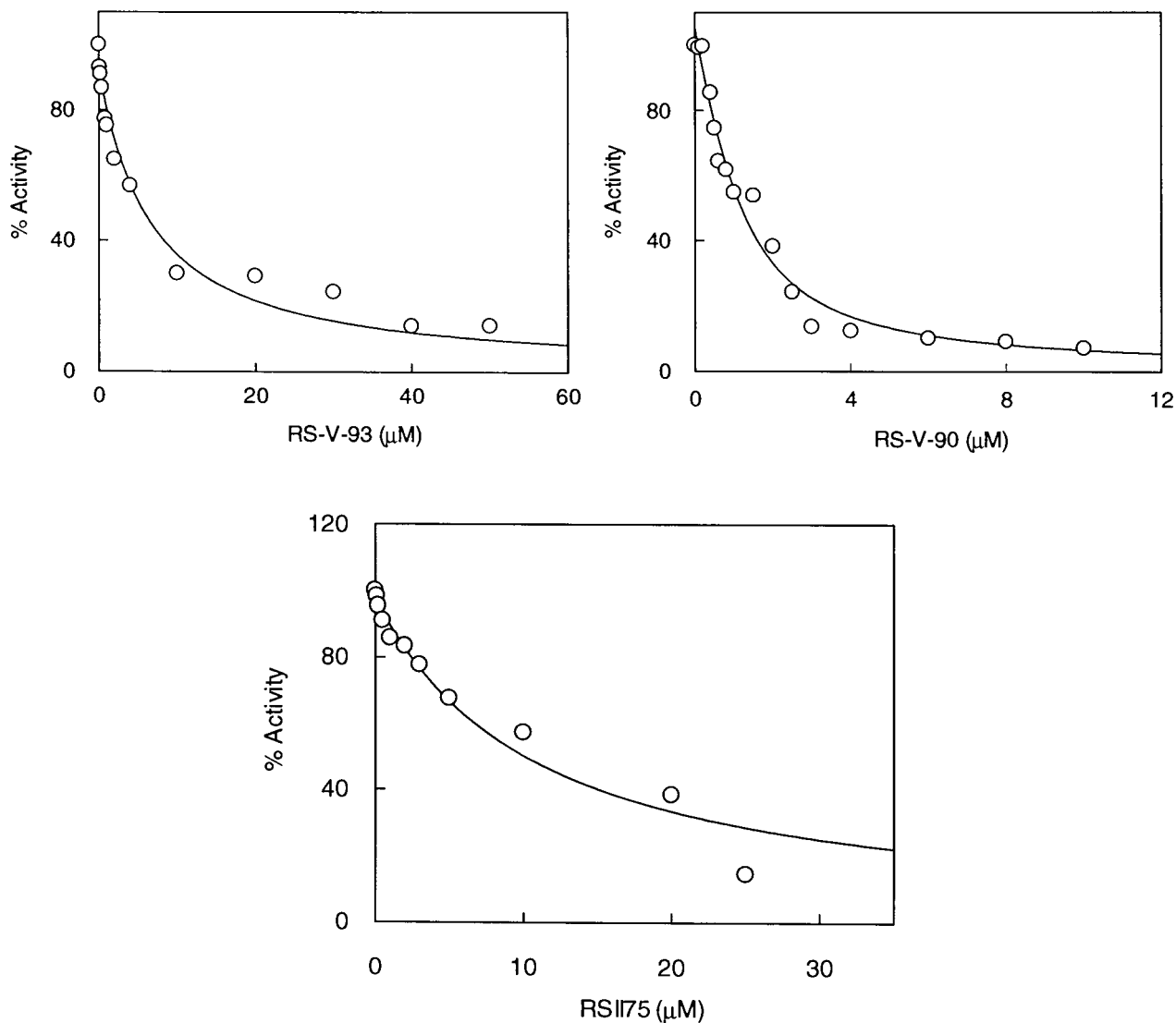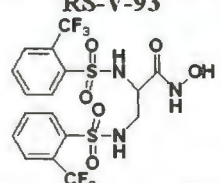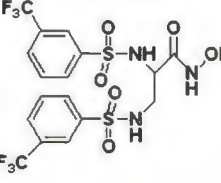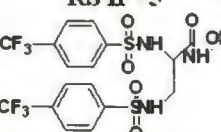
Figure 8.3. Determination of the inhibition constant (K_i) of hMMP-7 with DAPA Hydroxamate inhibitors. Steady state kinetic reactions of hMMP-7 for DAPA Hydroxamate inhibitors. The initial rates of the enzyme catalyzed hydrolysis reaction of TPL substrate were measured as a function of increasing concentration of inhibitor. [hMMP-7] = 0.3 µM, [TPL] = 20 µM. The solid smooth line is the best fit of the data according to Eq 3.10. The K_i values for RS-V-93, RS-V-90 and RS-II-75 are 6.0 ± 0.9 µM, 0.6 ± 0.08 µM and 10 ± 0.1 µM, respectively.

Table 8.1 shows the comparative account of the three different compounds, RS-V-93, RS-V-90 and RS-II-75. It has been very evident that the position of the CF_3 group dictates the inhibition constant (K_i) in the Table. In the case of RS-V-93, RS-V-90 and RS-II-75, CF_3 has been placed in the ortho, meta and para positions, respectively. The functional group in consideration here is an electron donating group. As observed, the functional group present at the ortho and para positions was not potent inhibitors of hMMP-7, while the meta position acted as a very potent inhibitor. When comparisons were sorted with the other two hMMP isozymes, it became obvious that RS-V-93 and RS-V-90 only inhibited hMMP-7. RS-II-75 inhibited hMMP-7 and 9 with comparable potency as compared to hMMP-10. Upon closer comparison of RS-V-93 and RS-V-90 with hMMP-7, it was noticed that the same group (CF_3 group) when placed in two different positions inhibited by ten-fold more potency. The logical reason for this would be that it is only at the meta position where the functional group gets enough temporal space to form an additional hydrogen bond with the enzyme to stabilize it more inside the active site. The CF_3 moieties in the other positions: (1) at the ortho position is pushed to the wall of the enzyme active site due to steric hindrance; and (2) at the para position, the distance restricted the formation of the hydrogen bond. Hence, the meta position was preferred over the other two positions.

Figure 8.4.A, B and C shows the Gaussian view of the three CF_3 DAPA Hydroxamate inhibitors. Amongst computational methods available for the estimation of the interaction between two molecules, molecular mechanics or electronic structure methods are the most preferred.
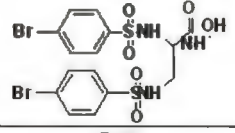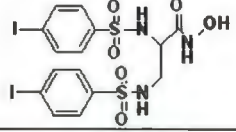
295

Table 8.1. Structures and inhibitory properties of DAPA Hydroxamate derivative inhibitors. The data shown for hMMP-9 and 10 were obtained from Reference 32.

Hydroxamates [DAPA]	MMP-7	MMP-9	MMP-10
RS-V-93	6.0	NI	NI
RS-V-90	0.602	NI	NI
RS II 75	10	7.9	23
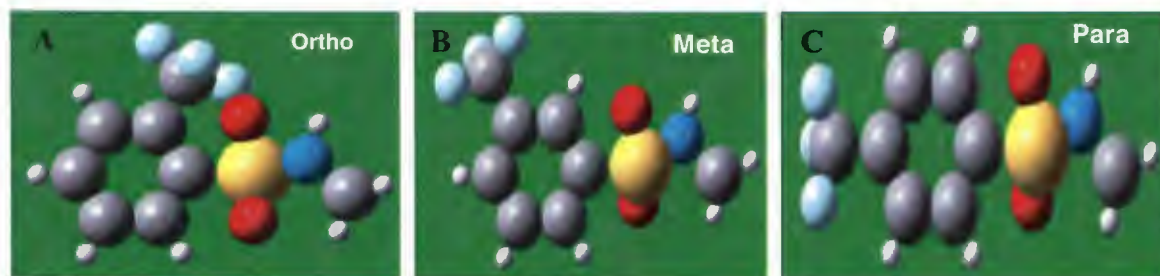
Figure 8.4.A. The Gaussian view of the ortho CF_3 DAPA Hydroxamate inhibitor. B. The Gaussian view of the meta CF_3 DAPA Hydroxamate inhibitor. C. The Gaussian view of the para CF_3 DAPA Hydroxamate inhibitor.

The most simple and easiest method to obtain the spatio-temporal distribution of the functional groups as well as their individual distribution, which dictated the dynamics of the interactions between the enzyme and the inhibitor side groups and accomodated their geometry optimization inside the enzyme active site cavity, was captured by the Gaussian 3.0 software package [33]. The parameters used render these methods computationally are

in-expensive, making them suited for small and large systems where other methods are not very practical and sensitive [34]. These data further supports and elaborate on the already explained inhibition data.

Figure 8.5 shows the inhibition constants (K_i) of hMMP-7 with three other DAPA Hydroxamate inhibitors. The K_i values for RS-II-19, RS-II-33 and RS-II-31 are 2.8 ± 0.18 μM, 0.521 ± 0.6 μM and 6.6 ± 0.03 μM, respectively. Table 8.2, as shown in RS-II-19, RS-II-33 and RS-II-31 have a non-substituted benzene ring and para-methoxy and para-nitro functional groups attached, respectively. In the case of hMMP-7 the methoxy at the para position behaves as a potent inhibitor. This trend is followed by the benzene non-substitute benzene derivatives and then the para-nitro containing derivatives. Since, a methoxy group is an electron-donating group whereas a nitro group is electron-withdrawing group, the more electron density near the sulfonyl group (as RS-II-19), allows a better and stronger hydrogen bond to be formed, thereby making a more potent inhibitor. Another striking feature observed here is that the worst hydrogen acceptor results in a poor inhibitor. A similar trend has been observed for hMMP-9 and 10.

Figure 8.6 shows the inhibition constant (K_i) of hMMP-7 with these then DAPA Hydroxamate inhibitors. The K_i values for M3, M1 and M2 are 0.24 ± 0.07 μM, 5.5 ± 0.12 μM and 1.3 ± 0.15 μM, respectively. The structures and inhibition constants are being shown in Table 8.3. According to the Periodic Table, all the functional groups attached in the para positions are electron withdrawing halides, from the smallest fluoride to the biggest iodide ion and electronegativity decreases as the size of the halide increases.
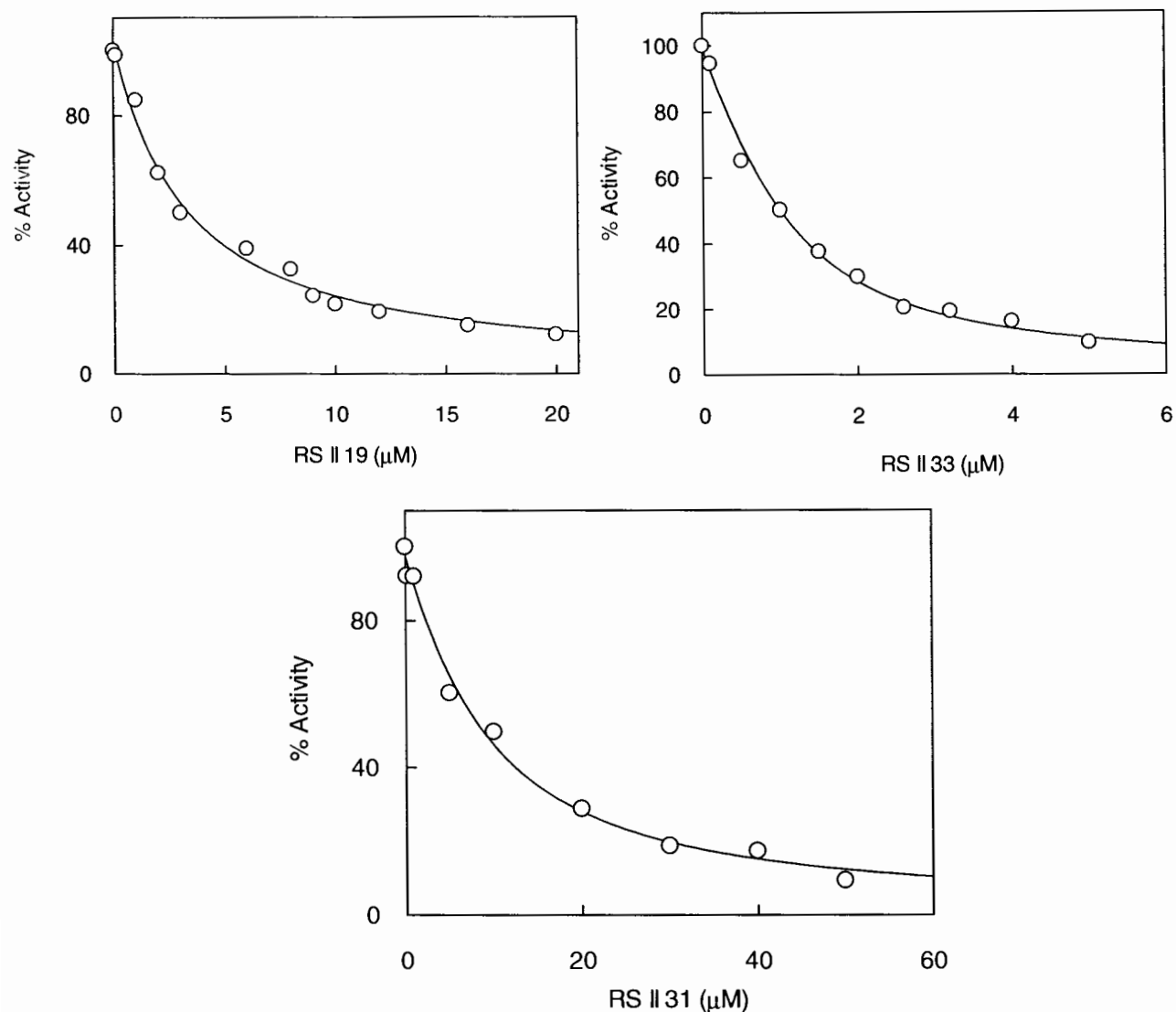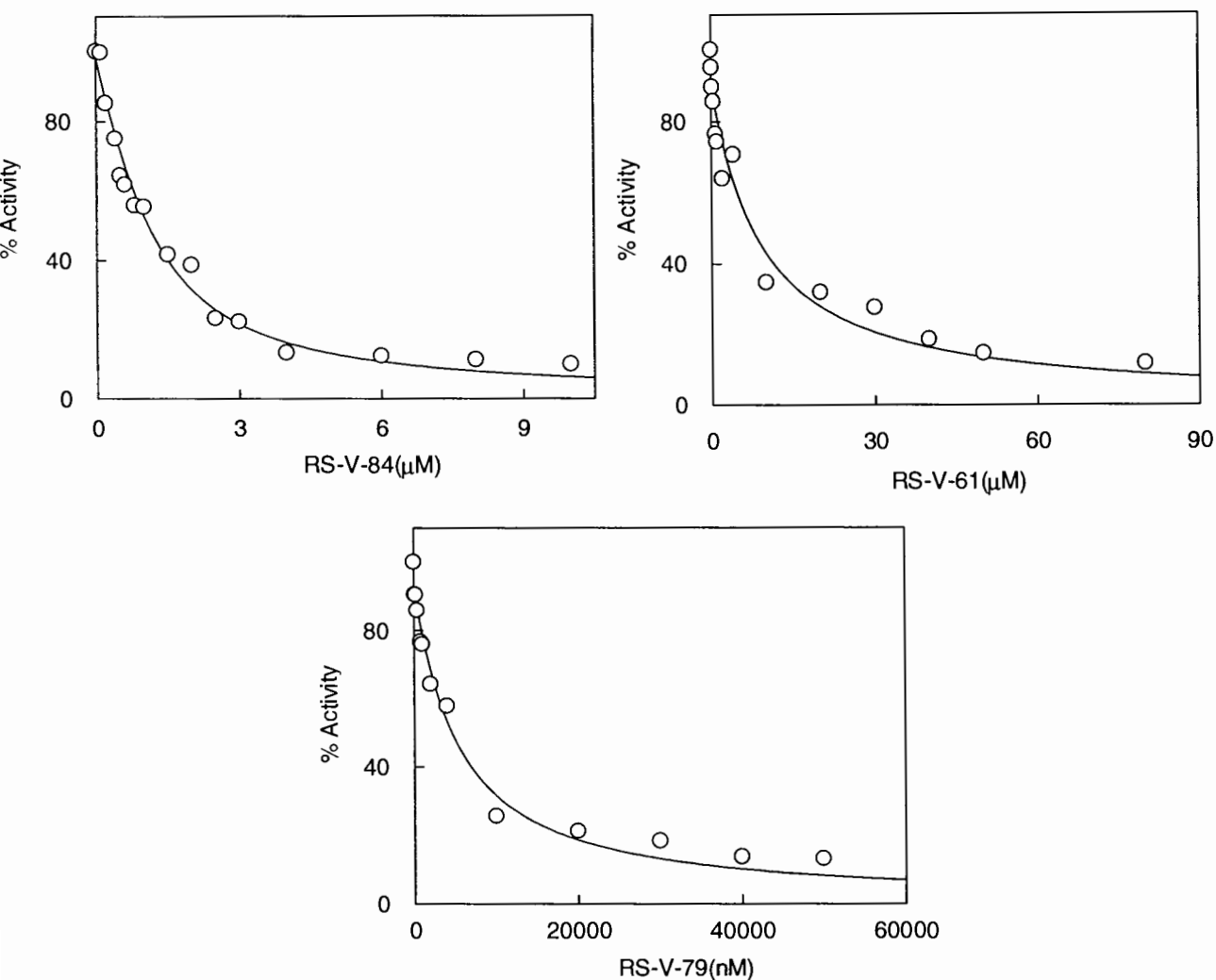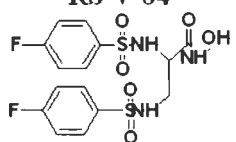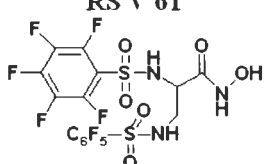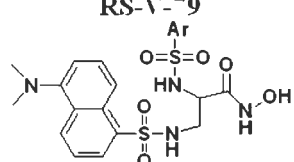
Figure 8.5. Determination of the inhibition constant (K_i) of hMMP-7 with DAPA Hydroxamate inhibitors. Steady state kinetic reactions of hMMP-7 for DAPA Hydroxamate ihibitors. The initial rates of the enzyme catalyzed hydrolysis reaction of TPL substrate were measured as a function of increasing concentration of inhibitor. [hMMP-7] = 0.3 μM, [TPL] = 20 μM. The solid smooth line is the best fit of the data according to Eq 3.10. The K_i values for RS-II-19, RS-II-33 and RS-II-31 are 2.8 ± 0.18 μM, 0.5 ± 0.6 μM & 6.6 ± 0.03 μM, respectively.

298

Figure 8.6. Determination of the inhibition constant (K$_i$) of hMMP-7 with DAPA Hydroxamate inhibitors. Steady state kinetic reactions of hMMP-7 for DAPA Hydroxamate inhibitors. The initial rates of the enzyme catalyzed hydrolysis reaction of TPL substrate were measured as a function of increasing concentration of inhibitor. [hMMP-7] = 0.3 μM, [TPL] = 20 μM. The solid smooth line is the best fit of the data according to Eq 3.10. The K$_i$ values for M3, M1 and M2 are 0.24 ± 0.07 μM, 5.5 ± 0.12 μM and 1.3 ± 0.15 μM, respectively.

299
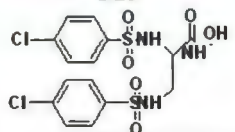
Table 8.2. Structures and inhibitory properties of DAPA Hydroxamate derivative inhibitors. The data shown for hMMP-9 and 10 were obtained from Reference 32.

Hydroxamates [DAPA]	MMP-7	MMP-9	MMP-10
RS II 19	2.8	0.227	0.356
RS 33	0.521	0.039	0.355
RS 31	6.6	1.7	22

Equipped with the knowledge of the pocket sizes of hMMP-7, 9 and 10 active sites [35], hMMP-7 is the smallest and most hydrophilic pocket, and thus, the smallest halide containing inhibitor is favored. For hMMP-10, a similar scenario is indicated as that of hMMP-7 but in the case of hMMP-9, which has a long, hydrophilic pocket, the larger halide-containing inhibitor is preferred.

Figure 8.7.A shows the Gaussian view of the basic structure. Figure 8.7.B shows the Gaussian view of the iodo Hydroxamate inhibitor. This illustration supports the kinetic data and gives a dimensional arrangement of the different molecules of the inhibitor in space. Figure 8.8 shows the inhibition constant (K_i) of hMMP-7 with DAPA Hydroxamate inhibitors. The K_i values for RS-V-84, RS-V-61 and RS-V-79 are 0.63 ± 0.07 µM, 8.6 ± 0.15 µM and 4.8 ± 0.6 µM, respectively. Table 8.4 shows the inhibition constant (K_i) of hMMP-7 with DAPA Hydroxamate inhibitors.

Table 8.3. Structures and inhibitory properties of DAPA Hydroxamate derivative inhibitors. The data shown for hMMP-9 and 10 were obtained from Reference 32.

Hydroxamates [DAPA]	MMP-7	MMP-9	MMP-10
M3	0.24	0.23	0.6
M1	5.5	0.15	1.33
M2	1.3	0.0026	1.6
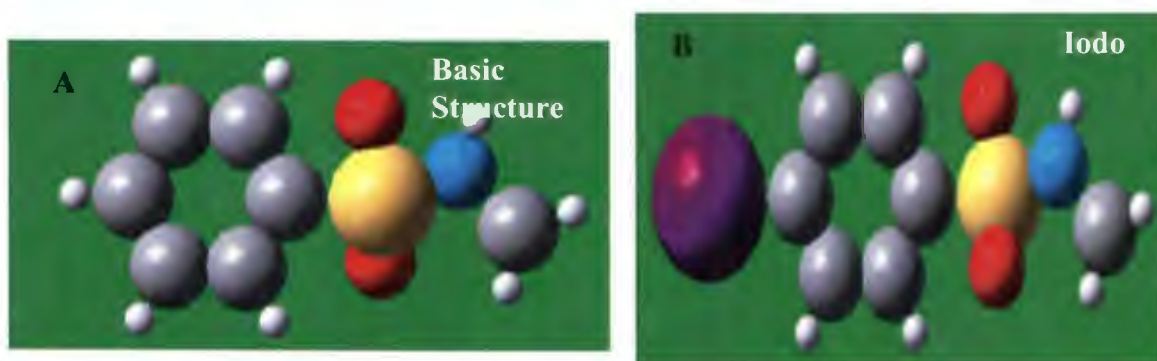
Figure 8.7.A. The Gaussian view of the basic structure. B. The Gaussian view of the iodo Hydroxamate inhibitors.

In Table 8.4 the RS-V-84 bears the fluoride groups at the para position; RS-V-61 bears many fluorides while RS-V-79 bears the di-methyl amine at the para position. The electronics, steric hindrance and additional hydrogen bonds were responsible for the high potency of RS-V-84 for hMMP-7. For hMMP-9, RS-V-61 and RS-V-79 are very poor inhibitors due to the bulky groups attached to the parent compound. But for hMMP-7 and

301

10 these inhibitors are better due to the small size of the pockets, which can be easily obstructed by this group of inhibitors.

Figure 8.9 shows the inhibition constant (K_i) of hMMP-7 with Ornithine Hydroxamate inhibitors. The K_i value of hMMP-7 for RS-V-99 is 5.0 ± 0.69 μM. Table 8.5 summarizes the inhibition of the isozymes by Ornithine Hydroxamate inhibitors. Unlike the DAPA halide containing Hydroxyl derivatives, in the group of Ornithine Hydroxamate inhibitors RS-V-99 acts as a potent inhibitor of hMMP-7 only. Figure 8.10.A and 8.10.B shows the Gaussian view of the Flouro and Iodo forms of the Ornithine Hydroxamate inhibitors. Figure 8.10.C shows the active site of hMMP-7 exhibiting the small pocket of the enzyme. Figure 8.11 shows the inhibition constant (K_i) of hMMP-7 with Ornithine Hydroxamate inhibitors. The K_i value for RS-II-80 is 7.0 ± 0.61 μM. Table 8.6 shows the inhibition constant (K_i) of hMMP-7 with Ornithine Hydroxamate inhibitors. RS-II-80 is the most potent inhibitor for hMMP-7 whereas for hMMP-9 and 10 the same inhibitor is a very poor inhibitor. RS-II-41 inhibits hMMP-9 and 10 to a moderate extent.

Figure 8.12 shows the inhibition constant (K_i) of hMMP-7 with Lysine Hydroxamate inhibitors. The K_i values for RS-VI-24 and RS-VI-22 are 3.1 ± 0.96 μM and 2.2 ± 0.37 μM, respectively. Table 8.7 shows the structure of the Lysine Hydroxamate inhibitors. Amongst all the functional groups only the fluoride and bromide Lysine Hydroxamate inhibitors are potent inhibitors of hMMP-7. CF_3 is a big molecule compared to the active site pocket of hMMP-7, and is a good inhibitor which blocks the small pocket very easily.
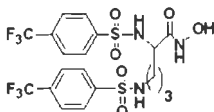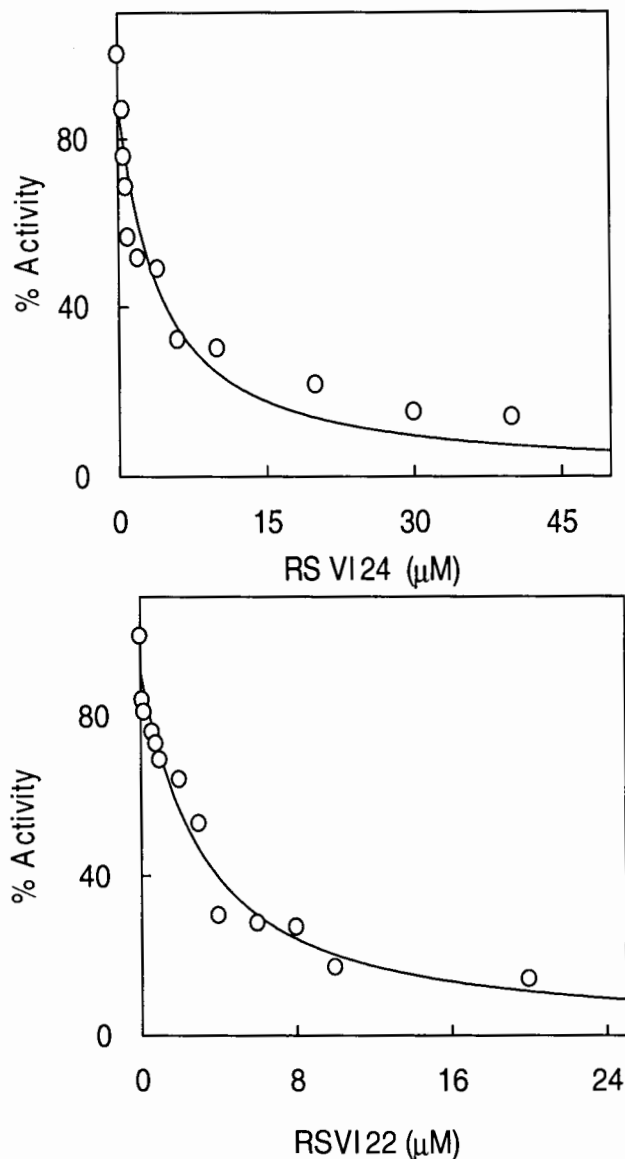
Figure 8.8. Determination of the inhibition constant (K_i) of hMMP-7 with DAPA Hydroxamate inhibitors. Steady state kinetic reactions of hMMP-7 for DAPA Hydroxamate inhibitors. The initial rates of the enzyme catalyzed hydrolysis reaction of TPL substrate were measured as a function of increasing concentration of inhibitor. [hMMP-7] = 0.3 μM, [TPL] = 20 μM. The solid smooth line is the best fit of the data according to Eq 3.10. The K_i values for RS-V-84, RS-V-61 and RS-V-79 are 0.63 $\pm$ 0.07 μM, 8.6 $\pm$ 0.15 μM & 4.8 $\pm$ 0.6 μM, respectively.

Table 8.4. Structures and inhibitory properties of DAPA Hydroxamate derivative inhibitors. The data shown for hMMP-9 and 10 were obtained from Reference 32.
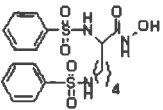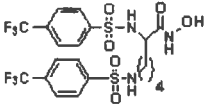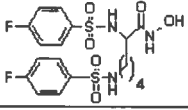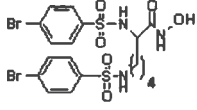
Hydroxamates [DAPA]	MMP-7	MMP-9	MMP-10
RS-V-84	0.625	2.75	4.57
RS-V-61	8.6	212	NI
RS-V-99	4.8	150	20
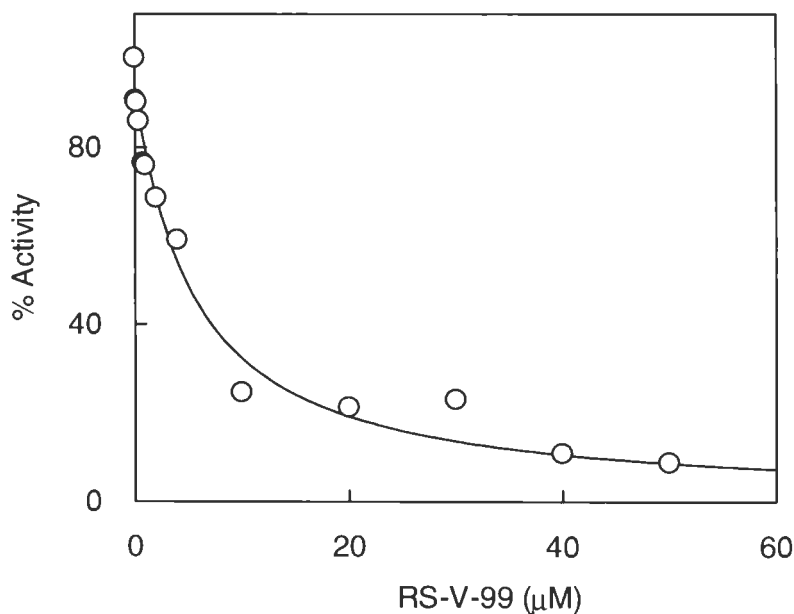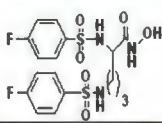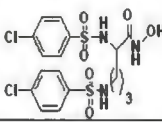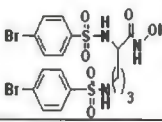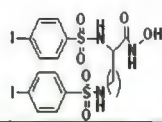
Figure 8.9. Determination of the inhibition constant (K_i) of hMMP-7 with Ornithine Hydroxamate inhibitor RS-V-99. Steady state kinetic reactions of hMMP-7 for Ornithine Hydroxamate inhibitor. The initial rates of the enzyme catalyzed hydrolysis reaction of TPL substrate were measured as a function of increasing concentration of inhibitor. [hMMP-7] = 0.3 μM, [TPL] = 20 μM. The solid smooth line is the best fit of the data according to Eq 3.10. The K_i value for RS-V-99 is 5.0 ± 0.69 μM.

304

Table 8.5. Structures and inhibitory properties of the Ornithine Hydroxamate derivative inhibitors. The data shown for hMMP-9 and 10 were obtained from Reference 32.

Hydroxamates [ORNITHINE]	MMP-7	MMP-9	MMP-10
RS-VI-19	17%	NI	20%
RS-VI-01	9%	NI	34.5
RS-VI-17	32%	9.3%	16.4%
RS V 99	5.0	221	NI

Para Fluoro Ornithine

Para Iodo Ornithine
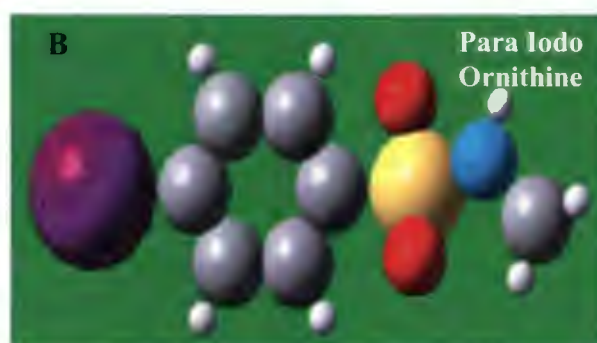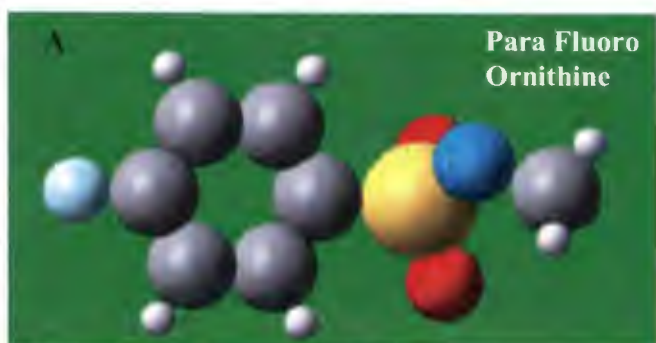
MMP-7 active site Pocket

Figure 8.10.A. The Gaussian view of the flouro form of Ornithine Hydroxamate inhibitor. B. The Gaussian view of the iodo form Ornithine Hydroxamate inhibitor. C. The active site of MMP-7. This figure is shown adapted from Reference 35.
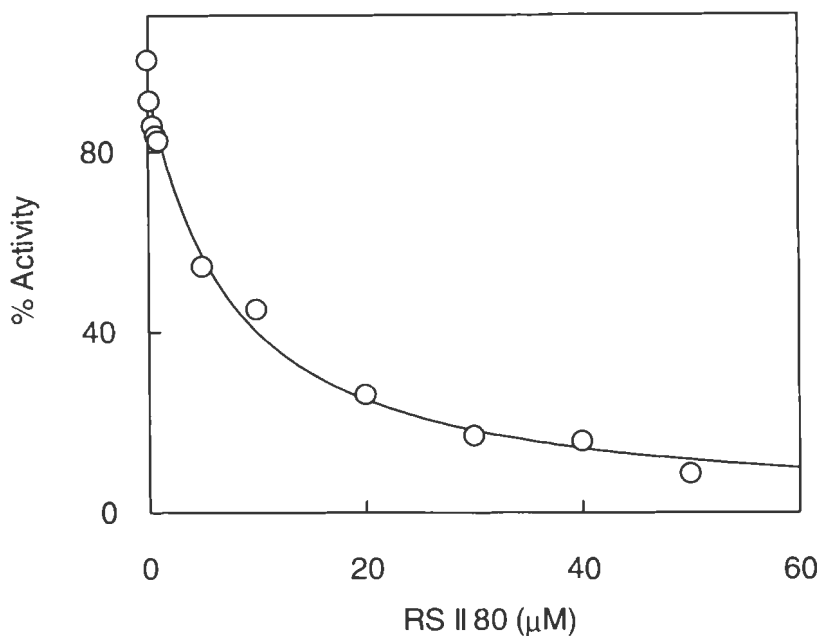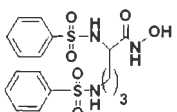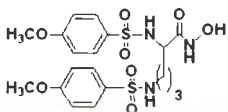
Figure 8.11. Determination of the inhibition constant (K_i) of hMMP-7 with the Ornithine Hydroxamate inhibitor of RS-II-80. Steady state kinetic reactions of hMMP-7 for the Ornithine Hydroxamate inhibitor. The initial rates of the enzyme catalyzed hydrolysis reaction of TPL substrate were measured as a function of increasing concentration of inhibitor. [hMMP-7] = 0.3 μM, [TPL] = 20 μM. The solid smooth line is the best fit of the data according to Eq 3.10. The K_i value for RS-Il-80 is 7.0 ± 0.61 μM.

Table 8.6. Structures and inhibitory properties of the Ornithine Hydroxamate derivative inhibitors. The data shown for hMMP-9 and 10 were obtained from Reference 32.
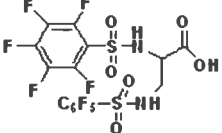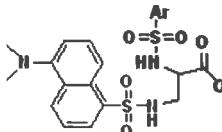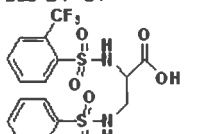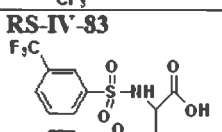
Hydroxamates [ORNITHINE]	MMP-7	MMP-9	MMP-10
RS 42	NI	NI	NI
RS 41	NI	4.2	16
RS II 80	7.0	329	337

306

Figure 8.12. Determination of the inhibition constant (K_i) of hMMP-7 with Lysine Hydroxamate inhibitors RS-VI-24 and RS-VI-22. Steady state kinetic reactions of hMMP-7 for Ornithine Hydroxamate inhibitors. The initial rates of the enzyme catalyzed hydrolysis reaction of TPL substrate were measured as a function of increasing concentration of inhibitor. [hMMP-7] = 0.3 μM, [TPL] = 20 μM. The solid smooth line is the best fit of the data according to Eq 3.10. The K_i values for RS-VI-24 and RS-VI-22 are 3.1 ± 0.96 μM and 2.2 ± 0.37 μM, respectively.

Table 8.8 shows the comparative account of DAPA, Ornithine and Lysine Hydroxamate inhibitors of hMMP-7. In the case of DAPA Hydroxamate inhibitors the

307

fluoro and the iodo functional group conjugated inhibitors proved to be very potent while the bromo inhibitor inhibits moderately. In case of Ornithine Hydroxamate inhibitors only the iodo form was a good inhibitor. In case of Lysine Hydroxamate inhibitors, the fluoro and bromo inhibitors were fair inhibitors of hMMP-7. The extra CH_2 group acts as a long spacer and helps in the formation of an additional hydrogen bond.

Table 8.7. Structures and inhibitory properties of the Lysine Hydroxamate derivative inhibitors. The data shown for hMMP-9 and 10 were obtained from Reference 32.
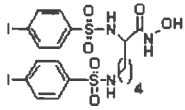
Hydroxamates [Lys]	MMP-7	MMP-9	MMP-10
RS-VI-54	44%	7.5%	34.5%
RS-VI-13	24%	NI	NI
RS-VI-24	3.1	NI	27.4%
RS-VI-22	2.2	NI	34.5
RS-VI-21	46%	NI	30.9%

Table 8.8. Comparative account of the DAPA, Ornithine, and Lysine Hydroxamate inhibitors with hMMP-7.

	DAPA	ORNI	LYS
FLUORO	Good	Poor	Fair
BROMO	Fair	Poor	Fair
IODO	Good	Good	Poor

308

Figure 8.13 shows the representation of the rearrangement of Enzyme-Inhibitor subunits binding pockets in presence of DAPA Hydroxamate inhibitors, Ornithine Hydroxamate inhibitors, and Lysine Hydroxamate inhibitors. It seems logical to imagine that while binding to hMMP-7, the R_α side chain of the DAPA Hydroxamate inhibitors would be placed at the S1 pocket and R_β side chain at the S1' pocket. With the Ornithine Hydroxamate inhibitors, the R_α side chain would be placed at the S1' pocket and R_δ side chain was exposed at the solvent and last but not the least, with the Lysine Hydroxamate inhibitors, the R_α side chain at the S1' pocket and R_ω side chain exposed in the solvent. Therefore, it was concluded that as the spacer length increased, the side chain gets more and more pushed to the solvent due to steric hindrance and thereby forms a less stabilized Enzyme-Inhibitor complex.

DAPA Hydroxamate

Ornithine Hydroxamate

Lysine Hydroxamate
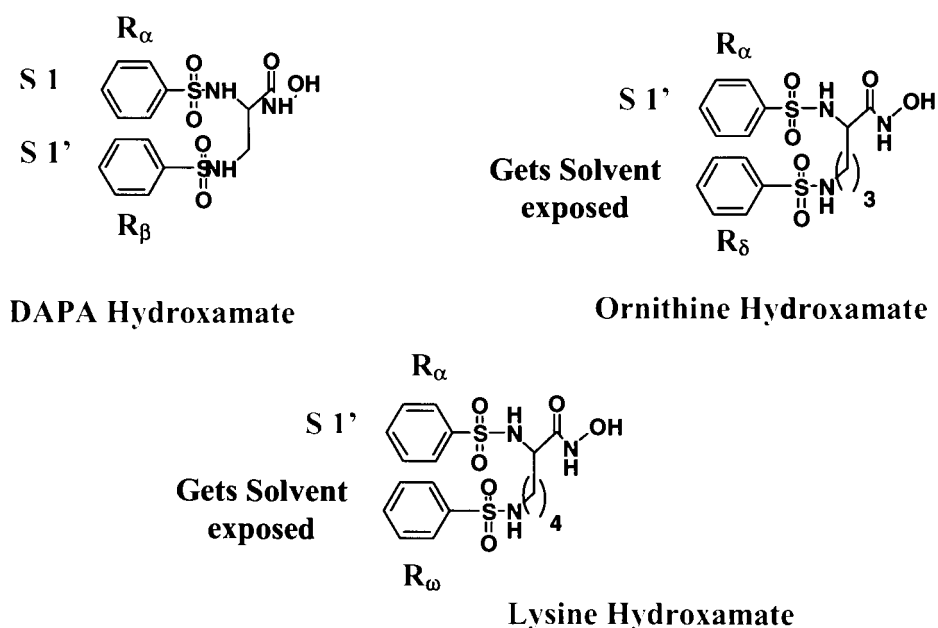
Figure 8.13. Representation of the rearrangement of Enzyme-Inhibitor subunits binding pockets in presence of DAPA Hydroxamates inhibitors, Ornithine Hydroxamates inhibitors and Lysine Hydroxamates inhibitors.

Table 8.9 shows the structures of the four DAPA Carboxylate inhibitors which show the poor potency as compared to the DAPA Hydroxamate inhibitors. All the functional groups are bulky in this category.

Table 8.9. Structures and inhibitory properties of DAPA Carboxylate derivative inhibitors. The data shown for hMMP-9 and 10 were obtained from Reference 32.
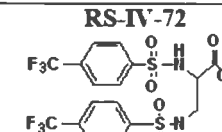
Carboxylates [DAPA]	MMP-7	MMP-9	MMP-10
RS-IV-53	NI	NI	NI
RS-IV-64	10%	NI	16%
RS-IV-87	NI	NI	34%
RS-IV-83	NI	NI	35%
RS-IV-72	1%	NI	7%

Figure 8.14 shows the inhibition constant (K_i) of hMMP-7 with DAPA Carboxylate inhibitor RS-III-77. The K_i value for RS-III- 77 is 0.327 ± 0.075 µM. Amongst all the halides in the group (Table 8.10), and even though the functional group is conjugated with a bulky group, it still acts as a very good inhibitor for hMMP-7. This is unlike the condition

observed in Table 8.9. The CF_3 group is more electron withdrawing than the Iodo group. The balance of the electonics and size of the functional groups played key roles in the potency of this inhibitor.
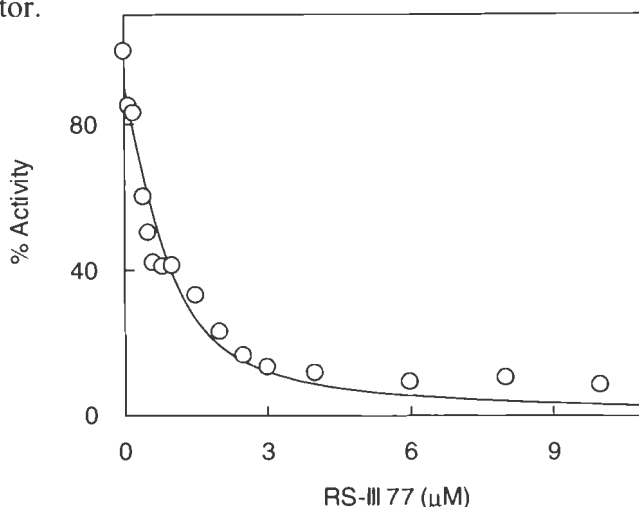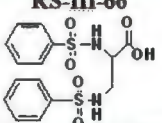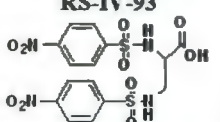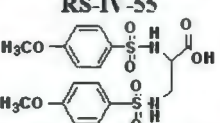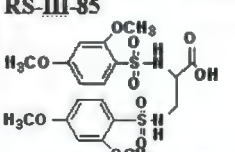
RS-III 77 (μM)

Figure 8.14. Determination of the inhibition constant (K_i) of hMMP-7 with DAPA Carboxylate inhibitor RS-III-77. Steady state kinetic reactions of hMMP-7 for the Ornithine Hydroxamate inhibitor. The initial rates of the enzyme catalyzed hydrolysis reaction of TPL substrate were measured as a function of increasing concentration of inhibitor. [hMMP-7] = 0.3 μM, [TPL] = 20 μM. The solid smooth line is the best fit of the data according to Eq 3.10. The K_i values for RS-III- 77 is   0.33 ± 0.08 μM.

Table 8.10. Structures and inhibitory properties of DAPA Carboxylate derivative inhibitors. The data shown for hMMP-9 and 10 were obtained from Reference 32.
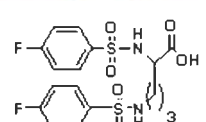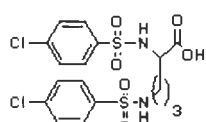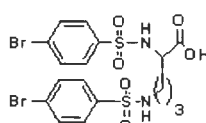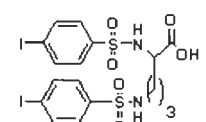
Carboxylates [DAPA]	MMP-7	MMP-9	MMP-10
RS-IV-2⁻	4%	NI	15.5%
RS-III-8⁻	10%	NI	10.9
RS-III-83	20%	5.6%	9.6
RS-III-⁻⁻	0.327	0.936	65

311

Table 8.11 shows the structures of more of DAPA Carboxylate derivative inhibitors. Only RS-IV-55 shows a fair potent inhibition of hMMP-10. Figure 8.15.A and 8.15.B show the Gaussian views of the para and iodo of the CF$_3$ of the Carboxylate inhibitor.

Table 8.11. Structures and inhibitory properties of DAPA Carboxylate derivative inhibitors. The data shown for hMMP-9 and 10 were obtained from Reference 32.
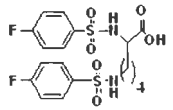
Carboxylates [DAPA]	MMP-7	MMP-9	MMP-10
RS-III-66	NI	NI	25%
RS-IV-93	6%	NI	NI
RS-IV-55	NI	NI	12.8
RS-III-85	ND	ND	ND
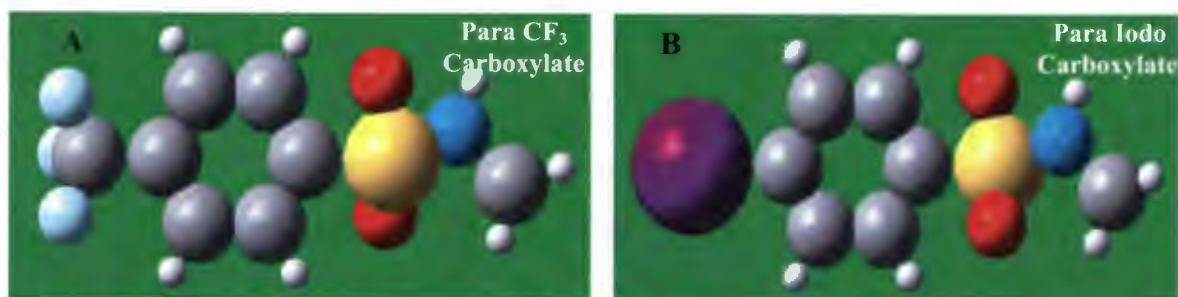
Figure 8.15.A. The Gaussian view of the para CF$_3$ of Carboxylate inhibitor. B. The Gaussian view of the iodo form DAPA Carboxylate inhibitor.

Table 8.12 and 8.13 show the structures and properties of more of the Ornithine Carboxylate inhibitors. Only RS-V-64 shows fair potency with hMMP-10, but it is not a good inhibitor for hMMP-7 and 9. Table 8.14 shows the structures and properties of the Lysine Carboxylate inhibitors.

Table 8.12. Structures and inhibitory properties of Ornithine Carboxylate derivative inhibitors. The data shown for hMMP-9 and 10 were obtained from Reference 32.
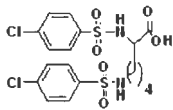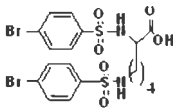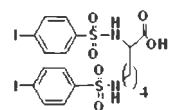
Carboxylates[ORNITHINE]	MMP-7	MMP-9	MMP-10
RS-V-83	7%	NI	14.5%
RS-V-80	19%	10%	50%
RS-V-64	25%	25.6%	4.9
RS-V-60	26%	42%	38%

Table 8.15 shows the comparative account of DAPA, Ornithine and Lysine Carboxylate inhibitors. Unlike Hydroxamate inhibitors, only Carboxylate inhibitors only the Iodo form behave as a potent inhibitor. The DAPA Carboxylate inhibitor shows the

most potency but the other two forms (e.g. the Ornithine and the Lysine) are poor inhibitors.

Table 8.13. Structures and inhibitory properties of Ornithine Carboxylate derivative inhibitors. The data shown for hMMP-9 and 10 were obtained from Reference 32.
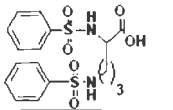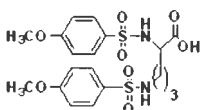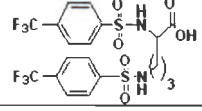
Carboxylates [Lys]	MMP-7	MMP-9	MMP-10
RS-VI-07	ND	ND	ND
RS-VI-03	9%	10%	25%
RS-V-100	14%	18.6%	NI
RS-V-97	15%	27%	4.1

Table 8.14. Structures and inhibitory properties of Lysine Carboxylate derivative inhibitors. The data shown for hMMP-9 and 10 were obtained from Reference 32.

Carboxylates[ORNITHINE]	MMP-7	MMP-9	MMP-10
RS-V-27	22%	43.4%	5.2
RS-V-29	19%	NI	28%
RS-V-92	NI	NI	28%

Table 8.15. Comparative account of the DAPA, Ornithine and Lysine Carboxylate inhibitors with hMMP-7.

	DAPA	ORNI	LYS
IODO	Good	Fair	Poor

Figure 8.16 shows the structure of Hydroxamates that form the five membered ring indicating more stability compared to the Carboxylates, which exist as a four membered ring. Innate differences in the structural stability of the inhibitors in the active-site pocket gave rise to the differences in the potency and variety in the inhibition pattern.

5 member ring   **4 member ring**
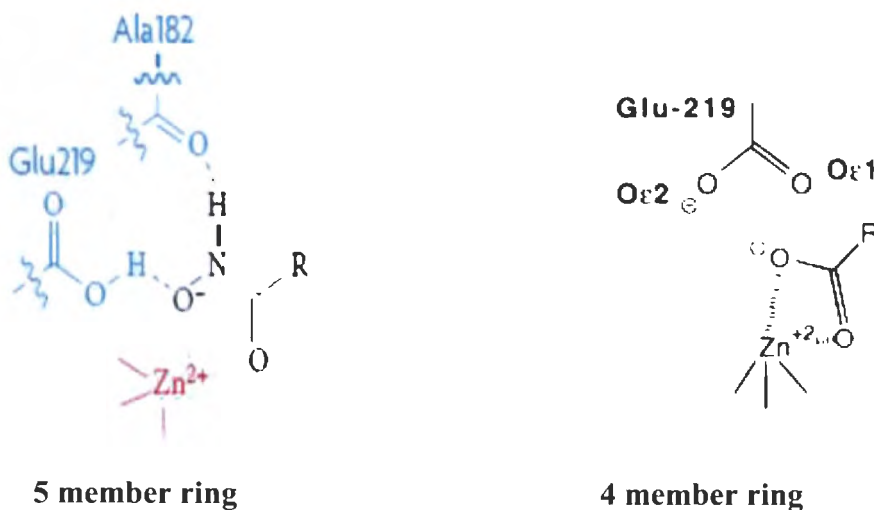
Figure 8.16. Structure of Hydroxamates form the 5 member ring indicating more stability compared to the Carboxylates 4 member ring. This figure has been adapted from Reference 404-405.

Figure 8.17 shows the inhibition constant (K_i) of hMMP-7 with the Miscellaneous Hydroxamate inhibitor for MH 9/14B. The K_i value for MH 9/ 14 B is 10.8 ± 0.83 µM. Table 8.16 shows the structures ans properties of the Miscellaneous inhibitors. None of the compounds in this category are good inhibitors except for MH 9/14 B, which seems to be a

fair inhibitor for hMMP-7. Table 8.17 shows the inhibition constant (K_i) of hMMP-7 with Methyl Red inhibitors. Neither of the inhibitors were good inhibitors for any of the hMMP isozymes.
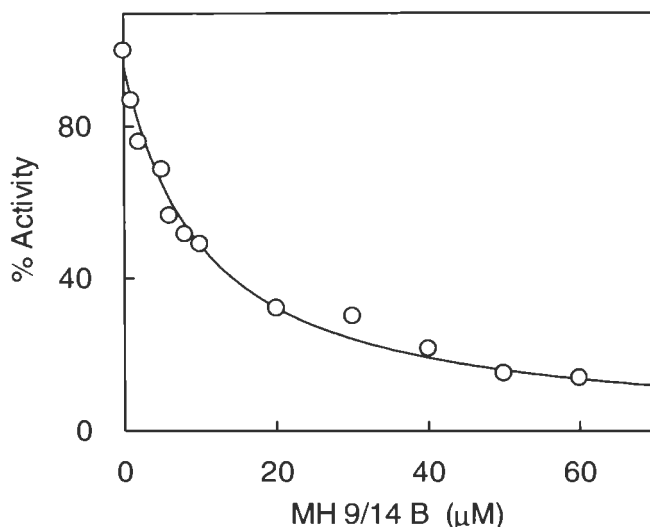

Figure 8.17. Determination of the inhibition constant (K_i) of hMMP-7 with Miscellaneous Hydroxamate inhibitor of MH 9/14 B. Steady-state kinetic reactions of hMMP-7 for the Miscellaneous Hydroxamate inhibitor. The initial rates of the enzyme catalyzed hydrolysis reaction of TPL substrate were measured as a function of increasing concentrations of inhibitor. [hMMP-7] = 0.3 μM, [TPL] = 20 μM. The solid smooth line is the best fit of the data according to Eq 3.10. The K_i value for MH 9/ 14 B is 10.8 ± 0.83 μM.

Table 8.16. Structures and inhibitory properties of the Miscellaneous inhibitors. The data shown for hMMP-9 and 10 were obtained from Reference 32.

Misc	MMP-7	MMP-9	MMP-10
MH 9 5	NI	NI	NI
MH 9 5B	NI	NI	NI
MH 9 14	NI	NI	NI
MH 9 14B	10.8	NI	NI

316

Table 8.17. Structures and inhibitory properties of the Methyl Red derivative inhibitors. The data shown for hMMP-9 and 10 were obtained from Reference 32.
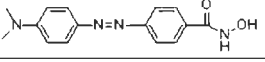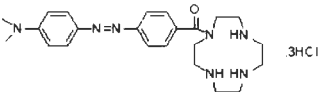
Methyl Red	MMP-7	MMP-9	MMP-10
MH 6 88	NI	NI	30%
MH 6 95 B	NI	15%	16%

Figure 8.18 shows the inhibition constant (K_i) of hMMP-7 with Cinnamic Acid O-Phenylene Diamine derivatives inhibitors. The K_i value for MH 7/ 23 is 3.9 ± 0.51 μM. Table 8.18 shows the structures and properties Cinnamic Acid O-Phenylene Diamine derivative inhibitors.
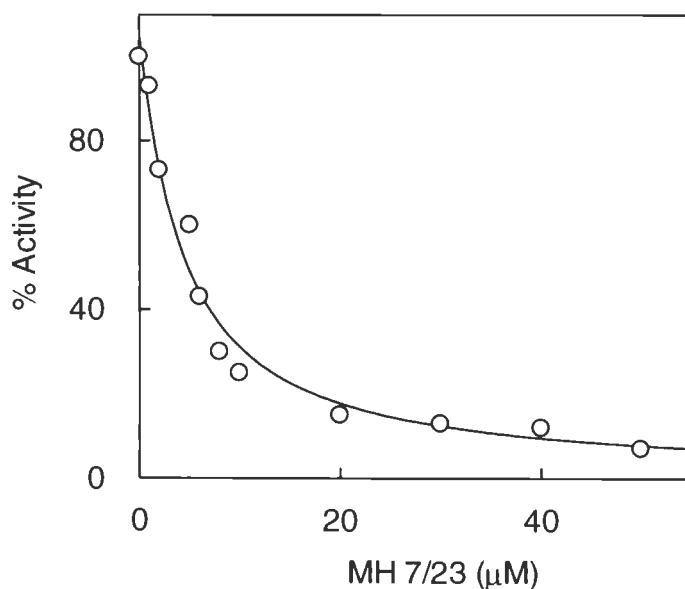

Figure 8.18. Determination of the inhibition constant (K_i) of hMMP-7 with Cinnamic Acid O-Phenylene Diamine derivative inhibitor MH 7/23. Steady-State Kinetic reactions of hMMP-7 for Cinnamic Acid O-Phenylene Diamine derivative inhibitor. The initial rates of the enzyme catalyzed hydrolysis reaction of TPL substrate were measured as a function of increasing concentration of inhibitor. [hMMP-7] = 0.3 μM, [TPL] = 20 μM. The solid smooth line is the best fit of the data according to Eq 3.10. The K_i value for MH 7/ 23 is 3.9 ± 0.51 μM.

Table 8.18. Structures and inhibitory properties of the Cinnamic Acid O-Phenylene Diamine derivative inhibitors. The data shown for hMMP-9 and 10 were obtained from Reference 32
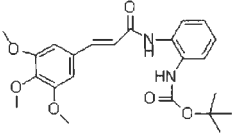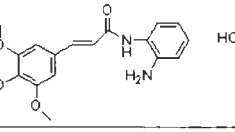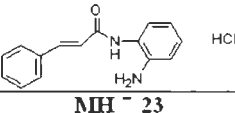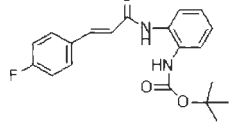
Cinnamic Acid Phenylene Diamine Derivatives	MMP-7	MMP-9	MMP-10
MH ⁻ 21	8.3	40%	NI
MH ⁻ 21 B	19%	NI	NI
MH ⁻ 22B	21%	24%	15.3%
MH ⁻ 23	3.9	NI	NI

Table 8.19 shows structures and properties of the Cinnamic Acid O-Phenylene Diamine derivatives inhibitors. These inhibitors do not inhibit the hMMP isozymes to a large extent. Tables 8.20 and 8.21 show the Inhibition constant (K_i) of hMMP-7 with Cinnamic Acid O-Phenylene Diamine derivative inhibitors. Table 8.22 shows the structures and properties of the Cinnamic Acid O-Phenylene Diamine Cyclene derivatives inhibitors. Figure 8.19 shows inhibition constant (K_i) of hMMP-7 with Cinnamic Acid O-Phenylene Diamine Cyclene derivative inhibitors. The K_i values for MH 7/ 35 and MH 7/ 36 are 3.6 ± 0.79 μM and 7.0 ± 0.84 μM respectively. The Cinnamic Acid O-Phenylene Diamine Cyclene derivatives MH 7/35 and MH 7/36 are good potential inhibitors for the enzyme i.e. hMMP-7 but not for the other hMMP isozymes [Table 8.23].

Table 8.19. Structures and inhibitory properties of the Cinnamic Acid O-Phenylene Diamine derivative inhibitors. The data shown for hMMP-9 and 10 were obtained from Reference 32.

Cinnamic Acid Phenylene Diamine Derivatives	MMP-7	MMP-9	MMP-10
MH ⁻ 30B	NI	19%	NI
MH ⁻ 31	23%	25%	NI
MH ⁻ 32	30%	35%	NI
MH ⁻ 33	19%	22%	NI

Table 8.20. Structures and inhibitory properties of the Cinnamic Acid O-Phenylene Diamine derivative inhibitors. The data shown for hMMP-9 and 10 were obtained from Reference 32.
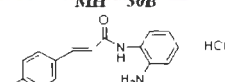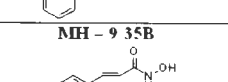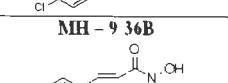
Cinnamic Acid Phenylene Diamine Derivatives	MMP-7	MMP-9	MMP-10
MH ⁻ 31B	NI	25%	NI
MH ⁻ 32B	39%	38%	NI
MH ⁻ 33B	35%	36%	NI
MH – 9 34B	7%	25%	NI
MH – 9 35B	NI	41%	NI
MH – 9 36B	NI	31%	NI

319

Table 8.21. Structures and inhibitory properties of the Cinnamic Acid O-Phenylene Diamine derivative inhibitors. The data shown for hMMP-9 and 10 were obtained from Reference 32.
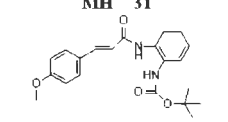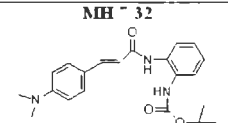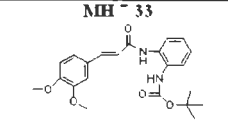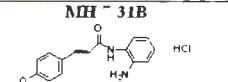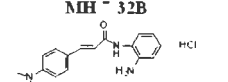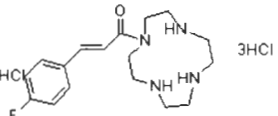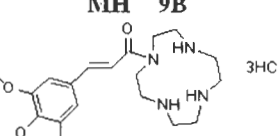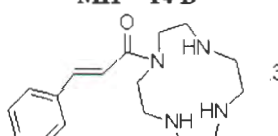
Cinnamic Acid Phenylene Diamine Derivatives	MMP-7	MMP-9	MMP-10
MH − 23B	9%	NI	33%
MH − 24	31%	NI	7%
MH − 24B	NI	NI	21%
MH − 30	NI	27%	NI

Table 8.22. Structures and inhibitory properties of the Cinnamic Acid O-Phenylene Diamine Cyclene derivative inhibitors. The data shown for hMMP-9 and 10 were obtained from Reference 32.
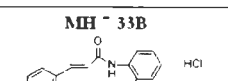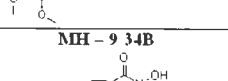
Cinnamic acid Phenylene Diamine cyclene Derivatives]	MMP-7	MMP-9	MMP-10
MH − 12	NI	22%	16%
MH − 9B	NI	7.5%	15%
MH − 14 B	9%	NI	NI

320

Figure 8.19. Determination of the inhibition constant (K_i) of hMMP-7 with Cinnamic Acid O-Phenylene Diamine Cyclene derivative inhibitors MH 7/35 and MH 7/36. Steady-state kinetic reactions of hMMP-7 for Cinnamic Acid O-Phenylene Diamine Cyclene derivatives inhibitors. The initial rates of the enzyme catalyzed hydrolysis reaction of TPL substrate were measured as a function of increasing concentration of inhibitor. [hMMP-7] = 0.3 µM, [TPL] = 20 µM. The solid smooth line is the best fit of the data according to Eq 3.10. The K_i values for MH 7/ 35 and MH 7/ 36 are 3.6 ± 0.79 µM and 7.0 ± 0.84 µM respectively.

Figure 8.20 shows the inhibition constant (K_i) of hMMP-7 with three Cinnamic

Acid O-Phenylene Diamine Cyclene derivatives inhibitors. The K_i values for MH 7/ 37,

MH 7/ 38 and MH 7/39 are 8.0 ± 0.1 µM, 0.4 ± 0.04 µM and 6.6 ± 0.84 µM, respectively.

MH 7/ 37 and MH 7/39 are comparable in potency, but MH 7/ 38 behaves as a very potent

inhibitor for hMMP-7. In the case of the other two hMMPs poor inhibition was observed [32] and tabulated in Table 8.24. Tables 8.2$\underline{5}$ and 8.26 show that Cinnamic Acid O-Phenylene Diamine Cyclene derivative inhibitors have no inhibitory properties.

Table 8.23. Structures and inhibitory properties of the Cinnamic Acid O-Phenylene Diamine Cyclene derivative inhibitors. The data shown for hMMP-9 and 10 were obtained from Reference 32.
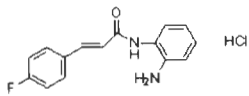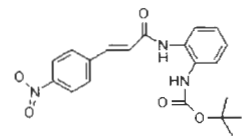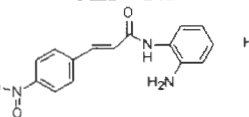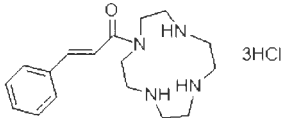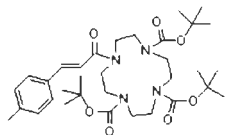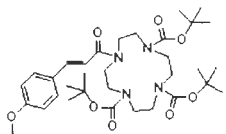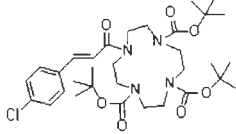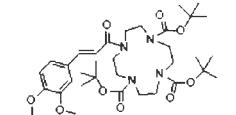
Cinnamic acid Phenylene Diamine cyclene Derivatives]	MMP-7	MMP-9	MMP-10
MH $^-$ 13 B 3HCl	NI	NI	17%
MH $^-$ 35	6.6	32%	NI
MH $^-$ 36	7.0	NI	8%

Table 8.24. Structures and inhibitory properties of the Cinnamic Acid O-Phenylene Diamine Cyclene derivative inhibitors. The data shown for hMMP-9 and 10 were obtained from Reference 32.
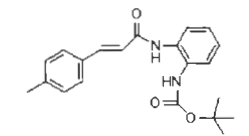
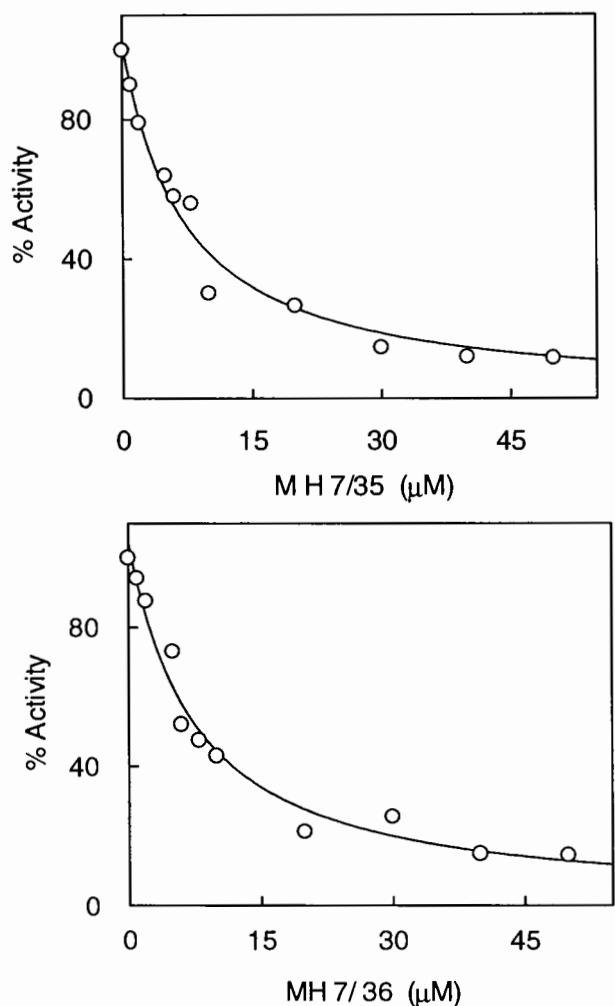| Cinnamic acid Phenylene Diamine cyclene Derivatives]	MMP-7	MMP-9	MMP-10
MH $^-$ 3$^-$	8.0	6%	17%
MH $^-$ 38	0.4	7.3%	7.6%
MH $^-$ 39	6.6	NI	NI
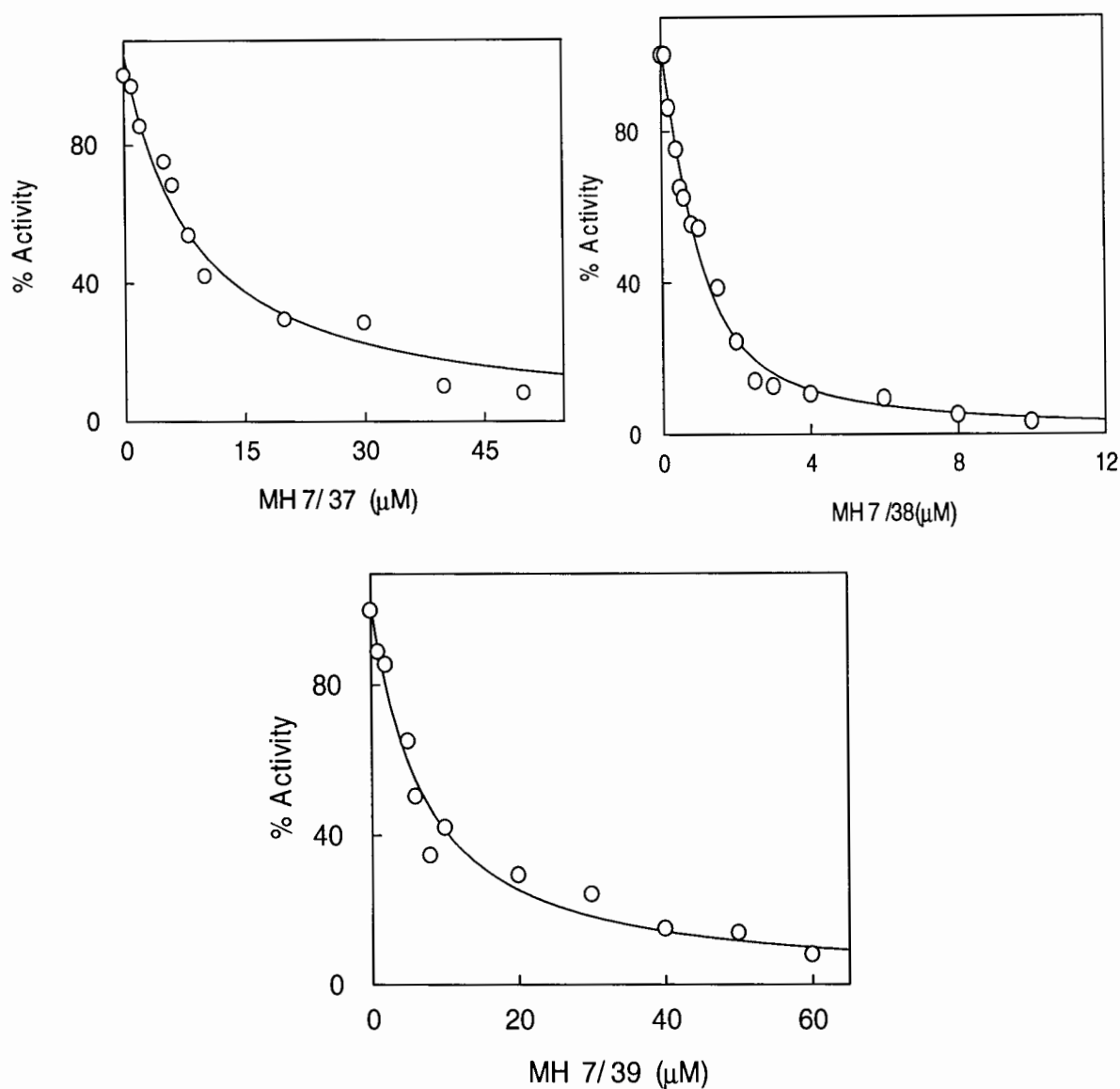
Figure 8.20. Determination of the inhibition constant (K_i) of hMMP-7 with Cinnamic Acid O-Phenylene Diamine Cyclene derivative inhibitors. Steady-State Kinetic reactions of hMMP-7 for Cinnamic Acid O-Phenylene Diamine Cyclene derivatives inhibitors. The initial rates of the enzyme catalyzed hydrolysis reaction of TPL substrate were measured as a function of increasing concentration of inhibitor. [hMMP-7] = 0.3 µM, [TPL] = 20 µM. The solid smooth line is the best fit of the data according to Eq 3.10. The K_i values for MH 7/37 and MH 7/38 and MH 7/39 are 8.0 ± 0.1 µM, 0.4 ± 0.04 µM and 6.6 ± 0.84 µM, respectively.

Table 8.25. Structures and inhibitory properties of the Cinnamic Acid O-Phenylene Diamine Cyclene derivative inhibitors. The data shown for hMMP-9 and 10 were obtained from Reference 32.

Cinnamic acid Phenylene Diamine cyclene Derivatives]	MMP-7	MMP-9	MMP-10
MH 9 21	NI	NI	NI
MH 9 21B	NI	NI	NI

Table 8.26. Structures and inhibitory properties of the Cinnamic Acid O-Phenylene Diamine Cyclene derivative inhibitors. The data shown for hMMP-9 and 10 were obtained from Reference 32.

Cinnamic acid Phenylene Diamine cyclene Derivatives]	MMP-7	MMP-9	MMP-10
MH ̄ 9	NI	NI	NI
MH ̄ 13	NI	NI	NI
MH 9 20B	NI	NI	NI

Figure 8.21 shows the inhibition constant (K_i) of hMMP-7 with Urea 2-Amino-5-Mercapto-Thiadiazole derivative inhibitor MH 7/28. The K_i value for MH 7/28 is 7.5 ± 0.11 µM. hMMP-9 and 10 was poorly inhibited (Table 8.27). Tables 8.28 and 8.29 show the structures and properties of the Urea 2-Amino-5-Mercapto-Thiadiazole derivative

inhibitors. This category did not act as good inhibitors for any of the hMMP isozymes.

Table 8.29 shows the inhibition constant (K_i) of hMMP-7 with Urea 2-Amino-5-Mercapto-Thiadiazole derivatives inhibitors. In this category we did not observe some potential candidates.
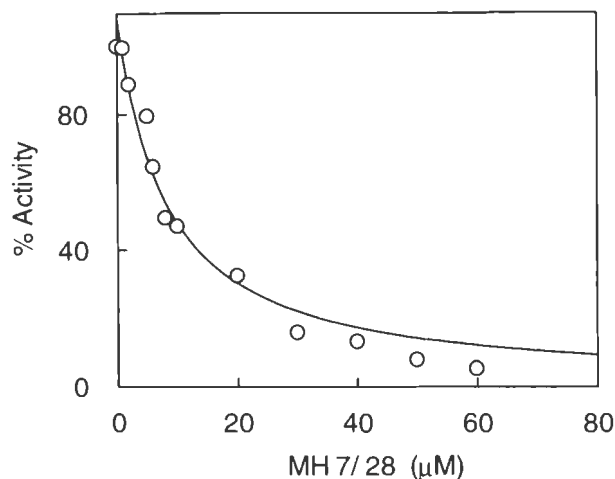
Figure 8.21. Determination of the inhibition constant (K_i) of hMMP-7 with Urea 2-Amino-5-Mercapto-Thiadiazole derivative inhibitor MH 7/28. Steady-State kinetic reactions of hMMP-7 for Urea 2-Amino-5-Mercapto -Thiadiazole derivative Inhibitor. The initial rates of the enzyme catalyzed hydrolysis reaction of TPL substrate were measured as a function of increasing concentration of inhibitor. [hMMP-7] = 0.3 μM, [TPL] = 20 μM. The solid smooth line is the best fit of the data according to Eq 3.10. The K_i value for MH 7/ 28 is 7.5 ± 0.11 μM.

Table 8.27. Structures and inhibitory properties of the Urea 2-Amino-5-Mercapto-Thiadiazole derivative inhibitors. The data shown for hMMP-9 and 10 were obtained from Reference 32.
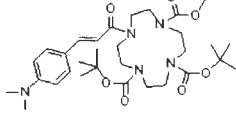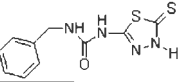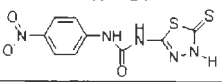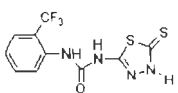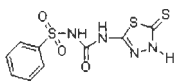
Urea Thiadiazole derivatives	MMP-7	MMP-9	MMP-10
MH 7/25	9%	25%	30%
MH 7/26	30%	19%	14%
MH 7/27	24%	15%	18%
MH 7/28	7.5	37%	NI

Table 8.28. Structures and inhibitory properties of the Urea 2-Amino-5-Mercapto-Thiadiazole derivative inhibitors. The data shown for hMMP-9 and 10 were obtained from Reference 32.
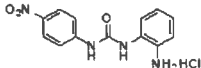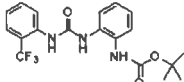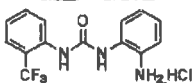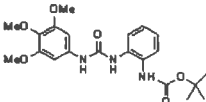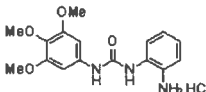
Urea Thiadiazole derivatives	MMP-7	MMP-9	MMP-10
MH – 8/16B	12%	NI	NI
MH – 8/17	Ni	Ni	23%
MH – 8/17B	12%	33%	10%
MH – 8/19	12%	NI	18%
MH – 8/19B	13%	NI	NI

Table 8.29. Structures and inhibitory properties of the Urea 2-Amino-5-Mercapto-Thiadiazole derivative inhibitors. The data shown for hMMP-9 and 10 were obtained from Reference 32.
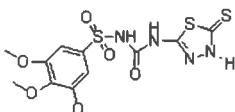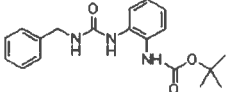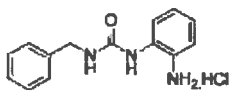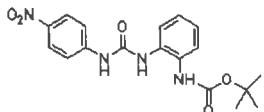
Urea Thiadiazole derivatives	MMP-7	MMP-9	MMP-10
MH – 8/2	30%	32%	10%
MH – 8/15	15%	NI	NI
MH – 8/15B	10%	40%	38%
MH – 8/16	19%	NI	NI

Figure 8.22 shows the inhibition constant (K_i) of hMMP-7 of the Urea 2-Amino-5-Mercapto-Thiadiazole Cyclene derivative inhibitor for MH 8/22. The K_i value for MH 8/22 is 0.4 ± 0.08 µM. Table 8.30 shows that MH 8/22 is the only derivative which is a potent inhibitor for hMMP-7 and is ineffective on hMMP-9 and 10. Table 8.31 shows the structures and properties of the Urea 2-Amino-5-Mercapto-Thiadiazole Cyclene derivative inhibitors. Amongst the derivatives only MH 8/24 inhibits hMMP-7 by 10%.

Figures 8.23, 8.24 and 8.25 show the structures of the Pyrimidine Trione derivatives Thioxopyrimidine Dione derivatives and Dimethyl Pyrimidine Trione [DPT] derivatives, respectively, that were tested.
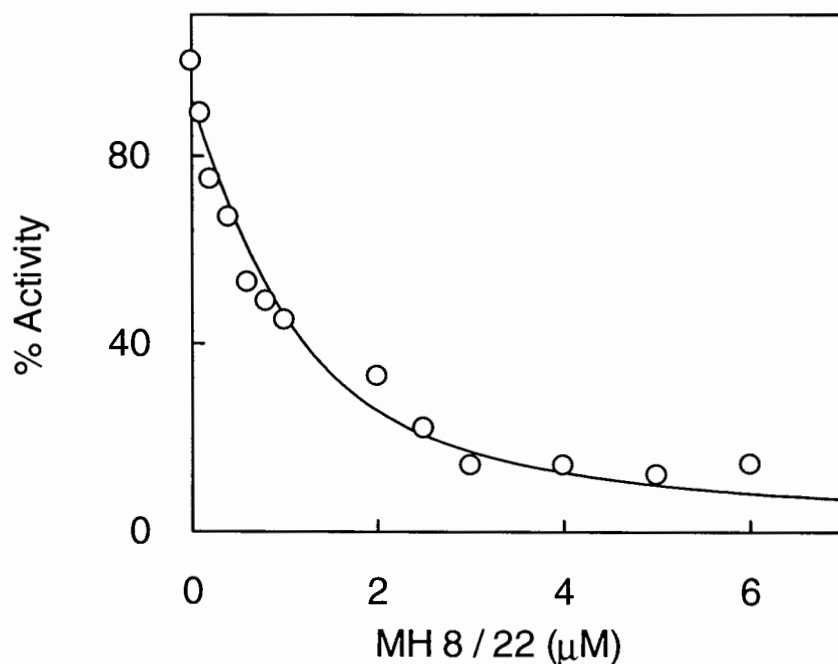
Figure 8.22. Determination of the inhibition constant (K_i) of hMMP-7 with Urea 2-Amino-5-Mercapto-Thiadiazole Cyclene derivative inhibitor MH 8/22. Steady-State kinetic reactions of hMMP-7 for Urea 2-Amino-5-Mercapto -Thiadiazole Cyclene derivative inhibitor. The initial rates of the enzyme catalyzed hydrolysis reaction of TPL substrate were measured as a function of increasing concentration of inhibitor. [hMMP-7] = 0.3 µM, [TPL] = 20 µM. The solid smooth line is the best fit of the data according to Eq 3.10. The K_i value for MH 8/ 22 is 0.4 ± 0.08 µM.

Table 8.30. Structures and inhibitory properties of the Urea 2-Amino-5-Mercato-Thiadiazole Cyclene derivative inhibitors. The data shown for hMMP-9 and 10 were obtained from Reference 32.
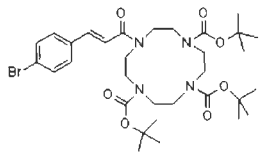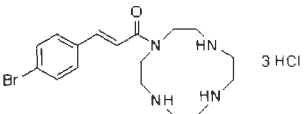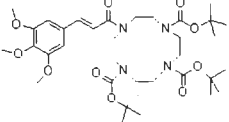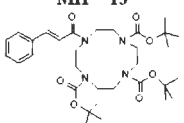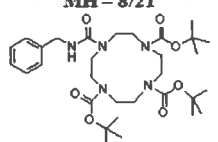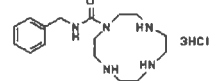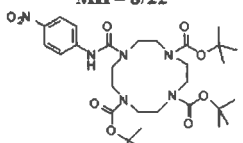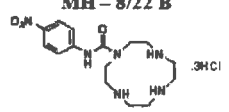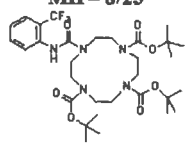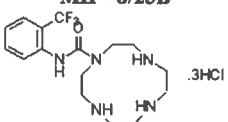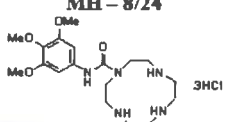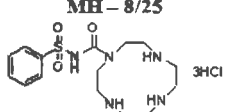
Urea Thiadiazole Cyclene Derivatives]	MMP-7	MMP-9	MMP-10
MH – 8/21	6%	NI	NI
MH – 8/21B	12%	NI	NI
MH – 8/22	0.4	NI	NI
MH – 8/22 B	6%	NI	NI

Table 8.31. Structures and inhibitory properties of the Urea 2-Amino-5-Mercato-Thiadiazole Cyclene derivative inhibitors. The data shown for hMMP-9 and 10 were obtained from Reference 32.
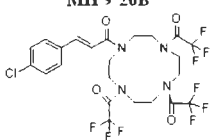
Urea Thiadiazole Cyclene Derivatives]	MMP-7	MMP-9	MMP-10
MH – 8/23	NI	NI	NI
MH – 8/23B	NI	NI	NI
MH – 8/24	10%	NI	NI
MH – 8/25	NI	NI	NI

MH 5-50   MH 5-51b   MH 5-52   MH 5-53

MH 5-54   MH 5-68   MH 5-69   MH 5-74

MH 5-75   MH 5-76   MDS 1-4   MDS 1-5

MDS 1-6   MDS 1-8   MDS 1-9   MDS 1-10

MDS 3-11   MDS 1-13   MDS 1-14   MDS 1-20

MDS 2-7   MDS 1-11   MDS 1-17   MDS 1-22
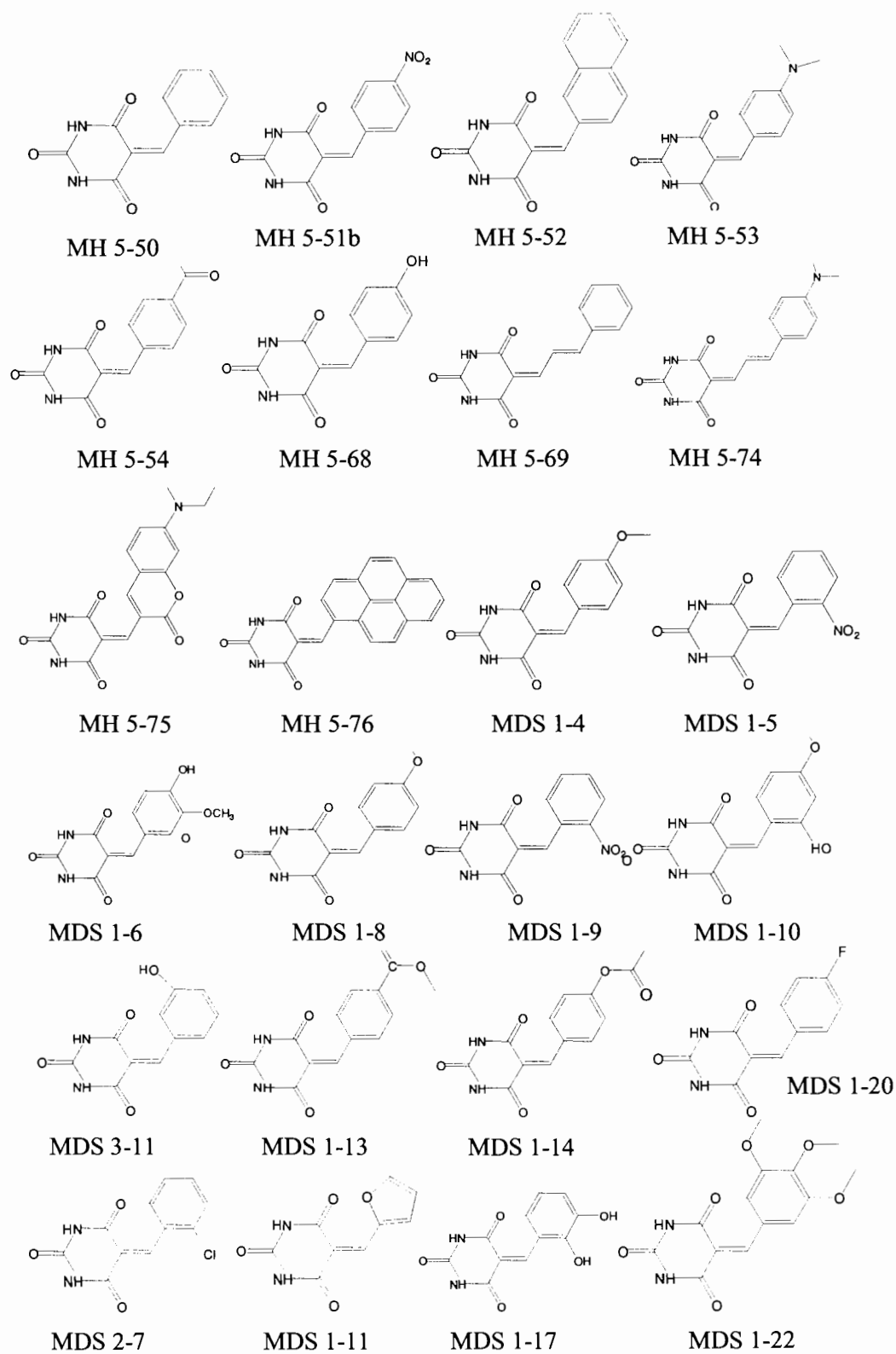
Figure 8.23. The structures of Pyrimidine Trione derivative inhibitors.

MDS 3-2   MDS 2-25   MDS 2-22   MDS 2-19

MDS 2-18   MDS 2-14   MDS 2-10   MDS 2-9

MDS 2-5   MDS 1-23   MDS 1-24   MDS 1-25

MDS 1-28
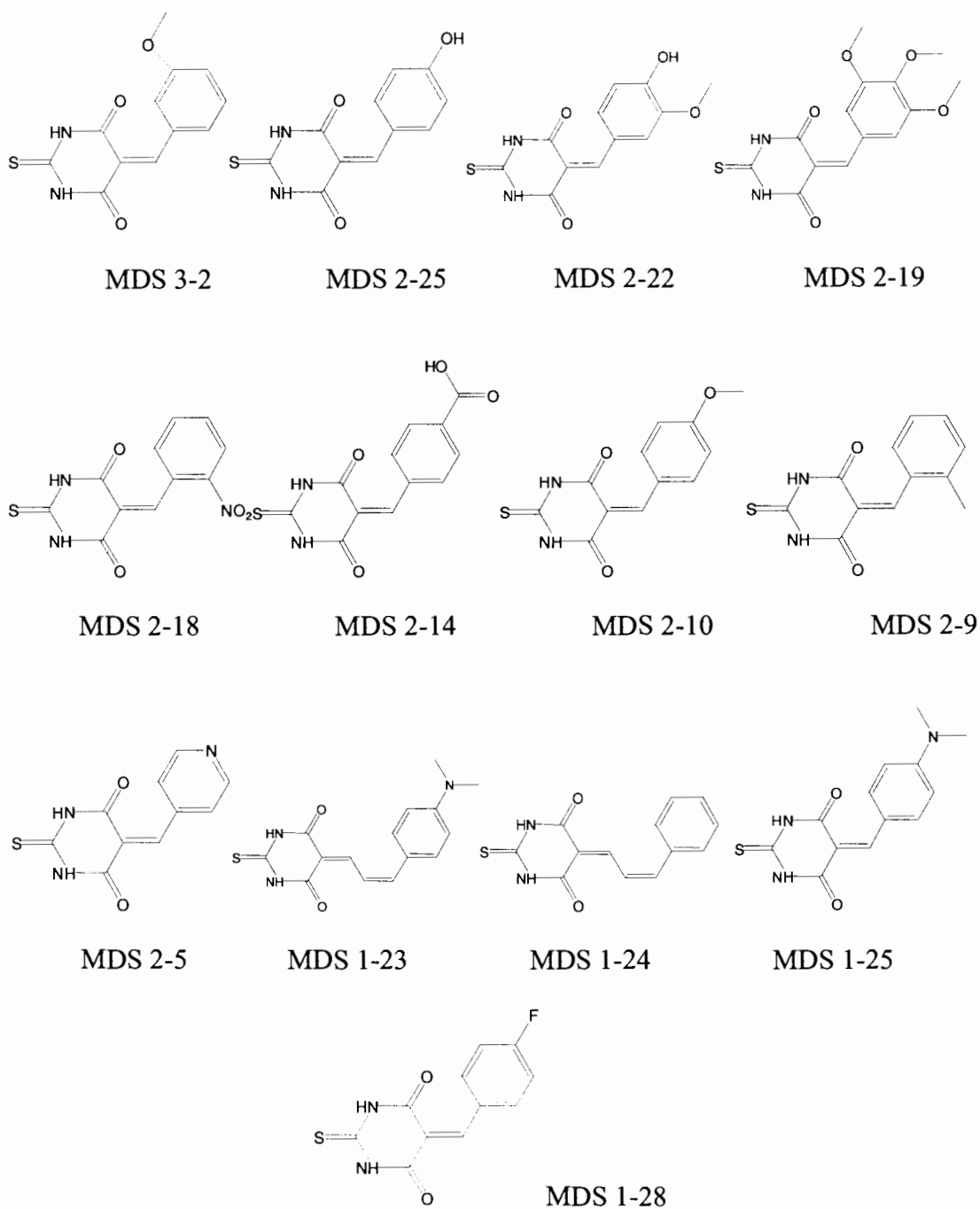
Figure 8.24. The structures of Thioxopyrimidine Dione derivative inhibitors.

MDS 3-10   MDS 3-3   MDS 2-2   MDS 2-1

MDS 3-25   MDS 3-12   MDS 3-19   MDS 3-14

MDS 3-16
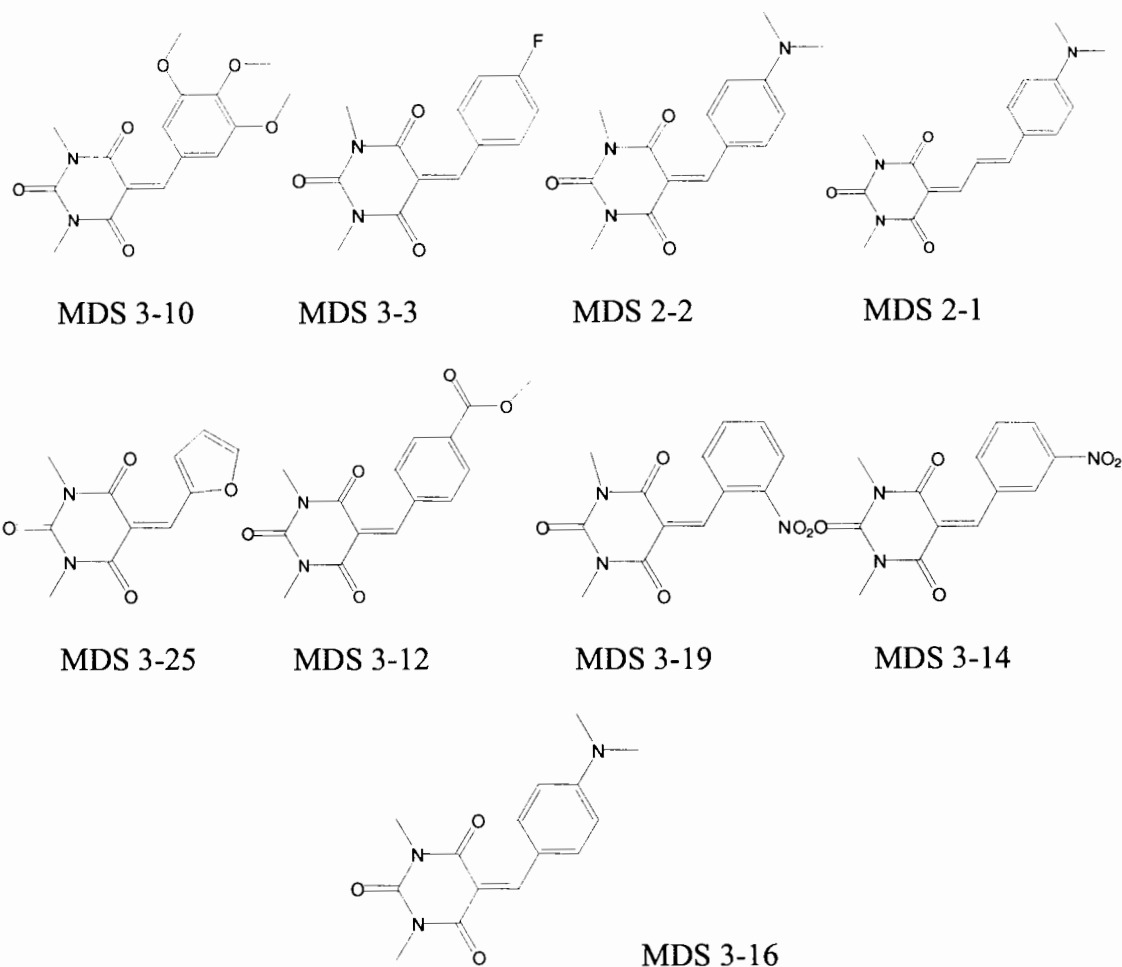
Figure 8.25. The structures of Dimethyl Pyrimidine Trione derivative [DPT] inhibitors.

Figure 8.26 shows the structures of the Miscellaneous inhibitor (supplied by Dr.Mallik's Research Team). None of these different categories of inhibitors inhibit any of the hMMP isozymes.

MH 5-71
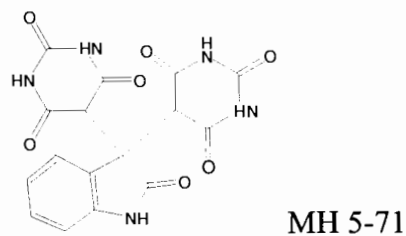
Figure 8.26. The structures of the Miscellaneous inhibitor.

There were 58 compounds, obtained from Dr Cook's Laboratory, with different functional groups that were screened. However, the preliminary synthesis shows that none of the inhibitors inhibited any the hMMP isozymes. Still this preliminary screening was important as new inhibitors can be designed based on this exhaustive study. There were six major categories into which the derivative of the inhibitors obtained from Dr Cook's Laboratory has been classified: (1) Benzene Thiols; (2) Benzyl Esters; (3) Hydrazone Methyl Phenols; (4) Phenol derivatives; (5) Thio Urea derivatives; and (6) Miscellaneous inhibitors.

Figure 8.27 shows the derivatives that have been categorized into a group of benzyl thiols. Due to the bulkiness in the functional group, the binding of these inhibitors could not form the stable MMP-Inhibitor complexes; hence, they turned out to be poor inhibitors for all three hMMP isozymes. Figures 8.28, 8.29 and 8.30 show the different groups of inhibitors like Benzyl Esters, Hydrazone Methyl Phenol and Phenol derivatives respectively. All these inhibitors have one common factor, the bulky nature of their attached groups. Due to serious steric hindrances amongst the groups none of these are potent inhibitors for the hMMP isozymes.

VYU-2-14   VYU-2-15   VYU-2-16   VYU-2-17   VYU-2-19
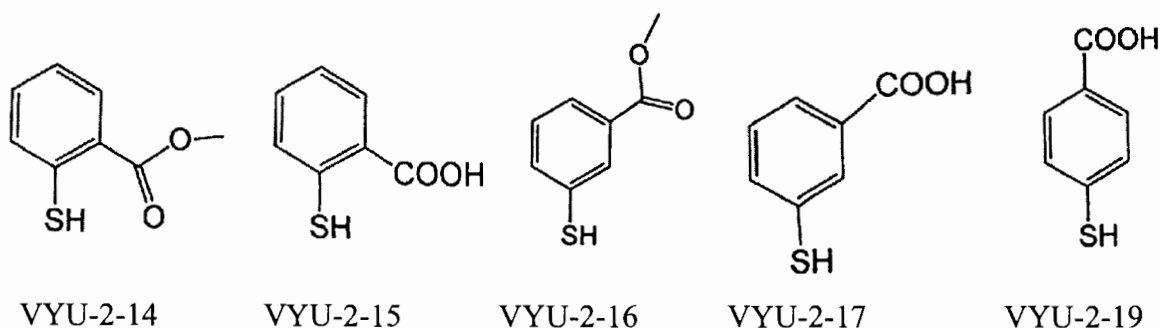
Figure 8.27. The structures of the five compounds that have been categorized as Benzene Thiols.

VYU-2-44   YU-2-46   VYU-2-48
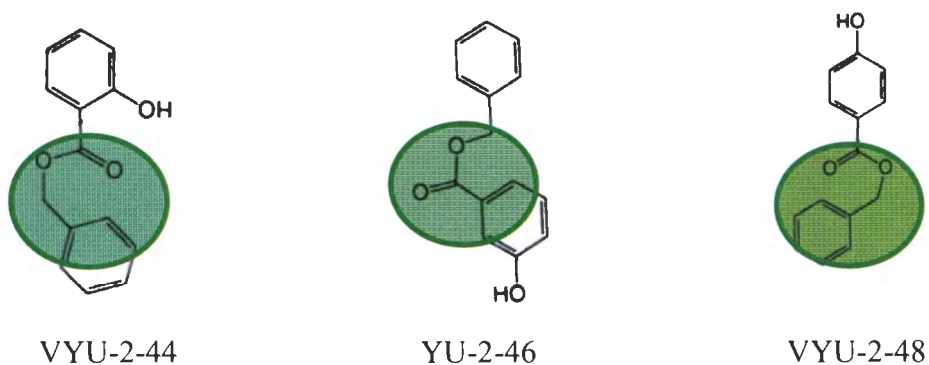
Figure 8.28. The structures of the five compounds that have been categorized as Benzyl Esters. The solid thick dark green colored circle indicates the two components to the inhibitors; a) Benzyl group and b) Ester.

TM-1-119   TM-1-121

TM-1-187   TM-1-234
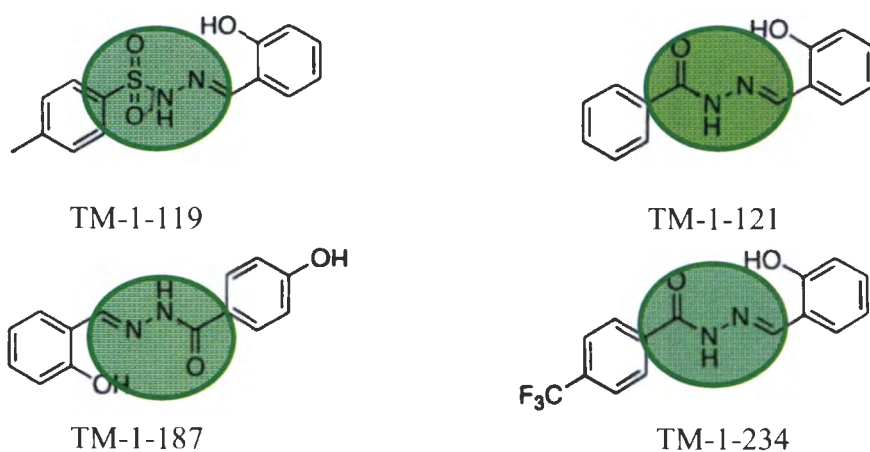
Figure 8.29. The structures of the four compounds which have been categorized as Hydrazone Methyl Phenols. The solid thick green colored circle indicates the functional group (Hydrazone Methyl Phenol) within the parent inhibitor.

VYU-2-10   VYU-2-11   VYU-2-20   VYU-2-23   VYU-2-62-2
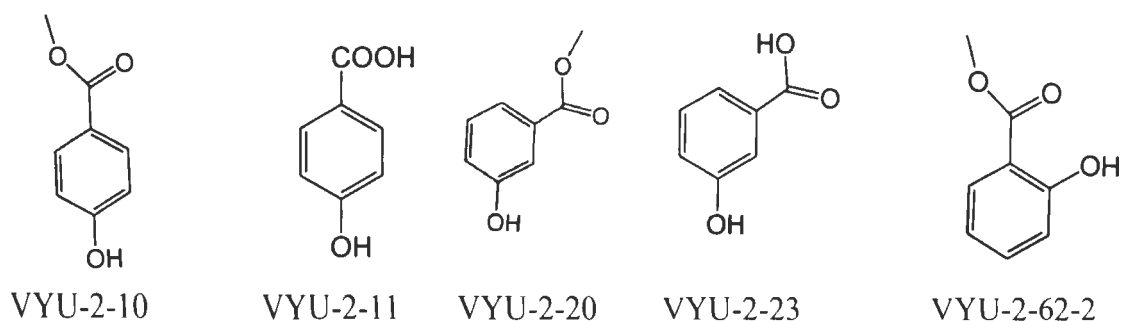
Figure 8.30. The structures of the five compounds which have been categorized as Phenol derivatives.

333

Figure 8.31 shows the nine compounds that have been categorized as Urea derivatives. Figure 8.32 shows the Miscelleneous inhibitor (supplied by Dr Cook's Research Team). Their elongated structure made them bulky and maneuvering these functional groups in the vicinity of the active-site of hMMPs might be difficult. Since hMMPs fall in the category of "soft proteins" [38], the rigid bulky inhibitors could not make significant hydrogen bonds with the solvent and the hMMPs. Hence these are in fact not potent inhibitors of the hMMP isozymes.
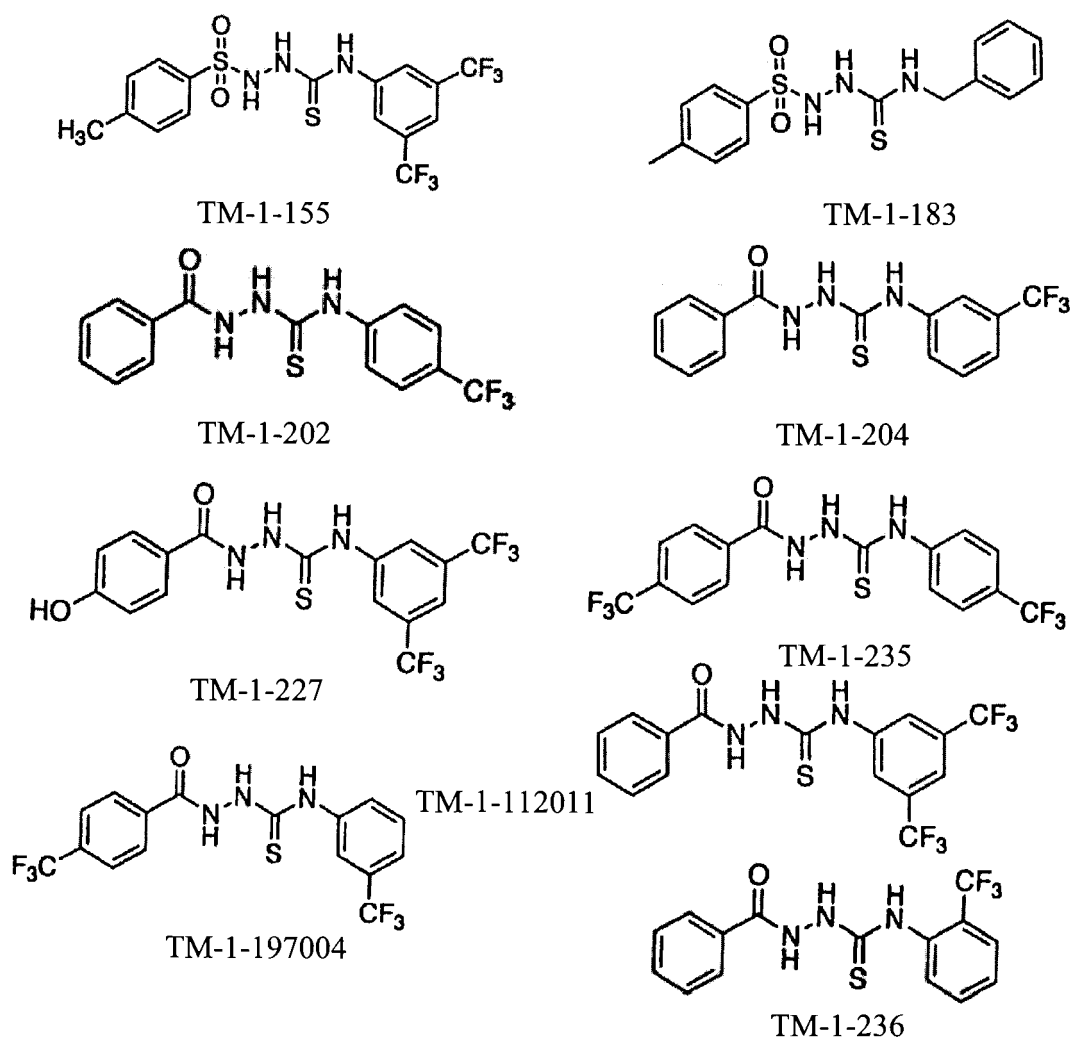
Figure 8.31. The structures of the nine compounds that have been categorized as Urea derivatives.
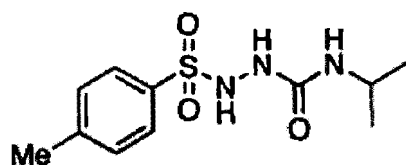
TM-1-185

Figure 8.32. The structure of the compound that was categorized as a Miscellaneous inhibitor.

A review of the inhibition results leads to the following conclusions which have been considered herein: (1) DAPA Hydroxamate inhibitors are the most potent Inhibitors amongst all the inhibitors assayed in the "High Throughput Screening' technique used in this study; (2) DAPA Carboxylate inhibitors are not as potent inhibitors as DAPA Hydroxamate inhibitors; and (3) There are potencies exhibited by all three hMMPs isozymes to different categories of inhibitors screened herein. A few factors that seem to dictate the binding for each of the three hMMPs are; (a) Size of the Inhibitor (specially the associated functional group); (b) The size of the hMMP active site pocket; (c) The hydrophobic or hydrophilic nature of the hMMP involved and the changes undergone by the inhibitor philicity in the solvent vicinity of the active site; and (d) The additional hydrogen bonds formed between the side groups of the inhibitor and the enzyme (amine groups in the backbone of the enzyme and the residues accessible in the active site pocket) determines the stability of the enzyme-inhibitor complex, and thereby, the potency of the concerned inhibitor perturbing the enzyme activity of the hMMP isozymes. After two decades of extensive research and the escalating database of information available on the structure-function relationship of the MMPs, it has become possible to endorse different advances towards blocking these enzymes [17]. The reason behind the failures in the

335

clinical trials of the first-generation MMPIs designed until now are being well studied and

are still being deliberated. For instance, the use of MMP inhibitors, in combination therapy

and in the early stages of disease onset, could be a novel approach geared towards

achieving improved clinical advantage. Nevertheless, the design of the first-generation

MMP inhibitors has demonstrated the synergy between medical chemistry, structural

biology and molecular modelling, which provides a persuasive means of accelerating the

lead optimization process.

8.3. References

1. Aranapakam, V., Grosu, G. T., Davis, J. M., Hu, B., Ellingboe, J., Baker, J. L., Skotnicki, J. S., Zask, A., DiJoseph, J. F., Sung, A., Sharr, M. A., Killar, L. M., Walter, T., Jin, G., and Cowling, R. J. (2003) Synthesis and structure-activity relationship of alpha-sulfonylhydroxamic acids as novel, orally active matrix metalloproteinase inhibitors for the treatment of osteoarthritis, *Med. Chem.* 46, 2361.
2. Engel, C. K., Pirard, B., Schimanski, S., Kirsch, R., Habermann, J., Klingler, O., Schlotte, V., Weithmann, K. U., and Wendt, K. U. (2005) Structural basis for the highly selective inhibition of MMP-13, *Chem. Biol.* 12 (2), 181-189.
3. Amin, E.A., and Welsh, W.J. (2001) Three-dimensional quantitative structure-activity relationship (3D-QSAR) models for a novel class of piperazine-based stromelysin-1 (MMP-3) inhibitors: Applying a "divide and conquer" strategy, *J. Med. Chem.* 44, 3849–3855.
4. Venkatesan, A. M., Davis, J. M., Grosu, G. T., Baker, J., Zask, A., Levin, J. I., Ellingboe, J., Skotnicki, J. S., DiJoseph, J. F., Sung, A., Jin, G., Xu, W., McCarthy, D.J., and Barone, D. J. (2004) Synthesis and Structure–Activity Relationships of 4-alkynyloxy Phenyl Sulfanyl, Sulfinyl, and Sulfonyl Alkyl Hydroxamates as Tumor Necrosis Factor-α Converting Enzyme and Matrix Metalloproteinase Inhibitors, *J. Med. Chem.* 47, 6255.
5. Whittaker, M., Floyd C. D., Brown, P., and Gearing, J. H. (1999) Design and therapeutic application of matrix metalloproteinase inhibitors, *Chem. Rev.* 99, 2735-2776.
6. Cheng, M., De, B., Pikul, S., Almstead, N. G., Natchus, M. G., Anastasio, M. V., McPhail, S. J., Snider, C. E., Taiwo, Y. O., Chen, L., Dunaway, C. M., Gu, F., Dowty, M. E., Mieling, G. E., Janusz, M. J., and Wang-Weigand, S. (2000) Design and Synthesis of Piperazine-Based Matrix Metalloproteinase Inhibitors, *J. Med. Chem.* 43, 369-380.

7. Tochowicz, A., Maskos, K., Huber, R., Oltenfreiter, R., Dive, V., Yiotakis, A., Zanda, M., Bode, W., and Goettig, P. (2007) Crystal structures of MMP-9 complexes with five inhibitors: contribution of the flexible Arg424 side-chain to selectivity, *J. Mol. Biol.* 371, 989-1006.

8. Seltzer, J. L., Akers, K. T., Weingarten, H., Grant, G. A., McCourt, D. W., and Eisen, A. Z. (1990) Cleavage specificity of human skin type IV collagenase (gelatinase). Identification of cleavage sites in type I gelatin, with confirmation using synthetic peptides, *J. Biol. Chem.* 265, 20409-20413.

9. Wu, J.-J., Lark, M. W., Chun, L. E., and Eyre, D. R. (1991) Sites of stromelysin cleavage in collagen types II, IX, X, and XI of cartilage, *J. Biol. Chem.* 266, 5625-5628.

10. Nagase, H., Fields, C. G., and Fields, G. B. (1994) Design and characterization of a fluorogenic substrate selectively hydrolyzed by stromelysin 1 (matrix metalloproteinase-3), *J. Biol. Chem.* 269, 20952-20957.

11. Bode, W. and Maskos, K. (2003). Structural basis of the matrix metalloproteinases and their physiological inhibitors, the tissue inhibitors of metalloproteinases. *J. Biol. Chem.* 384, 863-872.

12. O'Brien, P.M., Ortwine, D.F., Pavlovsky, A.G., Picard, J.A., Sliskovic, D.R., Roth, B.D., Dyer, R.D., Johnson, L.L., Man, C.F., and Hallak, H. (2000). Structure-activity relationships and pharmacokinetic analysis for a series of potent, systemically available biphenylsulfonamide matrix metalloproteinase inhibitors. *J. Med. Chem.* 43, 156-166.

13. Babine, R.E., and Bender, S.L. (1997) Molecular Recognition of Protein minus sign Ligand Complexes: Applications to Drug Design, *Chem. Rev. 97*, 1359-1472.

14. Wojtowicz-Praga, S.M., Dickson, R.B., and Hawkins, M.J. (1997) Matrix metalloproteinase inhibitors, *Invest. New Drugs.* 15, 61-75.

15. Winum, J., Scozzafava, A., Montero, J., and Supuran, C.T. (2006) Therapeutic potential of sulfamides as enzyme inhibitors, *Med. Res. Rev. 26*, 767-792.

16. Yang, S., Scannevin, R.H., Wang, B., Burke, S.L., Wilson, L.J., Karnachi, P., Rhodes, K.J., Lagu, B., and Murray, W.V. (2008) beta-N-Biaryl ether sulfonamide hydroxamates as potent gelatinase inhibitors: part 1. Design, synthesis, and lead identification, *Bioorg. Med. Chem. Lett.* 18, 1135-1139.

17. Borkakoti, N. (2004) Matrix metalloprotease inhibitors: design from structure, *Biochem. Soc. Trans.* 32 (1), 17-24.

18. Natchus, M.G., Bookland, R.G., De, B., Almstead, N.G., Pikul, S., Janusz, M.J., Heitmeyer, S.A., Hookfin, E.B., Hsieh, L.C., Dowty, M.E., Dietsch, C.R., Patel, V.S., Garver, S.M., Gu, F., Pokross, M.E., Mieling, G.E., Baker, T.R., Foltz, D.J., Peng, S.X., Bornes, D.M., Strojnowski, M.J., and Taiwo, Y.O. (2000) Development of new hydroxamate matrix metalloproteinase inhibitors derived from functionalized 4-aminoprolines, *J. Med. Chem.* 43, 4948-4963.

19. Gomis-Rüth, F.X., Maskos, K., Betz, M., Bergner, A., Huber, R., Suzuki, K., Yoshida, N., Nagase, H., Brew, K., Bourenkov, G.P., Bartunik, H., and Bode, W. (1997) Mechanism of inhibition of the human matrix metalloproteinase stromelysin-1 by TIMP-1, *Nature.* 389, 77-81.

337

20. Woessner, J.F., and Nagase, H. (2000) Matrix Metalloproteinases and TIMPs: protein profile. *Oxford: Oxford Univ. Press.*

21. Edwards, D.R. (2001) The tissue inhibitors of metalloproteinases (TIMPs). In *Matrix Metalloproteinase Inhibitors in Cancer Therapy ed. NJ Clendeninn, K Appelt. Totowa, NJ: Humana,* 67-84.

22. Yip, D., Ahmad, A., Karapetis, C., Hawkins,C.A., and Harper, P.G. (1999) Matrix metalloproteinase inhibitors: applications in oncology, *Invest. New Drugs.* 17, 387-399.

23. Macaulay, V.M., O'Byrne, K.J., Saunders, M.P., Braybrooke, J.P., Long, L., Gleeson, F., Mason, C.S., Harris, A.L., Brown, P. and Talbot, D.C. (1999) Phase I study of intrapleural batimastat (BB-94), a matrix metalloproteinase inhibitor, in the treatment of malignant pleural effusions, *Clin. Can. Res.* 5, 513-520.

24. Talbot, D.C., and Brown, P.D. (1996) Experimental and clinical studies on the use of matrix metalloproteinase inhibitors for the treatment of cancer. *Eur. J. Cancer.* 32A: 2528-2533.

25. Coussens, L. M., Fingleton, B., and Matrisian, L. M. (2002) Matrix metalloproteinase inhibitors and cancer: trials and tribulations, *Science.* 295, 2387-2392.

26. Zucker, S., Cao, J., and Chen, W. T. (2000) Critical appraisal of the use of matrix metalloproteinase inhibitors in cancer treatment, *Oncogene.* 19, 6642-6650.

27. Kruger, A. (2001) Hydroxamate-type matrix metalloproteinase inhibitor promotes liver metastasis, *Cancer Res.* 61, 1272-1275.

28. Vazquez, F. (1999) METH-1, a human ortholog of ADAMTS-1, and METH-2 are members of a new family of proteins with angio-inhibitory activity, *J. Biol. Chem.* 274, 23349-23357.

29. Kontogiogis, C.A., Papaionnou, P., and Hadjipavlou-Litina, D.J. (2005) Matrix metalloproteinase inhibitors: A review on pharmacophore mapping and (Q)Sars results, *Curr. Med. Chem.* 12, 339-355.

30. Brown, P. (1997) Matrix metalloproteinase inhibitors, *Angiogenesis.* 1, 142-154.

31. Mandal, M., Mandal, A., Das, S., Chakraborti, T., and Chakraborti, S. (2003) Clinical implications of matrix metalloproteinases, *Mol. Cell. Biochem.* 252, 305-329.

32. Conformational Changes and Catalysis in Matrix Metalloproteinase 9 and 10, Shakila Tobwala, PhD Dissertation, Department of Chemistry and Biochemistry, Year 2009.

33. Heth, C.L., Tallman, D.E., and Rasmussen, S.C. (2010) Electrochemical study of 3-(N-alkylamino) thiophenes: experimental and theoretical insights into a unique mechanism of oxidative polymerization, *J. Phys. Chem. B.* 114(16):5275-82.

34. Frisch, M. J.; Trucks, G. W.; Schlegel, H. B.; Scuseria, G. E.; Robb, M. A.; Cheeseman, J. R.; Montgomery, Jr., J. A.; Vreven, T.; Kudin, K. N.; Burant, J. C.; Millam, J. M.; Iyengar, S. S.; Tomasi, J.; Barone, V.; Mennucci, B.; Cossi, M.; Scalmani, G.; Rega, N.; Petersson, G. A.; Nakatsuji, H.; Hada, M.; Ehara, M.; Toyota, K.; Fukuda, R.; Hasegawa, J.; Ishida, M.; Nakajima, T.; Honda, Y.; Kitao, O.; Nakai, H.; Klene, M.; Li, X.; Knox, J. E.; Hratchian, H. P.; Cross, J. B.;

Bakken, V.; Adamo, C.; Jaramillo, J.; Gomperts, R.; Stratmann, R. E.; Yazyev, O.; Austin, A. J.; Cammi, R.; Pomelli, C.; Ochterski, J. W.; Ayala, P. Y.; Morokuma, K.; Voth, G. A.; Salvador, P.; Dannenberg, J. J.; Zakrzewski, V. G.; Dapprich, S.; Daniels, A. D.; Strain, M. C.; Farkas, O.; Malick, D. K.; Rabuck, A. D.; Raghavachari, K.; Foresman, J. B.; Ortiz, J. V.; Cui, Q.; Baboul, A. G.; Clifford, S.; Cioslowski, J.; Stefanov, B. B.; Liu, G.; Liashenko, A.; Piskorz, P.; Komaromi, I.; Martin, R. L.; Fox, D. J.; Keith, T.; Al-Laham, M. A.; Peng, C. Y.; Nanayakkara, A.; Challacombe, M.; Gill, P. M. W.; Johnson, B.; Chen, W.; Wong, M. W.; Gonzalez, C.; and Pople, J. A.; Gaussian, Inc., Wallingford CT, 2004.

35. Bode, W., Catalan, C. F., Tschesche, H., Grams, F., Nagase, H., and Maskos, K. (1999) Structural properties of matrix metalloproteinases, *Cell. Mol. Life. Sci.* 55, 639-652.

36. Kiyama, R., Tamura, Y., Watanabe, F., Tsuzuki, H., Ohtani, M., and Yodo, M. (1999) Homology modeling of gelatinase catalytic domains and docking simulations of novel sulfonamide inhibitors, *J. Med. Chem.* 42, 1723-1738.

37. Lovejoy, B., Welch, A.R., Carr, S., Luong, C., Broka, C., Hendricks, R.T., Campbell, J.A., Walker, K.A., Martin, R., Van Wart, H., and Browner, M.F. (1999) Crystal structures of MMP-1 and -13 reveal the structural basis for selectivity of collagenase inhibitors, *Nat. Struct. Biol.* 6, 217-221.

38. Norde, W. (1998) Driving forces for protein adsorption at solid surfaces. In: Malmsten, M. Jr (Ed.), Biopolymers at Interfaces. In: Surfactant Sci, vol. 75. *Marcel Dekker, New York*, pp: 27–54.

CHAPTER 9. SUMMARY AND FUTURE DIRECTIONS

9.1. Summary

The experimental results discussed in the previous chapters illustrated physico-chemical properties of three of the hMMP isozymes. It also gives an insight into the kinetic properties and the structural functional relationships existing between the hMMP isozymes and their different cognate ligands. Cognate ligands used in this study included Au-NPs, PLL, differently charged liposomes, cationic and anionic QDs, and small molecule inhibitors (SMIs).

9.1.1. Relationship between "rigid" and "flexible" surfaces on the differential modulation of functional and structural characteristics of Matrilysin (hMMP-7)

Many researchers have detailed protein detection and desensitization methods using decorated gold nanoparticles (Au-NPs) and quantum dots (QDs) [1]. It is the combination of the advantageous size and shape of these NPs that detection and desensitization of protein biomarkers for many diseases have been rigorously pursued. With the goal of desensitizing and alleviating the onset of carcinogenesis as well as metastasis, this study included the pathogenic enzyme of the MMP family (hMMP-7). MMP-7 is one of the enzymes whose expression is often linked to the pathogenesis of several types of human diseases. In this endeavor, one of the main objectives was to focus on the structural and functional consequences of interactions of hMMP-7 with different surface types of cationic macro-clusters. The results of the experimental data presented in Chapter 5 leads to the following conclusions: (1) The enzyme activity of hMMP-7 is enhanced by stoichiometric concentrations of PLL and inhibited at higher concentration of PLL; (2). Secondary

conformational changes were observed in hMMP-7 indicating that the protein becomes more helical and compact upon binding to the positively charged PLL; (3). Au-CNP acts as a very strong inhibitor for hMMP-7; (4). Again secondary conformational changes were observed in hMMP-7 upon binding to Au-CNP but the protein loses its secondary helical structure and is denatured; and (5). Inhibition of hMMP-7 by PLL is reversible whereas Au-CNP irreversibly denatures hMMP-7.

9.1.2. Molecular origin of the intrinsic selectivity in binding of human Matrix Metalloproteinase (hMMP) isozymes to differently charged lipid membranes

Biosensors based on antibody array technology have made rapid progress as possible means of quick and direct protein detection. Even though antibody array methodology may provide quick and simultaneous protein detection it has limitations. More recently, metallic films and Au-NPs have been proposed as sensing platforms to exploit the surface Plasmon phenomenon and its application in bio-specific interaction assays. However, these metal and glass substrates may not be the most desirable for *in vivo* applications and thus there use has been restricted to *in vitro* applications. Despite exhaustive research on MMPs and knowledge available on inhibitors of these pathogenic enzymes, efforts for many decades in developing diagnostic tools for these disease marker proteins remains unfulfilled. Based on the possibilities that the catalytic and regulatory features of hMMP isozymes (especially hMMP-7) may be fine tuned if localized on the plasma membranes *in vivo*, one goal was to investigate the potential interactions of LUVs (as model biological membranes) with three hMMPs, and elucidate the functional consequences of these interactions [2].

In pursuit of this goal, formulations of LUVs with varied lipid compositions were

341

studied. Unlike conventional usage of liposomes (i.e., serving as drug carriers), the LUVs were used to introduce selective ligands on the liposomal surface (as head groups) and "tap" the potentials of the lipid mobility (within liposomes) in promoting "multivalent" interactions between the liposomal ("reporter") head groups with the MMP isozymes. The liposomes also contain sensitized-dansyl groups as fluorescent probes to monitor the interactions. This approach was a natural extension towards the effort in designing highly potent and selective "two-prong" inhibitors exhibiting MMP isozymes selectivity [3].

In summary, the conclusions for the interaction of the hMMP isozymes and the differently charged lipid membranes are as follows: 1) All three hMMP isozymes bind to the differently charged LUVs with varying affinities but hMMP-7 has more specificity for the POPS liposomes; 2) Enzyme activity of hMMP-7 gets perturbed upon binding to the EPOPC (25 mol %) liposomes; 3) Enzyme activity of hMMP-9 or 10 does not get perturbed upon binding to the differently charged LUVs; 4) hMMP-7 binds to cationic liposome via strong electrostatics unlike MMP-9 and 10; 5) Both local negative charge density and organization of the LUVs influence the specificity with which hMMP-7 binds to anionic POPS LUVs; and 6) Poly-anionic PIP_2 (4 mol %) shows similar binding affinity as mono-anionic POPS (25 mol %).

9.1.3. Mechanistic studies to unravel the alternative binding modes of human Matrix Metalloproteinase (hMMP) isozymes to cationic and anionic quantum dots

Quantum dots can be tailored to pursuit improvement in the detection of changes in the conformations and dynamics of flexible globular proteins. These quantum dots are a form of semiconductor nanocrystals, which are novel functional nano-materials and possess outstanding electronic and spectral properties. Size distribution, shape, and surface

defects dictate the spectroscopic properties of quantum dots [4]. The capacity to modulate physiologically significant interactions is more widespread and frequent among proteins that have been studied so far.

Many of the approaches to experimentally evaluate the contributions of conformational dynamics in proteins were used to unravel the different binding modes of hMMP isozymes to cationic and anionic quantum dots. The multi-faceted and efficient use of quantum dots in medical therapy, industrial processes, and as diagnostic tools [5-6] requires a means to induce and maintain functional conformations of peptides and proteins on their surfaces. This study provides a detailed insight into the interactions of the MMP isozymes with differently charged QDs and contributes to the long term goal of possibly using QDs for detection of different stages of cancers.

Analysis of the experimental data presented, leads to the following conclusions: 1) Differently charged QDs bind to hMMP-7, 9 and 10; 2) Enzyme activity of all three hMMPs gets perturbed on binding to the cationic and anionic QDs; 3) Binding of hMMPs to the differently charged QDs is reversible with the restoration of the catalytic activities; 4) Binding of hMMP to CQD and AQD were mediated via electrostatics; and 5) Lifetime data indicate: [A]. The possibilities that the tryptophan residues of the MMP isozymes are in different micro-environments and as such the lifetime of each MMP decays with different lifetime values, and/or [B]. Each protein exists in two distinct conformations that exhibit different average lifetime decays.

9.2. Impact

Over the past few years sensitive, convenient, and precise-sensing methods have been

343

sought to serve as crucial tools for the detection of specific proteins. However, protein detection has been a challenging problem owing to the structural diversity and complexity of individual proteins. The most popular current technique for detection of proteins is ELISA [7]. Despite the high sensitivity of ELISA assays, the high cost of carrying out the test, antibody instability and a laborious quantification protocol are problematic [8]. A search for alternative procedures using NPs is being investigated.

Equipped with the knowledge about the interactions between the different NPs (Au-NPs, QDs, and LNPs) studied here and the hMMP isozymes, this information may be applicable to the development of highly specific diagnostic and desensitization protocols for the MMPs because of their biomedical relevance. Future research should be to develop Au-NPs / QDs or LNPs based detection and desensitization methods, which will find applications in the isozyme specific detection of Matrix Metalloproteinases (MMPs) that are involved in tissue remodeling. The successful completion of this research will provide insights into developing nano-particle based, highly specific, and facile diagnostic as well as desensitizing tools for MMPs and other biomarker proteins.

9.1.4. High throughput screening of small molecule inhibitors (SMI) with hMMP isozymes

The ECM plays a critical role for maintaining structure and integrity of tissue types in vertebrates [9-10]. However, under many progressive pathological conditions [9, 11-15], the well maintained balance between the active forms of the MMPs and the synthesis of TIMPs gets disrupted leading to pathogenesis. Consequently, the main approach for the identification of synthetic, potent MMPIs was design of substrate-based recognition peptide sequences [16]. The amino acid sequence at the cleavage site (both left hand side

and right hand side) was synthesized. Compounds in the first category were more potent inhibitors, and were used for the investigation of the pharmacological applications [9].

Research in this dissertation was to design isozyme selective small-molecule inhibitors for the hMMP isozymes. The rationale for designing the SMIs was to discover a few potent inhibitors that might prove to exhibit isozyme preference. Preference was based on the micro-environment of the active site pockets. It was based on the deep specificity pocket of one MMP over those with a smaller pocket, or the type of additional hydrogen bonds formed by the different inhibitor compounds in different MMP isozymes.

The following conclusions were drawn from the results presented: (1) DAPA Hydroxamate inhibitors are the most potent inhibitors of all the inhibitors assayed through the "high throughput screening' technique used in this study; (2) DAPA Carboxylate inhibitors are not as potent inhibitors as the DAPA Hydroxamate inhibitors; and (3) There are varied potency exhibited by all of the three hMMP isozymes to different categories of inhibitors screened. The few factors that seem to dictate the binding for each of the three hMMPs are (a) size of the inhibitor (especially the functional group associated), (b) The size of the hMMP active site pocket, (c) The hydrophobic or hydrophilic nature of the hMMP involved and the changes undergone by the inhibitor philicity in the solvent vicinity of the active site, and (d) The additional hydrogen bonds formed between the side groups of the inhibitor and the enzyme (amine groups in the backbone of the enzyme or the residues accessible in the active site pocket) determines the stability of the enzyme-inhibitor complex, and thereby the potency of the concerned inhibitor perturbing the enzyme activity of the hMMP isozymes.

9.3. Future Directions

In the pursuit of finding potent inhibitor(s) for the MMP family or inhibitors with isozyme selectivity, the natural progression would be to carry out chemo-invasion assay [17] using the potential inhibitors identified here for the three hMMP isozymes. The chemo-invasion assay could be used to assess tumor and endothelial cell invasion and its modulation with those potential inhibitors.

Many researchers have claimed that in angiogenesis, the endothelial cells start acting partially as the invasive tumor cells. They cross the BM with very high efficiency. The set of proteolytic enzymes, mainly MMPs and the uPa (see Introduction Section), involved in BM digestion needs to be further investigated. MMPs may be induced by oncogenes and inflammation indicates their central role in metastasis (see Introduction Section) and tumour progression through disruption of micro-environmental confinement. Hence, evaluation of cell migration and quantification to the chemotactic potential of the soluble mediators would be a very good step to study.

In this manner, the quest to discover the "drug" that would selectively inhibit MMP isozymes in a pool of pathogenic proteins may be achieved. This might be a very small step towards solving the enigma and this tantalizing possibility currently remains a distant mirage. MMPs play a critical role for a variety of physiological and pathological processes and appear to be some of the most promising targets for new drugs to combat cancer and in inflammatory diseases.

9.4. References

1. Hsieh, M.S., Ho, H.C., Chou, D.T., Pan, S., Liang, Y.C., Hsieh, T.Y., Lan, J.L., and Tsai, S.H. (2003) Expression of matrix metalloproteinase-9 (gelatinase B) in gouty

arthritis and stimulation of MMP-9 by urate crystals in macrophages, *J. Cell. Biochem.* 89, 791-799.

2. Mbamala, E. C.; Shaul, A. B.; and May, S. (2005) Domain formation induced by the adsorption of charged proteins on mixed lipid membranes, *Biophys. J.* 88 (3), 1702-1714.

3. Norel, R., Sheinerman, F., Petrey, D., and Honig, B. (2001) Electrostatic contributions to protein-protein interactions: fast energetic filters for docking and their physical basis, *Protein. Sci.* 10, 2147-2161.

4. Unni, C., Philip, D., and Gopchandran, K.G. (2008) Studies on optical absorption and photoluminescence of thiolglycerol-stabilized CdS quantum dots, *Spectrochimica Acta Part A.* 71, 1402–1407.

5. Warnement, M. R., Tomlinson, I. D., Chang, J. C., Schreuder, M.A., Luckabaugh, C.M., and Rosenthal, S.J. (2008) Controlling the reactivity of ampiphilic quantum dots in biological assays through hydrophobic assembly of PEG derivatives, *Bioconj. Chem.* 19, 1404-1413.

6. Kley, N., Ivanov, I., and Meier-Ewert, S. (2004) Genomics and proteomics tools for compound mode-of-action studies in drug discovery, *Pharmacogenomics.* 5, 395-404.

7. Jain, K. K. (2007) Applications of nanobiotechnology in clinical diagnostics, *Clin. Chem.* 53 (11), 2002-2009.

8. Willner, I., Basnar, B., and Willner, B. (2007) Nanoparticle-enzyme hybrid systems for nanobiotechnology, *FEBS. J.* 274, 302-309.

9. Whittaker, M., Floyd C. D., Brown, P., and Gearing, J. H. (1999) Design and therapeutic application of matrix metalloproteinase inhibitors, *Chem. Rev.* 99, 2735-2776.

10. Tschesche, H. (1995) Human neutrophil collagenase, *Methods in Enzymology*, 248, 431-449.

11. Nagase, H., Fields, C. G., and Fields, G. B. (1994) Design and characterization of a fluorogenic substrate selectively hydrolyzed by stromelysin 1 (matrix metalloproteinase-3), *J. Biol. Chem.* 269, 20952-20957.

12. Nagase, H. and Woessner, J.F. Jr. (1999) Matrix metalloproteinases, *J. Biol. Chem.* 274, 21491-21494.

13. Bottomley, K.M., Johnson, W.H. and Walter, D.S. (1998) Matrix metalloproteinase inhibitors in arthritis, *J. Enz. Inh.* 13, 79-102.

14. Dioszegi, M., Cannon, P. and Van Wart, H.E. (1995) Vertebrate collagenases, *Methods in Enzymology*, 248, 413-431.

15. Johnson, L.L., Dyer, R. and Hupe, D.J. (1998) Matrix metalloproteinases, *Curr. Opin. Chem. Biol.* 2, 466-471.

16. Babine, R.E., and Bender, S.L. (1997) Molecular Recognition of Protein minus sign Ligand Complexes: Applications to Drug Design, *Chem. Rev.* 97, 1359-1472.

17. Albini, A., an Benelli, R. (2007) The Chemoinvasion assay: a method to assess tumor and endothelial cell invasion and its modulation, *Nat. Prot.* 2(3), 504-511.

APPENDIX A. SUB-CLONING OF HUMAN ANNEXIN V WITHOUT A HEXA-HISTIDINE TAG

A.1. Introduction

A.1.1. Literature review about annexin family

The exploration of protein mediators of intracellular calcium signals has been instrumental in the identification of a number of soluble proteins, which help in binding proteins to phospholipid membranes in a calcium dependent manner [1]. Initially, these proteins (e.g. synexin, calelectrins, chromobindins, calpactins, calcimedins, endonexins, and lipocortins) were named for their sources or *in vitro* properties. The term annexin [2] is now used [3] to classify this group of proteins. Chemical properties and protein sequences differentiate the annexin family from the protein kinase C, calmodulin (EF hand), and phospholipase A_2 families of calcium-binding proteins that play a significant role in signal transduction.

A.1.2. Crystal structure of Annexins

Human annexin V was the first annexin to be characterized by its three-dimensional structure [4]. The molecular structures of human [5-7], chicken [8], and rat annexin V [9] have been solved in various crystal forms. Crystal structures have been determined for human annexin III [10], human annexin VI [11], annexin XII from *Hydra vulgaris* [12]. Also, the structures of N-terminally truncated forms of human annexin I [13], human annexin II [14], and annexin VII from *Dictyostelium discoideum* [15] have been determined. As expected from the high primary sequence homology, all annexin structures reveal the same protein topology (Figure A.1). Circular dichroism studies have shown most annexins to be almost entirely α-helical [16-17]. The polypeptide chain is folded into four

compact domains of similar structure (labelled from I to IV) corresponding to the four homologous amino-acid repeats, one exception is annexin VI. Each domain consists of five α-helices (labeled from A to E) wound into less than two turns of a right-handed super helix. Four helices are oriented approximately anti-parallel to each other while the fifth helix lies almost perpendicular to these. The connector between domains I and II is extended while domains I and II, and III and IV, respectively, are connected by short inter helical turns.

The four domains are arranged in a planar cyclic array. The molecules have a slightly curved, but overall flat shape, with a concave and a convex side. The N- and C-termini are placed on the concave side whereas all calcium ions defined in the various crystal structures are located on the convex face. The domains II and III, and I and IV generate two modules with approximately two-fold dyad symmetry due to tight contacts mediated by hydrophobic residues and thereby generating a channel. Well-ordered water molecules are buried in the structure, which is located predominantly within this channel. The pore has been identified as the calcium-selective ion conduction pathway by single channel measurements on annexin V [18–20]. Ion channel activity has also been reported for annexins I, II, VI and VII [21–23].

A.1.3. Role of metal ions in the stability and function of Annexins

Metal ions were found to be well defined in the molecular structures when annexins were crystallized at millimolar calcium concentrations. Hexagonal crystal forms of the human annexin V are exceptions where the calcium-binding sites are not well ordered [24]. Binding to phospholipids is dependent on calcium and is rapidly reversed by addition of the

349

calcium (Ca^{2+})chelators such as EDTA [25-29]. A hydrogen bond with the phospholipids is formed when the Ca^{2+} bound Gly28 securely anchors the membrane bound lipid to the metal bound loop [30]. Thus, Ca^{2+} along with the protein and PS membrane act to stabilize and promote protein–membrane association and protein-protein interaction in a synergetic manner [26, 31].
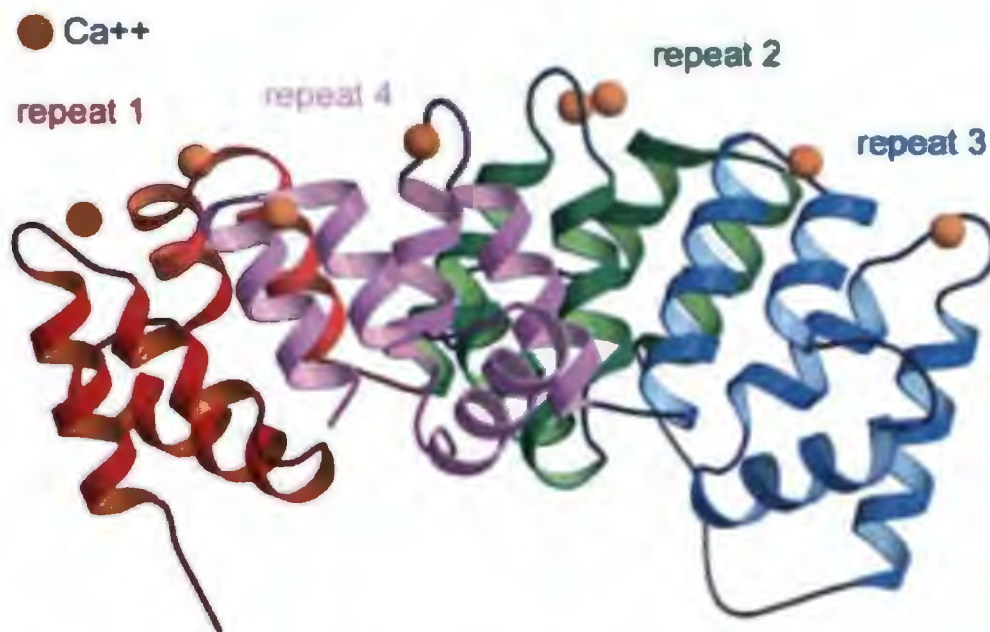
Figure A.1. The molecular structure of Annexin A1. It shows the ribbon representation of the three-dimensional fold of the Ca backbone of annexin A1 in the presence (left) or absence (right) of Ca^{2+} ions. In the X-ray structure the Ca^{2+}-bound annexin A1 is shown which has integrated into 3 of the folded core domains in the Ca^{2+} free protein (depicted in yellow in the right handed structure). This figure has been adapted from Ref 32.

A.1.4. Biological significance of Annexins

It is known that self-assembly of macro-molecules play a vital role in many biological processes [32]. Annexin A5 can self-organize into two-dimensional crystals adsorbed on a planar lipid surface or can form a two-dimensional array junction between lipid membranes. Annexins also play a major role in tumor development and progression,

and are involved in cell motility, tumor invasion, cell signaling pathways, metastasis, apoptosis, drug resistance, and angiogenesis. Annexins display tumor specific patterns of expression and symbolize prognostic biomarkers and potential diagnostics [33-34]. Annexins, expressed in most eukaryotic cell types, are closely related to membrane and calcium binding proteins. Annexins, despite their biochemical and structural similarities, have varied functions in normal cellular activities that including cell division, vesicle trafficking, apoptosis, growth regulation, and calcium signaling. There is sufficient evidence that suggests that changes in annexin expression levels or localization may contribute to many diseases and have pathological consequences [35-36]. Annexins thus have an indirect link to serious human disease classes that include cancer.

A.1.5. Relation of Annexins with Matrix Metalloproteinases

A recent study (Figure A.2) on annexin II (Anx II) has revealed that Matrilysin (matrix metalloprotease-7) cleaves membrane-bound annexin II and enhances binding of tissue-type plasminogen activator (tPA) to cancer cell surfaces [37]. Specific cleavage of annexin II by MMP-7 enhances the binding of tPA to cancer cell surfaces leading to activation of tPA-mediated pericellular proteolytic cascade on cancer cells. Moreover, Anx II has also been reported to play an important role in the patho-physiological action of macrophages during inflammatory processes [38]. Annexin XII (ANXII) plays an important role in mediating the action of estrogen and on the expression level of MMP-9.

A.1.6. Application of Annexins in biotechnology and biomedical therapeutics

Three dimensional structures of annexins [39], comprised of the protein core and a short N-terminal domain (annexins III, IV, V, VI and XII) or a form lacking the terminal.
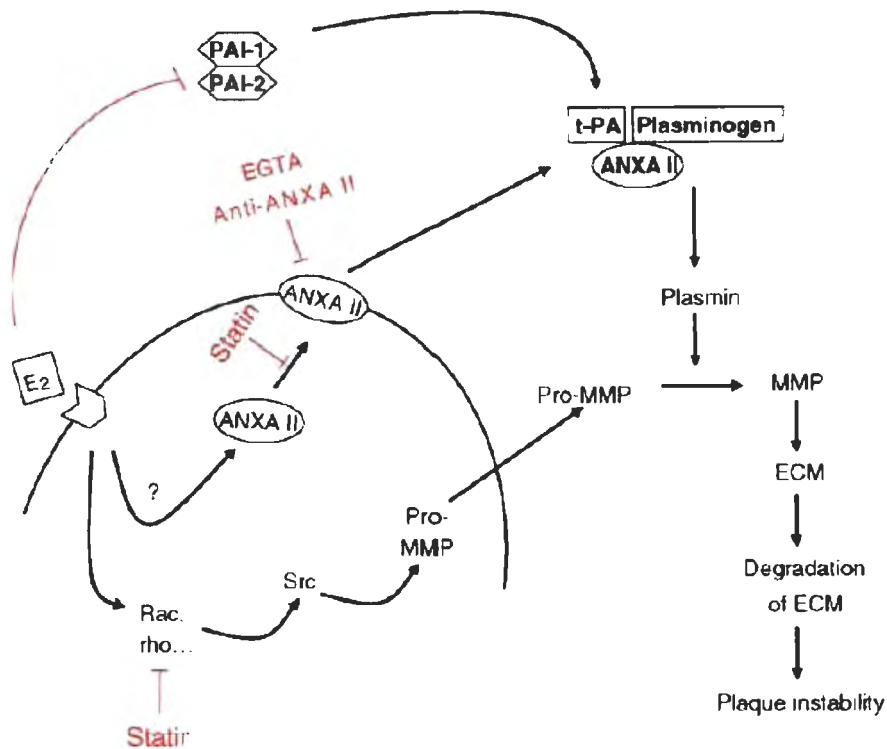
Figure A.2. The mechanism for E2-stimulated MMP production in macrophages. E2 increases MMP by increasing expression of ANXII, which inturn promotes the interaction of tPa and plasminogen leading to plasmin activation and conversion of pro-MMP to active MMP. Signaling of MMP leads to activation of rac and rho which in turn activate Src and pro-MMP. Statins inhibit the association of ANXII as well as translocation of rac and rho. This figure has been adapted from Ref 38.

Most of the known biological functions of annexin V (Anx V) can be attributed to its high affinity for negatively charged POPS phospholipids in the presence of physiological concentrations of calcium [40]. This feature has been exploited and Anx V is used to detect apoptosis conditions as the apoptotic cells rupture and the PS moieties become accessible to Annexin labeled with FITC.

A.1.7. Purification and implication of this work

Annexins generally are prepared by using a single-step anion exchange chromato-

graphy procedure [38]. The disadvantage in this method is that some portion of annexin V gets deleted and only the prominent domain, which has high affinity for the PS membrane, is included. The protein is purified with the help of either POPS-rich liposomes or beads [41]. Rapid expression and purification systems for recombinant proteins are well established and in many cases provide better and quicker isolation procedures and yield of specific proteins. The hexa-Histidine tag (His tag) is commonly used for making insoluble proteins express well in soluble fractions. Addition of a poly-histidine tag to Annexin V (or any protein), should provide a simple means of isolating proteins from other contaminating bacterial proteins using a single-step purification procedure. The size of the hexa-His tag (19.2 kDa) is smaller than other commonly used tags like Glutathione S Transferase (27.8 KDa) or Maltose-Binding Protein (44.9 KDa). Thus, this small tag should not interfere with the function Anx V to bind to POPS.

The cDNA encoding mature anx V has been isolated using a RT-PCR method on total RNAs from fresh human placenta [42]. The anx V cDNA was cloned into expression plasmid pET24a (+) under the T7 promoter and then transformed into *E.coli* BL21(DE3) [42] containing a His-tag at the N terminus. In another study, Sun *et. al* [43] cloned human annexin V cDNA into plasmid pET19b fused to a histidine tag with ten consecutive residues at the N-terminus. When expressed in *E. coli* BL21 (DE3) cells, the recombinant His10-annexin V accumulated in a soluble form in the cytoplasm and was purified using metal chelate affinity chromatography and anion-exchange chromatography. However, the presence of the His-tag lead to artifactual results in metal dependent experiments [44]. Thus use recombinant human annexin V for biophysical studies with MMPs [37-38], there

is a need to clone and over-express the recombinant human annexin V without a His tag.

A.2. Materials

Plasmid pOTB7 containing the full-length cDNA clone of human Annexin V (ATCC #: 2261) was purchased from Open Biosystems (Huntsville, AL-Catalog #: MHS1011-59192). *Bam HI* and *Nco I* restriction endonucleases, and T4 DNA ligase (Catalog #: M1801) were purchased from Promega (Madison, USA). Miniprep, Maxiprep and Qiaquick® purification kits were purchased from Qiagen (Valencia, CA). Primers were designed and the sequences were checked for hair-pin loop formation and secondary structure formation before having them custom synthesized at Integrated DNA technologies (IDT, San Diego, California). Recombinant *Pfu* DNA polymerase and DH5α *E. coli* competent cells were purchased from Stratagene (La Jolla, CA). Agarose ((Molecular Biology grade) was purchased from Bio-Rad (Hercules, CA). The plasmid pET3d was purchased from Novagen (Catalog # 69421-3). O'GeneRuler[TM] 1Kb DNA ladder Plus (catalog # SM1343) was purchased from Fermentas, Inc (Maryland). All other chemicals were of reagent grade, and were used without further purification.

A.3. Methods

A.3.1.Colony cracking technique

5 ml of overnight cultures of the colonies of interest was grown. A 1 ml aliquot of each overnight grown culture was placed in a 1.5 ml microfuge tube and the remaining cultures were refrigerated. The culture in the microfuge tube was centrifuged at 15,000 r.p.m. a Sorvall SS34 fixed angle rotor for 1 minute. The supernatant was removed. 50 μl of 1X lysis buffer (See below for the composition) was added to the cell pellet and

vortexed to completely resuspend the cells. The resuspended solution was boiled for 90 seconds at 100°C and centrifuged at 15,000 r.p.m. using a Sorvall SS34 fixed angle rotor for 10 minutes. 15 µl of the cleared supernatant was aliquoted in a new 1.5 ml microfuge tube. Restriction digests were setup of the sample at the 37°C temperature. After the digest, the samples were analyzed by agarose-gel electrophoresis. Plasmid-positive candidates were obtained from the refrigerated culture.

A.3.2. Preparation of the lysis buffer

The 10 ml of 1X lysis solution consists of 100 µl from 1M Tris-HCl (pH 8.0), 200 µl from 0.5 M EDTA (pH 8.0), 1.5 g sucrose, 20 mg lysozyme, 200 µl from 10 mg/ml RNAase A, 100 µl from 10 mg/ml BSA and 9.4 ml ddH$_2$O.

A.4. Results and Discussion

To evoke new biophysical studies with MMP isozymes in presence of high concentrations of metal ions, human Annexin V was cloned without a His tag. Figure A.3.A shows the plasmid map of pOTB7 vector. This is a mammalian non-expression vector that was used as a vehicle to transport the human Annexin V (hAnx V) gene. Figure A.3.B shows the sequence of the insert in pOTB7. The sequence matches with the existing sequence of hAnx V available in NCBI (Accession #: BC001429.2). This is the cDNA clone sequence: MGC: 2261. The sequence was carefully matched with the known sequence of hAnxV. The cDNA of hAnx V was in a glycerol stock, so to use it further in the subsequent experiment, the glycerol stock was streaked on an Agar plate containing chloramphenicol (50 µg/ml). The plate was incubated overnight and colonies were observed the next day. The plasmid DNA was isolated from a single colony using a

QIAquick® plasmid isolation kit. Samples (5 µl) of the plasmid DNA were either treated with restriction endonucleases *EcoRI* and *Hpa I* or untreated and separated by agarose-gel electrophoresis. It was concluded that the plasmid pOTB7 containing the full length clone of the coding sequence (CDS) of human Annexin V and was ready for further use.

The positive plasmid obtained from the above treatment was transformed into DH5α competent cells and plated on LB-Amp (100 µg/ml) plates. After overnight incubation at 37°C, Amp resistant colonies were observed. After the overnight incubation, Figure A.5 shows several Amp [R] colonies and they were selected for further use and plasmid DNA was purified from cells grown from these colonies using the Plasmid Isolation kit from Qiagen. The purified plasmids from the clonies were stored at -20°C.
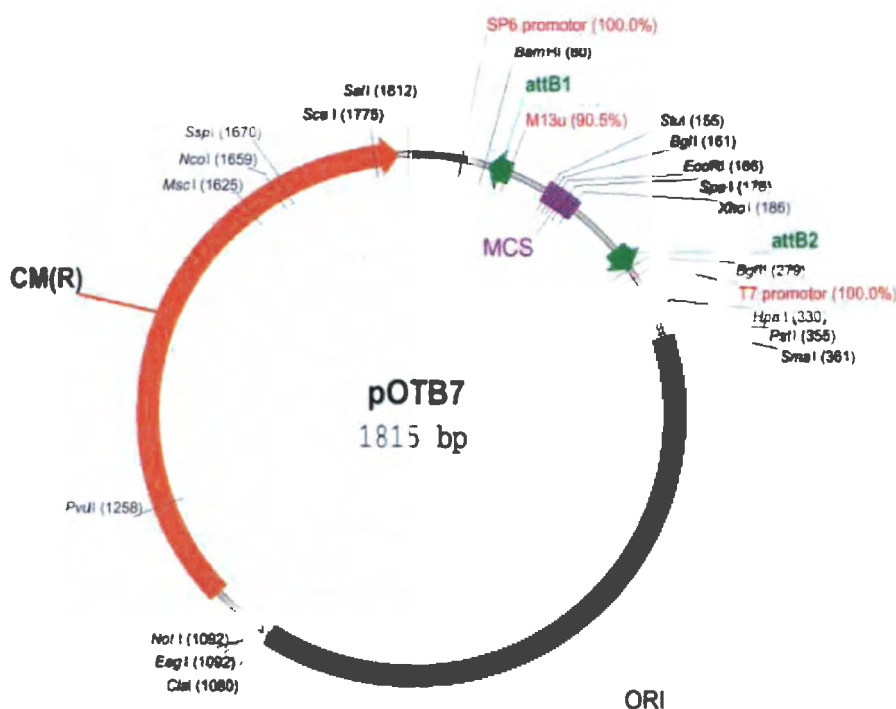
Figure A.3.A. Plasmid map of pOTB7 vector showing the restriction sites. The hAnx V sent by Open Biosystem was incorporated between the *Eco RI* and *Xho I*.

Figure A.3.B shows the human annexin A5, (cDNA clone MGC: 2261), complete CDS. The bases corresponding from 71 to 1033 bases constitutes of the CDS sequence of the human Annexin V clone [45].

```
ORIGIN
      1 ggcgcgctaa gcccgaggtt tcttctcttt tgcagtcctg cttcaccttc ccctgacctg
     61 agtagtcgcc atggcacagg ttctcagagg cactgtgact gacttccctg gatttgatga
    121 gcgggctgat gcagaaactc ttcggaaggc tatgaaaggc ttgggcacag atgaggagag
    181 catcctgact ctgttgacat cccgaagtaa tgctcagcgc caggaaatct ctgcagcttt
    241 taagactctg tttggcaggg atcttctgga tgacctgaaa tcagaactaa ctggaaaatt
    301 tgaaaaatta attgtggctc tgatgaaacc ctctcggctt tatgatgctt atgaactgaa
    361 acatgccttg aagggagctg gaacaaatga aaaagtactg acagaaatta ttgcttcaag
    421 gacacctgaa gaactgagag ccatcaaaca agtttatgaa gaagaatatg gctcaagcct
    481 ggaagatgac gtggtggggg acacttcagg gtactaccag cggatgttgg tggttctcct
    541 tcaggctaac agagaccctg atgctggaat tgatgaagct caagttgaac aagatgctca
    601 ggctttattt caggctggag aacttaaatg ggggacagat gaagaaaagt ttatcaccat
    661 ctttggaaca cgaagtgtgt ctcatttgag aaaggtgttt gacaagtaca tgactatatc
    721 aggatttcaa attgaggaaa ccattgaccg cgagacttct ggcaatttag agcaactact
    781 ccttgctgtt gtgaaatcta ttcgaagtat acctgcctac cttgcagaga ccctctatta
    841 tgctatgaag ggagctggga cagatgatca taccctcatc agagtcatgg tttccaggag
    901 tgagattgat ctgtttaaca tcaggaagga gtttaggaag aattttgcca cctctcttta
    961 ttccatgatt aagggagata catctgggga ctataagaaa gctcttctgc tgctctgtgg
   1021 agaagatgac taacgtgtca cggggaagag ctccctgctg tgtgcctgca ccaccccact
   1081 gccttccttc agcaccttta gctgcatttg tatgccagtg cttaacacat tgccttattc
   1141 atactagcat gctcatgacc aacacataca cgtcatagaa gaaaatagtg gtgcttcttt
   1201 ctgatctcta gtggagatct ctttgactgc tgtagtacta aagtgtactt aatgttacta
   1261 agtttaatgc ctggccattt tccatttata tatatttttt aagaggctag agtgctttta
   1321 gccttttta aaaactccat ttatattaca tttgtaacca tgatacttta atcagaagct
   1381 tagccttgaa attgtgaact cttggaaatg ttattagtga agttcgcaac taaactaaac
   1441 ctgtaaaatt atgatgattg tattcaaaag attaatgaaa ataaacatt tctgtccccc
   1501 tgaaaaaaaa aaaaaaaaaa aaaaaaaa
```

Figure A.3.B. The sequence of the insert that has been sent incorporated in plasmid map of pOTB7 vector within the restriction sites of *Eco RI* and *Xho I*. The nucleotides from 71 to 1033 correspond to the CDS sequence. It has been indicated in red.

Figure A.4 shows the pET3d vector map of the plasmid to which the ORF (bases 71-1033 of hAnx V) would be inserted. The pET3d vector contains an N-terminal T7-Tag sequence and *Bam HI* cloning site. The cloning / expression region of the coding strand transcribed by T7 RNA polymerase has been shown in the Figure A.4. There are two major reasons as to why pET3d was chosen to be the vector into which hAnx V clone was to be inserted. Firstly, there has been literature reports [46-47] stating that the rat Annexin V was expressed in pET3d [52]. Secondly, the plasmid contains a T7 promoter and cloning sites to put the insert DNA in the proper reading frame for expression.
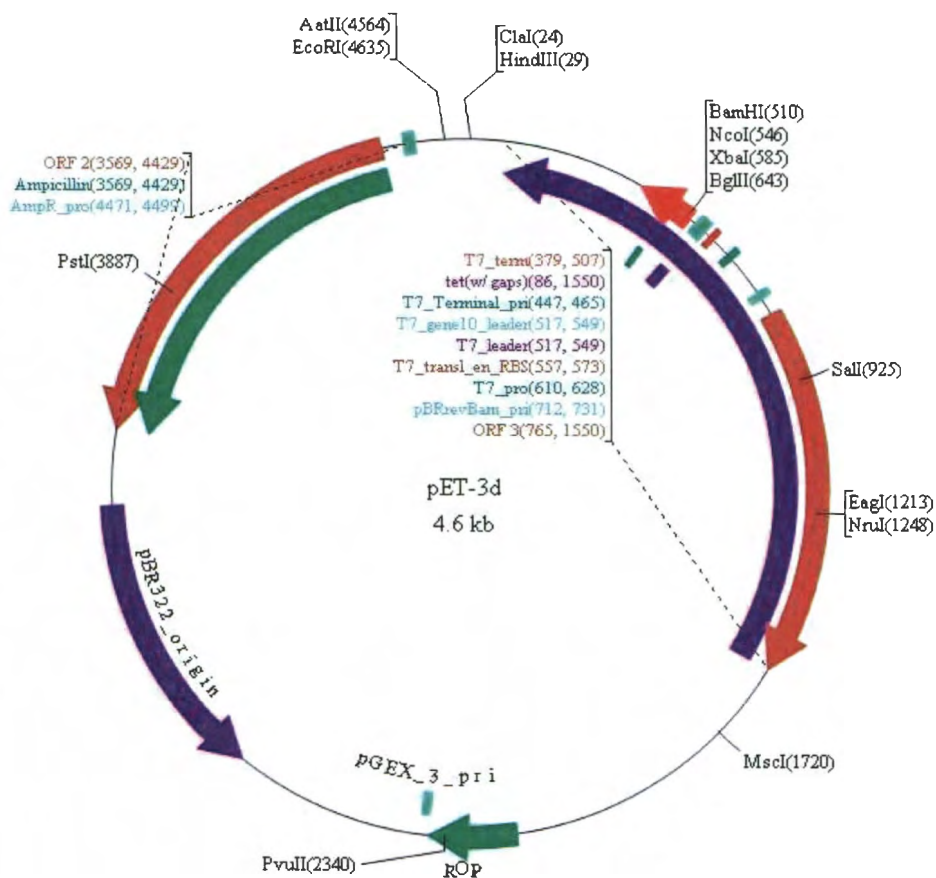
Figure A.4. Plasmid map of pET3d showing the backbone and the restriction sites. The restriction sites for the insertion of the gene of interest are *Bam HI* and *Nco I*.

Figure A.5.A shows the overview of the transformed pET3d colonies on LB-Amp plates grown overnight at 37°C, and a closer view of the colonies has also been shown in Figure A.5.B and C. The pET3d vector was treated with restriction endonucleases *Bam HI* and *Nco I*. Samples were loaded onto 1% agarose gel and electrophoresed. The pET3d plasmid was transformed into DH5α chemically competent cells, plated, incubated for overnight at 37°C, and Amp resistant colonies were obtained. The plasmid was isolated from Amp^R using the Maxi Plasmid Isolation kit. Taking about 2 µl of the DNA from the Maxi preparation stock, a restriction digest was setup. The restriction enzymes used were *Bam HI* and *Nco I*. The result verified the correct size of the DNA fragment for pET3d. Restriction fragments were separated on an agarose gel by electrophoresis. Staining of the gel with Ethidium Bromide and observation under UV light showed a 4.6 Kb band, indicating expected size of the plasmid DNA fragment.

At this point, purification of the vector from the gel was required in order to make the selection of the vector alone without the small fragment (0.036Kb) between *Bam HI* and *Nco I* site. DNA fragments purified with the QIAquick system would be ready for direct use in all applications, including sequencing, ligation and transformation, restriction digestion, labeling, microinjection, PCR and *in vitro* transcription. Figure A.6 shows the results of agarose gel used to separate the vector DNA after gel purification. Before storing the purified plasmid (pET3d) at -20°C, the absorbance at A_{260}, using Molecular Devices SpectraMax$^®$ Plus microplate reader or a quartz cuvette (1-cm path length), was measured. The excitation spectra measured was represented after subtraction of the buffer background (ddH$_2$0 was used as blank) and the difference data was converted in Absorbance units.
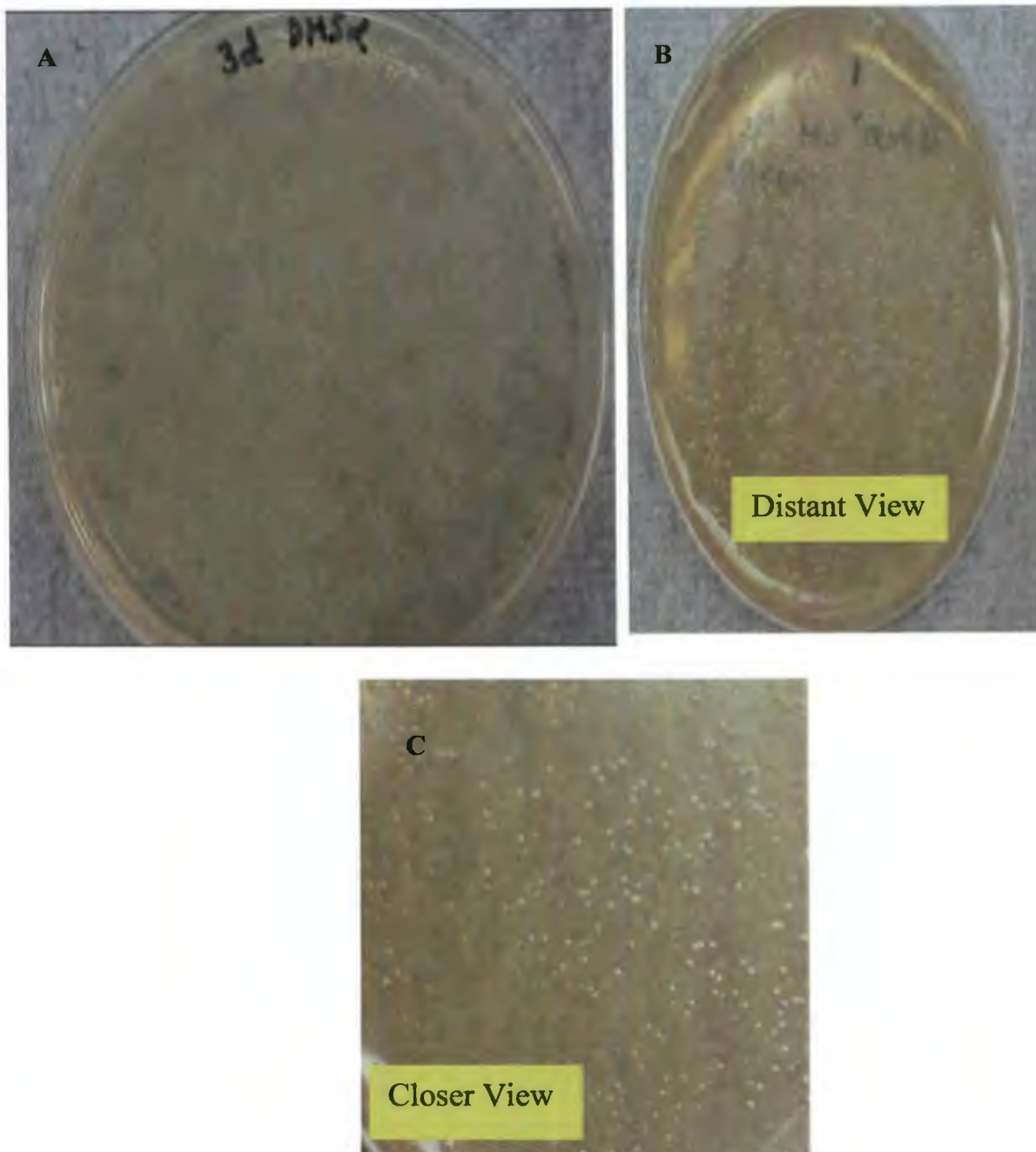
Figure A.5.A. Ampicillin containing plates with colonies of pET3d vector in DH5α. B. The distant view of the colonies of pET3d vector in DH5α. C. The closer view of the colonies of pET3d vector in DH5α.
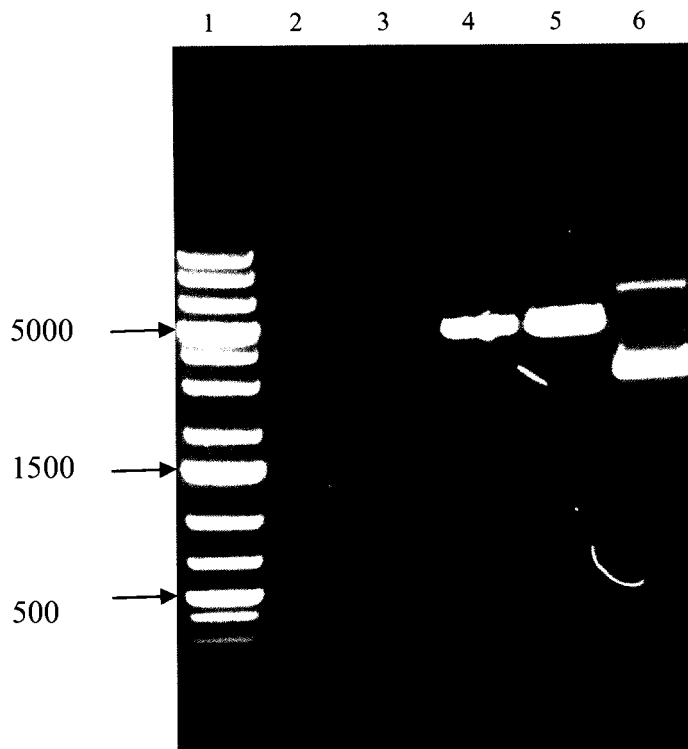
Figure A.6. Agarose gel showing the vector after gel purification. L to R: *Lane 1*: DNA ladder, *Lane 4*: pET3d vector after cut by *Bam HI* and *Nco I*, *Lane 5*: pET3d vector after cut by Bam *HI/ Nco I* (Duplicate), Lane *6*: Uncut pET3d vector.

The positive plasmid DNA of hAnx V was transformed into DH5α competent cells and the plasmid was isolated. The nucleotide fragment from the residue Met 1 to Asp 320 amino acids (71 to 1033 bases) was amplified by the hot start PCR method [48] using the above plasmid as the DNA template and synthesized primers. The bases corresponding from 75 to 95 for the forward primer and bases corresponding from 1033 to 1011 for the reverse primer [43] were chosen for the primer designs. The Forward and Reverse primers were obtained from IDT (Integrated data Technologies). The Forward Primer (Reference #: 47723739) and the Reverse Primer (Reference #: 47723740) were used. Figure A.7 shows the forward and the reverse primers designed for the PCR reaction.

Annexin V Forward primer:

℗-5' TGCATTCCATGGCACAGGTTCTCAGAGGCACTG   3' OH

Annexin V Reverse primer:

℗-5' TGCATTGGATCCTTAGTCATCTTCTCCACAGAGCAGCAGAAGAGC 3' OH

Figure A.7. Forward and reverse pimers designed for the sub-cloning of hAnx V.

While designing forward and reverse primers, various aspects playing a major role in the success of the amplification of the correct PCR product were considered. These primers are designed to have a sequence corresponding to the reverse complement of a region of template or target DNA to which the primer would anneal. When designing primers for PCR, it is often necessary to make predictions regarding the melting temperature (T_m) and propensity to form dimers with self or other primers in the reaction. The IDT DNA (Select Oligo analyzer) program was used to perform these calculations on both the primer sequences. The forward primer is 33 bases in length, while the reverse primer has 45 bases. The reverse primer is a little long as compared to the norms of primer design. This was due to the need to obtain a balance between a length of the primer and a match with the T_m values between the two primers. Both the primers ended with 3'G or C, or GC: this prevents "breathing" of ends and increases the efficiency of priming. T_m for both the primers was comparable (67-68°C). The T_m for both the primers were calculated using the Wu *et al.* [48] equation; this is an empirically derived equation, based on primer length and GC content, to determine optimal oligonucleotide annealing temperatures.

In designing these two primers care has been taken to incorporate the restriction sites for (*Bam HI* and *Nco I*) at the correct ends. *Nco I* (**CCATGG**) is incorporated at the 5' end of forward primer while *Bam HI* (**GGATCC**) in the reverse primer. This was done to obtain the PCR product in alignment with the reading frame of the vector (pET3d-Figure A.4). For better primer-template hybridization during annealing, random 6 bases (TGCATT) have been added in both the primers at the 5'end. The use of random extra bases is used in conditions where information, e.g. a motif binding site, restriction endonuclease site or GC clamp, is attached to 5' end. Such extensions do not generally alter annealing to the sequence specific portion of the primer [48-49].

After the PCR product was obtained (Figure A.8), the product was first analyzed by agarose-gel electrophoresis. The PCR fragment corresponded to 0.96 Kb in size when compared to the ladder. The PCR product was purified using Omega Product Purification Kit (Cat #: D6493-00). The absorbance at A_{260} was measured to estimate the amount of DNA present in the purified product (Figure A.9). The restriction enzyme (*Bam HI* and *Nco I*) treatment and subsequently agarose-gel electrophoresis established the presence of the correct purified PCR product.

Both the vector (gel purified pET3d) and the insert (purified PCR product) were ready to be used for the ligation procedure. Individual restriction reactions, in two separate eppendorf tubes (one for the vector and another one for the insert), were setup. The vector and the insert were treated with both *Bam HI* and *Nco I*. The vector and the insert after the double restriction enzyme digestion were used for the Ligation experiment.
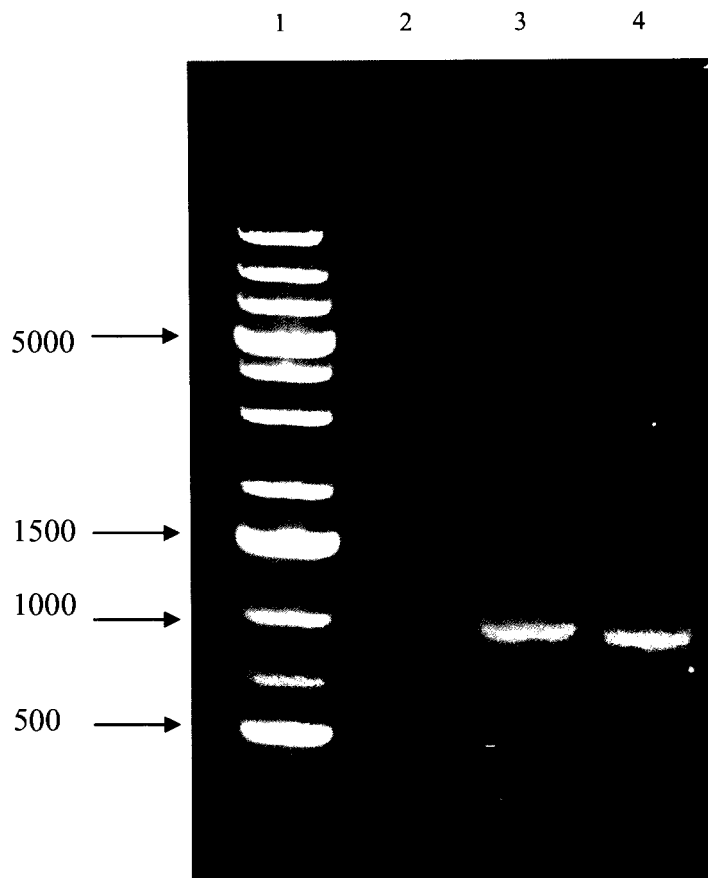
Figure A.8. Agarose gel showing the PCR amplified CDS of hAnx V. L to R: *Lane 1*: The DNA Ladder, *Lane 3*: The PCR amplified product, *Lane 4*: The PCR amplified product (duplicate).
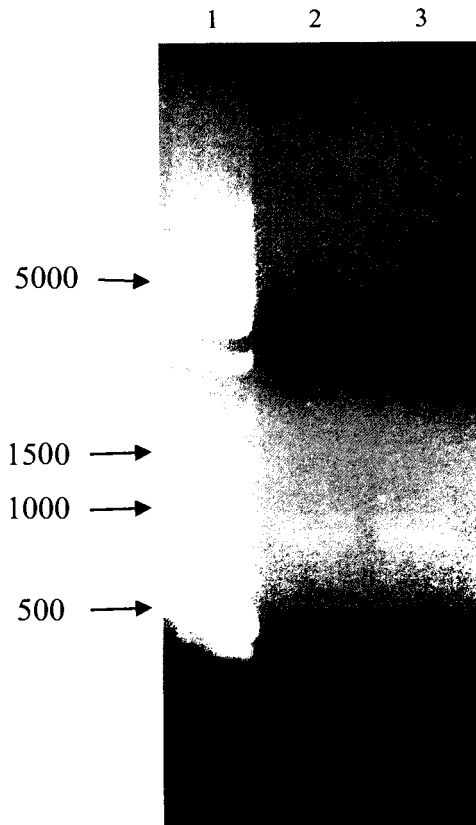
Figure A.9. Agarose gel showing the PCR amplified product of amplified CDS of hAnx V after purification. L to R: *Lane 1*: DNA ladder, *Lane 2*: PCR product after purification. *Lane 3*: PCR product after purification (duplicate).

The amount of vector and insert used in the ligation experiment were calculated according to the following calculation.

$$\text{ng of Insert} = \frac{\text{ng of vector * Kb size of the Insert}}{\text{Kb size of the vector}} * \frac{\text{molar ratio of Insert}}{\text{molar ratio of vector}} \quad \text{.......(A1)}$$

The molar ratio of vector to insert DNA with varying concentrations (1:1, 1:3 or 3:1) was used while cloning the fragment into the plasmid vector. Different ratios of the vector and insert were used to setup five different experiments. The eppendorf tubes were incubated for 16 hours at 15°C inside the Thermocycler. The ligated reaction mixture was used in the

transformation process along with the DH5α competent cells. After incubation overnight at 37°C, colonies in the agar plate containing Ampicillin were observed. However, just to pursue the matter more extensively and prevent missing out any positive clones, all the colonies (53 colonies) obtained in the two agar test plates were hand picked. 5 ml started culture of LB broth containing Ampicillin as the antibiotic was grown for 10-12 hours at 37°C with constant stirring at 250 r.p.m. in a shaker. After the primary culture looked turbid, cells were centrifuged down (8,000 r.p.m using a Sorvall SLA 1500 fixed angle rotor) to form a pellet at the bottom of the centrifuge tube. The pellets were processed to obtain the plasmid using a technique known as "Colony Cracking Technique" (see the Methods Section). For future references, master plates were prepared of all the 53 colonies.

It is essential to use a technique that allows simultaneous rapid screening of a large number of potential positive clones without requiring DNA amplification or using expensive restriction enzymes. A technique that fulfils these criteria is known as "Colony Cracking". This technique is a very fast yet a very crude procedure [50] to determine the positive clones. Figure A.10 shows the agarose gel of all the 53 clones double treated with the two restriction enzymes. It is very evident from the gel that Clone # 2 (Figure A.10.A), Clone # 21 and Clone # 36 (Figure A.10.B) seemed to be the positive clones. The plasmids extracted from the Colony Cracking technique were treated with *Bam HI and Nco I*, later agarose-gel electrophoresis confirmed the positive clones for hAnx V from the 53 clones. Figure A.11 shows the photos of Master Plates: [A]. Master Plate-1 [B]. Master Plate-2 and [C]. Control Plate. The 53 colonies obtained after plating the ligation reaction mixture in the LB-Amp plate were hand picked and streaked in the master plate-1 and master plate-2.
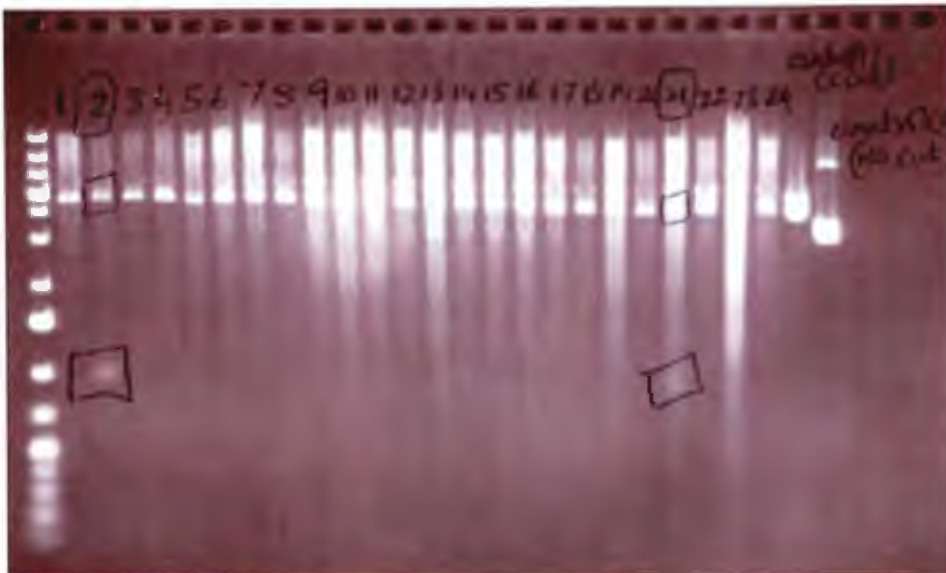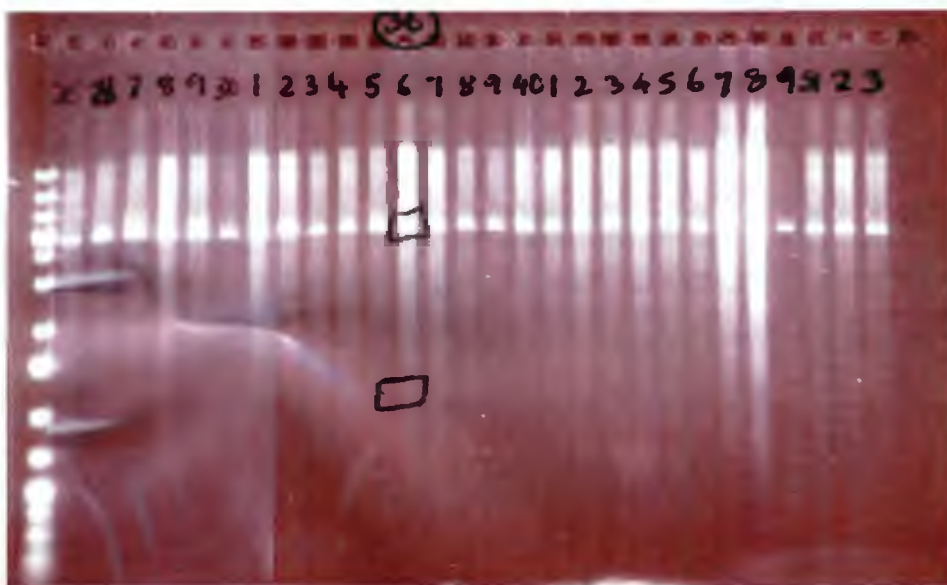
Figure A.10.A. Agarose gel showing the positive clones using Colony Cracking procedure from Gel 1. B. Agarose gel showing the positive clones using Colony Cracking procedure from Gel 2. In both the Gels the square boxes indicate the bands of the vector and insert of the positive clones.

Here, the numbering in the plate has been done as the indication goes from Left to right (L to R) in Plate-1 and Plate-2. Figure A.11.C shows the control plate. No colonies were observed indicating that there is no contamination in the plates used (negative control). The positive clones were also used to provide starter cultures in 5ml tubes. These were grown for 8-10 hours at 37°C (Figure A.11.D) and the plasmid was isolated from the three positive clones (Figure A.10.A and B). Again restriction digest was setup (*Bam HI and Nco I*). Figure A.12. C shows the agarose-gel electrophoresis with *Bam HI* and *Nco I* cut in hAnx V cloned in pET3d vector. The figure shown here is that of Colony # 2 (as one of the positive clones) but a similar treatment was done to colony # 21. Figure A.12.A shows the vector map of the pET3d vector alone using Serial Cloner software. Figure A.12.B shows the vector map of the linear insert of hAnx V constructed using Serial Cloner. Figure A.12 A and B corroborates with the experimental result obtained in Figure A.12.C.

The sequencing results were analyzed using Clustal W2 [51] for sequence alignment. In conjunction with results from Figure A.11 and A.12, Colony # 2 and 21 were sent for sequencing from the McLab (San Francisco, CA). Different samples of the same positive clones were anayzed: Colony # 2 was picked up and two separate plasmid preparations were done and were named as P2-1, P2-2. Similarly, Colony # 21 was picked up and two separate plasmid preparations were done and were named as P21-1, P21-2. All 8 samples were used to sequence with the forward and the reverse primers. Using Clustal W2 software, the alignment of the sequences and comparison with the Reference sequence (NM_001154) were noted. The % identity between the reference sequence and the existing

sequence of hAnx V available in NCBI were compared (Accession #: BC001429.2). There was 100% sequence identity between the two known sequences (NM_001154 and BC001429.2).

The 8 sample sequences are aligned together in a single multiple alignment, so that the forward primer sequence and the reverse-complement sequence determined from the reverse primer are both aligned with the same starting sequence. This was done to facilitate the easy observation and comparison of these aligned sequences, which would determine the consensus sequence. The sequence homology amongst these 8 sample sequences with the reference sequence varied between 94 to 99%. The single sequence alignment of one of the best matched sequences (99% identity match with the Reference sequence) with the reference sequence of hAnx V is shown in Figure A.13. While detecting the bases during sequencing, due to the proximity of the forward and reverse primers, no signal for the initial and last few bases was reliably detected. This led to the occurrence of less number of bases (846 bases) than the actual 963 bases. For obtaining sequences near the 5' and 3' ends, the Universal Forward and Universal Reverse primers should have been used.

Figure A.14 shows the consensus sequence obtained. The resultant sequence has 846 nocleotides (Reference Sequence has 963 nucleotides). Figure A.15 shows the protein sequence from the consensus Sequence (Figure A.14). The translated protein had 282 amino acids (Reference hAnx V protein has 320 amino acids) and matched the sequence of amino acids in the reference protein.
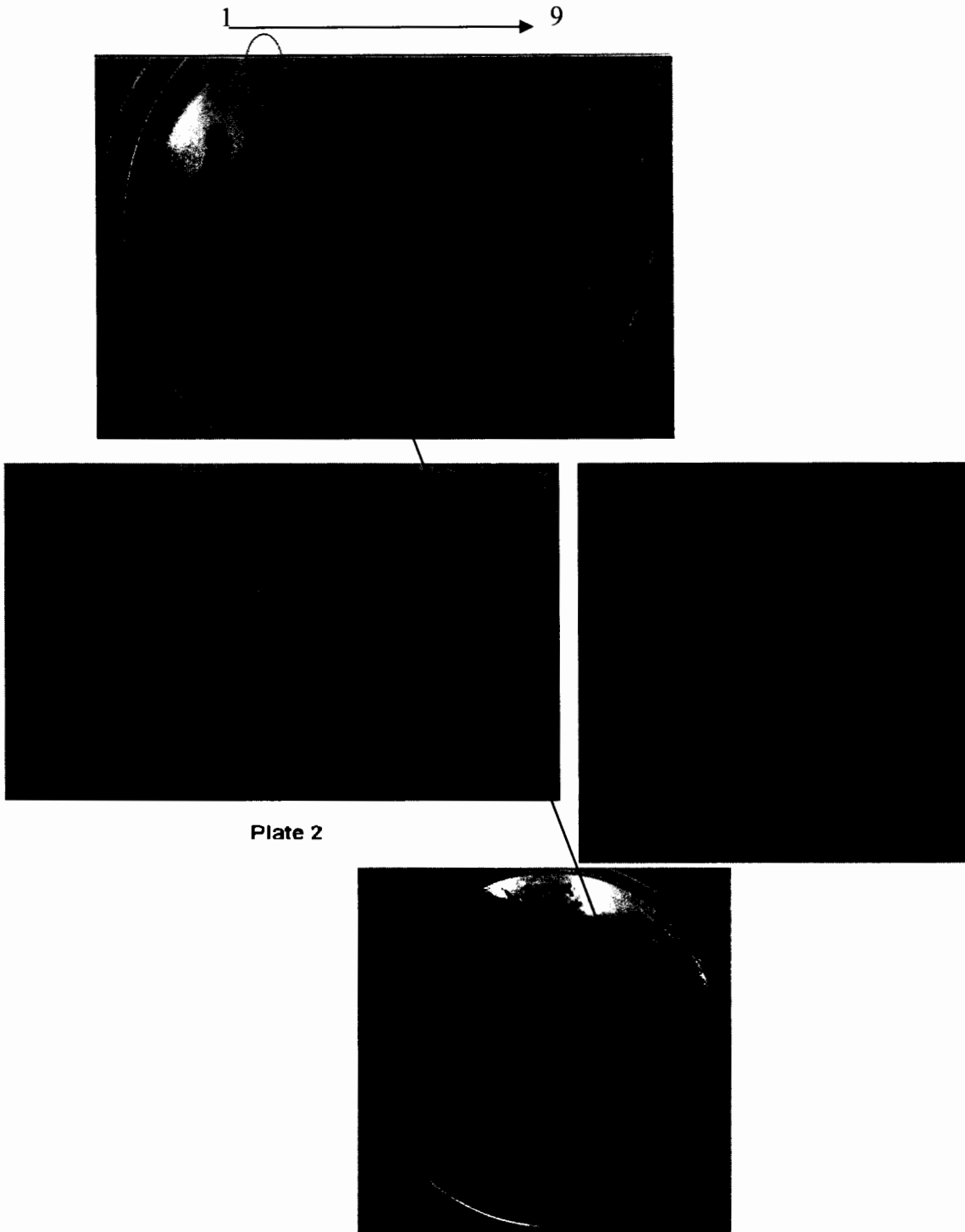
Figure A.11. Photos of Master Plates: A. Master Plate [1] B. Master Plate [2] C. Control Plate. D. The ampicillin containing agar plate with the colony picked up from Master plate 1 (Colony # 2) was transformed in fresh DH5α cells. The spread of isolated colonies are being observed of the positive clone (Colony # 2).

Figure A.12. Agarose gel showing the *Bam HI* and *Nco I* cut in hAnx V cloned in pET3d vector. A. The vector map of the pET3d vector alone using Serial Cloner. B. The vector map of the linear insert that should be ligated to pET3d vector using Serial Cloner. C. The Agarose gel showing the bands of the vector and the insert after treatment with double digest of *Bam HI* and *Nco I* restriction enzymes. The DNA shown in the figure is from Colony # 2 but similar treatment was done to colony # 21. L to R: *Lane 1*: DNA Ladder, *Lane 2*: pET3d vector and the hAnx V Insert after *Bam HI* and *Nco I* treatment.

```
CLUSTAL 2.0.12 multiple sequence alignment


Ref        ATGGCACAGGTTCTCAGAGGCACTGTGACTGACTTCCCTGGATTTGATGAGCGGGCTGAT 60
RP21-2     ------------------------------------------------------------


Ref        GCAGAAACTCTTCGGAAGGCTATGAAAGGCTTGGGCACAGATGAGGAGAGCATCCTGACT 120
RP21-2     ------------------TATGAAAGGCTTGGGCACAGATGAGGAGAGCATCCTGACT 40
                             ******************************************


Ref        CTGTTGACATCCCGAAGTAATGCTCAGCGCCAGGAAATCTCTGCAGCTTTTAAGACTCTG 180
RP21-2     CTGTTGACATCCCGAAGTAATGCTCAGCGCCAGGAAATCTCTGCAGCTTTTAAGACTCTG 100
           ************************************************************


Ref        TTTGGCAGGGATCTTCTGGATGACCTGAAATCAGAACTAACTGGAAAATTTGAAAAATTA 240
RP21-2     TTTGGCAGGGATCTTCTGGATGACCTGAAATCAGAACTAACTGGAAAATTTGAAAAATTA 159
           ************************************************************


Ref        ATTGTGGCTCTGATGAAACCCTCTCGGCTTTATGATGCTTATGAACTGAAACATGCCTTG 300
RP21-2     ATTGTGGCTCTGATGAAACCCTCTCGGCTTTATGATGCTTATGAACTGAAACATGCCTTG 219
           ************************************************************


Ref        AAGGGAGCTGGAACAAATGAAAAAGTACTGACAGAAATTATTGCTTCAAGGACACCTGAA 360
RP21-2     AAGGGAGCTGGAACAAATGAAAAAGTACTGACAGAAATTATTGCTTCAAGGACACCTGAA 279
           ************************************************************


Ref        GAACTGAGAGCCATCAAACAAGTTTATGAAGAAGAATATGGCTCAAGCCTGGAAGATGAC 420
RP21-2     GAACTGAGAGCCATCAAACAAGTTTATGAAGAAGAATATGGCTCAAGCCTGGAAGATGAC 339
           ************************************************************


Ref        GTGGTGGGGGACACTTCAGGGTACTACCAGCGGATGTTGGTGGTTCTCCTTCAGGCTAAC 480
RP21-2     GTGGTGGGGGACACTTCAGGGTACTACCAGCGGATGTTGGTGGTTCTCCTTCAGGCTAAC 399
           ************************************************************


Ref        AGAGACCCTGATGCTGGAATTGATGAAGCTCAAGTTGAACAAGATGCTCAGGCTTTATTT 540
RP21-2     AGAGACCCTGATGCTGGAATTGATGAAGCTCAAGTTGAACAAGATGCTCAGGCTTTATTT 459
           ************************************************************


Ref        CAGGCTGGAGAACTTAAATGGGGGACAGATGAAGAAAAGTTTATCACCATCTTTGGAACA 600
RP21-2     CAGGCTGGAGAACTTAAATGGGGGACAGATGAAGAAAAGTTTATCACCATCTTTGGAACA 519
           ************************************************************


Ref        CGAAGTGTGTCTCATTTGAGAAAGGTGTTTGACAAGTACATGACTATATCAGGATTTCAA 660
RP21-2     CGAAGTGTGTCTCATTTGAGAAAGGTGTTTGACAAGTACATGACTATATCAGGATTTCAA 579
           ************************************************************


Ref        ATTGAGGAAACCATTGACCGCGAGACTTCTGGCAATTTAGAGCAACTACTCCTTGCTGTT 720
RP21-2     ATTGAGGAAACCATTGACCGCGAGACTTCTGGCAATTTAGAGCAACTACTCCTTGCTGTT 639
           ************************************************************


Ref        GTGAAATCTATTCGAAGTATACCTGCCTACCTTGCAGAGACCCTCTATTATGCTATGAAG 780
RP21-2     GTGAAATCTATTCGAAGTATACCTGCCTACCTTGCAGAGACCCTCTATTATGCTATGAAG 699
           ************************************************************


Ref        GGAGCTGGGACAGATGATCATACCCTCATCAGAGTCATGGTTTCCAGGAGTGAGATTGAT 840
RP21-2     GGAGCTGGGACAGATGATCATACCCTCATCAGAGTCATGGTTTCCAGGAGTGAGATTGAT 759
           ************************************************************


Ref        CTGTTTAACATCAGGAAGGAGTTTAGGAAGAATTTTGCCACCTCTCTTTATTCCATGATT 900
```

372

```
RP21-2      CTGTTTAACATCAGGAAGAG--TTAGGAAGAATTTTGCCACCTCTCTTTATTCCATGATT 817
            *****************     **************************************

Ref         AAGGGAGATACATCTGGGGACTATAAGAAAGCTCTTCTGCTGCTCTGTGGAGAAGATGAC 960
RP21-2      AAGGGAGATAC--CTGGGTA---------------------------------------- 835
            ***********   ***** *

Ref         TAA 963
RP21-2      ---
```

Figure A.13. The sample (RF 21-1) sequence aligned with the Reference sequence. The reverse-complement sequence determined from the reverse primer has been aligned with the same starting sequence. The blue color represents the reference sequence; green color represents the sample sequence. The red colored star represents the homology amongst the sequences.

```
TTTGATGA GCGGGCTGAT GCAGAAACTC TTCGGAAGGC TATGAAAGGC TTGGGCACAG
ATGAGGAGAG CATCCTGACT CTGTTGACAT CCCGAAGTAA TGCTCAGCGC CAGGAAATCT
CTGCAGCTTT TAAGACTCTG TTTGGCAGGG ATCTTCTGGA TGACCTGAAA TCAGAACTAA
CTGGAAAATT TGAAAAATTA ATTGTGGCTC TGATGAAACC CTCTCGGCTT TATGATGCTT
ATGAACTGAA ACATGCCTTG AAGGGAGCTG GAACAAATGA AAAAGTACTG ACAGAAATTA
TTGCTTCAAG GACACCTGAA GAACTGAGAG CCATCAAACA AGTTTATGAA GAAGAATATG
GCTCAAGCCT GGAAGATGAC GTGGTGGGGG ACACTTCAGG GTACTACCAG CGGATGTTGG
TGGTTCTCCT TCAGGCTAAC AGAGACCCTG ATGCTGGAAT TGATGAAGCT CAAGTTGAAC
AAGATGCTCA GGCTTTATTT CAGGCTGGAG AACTTAAATG GGGGACAGAT GAAGAAAAGT
TTATCACCAT CTTTGGAACA CGAAGTGTGT CTCATTTGAG AAAGGTGTTT GACAAGTACA
TGACTATATC AGGATTTCAA ATTGAGGAAA CCATTGACCG CGAGACTTCT GGCAATTTAG
AGCAACTACT CCTTGCTGTT GTGAAATCTA TTCGAAGTAT ACCTGCCTAC CTTGCAGAGA
CCCTCTATTA TGCTATGAAG GGAGCTGGGA CAGATGATCA TACCCTCATC AGAGTCATGG
TTTCCAGGAG TGAGATTGAT CTGTTTAACA TCAGGAAGGA GTTTAGGAAG AATTTTGCCA
CCTCTCTT
```

Figure A.14. The Consensus sequence from the single multiple alignments. The sequence has 846 nucleotides.

```
FDERADAETLRKAMKGLGTDEESILTLLTSRSNAQRQEISAAFKTLFGRDLLDDLK
SELTGKFEKLIVALMKPSRLYDAYELKHALKGAGTNEKVLTEIIASRTPEELRAIKQ
VYEEEYGSSLEDDVVGDTSGYYQRMLVVLLQANRDPDAGIDEAQVEQDAQALFQA
GELKWGTDEEKFITIFGTRSVSHLRKVFDKYMTISGFQIEETIDRETSGNLEQLLLA
VVKSIRSIPAYLAETLYYAMKGAGTDDHTLIRVMVSRSEIDLFNIRKEFRKNFATSL
```

Figure A.15. The hAnx V protein sequence from the Consensus sequence. The protein has 282 amino acids.

373

The cloning of human Annexin V could be presumably over-expressed in BL21 chemically competent cells and isolated using anionic-exchange chromatography or using the protocol of purifying annexins without the use of phospholipids [52]. The protein could possibly be purified in decent quantities from inclusion bodies. The sub-cloned, expressed and purified human annexin V without the Hexa-Histidine tag could then be used for biophysical studies with MMP isozymes in presence of calcium or other metal ion.

A.5. References

1. Pikula, J.B. (2003) In Annexins: Biological importance and Annexin-related pathologies, *Kluwer Acadeic/ Planum Publishers, NY, USA.*
2. Swairjo, M.A., and Seaton, B.A. (1994) Annexin structure and membrane interactions: A molecular perspective, *Annu.Rev. Biophys. Biomol. Struct.* 23: 193-213.
3. Geisow, M.J., and Walker, J. H. (1986) New proteins involved in cell regulation by Ca^{2+} and phospholipids, *Trends Biol. Sci.* 11, 420-425.
4. Liemann,S., and Huber, R. (1997) Three-dimensional structure of annexins, *Cell. Mol .Life. Sci.* 53, 516-521.
5. Moss, S. E., Edwards H. C., and Crumpton M. J. (1991) Diversity in the annexin family. In: Novel calcium-binding proteins, pp:535–566, Heizmann, C. W. (Ed.), *Springer-Verlag,Berlin.*
6. Liemann, S., and Lewit-Bentley A. (1995) Annexins: a novel family of calcium- and membrane-binding proteins in search of a function, *Structure.* 3, 233–237.
7. Raynal, P., and Pollard, H. B. (1994) Annexins: the problem of assessing the biological role for a gene family of multifunctional calcium- and phospholipid-binding proteins, *Biochim. Biophys. Acta.* 1197, 63–93.
8. Bewley, M. C., Boustead, C. M., Walker, J. H., Waller, D. A. and Huber, R. (1993) Structure of chicken annexin V at 2.25-A° resolution, *Biochemistry.* 32, 3923–3929.
9. Concha, N. O., Head, J. F., Kaetzel, M. A., Dedman, J. R., and Seaton, B. A. (1993) Rat annexin V crystal structure: Ca^{2+}- induced conformational changes, *Science.* 261, 1321–1324.
10. Favier-Perron, B., Lewit-Bentley, A. and Russo-Marie, F. (1996) The high-resolution crystal structure of human annexin III shows subtle differences with annexin V, *Biochemistry.* 35, 1740–1744.
11. Benz, J., Bergner, A., Hofmann, A., Demange, P., Gottig, P., Liemann, S. (1996) The structure of recombinant human annexin VI in crystals and membrane-bound, *J. Molec. Biol.* 260,638–643.

12. Luecke, H., Chang, B. T., Maillard, W. S., Schlaepfer, D. D., and Haigler, H. T. (1995) Crystal structure of the annexin XII hexamer and implications for bilayer insertion, *Nature.* 378, 512–515.

13. Weng, X., Luecke, H., Song, I. S., Kang, D. S., Kim, S. H. and Huber, R. (1993) Crystal structure of human annexin I at 2.5A° resolution, *Prot. Sci.* 2, 448–458.

14. Burger, A., Berendes, R., Liemann, S., Benz, J., Hofmann, A., Gottig, P. (1996) The crystal structure and ion channel activity of human annexin II, a peripheral membrane protein, *J. Molec. Biol.* 257, 839–847.

15. Liemann, S., Bringemeier, I., Benz, J., Gottig, P., Hofmann, A., Hube, R. (1997) Crystal structure of the C-terminal tetrad repeat from synexin (annexin VII) of *Dictyostelium discoideum, J. Molec. Biol.* 270, 79-88.

16. Sopkova, J., Gallay, J., Vincent, M., Pancoska, P., and Lewit-Bentley, A. (1994) The dynamic behavior of annexin V as a function of calcium ion binding: a circular dichroism, UV absorption, and steady-state and time-resolved fluorescence study, *Biochemistry.* 33, 4490–4499.

17. Geisow, M. J. (1986) Common domain structure of Ca^{2+} and lipid-binding proteins, *FEBS Lett.* 203, 99–103.

18. Burger, A., Voges, D., Demange, P., Perez, C. R., Huber, R., and Berendes, R. (1994) Structural and electrophysiological analysis of annexin V mutants. Mutagenesis of human annexin V, an *in vitro* voltage-gated calcium channel, provides information about the structural features of the ion pathway, the voltage sensor and the ion selectivity filter, *J. Molec. Biol.* 237, 479–499.

19. Berendes, R., Voges, D., Demange, P., Huber, R., and Burger, A. (1993) Structure-function analysis of the ion channel selectivity filter in human annexin V, *Science.* 262, 427–430.

20. Liemann, S., Benz, J., Burger, A., Voges, D., Hofmann, A., and Huber, R. (1996) Structural and functional characterization of the voltage sensor in the ion channel human annexin V, *J. Molec. Biol.* 258, 555–561.

21. Pollard, H. B., Guy, H. R., Arispe, N., de la Fuente, M., Lee, G., and Rojas, E. M. (1992) Calcium channel and membrane fusion activity of synexin and other members of the Annexin gene family, *Biophys. J.* 62, 15–18.

22. Voges, D., Berendes, R., Demange, P., Benz, J., Gottig, P., and Liemann, S. (1995) Structure and function of the ion channel model system annexin V, *Adv. Enzymol.* 71, 209–239.

23. Rojas, E., Pollard, H. B., Haigler, H. T., Parra, C., and Burns, A. L. (1990) Calcium-activated endonexin II forms calcium channels across acidic phospholipid bilayer membranes, *J. Biol. Chem.* 265, 21207–21215.

24. Huber, R., Romisch, J., and Paques, E. P. (1990) The crystal and molecular structure of human annexin V, an anticoagulant protein that binds to calcium and membranes, *EMBO. J.* 9, 3867–3874.

25. Sopkova, J., Renouard, M., and Lewit-Bentley, A. (1993) The crystal structure of a new high-calcium form of annexin V, *J. Molec. Biol.* 234, 816–825.

26. Brooks, N.D., Grundy, J.E., Lavigne, N., Derry, M.C., Restall, C.M., MacKenzie, C.R., Waisman, C.M., Pryzdial, L.G. (2002) Ca^{2+}-dependent and phospholipid-independent binding of annexin 2 and annexin 5, *Biochem. J.* 367, 895.

27. Klee, C. B. (1988) Ca^{2+}-dependent phospholipid- (and membrane-)binding proteins, *Biochemistry.* 27, 6645–6653.

28. Lewit-Bentley, A., Morera, S., Huber, R., and Bodo, G. (1992) The effect of metal binding on the structure of annexin V and implications for membrane binding, *Eur. J. Biochem.* 210, 73–77.

29. Mo, Y., Compos, B.A., Mealy, T.R., Commodore, L., Head, J.F., Dedman, J.R., and Seaton, B.A. (2003) Interfacial Basic Cluster in Annexin V Couples Phospholipid Binding and Trimer Formation on Membrane Surfaces, *J. Biol. Chem.* 278 (4), 2437-2443.

30. Jin, M., Smith, C., Hsieh, Heng-Yu., Gibson, D.F., and Tait, J.F. (2004) Essential Role of B-helix Calcium Binding Sites in Annexin V-Membrane Binding, *J. Biol. Chem.* 279 (39), 40351-40357.

31. Huber, R., Berendes, R., Burger, A., Schneider, M., Karshikov, A., Luecke, H. (1992) Crystal and molecular structure of human annexin V after refinement. Implications for structure, membrane binding and ion channel formation of the annexin family of proteins, *J. Molec. Biol.* 223, 683–704.

32. Rescher, U., Ruhe, D., Ludwig, C., Zobiack, N., and Gerke, V. (2004) Annexin 2 is a phosphatidylinositol (4,5)-bisphosphate binding protein recruited to actin assembly sites at cellular membranes, *J. Cell. Sci.* 117 (16), 3473-3480.

33. Brumatti, G., Sheridan, C., and Martin, S.J. (2008) Expression and purification of recombinant annexin V for the detection of membrane alterations on apoptotic cells, *Methods.* 44, 235-240.

34. Hayes, M.J., and Moss, S.E. (2004) Annexins and diseases, *Biochem. Biophys. Res. Comm.* 322, 1166-1170.

35. Mussunoor, S., and Murray, G. (2008) The role of annexins in tumour development and progression, *J. Pathol.* 216, 131-140.

36. Morgan, R.O., and Fernandez, M.P. (1995) Molecular phylogeny of annexins and identification of a primitive homologue in *Giardia lambia*, *Mol. Biol. Evol.* 12 (6), 967-979.

37. Crumpton, M. J., and Dedman, J. R. (1990) Protein terminology tangle, *Nature* .345:212-223.

38. Wang, F., He, Xiao-Wen., Yan, Hong-Li., Huang, J.J., Zhang, Yi., Jiang, Lei., Gao, Y.J., and Sun, S.H. (2006) Non-fusion expression in *Escherichia coli*: Single-step purification of recombinant human annexin A5 for the detection of apoptosis, *Prot. Exp. Purif.* 45, 80-87.

39. Tsunezumi, J., Yamamoto, K., Higashi, S., and Miyazaki, K. (2008) Matrilysin (matrix metalloproteinase-7) cleaves membrane-bound annexin II and enhances binding of tissue-type plasminogen activator to cancer cell surfaces, *FEBS Lett.* 275, 4810-4823.

40. Hwang, J., Hodis, H.N., Hsiai, T.K., Asatryan, l., and Sevanian,A. (2006) Role of annexin II is estrogen-induced macrophage matrix metalloproteinase-9 activity: The modulating effect of statins, *Atherosclerosis.* 189, 76-82.

41. Pollard, H. B., and Rojas, E. (1988) Ca^{2+} activated synexin forms highly selective, voltage-gated Ca^{2+} channels in phosphatidylserine bilayer membranes, *Proc. Natl Acad. Sci.* 85, 2974–2978.

42. Cabrita, L.D., Dai, W., and Bottomley, S.P. (2006) A family of *E.coli* expression vectors for laboratory scale and high throughout soluble protein production, *BMC Biotech.* 6,12-19.

43. Sun, J. X., Shen, X.C., and Wu, X.F. (1999) Cloning and Expression of Annexin V cDNA in E.coli, *Sheng Wu Hua Xue Yu Sheng Wu Wu Li Xue Bao (Shanghai)*, 31(2), 163-166.

44. Zhang, L. N., Yang, X., and Hua, Z.C. (2000) Expression and purification of recombinant human annexin V in *Escherichia coli*, *Prep. Biochem. Biotechnol.* 30(4), 305-312.

45. Kaneko, N., Ago, H., Matsuda, R., Inagaki, E., and Miyano, M. (1997) Crystal structure of Annexin V with its ligand K-201 as calcium channel activity inhibitor, *J. Mol. Biol.* 274, 16-20.

46. Sohma, H., Ohkawa,H., Akino, T., and Kuroki, Y. (2001) Binding of annexins to lung lamellar bodies and the PMA-stimulated secretion of annexin V from alveolar type II cells, *J. Biochem.* 130, 449-455.

47. Chung, L., Dinakarpandian, D., Yoshida, N., Lauer-Fields, J.L., Fields, G.B., Visse, R. and Nagase, H. (2004). Collagenase unwinds triple-helical collagen prior to peptide bond hydrolysis, *EMBO J.* 23, 3020-3030.

48. Wu, D.Y., W. Ugozzoli, B.K. Pal, J. Qian, and R.B. Wallace. (1991) The effect of temperature and oligonucleotide primer length on specificity and efficiency of amplification by the polymerase chain reaction, *DNA Cell. Biol.* 10 (3), 233-238.

49. Sheffield, V.C., Cox, D.R., Lerman, L.S., and Myers, R.M. 1989. Attachment of a 40 base pair G+C rich sequence (GC-clamp) to genomic DNA fragments by polymerase chain reaction results in improved detection of single base changes, *Proc. Natl. Acad. Sci.* 86: 232-236.

50. Iwasaki, A., Suda, M., Nakao, H., Nagoya, T., Saino, Y., Arai, K., Mizoguchi, T., Sato, F., Yoshizaki, H., Hirata, M., Miyata, T., Shidara, Y., Murata, M., and Maki, M. (1987) Structure and expression of cDNA for an inhibitor of blood coagulation isolated from human placenta: a new lipocortin-like protein, *J. Biochem.* 102, 1261-1273.

51. Larkin, M.A., Blacksbields, G., Brown, N.P., Chenna, R, McGettigan, P.A., McWilliam, H., Valentin, F., Wallace, I.M., Wilm, A., Lopez, R., Thompson, J.D., Gibson, T.J., and Higgins, D.G. (2007) Clustal W and Clustal X version 2.0, *Bioinformatics.* 23, 2947-2948.

52. Elegbede, A.I., Srivastava, D. K., and Hinderliter, A. (2006) Purification of recombinant annexins without the use of phospholipids, *Protein. Expr. Purif.* 50(2), 157-162.

377